



PhD thesis

Kristoffer Szilas^{1,2,3}

Geochemistry of Archaean supracrustal belts in SW Greenland

Academic advisor: Robert Frei¹

External advisors: Minik T. Rosing²,

Thomas F. Kokfelt³ & Anders Scherstén⁴

Submitted: April 16th 2012

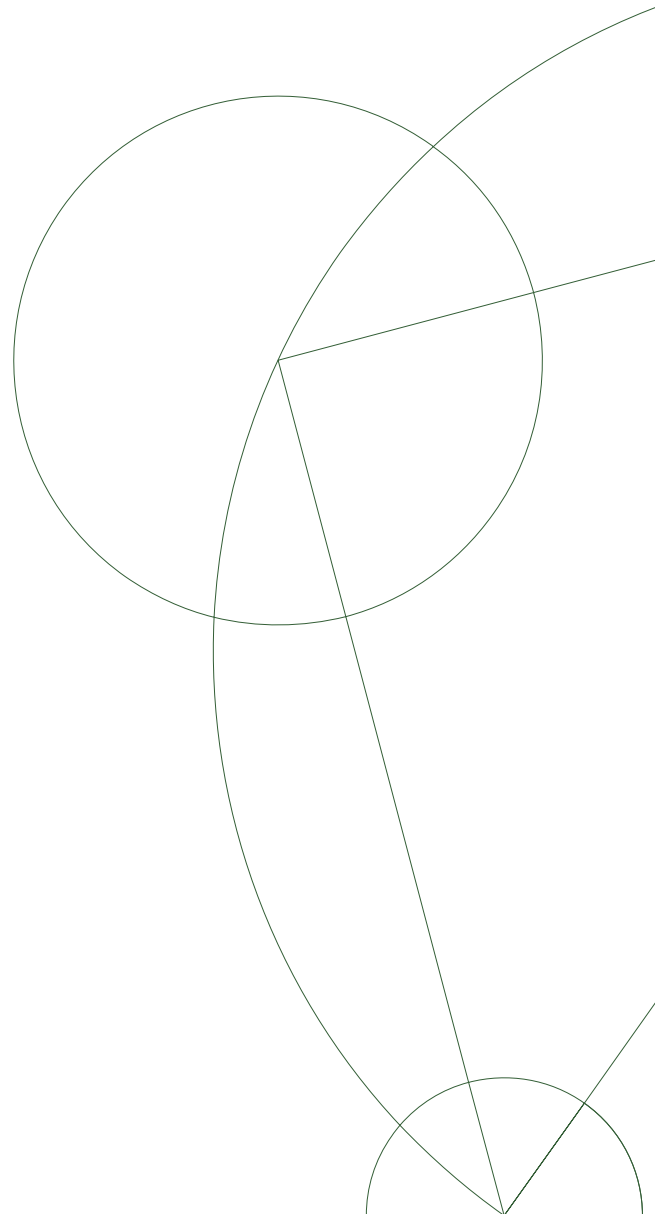
Affiliations:

¹Department of Geography and Geology, University of Copenhagen, Øster Voldgade 10, 1350, Copenhagen K, Denmark

²Natural History Museum of Denmark, Øster Voldgade 5-7, 1350, Copenhagen K, Denmark

³Geological Survey of Denmark and Greenland, Øster Voldgade 10, 1350, Copenhagen K, Denmark

⁴Department of Geology, Lund University Sölvegatan 12, 223 62 Lund, Sweden



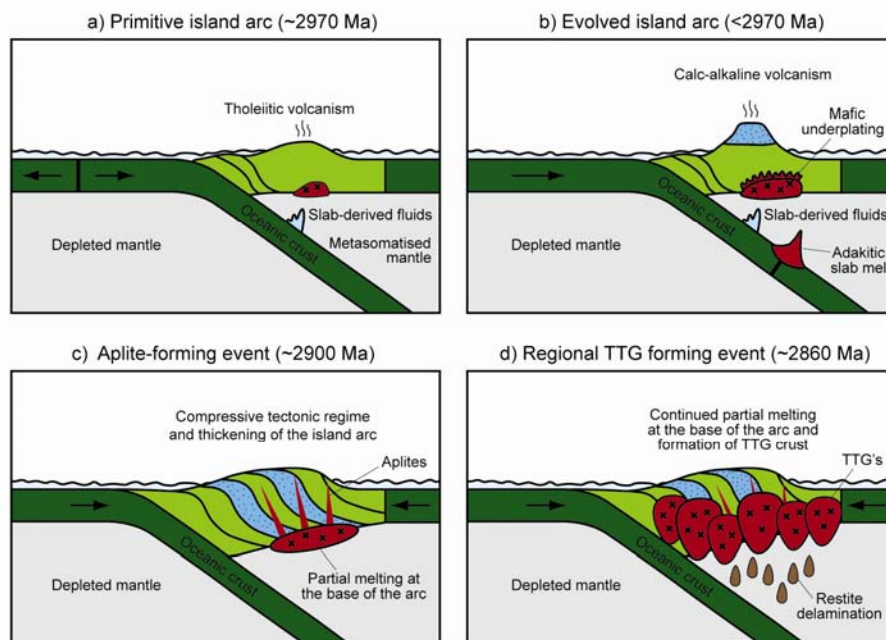
Contents

Abstract	I
Summary	II
Resumé (in Danish)	IV
Preface and acknowledgements	VI
Objectives	VIII
1. Introduction to the Archaean Eon	
1.1. Events in the early Earth	1
1.2. The cratonic crust	3
1.3. The sub-cratonic mantle	8
1.4. Archaean supracrustal belts	11
1.5. The geodynamic settings of supracrustal rocks	14
1.6. Previous work on Archaean supracrustal belts in SW Greenland	18
2. Discussion of the thesis papers	
2.1. Paper I: Remnants of arc-related Mesoarchaeoan oceanic crust in the Tartoq Group of SW Greenland	26
2.2. Paper II: Complex calc-alkaline volcanism recorded in Mesoarchaeoan supracrustal belts north of Frederikshåb Isblink, southern West Greenland: implications for subduction zone processes in the early Earth	29
2.3. Paper III: Origin of Mesoarchaeoan arc related rocks with boninite/komatiite affinities from southern West Greenland	31
3. Conclusions and future work	33
References	35
Curriculum Vitae	41
Annex	
Paper I: Remnants of arc-related Mesoarchaeoan oceanic crust in the Tartoq Group of SW Greenland	
Supplementary material for Paper I	
Paper II: Complex calc-alkaline volcanism recorded in Mesoarchaeoan supracrustal belts north of Frederikshåb Isblink, southern West Greenland: implications for subduction zone processes in the early Earth	
Supplementary material for Paper II	
Paper III: Origin of Mesoarchaeoan arc related rocks with boninite/komatiite affinities from southern West Greenland	
Supplementary material for Paper III	

Abstract

This PhD thesis investigates the petrogenesis of Mesoarchaeon (c. 3200-3000 Ma) supracrustal rocks from SW Greenland, using whole-rock geochemical, Sm-Nd and Lu-Hf isotope data. The main findings, for each of the three study areas, are the following:

- (1) The Tartoq Group contains a lithological assemblage of pillow lavas, shallow mafic sills/dykes, deeper level gabbros, and serpentinites of harzburgitic composition. This rock assemblage is interpreted as representing a section through oceanic crust. Whole-rock Lu-Hf isotope data yields an errorchron of 3189 ± 65 Ma. The geochemical data indicates an arc-affinity, similar to that of modern forearc- to backarc mafic magmas.
- (2) The Ikkattup Nunaa supracrustal association comprises basaltic and andesitic amphibolites, which display pillow lava and volcanoclastic structures, respectively. Whole-rock Lu-Hf data yield an errorchron of 2990 ± 41 Ma. The geochemical data are consistent with mixing of mafic and felsic magmas and mantle metasomatism in a process similar as that seen in modern island arcs. The graphical abstract below illustrates a model for the formation of the Ikkattup Nunaa supracrustal association, as an example of the processes that that may have operated in the Mesoarchaeon Era.
- (3) The Nunatak 1390 area comprises mafic and ultramafic rocks. The latter have geochemical features that are practically identical to Ti-enriched komatiites described in the literature. However, they show mixing with a slab-melt component and have Nd isotope compositions similar to the mafic rocks. The petrogenesis of these ultramafic rocks is suggested to reflect flux-melting of a strongly depleted mantle source in a similar way as modern boninites. In conclusion, all of the three studied areas contain characteristics that are entirely compatible, and best explained, by formation in an arc setting. Thus, it is suggested that modern-style subduction zone processes were in operation since at least the Mesoarchaeon Era.



Graphical abstract. Model for the formation of Mesoarchaeon calc-alkaline volcanic rocks in SW Greenland. a) Primitive island arc stage, which was dominated by tholeiitic basalts with characteristic negative Nb-anomalies. b) Evolved island arc stage where calc-alkaline andesites were formed by slab melt metasomatism and mixing of mafic melts with felsic melts produced by partial melting of the base of the arc due to mafic underplating. c) Convergent stage where the island arc crust was stacked and thickened, so that the base reached granulite facies metamorphic conditions and underwent partial melting to produce intrusive aplites. d) Large scale melting of the base of the island arc crust produced TTG batholiths.

Summary

This PhD thesis investigates the petrogenesis of Mesoarchaeoan (c. 3200-3000 Ma) supracrustal rocks from SW Greenland by whole-rock geochemical, Sm-Nd and Lu-Hf isotope, and U-Pb zircon data. The foundation of this PhD thesis is the three papers found in the Annex. Additionally, three preceding chapters provide a general introduction to the Archaean Eon, previous work on supracrustal belts in SW Greenland, a discussion of the three papers, and finally conclusions and suggestions for future work in this region. The three papers present field- and geochemical data from the Tartoq Group, the Ikkattup Nunaa supracrustal association and the Nunatak 1390 area. The main findings are the following:

The Tartoq Group crops out as a series of blocks and slivers that are imbricated with originally intrusive Mesoarchaeoan tonalite-trondhjemite-granodiorite (TTG) orthogneisses along the southern margin of the North Atlantic craton. It comprises an assemblage of supracrustal rocks, of mainly tholeiitic basalt composition, which includes pillow lavas, sills/dykes, gabbros, and serpentinites. This rock assemblage resembles that of Phanerozoic ophiolites (ocean floor). The metamorphic grade ranges from greenschist- to upper amphibolites-facies. LA-ICP-MS U-Pb zircon dating of an intrusive TTG sheet yields a minimum age of 2986 ± 4 Ma for the Tartoq Group. This age is consistent with a MC-ICP-MS Lu-Hf whole-rock errorchron of 3189 ± 65 Ma and a Sm-Nd errorchron of 3068 ± 220 Ma for the supracrustal rocks. Overall the geochemical features of the Tartoq Group rocks are characterised by chondrite-normalized REE patterns with La_{CN}/Sm_{CN} of 0.67-1.96 and rather flat primitive mantle-normalized multi-element patterns, except for scattered LILE contents, and generally negative Nb-anomalies with Nb/Nb* of 0.26-1.31. Th/Yb varies between 0.06 and 0.47 and Nb/Yb between 0.45 and 4.4, indicative of an arc affinity when compared to rocks from modern settings. The geochemical signatures of the Tartoq Group rocks thus resemble rocks from modern forearc ophiolites, as well as Archaean supracrustal rocks found elsewhere in SW Greenland, such as the Isua and Ivisartoq supracrustal belts in the Nuuk region. Therefore the Tartoq Group likely represents remnants of dismembered Mesoarchaeoan suprasubduction zone oceanic crust.

The Ikkattup Nunaa Supracrustal Association is a collective name that is proposed for the three Mesoarchaeoan supracrustal belts of Ravns Storø, Bjørnesund and Perserajørsuaq. It is situated north of Frederikshåb Isblink and south of the Fiskerhæset complex in SW Greenland. The Ikkattup Nunaa Supracrustal Association mainly comprises tholeiitic amphibolites and calc-alkaline leucoamphibolites of basaltic and andesitic composition, respectively. Primary structures such as pillow lavas and tuffs are well preserved in the Ravns Storø supracrustal belt. The supracrustal lithologies are cut by aplite sheets of TTG composition with LA-ICP-MS U-Pb zircon ages of c. 2900 Ma. Whole-rock MC-ICP-MS Lu-Hf and Sm-Nd errorchrons based on amphibolites and leucoamphibolites from the Ravns Storø and Bjørnesund supracrustal belts combined yield ages of 2990 ± 41 Ma for the Lu-Hf system and 3020 ± 78 Ma for the Sm-Nd system. The leucoamphibolites form apparent geochemical mixing trends between the tholeiitic amphibolites and TTG gneisses as end-members. By assimilation-fractional crystallisation (AFC) modelling it can be shown that one group of leucoamphibolites can be explained by contamination of the parental melts by a TTG-like end-member and another group of high P_2O_5 , La and Nb leucoamphibolites can be explained by contamination involving a hypothetical low-silica adakite end-member. However, the leucoamphibolites are juvenile with $\epsilon Nd_{(2970 \text{ Ma})}$ from +2.1 to +3.5 and $\epsilon Hf_{(2970 \text{ Ma})}$ of +3.5 to +4.3. Thus, the mafic source of the felsic contaminant melts must have been derived from a depleted mantle source more or less at the same time (<60 Ma) as the volcanism took place. Our preferred interpretation of the

whole-rock geochemical and isotope data is that the protoliths of the supracrustal rocks formed in an island arc setting, where early tholeiitic volcanism gave way to calc-alkaline volcanism in a maturing arc. The apparent contamination trends are thus explained by *in situ* partial melting of basaltic arc crust to form juvenile TTG- and adakite-melts that mixed with mafic magmas or contaminated their mantle source to produce the calc-alkaline leucoamphibolite protolith. This model has important implications for the general interpretation of Archaean supracrustal belts, because AFC and geochemical mixing trends towards a TTG end-member are not uniquely diagnostic of crustal contamination, but may rather reflect processes operating at source levels in arcs, such as melting-assimilation-storage-homogenisation (MASH) or slab-melt (low-silica adakite) metasomatism of their mantle source. Therefore, this study supports the operation of subduction zone processes since the Mesoarchaeon Era.

The Nunatak 1390 is not a supracrustal belt by itself, as the outcrop is only about 6 km², but it might be correlated to similar rocks west of it. The Nunatak 1390 supracrustal rocks have a minimum age of c. 2900 Ma defined by LA-ICP-MS U-Pb zircon ages of cross-cutting aplite sheets of TTG composition. The supracrustal rocks comprise pillowed and layered amphibolites and ultramafic rocks with amphibolite facies mineral assemblages and a peak metamorphic temperature of approximately 550°C. The mafic sequence has relatively flat trace element patterns (La_N/Sm_N of 0.70-2.4) and mostly negative Nb-anomalies (Nb/Nb^* of 0.30-1.0). The mafic sequence can be divided into a high- and low-Ti group, where the former group has lower MgO, and significantly higher contents of incompatible elements such as TiO_2 , P_2O_5 , Zr, Nb and Th. The ultramafic rocks, consisting of serpentine, chlorite, magnetite and amphibole, have similar major and trace element compositions as Ti-enriched/Karasjok-type komatiites described in the literature. The low-Ti group of the mafic sequence appears to have been derived from a N-MORB source, whereas the high-Ti group and the ultramafic rocks appear to have been derived from a mantle source that is more enriched than the N-MORB source. However, there is no difference in the initial ϵNd of the mafic and ultramafic rocks. Additionally, AFC modelling suggests that the enrichment was caused by introduction of a juvenile low-silica adakite melt component into their mantle source region. Accordingly, we propose that the mafic and ultramafic rocks were derived from a similar mantle source, but that the ultramafic rocks were derived from a previously depleted mantle source that was refertilised by slab melts and fluids in a subduction zone setting. Thus, the high MgO contents of the ultramafic rocks may reflect second-stage melting of refractory mantle, in a process that is similar to the formation of modern boninites. The implication of this model is that rock of komatiitic composition may not always be derived from deep mantle plumes, as has otherwise been the consensus view for the last three decades. Komatiitic rocks could instead reflect shallow melting of refractory mantle that was fluxed by melts and fluids in a subduction zone setting, and thus represent Archaean equivalents of modern boninites. This scenario is likely for at least the Ti-enriched type of komatiite-like ultramafic rocks that we have identified in the Nunatak 1390 supracrustal sequence and such a model is supported by the recent literature that is continuously documenting new evidence for a hydrous origin of komatiites.

In conclusion all of the three studied areas contain geochemical- and field characteristics that are entirely compatible, and best explained, by formation in a subduction zone geodynamic setting. Therefore this study confirms previous work on Archaean supracrustal rocks from SW Greenland, which suggest that accretion of island arc complexes resulted in thickened mafic crust. Partial melting of these supracrustal lithologies in the lower crust resulted in formation of TTG intrusions in a convergent tectonic environment.

Resumé (in Danish)

Denne PhD-afhandling undersøger petrogenesen af Midtarkæiske (ca. 3200-3000 Ma) suprakrustale bjergarter fra SV Grønland ved geokemiske, Sm-Nd og Lu-Hf isotop, og U-Pb zirkon data. Hovedparten af denne PhD-afhandling består af de tre publikationer, som findes i Annexet. Derudover giver tre forudgående kapitler en generel introduktion til det Arkæiske Eon, tidligere studier af suprakrustale bælter i SV Grønland, en diskussion af de tre publikationer, og endelig konklusioner og forslag til fremtidigt arbejde i denne region. De tre publikationer præsenterer feltobservationer og geokemiske data fra Tartoq-gruppen, Ikkattup Nunaa suprakrustal associationen samt Nunatak 1390. De vigtigste konklusioner er følgende:

Tartoq-gruppen udgøres af en serie af blokke og skiver, som er imbrikerede med oprindeligt intrusive Mesoarkæiske tonalit-trondhjemit-granodiorit (TTG) orthognejser langs den sydlige margin af det Nordatlantiske craton. Den omfatter en samling af suprakrustale bjergarter af hovedsagelig tholeiitisk basalt sammensætning, som består af pude lava, horisontale eller vertikale gangbjergarter, gabbroer, og serpentinit. Denne samling af bjergarter minder om Phanerozoiske ofioliter (havbundsskorpe). Den metamorfe grad varierer fra grønstens- til øvre amfibolit-facies. LA-ICP-MS U-Pb zirkon datering af en intrusiv TTG gnejs giver en minimumsalder på 2986 ± 4 Ma for Tartoq-gruppen. Denne alder underbygges af en MC-ICP-MS Lu-Hf isokron på 3189 ± 65 Ma og en Sm-Nd isokron på 3068 ± 220 Ma for de suprakrustale bjergarter. Den samlede geokemiske signatur af Tartoq-gruppen er karakteriseret ved kondrit-normaliserede REE mønstre med La_{CN}/Sm_{CN} på 0,67-1,96 og forholdsvis flade primitive kappe-normaliserede multi-element mønstre, bortset fra variabelt LILE-indhold, og generelt negative Nb-anomalier med Nb/Nb* mellem 0,26 og 1,31. Th/Yb varierer mellem 0,06 og 0,47 og Nb/Yb varierer mellem 0,45 og 4,4, hvilket tyder på en vulkanisk øbue affinitet når man sammenligner med bjergarter fra moderne geologiske miljøer. De geokemiske signaturer for Tartoq-gruppen ligner dermed bjergarter fra moderne forlands ofioliter, samt Arkæiske suprakrustale bjergarter fra andre steder i SV Grønland, såsom Isua og Ivisaartok suprakrustalerne i Nuuk regionen. Samlet set er det sandsynligt at Tartoq-gruppen repræsenterer resterne af opbrudt Midtarkæisk suprasubduktionszone oceanisk skorpe.

Ikkattup Nunaa suprakrustal associationen er et samlet navn, som foreslås for de tre Midtarkæiske suprakrustale bælter: Ravns Storø, Bjørnesund og Perserajoorsuaq. Det ligger nord for Frederikshåb Isblink og syd for Fiskeræset komplekset i SV Grønland. Ikkattup Nunaa suprakrustal associationen består hovedsagelig af tholeiitiske amfiboliter og calc-alkaline leucoamfiboliter af henholdsvis basaltisk og andesitisk sammensætning. Primære strukturer såsom pudelava og tuffer og velbevarede i Ravns Storø suprakrustal bæltet. De suprakrustale enheder skæres af aplitgange med TTG sammensætning, som har LA-ICP-MS U-Pb zirkon aldrer på ca. 2900 Ma. MC-ICP-MS Lu-Hf og Sm-Nd isokroner baseret på amfiboliter og leucoamfiboliter fra Ravns Storø og Bjørnesund suprakrustalerne resulterer samlet i alderen 2990 ± 41 Ma for Lu-Hf systemet og 3020 ± 78 Ma for Sm-Nd systemet. Leucoamfiboliterne danner tilsyneladende geokemiske blandinger mellem de tholeiitiske amfiboliter og TTG gnejserne, som repræsenterer endeled. Ved assimilations-fraktioneret krystallisations (AFK) modellering kan man vise, at én gruppe af leucoamfiboliterne kan forklares med kontaminering af udgangssmelterne med et TTG-lignende endeled og at en anden gruppe af højt P_2O_5 , La og Nb leucoamfiboliter kan forklares med kontaminering af et hypotetisk lav-silica adakit endeled. Det viser sig dog at leucoamfiboliterne er juvenile med $\epsilon Nd_{(2970 \text{ Ma})}$ fra 2,1 til 3,5 og $\epsilon Hf_{(2970 \text{ Ma})}$ fra 3,5 til 4,3. Dette betyder at den mafiske kilde til den felsiske kontaminant må være afledt fra en forarmet kappe-kilde mere eller mindre samtidigt med (<60 Ma) at vulkanismen fandt sted. Vores foretrukne tolkning af de geokemiske og isotopiske data er at protoliten til de

suprakrustale bjergarter blev dannet i et vulkansk øbue miljø, hvor tidlig tholeiitisk vulkanisme blev afløst af calc-alkalin vulkanisme efterhånden som øbuen udviklede sig. De tilsyneladende kontaminations tendenser kan således forklares ved *in situ* delvis opsmeltning af basaltisk øbueskorpe som dannede juvenile TTG- og adakitiske smelter, der blandede sig med mafiske magma eller forurenede deres kappe-kilde og dermed resulterede i protoliten til de calc-alkaline leucoamfiboliter. Denne model har stor betydning for den generelle tolkning af andre Arkæiske suprakrustale bæltet, fordi AFK og geokemiske blandingstendenser, som tyder på et TTG endeled ikke er nødvendigvis diagnostisk for skorpekontaminering, men kan derimod reflektere processer, som opererer i kappe-kilden i vulkanske øbuer, såsom smeltning-assimilering-lagring-homogenisering eller subduktionsplade-smelte- (lav-silica adakit) overprægning af deres kappe-kilde. Derfor underbygger dette studie at subduktionszoneprocesser har fundet sted siden den Midtarkæiske Era.

Nunatak 1390 er ikke i sig selv et suprakrustalt bælte, da det kun udgør et areal på ca. 6 km², men det kan muligvis korreleres med tilsvarende bjergarter længere mod vest. Nunatak 1390 suprakrustalerne har en minimumsalder på ca. 2900 Ma, defineret ved LA-ICP-MS U-Pb zirkon-aldre af skærende aplitgange af TTG sammensætning. Suprakrustalerne omfatter pudelavaer og lagdelte amfiboliter, samt ultramafiske bjergarter med amfibolit-facies mineralogisk sammensætning og maksimale metamorfe temperaturer på omkring 550°C. Den mafiske sekvens har relativt flade sporelementsmønstre (La_N/Sm_N mellem 0,70 og 2,4) og for det meste negative Nb-anomalier (Nb/Nb^* mellem 0,30 og 1,0). Den mafiske sekvens kan opdeles i en høj- og lav-Ti-gruppe, hvor den førstnævnte gruppe har lavere MgO og signifikant højere indhold af inkompatible elementer, såsom TiO_2 , P_2O_5 , Zr, Nb og Th. De ultramafiske bjergarter, bestående af serpentin, klorit, magnetit og amfibol har sporelementsmønstre, som er næsten identiske med såkaldte Ti-berigede/Karasjok-type komatiitter beskrevet i litteraturen. Lav-Ti gruppen i den mafiske sekvens er tilsyneladende afledt fra en N-MORB kappe-kilde, hvorimod høj-Ti-gruppen, og de ultramafiske bjergarter synes at være afledt af en kappe-kilde, som var mere beriget end N-MORB kilden. Der er imidlertid ingen forskel i deres initiale ϵNd værdier. Derudover tyder AFK-modellering på at berigelsen var forårsaget af overprægning af kappe-kilden med juvenile lav-silica adakite smelter. Derfor foreslås det at både de mafiske og ultramafiske bjergarter blev afledt fra den samme kappe-kilde, men at de ultramafiske bjergarter var afledt fra en tidligere forarmet kappe-kilde, der blev overpræget af smelter og fluider i en subduktionszone. Det høje MgO-indhold i de ultramafiske bjergarter afspejler således muligvis en to-trins opsmeltning af kappen i en proces, der svarer til dannelsen af moderne boniniter. Implikationen af denne model er, at komatiitter ikke nødvendigvis dannes som følge af dybe kappediapirer, som det ellers har været konsensus i de sidste tre årtier. Komatiitter kunne derimod afspejle delvis opsmeltning af refraktorisk kappe, der blev fluxet med smelter og fluider i en subduktionszone og dermed repræsenterer Arkæiske ækvivalenter af moderne boniniter. Denne model er mulig for i hvert fald den Ti-berigede type af komatiitter, som vi har identificeret på Nunatak 1390 og en sådan model er understøttet af den nyere litteratur, som løbende dokumenterer nye beviser for en volatilrig oprindelse af komatiitter.

Konklusionen for de tre undersøgte områder, baseret på geokemiske data og feltobservationer, er at disse bjergarter er fuldstændigt kompatible med, og kan lettest forklares ved, dannelse i et subduktionszone miljø. Derfor bekræfter denne afhandling tidligere studier af de Arkæiske suprakrustale bjergarter i SV Grønland, som antyder at amalgamering af vulkaniske øbue-komplekser resulterede i fortykket mafiske skorpe. Delvis opsmeltning af disse suprakrustale enheder i den nedre skorpe resulterede i dannelsen af TTG intrusioner i et konvergerende tektonisk miljø.

Preface and acknowledgements

My interest in Archaean geology began when I was hired by the exploration company NunaMinerals A/S, as a field assistant for Jeroen van Gool, who was then working at the Geological Survey of Denmark and Greenland (GEUS). Fieldwork together with him and Claus Østergaard on Storø in SW Greenland greatly motivated me to get into this area of geoscience, because I realised how little was actually known about this period of Earth's history. During the three summers of fieldwork that I did for NunaMinerals I met legendary geologists such as Minik Rosing, Clark Friend and Allen Nutman, who are pioneers in the Archaean geology of SW Greenland.

Christian Knudsen from GEUS convinced me to do a MSc project about the Storø supracrustal belt, where I would study the geochemistry of supracrustal rocks and investigated the relation between hydrothermal alteration zones and gold mineralisation in these rocks. Anders Scherstén at GEUS and Jens Konnerup-Madsen at the Geological Institute of Copenhagen were my supervisors for the project. During this work I also had many productive discussions with Jeroen van Gool, Adam Garde, Denis Schlatter and Jochen Kolb at GEUS, who were all very helpful in guiding my project in the right direction. I finished my MSc thesis and then applied for the present PhD project at GEUS. This was financed by the so-called GEOCENTER, so I would have a supervisor in each of the three research institutes; Minik Rosing at the Natural History Museum, Robert Frei at the Geological Institute and Anders Scherstén at GEUS. When Anders later resigned from GEUS to work at Lund University in Sweden, I also got Thomas Kokfelt as a supervisor at GEUS.

As the title of my PhD thesis suggests this project was rather broadly defined with very few initial constraints. The idea was simply to do field work on the GEUS lead campaigns in the summers of 2009 and 2010 and characterise the samples that were collected. My task was to find out what information this data could provide about the petrogenesis of Archaean supracrustal belts in SW Greenland. Obviously nothing was guaranteed, but each of the three thesis areas happened to be unique and presented excellent opportunities to study the Archaean geodynamic environments of SW Greenland. Eventually, after three exciting years of studies, I have complied, presented and interpreted all of the data that was generated by the present PhD project.

During this time I visited the University of Alberta in Edmonton, Canada, for two months where I worked in Robert Creaser's Re-Os isotope laboratory. Unfortunately, this work is not included in my PhD thesis, because there were some spike-problems at the laboratory at the time, so the data ended up not being useful in this study. Fortunately, Anders Scherstén had a contact to Carsten Münker's laboratory in Bonn, Germany, so I could take a short trip there to learn another method. Their MC-ICP-MS laboratory was a great experience for me and I was introduced by Elis Hoffmann to the Sm-Nd and Lu-Hf methods that they routinely use. He was doing a PhD thesis about the Isua supracrustal belt at the time and our work shared many of the questions we wished to answer. He became a great college and friend and I am grateful for all of the help that I got from him during my thesis work.

I am also happy that I have been able to participate I conferences such as the Fifth International Archean Symposium in Perth, the 2011 European Geophysical Union conference and the 2011 Goldschmidt conference. During these conferences I not only learned a lot about the Archaean Earth, but I also developed a large network with scientist in this field of research. For instance this resulted in me being invited to Oulu in Finland by Wolfgang Maier to present some of my work during a workshop on Archaean geology and metallogeny in the spring of 2010. Through these various meetings I now have a good network with young geoscientists such as Vincent van Hinsberg (Holland), Elis

Hoffman (Germany), Esa Heilimo (Finland), who all work with similar research as I do and I am sure that we will collaborate much in the future.

I appreciate the many fruitful discussions during field work in Greenland with Vincent van Hinsberg, Alex Kisters, Brian Windley and Ali Polat. I would also like to thank Tomas Næraa, whom I have shared an office with at GEUS, for many interesting discussions about Archaean geology over the years. I would also like to thank the technicians, who helped me out with the laborious zircon separation work at GEUS: Fiorella Aguilera and Mojagan Alaei.

Finally, I would like to thank my friends and family who have supported me in this long journey. Although they may not always have understood what it is that I have been doing for all of these years, they respect the time and effort I have put in to this work. Personally, I am proud to have provided yet another piece to the puzzle of the early Earth, however small my contribution may be.

Objectives

The aim of this PhD thesis was to describe the geochemical characteristics of Archaean supracrustal rocks from SW Greenland by their whole-rock major and trace element contents. Sm-Nd and Lu-Hf isotope data is used in order to date the supracrustal rocks directly by isochrons and to evaluate their mantle source and degree of crustal contamination. Additionally, U-Pb zircon dating provides minimum ages for the supracrustal rocks from cross-cutting granitoid sheets. The above geochemical methods would serve as tools to investigate the main question that this study attempts to answer:

“What was the geodynamic setting in which the Mesoarchaeoan supracrustal belts of SW Greenland formed”?

The hypothesis that I set out to test was basically if the geochemical data are compatible with a subduction zone setting, as proposed by previous work in the region, or if the data are in fact better explained by alternative models like plume-related tectonic processes, as suggested for some Archaean supracrustal belts in other parts of the world.

The thesis consists of a synopsis with three chapters; The first serves as a general introduction to the different elements of Archaean geology and discusses possible interpretations of the Archaean rock record. The second chapter discusses the three thesis papers. The third chapter provides conclusions based on the three papers, as well as on the literature outlined in the first section and provides a platform of understanding on which future research in the region can be based.

1. Introduction to the Archaean Eon

In the following sections I briefly outline the evolution and current understanding of the Archaean Earth and its main components: the cratonic crust, the sub-cratonic mantle and the supracrustal belts. The latter represent the uppermost portion of the lithosphere and constitute the main topic of this thesis. The Archaean Eon is defined here as the time period from about 3800 to 2500 Ma in Earth's history. Supracrustal belts are defined as remnants of sedimentary, volcanic and shallow intrusive geological environments of the early Earth.

It is important to point out that the three papers presented in the Annex represent the foundation of this PhD thesis and that Chapters 1, 2 and 3 serve as an introduction and summary of the findings of the three papers. Therefore, for the results and the detailed discussions, the reader is referred to the papers in the Annex. The actual geochemical data that form the basis of this work can be found as supplementary material after each paper.

1.1. Events in the early Earth

According to our current best understanding of the early Solar System it formed at 4567.2 ± 0.6 Ma, which is the Pb-isotopic age obtained from chondritic meteorites (Amelin et al., 2002). Within a few million years, the Earth grew through accretion of increasingly bigger planetesimals in the Solar Nebula (Kleine et al., 2002; Yin et al., 2002). Recent isotopic studies have shown that the Earth had differentiated into core, mantle and crust less than 30 Ma after formation of the Solar System (Boyet and Carlson, 2005; Jacobsen, 2005). The formation of the Moon is intimately related to the early differentiation of the Earth, because it is believed to be the result of a collision of a Mars-sized body with the proto-Earth during the so-called 'Giant Impact' (Stevenson, 1987; Canup, 2004). The timing of this event is also believed to be less than 30 Ma after the initiation of the Solar System and marks the end of major Earth accretion (Schoenberg et al., 2002). Table 1 below shows some of the most important events in early history of the Earth.

The time period from the formation of Earth to the beginning of the Archaean Eon is called the Hadean Eon after the Greek word Hades, which means 'unseen' and refers to 'hell' in Greek mythology. This name was chosen because it was believed that the young Earth was completely molten and no rocks were preserved from this time. It is thought that due to the higher contents of undecayed radioactive elements in the Hadean, only low K, U and Th high-Mg basalt could have formed a thermally stable crust, but from isotopic considerations this protocrust must have been completely recycled into the mantle between 3800 and 3500 Ma (Kamber, 2007). Additionally, the 'Late Heavy Bombardment' (LHB), which was a period of abundant meteorite impacting down to c. 3900 Ma (Tera et al., 1974; Kring and Cohen, 2002), was thought to have destroyed any geological record prior to this.

However, rocks and minerals are in fact preserved from the Hadean Eon on Earth, such as granitoid rocks from the Acasta Gneiss Complex in Canada dated at 4031 Ma (Bowring and van Schmus, 1984; Iizuka et al., 2007), which contains c. 4200 Ma inherited zircon. These zircon grains have trace element chemistry that suggests crystallisation from granitic melts (Iizuka et al., 2006). Detrital zircons from the Jack Hills metasediments in Australia date back to 4404 Ma and thus provide evidence for even older granitoid rocks (Compston and Pidgeon, 1986; Wilde et al., 2001; Harrison et al., 2005). Hadean granitoids that hosted zircon are interpreted as having formed by internal thermal differentiation of basaltic crust rather than due to subduction-related continental crust formation (Kamber, 2007; Rollinson, 2008a; Kemp et al., 2010). However, Bizzarro et al. (2012) recently showed that the Hf-isotope composition

of chondrites may need to be changed, so that the enriched and depleted reservoirs of the crust-mantle system can be traced back all the way to 4300 Ma, implying that plate tectonic processes may have been in operation throughout most of Earth's history.

The boundary between the Hadean and Archaean is not strictly defined in the rock record, but is rather represented by the end of the LHB and is thus difficult to date precisely (Zahnle et al., 2007). However, recently it has been questioned whether the LHB even existed (Norman, 2009), in which case this boundary should probably be defined as the age of the oldest preserved supracrustal rocks.

Event	Time	Reference
Formation of the Solar System	~ 4567 Ma	Amelin et al. (2002)
Accretion of the Earth	~ 4556 Ma	Yin et al. (2002)
Mantle and proto crust differentiation	> 4537 Ma	Boyet and Carlson (2005)
End of core formation	~ 4537 Ma	Jacobsen (2005)
The Giant Impact and Moon formation	~ 4537 Ma	Schoenberg et al. (2002)
Oldest preserved zircons on Earth	< 4400 Ma	Wilde et al. (2001)
Oldest preserved granitoids on Earth	< 4030 Ma	Iizuka et al. (2007)
The Late Heavy Bombardment	~ 3900 Ma	Kring and Cohen (2002)
Oldest preserved supracrustal rocks on Earth	~ 3800 Ma	Friend and Nutman (2010)

Table 1. The timing of some important events in the early Earth.

It has been proposed that supracrustal rocks with an age of 4280 Ma are present in the Nuvvuagittuq greenstone belt in the Superoir Province (O'Neil, 2009). However, this isochron age is based on the short-lived ^{146}Sm - ^{142}Nd system and may reflect the age of the mantle reservoir that the rocks were extracted from rather than their extrusion age. Orthogneisses that are folded with the supracrustal rocks provide U-Pb zircon ages of 3750 Ma (Cates and Mojzsis, 2007). Thus, more research is required on these supracrustal rocks before their age can be confidently determined and at the moment this is outcrop remain controversial and will not be discussed further in this thesis.

The oldest non-controversial supracrustal rocks currently known on Earth are found in the North Atlantic craton. The largest and best preserved outcrops are located in SW Greenland and have been dated by cross-cutting granitoid sheets to be older than about 3800 Ma (Baadsgaard, 1973; Nutman et al., 1996; Manning et al., 2006). There have been some discussion about which outcrop actually contains the oldest supracrustal rocks, but it is generally agreed that the Isua supracrustal belt represents the largest and most coherent outcrop of rocks with an age older than c. 3800 Ma (Myers and Crowley, 2000; Kamber et al., 2005; Nutman and Friend, 2009b; Friend and Nutman, 2010). Of great interest is the occurrence of banded iron formation and clastic sediments. These rocks are important because they give constraints on the temperature of Earth's surface at the time.

Solar phycisists are confident that the young Sun was some 25% less luminous than it is now (Schwarzschild, 1958). For this reason Earth should have been frozen solid at its surface around 3800 Ma, but the presence of sediments in the Isua supracrustal belt proves otherwise. This problem has been termed the 'faint young Sun paradox' (Sagen and

Mullen, 1972; Sagen and Chyba, 1997). Several possible explanations have been proposed over the years for this paradox, such as high levels of greenhouse gasses in the atmosphere (e.g. Kiehl and Dickinson, 1987) or lower albedo due to changes in the cloud cover (Rondanelli and Lindzen, 2010; Rosing et al., 2010). However, recent work on serpentinites from the Isua supracrustal belt show that Earth's oceans were up to 26% more voluminous at that time (Pope et al., 2012). This result is consistent with the observation that most Archaean supracrustal belts show signs of subaqueous volcanism (de Wit and Ashwal, 1997). This in turn would mean that the continents were flooded and that Earth's surface albedo would be significantly lower than at present and could thus solve the paradox. However, this still assumes that the cloud cover would have to be lower than now. It has been observed that the present cloud cover appears to be linked in some way to the cosmic ray flux that reaches Earth (Svensmark and Friis-Christensen, 1997). Therefore a possible mechanism that could yield a low cloud cover is the idea is that cosmic rays produce ions in the atmosphere that could cause an increase in cloud nucleation. Because the cosmic rays flux on Earth is modulated by the magnetic field of the Sun, and given that the magnetic activity would have been far greater in the young Sun, it is a possibility that the cloud cover on Earth would have been much lower than at present (Karooff and Svensmark, 2010). At the moment this hypothesis remains controversial, but experiments are currently trying to quantify this mechanism at the CERN facility in Geneva.

The end of the Archaean Eon and the transition to the Proterozoic Eon has been set at 2500 Ma, although it is not determined by any stratigraphic boundary; it roughly coincides with the Great Oxidation Event, when oxygen levels rose significantly in the early atmosphere (Canfield, 2005; Anbar et al., 2007).

1.2. The cratonic crust

Earth is the only planet in the Solar System that has an extensive granitoid crust (Campbell and Taylor, 1983). This is likely related to three facts: (1) Earth is the only planet on which water primarily exists in a liquid state due to its size, distance from the sun and its atmospheric composition (Zahnle et al., 2007), (2) the operation of plate tectonic processes, which affects the shallow mantle by introducing hydrated phases (e.g. Rüpke et al., 2004), and (3) life produces oxygen through photosynthesis, which changes the oxidation state of the atmosphere and hydrosphere and therefore promotes reaction with rocks at the surface, which in turn can affect the mantle during recycling (Rosing et al., 2006). All of the above were likely important for the formation of Earth's granitoid crust, and although there is no agreement on their relative importance, liquid water probably had the greatest impact on the development of the continental crust by lowering the mantle solidus, and enhancing melt production and differentiation (Gaetani and Grove, 1998; Katz et al., 2003).

Areas where rocks of Archaean (and Proterozoic) age are extensively represented are known as cratons, which comprise vast volumes of gneisses of tonalite-trondhjemite-granodiorite (TTG) composition (e.g. Condie and Pease, 2008). Cratons are stable parts of the continental lithosphere that survived the Wilson Cycles of rifting and collision of the continents through time (Wilson, 1966), and form the Archaean and Proterozoic cores of the continents. Thus, they are tectonically inactive regions, which expose the oldest rocks preserved on Earth. The cratons are commonly surrounded by younger orogenic belts, which are the tectonically active parts of the lithosphere (Fig. 1).

Seismic data show that the continental crust in cratons is 41 km thick on average (Christensen and Mooney, 1995). Such cratonic crust is underlain by thick buoyant cratonic mantle (Section 1.3), which is believed to be the main

reason why this old continental crust maintained long-term stability and was not reworked during the orogenic cycles (Jordan, 1978). Archaean supracrustal belts are located within the cratonic crust, and comprise volcanic, shallow intrusive and sedimentary rocks that are generally located in belts or extensive enclaves within the TTG gneisses (Section 1.4; Condie, 1981). Supracrustal belts are usually dominated by mafic rocks of tholeiitic basalt composition, which have experienced greenschist- or granulite-facies metamorphism.

It is now well established that rocks of TTG composition can be produced by polybaric partial melting of hydrous mafic rocks, such as those found in Archaean supracrustal belts (Rapp and Watson, 1995; Foley et al., 2002; Clemens et al., 2006). There is usually a distinct depletion in heavy rare earth elements (HREE) in TTGs. This can be explained by melting of garnet amphibolite or eclogite, which leaves garnet in the residue and retains the HREEs. Thus, there appears to be a genetic link between the mafic rocks found in Archaean supracrustal belts and the cratonic crust (e.g. Rollinson, 2010). Although the specific tectonic setting of the formation of the Archaean continental crust is still debated (Section 1.5), the data are compatible with a broad range of P-T conditions (Moyen, 2011). Whatever the exact setting, this partial melting process would lead to vast amounts of depleted eclogite/pyroxenite cumulates, which might reside deep in the mantle (Barth et al., 2002) or alternatively might be melted by catalytic reactions with the mantle (Bédard, 2006).

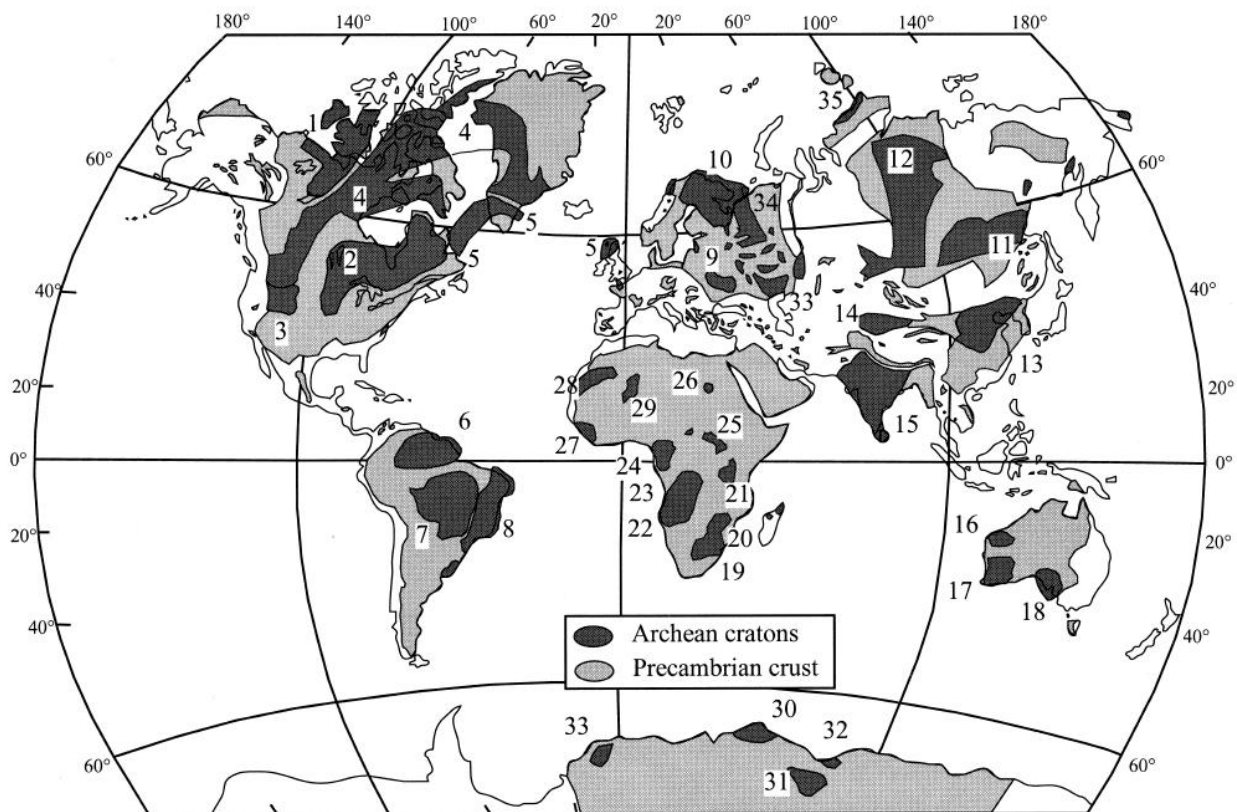


Figure 1. Worldwide distribution of Archaean cratons and areas underlain by Precambrian/Proterozoic crust. Continental areas that are left blank are of Phanerozoic age. The Archaean cratons are labelled as follows: 1) Slave Province, 2) Superior, 3) Wyoming, 4) Kaminak (Hearne), 5) North Atlantic (Nain, Godthaab, Lewisian), 6) Guiana, 7) Central Brazil (Guapore), 8) Atlantic (São Francisco), 9) Ukrainian, 10) Baltic (Kola), 11) Aldan, 12) Anabar, 13) Sino-Korean, 14) Tarim, 15) Indian, 16) Pilbara, 17) Yilgarn, 18) Gawler, 19) Kaapvaal, 20) Zimbabwe, 21) Zambian, 22) Angolan, 23) Kasai, 24) Gabon, 25) Kibalian, 26) Uweinat, 27) Liberian, 28) Maritanian, 29) Ouzzalian, 30) Napier Complex, 31) Prince Charles Mountains, 32) Vestfold Hills, 33) Heimefront Ranges, 34) deeply buried Archaean rocks of the East European Shield, 35) Tajmyr. Figure from Kusky and Polat (1999).

The fact that the average composition of the continental crust is andesitic (Rudnick and Gao, 2003) has led some workers to propose that the crust formed directly in volcanic arcs as high-Mg andesites (Kelemen, 1995) and accretion of such rocks lead to the formation of the continental crust. It has been suggested that alternatively, the net flux from the mantle was felsic in the Archaean (TTGs), but mafic today, so that the andesitic average composition simply represents a time-integrated average (Rollinson, 2008b). However, a recent study of the Kohistan arc has shown that the overall bulk composition of mature oceanic arcs is in fact andesitic (Jagoutz and Schmidt, 2012). Although melts from the mantle are initially mafic they can result in crust of andesitic composition by either fractionating ultramafic cumulates, which can delaminate, or they can further partially melt by mafic underplating leaving a pyroxenite residue to delaminate.

Three geodynamic environments of Archaean continental crust formation have been proposed (Fig. 2): (a) above a mantle plume, which supplied mafic material and heat for partial melting of hydrous basalt (e.g. Condie, 2000; Bédard, 2006), (b) direct slab melts (adakites) that formed TTG crust (Martin et al., 2005; Martin and Moyen, 2002; 2005) and (c) stacking or underplating of oceanic crust to cause thickening and partial melting at the base of this crust (Kerrick and Polat, 2006; Nagel et al., 2012), perhaps combined with crustal relamination (Hacker et al., 2011).

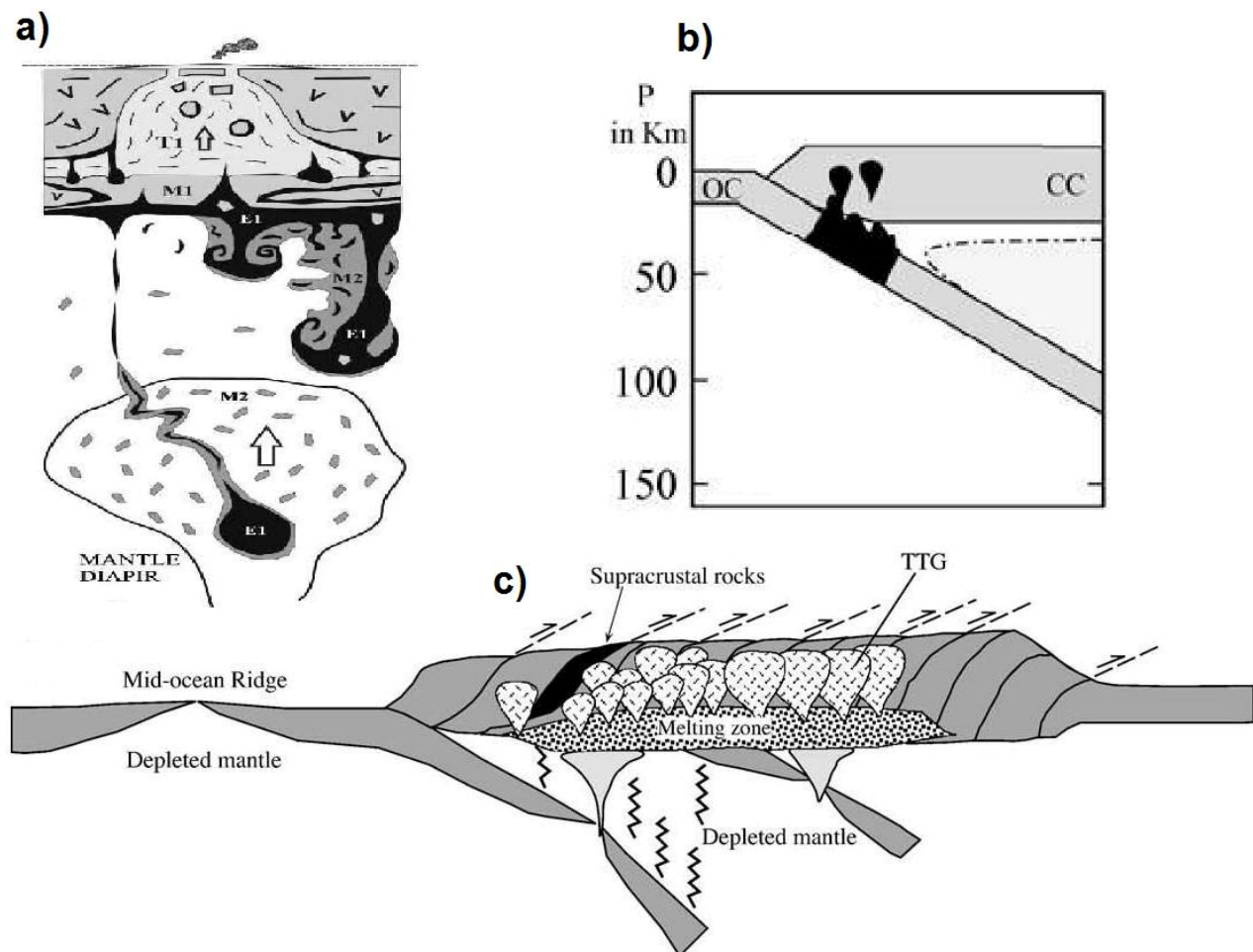


Figure 2. Different models of continental crust formation. a) Plume-related differentiation of a mafic oceanic plateau, which could catalyse the restites by reaction with the mantle (Bédard, 2006). b) Slab-melt model where TTGs are directly derived by partial melting of the subducting slab (Martin and Moyen, 2005). c) Modern-style subduction with mafic underplating (Kerrick and Polat, 2006). For detailed explanations of each model the reader is referred to the cited papers.

The geodynamic setting of TTG formation is likely related to the same setting in which the subcontinental lithospheric mantle (SCLM) formed, because of similar formation ages (Shirey and Walker, 1998; Nasir and Rollinson, 2009; Section 1.3). Additionally, TTG formation is almost certainly related to the setting in which supracrustal rocks formed, because they represent the source material of the TTG melts (Section 1.5). Although there is still debate about the specific setting of TTG formation, the adakite model (b) mentioned above has been significantly weakened by the mismatch in the geochemistry between TTGs and adakites (Smithies, 2000; Kamber et al., 2002). However, there are certain adakites of the high-silica type that resemble Archaean TTG crust (Martin et al., 2005). Nevertheless, such a model is still incompatible with the wide range in estimated pressure and temperature conditions of TTGs (Moyen, 2011) and the fact that Hf-isotopic evidence from zircon, suggests long residence times (>200 Ma) before juvenile mafic crust is partially melted to form TTGs, as well as indicating mixed mafic sources (Næraa, 2011). Recent thermodynamic calculations and trace element modelling of TTG residues suggest that melting took place within a thickened mafic crust rather than by direct slab melting (Nagel et al., 2012). Given that TTGs can form by partial melting of hydrous mafic rocks under a broad range of P-T conditions (Moyen, 2011), both the plume model (a) and the arc underplate model (c) could be reasonable solutions to this long-lasting geological problem and it thus remains a task for future research to resolve this issue.

The rate of formation of the continental crust is a matter of debate, and several models have been proposed ranging from very little growth during the Archaean to total growth and even a decline in volume after the Archaean (e.g. Fyfe, 1978; Armstrong, 1981; Collerson and Kamber, 1999). Another matter of debate is, if the growth of the continental crust was continuous or occurred as distinct events in response to Wilson Cycles of supercontinent formation as suggested by the peaked U-Pb zircon ages recorded in global studies (Condie, 1998; Rino et al., 2004).

The present crustal growth in volcanic arcs is argued to be balanced by the rate of subduction erosion and recycling of material into the mantle (Plank and Langmuir, 1998; Scholl and von Huene, 2007, 2009). If true, the peaks recorded in the global zircon data reflect events of reworking during supercontinent formation rather than a juvenile crustal input (Hawkesworth et al., 2009, 2010). In support of this view, recent worldwide zircon Hf-isotope data (Fig. 3) suggest that over 70 % of the juvenile input to the continental crust was added during the Archaean and that growth on average was continuous rather than episodic (Belousova et al., 2010). This means that the net growth rate of the continental crust has declined since the Archaean and that the significance of recycling has increased through time until our current steady state where it dominates. This result has recently been confirmed by Dhuime et al. (2012).

An interesting observation is that Archaean TTG crust formation worldwide, appears to be postdated by intrusion of so-called sanukitoids (Heilimo et al., 2010; Halla, 2011). These granitoid rocks are characterised by a high contents of incompatible trace elements in combination with a high contents of compatible trace elements such as MgO, Cr and Ni (Stern et al., 1989). They are generally interpreted as melts of a crustally contaminated mantle, perhaps in a similar way as high-Mg andesites in a subduction zone environment (Halla, 2005; Kovalenko et al., 2005). Sanukitoid magmatism is commonly attributed to slab break-off (Halla, 2009; Heilimo et al., 2012), but it is also a possibility that sanukitoids represent melting of metasomatised subcontinental lithospheric mantle during the rebound of a craton after the tectonic activity ceases. Although sanukitoid magmatism postdating TTG formation appears to be the rule rather than the exception, such rocks have so far only been identified in one place in the Archaean craton of Greenland (Steenfelt et al., 2005).

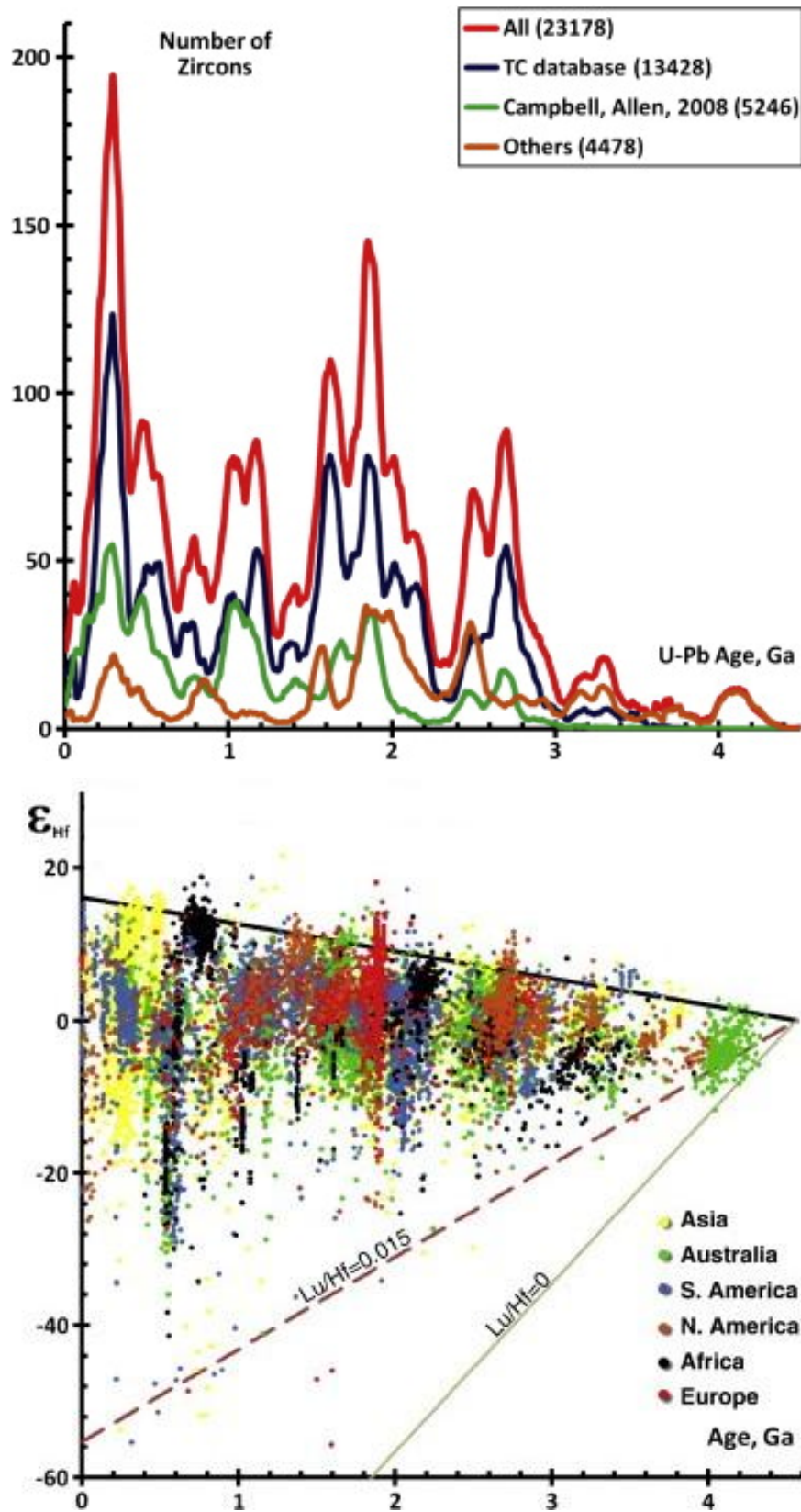


Figure 3. Top) Comparison of zircon U-Pb age distributions for data collected from different sources. A complete list of references is provided in the cited paper. Bottom) Plot of ϵ_{Hf} vs age with data coloured by continent, which overall shows a continuous juvenile input. Figure from Belousova et al. (2010).

1.3. The sub-cratonic mantle

The lithospheric mantle directly under the cratons is commonly referred to as the cratonic root or keel. It is considered to be part of the so-called tectosphere that is physically isolated and compositionally distinct from the ambient asthenospheric mantle (Jordan, 1975, 1978; Walker et al., 1989). This cratonic mantle is composed of highly depleted Mg-rich peridotite (Carlson et al., 2005) and has a lower temperature and higher viscosity when compared with the ambient convecting asthenospheric mantle (Jordan, 1988; Mareschal and Jaupart, 2004). In the following I will refer to this isolated lithospheric portion of mantle as the subcontinental lithospheric mantle (SCLM).

Evidence for the existence of the SCLM mainly comes from the xenolith record and from seismic data. Xenoliths brought to the surface by rapid extrusion of kimberlite and basalt dykes consist of either peridotites such as lherzolite and harzburgite, which are believed to represent the main portion of the SCLM, or they consist of eclogites, which are interpreted to be remnants of subducted oceanic crust (Lee, 2006). It is worth noting that there appears to be a secular change in the depletion of peridotite xenoliths from the SCLM (Fig. 4). This could be a function of decreasing mantle temperature since the mid-Archaeon (Herzberg et al., 2010). However, Proterozoic xenolith compositions might reflect re-enrichment of originally Archaean SCLM and thus represent an abrupt change in the formation mechanism of SCLM rather than an apparent continuum (Griffin et al., 2003, 2009).

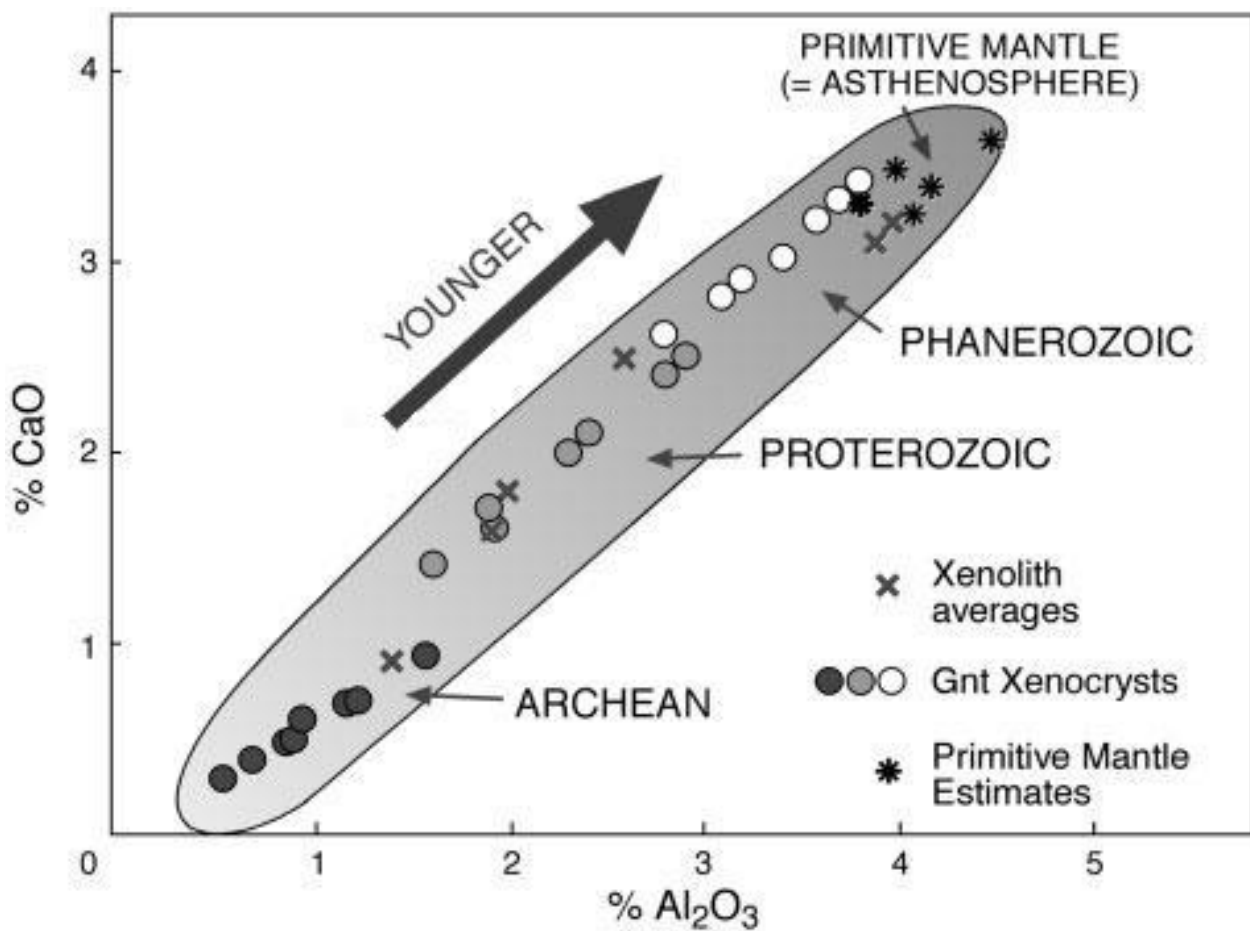


Figure 4. The composition of SCLM through time. Figure from Griffin et al. (2009).

Seismic tomography shows that the SCLM reaches depths to 250 km, under which ambient mantle prevails (Polet and Anderson, 1995; Simmons et al., 2009; Jordan, 2011). According to the isopycnal hypothesis (Jordan, 1988), the low density and high viscosity of the SCLM caused by its Mg-rich and depleted nature has made it buoyant and stable since the Archaean in contrast to the Fe-rich ambient convecting asthenospheric mantle. This has kept these two types of mantle isolated from each other since the formation of the Archaean SCLM, and despite the significant cooling it must have experienced over time, the Mg-rich composition has kept it buoyant, although highly viscous.

In the case of the Kaapvaal craton in South Africa (Fig. 1), it was concluded that the lithosphere stabilised before 3500 Ma and reached a thickness of over 200 km (Pearson et al., 1995), which is consistent with ages of 3800 Ma for SCLM from the Zimbabwe craton (Näglér et al., 1997). Griffin et al. (2010) suggested that 70% of the SCLM is of Archaean origin (Fig. 5) and Re-Os depletion ages on peridotite xenoliths show that the ages of the cratonic crust and mantle coincide in most cases (Shirey and Walker, 1998). This obviously has important implications for the rate of continental growth and craton stabilisation and is in part supported by Hf-isotopic data from zircon (Belousova et al., 2010). Therefore, the coupled formation of the cratonic crust and mantle must be accounted for in any genetic model. It should also be kept in mind that it is possible that the temperature of the ambient convecting mantle peaked around 3000 to 2500 Ma, because internal heating exceeded surface heat loss (Herzberg et al., 2010). This could have important implications on geodynamic models for the formation of SCLM.

There are generally three models for the formation of the SCLM (Fig. 6), which are in some ways similar to the proposed settings of TTG formation (Fig. 2): (1) high-degree melting at temperatures over 1650 °C in a plume head, (2) accretion of oceanic lithosphere and (3) accretion of arc lithosphere.

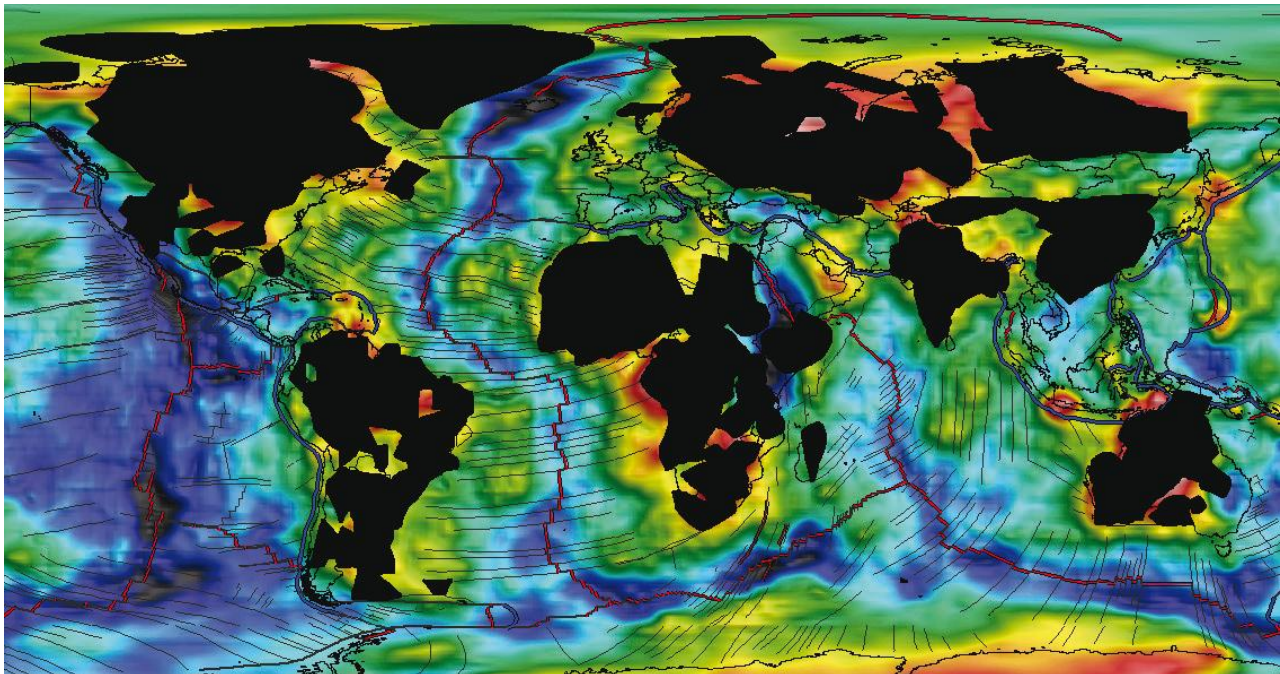


Figure 5. The interpreted extent (70%) of original Archaean SCLM (black) superimposed on a global tomography image at 100-150 km depth. Figure from Griffin et al. (2010). Blue colours are seismic slow/warm and red are fast/cold.

The SCLM has been proposed to be genetically related to Archaean MORB formation, and may represent the mantle restite after such extraction from a primitive mantle (Bernstein et al., 1998; Rollinson, 2010). Primary magmas derived by about 30% partial melting of such mantle would have 18-24 wt.% MgO and would leave a depleted harzburgite residue that could explain at least some parts of the SCLM (Herzberg et al., 2010).

However, the degree of depletion of the Archaean mantle, as observed in xenoliths from the SCLM (e.g. Wittig et al., 2010), is too large to have been caused by basalt extraction and thus komatiites have been proposed as a better suited melt to be responsible for the depleted mantle restite that now constitutes the SCLM (Arndt et al., 2009). Nevertheless, even the most MgO-rich komatiitic melts cannot have been in equilibrium with the extremely depleted SCLM peridotite xenoliths (Parman et al., 2004), and they also make up only a small fraction of the rock assemblages found in supracrustal belts. In an oceanic setting, the mantle residue would be relatively dry and with less silica than in an arc environment, where fluid/melt metasomatism would lead to more silica and thus secondary pyroxene.

The problem with the first model is that it predicts deep melting and thus the signature of garnet in the peridotite residue. This is not observed because the geochemical composition of peridotite xenoliths shows low-pressure melt depletion (Canil, 2004; Lee, 2006; Wittig et al., 2008). Thus, the two latter models are more likely, because they predict low-pressure depletion.

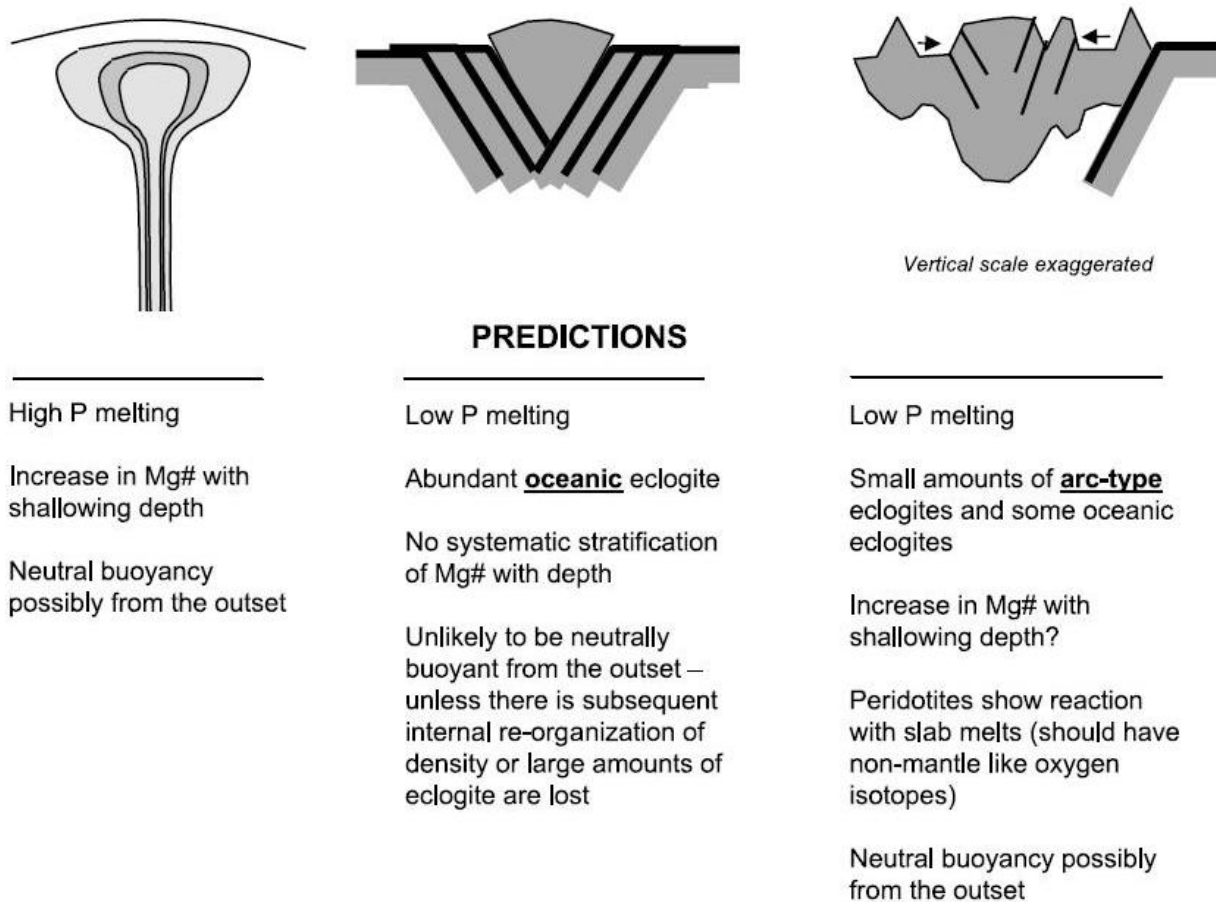


Figure 6. The three main models for the formation of the SCLM and the predictions of each model. From left to right: plume setting, oceanic crust accretion and island arc accretion. Figure from Lee (2006).

Boninitic mantle residue found in Phanerozoic arcs actually provide a better match with Archaean SCLM xenoliths (Parman et al., 2004). Consequently this supports accretion of arc lithosphere with a high degree of melt depletion as the source of cratonic SCLM. Thus a two-stage process is likely, such as that observed during formation of modern boninites (König et al., 2010), where previously depleted mantle is flux-melted in a subduction zone setting to yield very MgO-rich melts that further deplete the mantle to compositions compatible with that of the SCLM. A subduction zone setting is also supported by the observation that dunite restite has been enriched by Si-rich fluids after melt extraction causing the SCLM to retain its high Mg#, but forming significant amounts of orthopyroxene during reaction of silica and olivine (Kelemen et al., 1998; Hanghøj et al., 2001; Bernstein et al., 2007). This could have happened by fluid/melt refertilisation of previously depleted mantle to cause additional depletion as by the process of boninite formation (Parman et al., 2004; König et al., 2010).

The subduction zone model for the formation of the Archaean SCLM is additionally supported by the compositions of cratonic peridotites, which suggest depletion in the spinel stability field (Pearson and Wittig, 2008), as well as by more general case studies that establish a petrogenetic and temporal coupling between cratonic crust and mantle (Schmitz et al., 2004; Wittig et al., 2008). Other lines of evidence for a subduction zone setting come from eclogite inclusions in diamonds (Shirey et al., 2004; Shirey and Richardson, 2011) and from the V-contents in spinel-facies peridotites from the SCLM, which suggest that they formed under more oxidising conditions than MORB mantle source and are thus likely related to a convergent margin setting (Canil, 2002). Finally, numeric modelling (Gray and Pysklywec, 2010) shows that the thickness of the SCLM, which may be up to 250 km (Simmons et al., 2009; Jordan, 2011), is best explained by imbrication and underplating of the lithospheric mantle during continental collision events as would be expected in the arc hypothesis (e.g. Helmstaedt, 2009).

1.4. Archaean supracrustal belts

Supracrustal belts comprise volcanic, shallow intrusive and sedimentary rocks (e.g. Fig. 7). They occur within the TTG dominated gneisses of every craton as large enclaves, and as individual belts that can be traced for several tens of km along strike (Condie, 1981). The TTGs often have intrusive relationships with the supracrustal belts, at least in SW Greenland (Section 1.6). Such volcano-sedimentary outcrops are commonly known as greenstone belts, because many preserve greenschist-facies metamorphic assemblages, which have a green colour due to their high chlorite contents (Condie, 1981). Here we are only concerned with greenstone belts of Archaean age, and we use the term supracrustal belt, as it does not imply a specific metamorphic grade.

Supracrustal belts provide the only source of information about the conditions of the atmosphere and hydrosphere in the Archaean Eon, because they consist of rocks that interacted with Earth's surface conditions shortly after their formation. Hydrothermal alteration, which is caused by reactions between rocks and for instance seawater, can provide information about the chemical conditions that were present in the Archaean hydrosphere (e.g. Hessler et al., 2004; Pope et al., 2012). Supracrustal belts are also important for the study of the earliest signs of life on this planet, because they host chemical precipitates such as banded iron formation (BIF) that may have formed via microbial activity (e.g. Koehler et al., 2010), as well as a range of sedimentary rocks such as turbidites, shales and carbonates that may preserve signs of life. However, this field of research is controversial, because there is much disagreement about the interpretation of hydrothermal and metamorphic effects on such rocks (Myers and Crowley, 2000).

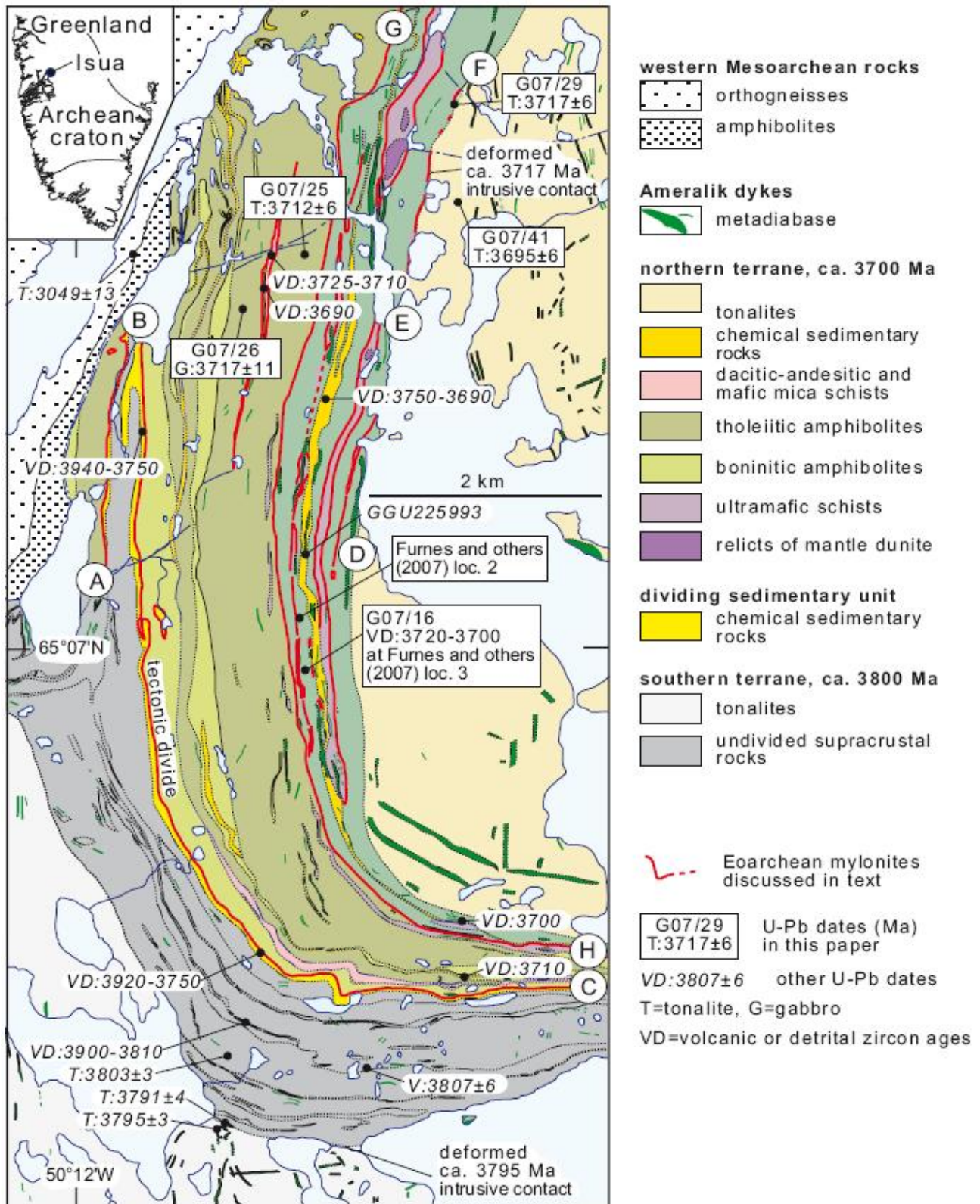


Figure 7. Example of an Archean supracrustal belt (Isua). This map illustrates the complexity of composite supracrustal belts, which require detailed mapping in order to make meaningful interpretations of the geochemical and geochronological data of the various lithological units. Figure from Friend and Nutman (2010).

A small outcrop of supracrustal rocks on the island of Akilia about 20 km south of Nuuk in SW Greenland has received much attention due to claims of evidence of life older than 3850 Ma (Mojzsis et al., 1996). However, these rocks are highly deformed and metasomatised and therefore these claims have generally been abandoned (Whitehouse and Kamber, 2004). A more convincing case for indications of early life is found in the Isua supracrustal belt about 120 km northeast of Nuuk in SW Greenland, which comprise better preserved rocks. Carbon-isotopic fractionations and high U-contents in graphite-bearing shales and greywackes support photosynthetic microbial activity some 3800 Ma ago (Schidlowski, 1988; Rosing, 1999; Rosing and Frei, 2004).

More importantly for the present study, however, is the fact that the igneous rocks found within supracrustal belts provide information about the geodynamic setting that existed during the Archaean Eon. Mafic igneous rocks provide constraints on their mantle source, and can thus be used as a record of the mantle evolution through time (Walter, 2003). Archaean oceanic crust was probably 25-30 km thick and formed by about 30% partial melting of ambient mantle (Sleep and Windley, 1982; Herzberg et al., 2010). Because the formation of TTGs is likely related to partial melting of the mafic rocks found in the supracrustal belts (Section 1.2), they may have formed in the same geodynamic setting. The specific environment of formation of TTGs remains unconstrained due to the variable temperature and pressure conditions they record for their source (Moyen, 2011). Thus the supracrustal source rocks may provide an indirect way to understand the setting and formation mechanism of the continental crust. Unusual supracrustal rock types such as high-Mg andesites, boninites, adakites and komatiites can be used to infer specific magmatic processes and are thus important to distinguish between different tectonic environments. Polat et al. (2009b) showed that supracrustal rocks provide evidence for a whole range of geodynamic environments that are also found in modern geological settings. Supracrustal belts, as in the Fiskensæset region of SW Greenland, sometimes contain layered gabbro-anorthosite complexes. They are poorly understood, but are proposed to be related to fractional crystallisation of hydrous magmas in an arc setting, where plagioclase is crystallising later than olivine and pyroxene and is thus concentrated in the final melt to form anorthosite plutons (e.g. Polat et al., 2009a; Hoffmann et al., 2012). A modern analogues to such Archaean anorthosite complexes have been identified in arc environments, such as the Fiordland Mesozoic arc in New Zealand (Gibson, 1990; Gibson and Ireland, 1999) and the Cretaceous Kohistan arc in Pakistan (Coward et al., 1982; Jagoutz et al., 2007).

Archaean supracrustal belts are dominated by volcanic rocks of tholeiitic basalt composition that differ from modern mid-ocean ridge basalt (MORB) by having higher Fe, Ni, Cr and Co (Condie, 1981). Similarities between Archaean tholeiitic basalts and modern back-arc basalts and island arc tholeiitic basalts have long been recognized (e.g. Hart et al., 1970; Glikson, 1971; Hart and Brooks, 1977; Gill, 1979; Condie, 1985). Many recent studies have also pointed out the similarities between the supracrustal rocks in SW Greenland and those in modern suprasubduction zone settings (e.g. Garde, 2007; Polat et al., 2008a; Windley and Garde, 2009; Papers I, II and III in the Annex). In particular they have documented evidence of arc-type processes such as fluid-fluxed melting of mantle, slab melting (adakites), high-Mg andesites, underplating and melting-assimilation-homogenisation-storage (MASH). These processes collectively point to an arc-like geodynamic setting during the Archaean, which might have been operating as far back as 3800 Ma in this region (e.g. Friend and Nutman, 2010; Dilek and Furnes, 2011; Hoffmann et al., 2011; Polat et al., 2011). However, elsewhere in the world deep mantle plumes have been invoked to explain supracrustal belts of oceanic plateau affinity and intracratonic basins (e.g. Bédard, 2006; Arndt et al., 2009; van Kranendonk, 2011a, 2011b). In the following section we will discuss these two vastly different models.

1.5. The geodynamic settings of supracrustal rocks

Just as there are different schools of thought on the genesis of the cratonic crust and mantle there are various geodynamic models for the formation of Archaean supracrustal belts. However, it would be logical to assume that these three lithospheric components formed in the same geodynamic environment given their spatial and temporal relationships (e.g. van Kranendonk, 2004; Condie and Pease, 2008). As mentioned previously, the cratonic crust could have formed either in a mantle plume or a subduction zone setting (Section 1.2), whereas much evidence favours a subduction zone setting for the formation of the cratonic mantle (Section 1.3). In the same way the formation of Archaean supracrustal belts has also been attributed to either a plume or subduction-related geodynamic setting (e.g. Polat et al., 2009b). This debate has been polarised into one group that claims uniformitarian principles according to which horizontal tectonics were operating as far back as the earliest supracrustal rock record (e.g. Isua at c. 3800 Ma; Friend and Nutman, 2010; Dilek and Furnes, 2011; Polat et al., 2011) and another group that argues that mantle plumes and thereby vertical tectonics were responsible for the formation of most Archaean supracrustal belts (e.g. Bédard, 2006; van Kranendonk, 2011b).

A horizontal tectonic regime for the Archaean craton of SW Greenland was invoked from field relationships in some of the earliest work in this region (Bridgwater et al., 1974). This was in stark contrast to coeval work in the Archaean of southern Africa, which invoked vertical tectonics (Anhaeusser, 1973). It would appear that these two fundamentally different models for the Archaean have persisted to this day (Windley and Garde, 2009; van Kranendonk, 2011b).

Modern subduction zones are places along which sediments, oceanic crust and lithospheric mantle are returned and re-equilibrated with the ambient mantle (Stern, 2002). Thus, the isotopic evolution recorded by mantle-derived magmas serves as a window into the differentiation of Earth through time (Vervoort and Blichert-Toft, 1999; Bennett, 2003). For this reason, systematic studies of supracrustal belts throughout the Archaean Eon are important for understanding the secular changes of the Earth. However, geochemical data alone do not provide reliable and unambiguous arguments that prove the existence of a particular geodynamic environment; rock assemblages, field relationships and structures also provide critical and often diagnostic criteria.

One of the most important pieces of evidence for uniformitarian principles and horizontal tectonics is the possible occurrence of Archaean ophiolites. These would provide undeniable evidence for spreading of oceanic crust in a mid-ocean ridge or back-arc, as well as representing evidence for obduction at subduction zones, and thus the operation of plate tectonics. Therefore the occurrence of Archaean ophiolites is much debated and is still a controversial subject. Many scientists are in favour of the existence of Archaean ophiolites (e.g. Shervais, 2001, 2006; de Wit, 2004; Cawood et al., 2006; Condie and Kröner, 2008; Dilek and Polat, 2008; Metcalf and Shervais, 2008; Polat et al., 2009a, 2009b; Windley and Garde, 2009; Dilek and Furnes, 2011; Kusky et al., 2011; Paper I in the Annex), whereas some negate the possibility of Archaean plate tectonics (e.g. Bickle et al., 1994; Davies, 1999; McCall, 2003; Stern, 2005, 2008; Hamilton, 1998, 2011).

The main arguments against horizontal tectonics in the Archaean hinge on the lack of complete ophiolite successions (Penrose definition *sensu stricto*; Anonymous, 1972), lack of unequivocal sheeted dyke complexes, and lack of blueschists and eclogites of Archaean age (e.g. Stern, 2005, 2008). However, these arguments against Archaean tectonics have become out-of-date, because it is now known that at Phanerozoic subduction zones in the Western

Pacific, the ultramafic rocks, gabbros, sheeted dykes and most of the basalts of the ocean floor are typically subducted, and only the upper basalts and sediments belonging to ocean plate stratigraphy are accreted (e.g. Kimura and Ludden, 1995; Shervais, 2006) and this was also likely in the Archaean (Hoffman and Ranalli, 1988).

This dismembering of the oceanic crust is probably the main reason why ophiolites are rare in accretionary orogens; for example, in southern Japan there are over 1000 slices of Mesozoic-Cenozoic accreted ocean floor, mostly meta-basalts, but only four ophiolites (Maruyama, 1997). Moreover, sheeted dykes would arguably only form at slow spreading rates, as at present, whereas higher mantle temperatures and faster spreading rates would be unfavourable for the formation of such dykes (Bickle, 1986). Furthermore sheeted dykes only develop under brittle conditions and require a balance of magma supply and spreading rate that may not always have been met in the Archaean (Abbott, 1996; Robinson et al., 2008).

As for the lack of blueschist- and eclogite-facies rocks, it is now widely accepted that the hotter mantle in the Archaean (Herzberg et al., 2010) led to a steeper geothermal gradient, which may have prevented the formation of low-T/high-P blueschist- and eclogite-facies rocks (Ernst, 2003; Brown, 2008). However, locally evidence for such rocks of Archaean age is found although their preservation is obviously rare (Moyen et al., 2006; Lana et al., 2010; Mints et al., 2010).

One of the problems in identifying ophiolites is that the Penrose definition (Anonymous, 1972) represents a hypothetical idealised section through oceanic crust. This hampers the possibility to term oceanic crust as ophiolite, despite other lines of evidence for such an origin. A new ophiolite classification scheme has therefore been proposed (Dilek, 2003; Dilek and Furnes, 2011), which is shown in Figure 8. This essentially discards the old Penrose classification and expands the term ophiolite to encompass any section of oceanic crust regardless of its tectonic origin. However, the generally high degree of metamorphism and hydrothermal alteration, as well as strong deformation, makes complete ophiolite sections of Archaean age both rare and difficult to recognise. Additionally, it can be a challenge to determine whether or not such rocks are coeval.

The two oldest uncontroversial ophiolites are Paleoproterozoic in age (c. 2000 Ma). The Jormua ophiolite in Finland contains pillow lavas, gabbros, sheeted dykes and ultramafic rocks and is interpreted to have formed in an incipient ocean setting (Kontinen, 1987; Peltonen et al., 1998). The Purtunq ophiolite in Quebec likewise contains pillowed and massive volcanic rocks, sheeted dykes, gabbros, ultramafic layered cumulates and plagiogranites, and generally has similar geochemical characteristics as modern MORBs and ocean island basalts (OIB) settings (Scott et al., 1992).

All proposed Archaean ophiolites are still highly debated, such as the Dongwanzi complex in the North China Craton. This was suggested to be a 2505 Ma old ophiolite containing harzburgites, ultramafic cumulates, gabbros, sheeted dykes, pillow lavas and BIF (Kusky et al., 2001, 2011). There is geochemical evidence for a suprasubduction zone (SSZ) ophiolitic origin of picrites and peridotites in the same area, as well as a Lu-Hf isochron that is consistent with the age of 2500 Ma (Polat et al., 2005, 2006). However, the validity of this ophiolite was questioned by Zhai et al. (2002) due to a different interpretation of the field relationships, because they were unable to identify pillow lavas and sheeted dykes. Additionally, it was suggested that the complex is not a coeval sequence of rocks, because several mafic dykes have U-Pb zircon ages just over 300 Ma (Zhao et al., 2007). Nutman et al. (2010) also regard the claim of the Dongwanzi ophiolite as being invalid, due to geochemical and field constraints, and so it is apparently still a controversial case.

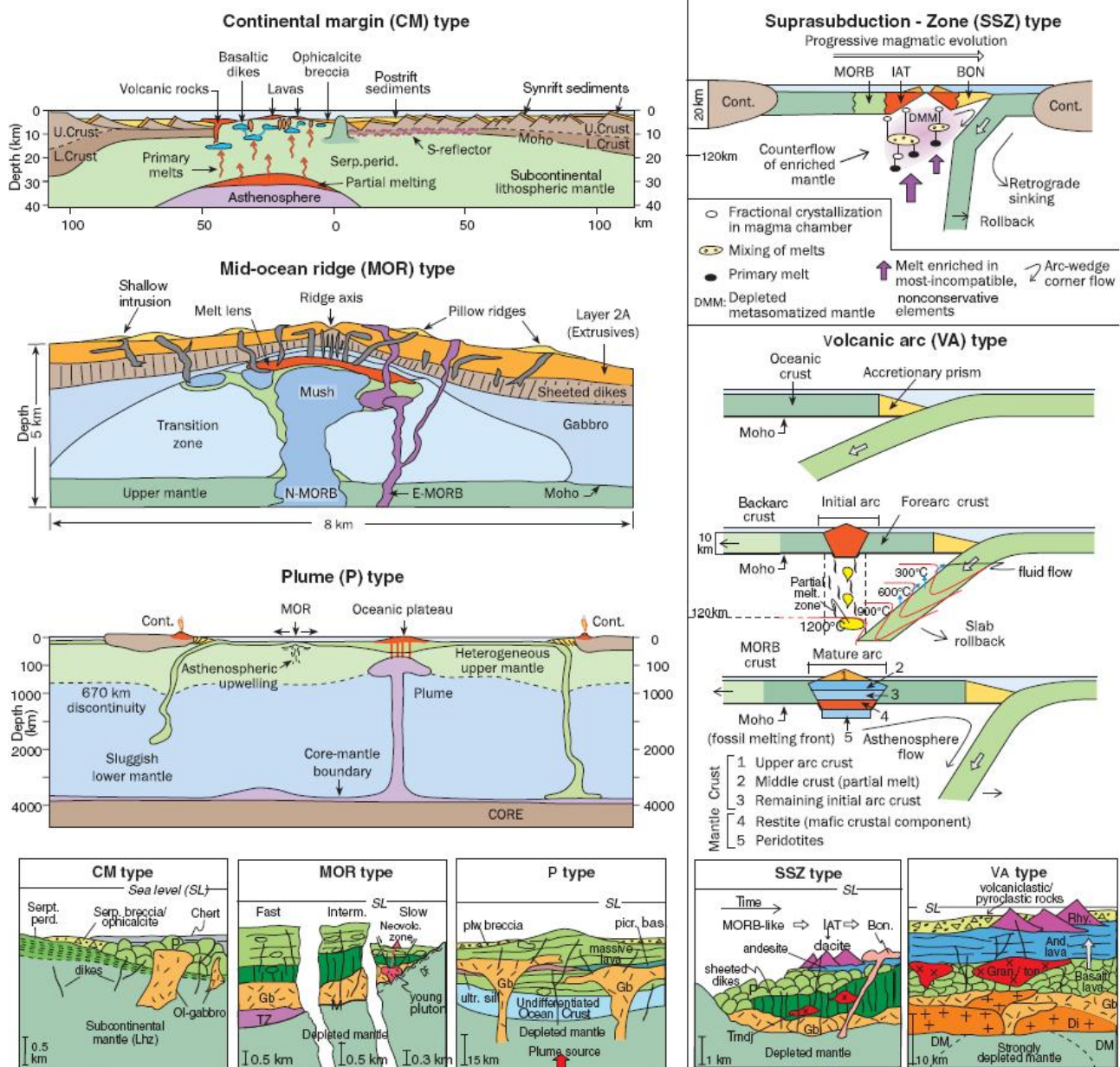


Figure 8. Schematic sections through different types of ophiolites. The lithological association can be used in combination with the distinct geochemical features to provide evidence for a particular geodynamic environment of formation. This model can be applied directly to supracrustal belts as will be shown in Section 2.1. Figure from Dilek and Furnes (2011).

The Palaeoarchaean Jamestown Ophiolite Complex in South Africa was first described as 3 km-thick tectono-magmatic sequence containing most components of an ophiolite (de Wit et al., 1987). However, some of the components are up to 120 Ma different in age, and are separated by major shear zones; thus it is no longer regarded as a true ophiolite (de Wit et al., 2011).

Keto and Kurki (1967) and Maruyama et al. (1991) suggested that the c. 3800 Ma Isua supracrustal belt in SW Greenland contains an ophiolitic assemblage within an accretionary complex. This was supported by detailed field relations including the critical recognition of ocean plate stratigraphy (Komiya et al., 1999), which therefore provide the oldest evidence of seafloor-spreading on Earth. Recently, Furnes et al. (2007a, 2007b, 2009) also described a sheeted dyke complex at Isua and interpreted the supracrustal rocks as a SSZ ophiolite containing pillow lavas, sheeted dykes,

gabbros and ultramafic rocks. However, this claim was disputed by others (Nutman and Friend, 2007; Hamilton, 2007; Friend and Nutman, 2010), who pointed out that the geochemical composition of the sheeted dykes is different from the pillow lavas that they are supposed to feed, that field evidence negates a sheeted dyke origin for these rocks and the dykes are more likely to represent the so-called Ameralik dykes (<3500 Ma)

As shown above, all proposed Archaean ophiolites currently remain controversial. However, the geochemical data and the lithological assemblage of the Tartoq Group in SW Greenland provides more robust evidence for a dismembered section through arc-related oceanic crust, and thus this is essentially an Archaean ophiolite (Section 2.1 and Paper I in the Annex).

It has long been recognized that the majority of the best-studied ophiolites (e.g. Oman, Cyprus and western Newfoundland) formed in SSZ settings rather than at mid-ocean ridges (MOR) (e.g. Miyashiro, 1973; Pearce et al., 1984; Elthon, 1991; Pearce, 2003) and thus they are thus not actual MOR analogues of the proposed Penrose ophiolite sequence. Dilek and Furnes (2011) examined several Archaean supracrustal belts that were previously suggested to be ophiolites and concluded that such assemblages can develop in a range of tectonic settings, including subduction zones, mid-ocean ridges and plume-type oceanic plateaus, and could indeed represent ophiolite sections according to the new definition (Dilek, 2003). The ongoing controversy demonstrates that there is still much need of identification and detailed analysis of possible ophiolitic assemblages of Archaean age (e.g. Shervais, 2001).

There are also other more indirect lines of evidence for subduction zone processes in the Archaean Eon. For example 2900 Ma-old sulfide minerals in diamonds with geochemical characteristics of a basaltic protolith provide evidence that subduction-related crustal recycling was active since at least the mid-Archaean (Richardson et al., 2001). This age can be extended back to 3520 Ma from similar evidence in diamonds, which suggests a subduction wedge origin is possible (Westerlund et al., 2006). The LITHOPROBE seismic profile across the Canadian craton illustrates dipping reflectors (Lewry et al., 1994), which have been interpreted to be remnants of a fossil subduction zone. Additionally, numeric modelling shows that the structure of the SCLM is best explained by imbrication and underplating of the lithospheric mantle during continental collision events (Helmstaedt, 2009; Gray and Pysklywec, 2010).

The above view that subduction-related processes were in operation throughout much if not all of the Archaean has been challenged by workers supporting vertical tectonics and a mantle plume-dominated early Earth (Bickle et al., 1994; Davies, 1999; McCall, 2003; Bédard, 2006; Stern, 2005, 2008; Hamilton, 1998, 2011). A plume-dominated geodynamic environment, such as the one invoked for oceanic plateaus, has been proposed for a number of Archaean supracrustal belts as an alternative to the ophiolite and subduction-related models. Of particular importance is the assumed relation between komatiites and hot mantle plumes (Arndt et al., 2008). The presence of komatiites in some supracrustal belts has commonly been taken as evidence of plume-related petrogenetic processes. This is partly because of the presence of well-preserved Cretaceous komatiites on Gorgona, which is interpreted as being related to a mantle plume (Arndt et al., 1997). However, the dogma that komatiites are always related to deep mantle plumes will be challenged in Section 2.3 and Paper III in the Annex.

Given that there are problems in proving incontrovertibly the existence of deep mantle plumes even in recent volcanic rocks (Fougler, 2005, 2012; Fougler and Jurdy, 2007; Fitton, 2007; Koppers, 2011), it is somewhat speculative to consider whether or not they existed in the Archaean Eon. However, although much evidence supports the idea that subduction zone processes were in operation throughout the Archaean Eon in SW Greenland, this does not preclude that

a mantle plume setting may have existed locally in other regions, such as in southern Africa (van Kranendonk, 2011a, 2011b), western Australia (Smithies et al., 2005a; van Kranendonk, 2007a, 2007b), and parts of the Superior Province (Polat et al., 2009b; Wyman and Kerrich, 2010).

In the following section I will provide an overview of recent work on supracrustal belts in SW Greenland as a final introduction to the discussion of the three papers in Section 2 of this thesis.

1.6. Previous work on Archaean supracrustal belts in SW Greenland

The ancient age of the gneisses in the Nuuk region was unknown until the first geochronological data were published. Pb-Pb and Rb-Sr isotopes provided ages of c. 3600-3750 Ma of gneissic protoliths, collectively named the Amîtsoq gneisses (Black et al., 1971; Moorbath et al., 1972; Baadsgaard, 1973). It was realised that supracrustal rocks that were intruded by these gneisses had to be even older and that this area represents a unique fragment of the early Earth. During some of the first geological mapping in the Nuuk region (e.g. McGregor and Mason 1977; Hall et al., 1987), the Eoarchaeon supracrustal stratigraphy was divided into the Isua supracrustal belt and the Akilia association. These supracrustal rocks are still regarded as the oldest mafic components in the region (>3800 Ma). The Ameralik basic dykes, the Malene supracrustal rocks and the Fiskensæset complex, were known to be older than the Nûk gneisses (c. 2900 Ma), but direct dating of mafic rocks was difficult at that time and the relative ages of the different components could not be separated.

Nutman et al. (1996) introduced the term ‘Itsaq Gneiss Complex’ to include all early Archaean rocks in the Nuuk region (Amîtsoq gneisses, Isua supracrustal belt and Akilia association), despite the fact that they are unrelated and span a period of about 150 Ma (Friend and Nutman, 2005a). They furthermore included the Itsaq Gneiss Complex in the Akulleq terrane and termed the gneisses west of this as the Akia terrane (including the Nûk gneisses) and the rocks east of it as the Tasiarsuaq terrane. These terranes were defined by their different tectono-metamorphic histories and as new U-Pb zircon data were published this model was further refined. The Nuuk region now comprises the following terranes: Færingehavn, Isukasia, Qarliit Tasersuat, Aasivik, Tre Brødre, Tasisarsuaq, Akia and Kapisilik (Nutman et al., 1989, 1993; Friend and Nutman, 1991; Nutman et al., 2004; Friend and Nutman, 2005b). Later, Windley and Garde (2009) proposed in their block model for SW Greenland, in which several large shear zones divide the region into a series of tilted blocks that each display northerly granulite-facies and southerly amphibolite-facies metamorphic conditions. However, such a block model is not compatible everywhere with recent work on the metamorphic grade of supracrustal rocks, which show distinctly different metamorphic grade patterns (Schumacher et al., 2011).

In the following, I will give a short overview of the various supracrustal belts in SW Greenland and the most recent literature describing them, starting with the Isua supracrustal belt and moving southwards to the Tartoq Group (Fig. 9).

Most of this region has experienced amphibolite- to granulite-facies metamorphic conditions, but amphibolite-facies dominates the supracrustal lithologies due to retrogression (Wells, 1976; Schumacher et al., 2011). It should be noted that the surrounding TTG gneisses are intrusive into the supracrustal belts in almost all cases, although these contacts are commonly later deformed. Few of the supracrustal belts appear to be located along tectonic contacts between orthogneisses of different terranes, such as the Storø composite supracrustal belt described below.

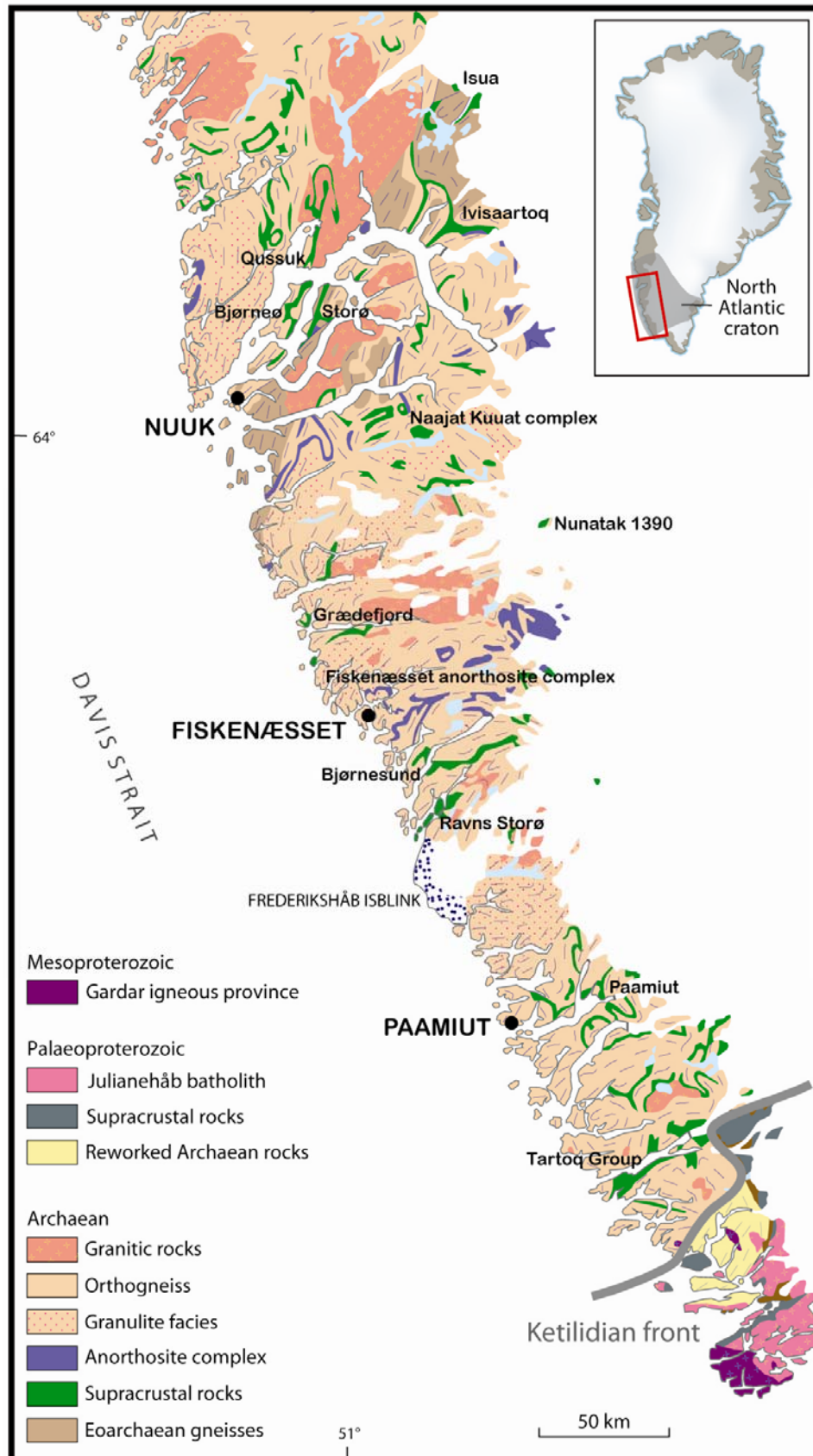


Figure 9. Geological map of the North Atlantic craton in SW Greenland. The supracrustal belts described in this section are named in the map together with important place names. Based on Allaart (1982) and recent GEUS data.

The Isua supracrustal belt is located by the inland ice about 150 km NE of the capital of Greenland, Nuuk (Fig. 9). It is generally considered to be the oldest extensive outcrop of volcanic and sedimentary rocks on Earth (Nutman et al., 1996; Myers and Crowley, 2000; Kamber et al., 2005; Nutman and Friend, 2009a). In detail the Isua supracrustal is a composite that consists of two distinct packages of supracrustal rocks, which are separated by a mylonite (Fig. 7). The two packages have been dated at c. 3800 Ma and c. 3700 Ma, respectively (Friend and Nutman, 2010). The Isua supracrustal belt comprises tholeiitic basalts with pillow lavas, gabbros and boninite-like picrites (Polat et al., 2002), as well as BIF and clastic sediments (Nutman and Friend, 2009b). Bennett et al. (1993) showed the existence of a highly depleted mantle reservoir from Sm-Nd systematic in these rocks. Furthermore, positive ^{142}Nd -anomalies in metasedimentary rocks, amphibolites and orthogneisses at Isua imply derivation from a mantle source that was previously depleted during the lifetime of this short-lived Sm-Nd isotopic system in the Hadean (Caro et al., 2006). Hoffmann et al. (2011) ascribed decoupling of the Hf and Nd isotopic system in mafic rocks to modern arc-type processes, whereas Rizo et al. (2011) invoked a deep-seated Mg-perovskite origin for this decoupling. In a recent O-isotope study of serpentinites from the Isua supracrustal belt it was shown that the oceans were about 26% more voluminous at 3800 Ma than at present (Pope et al., 2012). This is a good example of just how much new information the Isua supracrustal belt still contains and it will likely continue to be intensely studied, because it represents an unusually well preserved window into the early Earth.

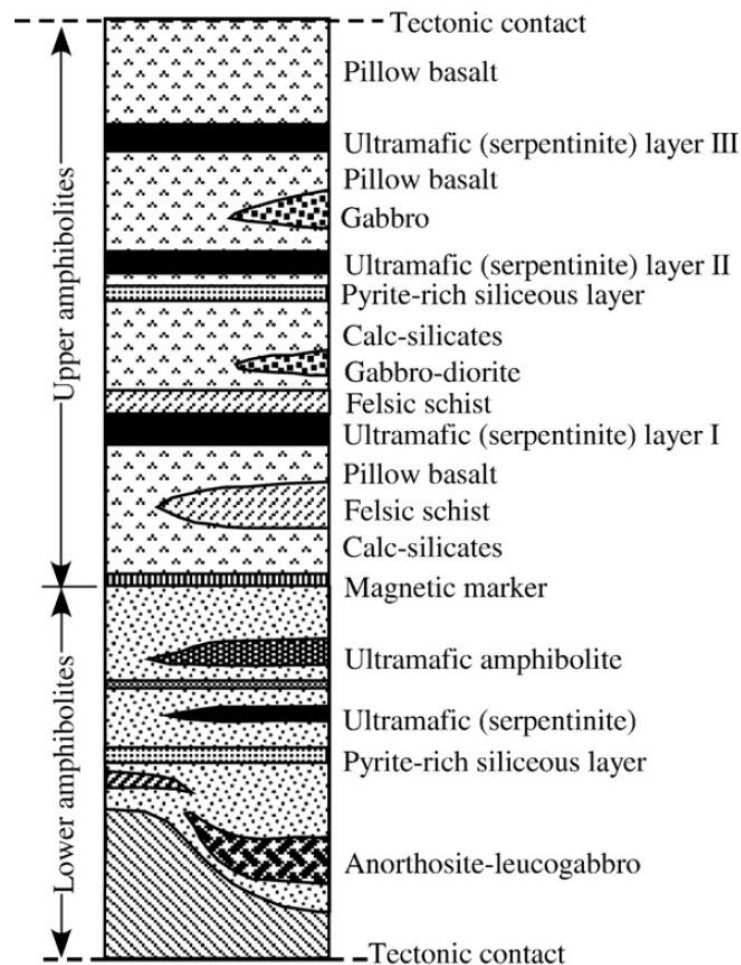


Figure 10. Stratigraphic section through the Ivisârtoq supracrustal belt, which resembles that of an ophiolite (Fig. 8). Figure from Polat et al. (2009c).

The Ivisârtoq supracrustal belt (Chadwick, 1985) is located about 30 km south of the Isua supracrustal belt at the end of Godthåbsfjord (Fig. 9). It has been dated at c. 3075 Ma from volcano-sedimentary rocks (Friend and Nutman, 2005b). This belt has recently been studied in detail by Ali Polat and co-workers (Polat et al., 2007, 2008a, 2008b; Ordóñez-Calderón et al., 2008, 2009), who concluded that the tholeiitic pillow lavas, gabbros, picrites and sedimentary rocks represent dismembered SSZ oceanic crust (Fig. 10).

The Qussuk supracrustal belt is located about 70 km NNE of Nuuk (Fig. 9) and has mainly been studied by the Geological Survey of Denmark and Greenland (GEUS). It has been dated at c. 3070 Ma from a volcano-sedimentary schist (Garde, 2007a). It contains tholeiitic basalt and calc-alkaline andesite rocks, with well preserved volcanoclastic textures, as well as aluminous schists, interpreted to represent hydrothermal alteration zones, and associated with Au mineralisation (Garde, 1997; Garde, 2005; Andreasen, 2007; Garde et al., 2007; Garde, 2008). Schlatter and Christensen (2010) propose that this association is only spatial/structural and not primary, however Garde et al. (2012) show field, geochemical and geochronological evidence that supports an epithermal origin of both the alteration and Au mineralisation.

The Bjørneøen supracrustal belt is located a few km south of Qussuk (Fig. 9). This supracrustal belt has been proposed to be co-genetic with the Qussuk supracrustal belt, because of their similar ages and lithologies (Garde, 2007b, 2008). Garde et al. (2012) show that these two supracrustal belts are in fact likely to be a direct continuation of the same arc system. Bjørneøen is dominated by tholeiitic basalts with pillow lava structures and bedded volcano-sedimentary rocks (Hollis et al., 2005; Garde et al., 2007b; Stendal, 2007). This belt has mainly received attention due to volcanogenic massive sulfide and Au mineralisation (e.g. Smith, 1998).



Figure 11. Primary volcanic structures in the Bjørnesund supracrustal belt. Left: pillow lavas. Right: volcanoclastic fragments. From Hollis et al. (2005).

The Storø composite supracrustal belt is located a few km east of Bjørneøen in Godthåbsfjord and about 30 km NE of Nuuk (Fig. 9). This supracrustal belt is located on the contact between the Tre Brødre and Færringehavn terranes. The sequence likely represents a composite of two discrete supracrustal belts, because U-Pb data in zircons extracted from gabbros associated with anorthosite contain ages >2900 Ma (K. Szilas, unpublished data). Due to a significant Au prospect claimed by NunaMinerals A/S, this composite supracrustal belt has received much scientific attention in an attempt to explain the favourable conditions of Au mineralisation (e.g. Pedersen, 1996; Hollis, 2005; Juul-Pedersen et

al., 2007; Nutman et al., 2007; Persson, 2007; van Gool et al., 2007; Szilas, 2008; Ordóñez-Calderón et al., 2011). The ages of the Storø composite supracrustal belt is not precisely established, but a maximum age for the younger sequence is 2800-2850 Ma from U-Pb dating of detrital zircons in quartzites (van Gool et al., 2007). A minimum age of c. 2700 Ma is indicated by Re-Os dating of arsenopyrite (Scherstén et al., 2012) related to an early phase of Au mineralisation. The Storø composite supracrustal belt mainly comprises tholeiitic basalts and various clastic sedimentary rocks, as well as Fe-rich garnetites (van Gool et al., 2007). Aluminous schists situated between the basalts and the sedimentary rocks may have formed by extreme hydrothermal leaching of basaltic rocks during reaction with seawater (Eilu et al., 2006; Knudsen et al., 2007; Szilas, 2008). The older part of the sequence comprise gabbros and anorthosite.

The Naajat Kuuat Complex, located about 60 km east of Nuuk (Fig. 9), is a layered anorthosite-gabbro complex of arc-affinity and comprises anorthosite, amphibolite and ultramafic rocks (Hoffmann et al., 2012). The complex has a c. 2985 ± 59 Ma Lu-Hf isochron age and is thus similar in age and composition to the larger Fiskensæset anorthosite complex farther south (Hoffmann et al., 2012).

Nunatak 1390 is located about 100 km ESE of Nuuk (Fig. 9). It is not large enough to constitute a supracrustal belt on its own, but it may be correlated with similar enclaves west of it (Escher and Myers, 1975; Chadwick and Coe, 1984; Kolb et al., 2009). A minimum age is defined by intrusive TTG aplites with U-Pb ages of about 2900 Ma (Paper III in the Annex). The outcrop is dominated by tholeiitic amphibolites and ultramafic rocks. The latter have compositions similar to Ti-enriched komatiites, but show evidence of a slab melt component and may thus rather represent boninites (Paper III in the Annex). Pillow lavas are locally present, but strong deformation has given rise to layered amphibolites in the central part and hydrothermal alteration associated with sulfides and tourmaline (Stendal, 2007; Stendal and Scherstén, 2007; Scherstén and Stendal, 2008). This area will be discussed further in Section 2.3 and Paper III in the Annex.



Figure 12. Ocelli in amphibolite at Grædefjord. These felsic inclusions in mafic rocks may represent immiscible liquids that were injected into a magma chamber during mingling of melts of different composition. Similar ocelli structures have been reported from the Isua and Ivisârtôq supracrustal belts. Photo by K. Szilas.

The Grædefjord supracrustal belt, located about 25 km north of Fiskeneset (Fig. 9), comprises amphibolites, leucoamphibolites, and ultramafic rocks with possible primary volcanoclastic bombs, fiamme textures and pillow structures (Wilf, 1982; Kolb et al., 2010). The age of the Grædefjord supracrustal belt is poorly constrained, but intrusive TTG aplites have U-Pb ages of c. 2890 Ma and a strong 2720 Ma metamorphic overprint (K. Szilas unpublished data). Tholeiitic and calc-alkaline rocks dominate the belt, and thin layers of ultramafic rock are similar to the boninite-like rocks presented from Nunatak 1390 (Paper III in the Annex). Ocelli-bearing amphibolites that show evidence of immiscible felsic melt droplets (K. Szilas, unpublished data), are similar to rocks found in the Ivisârtoq (Polat et al., 2009c) and Isua (Appel et al., 2009) supracrustal belts. However, it is not yet known if these felsic melt inclusions represent plagiogranites (e.g. Rollinson, 2009) or melts derived from a subducting slab (adakites).

The Fiskeneset anorthosite complex, located about 25 km north of Frederikshåb Isblink (Fig. 9), consist of sheets of anorthosite that intruded a layered leucogabbro, gabbro, and ultramafic sequence (Windley et al., 1973; Myers, 1985). The Fiskeneset anorthosite complex yield a Sm-Nd isochron age of 2973 ± 28 Ma (Polat et al., 2010). Common intrusive relations show that the anorthosite intruded the supracrustal rocks, and the protoliths of the regional TTG orthogneisses intruded the anorthosite complex (Kalsbeek and Myers, 1973; Bridgwater et al., 1976). Geochemical evidence indicates that these rocks formed in an arc-related geodynamic environment (Polat et al., 2009a) and were possibly derived from an aluminous mantle source (Rollinson et al., 2010).

The Bjørnesund supracrustal belt is located on both sides of Bjørnesund fjord in southern West Greenland a few km south of the Fiskeneset complex (Fig. 9). It comprises amphibolites, leucoamphibolites and minor anorthosite sheets along the northern contact with the surrounding TTG orthogneisses.



Figure 13. Well preserved pillow lava structures at Ravns Storø. The individual pillows are facing up with flat tops. Photo by Brian Windley.

Pulvertaft (1972) reported pillow lavas west of Bjørnesund fjord, but this supracrustal belt has experienced a high degree of deformation and primary structures are generally rare. Keulen et al. (2011) proposed that the Bjørnesund supracrustal belt can be correlated with the Ravens Storø supracrustal belt located a few km to the south. This relationship is supported by their similar geochemical and isotopic signatures (Paper II in the Annex). Retrogression from granulite-facies is evident by orthopyroxene pseudomorph in hornblende (McGregor and Friend, 1992). Intrusive TTG aplites yield minimum ages of c. 2900 Ma, and the supracrustal rocks have Nd- and Hf-isochron ages of about 2970 Ma (Paper II in the Annex). This area will be discussed further in Section 2.2.

The Ravens Storø supracrustal belt, located immediately north of Frederikshåb Isblink (Fig. 9), is one of the best preserved supracrustal belts in SW Greenland. This belt contains pillow lavas, lithic tuffs and zoned agglomerated bombs (Windley, 1968; Friend, 1975; Paper II in the Annex). Tholeiitic amphibolites and calc-alkaline leucoamphibolites comprise the majority of the supracrustal belt, but locally ultramafic rocks and aluminous schists occur along the southern margin of the belt (Friend, 1976). Intrusive TTG aplites with U-Pb ages of c. 2900 Ma provide a minimum age of the supracrustal belt, which has a Nd- and Hf-isochron age of about 2970 Ma (Paper II in the Annex). This area will be discussed further in Section 2.2.



Figure 14. Possible spinifex-texture in ultramafic rocks from the Paamiut supracrustal belt.
Photo by Jochen Kolb.

The Paamiut supracrustal belt, located about 30 km south of Frederikshåb Isblink in South-West Greenland (Fig. 9), was termed the Kvanefjord amphibolites by Escher (1971). It consists of several blocks and enclaves that comprise tholeiitic basalt, calc-alkaline andesite and komatiite-like ultramafic rocks (Higgins, 1990; Klausen et al., 2011; Kolb, 2011). The supracrustal rocks have a minimum age defined by TTG aplites that intruded at c. 2930 Ma (Klausen et al., 2011), however the region is dominated by 2850-2770 Ma granodioritic gneisses (Friend and Nutman, 2001). The rocks generally record amphibolites-facies metamorphic grade, but there is local evidence for retrogression from the granulite-facies (McGregor and Friend, 1997). It is worth noting that the ultramafic rocks in the Paamiut region are geochemically similar to the boninite-like rocks found on Nunatak 1390 (Paper III in the Annex), as well as ultramafic rocks in the Grædefjord supracrustal belt (K. Szilas unpublished data), and thus may have a similar origin. However, in the Paamiut region, certain outcrops of such ultramafic rocks contain what appear to be pseudomorphs after spinifex textures, as seen in Fig. 14 (Kolb, 2011).

The Tartoq Group, located adjacent to Sermiligaarsuk fjord in South-West Greenland, was mapped by the Geological Survey of Greenland (GGU) in the 1960's (Higgins, 1968, 1990; Higgins and Bondesen, 1966; Berthelsen and Henriksen, 1975). Its Mesoarchaeon minimum age was established by U-Pb dating of an intrusive TTG sheet at 2944 Ma (Nutman and Kalsbeek, 1994). Gold-anomalies have lead to prospecting by exploration companies and detailed mapping in areas of mineral potential (e.g. Petersen, 1992). XRF and AAS geochemical data were reported in an unpublished M.Sc. thesis (Lie, 1994), but no detailed modern geochemical and isotopic studies have been carried out prior to the study presented in Section 2.1 and Paper I in the Annex. The Tartoq Group stands out from the above-mentioned supracrustal belts by having the lowest degree of metamorphism found anywhere in the North Atlantic craton of Greenland. However, it also has the largest range in metamorphic grade (greenschist- to upper-amphibolite-facies) of any single supracrustal sequence in the craton (van Hinsberg et al., 2010). The rocks mainly comprise metamorphosed tholeiitic basalts, and prominent subaqueous lava flows, shallow mafic sills/dykes, and deeper level gabbroic intrusives, and serpentinites of harzburgitic composition. Therefore Szilas et al. (2011) suggested that the Tartoq Group represents a section through Mesoarchaeon oceanic crust and is thus essentially an Archaean ophiolite. This possibility will be discussed further in Section 2.1 and in Paper I in the Annex.

2. Discussion of the thesis papers

In the following sections I summarise the three thesis papers found in the Annex and discuss the implication of these studies for the geodynamic setting of SW Greenland. I will not present the results here as this is done in the papers. The data that form the basis of these studies are presented as supplementary material after each paper.

2.1. Paper I: Remnants of arc-related Mesoarchaeoan oceanic crust in the Tartoq Group of SW Greenland

This paper is in press in Gondwana Research

DOI: 10.1016/j.gr.2011.11.006

Szilas et al. (2011) recently suggested from preliminary data that the Tartoq Group of SW Greenland may represent a >3000 Ma dismembered ophiolite sequence. As mentioned in Section 1.5, one of the problems in accepting the existence of Archaean ophiolites, is that many authors are still confined by the 1972 Penrose definition for ophiolites (Anonymous, 1972). However, this is out-dated and should be replaced by the new classification of Dilek (2003). In a review of several well studied supracrustal belts from SW Greenland (Isua and Ivisârtôq) it was concluded that they indeed resemble modern suprasubduction zone (SSZ) ophiolites, although they represent incomplete sections (Polat et al., 2011). It is thus mainly the high degree of deformation, as well as metamorphism and hydrothermal alteration that makes it difficult to preserve a complete ophiolite section of this age, and further makes it a challenge to determine if such a rock assemblage is coeval or not.

In Paper I, we present the first comprehensive modern major-, trace- and isotope-geochemical data set for the Tartoq Group and show that these well preserved supracrustal rocks indeed have the lithological, compositional and structural characteristics that make them a prime candidate for a near-complete Archaean ophiolite complex. A well constrained Lu-Hf errorchron for the mafic association of the Tartoq Group suggests an age of 3189 ± 65 Ma for these rocks.

Th/Yb vs. Nb/Yb has been used to detect a crustal contamination signature in volcanic rocks and its use for Archaean supracrustal rocks was reviewed by Pearce (2008). He concluded that essentially all Archaean tholeiitic suites contain evidence for a crustal input. However, TTGs contain an order of magnitude higher Th content than the supracrustal rocks, which they envelop and mobility of Th has been documented in Archaean supracrustal belts (Frei et al., 2002; Polat and Hofmann, 2003). In addition Yb and MgO are inversely correlated and because MgO-rich samples are likely more prone to alteration, it is possible that the Th/Yb ratio is not recording the primary magmatic abundances of these two elements. This in turn suggests that the use of the Th/Yb-Nb/Yb diagram is perhaps less diagnostic than previously argued by Pearce (2008), at least for MgO-rich rocks which have experienced extensive alteration and metasomatism. Nevertheless, there appears to be a sub-vertical trend in Th/Yb ratio for the mafic association of the Tartoq Group. The greenstones and pillow lavas have the most MORB-like ratios and extend into the field of arc lavas, which suggests interaction with a subduction zone component (Fig. 15). The transitional greenschists appear to plot

towards local TTG crust and some of the felsic schists plot towards the mafic association. This likely reflects mechanical mixing of the two end members during deformation that resulted in the TTG mylonites and the felsic schists. This must be a late feature given the presence of zircon grains in the felsic schists, which are younger than the minimum age of the Tartoq Group defined by intrusive TTGs with U-Pb ages of 2986 ± 4 Ma.

It is generally accepted that subduction zones have been operating since around 3200 Ma (Condie, 1981; de Wit, 1998; Smithies et al., 2005b; Kerrich and Polat, 2006; Moyen et al., 2006; van Kranendonk et al., 2007b; Pease et al., 2008) and possibly even as early as 3800 Ma (Komiya et al., 1999; Polat et al. 2002; Dilek and Polat, 2008; Furnes et al., 2009). The former minimum age for subduction zones on Earth is also suggested by this study on the mafic association of the Tartoq Group. Their geochemical characteristics support them as being intermediate between mid-ocean ridge basalt (MORB) and island arc tholeiite (IAT) with a possible relation to a back-arc basin (BAB) environment. It can be argued that rocks formed in a BAB setting are more likely to be preserved than true MORB, because crust will tend to be thinner and already located in a compressional tectonic setting (Martinez and Taylor, 2003; Taylor and Martinez, 2003). This is confirmed by the fact that many of the best preserved ophiolites formed in supra subduction zone (SSZ) settings rather than as MORB and have IAT geochemical signatures (Dilek and Polat, 2008). The Izu-Bonin-Mariana arc-trench system is considered the best modern analogue for formation of SSZ ophiolites and such a setting of accretion of island arc complexes could be a modern analogue of at least some Archaean supracrustal belts (Dilek and Furnes, 2011).

Polat et al. (2011) presented data from the Isua and Ivisârtoq supracrustal belts in SW Greenland and argued that they resemble modern SSZ mafic assemblages and thus that subduction zone environments may have existed throughout the Archaean Eon. Because the Tartoq Group mafic assemblage is essentially overlapping the rocks from the Isua and Ivisârtoq supracrustal belts, we follow the same line of reasoning and suggest that the Tartoq Group rocks have likely formed in a SSZ setting, assuming that the principle of uniformitarianism can be applied to the Mesoarchaeon. Although different tectonics settings have been proposed for the Archaean including both subduction zones and mantle plumes (e.g. Zegers and van Keken, 2001; Bédard, 2006; Kerrich and Polat, 2006; Rollinson and Whitehouse, 2011), it appears that the observed data for the Tartoq Group are entirely consistent with a modern SSZ environment. Therefore this suggests that some form of plate tectonic processes were in operation since at least 3200 Ma, which is consistent with the general consensus (Condie, 1981; de Wit, 1998; Smithies et al., 2005b; Kerrich and Polat, 2006; Moyen et al., 2006; Pease et al., 2008).

Our field interpretation of the serpentinites as cumulates or relict mantle related to the mafic association and not intrusive sills as previously proposed by Berthelsen and Henriksen (1975) is supported by their high MgO (c. 30-40 wt.%). The high MgO contents is far too high for even komatiitic magmas and suggests that they represent olivine-rich cumulates or mantle as their CIPW-norm also suggests. These rocks are rather Fe-rich compared with examples of Archaean SCLM, but they are highly depleted in CaO, Al_2O_3 and incompatible elements as expected for mantle rocks. However, we are not able to confidently determine if the serpentinites are cumulates or tectonized mantle and further work is needed on these rocks.

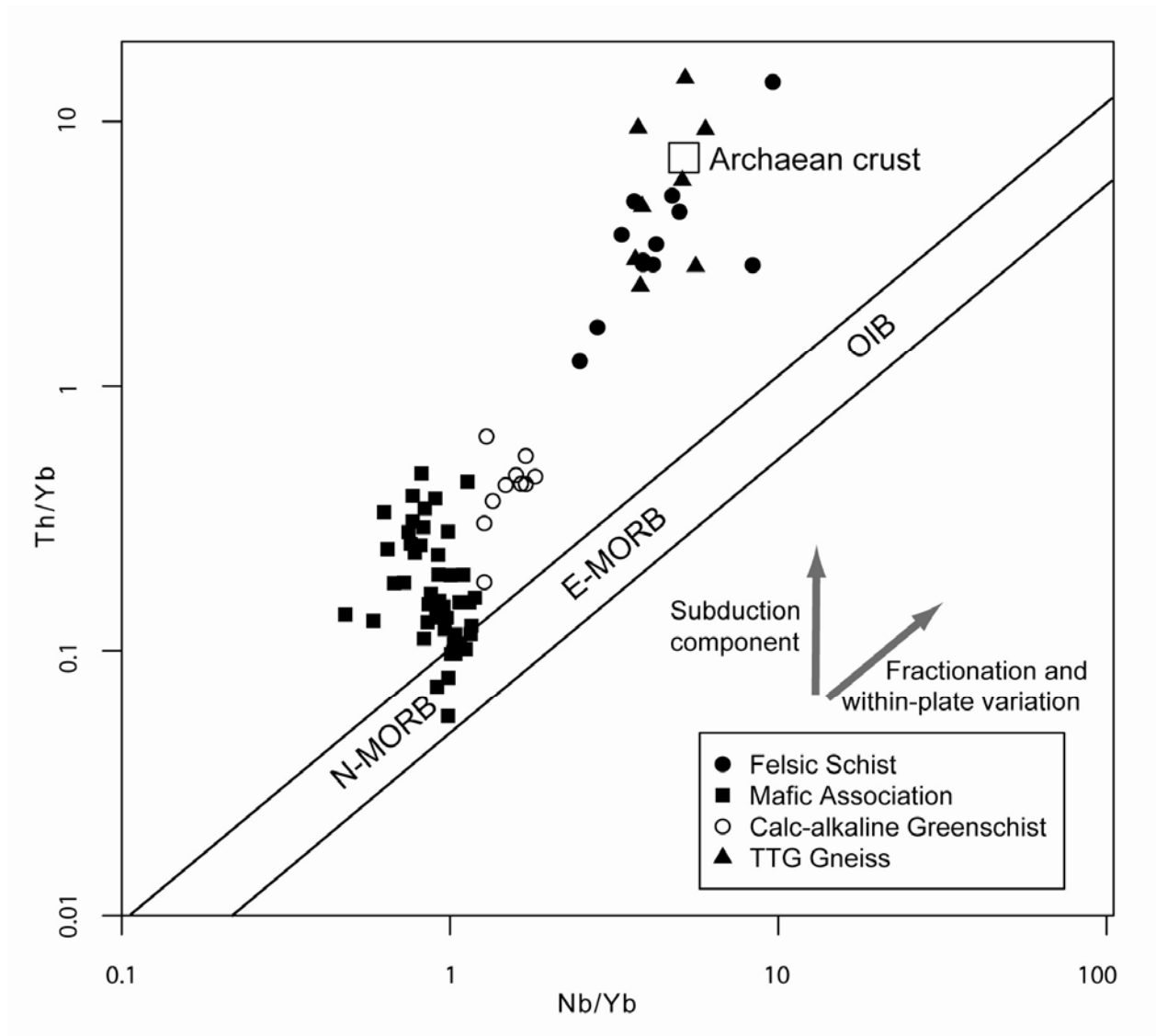


Figure 15. Th/Yb vs. Nb/Yb diagram of Pearce (2008). The mafic sequence of the Tartoq Group shows a subvertical arc trend, whereas the felsic components show possible mechanical mixing towards local TTG crust.

The conclusion of Paper I is therefore that we consider the Tartoq Group mafic association of pillow lavas, sills/dykes and gabbros as a co-genetic sequence due to their similar trace element characteristics. We suggest that they formed as oceanic crust in a tectonic setting similar to that of a modern suprasubduction zone, such as a fore-arc or back-arc basin.

Future studies on the Tartoq Group should focus on the serpentinites and establish if they indeed represent mantle rocks, and thus confirm the ophiolite model. One approach could be to determine the composition of chromites, which have been shown to be diagnostic of certain tectonic environments (e.g. Rollinson, 2008c; Pagé et al., 2012). Re-Os age dating would also be important in order to establish if the serpentinites are cogenetic with the mafic sequence.

2.2. Paper II: Complex calc-alkaline volcanism recorded in Mesoarchaeoan supracrustal belts north of Frederikshåb Isblink, southern West Greenland: implications for subduction zone processes in the early Earth

This paper is in press in Precambrian Research

DOI: 10.1016/j.precamres.2012.03.013

In this paper we present new geochemical and isotopic data from the three Mesoarchaeoan supracrustal belts of Ravns Storø, Bjørnesund and Perserajorsuaq. The collective name ‘Ikkattup Nunaa Supracrustal Association’ is proposed for this co-magmatic assemblage of rocks. The study area is located north of Frederikshåb Isblink in southern West Greenland, just a few km south of the Fiskenæsset complex. The supracrustal rocks mainly comprise amphibolites with a tholeiitic basalt composition and leucoamphibolites with a calc-alkaline andesite composition. Both lithological units are cut by aplite sheets of TTG composition with U-Pb zircon ages of c. 2900 Ma, which provides the minimum age of the supracrustal rocks. Lu-Hf and Sm-Nd isochrons based on whole-rock amphibolite and leucoamphibolite samples yield ages of 2990 ± 41 Ma and 3020 ± 78 Ma, respectively. Of particular interest in this study is the origin of the andesitic leucoamphibolites, because such rocks are rare in Archaeoan supracrustal belts, but may provide important constraints on the geodynamic environment of formation.

The petrogenesis of calc-alkaline andesites is much debated, even in modern subduction zone settings (e.g. Kelemen et al., 2003; and references therein). The observation of disequilibrium textures in modern calc-alkaline arc rocks suggests the operation of complex processes for their formation, which have been ascribed to both differentiation of water-rich magmas (Green and Ringwood, 1967; Sisson and Grove, 1993; Grove et al., 2003), degassing-induced crystallisation (Frey and Lange, 2010), and mixing of felsic and mafic magmas (Anderson, 1975; Eichelberger, 1978; Tatsumi and Suzuki, 2009). Although all of these effects could potentially contribute to the documented disequilibrium features in arc magmas, mixing is strongly supported by recent work on melt inclusions and quenched glasses from volcanic arcs, which show a strong bimodal distribution (Reubi and Blundy, 2009; Kovalenko et al., 2010). This conclusion is supported by mineral-scale isotope and trace element variations (e.g. Davidson et al., 2005, 2007).

Archeoan examples of andesites are fairly rare, but have been described from several supracrustal belts worldwide (e.g. Barley et al., 1998; Polat and Münker, 2004; Wang et al., 2004; Manikyamba et al., 2009; Mtoro et al., 2009; Klausen et al., 2011; Leclerc et al., 2011). Such rocks are often reported to have an adakitic (slab-melt) affinity as originally been defined by Defant and Drummond (1990). However, this term has been misused in the literature to include rocks with similar geochemical characteristics, but with no relations to subduction zones (Castillo, 2012).

The leucoamphibolites from the three supracrustal belts in the present study show apparent geochemical mixing trends between tholeiitic amphibolites and TTG gneisses, as the compositional end-members. By assimilation-fractional-crystallisation (AFC) modelling we can show that one group of the leucoamphibolites can indeed be explained by contamination of their parental melts by a TTG-like end-member. Another group of high P_2O_5 , La and Nb leucoamphibolites can be explained by contamination involving a hypothetical low-silica adakite end-member. However, the leucoamphibolites are juvenile with $\epsilon Nd_{(2970Ma)}$ from +2.1 to +3.5 and $\epsilon Hf_{(2970Ma)}$ of +3.5 to +4.3. Thus,

the mafic source of the felsic contaminant melts must have been derived from a depleted mantle source more or less at the same time (<60 Ma) as the volcanism took place.

Our preferred interpretation of the geochemical and isotopic data is that the protoliths of the supracrustal rocks formed in an island arc setting, where early tholeiitic volcanism gave way to calc-alkaline volcanism in a maturing arc (Fig. 16). The apparent AFC trends are thus explained by *in situ* partial melting of basaltic arc crust to form juvenile TTG- and adakite-melts that mixed with mafic magmas or contaminated their mantle source to produce the calc-alkaline leucoamphibolite protolith.

The proposed petrogenetic model for the 'Ikkattup Nunaa Supracrustal Association' has important implications for the general interpretation of other Archaean supracrustal belts. AFC and geochemical mixing trends towards a TTG end-member are not uniquely diagnostic of crustal contamination, but may rather reflect processes operating at source levels in arcs, such as melting-assimilation-storage-homogenisation (MASH) or slab-melt (low-silica adakite) metasomatism of their mantle source. Therefore this study supports the operation of subduction zone processes since at least the Mesoarchaeon and provides insights to a specific process of andesite formation, which is also observed in modern arc settings.

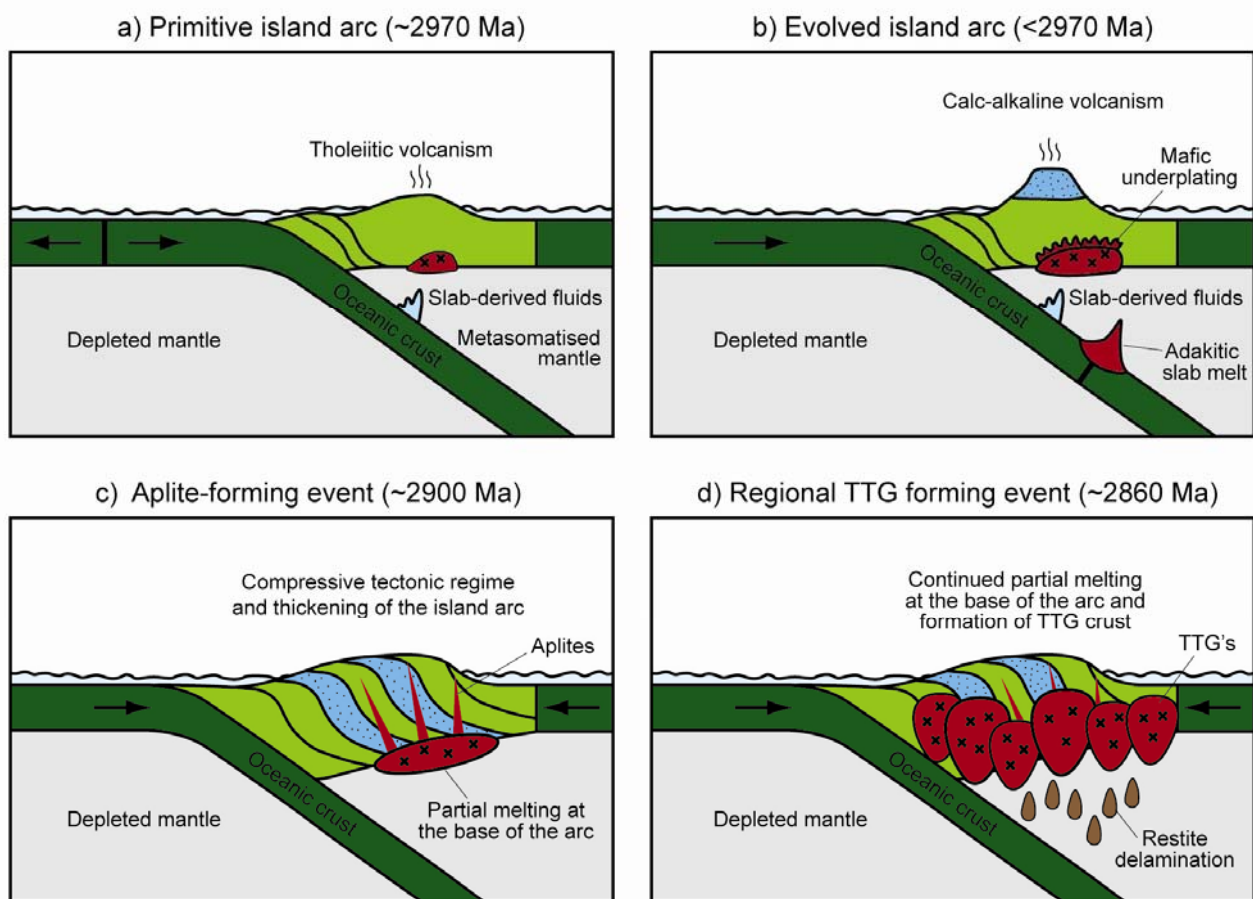


Figure 16. Model for the formation of Mesoarchaeon calc-alkaline volcanic rocks in SW Greenland. a) Primitive island arc stage, which was dominated by tholeiitic basalts with characteristic negative Nb-anomalies. b) Evolved island arc stage where calc-alkaline andesites were formed by slab melt metasomatism and mixing of mafic melts with felsic melts produced by partial melting of the base of the arc due to mafic underplating. c) Convergent stage where the island arc crust was stacked and thickened, so that the base reached granulite facies metamorphic conditions and underwent partial melting to produce intrusive aplites. d) Large scale melting of the base of the island arc crust produced TTG batholiths.

2.3. Paper III: Origin of Mesoarchaeoan arc related rocks with boninite/komatiite affinities from southern West Greenland

This paper is in press in Lithos

DOI: 10.1016/j.lithos.2012.03.023

We report elemental and Sm-Nd isotope whole-rock geochemical data on supracrustal rocks from Nunatak 1390 in southern West Greenland. Additionally, we present the metamorphic temperature history for these rocks, as derived from tourmaline thermometry on a tourmalinite inlier, as well as *in situ* U-Pb, Hf and O isotopic data from zircon extracted from intrusive TTG gneisses. The Nunatak 1390 supracrustal rocks have a minimum age of c. 2900 Ma defined by U-Pb zircon ages of cross-cutting aplite sheets of TTG composition. The supracrustal rocks comprise pillowed and layered amphibolites and ultramafic rocks with amphibolites-facies mineral assemblages and a peak metamorphic temperature of approximately 550°C. The mafic sequence has relatively flat trace element patterns (La_N/Sm_N of 0.70-2.4) and mostly negative Nb-anomalies (Nb/Nb^* of 0.30-1.0), which resembles modern island arc tholeiites (IAT). The mafic sequence can be divided into a high- and low-Ti group, where the former group has lower MgO, and significantly higher contents of incompatible elements, such as TiO_2 , P_2O_5 , Zr, Nb and Th. The ultramafic rocks have similar major and trace element compositions as Ti-enriched/Karasjok-type komatiites (Fig. 17). Recently similar rocks have been described from the Paamiut region in SW Greenland and some of these rocks have the critical spinifex textures that define komatiites (Fig. 14; Klausen et al., 2011; Kolb, 2011). These rocks have similar geochemical characteristics as the Nunatak 1390 ultramafic rocks, so it is possible that they were originally komatiites *sensu stricto*, but have later been metamorphosed and deformed beyond recognition.

Komatiites are ultramafic volcanic rocks of mostly Archaean age and have traditionally been related to deep mantle plumes (Arndt and Nisbet, 1982; Arndt, 1994; Arndt et al., 2008). However, an alternative interpretation of the geodynamic environment of formation for komatiites has been presented by Grove et al. (1999) and Parman et al. (2001, 2004). These workers propose that the Mg-rich komatiitic magmas formed by fluid fluxed melting of previously depleted mantle and thus, that komatiites essentially represent Archaean equivalents of modern boninites. This model is supported by the presence of igneous augite in komatiites, which is mainly produced by hydrous melts (Parman et al., 1997; Parman and Grove, 2004). Another piece of evidence for the primary volatile contents of komatiites is the presence of volcanoclastic textures in komatiites from the Barberton Greenstone Belt (Stiegler et al., 2010). Even stronger evidence for an elevated water content of komatiites comes from magmatic amphibole, which has textures and compositions that are primary (Stone et al., 1997). Moreover, *in situ* trace element and Boron isotopic data suggests that these volatiles were not mantle-derived (Fiorentini et al., 2008, 2011; Gurenko and Kamenetsky, 2011). Finally, water-rich melt inclusions in olivine have been reported in late Cretaceous komatiites on Gorgona Island (Kamenetsky et al., 2010). Thus, there seems to be growing evidence for an alternative explanation for the origin of komatiites, which is markedly different from the deep mantle plume model, which has been the consensus view for three decades (Arndt and Nisbet, 1982).

The low-Ti group of the mafic sequence on Nunatak 1390 appears to have been derived from an N-MORB source, whereas the high-Ti group and the ultramafic rocks appear to have been derived from a mantle source that is

more enriched than the N-MORB source. However, there is no difference in the initial ϵ_{Nd} of the mafic and ultramafic rocks. Additionally, AFC modelling suggests that the enrichment was caused by introduction of juvenile low-silica adakite melts into the mantle source region. Accordingly, we propose that the mafic and ultramafic rocks were derived from a similar mantle source, but that the source of the ultramafic rocks was previously depleted and later refertilised by slab melts in a subduction zone setting. Thus, the high MgO contents of the komatiites may simply reflect second-stage melting of refractory mantle in a process that is similar to that which is responsible for the formation of modern boninites.

The implication of this model is that komatiites are not restricted to deep mantle plumes, but could instead reflect shallow melting of refractory mantle that was fluxed by melts and fluids in a subduction zone setting, and thus represent Archaean equivalents of modern boninites. This scenario is likely for at least the Ti-enriched type of komatiites that we have identified in the Nunatak 1390 supracrustal sequence and such a model is supported by the recent literature that is continuously documenting new evidence for a hydrous origin of komatiites.

Perhaps some of the ultramafic enclaves and inclusions found in TTGs represent refractory rocks such as mantle restites or komatiitic/boninitic rocks, which have melting temperatures that are higher than the sedimentary and mafic rocks that comprise the main portion of supracrustal belts. If this is the case then supracrustal belts could be viewed as remnants of mafic crust that should have been melted by whatever process is responsible for TTG formation, and these preserved mafic relicts escaped such melting by sheer coincidence.

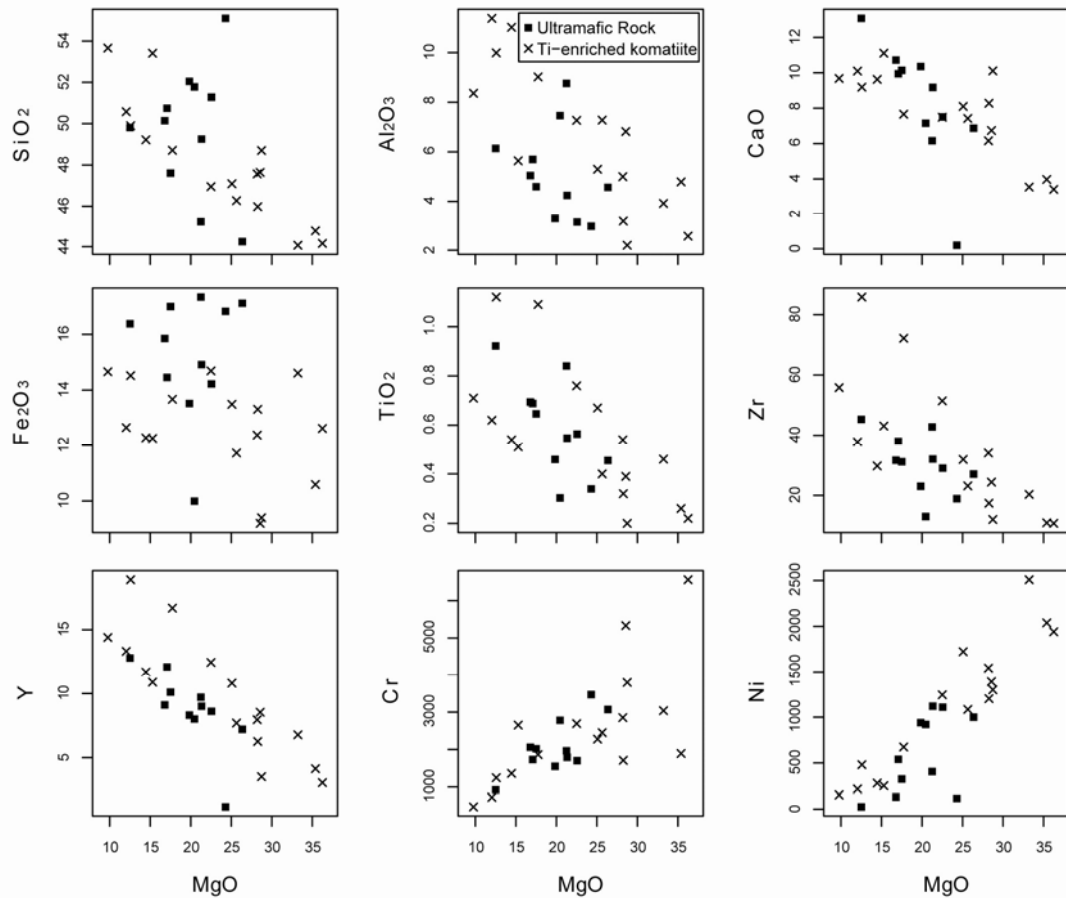


Figure 17. Harker diagrams showing the similarity between the ultramafic rocks found on Nunatak 1390 and Ti-enriched komatiites from the Murchinson Terrane in Western Australia described by Barley et al. (2000).

3. Conclusions and future work

The geochemical evidence from the supracrustal belts of SW Greenland exclusively points to a subduction zone setting and thus support the existence of uniformitarian tectonic processes throughout most of the Archaean Eon (e.g. Dilek and Furnes, 2011; Friend and Nutman, 2010; Furnes et al., 2009; Garde, 2007a, 2007b; Hoffmann et al., 2011; Polat et al., 2002, 2008a, 2008b, 2010, 2011; Windley and Garde, 2009; Papers I, II and III in the Annex). This has important consequence in the global framework, because other Archaean cratons have been interpreted in terms of a distinctly different plume-driven geodynamic setting that is not compatible with uniformitarian principles (e.g. Bickle et al., 1994; Davies, 1999; McCall, 2003; Bédard, 2006; Stern, 2005, 2008; Hamilton, 1998, 2011; van Kranendonk, 2011b).

Although the geochemical data of TTGs bear some resemblance to arc related magmas, due to their enriched trace element patterns and negative Nb, Ta and Ti anomalies, it is not possible to discriminate between a plume and arc setting, because these geochemical characteristics can arise under widely different temperature and pressure conditions (Moyen, 2011). Thus, we must turn to the SCLM xenolith and supracrustal rock records to establish what geodynamic setting was dominating during the Archaean.

Eclogite xenoliths with ages of up to 3000 Ma suggests that subduction of basaltic slabs was occurring at least since then (Shirey and Richardson, 2011). The peridotite xenolith data worldwide supports shallow melt depletion (Section 1.3; Canil, 2004; Wittig et al., 2008). A particularly important observation is that the extreme depletion seen in peridotite xenoliths cannot be explained with a single-stage melt extraction. Not even komatiites are mafic enough to be in equilibrium with the SCLM and thus cannot account for the observed depletion. Thus, a two-stage process is required, and the fact that Phanerozoic boninite mantle restite overlaps more or less with the Archaean SCLM xenolith record, suggests that a similar process could be responsible for the formation of SCLM (Parman et al., 2004). Additionally, numeric modelling shows that it would be possible to thicken the SCLM during arc accretionary processes to cause the presently observed structure of the cratons (Gray and Pysklywec, 2010). Accordingly, the peridotite and eclogite xenolith data supports the formation of the SCLM during subduction zone processes.

The global Archaean supracrustal rock record, on the other hand, has been interpreted in terms of both mantle plume and subduction zone processes. It appears to be a possibility that both settings were operating during the Archaean, but each setting may have been dominating over the other in different regions of the world. However, evidence from supracrustal belts in SW Greenland collectively points to a model where arc accretion was important throughout the Archaean, at least in this region due to the follow lines of evidence:

(1) Structural observations support terrane collision and horizontal accretion of both TTG crust and supracrustal belts during the Archaean in SW Greenland (Bridgwater et al., 1974; Myers, 1985; Komiya et al., 1999; Hamner and Greene, 2002; Windley and Garde, 2009; Kisters et al., 2011).

(2) The geochemical data of mafic supracrustal rocks in SW Greenland is similar to primitive Phanerozoic island arc rocks (Dilek and Polat, 2008; Dilek and Furnes, 2011; Polat et al., 2011; Papers I, II and III in the Annex). In particular their negative Nb-anomalies and their high Th/Yb ratios are distinctive of island arc settings.

(3) Calc-alkaline andesites found in supracrustal belts indicate the presence of slab melts in their mantle source or mixing with juvenile felsic melts in magma chambers prior to eruption (Section 2.2; Klausen et al., 2011; Paper II in the Annex).

(4) Ultramafic rocks in SW Greenland have compositional similarities with high-Ti/Karasjok-type komatiites (Section 2.3; Paper III in the Annex). These rocks are possibly an Archaean equivalent of modern boninites, which form by melting of a previously depleted mantle source that has been refertilised by a slab fluid/melt component in subduction zones (König et al., 2010; Parman et al., 2004).

(5) Hf isotopic data from zircon in TTGs show evidence of mixing of sources during compressional events and have long residence times (Paper III in the Annex; Næraa, 2011, 2012).

Based on this thesis work it can be concluded that modern-style subduction zone processes were likely in operation since at least the Mesoarchaean in SW Greenland. This conclusion is fairly uncontroversial and is supported by a wide range of evidence worldwide, such as from the geochemical characteristics of supracrustal belts in other cratons (e.g. Smithies et al., 2005b; Polat et al., 2006), metamorphic studies of supracrustal rocks (Moyen et al., 2006; Kisters et al., 2010), dipping seismic reflectors in the Canadian craton (Lewry et al., 1994), SCLM xenoliths pointing to shallow melt depletion in subduction zones (Canil, 2004; Lee, 2006; Wittig et al., 2008), numeric modelling of the SCLM that are best explained by imbrication and underplating during accretionary processes (Gray and Pysklywec, 2010) and eclogitic inclusions in diamonds suggest that subducting slabs became abundant in the SCLM after 3000 Ma (Shirey and Richardson, 2011).

Accepting the above conclusion that the studied supracrustal belts of SW Greenland collectively points to a subduction zone geodynamic environment, we have to think about what direction the next steps of research should take. The present PhD thesis and the extensive number of publications about the supracrustal belts in SW Greenland in recent years have substantially increased our understanding of such volcanic rocks and their tectonic environment of formation. Similarly much geochronological work has been done on the TTG gneisses in SW Greenland and it is now clear that they are derived from supracrustal rocks by partial melting at the base of tectonically thickened mafic crust (Nagel et al., 2012). Therefore, one obvious path would be to do similar studies in the essentially unknown SE part of the Archaean craton of Greenland to test if a similar picture will emerge.

Another important piece of the Archaean puzzle that remains poorly understood, even in the relatively well studied SW Greenland region, is the petrogenesis of ultramafic enclaves found both within the supracrustal belts and the TTG gneisses. Firstly, a thorough characterisation would be needed of these ultramafic rocks, employing whole-rock, platinum group element, electron microprobe and Re-Os isotopic analysis. Possible origins of these refractory Mg-rich rocks could be komatiite/boninite lavas, cumulate rocks or mantle peridotite.

Of particular interest would be to develop a consistent model that explains the formation of the TTG orthogneiss terrane, the subcontinental lithospheric mantle and the supracrustal belts in order to determine the geodynamic setting that was operating during the Archaean Eon.

References

- Abbott, D.H., 1996. Plumes and hotspots as sources of greenstone belts. *Lithos* 37, 113-127.
- Allaart, J.H., 1982. Geological map of Greenland. 1:500 000. Sheet 2, Frederikshåb Isblink – Søndre Strømfjord, Geological Survey of Greenland, Copenhagen.
- Amelin, Y., Krot, A.N., Hutcheon, I.D., Ulyanov, A.A., 2002. Lead isotopic ages of chondrules and calcium-aluminum-rich inclusions. *Science* 297, 1678-1683.
- Anbar, A.D., Duan, Y., Lyons, T.W., Arnold, G.L., Kendall, B., Creaser, R.A., Kaufman, A.J., Gordon, G.W., Scott, C., Garvin, J., Buick, R., 2007. A whiff of oxygen before the Great Oxidation Event? *Science* 317, 1903-1906.
- Anderson, A.T., 1975. Magma mixing: petrological process and volcanological tool. *Journal of Volcanology and Geothermal Research* 1, 3-33.
- Andreasen, B., 2007. Mineralogical and geochemical investigations of gold-bearing Mesoproterozoic supracrustal rocks from the Qussuk area, southern West Greenland, Mineral resource assessment of the Archaean Craton (66° to 63°30'N) SW Greenland, Contribution no. 6. Danmark og Grønlands Geologiske Undersøgelse Rapport 2007/79, 77 pp.
- Anhaeusser, C.R., 1973. The evolution of the early Precambrian crust of southern Africa. *Philosophical Transactions of the Royal Society of London*, A, 273, 359-388.
- Anonymous, 1972. Penrose field conference on ophiolites. *Geotimes* 17, 24-25.
- Appel, P.W.U., Polat, A., Frei, R., 2009. Dacitic ocelli in mafic lavas, 3.8–3.7 Ga Isua greenstone belt, West Greenland: Geochemical evidence for partial melting of oceanic crust and magma mixing. *Chemical Geology* 258, 105-124.
- Armstrong, R.L., 1981. Radiogenic isotopes: the case for crustal recycling on a near-steady-state no-continental growth Earth. *Philosophical Transactions of the Royal Society of London Series A* 301, 443-471.
- Arndt, N.T., 1994. Archean komatiites. In: Condie, K.C. (ed.), *Archean Crustal Evolution*. Elsevier (Amsterdam), 11-44.
- Arndt, N.T., Nisbet, E.G., 1982. Komatiites. Allen and Unwin, London, 526 pp.
- Arndt, N.T., Kerr, A.C., Tarney, J., 1997. Dynamic melting in plume heads: the formation of Gorgona komatiites and basalts. *Earth and Planetary Science Letters* 146, 289-301.
- Arndt, N.T., Leshner, C.M., Barnes, S.J., 2008. Komatiites. Cambridge University Press, 488 pp.
- Arndt, N.T., Coltice, N., Helmstaedt, H., Gregoire, M., 2009. Origin of Archean subcontinental lithospheric mantle: Some petrological constraints. *Lithos* 109, 61-71.
- Baadsgaard, H., 1973. U-Th-Pb dates on zircons from the early Precambrian Amitsoq gneisses, Godthaab district, West Greenland. *Earth and Planetary Science Letters* 19, 22-28.
- Barley, M.E., Loader, S.E., McNaughton, N.J., 1998. 3430 to 3417 Ma calc-alkaline volcanism in the McPhee Dome and Kelly Belt, and growth of the eastern Pilbara Craton. *Precambrian research* 88, 3-23.
- Barley, M.E., Kerrich, R., Reudavy, I., Xie, Q., 2000. Late Achaean Ti-rich Al-depleted komatiites and komatiitic volcanoclastic rocks from the Murchison Terrane in Western Australia. *Australian Journal of Earth Sciences* 47, 873-883.
- Barth, M.G., Foley, S.F., Horn, I., 2002. Partial melting in Archean subduction zones: Constraints from experimentally determined trace element partition coefficients between eclogitic minerals and tonalitic melts under upper mantle conditions. *Precambrian Research* 113, 323-340.
- Bédard, J.H., 2006. A catalytic delamination-driven model for coupled genesis of Archean crust and sub-continental lithospheric mantle. *Geochimica et Cosmochimica Acta* 70, 1188-1214.
- Belousova, E.A., Kostitsyn, Y.A., Griffin, W.L., Begg, G.C., O'Reilly, S.Y., Pearson, N.J., 2010. The growth of the continental crust: Constraints from zircon Hf-isotope data. *Lithos* 119, 457-466.
- Bennet, V.C., Nutman, A.P., McCulloch, M.T., 1993. Nd isotopic evidence for transient, highly depleted mantle. *Earth and Planetary Science Letters* 119, 299-317.
- Bennett, V.C., 2003. Compositional Evolution of the Mantle. In: Carlson, R.W. (ed.), *Treatise on Geochemistry* (Elsevier) 2.13, 493-519.
- Bernstein, S., Kelemen, P.B., Brooks, C.K., 1998. Depleted spinel harzburgites xenoliths in Tertiary dykes from East Greenland: restites from high degree melting. *Earth and Planetary Science Letters* 154, 221-235.
- Bernstein, S., Kelemen, P.B., Hangoj, K., 2007. Consistent olivine Mg# in cratonic mantle reflects Archean mantle melting to the exhaustion of orthopyroxene. *Geology* 35, 459-462.
- Berthelsen, A., Henriksen, N., 1975. Geological map of Greenland, 1:100,000 Ivittuut 61 V.1 Syd (with description). Geological Survey of Greenland, Copenhagen, 169 pp.
- Bickle, M.J., 1986. Implications of melting for stabilisation of the lithosphere and heat loss in the Archaean. *Earth and Planetary Science Letters* 80, 314-324.
- Bickle, M.J., Nisbet, E.G., Martin, A., 1994. Archean greenstone belts are not oceanic crust. *The Journal of Geology* 102, 121-138.
- Bizzarro, M., Connelly, J.N., Thrane, K., Borg, L.E., 2012. Excess hafnium-176 in meteorites and the early Earth zircon record. *Geochemistry, Geophysics, Geosystems* 13, no. 3, 1-10.
- Black, L.P., Gale, N.H., Moorbath, S., Pankhurst, R.J., McGregor, V.R., 1971. Isotopic dating of very early Precambrian amphibolite facies gneisses from the Godthaab district, West Greenland. *Earth and Planetary Science Letters* 12, 245-259.
- Bowring, S.A., van Schmus, W.R., 1984. U-Pb zircon constraints on evolution of Wopmay Orogen, N.W.T. Geological Association of Canada/Mineralogical Association of Canada, Abstract 9.
- Boyett, M., Carlson, R.W., 2005. ¹⁴²Nd evidence for early (>4.53 Ga) global differentiation of the silicate Earth. *Science* 309, 576-581.
- Bridgwater, D., McGregor, V.R., Myers, J.S., 1974. A horizontal tectonic regime in the Archaean of Greenland and its implications for early crustal thickening. *Precambrian Research* 1, 179-197.
- Bridgwater, D., Keto, L., McGregor, V.R., Myers, J.S., 1976. Archaean gneiss complex of Greenland. In: Escher, A., Watt, W.S. (eds.), *Geology of Greenland, Grønlands Geologiske Undersøgelse*, Copenhagen, 18-75.
- Brown, M., 2008. Characteristic thermal regimes of plate tectonics and their metamorphic imprint throughout Earth history: when did Earth first adopt a plate tectonics mode of behaviour? In: Condie K.C., Pease V. (eds.), *When did Plate Tectonics begin on Planet Earth?* Geological Society of America, Special Paper 440.
- Campbell, I.H., Taylor, S.R., 1983. No water, no granites – No oceans, no continents. *Geophysical Research Letters* 10, 1061-1064.
- Canfield, D.E., 2005. The Early History of Atmospheric Oxygen: Homage to Robert M. Garrels. *Annual Reviews of Earth and Planetary Science* 33, 1-36.
- Canil, D., 2002. Vanadium in peridotites, mantle redox and tectonic environments: Archean to present. *Earth and Planetary Science Letters* 195, 75-90.
- Canil, D., 2004. Mildly incompatible elements in peridotites and the origins of mantle lithosphere. *Lithos* 77, 375-393.
- Canup, R.M., 2004. Dynamics of Lunar formation. *Annual Reviews of Astronomy and Astrophysics* 42, 441-475.
- Carlson, R.W., Pearson, D.G., James, D.E., 2005. Physical, chemical, and chronological characteristics of continental mantle. *Reviews of Geophysics* 43, RG1001, 1-24.
- Caro, G., Bourdon, B., Birck, J.-L., Moorbath, S., 2006. High-precision ¹⁴²Nd/¹⁴⁴Nd measurements in terrestrial rocks: Constraints on the early differentiation of the Earth's mantle. *Geochimica Cosmochimica Acta* 70, 164-191.
- Castillo, P.R., 2012. Adakite petrogenesis. *Lithos* 134-135, 304-316.
- Cates, N.L., Mojzsis, S.J., 2007. Pre-3750 Ma supracrustal rocks from the Nuvvuagittuq supracrustal belt, northern Québec. *Earth and Planetary Science Letters* 255, 9-21.
- Cawood, P.A., Kröner, A., Pisarevsky, S., 2006. Precambrian plate tectonics: criteria and evidence. *Geological Society of America, GSA Today* 17, 4-10.
- Chadwick, B., Coe, K., 1984. Archean crustal evolution in southern West Greenland: a review based on observations in the Buksefjorden region. *Tectonophysics* 105, 121-130.
- Chadwick, B., 1985. Contrasting styles of tectonism and magmatism in the Late Archean crustal evolution of the northeastern part of the Ivsaartoq region, inner Godthåbsfjord region, southern West Greenland. *Precambrian Research* 27, 215-238.
- Christensen, N.I., Mooney, W.D., 1995. Seismic velocity structure and composition of the continental crust: a global view. *Journal of Geophysical Research* 100, 9761-9788.
- Clemens, J.D., Yearon, L.M., Stevens, G., 2006. Barberton (South Africa) TTG magmas: Geochemical and experimental constraints on source-rock petrology, pressure of formation and tectonic setting. *Precambrian Research* 151, 53-78.
- Collerson, K.D., Kamber, B., 1999. Evolution of the continents and the atmosphere inferred from Th-U-Nb systematics of the depleted mantle. *Science* 283, 1519-1922.
- Compston, W., Pidgeon, R.T., 1986. Jack Hills, evidence of more very old detrital zircons. *Nature* 321, 766-769.
- Condie, K.C., 1981. Archean Greenstone Belts. Elsevier (Amsterdam), 435 pp.
- Condie, K.C., 1985. Secular variation in the composition of basalts: an index to mantle evolution. *Journal of Petrology* 26, 545-563.
- Condie, K.C., 1998. Episodic continental growth and supercontinents: a mantle avalanche connection? *Earth and Planetary Science Letters* 163, 97-108.
- Condie, K.C., 2000. Episodic continental growth models: afterthoughts and extensions. *Tectonophysics* 322, 153-162.
- Condie, K.C., Kröner, A., 2008. When did plate tectonics begin? Evidence from the geologic record. In: Condie K.C., Pease V. (eds.), *When did Plate Tectonics begin on Planet Earth?* Geological Society of America, Special Paper 440.
- Condie K.C., Pease V., 2008. When did plate tectonics begin on planet Earth? Geological Society of America, Special Paper 440.
- Coward, M.P., Jan, M.Q., Rex, D., Tarney, J., Thirwall, M., Windley, B.F., 1982. Geotectonic framework of the Himalaya of N. Pakistan. *Journal of the Geological Society (London)* 139, 299-308.
- Davies, G.F., 1999. Dynamic Earth plates, plumes and mantle convection. Cambridge University Press, 458 pp.
- Davidson, J.P., Hora, J.M., Garrison, J.M., Dungan, M.A., 2005. Crustal forensics in arc magmas. *Journal of Volcanology and Geothermal Research* 140, 157-170.
- Davidson, J.P., Morgan, D.J., Charlier, B.L.A., Harlou, R., Hora, J.M., 2007. Microsampling and isotopic analysis of igneous rocks: implications for the study of magmatic systems. *Annual Reviews of Earth and Planetary Sciences* 35, 273-311.
- Defant, M.J., Drummond, M.S., 1990. Derivation of some modern arc magmas by melting of young lithosphere. *Nature* 347, 662-665.
- Dhuime, B., Hawkesworth, C.J., Cawood, P.A., Storey, C.D., 2012. A change in the geodynamics of Continental Growth 3 Billion Years Ago. *Science* 335, 1334-1336.
- Dilek, Y., 2003. Ophiolite concept and its evolution. In: Dilek, Y., Newcomb, S., (eds.), *Ophiolite Concept and the Evolution of Geological Thought*. Geological Society of America, Special Paper 373, 1-16.
- Dilek, Y., Polat, A., 2008. Suprasubduction zone ophiolites and Archean tectonics. *Geology* 36, 431-432.
- Dilek, Y., Furnes, H., 2011. Ophiolite genesis and global tectonics: geochemical and tectonic fingerprinting of ancient oceanic lithosphere. *Geological Society of America Bulletin* 123, 387-411.
- de Wit, M.J., Ashwal, L.D., (eds.), 1997. Greenstone belts. Oxford Monographs on Geology and Geophysics 35, 809 pp.
- de Wit, M.J., 1998. On Archean granites, greenstones, cratons, and tectonics: does the evidence demand a verdict? *Precambrian Research* 91, 181-226.
- de Wit, M.J., Hart, R.A., Hart, R.J., 1987. The Jamestown ophiolite complex, Barberton mountain belt: a section through 3.5 Ga oceanic crust. *Journal of African Earth Science* 6, 681-730.
- de Wit, M.J., 2004. Archean Greenstone Belts Do Contain Fragments of Ophiolites. *Developments in Precambrian Geology* 13, 599-614.
- de Wit, M.J., Furnes, H., Robins, B., 2011. Geology and tectonostratigraphy of the Onverwacht Suite, Barberton Greenstone Belt, South Africa. *Precambrian Research* 186, 1-27.
- Eichelberger, J.C., 1978. Andesitic volcanism and crustal evolution. *Nature* 275, 21-27.
- Eilu, P., Garofalo, P., Appel, P.W.U., Heijlen, W., 2006. Alteration patterns in Au-mineralised zones of Storö, Nuuk region – West Greenland. *Danmarks og Grønlands Geologiske Undersøgelse Rapport* 2006/30, 73 pp.

- Elthon, D., 1991. Geochemical evidence for formation of the Bay of Islands ophiolite above a subduction zone. *Nature* 354, 140-143.
- Ernst, W.G., 2003. High-pressure and ultrahigh-pressure metamorphic belts - Subduction, recrystallization, exhumation, and significance for ophiolite studies. In: Dilek, Y., Newcomb, S., (eds.), *Ophiolite Concept and the Evolution of Geological Thought*. Geological Society of America, Special Paper 373, 365-384.
- Escher, J.C., 1971. The geology of Akuliarq with particular bearing on the origin and evolution of the supracrustal Kvanefjord belt, Frederikshåb area, South-West Greenland. Unpublished thesis, University of Lausanne.
- Escher, J.C., Myers, J.S., 1975. New evidence concerning the original relationships of early Precambrian volcanics and anorthosites in the Fiskensætt region, southern West Greenland. *Rapport Grønlands Geologiske Undersøgelse* 75, 72-76.
- Fiorentini, M.L., Beresford, S.W., Delouie, E., Hanski, E., Stone, W.E., Pearson, N., 2008. The role of mantle-derived volatiles in the petrogenesis of Palaeoproterozoic ferro picrites in the Pechenga Greenstone Belt, northwestern Russia: insights from in-situ microbeam and nanobeam analysis of hydromagmatic amphibole. *Earth and Planetary Science Letters* 268, 2-14.
- Fiorentini, M.L., Beresford, S.W., Stone, W.E., Delouie, E., 2011. Evidence of water degassing in Archean komatiites. *Goldschmidt conference abstract* 2011.
- Fitton, J.G., 2007. The OIB paradox. *Geological Society of America, Special Paper* 430, 387-412.
- Foley, S.F., Tiepolo, M., Vannucci, R., 2002. Growth of early continental crust controlled by melting of amphibolite in subduction zones. *Nature* 417, 837-840.
- Fouglér, G.R., 2005. Mantle plumes: Why the current scepticism? *Chinese Science Bulletin* 50, 1555-1560.
- Fouglér, G.R., 2012. Are 'hot spots' hot spots? *Journal of Geodynamics* 58, 1-28.
- Fouglér, G.R., Jurdy, D.M., (eds), 2007. *Plates, Plumes and Planetary Processes*. Geological Society of America, Special Publications 430, 997 pp.
- Frei, R., Rosing, M.T., Waigat, T.E., Ulfbeck, D.G., 2002. Hydrothermal-metasomatic and tectono-metamorphic processes in the Isua supracrustal belt (West Greenland): a multi-isotopic investigation of their effects on the Earth's oldest oceanic crustal sequence. *Geochimica et Cosmochimica Acta* 66, 467-486.
- Friend, C.R.L., 1975. The geology and geochemistry of the Prekretildian basement complex in the Ravns Storø area, Fiskensætt region, southern West Greenland. Unpublished Ph.D. thesis, University London, 233 pp.
- Friend, C.R.L., 1976. Field relationships and petrology of leucocratic schists from the Ravns Storø Group near Fiskensætt. *Rapport Grønlands Geologiske Undersøgelse* 73, 81-85.
- Friend, C.R.L., Nutman, A.P., 1991. Refolded nappes formed during the late Archean terrane assembly, Godthåbsfjord, southern west Greenland. *Journal of the Geological Society (London)* 148, 507-519.
- Friend, C.R.L., Nutman, A.P., 2001. U-Pb zircon study of tectonically bounded blocks of 2940-2840 Ma crust with different metamorphic histories, Paamiut region, South-West Greenland: implication for the tectonic assembly of the North Atlantic craton. *Precambrian Research* 105, 143-164.
- Friend, C.R.L., Nutman, A.P., 2005a. Complex 3670-3500 Ma orogenic episodes superimposed on juvenile crust accreted between 3850 and 3690 Ma, Itsaq Gneiss complex, southern West Greenland. *The Journal of Geology* 113, 375-397.
- Friend, C.R.L., Nutman, A.P., 2005b. New pieces to the Archean jigsaw puzzle in the Nuuk region, southern West Greenland: steps in transforming a simple insight into a complex regional tectonothermal model. *Journal of the Geological Society (London)* 162, 147-162.
- Friend, C.R.L., Nutman, A.P., 2010. Eoarchean ophiolites? New evidence for the debate on the Isua supracrustal belt, southern West Greenland. *American Journal of Science* 310, 826-861.
- Frey, H.M., Lange, R.A., 2010. Pseudomorph complexity in andesites and dacites from the Tequila volcanic field, Mexico: resolving the effects of degassing vs. magma mixing. *Contributions to Mineralogy and Petrology* 162, 415-445.
- Furnes, H., de Wit, M.J., Staudigel, H., Rosing, M., Muehlenbachs, K., 2007a. A vestige of Earth's oldest ophiolite. *Science* 315, 1704-1707.
- Furnes, H., de Wit, M.J., Staudigel, H., Rosing, M., Muehlenbachs, K., 2007b. Response to comments on "A vestige of Earth's oldest ophiolite". *Nature* 318, 746e.
- Furnes, H., Rosing, M., Dilek, Y., de Wit, M., 2009. Isua supracrustal belt (Greenland) – A vestige of a 3.8 Ga suprasubduction zone ophiolite, and the implications for Archean geology. *Lithos* 113, 115-132.
- Fyfe, W.S., 1978. The evolution of the Earth's crust: modern plate tectonics to ancient hot spot tectonics? *Chemical Geology* 23, 89-114.
- Gaetani, G.A., Grove, T.L., 1998. The influence of water on melting of mantle peridotites. *Contributions to Mineralogy and Petrology* 131, 323-346.
- Garde, A.A., 1997. Accretion and evolution of an Archean high-grade grey gneiss – amphibolite complex: the Fiskefjord area, southern West Greenland. *Geology of Greenland Survey Bulletin* 177, 115 pp.
- Garde, A.A., 2005. A mid-Archean island arc complex with gold mineralisation at Qussuk, Akia terrane, southern West Greenland. In: Hollis, J.A. (ed.), *Greenstone Belts in the Central Godthåbsfjord region, Southern West Greenland*. Danmark og Grønlands Geologiske Undersøgelse Rapport 128, 23-36.
- Garde, A.A., 2007a. A mid-Archean island arc complex in the eastern Akia terrane, Godthåbsfjord, southern West Greenland. *Journal of the Geological Society (London)* 164, 565-579.
- Garde, A.A., 2007b. A relict island arc complex with synvolcanic epithermal alteration in western Godthåbsfjord, southern West Greenland: field work in 2006 at Qussuk and Bjørnøen. In: Stendal, H. (ed.), *Characterisation of selected geological environments. Mineral resource assessment of the Archean Craton (66° to 63°30'N) SW Greenland contribution no. 1*. Danmarks og Grønlands Geologiske Undersøgelse Rapport 2007/20, 13-40.
- Garde, A.A., Stendal, H., Stendal, B.M., 2007. Pre-metamorphic hydrothermal alteration with gold in a mid-Archean island arc, Godthåbsfjord, West Greenland. *Geological Survey of Denmark and Greenland Bulletin* 13, 37-40.
- Garde, A.A., 2008. Geochemistry of Mesoarchean andesite rocks with epithermal gold mineralization at Qussuk and Bjørnøen, southern West Greenland, Mineral resource assessment of the Archean Craton (66° to 63°30'N) SW Greenland, Contribution no. 8. Danmark og Grønlands Geologiske Undersøgelse Rapport 2008/5, 52 pp.
- Garde, A.A., Whitehouse, M., Christensen, R., 2012. Mesoarchean epithermal gold mineralization preserved at upper amphibolites-facies grade, Qussuk, southern West Greenland. *Economic Geology* (in press).
- Gibson, G.M., 1990. Uplift and exhumation of middle and lower crustal rocks in an extensional tectonic setting, Fiordland, New Zealand. In: Salisbury, M.H., Fountain, D.M. (eds.), *Exposed Cross-Sections of Continental Crust*. Kluwer, 77-101.
- Gibson, G.M., Ireland, T.R., 1999. Black Giants anorthosite, New Zealand: a Paleozoic analogue of Archean stratiform anorthosites and implications for the formation of Archean high-grade gneiss terranes. *Geology* 27, 131-134.
- Gill, R.C.O., 1979. Comparative petrogenesis of Archean and modern low-K tholeiites. A critical review of some geochemical aspects. In: Ahrens, L.H. (ed.), *Origin and Distribution of the Elements. Physics and Chemistry of the Earth* 11, Pergamon, Oxford, 431-447.
- Glikson, A.Y., 1971. Primitive Archean element distribution patterns: chemical evidence and geotectonic significance. *Earth and Planetary Science Letters* 12, 309-320.
- Gray, R., Pysklywee, R.N., 2010. Geodynamic models of Archean continental collision and formation of mantle lithosphere keels. *Geophysical Research Letters* 37, L19301 1-5.
- Green, T.H., Ringwood, A.E., 1967. Crystallization of basalt and andesite under high pressure hydrous conditions. *Earth and Planetary Science Letters* 3, 481-489.
- Griffin, W.L., O'Reilly, S.Y.O., Abe, N., Aubach, S., Davies, R.M., Pearson, N.J., Doyle, B.J., Kivi, K., 2003. The origin and evolution of Archean lithospheric mantle. *Precambrian Research* 127, 19-41.
- Griffin, W.L., O'Reilly, S.Y., Afonso, J.C., Begg, G.C., 2009. The composition and evolution of lithospheric mantle: a re-evaluation and its tectonic implication. *Journal of Petrology* 50, 1185-1204.
- Griffin, W.L., O'Reilly, S.Y., Afonso, J.C., Begg, G.C., 2010. The evolution and extent of Archean continental lithosphere: implications for tectonic models. In: Taylor, I.M., Knox-Robinson, C.M. (eds.), *Fifth International Archean Symposium, Abstracts* 21-24.
- Grove, T.L., Parman, S.W., Dann, J.C., 1999. Conditions of magma generation for Archean komatiites from the Barberton Mountainland, South Africa. In: Fei, Y., Bertka, C.M., Mysen, B.O. (eds.), *Mantle Petrology: Field Observations and High-Pressure Experimentation; a Tribute to Francis R. (Joe) Boyd*, Vol. 6. Geochemical Society, Houston, 155-167.
- Grove, T.L., Elkins-Tanton, L.T., Parman, S.W., Chatterjee, N., Müntener, O., Gaetani, G.A., 2003. Fractional crystallization and mantle-melting controls on calc-alkaline differentiation trends. *Contributions to Mineralogy and Petrology* 145, 515-533.
- Gurenko, A.A., Kamenetsky, V.S., 2011. Boron isotopic composition of olivine-hosted melt inclusions from Gorgona komatiites, Colombia: New evidence supporting wet komatiite origin. *Earth and Planetary Science Letters* 312, 201-212.
- Hacker, B.R., Kelemen, P.B., Behn, M.D., 2011. Differentiation of the continental crust by reamination. *Earth and Planetary Science Letters* 307, 501-516.
- Hall, R.P., Hughes, D.J., Friend, C.R.L., 1987. Mid-Archean basic magmatism of southern West Greenland. In: Park, R.G., Tarney, J. (eds.), *Evolution of the Lewisian and Comparable Precambrian High Grade Terrains*. Geological Society (London), Special Publications 27, 261-275.
- Halla, J., 2005. Late Archean high-Mg granitoids (sanukitoids) in the southern Karelian domain, eastern Finland: Pb and Nd isotopic constraints on crust-mantle interactions. *Lithos* 79, 161-178.
- Halla, J., van Hunen, J., Heilimo, E., Hölttä, P., 2009. Geochemical and numerical constraints on Neoproterozoic plate tectonics. *Precambrian Research* 174, 155-162.
- Halla, J., 2011. Sanukitoid granitoids as indicators of accretionary tectonics from the late Mesoproterozoic to the Archean-Proterozoic boundary. *Geophysical Research Abstracts* 13, EGU2011-7916.
- Hamilton, W.B., 1998. Archean magmatism and deformation were not products of plate tectonics. *Precambrian Research* 91, 143-179.
- Hamilton, W.B., 2007. Comment on "A vestige of Earth's oldest ophiolite". *Science* 318, 746d.
- Hamilton, W.B., 2011. Plate tectonics began in Neoproterozoic time, and plumes from deep mantle have never operated. *Lithos* 123, 1-20.
- Hamner, S., Greene, D.C., 2002. A modern structural regime in the Paleoproterozoic (~ 3.64 Ga): Isua Greenstone Belt, southern West Greenland. *Tectonophysics* 246, 201-222.
- Hanghøj, K., Kelemen, P., Bernstein, S., Blusztajn, J., Frei, R., 2001. Osmium isotopes in the Wiedemann Fjord mantle xenoliths: A unique record of cratonic mantle formation by melt depletion in the Archean. *Geochimica et Cosmochimica Acta* 65, 1525-1527.
- Harrison, T.M., Blichert-Toft, J., Müller, W., Albarède, F., Holden, P., Mojzsis, S.J., 2005. Heterogeneous Hadean hafnium: Evidence of continental crust at 4.4 to 4.5 Ga. *Science* 310, 1947-1950.
- Hart, S.R., Brooks, C., Krogh, T.E., Davis, G.L., Nava, D., 1970. Ancient and modern volcanic rocks: A trace element model. *Earth and Planetary Science Letters* 10, 17-28.
- Hart, S.R., Brooks, C., 1977. The geochemistry and evolution of Early Precambrian mantle. *Contributions to Mineralogy and Petrology* 61, 109-128.
- Hawkesworth, C., Cawood, P., Kemp, T., Storey, C., Dhuime, B., 2009. A matter of preservation. *Science* 323, 49-50.
- Hawkesworth, C., Dhuime, B., Pietranik, A.B., Cawood, P.A., Kemp, A.I.S., Storey, C.D., 2010. The generation and evolution of the continental crust. *Journal of the Geological Society (London)* 167, 229-248.
- Heilimo, E., Halla, J., Hölttä, P., 2010. Discrimination and origin of the sanukitoid series: Geochemical constraints from the Neoproterozoic western Karelian Province (Finland). *Lithos* 115, 27-39.
- Heilimo, E., Halla, J., Andersen, T., Huhma, H., 2012. Neoproterozoic crustal recycling and mantle metasomatism: Hf-Nd-Pb-O isotope evidence from sanukitoids of the Fennoscandian shield. *Precambrian Research* (in press).
- Helmstaedt, H., 2009. Crust-mantle-coupling revisited: The Archean Slave craton, NWT, Canada. *Lithos* 112, 1055-1068.
- Herzberg, C., Condie, K., Korenaga, J., 2010. Thermal history of the Earth and its petrological expression. *Earth and Planetary Science Letters* 292, 79-88.
- Hessler, A.M., Lowe, D.R., Jones, R.L., Bird, D.K., 2004. A lower limit for atmospheric carbon dioxide levels 3.2 billion years ago. *Nature* 428, 736-738.
- Higgins, A.K., 1968. The Tartoq Group on Nuna Qagertog and in the Ilerdsk area, South-West Greenland. *Rapport Grønlands Geologiske Undersøgelse* 17, 17 pp.
- Higgins, A.K., 1990. Descriptive text to 1:100000 sheets Neria 61 V.1 N and Midternæs 61 V.2 N. *Grønlands Geologiske Undersøgelse*, 23 pp.

- Higgins, A.K., Bondesen, E., 1966. Supracrustals of pre-Ketilidian age (the Tartoq Group) and their relationships with Ketilidian supracrustals in the Ivigtut region, South-West Greenland. *Rapport Grønlands Geologiske Undersøgelse* 8, 21 pp.
- Hoffman, P.F., Ranalli, G., 1988. Archean oceanic flake tectonics. *Geophysical Research Letter* 15, 1077-1080.
- Hoffmann, J.E., Münker, C., Polat, A., Rosing, M.T., Schulz, T., 2011. The origin of decoupled Hf-Nd isotope compositions in Eoarchean rocks from southern West Greenland. *Geochimica Cosmochimica Acta* 75, 6610-6628.
- Hoffmann, J.E., Svahnberg, H., Piazzolo, S., Scherstén, A., Münker, C., 2012. The geodynamic evolution of Mesoarchean anorthositic complexes inferred from the Naajat Kuuat Complex, southern West Greenland. *Precambrian Research* 196, 149-170.
- Hollis, J.A., (ed.), 2005. Greenstone belts in the central Godthåbsfjord region, southern West Greenland: geochemistry, geochronology and petrography arising from 2004 fieldwork, and digital map data. *Danmarks og Grønlands Geologiske Undersøgelse Rapport* 2005/42, 215 pp.
- Hollis, J.A., van Gool, J.A.M., Steenfelt, A., Garde, A.A., 2005. Greenstone belts in the central Godthåbsfjord region, southern West Greenland. *Geological Survey of Denmark and Greenland Bulletin* 7, 65-68.
- Iizuka, T., Horie, K., Komiya, T., Maruyama, S., Hirata, T., Hidaka, H., Windley, B.F., 2006. 4.2 Ga zircon xenocryst in an Acasta gneiss from northwestern Canada: Evidence for early continental crust. *Geology* 34, 245-248.
- Iizuka, T., Komiya, T., Ueno, Y., Katayama, I., Uehara, Y., Maruyama, S., Hirate, T., Johnson, S.P., Dunkley, D.J., 2007. Geology and zircon geochronology of the Acasta Gneiss Complex, northwestern Canada: New constraints on its tectonothermal history. *Precambrian Research* 153, 179-208.
- Jacobsen, S.B., 2005. The Hf-W isotopic system and the origin of the Earth and Moon. *Annual Reviews of Earth and Planetary Science* 33, 531-570.
- Jagoutz, O., Müntener, O., Ulmer, P., Pettkie, T., Burg, J.-B., Dawood, H., Hussain, S., 2007. Petrology and mineral chemistry of lower crustal intrusions: the Chilas Complex, Kohistan (NW Pakistan). *Journal of Petrology* 48, 1895-1953.
- Jagoutz, O., Schmidt, M.W., 2012. The formation and bulk composition of modern juvenile continental crust: The Kohistan arc. *Chemical Geology* 298, 79-96.
- Jordan, T.H., 1975. The continental tectosphere. *Reviews of Geophysics and Space Physics* 13, 1-12.
- Jordan, T.H., 1978. Composition and development of the continental tectosphere. *Nature* 274, 544-548.
- Jordan, T.H., 1988. Structure and formation of the continental tectosphere. *Journal of Petrology, Special Lithosphere Issue*, 11-37.
- Jordan, T.H., 2011. Really now, how thick are the cratons? Geological Society of America, Annual Meeting, Abstract no. 125-4.
- Juul-Pedersen, A., Frei, R., Appel, P.W.U., Persson, M., Konnerup-Madsen, J., 2007. A shear zone related greenstone belt hosted gold mineralisation in the Archean of West Greenland. A petrographic and combined Pb-Pb and Rb-Sr geochronological study. *Ore Geology Reviews* 32, 20-36.
- Karoff, C., Svensmark, H., 2010. How did the Sun affect the climate when life evolved on the Earth? Solar and Stellar Astrophysics, arXiv:1003.6043v1
- Kalsbeek, F., Myers, J.S., 1973. The geology of the Fiskensæst region. *Rapport Grønlands Geologiske Undersøgelse* 51, 5-18.
- Kamber, B.S., Ewart, A., Collerson, K.D., Bruce, M.C., McDonald, G.D., 2002. Fluid-mobile trace element constraints on the role of slab melting and implications for Archaean crustal growth. *Contributions to Mineralogy and Petrology* 144, 38-56.
- Kamber, B.S., Whitehouse, M.J., Bolhar, R., Moorbath, S., 2005. Volcanic resurfacing and the early terrestrial crust: Zircon U-Pb and REE constraints from the Isua Greenstone Belt, southern West Greenland. *Earth and Planetary Science Letters* 240, 276-290.
- Kamber, B.S., 2007. The enigma of the terrestrial protocrust: evidence for its former existence and the importance of its complete disappearance. In: *Earth's Oldest Rocks* van Kranendonk, M.J., Smithies, R.H., Bennett, V.C. (eds.), *Developments in Precambrian Geology* 15, 75-89.
- Kamenetsky, V.S., Gurenko, A.A., Kerr, A.C., 2010. Composition and temperature of komatiites melts from Gorgona Island, Colombia, constrained from olivine-hosted melt inclusions. *Geology* 38, 1003-1006.
- Katz, R.F., Spiegelman, M., Langmuir, C.H., 2003. A new parameterization of hydrous mantle melting. *Geochemistry Geophysics Geosystems* 4, 1073. DOI: 10.1029/2002GC000433.
- Kemp, A.I.S., Wilde, S.A., Hawkesworth, C.J., Coath, C.D., Nemchin, A., Pidgeon, R.T., Vervoort, J.D., DuFrane, S.A., 2010. Hadean crustal evolution revisited: New constraints from Pb-Hf isotope systematics of the Jack Hills zircons. *Earth and Planetary Science Letters* 296, 45-56.
- Kerrick, R., Polat, A., 2006. Archean greenstone-tonalite duality: thermodynamic mantle convection models or plate tectonics in the early Earth global dynamics. *Tectonophysics* 415, 141-165.
- Kelemen, P.B., 1995. Genesis of high Mg# andesites and the continental crust. *Contributions to Mineralogy and Petrology* 120, 1-19.
- Kelemen, P.B., Hart, S.R., Bernstein, S., 1998. Silica enrichment in the continental upper mantle via melt/rock reaction. *Earth and Planetary Science Letters* 164, 387-406.
- Kelemen, P.B., Hanghøj, K., Greene, A., 2003. One view of the geochemistry of subduction-related magmatic arcs, with an emphasis on primitive andesite and lower crust. In: *Rudnick R.L. (ed.), The Crust, Vol. 3, Treatise on Geochemistry*. Oxford, UK, Elsevier-Peramgon, 593-659.
- Keto, L., Kurki, J., 1967. Report on the exploration activity at Isua 1967. *Kryolitselskabet Øresund A/S Prospekterings report*. Lodged as report 20024 at the Geological Survey of Denmark and Greenland.
- Keulen, N., Schumacher, J.C., van Hinsberg, V.J., Szilas, K., Windley, B.F., Kokfelt, T.F., Schlatter, D.M., Scherstén, A., 2011. The Bjørnesund anorthositic-greenstone belt – a link between the Fiskensæst Complex and the Ravn Storø metavolcanic belt, southern West Greenland. *Geophysical Research Abstracts*, vol. 13, EGU2011-8525-1.
- Kiehl, J.T., Dickinson, R.E.A., 1987. A study of the radiative effects of enhanced atmospheric CO₂ and CH₄ on early Earth surface temperatures. *Journal of Geophysical Research* 92, 2991-2998.
- Kisters, A.F.M., Belcher, R.W., Poujol, M., Dziggel, A., 2010. Continental growth and convergence-related arc plutonism in the Mesoarchaean: Evidence from the Barberton granitoid-greenstone terrain, South Africa. *Precambrian Research* 178, 15-26.
- Kisters, A.F.M., Szilas, K., van Hinsberg, V.J., 2011. Structural geology and emplacement of the Tartoq Group, SW Greenland. In: Kolb, J. (ed.), *Controls of hydrothermal quartz vein mineralisation and wall rock alteration in the Paamiut and Tartoq areas, South-West Greenland*. *Danmarks og Grønlands Geologiske Undersøgelse Rapport* 2011/114, 116-147.
- Kimura, G., Ludden, J., 1995. Peeling oceanic crust in subduction zones. *Geology* 23, 217-220.
- Klausen, M.B., Kokfelt, T.F., Keulen, N., Berger, A., Schumacher, J.C., 2011. Tholeiitic 'komatiite'-basalt and calc-alkaline andesite-dacite succession in the Archaean Kvanefjord Area (South-West Greenland): A composite oceanic and volcanic arc suite? *EGU Geophysical Research Abstracts* 13, EGU2011-10661.
- Kleine T. Münker C., Mezger K., Palme H., 2002. Rapid accretion and early core formation on asteroids and the terrestrial planets from Hf-W chronometry. *Nature* 418, 952-955.
- Knudsen, C., van Gool, J.A.M., Østergaard, C., Hollis, J., Rink-Jørgensen, M., Persson, M., Szilas, K., 2007. Gold-hosting supracrustal rocks on Storø, southern West Greenland: lithologies and geological environment. *Geological Survey of Denmark and Greenland Bulletin* 13, 41-44.
- Koehler, I., Konhäuser, K., Kappler, A., 2010. Role of Microorganisms in Banded Iron Formations. *Geomicrobiology: Molecular and Environmental Perspective* 2010, 309-324.
- Kolb, J., Stensgaard, B.M., Schlatter, D.M., Dziggel, A., 2009. Controls of hydrothermal quartz vein mineralisation and wall rock alteration between Ameralik and Sermilik, southern West Greenland. *og Grønlands Geologiske Undersøgelse Rapport* 2009/25.
- Kolb, J., Dziggel, A., Koppeltberg, M., Stoltz, N.B., Kisters, A.F.M., Bergen, A., 2010. Controls on hydrothermal quartz vein mineralisation and wall rock alteration between Sermilik and Grædefjord, southern West Greenland. *Danmarks og Grønlands Geologiske Undersøgelse Rapport* 2010/47, 73 pp.
- Kolb, J., (ed.), 2011. Controls of hydrothermal quartz vein mineralisation and wall rock alteration in the Paamiut and Tartoq areas, South-West Greenland. *Danmarks og Grønlands Geologiske Undersøgelse Rapport* 2011/114, 176 pp.
- Komiya, T., Maruyama, S., Masuda, T., Nohda, S., Hayashi, M., Okamoto, K., 1999. Plate tectonics at 3.8-3.7 Ga: field evidence from the Isua accretionary complex, southern West Greenland. *Journal of Geology* 107, 515-554.
- König, S., Münker, C., Schuth, S., Luguet, A., Hoffmann, J.E., Kuduon, J., 2010. Boninites as windows into trace element mobility in subduction zones. *Geochimica Cosmochimica Acta* 74, 684-704.
- Kontinen, A., 1987. An early Proterozoic ophiolite - the Jormua mafic-ultramafic complex, Northeastern Finland. *Precambrian Research* 35, 313-341.
- Koppers, A.A.P., 2011. Mantle plumes persevere. *Nature Geoscience* 4, 816-817.
- Kovalenko, A., Clemens, J.D., Savatenko, V., 2005. Petrogenetic constraints for the genesis of Archaean sanukitoid suites: geochemistry and isotopic evidence from Karelia, Baltic Shield. *Lithos* 79, 147-160.
- Kovalenko, V.I., Naumov, V.B., Gurnis, A.V., Dorofeeva, V.A., Yarmolyuk, V.V., 2010. Average composition of basic magmas and mantle sources of island arcs and active continental margins estimated from the data on melt inclusions and quenched rock glasses. *Petrology* 18, 1-26.
- Kring, D.A., Cohen, B.A., 2002. Cataclysmic bombardment throughout the inner solar system 3.9-4.0 Ga. *Journal of Geophysical Research* 107, 4-1 to 4-6.
- Kusky, T.M., Polat, A., 1999. Growth of granite-greenstone terranes at convergent margins, and stabilization of Archean cratons. *Tectonophysics* 305, 43-73.
- Kusky, T.M., Li, J.-H., Tucker, R.D., 2001. The Archean Dongwanzi Ophiolite Complex, North China Craton: 2.505-Billion-Year-Old Oceanic Crust and Mantle. *Science* 292, 1142-1145.
- Kusky, T.M., Lu, W., Dilek, Y., Robinson, P., Songbai, P., X. H., 2011. Application of the modern ophiolite concept with special reference to Precambrian ophiolites. *Science China Earth Science* 54, 315-341.
- Lana, C., Kisters, A., Stevens, G., 2010. Exhumation of Mesoarchean TTG gneisses from the middle crust: Insights from the Steynsdorp core complex, Barberton granitoid-greenstone terrain, South Africa. *Geological Society of America* 122, 183-197.
- Leclerc, F., Bédard, J.H., Harris, L.B., McNicoll, V.J., Goulet, N., Roy, P., Houle, P., 2011. Tholeiitic to calc-alkaline cyclic volcanism in the Roy Group, Chibougamau area, Abitibi Greenstone Belt – revised stratigraphy and implications for VHMS exploration. *Canadian Journal of Earth Sciences* 48, 661-694.
- Lee, C.-T.A., 2006. Geochemical/Petrological Constraints in the Origin of Cratonic Mantle. *Geophysical Monograph Series* 164, 1-26.
- Lewry, J.F., Hajnal, Z., Green, A., Lucas, S.B., White, D., Stauffer, M.R., Ashton, K.E., Weber, W., Clowes, R., 1994. Structure of a Paleoproterozoic continent-continent collision zone: a LITHOPROBE seismic reflection profile across the Trans-Hudson Orogen, Canada. *Tectonophysics* 232, 143-160.
- Lie, A., 1994. Guld-mineralisering i det Arkæiske Nuuluk grønstensbælte, Tårtoq-gruppen, Sydvest Grønland. Unpublished M.Sc. thesis, University of Aarhus, 126 pp.
- Manning, C.E., Mojzsis, S.J., Harrison, T.M., 2006. Geology, age and origin of supracrustal rocks at Akilia, West Greenland. *American Journal of Science* 306, 303-366.
- Manikyamba, C., Kerrich, R., Khanna, T.C., Satyanarayanan, M., Krishna, A.K., 2009. Enriched and depleted arc basalts, with Mg-andesites and adakites: A potential paired arc-back-arc of the 2.6 Ga Huttli greenstone terrane, India. *Geochimica Cosmochimica Acta* 73, 1711-1736.
- Mareschal, J.C., Jaupart, C., 2004. Variations of surface heat flow and lithospheric thermal structure beneath the North American craton. *Earth and Planetary Science Letters* 223, 65-77.
- Martin, H., Moyaen, J.-F., 2002. Secular changes in tonalite-trondhjemite-granodiorite composition as markers of the progressive cooling Earth. *Geology* 30, 319-322.
- Martin, H., Moyaen, J.-F., 2005. The Archaean-Proterozoic transition: sanukitoid and clopset type magmatism. *Mineralogical Society of Poland Special Paper* 26, 57-68.
- Martin, H., Smithies, R.H., Rapp, R., Moyaen, J.-F., Champion, D., 2005. An overview of adakite, tonalite-trondhjemite-granodiorite (TTG) and sanukitoid: relationships and some implications for crustal evolution. *Lithos* 79, 1-24.
- Martinez, F., Taylor, B., 2003. Controls on back-arc crustal accretion: insights from the Lau, Manus and Mariana basins. In: *Larter, R.D. and Leat, P.T. (eds.), Intra-oceanic subduction systems: tectonic and magmatic processes*. Geological Society (London), Special Publications 219, 19-54.

- Maruyama, S., 1997. Pacific-type orogeny revisited: Miyashiro-type orogeny proposed. *The Island Arc* 6, 91-120.
- Maruyama, S., Masuda, T., Appel, P., 1991. The oldest accretionary complex on Earth: Isua, Greenland. *Geological Society of America, Abstract with Program*, A429-430.
- McCall, G.J.H., 2003. A critique of the analogy between Archaean and Phanerozoic tectonics based on regional mapping of the Mesozoic-Cenozoic plate convergent zone in the Makran, Iran. *Precambrian Research* 127, 5-17.
- McGregor, V.R., Mason, B., 1977. Petrogenesis and geochemistry of metabasaltic and metasedimentary enclaves in the Amitsoq gneisses, West Greenland. *American Mineralogist* 62, 887-904.
- McGregor, V.R., Friend, C.R.L., 1997. Field recognition of rocks totally retrogressed from granulite facies: an example from Archaean rocks in the Paamiut region, South-West Greenland. *Precambrian Research* 86, 59-70.
- McGregor, V.R., Friend, C.R.L., 1992. Late Archean prograde amphibolite- to granulite-facies relations in the Fiskensæset region, southern West Greenland. *Journal of Geology* 100, 207-219.
- Metcalfe, R.V., Shervais, J.W., 2008. Suprasubduction-zone ophiolites: Is there really an ophiolite conundrum? In: Wright, J.E., Shervais, J.W., (eds.), *Ophiolites, Arcs, and Batholiths: A Tribute to Cliff Hopson*. Geological Society of America, Special Paper 438, 191-222.
- Mints, M.V., Belousova, E.A., Konilov, A.N., Natapov, L.M., Shchipansky, A.A., Griffin, W.L., O'Reilly, S.Y.O., Dokukina, K.A., Kaulina, T.V., 2010. Mesoarchean subduction processes: 2.87 Ga eclogites from the Kola Peninsula, Russia. *Geology* 38, 739-742.
- Miyashiro, A., 1973. The Troodos complex was probably formed in an island arc. *Earth and Planetary Science Letters* 19, 218-224.
- Mojzsis, S.J., Arrhenius, G., McKeegan, K.D., Harrison, T.M., Nutman, A.P., Friend, C.R.L., 1996. Evidence for life on Earth before 3800 million years ago. *Nature* 384, 55-59.
- Moorbath, S., O'Nions, R.K., Pankhurst, R.J., Gale, N.H., McGregor, V.R., 1972. Further rubidium-strontium age determinations on the very early Precambrian rocks of the Godthåb district: West Greenland. *Nature* 240, 78-82.
- Moyen, J.-F., 2011. The composite Archaean grey gneisses: Petrological significance, and evidence for a non-unique tectonic setting for Archaean crustal growth. *Lithos* 123, 21-36.
- Moyen, J.-F., Stevens, G., Kisters, A.F.M., 2006. Record of mid-Archaean subduction from metamorphism in the Barberton terrain, South Africa. *Nature* 442, 559-562.
- Mtoto, M., Maboko, M.A.H., Many, S., 2009. Geochemistry and geochronology of the bimodal volcanic rocks of the Suguti area in the southern part of the Musoma-Mara Greenstone Belt, Northern Tanzania. *Precambrian Research* 174, 241-257.
- Myers, J.S., 1985. Stratigraphy and structure of the Fiskensæset Complex, southern West Greenland. *Grønlands Geologiske Undersøgelse Bulletin* 150, 72 pp.
- Myers, J.S., Crowley, J.L., 2000. Vestiges of life in the oldest Greenland rocks? A review of early Archean geology in the Godthåbsfjord region, and reappraisal of field evidence for > 3850 Ma life on Akilia. *Precambrian Research* 103, 101-124.
- Nagel, T., Hoffmann, J.E., Münker, C., 2012. Generation of Eoarchean TTGs from thickened mafic arc crust. *Geology* (in press). DOI: 10.1130/G32729.1.
- Nägler, T.F., Kramers, J.D., Kamber, B.S., Frei, R., Prendergast, M.D.A., Growth of subcontinental lithospheric mantle beneath Zimbabwe started at or before 3.8 Ga: Re-Os study on chromites. *Geology* 25, 983-986.
- Næraa, T., 2011. Zircon U/Pb, Hf and O isotope systematics from the Archaean basement in the Nuuk region, southern West Greenland – constraints on the early evolution of the continental crust. Unpublished Ph.D. thesis, University of Copenhagen, 195 pp.
- Næraa, T., Schersten, A., Rosing, M.T., Kemp, A.I.S., Hoffmann, J.E., Kokfelt, T.F., Whitehouse, M., 2012. Hafnium isotope evidence for a transition in the geodynamics of continental growth after 3.2 Ga. *Nature* (accepted).
- Nasir, S., Rollinson, H., 2009. The nature of the subcontinental lithospheric mantle beneath the Arabian Shield: Mantle xenoliths from southern Syria. *Precambrian Research* 172, 323-333.
- Norman, M.D., 2009. The lunar cataclysm: reality or "mythconception"? *Elements* 5, 23-28.
- Nutman, A.P., Friend, C.R.L., Baadsgaard, H., McGregor, V.R., 1989. Evolution and assembly of Archean gneiss terranes in the Godthåbsfjord region, southern West Greenland: structural, metamorphic and isotopic evidence. *Tectonics* 8, 573-589.
- Nutman, A.P., Friend, C.R.L., Kinny, P.D., McGregor, V.R., 1993. Anatomy of an Early Archean gneiss complex: 3900 to 3600 Ma crustal evolution in southern West Greenland. *Geology* 21, 415-418.
- Nutman, A.P., Kalsbeek, F., 1994. A minimum age of 2944 ± 7 Ma for the Tartoq Group, South-West Greenland. *Rapport Grønlands Geologiske Undersøgelse* 161, 35-38.
- Nutman, A.P., McGregor, V.R., Friend, C.R.L., Bennett, V.C., Kinny, P.D., 1996. The Itsaq gneiss complex of southern West Greenland; the world's most extensive record of early crustal evolution (3900-3600 Ma). *Precambrian Research* 78, 1-39.
- Nutman, A.P., Friend, C.R.L., Barker, S.L.L., McGregor, V.R., 2004. Inventory and assessment of Palaeoarchaean gneiss terrains and detrital zircons in southern West Greenland. *Precambrian Research* 135, 281-314.
- Nutman, A.P., Friend, C.R.L., 2007. Comment on "A vestige of Earth's oldest ophiolite". *Science* 318, 746c.
- Nutman, A.P., Christiansen, O., Friend, C.R.L., 2007. 2635 Ma amphibolite facies gold mineralization near a terrane boundary (suture?) on Storø, Nuuk region, southern West Greenland. *Precambrian Research* 159, 19-32.
- Nutman, A.P., Friend, C.R.L., 2009a. Detrital zircon sedimentary provenance ages for the Eoarchaean Isua supracrustal belt southern West Greenland: Juxtaposition of a ca. 3700 Ma juvenile arc against an older complex with 3920-3760 Ma components. *Precambrian Research* 172, 212-233.
- Nutman, A.P., Friend, C.R.L., 2009b. New 1:20,000 scale geological maps, synthesis and history of investigation of the Isua supracrustal belt and adjacent orthogneisses, southern West Greenland: A glimpse of Eoarchaean crust formation and orogeny. *Precambrian Research* 172, 189-211.
- Nutman, A.P., Wan, Y., Du, L., Friend, C.R.L., Dong, C., Xie, H., Wang, W., Sun, H., Liu, D., 2010. Multistage late Neoproterozoic crustal evolution of the North China Craton, eastern Hebei. *Precambrian Research* 189, 43-65.
- O'Neil, J., 2009. The Geology of Nuvvuagittuq Greenstone Belt and its Implications for the early Earth's Evolution. Unpublished PhD-thesis, McGill University, 194 pp.
- Ordóñez-Calderón, J.C., Polat, A., Fryer, B.J., Gagnon, J.E., Raith, J.G., Appel, P.W.U., 2008. Evidence for HFSE and REE mobility during calc-silicate metasomatism, Mesoarchean (~3075 Ma) Ivisartaq greenstone belt, southern West Greenland. *Precambrian Research* 161, 317-340.
- Ordóñez-Calderón, J.C., Polat, A., Fryer, B.J., Appel, P.W.U., van Gool, J.A.M., Dilek, Y., Gagnon, J.E., 2009. Geochemistry and geodynamic origin of the Mesoarchean Ujarassuit and Ivisartaq greenstone belts, SW Greenland. *Lithos* 113, 133-157.
- Ordóñez-Calderón, J.C., Polat, A., Fryer, B.J., Gagnon, J.E., 2011. Field and geochemical characteristics of Mesoarchean to Neoproterozoic volcanic rocks in the Storø greenstone belt, SW Greenland: Evidence for accretion of intra-oceanic volcanic arcs. *Precambrian Research* 184, 24-42.
- Pagé, P., Barnes, S.-J., Bédard, J.H., Zientek, M.L., 2012. In situ determination of Os, Ir and Ru in chromites formed from komatiite, tholeiite and boninite magmas: Implications for chromite control of Os, Ir and Ru during partial melting and crystal fractionation. *Chemical Geology* 302-303, 3-15.
- Parman, S.W., Dann, J.C., Grove, T.L., de Wit, M.J., 1997. Emplacement conditions of komatiite magmas from the 3.49 Ga Komati formation, Barberton Greenstone Belt, South Africa. *Earth and Planetary Science Letters* 150, 303-323.
- Parman, S.W., Grove, T.L., Dann, J.C., 2001. The production of Barberton komatiites in an Archean subduction zone. *Geophysical Research Letters* 28, 2513-2516.
- Parman, S.W., Grove, T.L., 2004. Harzburgite melting with and without H₂O: experimental data and predictive modeling. *Journal of Geophysical Research: Solid Earth* 109, B02201.
- Parman, S.W., Grove, T.L., Dann, J.C., de Wit, M.J., 2004. A subduction origin for komatiites and cratonic lithospheric mantle. *South African Journal of Geology* 107, 107-118.
- Pearce, J.A., 2003. Supra-subduction zone ophiolites: The search for modern analogues. In: Dilek, Y., Newcomb, S., (eds.), *Ophiolite Concept and the Evolution of Geological Thought*. Geological Society of America, Special Paper 373, 269-293.
- Pearce, J.A., 2008. Geochemical fingerprinting of oceanic basalts with applications to ophiolite classification and the search for Archean oceanic crust. *Lithos* 100, 14-48.
- Pearce, J.A., Lippard, S.J., Roberts, S., 1984. Characteristics and tectonic significance of supra-subduction zone ophiolites. *Geological Society (London), Special Publications* 16, 77-94.
- Pearson, D.G., Carlson, R.W., Shirey, S.B., Boyd, F.R., Nixon, P.H., 1995. Stabilisation of Archaean lithospheric mantle: A Re-Os isotope study of peridotite xenoliths from the Kaapvaal craton. *Earth and Planetary Science Letters* 134, 341-357.
- Pearson, D.G., Wittig, N., 2008. Formation of Archaean continental lithosphere and its diamonds: the root of the problem. *Journal of the Geological Society (London)* 165, 895-914.
- Pease, V., Percival, J., Smithies, H., Stevens, G., van Kranendonk, M., 2008. When did plate tectonics begin? Evidence from the orogenic record. In: Condie K.C., Pease V. (eds.), *When did Plate Tectonics begin on Planet Earth?* Geological Society of America, Special Paper 440.
- Pedersen, N.H., 1996. Guld mineraliseringer på Storø, Sydligge Vestgrønland. GEUS open file series 95/10, 73-75.
- Peltonen, P., Kontinen, A., Huhma, H., 1998. Petrogenesis of the mantle sequence of the Jormua Ophiolite (Finland): melt migration in the upper mantle during Palaeoproterozoic continental break-up. *Journal of Petrology* 39, 297-329.
- Persson, M.F., 2007. Metamorphic and geochronological evolution of Au-bearing rocks on central Storø, Nuuk region, West Greenland. Unpublished M.Sc. thesis, University of Copenhagen, 91 pp.
- Petersen, J.S., 1992. Nuuluk-Ilerlak gold and massive-sulfide project, Taartoq Archaean greenstone belt, SW Greenland. Field report, Nunaol A/S, 164 pp.
- Plank, T., Langmuir, C.H., 1998. The chemical composition of subducting sediment and its consequences for the crust and mantle. *Chemical Geology* 145, 325-394.
- Polat, A., Hofmann, A.W., Rosing, M.T., 2002. Boninite-like volcanic rocks in the 3.7-3.8 Ga Isua greenstone belt, West Greenland: geochemical evidence for intra-oceanic subduction zone processes in the early Earth. *Chemical Geology* Volume 184, 231-254.
- Polat, A., Hofmann, A.W., 2003. Alteration and geochemical patterns in the 3.7-3.8 Ga Isua greenstone belt, West Greenland. *Precambrian Research* 126, 197-218.
- Polat, A., Münker, C., 2004. Hf-Nd isotope evidence for contemporaneous subduction processes in the source of late Archean arc lavas from the Superior Province, Canada. *Chemical Geology* 213, 403-429.
- Polat, A., Kuský, T., Li, J., Fryer, B., Kerrich, R., Patrick, K., 2005. Geochemistry of Neoproterozoic (ca. 2.55-2.5 Ga) volcanic and ophiolitic rocks in the Wutaishan greenstone belt, central orogenic belt, North China craton: Implication for geodynamic setting and continental growth. *Geological Society of America Bulletin* 117, 1387-1399.
- Polat, A., Herzberg, C., Münker, C., Rodgers, R., Kuský, T., Li, J., Fryer, B., Delaney, J., 2006. Geochemical and petrological evidence for a suprasubduction zone origin of Neoproterozoic (ca. 2.5 Ga) peridotites, central orogenic belt, North China craton. *Geological Society of America Bulletin* 118, 771-784.
- Polat, A., Appel, P.W.U., Frei, R., Pan, Y., Dilek, Y., Ordóñez-Calderón, J.C., Fryer, B., Hollis, J.A., Raith, J.G., 2007. Field and geochemical characteristics of the Mesoarchean (~3075 Ma) Ivisartaq greenstone belt, southern West Greenland: Evidence for seafloor hydrothermal alteration in supra-subduction oceanic crust. *Gondwana Research* 11, 69-91.
- Polat, A., Frei, R., Appel, P.W.U., Fryer, B., Dilek, Y., Ordóñez-Calderón, J.C., 2008a. An overview of the lithological and geochemical characteristics of the Mesoarchean (ca. 3075 Ma) Ivisartaq greenstone belt, southern West Greenland. In: Condie, K.C., Pease, V. (eds.), *When did plate tectonics begin on planet Earth?* Geological Society of America, Special Paper 440, 51-76.
- Polat, A., Frei, R., Appel, P.W.U., Dilek, Y., Fryer, B., Ordóñez-Calderón, J.C., Yang, Z., 2008b. The origin and compositions of Mesoarchean oceanic crust: Evidence from the 3075 Ma Ivisartaq greenstone belt, SW Greenland. *Lithos* 100, 293-321.
- Polat, A., Appel, P.W.U., Fryer, B., Windley, B.F., Frei, R., Samson, I.M., Huang, H., 2009a. Trace element systematics of the Neoproterozoic Fiskensæset anorthositic complex and associated meta-volcanic rocks, SW Greenland: evidence for a magmatic arc origin. *Precambrian Research*, 175, 87-115.

- Polat, A., Kerrich, R., Windley, B.F., 2009b. Archean crustal growth processes in southern West Greenland and the southern Superior Province: geodynamic and magmatic constraints. In: Cawood, P.A., Kröner, A. (eds.), *Earth Accretionary Systems in Space and Time*. Geological Society (London), Special Publications 318, 155-191.
- Polat, A., Frei, R., Fryer, B., Appel, P.W.U., 2009c. The origin of geochemical trends and Eoarchean (ca. 3700 Ma) zircons in Mesoarchean (ca. 3075 Ma) ocelli-hosting pillow basalts, Ivisartoq greenstone belt, SW Greenland: Evidence for crustal contamination versus crustal recycling. *Chemical Geology* 268, 248-271.
- Polat, A., Frei, R., Scherstén, Appel, P.W.U., 2010. New age (ca. 2970 Ma), mantle source composition and geodynamic constraints on the Archean Fiskeneset anorthosite complex, SW Greenland. *Chemical Geology* 277, 1-20.
- Polat, A., Appel, P.W.U., Fryer, B.J., 2011. An overview of the geochemistry of Eoarchean to Mesoarchean ultramafic to mafic volcanic rocks, SW Greenland: Implication for mantle depletion and petrogenetic processes at subduction zones in the early Earth. *Gondwana Research* 20, 255-283.
- Polet, J., Anderson, D.L., 1995. Depth extent of cratons as inferred from tomographic studies. *Geology* 23, 205-208.
- Pope, E.C., Bird, D.K., Rosing, M.T., 2012. Isotope composition and volume of Earth's early oceans. *Proceedings of the National Academy of Sciences of the United States of America* 109, 4371, 1-6.
- Pulvertaft, I.C.R., 1972. Preliminary report on the geology of the area between Kigutilik and Bjørnesund (62° V 1). Grønlands Geologiske Undersøgelse Arkiv.
- Rapp, R.P., Watson, E.B., 1995. Dehydration melting of metabasalt at 8-32 kbar: Implications for continental growth and crust-mantle recycling. *Journal of Petrology* 36, 891-931.
- Reubi, O., Blundy, J., 2009. A dearth of intermediate melts at subduction zone volcanoes and the petrogenesis of arc andesites. *Nature Letters* 461, 1269-1274.
- Richardson, S.H., Shirey, S.B., Harris, J.W., Carlson, R.W., 2001. Archean subduction recorded by Re-Os isotopes in eclogitic sulfide inclusions in Kimberley diamonds. *Earth and Planetary Science Letters* 191, 257-266.
- Rino, S., Komiya, T., Windley, B.F., Katamaya, I., Motoki, A., Hirata, T., 2004. Major episodic increases of continental crustal growth determined from zircon ages of river sands: implications for mantle overturns in the early Precambrian. *Physics of the Earth and Planetary Interiors* 146, 369-394.
- Rizo, H., Boyet, M., Blichert-Toft, J., Rosing, M., 2011. Combined Nd and Hf isotopes evidence for deep-seated source of Isua lavas. *Earth and Planetary Science Letters* 312, 267-279.
- Robinson, P.T., Malpas, J., Dilek, Y., Zhou, M., 2008. The significance of sheeted dike complexes in ophiolites. *Geological Society of America, GSA Today* 18, 4-10.
- Rollinson, H., 2008a. Ophiolitic trondhjemites: a possible analogue for Hadean felsic 'crust'. *Terra Nova* 20, 364-369.
- Rollinson, H., 2008b. Secular evolution of the continental crust: Implications for crust evolution models, Geochemistry, Geophysics, Geosystems 9, Q12010. DOI: 10.1029/2008GC002262.
- Rollinson, H., 2008c. The geochemistry of mantle chromitites from the northern part of the Oman ophiolite: inferred parental melt composition. *Contributions to Mineralogy and Petrology* 156, 273-288.
- Rollinson, H., 2009. New models for the genesis of plagiogranites in the Oman ophiolite. *Lithos* 112, 603-614.
- Rollinson, H., 2010. Coupled evolution of Archean continental crust and subcontinental lithospheric mantle. *Geology* 38, 1083-1086.
- Rollinson, H., Reid, C., Windley, B., 2010. Chromitites from the Fiskeneset anorthosite complex, West Greenland: clues to late Archaean mantle processes. In: Kusky, T.M., Zhai, M.-G., Xiao, W. (eds.), *The Evolving Continents: Understanding Processes of Continental Growth*. Geological Society (London), Special Publications 338, 197-212.
- Rollinson, H., Whitehouse, M., 2011. The growth of the Zimbabwe Craton during the late Archaean: an ion microprobe U-Pb zircon study. *Journal of the Geological Society (London)* 168, 941-952.
- Rondanelli, R., Lindzen, R.S., 2010. Can thin cirrus clouds in the tropics provide a solution to the faint young Sun paradox? *Journal of Geophysical Research* 115.
- Rosing, M.T., 1999. 13C-depleted carbon microparticles in > 3700-Ma sea-floor sedimentary rocks from West Greenland. *Science* 283, 674-676.
- Rosing, M.T., Rose, N.M., Bridgewater, D., Thomsen, H.S., 1996. Earliest part of Earth's stratigraphic record: a reappraisal of the > 3.7 Ga Isua (Greenland) supracrustal sequence. *Geology* 24, 43-46.
- Rosing, M.T., Frei, R., 2004. U-rich Archaean sea-floor sediments from Greenland – indications of > 3700 Ma oxygenic photosynthesis. *Earth and Planetary Science Letters* 217, 237-244.
- Rosing, M.T., Bird, D.K., Sleep, N.H., Glassley, W., Albareda, F., 2006. The rise of continents – An essay on the geologic consequences of photosynthesis. *Palaeogeography, Palaeoclimatology, Palaeoecology* 232, 99-113.
- Rudnick, R.L., Gao, S., 2003. Composition of the continental crust. In: Holland, H.D., Turekian, K.K. (eds.), *Treatise on Geochemistry* (Elsevier), 3.01, 1-63.
- Rüpke, L.H., Morgan, J.P., Hort, M., Connolly, J.A.D., 2004. Serpentine and the subduction zone water cycle. *Earth and Planetary Science Letters* 223, 17-34.
- Sagan, C., Mullen, C., 1972. Earth and Mars: Evolution of Atmospheres and Surface Temperatures. *Science* 177, 52-56.
- Sagan, C., Chyba, C., 1997. The early faint sun paradox: organic shielding of ultraviolet-labile greenhouse gases. *Science* 276, 1217-1221.
- Scherstén, A., Stendal, H., 2008. Geochemistry of the Tasiarsuaq 'greenstone-granite' terrane, southern West Greenland. *Danmarks og Grønlands Geologiske Undersøgelse Rapport 2008/15*, 40 pp.
- Scherstén, A., Szilas, K., Creaser, R.A., van Gool, J.A.M., Næraa, T., Østergaard, C., 2012. Re-Os and U-Pb constraints on gold mineralisation events in the Meso- to Neoproterozoic Storö greenstone belt, Storö, southern West Greenland. *Precambrian Research*, 200-203, 149-162.
- Schidlowski, M., 1988. A 3,800-million-year isotopic record of life from carbon in sedimentary rocks. *Nature* 333, 313-318.
- Schlatter, D.M., Christensen, R., 2010. Geological, petrological and litho-geochemical investigations on the Qussuk gold mineralization, southern West Greenland. *Danmark og Grønlands Geologiske Undersøgelse 2010/10*, 53 pp.
- Schmitz, M.D., Bowring, S.A., de Wit, M.J., Gartz, V., 2004. Subduction and terrane collision stabilize the western Kaapvaal craton tectosphere 2.9 billion years ago. *Earth and Planetary Science Letters* 222, 363-376.
- Schoenberg, R., Kamber, B.S., Collerson, K.D., Eugster, O., 2002. New W-isotope evidence for rapid terrestrial accretion and very early core formation. *Geochimica Cosmochimica Acta* 66, 3151-3160.
- Scholl, D.W., von Huene, R., 2007. Crustal recycling at modern subduction zones applied to the past – issues of growth and preservation of continental basement crust, mantle geochemistry, and supercontinent reconstruction. In: Hatcher, R.D., Carlson, M.P., McBride, J.H., Catalán, J.R.M. (eds.), *4-D framework of continental crust*. Geological Society of America, Memoirs 200, 9-32.
- Scholl, D.W., von Huene, R., 2009. Implications of estimated magmatic additions and recycling losses at the subduction zones of accretionary (non-collisional) and collisional (suturing) orogens. In: Cawood, P.A., Kröner, A. (eds.), *Earth Accretionary Systems in Space and Time*. Geological Society (London), Special Publications 318, 105-125.
- Schumacher, J.C., van Hinsberg, V.J., Keulen, N., 2011. Metamorphism in supracrustal and ultramafic rocks in southern West Greenland and South-West Greenland 64 – 61.5°N. *Danmarks og Grønlands Geologiske Undersøgelse Rapport 2011/6*, 30 pp.
- Schwarzchild, M., 1958. *Structure and Evolution of the Stars*. Princeton University Press.
- Scott, D.J., Helmstaedt, H., Bickle, M.J., 1992. Pirtunig ophiolite, Cape Smith belt, northern Quebec, Canada: A reconstructed section of Early Proterozoic oceanic crust. *Geology* 20, 173-176.
- Shervais, J.W., 2001. Birth, death, and resurrection: The life cycle of suprasubduction zone ophiolites. *Geochemistry, Geophysics, Geosystems* (G3) 2. DOI: 10.1029/2000GC000080.
- Shervais, J.W., 2006. The significance of subduction-related accretionary complexes in early Earth processes. *Geological Society of America, Special Paper* 404, 173-192.
- Shirey, S.B., Walker, R.J., 1998. The Re-Os isotope system in cosmochemistry and high-temperature geochemistry. *Annual Review of Earth and Planetary Sciences* 26, 423-500.
- Shirey, S.B., Richardson, S.H., Harris, J.W., 2004. Integrated models of diamond formation and craton evolution. *Lithos* 77, 923-944.
- Shirey, S.B., Richardson, S.H., 2011. Start of the Wilson Cycle at 3 Ga shown by diamonds from subcontinental mantle. *Science* 333, 434-436.
- Simmons, N.A., Forte, A.M., Grand, S.P., 2009. Joint seismic, geodynamic and mineral physical constraints on three-dimensional mantle heterogeneity: Implications for the relative importance of thermal versus compositional heterogeneity. *Geophysical Journal International* 177, 1284-1304.
- Sisson, T.W., Grove, T.L., 1993. Experimental investigations of the role of H₂O in calc-alkaline differentiation and subduction zone magmatism. *Contributions to Mineralogy and Petrology* 113, 143-166.
- Sleep, N., Windley, B.F., 1982. Archean plate tectonics: constraints and inferences. *Journal of Geology* 90, 363-379.
- Smith, G.M., 1998. *Geology and mineral potential of the Bjørneøen supracrustal belt, Nuukfjord, West Greenland*. Unpublished report, Nunaöls A/S. GEUS report file 21649, 13 pp.
- Smithies, R.H., 2000. The Archaean tonalite-trondhjemite-granodiorite (TTG) series is not an analogue of Cenozoic adakite. *Earth and Planetary Science Letters* 182, 115-125.
- Smithies, R.H., van Kranendonk, M.J., Champion, D.C., 2005a. It started with a plume – early Archaean basaltic proto-continental crust. *Earth and Planetary Science Letters* 238, 284-297.
- Smithies, R.H., Champion, D.C., van Kranendonk, M.J., Howard, H.M., Hickman, A.H., 2005b. Modern-style subduction processes in the Mesoarchaean: geochemical evidence from the 3.12 Ga Whundo intraoceanic arc. *Earth and Planetary Science Letters* 231, 221-237.
- Stendal, H. (ed.), 2007. Characterisation of selected geological environments. Mineral resource assessment of the Archaean Craton (66° to 63°30'N) SW Greenland contribution no. 1. *Danmarks og Grønlands Geologiske Undersøgelse Rapport 2007/20*, 90 pp.
- Stendal, H., Scherstén, A., 2007. A well-preserved bimodal volcanic succession in the Tasiarsuaq terrane, South-West Greenland. *Geological Survey of Denmark and Greenland Bulletin* 13, 53-56.
- Steenfelt, A., Garde, A.A., Møyn, J.-F., 2005. Mantle wedge involvement in the petrogenesis of Archaean grey gneisses in West Greenland. *Lithos* 79, 207-228.
- Stern, R.A., Hanson, G.N., Shirey, S.B., 1989. Petrogenesis of mantle-derived LILE-enriched Archean monzodiorites and trachyandesites (sanukitoids) in southwestern Superior. *Canadian Journal of Earth Sciences* 26, 1688-1712.
- Stern, R.J., 2002. Subduction zones. *Reviews of Geophysics* 40, 4, 1-38.
- Stern, R.J., 2005. Evidence from ophiolites, blueschists, and ultrahigh-pressure metamorphic terranes that the modern episode of subduction tectonics began in Neoproterozoic time. *Geology* 33, 577-560.
- Stern, R.J., 2008. Modern-style plate tectonics began in Neoproterozoic time: an alternative interpretation of Earth's tectonic history. In: Condie K.C., Pease V. (eds.), *When did Plate Tectonics begin on Planet Earth?* Geological Society of America, Special Paper 440.
- Stevenson, D.J., 1987. Origin of the Moon – the collision hypothesis. *Annual Reviews of Earth and Planetary Science* 15, 271-315.
- Stiegler, M.T., Lowe, D.R., Byerly, G.R., 2010. The petrogenesis of volcanoclastic komatiites in the Barberton Greenstone Belt, South Africa; a textural and geochemical study. *Journal of Petrology* 51, 947-972.
- Stone, W.E., Deloule, E., Larson, M.S., Leshar, C.M., 1997. Evidence for hydrous high-MgO melts in the Precambrian. *Geology* 25, 143-146.
- Svensmark, H., Friis-Christensen, E., 1997. Variation of cosmic ray flux and global cloud coverage – a missing link in solar-climate relationships. *Variation of cosmic ray flux and global cloud coverage – a missing link in solar-climate relationships*. *Journal of Atmospheric and Terrestrial Physics* 59, 1225.
- Szilas, K., 2008. *Geochemistry of the late Archaean Storö supracrustal belt and alteration zones associated with gold mineralisation, Nuuk region, southern West Greenland*. University of Copenhagen, 42 pp.
- Szilas, K., van Hinsberg, V.J., Kisters, A.F.M., Kokfelt, T.F., Scherstén, A., Windley, B.F., 2011. Remnants of Mesoarchaean oceanic crust in the Tartoq Group, North Atlantic Craton, SW Greenland. *Geological Survey of Denmark and Greenland Bulletin* 23, 57-60.
- Tatsumi, Y., Suzuki, T., 2009. Tholeiitic vs calc-alkaline differentiation and evolution of arc crust: constraints from melting experiments on a basalt from the Izu-Bonin-Mariana arc. *Journal of Petrology* 50, 1575-1603.
- Taylor, B., Martinez, F., 2003. Back-arc basin basalt systematics. *Earth and Planetary Science Letters* 210, 481-497.
- Tera, F., Papanastassiou, D.A., Wasserburg, G.J., 1974. Isotopic evidence for a terminal lunar cataclysm. *Earth and Planetary Science Letters* 22, 1-21.

- van Gool, J.A.M., Scherstén, A., Østergaard, C., Næraa, T., 2007. Geological setting of the Storø gold prospect, Godthåbsfjord region, southern West Greenland. *Danmarks og Grønlands Geologiske Undersøgelse Rapport* 2007/83, 158 pp.
- van Hinsberg, V.J., Szilas, K., Kisters, A.F.M., 2010. The Tartoq Group, SW Greenland: Mineralogy, textures and a preliminary metamorphic to hydrothermal history. *Danmarks og Grønlands Geologiske Undersøgelse Rapport* 2010/120, 52 pp.
- van Kranendonk, M.J., 2004. Archaean tectonics 2004: a review. *Precambrian Research* 131, 143-151.
- van Kranendonk, M.J., Smithies, R.H., Hickman, A.H., Champion, D.C., 2007a. Paleoproterozoic development of a continental nucleus: the East Pilbara terrane of the Pilbara Craton, western Australia. In: van Kranendonk, M.J., Smithies, R.H., Bennett, V. (eds.), *Earth's Oldest Rocks. Developments in Precambrian Geology, Series 15*, Elsevier (Amsterdam), 307-337.
- van Kranendonk, M.J., Smithies, R.H., Hickman, A.H., Champion, D.C., 2007b. Review: secular tectonic evolution of Archean continental crust: interplay between horizontal and vertical processes in the formation of the Pilbara Craton, Australia. *Terra Nova* 19, 1-38.
- van Kranendonk, M.J., 2011a. Onset of plate tectonics. *Science* 333, 413-414.
- van Kranendonk, M.J., 2011b. Cool greenstone drips and the role of partial convective overturn in Barberton greenstone belt evolution. *Journal of African Earth Science* 60, 346-352.
- Vervoort, J.D., Blichert-Toft, J., 1999. Evolution of the depleted mantle: Hf isotope evidence from juvenile rocks through time. *Geochimica et Cosmochimica Acta* 63, 533-556.
- Walker, R.J., Carlson, R.W., Shirey, S.B., Boyd, F.R., 1989. Os, Sr, Nd, and Pb isotope systematics of southern African peridotites xenoliths: implications for the chemical evolution of subcontinental mantle. *Geochimica et Cosmochimica Acta* 53, 1583-1595.
- Walter, M.J., 2003. Melt Extraction and Compositional Variability in Mantle Lithosphere. In: Carlson, R.W. (ed.), *Treatise on Geochemistry* (Elsevier) 2.08, 363-394.
- Wang, Z., Wilde, S.A., Wang, K., Yu, L., 2004. A MORB-arc basalt-adakite association in the 2.5 Ga Wutai greenstone belt: late Archean magmatism and crustal growth in the North China Craton. *Precambrian Research* 131, 323-343.
- Wells, P.R.A., 1976. Late Archean metamorphism in the Buksefjorden region, southwest Greenland. *Contributions to Mineralogy and Petrology* 56, 229-242.
- Westerlund, K.J., Shirey, S.B., Richardson, S.H., Carlson R.W., Gurney, J.J., Harris, J.W., 2006. A subduction wedge origin for Paleoproterozoic peridotitic diamonds and harzburgites from Panda kimberlite, Slave craton: evidence from Re-Os isotope systematics. *Contributions to Mineralogy and Petrology* 152, 275-294.
- Whitehouse, M., Kamber, B.S., 2004. Assigning Dates to Thin Gneissic Veins in High-Grade Metamorphic Terranes: A Cautionary Tale from Akilia, Southwest Greenland. *Journal of Petrology* 46, 291-318.
- Wilde, S.A., Valley, J.W., Peck, W.H., Graham, C.M., 2001. Evidence from detrital zircons for the existence of continental crust and oceans on the Earth 4.4 Gyr ago. *Nature* 409, 175-178.
- Wilf, C.L., 1982. *Geokemien af de grå amphiboliter, en del af en supracrustal bjergartsenhed, ved Grædeffjorden, nord for bygden Qeqertarsuaq (Fiskenæsset) i den centrale del af Sydvestgrønland*. Unpublished M.Sc. thesis, University of Aarhus, 145 pp.
- Wilson, J.T., 1966. Did the Atlantic close and then re-open? *Nature* 211, 676-681.
- Windley, B.F., 1968. New field relations from the early Precambrian of West Greenland. *Grønlands Geologiske Undersøgelse Rapport* 15, 27-31.
- Windley, B.F., Herd, R.K., Bowden, A.A., 1973. The Fiskenæsset Complex, West Greenland, Part I: A preliminary study of the stratigraphy, petrology, and whole rock chemistry from Qeqertarsuaq. *Grønlands Geologiske Undersøgelse Bulletin* 106, 80 pp.
- Windley, B.F., Garde, A.A., 2009. Arc-generated blocks with crustal sections in the North Atlantic craton of West Greenland: crustal growth in the Archean with modern analogues. *Earth Science Reviews* 93, 1-30.
- Wittig, N., Pearson, D.G., Webb, M., Ottley, C.J., Irvine, G.J., Kopylova, M., Jensen, S.M., Nowell, G.M., 2008. Origin of cratonic lithospheric mantle roots: A geochemical study of peridotites from the North Atlantic Craton, West Greenland. *Earth and Planetary Science Letters* 274, 24-33.
- Wittig, N., Webb, M., Pearson, D.G., Dale, C.W., Ottley, C.J., Hutchison, M., Jensen, S.M., Luguet, A., 2010. Formation of the North Atlantic craton: Timing and mechanisms constrained from Re-Os isotope and PGE data of peridotite xenoliths from SW Greenland. *Chemical Geology* 276, 166-187.
- Wyman, D., Kerrich, R., 2010. Mantle plume – volcanic arc interaction: consequences for magmatism, metallogeny, and cratonization in the Abitibi and Wawa subprovinces, Canada. *Canadian Journal of Earth Sciences* 47, 565-589.
- Yin, Q., Jacobsen, S.B., Tamashita, K., Blichert-Toft, J., Telouk, P., Albarede, F., 2002. A short timescale for terrestrial planet formation from Hf-W chronometry of meteorites. *Nature* 418, 949-952.
- Zahnle, K., Arndt, N., Cockell, C., Halliday, A., Nisbet, E., Selsis, F., Sleep, N.H., 2007. Emergence of a habitable planet. *Space Science Reviews* 129, 35-78.
- Zegers, T.E. and van Keken, P.E. 2001. Middle Archean continent formation by crustal delamination. *Geology* 29, 1083-1086.
- Zhai, M., Zhao, G., Zhang, Q., 2002. Is the Dongwanzi Complex an Archean Ophiolite? *Science* 295, 923a.
- Zhao, G., Wilde, S.A., Li, Sanzhong, L., Sun, M., Grant, M.L., Li, X., 2007. U-Pb zircon age constraints on the Dongwanzi ultramafic-mafic body, North China, confirm it is not an Archean ophiolite. *Earth and Planetary Science Letters* 255, 85-93.

Curriculum Vitae



Name: **Kristoffer Szilas**

Year of birth: 1982 in Valby, Denmark

Nationality: Danish

Current address: Rungsted Plads 11 3. tv., 2200 Copenhagen N, DENMARK

E-mail address: ksz@geus.dk or Kristoffer_Szilas@Hotmail.com

Cell phone: +45 22164512

Languages (Speaking/Writing)

Danish: Mother tongue/Excellent

English: Excellent/Excellent

Hungarian: Good/Fair

German: Fair/Fair

Educational background

2006 B.Sc., Geology. Project about porphyry copper deposits.

2008 M.Sc., Geology. Thesis titled: "Geochemicatrty of the late Archaean Storø supracrustal belt and alteration zones associated with gold mineralisation, Nuuk region, southern West Greenland".

2012 Ph.D., Geology. Thesis titled: "Geochemistry of Archaean supracrustal belts in SW Greenland".

The Ph.D. thesis will be submitted on April 16th 2012 and will be defended on June 7th 2012.

The two external opponents will be Hugh Rollinson (University of Derby) and Jaana Halla (University of Helsinki).

Field experience

2004 Structural field course at Mors, Denmark.

2005 Hard rock/endogene field course in Bygland, Norway.

2006 Five weeks of field work for NunaMinerals A/S on Storø and Bjørneø in Godthåbsfjord, SW Greenland.

2007 Six weeks of field work for NunaMinerals A/S on Storø in the Nuuk region and around Paamiut in SW Greenland.

2008 Six weeks of field work for NunaMinerals A/S on Storø, Qussuk, Nordlandet, Ivisaartoq and Isua in SW Greenland.

2009 Four weeks of field work with GEUS (The Geological Survey of Denmark and Greenland) in the Grædefjord, Bjørnesund, Ravns Storø and Tartoq supracrustal belts of SW Greenland.

2010 Five weeks of field work with GEUS (The Geological Survey of Denmark and Greenland) in the Tartoq Group supracrustal rocks of SW Greenland.

Analytical experience

Clean lab/wet chemistry experience with rock dissolution and chromatographic element separation.

Isotope measurements of Sm-Nd (TIMS), Lu-Hf and Sm-Nd (MC-ICP-MS) and Re-Os (N-TIMS).

Zircon separation and *in situ* U-Pb dating (LA-ICP-MS).

Experience with SEM and EMP imaging and characterisation of minerals, as well as regular polarizing microscope.

Work shops, short-courses and conferences

2007 Short-course on epithermal mineral deposits by Jeffrey W. Hedenquist in Turku, Finland.

2008 Short-course on VMS mineral deposits by Mark Hannington in Turku, Finland.

2009 Workshop titled: "Archaean environment: the habitat of early life" in Mekrijärvi, Finland.

2010 Fifth International Archean Symposium in Perth, Australia.

2011 European Geosciences Union Conference (**one talk and two posters**) in Vienna, Austria.

2011 Goldschmidt Conference (**invited speaker**) in Prague, Czech Republic.

2012 Goldschmidt Conference (**talk**) in Montréal, Canada.

Teaching material/other publications

Mojzsis, S.J., Hanski, E., Maier, W.D., **Szilas, K.**, O'Brian, H., 2011. Shortcourse notes on Archaean geology. Oulu University, Finland. 150 pp.

Publications (peer-reviewed journals)

Szilas, K., Hoffmann, J.E., Scherstén, A., Kokfelt, T.F., Kisters, A.F.M., Rosing, M.T., Frei, R., Münker, C. Geochemistry of the Mesoarchaeoan Grædefjord supracrustal belt, SW Greenland: origin of calc-alkaline ocelli-bearing rocks (**in prep.**).

Keulen, N., Schumacher, J., **Szilas, K.**, van Hinsberg, J., Kokfelt, T.F. Structural evolution of the Ravns Storø-Bjørnesund region, southern West Greenland. *Precambrian Research* (**submitted**).

Kisters, A.F.M., van Hinsberg, V.J., **Szilas, K.** Geology of an Archaean accretionary complex – the structural record of burial and return flow in the Tartoq Group of South West Greenland. *Precambrian Research* (**submitted**).

Szilas, K., Hoffmann, J.E., Scherstén, A., Rosing, M.T., Kokfelt, T.F., Windley, B.F., van Hinsberg, V.J., Næraa, T., Keulen, N., Frei, R., Münker, C., 2012. Complex calc-alkaline volcanism recorded in Mesoarchaeoan supracrustal belts north of Frederikshåb Isblink, southern West Greenland: implications for subduction zone processes in the early Earth. *Precambrian Research* (**in press**). DOI: 10.1016/j.precamres.2012.03.013.

Szilas, K., Scherstén, A., Næraa, T., Stendal, H., Rosing, M.T., Kokfelt, T.F., V.J., Frei, R., 2012. Origin of Mesoarchaeoan arc related rocks with boninite/komatiite affinities from southern West Greenland. *Lithos* (**in press**). DOI: 10.1016/j.lithos.2012.03.023.

Scherstén, A., **Szilas, K.**, Creaser, R.A., van Gool, J.A.M., Næraa, T., Østergaard, C., 2012. Re-Os and U-Pb constraints on gold mineralisation events in the Meso- to Neoproterozoic Storø greenstone belt, Storø, southern West Greenland. *Precambrian Research*, 200-203, 149-162.

Szilas, K., van Hinsberg, J., Kisters, A.F.M., Hoffmann, E., Kokfelt, T.F., Scherstén, A., Windley, B.F., Münker, C., 2011. Remnants of arc-related Mesoarchaeoan oceanic crust in the Tartoq Group, SW Greenland. *Gondwana Research* (**in press**). DOI: 10.1016/j.gr.2011.11.006.

Szilas, K., van Hinsberg, V.J., Kisters, A.F.M., Kokfelt, T.F., Scherstén, A., Windley, B.F., 2011. Remnants of Mesoarchaeoan oceanic crust in the Tartoq Group, South-West Greenland. *Geological Survey of Denmark and Greenland Bulletin* 23, 57-60.

Conference abstracts

Szilas, K., Hoffmann J.E., Scherstén, A., 2012. Complex calc-alkaline volcanism recorded in Mesoarchaeoan supracrustal belts in SW Greenland. *Goldschmidt Conference Abstracts*.

Szilas, K., van Hinsberg, V.J., Kisters, A.F.M., 2011. Mesoarchaeoan suprasubduction zone ophiolite in the Tartoq Group, SW Greenland. *Goldschmidt Conference Abstracts* (**Invited speaker**).

Scherstén, A., **Szilas, K.**, Creaser, R.A., Næraa, T., 2011. Re-Os constraints on gold mineralisation events in the Neoproterozoic Storø supracrustal belt, southern West Greenland. *Goldschmidt Conference Abstracts*.

van Hinsberg, **Szilas, K.**, Wood, B.J., 2011. Towards a quantitative record of Archaean ocean water chemistry: An element partitioning approach. *Goldschmidt Conference Abstracts*.

Szilas, K., Garde, A.A., Scherstén, A., van Gool, J.A.M., Østergaard, C., 2011. Mesoarchaeoan premetamorphic hydrothermal alteration of tholeiitic basalt resulting in aluminous lithologies, Storø supracrustal belt, Nuuk region, southern West Greenland. *Geophysical Research Abstracts*, vol. 13, EGU2011-12125-1.

Szilas, K., Scherstén, A., Hoffmann, J.E., Kokfelt, T.F., van Hinsberg, V.J., Windley, B.F., Münker, C., 2011. Linking the Ravns Storø and Bjørnesund supracrustal belts (SW Greenland) using Lu-Hf and Sm-Nd isotopic data and whole-rock geochemistry. *Geophysical Research Abstracts*, vol. 13, EGU2011-11114-1.

Szilas, K., van Hinsberg, V.J., Kisters, A.F.M., Kokfelt, T.F., Scherstén, A., Windley, B.F., 2011. Remnants of Mesoarchaeoan oceanic crust in the Tartoq Group, North Atlantic Craton, SW Greenland. *Geophysical Research Abstracts*, vol. 13, EGU2011-3170-2.

Reports

Szilas, K., Scherstén, A., Kokfelt, T.F., 2011. Geochemistry of Archaean supracrustal belts in SW Greenland. In: Kokfelt, T.F. (ed.), Geochemistry of supracrustal rocks and associated intrusive TTG suites of the Archaean craton in South-West Greenland and southern West Greenland, 61°30' - 64°N. Danmarks og Grønlands Geologiske Undersøgelse Rapport 2011/10.

Szilas, K., Kokfelt, T.F., Næraa, T., Scherstén, A., 2011. Geochemistry of Archaean felsic crust in SW Greenland. In: Kokfelt, T.F. (ed.), Geochemistry of supracrustal rocks and associated intrusive TTG suites of the Archaean craton in South-West Greenland and southern West Greenland, 61°30' - 64°N. Danmarks og Grønlands Geologiske Undersøgelse Rapport 2011/10.

Kisters, A.F.M., **Szilas, K.**, van Hinsberg, V.J., 2011. Structural geology and emplacement of the Tartoq Group, SW Greenland. In: Kolb, J. (ed.), Controls of hydrothermal quartz vein mineralisation and wall rock alteration in the Paamiut and Tartoq areas, South-West Greenland. Danmarks og Grønlands Geologiske Undersøgelse Rapport 2011/114, 116-147.

van Hinsberg, V.J., **Szilas, K.**, Kisters, A.F.M., 2010. The Tartoq Group, SW Greenland: Mineralogy, textures and a preliminary metamorphic to hydrothermal history. Danmarks og Grønlands Geologiske Undersøgelse Rapport 2010/120, 52 pp.

List of completed courses

B.Sc. level (course name, date, Danish grade*, ECTS-points)

Mathematics for geologists, 01/2004, 10, 7.5
Chemistry for geologists, 01/2004, 7, 7.5
Geology 1A, 01/2004, 12, 12.5
Geological summer course A, 06/2004, Passed, 5
Geostatistics for geologists, 06/2004, Passed, 5
Geology 1A 2nd semester, 06/2004, 12, 17.5
Physics for geologists, 06/2004, Passed, 5
Geographical information systems (GIS), 10/2004, 7, 7.5
Geology 2 MI: Mineralogy, 11/2004, 10, 10
Geology 2 PA: Palaeontology, 01/2005, 12, 10
Geology 3.1 Endogene geology, 04/2005, 12, 10
Climate, soil and water, 04/2005, 7, 7.5
Geology 4.1 Exogene geology, 06/2005, 12, 10
Geological used geophysics, 07/2005, Passed, 5
Summer course B.Sc., 09/2005, Passed, 7.5
Geochemistry, 11/2005, 12, 7.5
Hydrogeology, 01/2006, Passed, 5
Geology 4.2a Exogene geology, 01/2006, 7, 7.5
Structural geology, 04/2006, Passed, 5
Geology 3.2a + 3.3a, 04/2006, 12, 17.5
B.Sc. project in endogene geology, 06/2006, 12, 10

M.Sc. level (course name, date, Danish grade*, ECTS-points)

Base course: Deep Earth, 11/2006, 12, 15
M.Sc. course: Structures of minerals, 01/2007, 12, 7.5
Laboratory course: Laboratory methods, 03/2007, 10, 7.5
M.Sc. course: Igneous and metamorphic, 05/2007, Passed, 7.5
Line project: Deep Earth, 08/2007, 12, 7.5
Geological field course C, 11/2007, Passed, 10
M.Sc. course: The dynamic inner earth, 02/2008, Passed, 7.5
M.Sc. project in endogen geology, 11/2007, 10, 60

Ph.D. level (course name, date, Danish grade*, ECTS-points)

Field Mapping of Ore Deposits, 05/2009, Passed, 7
Calculating Metamorphic Mineral Equilibria, 07/2009, Passed, 5
Archaean Environments, 08/2009, Passed, 3

Mineral Resources, 09/2009, Passed, 5
 Terrestrial Planets, 10/2009, Passed, 10
 Geochemistry for geophysicists, 11/2011, Passed, 5

*Note on the Danish grading system:

The 7-step-scale was designed to be compatible with the ECTS-scale			Equivalents	
Grade	Description		ECTS	U.S.
12	Excellent	High level of command of all aspects	A	A+
10	Very good	High level of command of most aspects	B	A-, A
7	Good	Good command – some weaknesses	C	B, B+
4	Fair	Some command – some major weaknesses	D	C, C+, B-
2	Adequate	The minimum requirements for acceptance	E	D-, D, D+, C-
0	Inadequate	Does not meet the minimum requirements	Fx	F
-3	Unacceptable	Unacceptable in all respects	F	F

Annex

Paper I:

Remnants of arc-related
Mesoarchaeoan oceanic crust in the
Tartoq Group of SW Greenland

Gondwana Research (in press)
DOI: 10.1016/j.gr.2011.11.006



Contents lists available at SciVerse ScienceDirect

Gondwana Research

journal homepage: www.elsevier.com/locate/gr

Remnants of arc-related Mesoarchaeoan oceanic crust in the Tartoq Group of SW Greenland

Kristoffer Szilas ^{a,b,c,*}, Vincent J. Van Hinsberg ^d, Alex F.M. Kisters ^e, J. Elis Hoffmann ^{f,g}, Brian F. Windley ^h, Thomas F. Kokfelt ^a, Anders Scherstén ⁱ, Robert Frei ^{b,j}, Minik T. Rosing ^{c,j}, Carsten Münker ^g

^a Geological Survey of Denmark and Greenland - GEUS, Øster Voldgade 10, 1350 Copenhagen K, Denmark

^b Department of Geography and Geology, University of Copenhagen, Øster Voldgade 10, 1350 Copenhagen K, Denmark

^c Natural History Museum of Denmark, Øster Voldgade 5-7, 1350 Copenhagen K, Denmark

^d Department of Earth Sciences, University of Oxford, South Parks Road, Oxford, United Kingdom

^e Department of Earth Sciences, Stellenbosch University, Matieland 7602, South Africa

^f Steinmann Institut für Geologie, Universität Bonn, Poppelsdorfer Schloss, 53115 Bonn, Germany

^g Geologisch-Mineralogisches Institut, Universität zu Köln, Zùlpicher Str. 49b, 50674 Köln, Germany

^h Department of Geology, University of Leicester, University Road, Leicester, LE1 7RH, United Kingdom

ⁱ Department of Earth and Ecosystem Sciences Division of Geology, Lund University, Sölvegatan 12, 223 62 Lund, Sweden

^j Nordic Center for Earth Evolution, NordCEE, Denmark

ARTICLE INFO

Article history:

Received 11 July 2011

Received in revised form 12 November 2011

Accepted 13 November 2011

Available online xxxx

Keywords:

Archean

Greenland

Tartoq Group

Geochronology

Supracrustal belt

Oceanic crust

ABSTRACT

The Tartoq Group, located in SW Greenland, consists of supracrustal rocks of mainly tholeiitic basaltic composition, including pillow lavas, sills/dykes and gabbros, as well as ultramafic rocks. Metamorphic grade ranges from greenschist facies to granulite facies. The Tartoq Group crops out as a series of blocks and slivers that are imbricated with originally intrusive Mesoarchaeoan TTG orthogneisses. The supracrustal rocks form part of a SE vergent fold and thrust belt consistent with the imbrication of TTG gneisses and supracrustal rocks along a convergent margin. LA-ICP-MS U–Pb zircon dating of an intrusive TTG sheet yields a minimum age of 2986 ± 4 Ma for the Tartoq Group. This age is consistent with MC-ICP-MS Lu–Hf and Sm–Nd isotopic whole-rock data for mafic samples from different blocks of the Tartoq Group, which yield errorchron ages of 3189 ± 65 Ma and 3068 ± 220 Ma, respectively. The mafic supracrustal rocks of the Tartoq Group have chondrite-normalized REE patterns with $\text{La}_{\text{CN}}/\text{Sm}_{\text{CN}}$ of 0.67–1.96 and rather flat primitive mantle-normalized multi-element patterns, except for scattered LILE contents, and generally negative Nb-anomalies with Nb/Nb^* of 0.26–1.31. Th/Yb varies between 0.06 and 0.47 and Nb/Yb between 0.45 and 4.4 indicative of an arc affinity when compared to rocks from modern settings. The similar geochemistry of the different lithological units, together with their coeval formation, as evident from trace element geochemical trends, supports a co-magmatic origin for the rock assemblage and their formation as imbricated relics of oceanic crust. Accordingly, we propose that the Tartoq Group represents remnants of Mesoarchaeoan oceanic crust, which formed in a suprasubduction zone geodynamic environment.

© 2011 International Association for Gondwana Research. Published by Elsevier B.V. All rights reserved.

1. Introduction

The identification of the geodynamic environments in which Archean supracrustal belts have formed is highly controversial. Many of the uncertainties relate to later overprints of the rock record in form of deformation, metamorphism and alteration processes. The majority of Archean supracrustal belts are strongly deformed and tectonically dismembered, and thus, individual belts may comprise a composite of rocks with several different origins. Before any definite conclusions about the possible tectonic setting can be drawn, it is

critical to establish whether or not a suite of rocks are co-magmatic and to what extent tectonic processes have disrupted the original sequence. Moreover, geochemical fingerprinting of igneous rock suites (e.g., [Condie and Kröner, 2011](#)) relies on the assumption of uniformitarian principles, but it is uncertain to what extent processes on the modern Earth can be extrapolated to the Archean rock record. Many geoscientists maintain that modern tectonic environments such as subduction zones were responsible for the formation of even the earliest recorded supracrustal rocks (e.g. Isua supracrustal belt at c. 3800 Ma; [Polat et al., 2002, 2011](#); [Dilek and Polat, 2008](#); [Friend and Nutman, 2010](#); [Hoffmann et al., 2011](#)). At the same time, there is a strong school of thought proposing that subduction zone processes only started to operate much later in the Meso- or even Neoproterozoic (e.g. [Hamilton, 1998, 2011](#); [Davies, 1999](#); [McCall, 2003](#); [Stern, 2005, 2008](#)).

* Corresponding author at: Geological Survey of Denmark and Greenland - GEUS, Øster Voldgade 10, 1350 Copenhagen K, Denmark.

E-mail address: ksz@geus.dk (K. Szilas).

Previous controversies regarding the co-magmatic origin of Archaean rock suites such as the Isua supracrustal belt (e.g. Furnes et al., 2007; Nutman and Friend, 2007; Hamilton, 2007; Furnes et al., 2009; Friend and Nutman, 2010), the Jamestown “ophiolite” (De Wit et al., 1987; Lowe and Byerly, 2007; Van Kranendonk et al., 2009) and the Dongwanzi complex (Kusky et al., 2001, 2011; Zhai et al., 2002; Zhao et al., 2007) highlight the difficulties in establishing whether or not the rock assemblages in such supracrustal belts are co-magmatic and how to interpret their geodynamic environment of formation. The problems outlined above demonstrate that more work on Archaean supracrustal belts is needed and that careful studies of such rocks may provide answers as to when and how the Earth arrived at its present style of plate tectonics.

In this paper we aim to contribute to the knowledge of the Archaean supracrustal rock record by presenting the first comprehensive modern major-, trace-, and isotope-geochemical data set, together with new field observations, for the Mesoarchaeoan Tartoq Group in SW Greenland. We interpret this assemblage of mafic to ultramafic rocks, ranging from pillow lavas through sills/dykes to gabbros and ultramafic cumulate/mantle restite, as lithological units which collectively represent a section through oceanic crust. The majority of samples yield a well-defined Lu–Hf errorchron and we take this as evidence of them being co-magmatic, although there is room for some parts of the Tartoq Group to be slightly younger or older than the age of c. 3190 Ma that we present here as the likely formation age. The similarity in geochemistry of the various lithological units supports the rocks as having formed in the same tectonic environment, which we propose was an arc to backarc setting according to classifications based on modern suites of rocks. Additionally, we find structural evidence of horizontal deformation in support of a convergent margin setting.

2. Geological background

The Tartoq Group is located adjacent to Sermiligaarsuk fjord in SW Greenland and crops out within an area of approximately 1000 km²

(Fig. 1). It consists of several fault-bound supracrustal blocks that are imbricated with originally intrusive, Archaean orthogneisses of tonalite–trondhjemite–granodiorite (TTG) composition. A U–Pb zircon age of 2944 ± 7 Ma from an intrusive TTG sheet confirms the Archaean age of the Tartoq Group (Nutman and Kalsbeek, 1994).

The metavolcanic rocks are characterised by the lowest degree of metamorphism found anywhere in the North Atlantic craton of Greenland, but they also have the largest range in metamorphic grade found within a single supracrustal sequence in this region. The metamorphic conditions range from greenschist to granulite facies conditions (Van Hinsberg et al., 2010), thus meta- is taken as being an implicit prefix for all lithological units throughout this paper. Lithological units of the Tartoq Group include greenschists, amphibolites and minor ultramafic rocks and their field relations are well described from 1:20,000-scale mapping in an almost totally exposed terrain (e.g. Higgins and Bondesen, 1966; Higgins, 1968; Berthelsen and Henriksen, 1975; Higgins, 1990; Petersen, 1992; Van Hinsberg et al., 2010). Most rocks have undergone variable degrees of retrogression and hydrothermal overprint, and hydrothermal fluid flow has extensively affected rocks in high strain zones, giving rise to gold mineralisation in strongly carbonated rocks (Appel and Secher, 1984; King, 1985; Petersen, 1992; Evans and King, 1993).

Berthelsen and Henriksen (1975) and Kisters et al. (2011) describe the Tartoq Group as allochthonous slivers of supracrustal rocks in a TTG-dominated terrain with, for the most part, originally intrusive contacts that have almost invariably been subsequently tectonized. Both internal contacts within the supracrustal belts as well as the TTG-supracrustal contacts are characterized by early mylonitic and late cataclastic fabrics resulting from the final structural assembly of the TTG-supracrustal terrain. Internal thrust zones are commonly delineated by felsic schists. The abundant carbonate-rich mylonites and felsic schists were previously described as metasediments, but are here interpreted as sheared TTG sheets and strongly carbonated deformation zones, respectively, and thus they are not primary lithological units of the Tartoq Group (see Sections 5.1 and 6.1). The

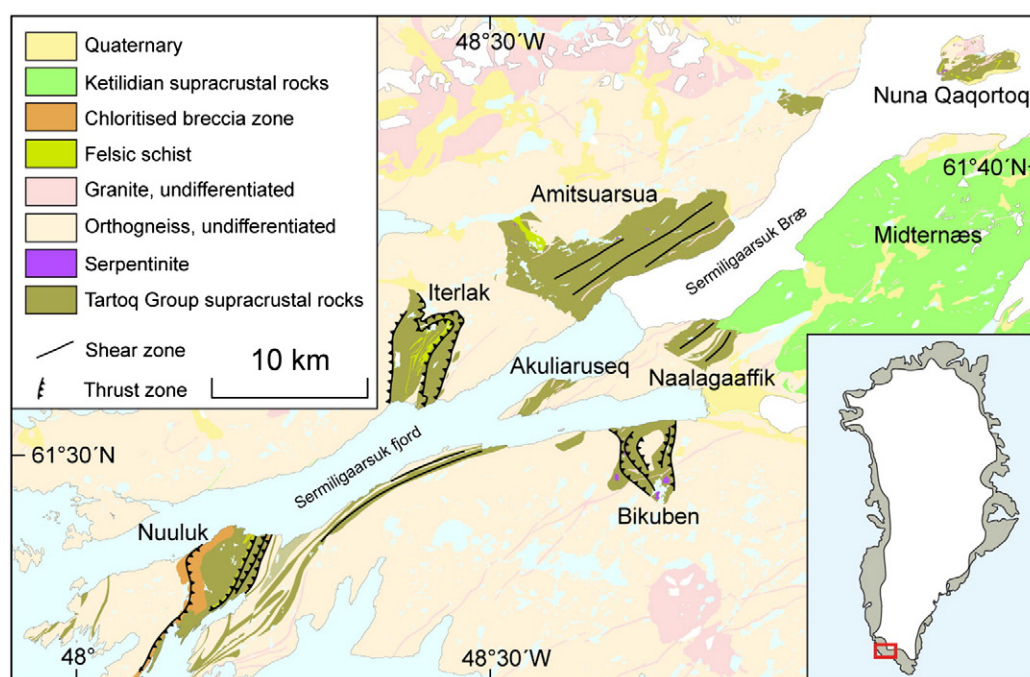


Fig. 1. Map of Sermiligaarsuk fjord showing the supracrustal blocks, which comprise the Tartoq Group and are situated within Archaean TTG orthogneisses. Younger supracrustal rocks of the Ketilidian orogen crop out to the east and are unconformable on top of the Tartoq Group. Several large thrust- and shear zones have been identified, which are often associated with felsic schists and TTG mylonites.

common subhorizontal structures suggest lateral accretion and the present localized, moderate to steep dips are the result of late-stage F3 refolding.

The Tartoq Group is intruded by late syn-tectonic granitic sheets, as well as fine-grained aplites and coarse-grained dolerite dykes ranging from Archaean to Mesozoic in age (Higgins, 1990). The supracrustal blocks have additionally been affected by late thrusting and carbonate alteration that postdates the TTG formation, but predates the ca. 1800 Ma Ketilidian orogen (Van Hinsberg et al., 2010; Kisters et al., 2011).

Except for some gold exploration (e.g. Petersen, 1992; Evans and King, 1993), there have been very few geological studies of the Tartoq Group since it was mapped in the 1960's, and thus this study provides the first modern geological data.

3. Samples and petrography

About 400 samples were collected in the Tartoq Group during fieldwork in 2009 and 2010 in a joint project between the Greenland Bureau of Minerals and Petroleum (BMP) and the Geological Survey of Denmark and Greenland (GEUS).

The main lithological units vary with metamorphic grade in the different supracrustal block sections, but in general the most common units are homogeneous mafic greenschists and amphibolites; serpentinites are only an important constituent in the Bikuben block (Fig. 1).

The samples have been grouped into the following lithological units as recognised in the field: greenschist, greenstone, amphibolite, gabbro, pillow lava, serpentinite, felsic schist, TTG gneiss and TTG mylonite.

The greenschists consist of chlorite–plagioclase–quartz, chlorite–plagioclase–epidote–quartz or actinolite–chlorite–quartz ± epidote. Altered equivalents of these rocks contain carbonate and sulfides (pyrite and pyrrhotite). Commonly a schistose chlorite foliation has overprinted the primary textures and with increasing carbonation these rocks take on a characteristic “crumbly” or “knobbly” texture, as described in previous works (Petersen, 1992; Van Hinsberg et al., 2010). This irregular texture shows abundant voids due to preferred

weathering of carbonate veins that were introduced during a late (D_2) deformation and associated fluid flow alteration. In high-strain zones, primary textures and the late-stage alteration are overprinted by a pervasive chlorite foliation (S_2). In these zones, deformation and associated fluid flow have resulted in complete transposition of fabrics and formation of almost pure ankerite schist with variable silicification that hosts gold mineralisation (Petersen, 1992).

The greenstones are essentially a subgroup of the greenschists, which are characterized by semi-ophitic textures visible in thin sections and sometimes even in hand samples (Fig. 2a). They form sheets which display grain-size variations with coarse centres and finer grained (chilled?) margins. The rocks have escaped carbonate alteration and are likely the precursors of a large proportion of the variably altered greenschists, because they often have mutual gradational contacts (Section 5.1). The greenstone samples were collected within 200 m of each other, but they are from several different sheets.

The amphibolites are typically medium-grained and consist of hornblende–plagioclase–quartz or hornblende–chlorite–plagioclase–quartz at lower grades with biotite in altered samples. A gabbroic texture is commonly present (Fig. 2b), especially in the northern part of the Ilerlak block (Fig. 1), and such rocks have been grouped together with greenschist facies equivalents as gabbros.

Some amphibolites from Nuna Qaqortoq have relict pillow structures (c.f. Higgins, 1968; Berthelsen and Henriksen, 1975; Higgins, 1990) outlined by a quartz-rich network between the pillows and have been grouped separately as pillow lavas. They consist of fine-grained amphibole–plagioclase–quartz typically with a distinct foliation and often have coarser grained margins. Pillow-like structures have also been reported in greenschists from other blocks, but strong carbonate alteration, deformation and generally a fine grain size make them equivocal for definition, and so they have not been included in the pillow lava group, but simply classified as greenschists. The pillow lava samples were collected from within 300 m of each on Nuna Qaqortoq. The amphibolites with the highest metamorphic grade occur in the Bikuben block (Fig. 1) and they are commonly garnet and clinopyroxene bearing, with local evidence of partial melting. Conditions of their

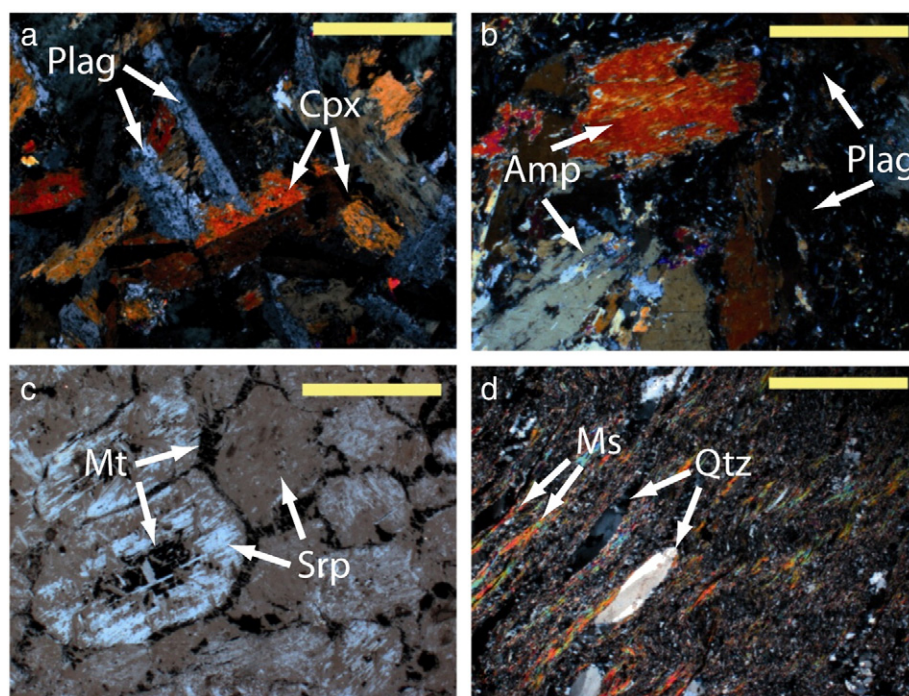


Fig. 2. (a) Greenstone thin section in crossed polarizers showing plagioclase, amphibole and chlorite. (b) Gabbro thin section in crossed polarizers showing plagioclase and amphibole. (c) Serpentinite in thin section with crossed polarizers. Possible lizardite–pseudomorphs after olivine outlined by magnetite. (d) Felsic schist in thin section in crossed polarizers showing fine-grained quartz and plagioclase separated by layers of muscovite. Abbreviations: Amphibole (Amp), clinopyroxene (Cpx), magnetite (Mt), muscovite (Ms), plagioclase (Plag), quartz (Qtz), serpentine (Srp). 25 × magnification, scale bar is 1 mm wide.

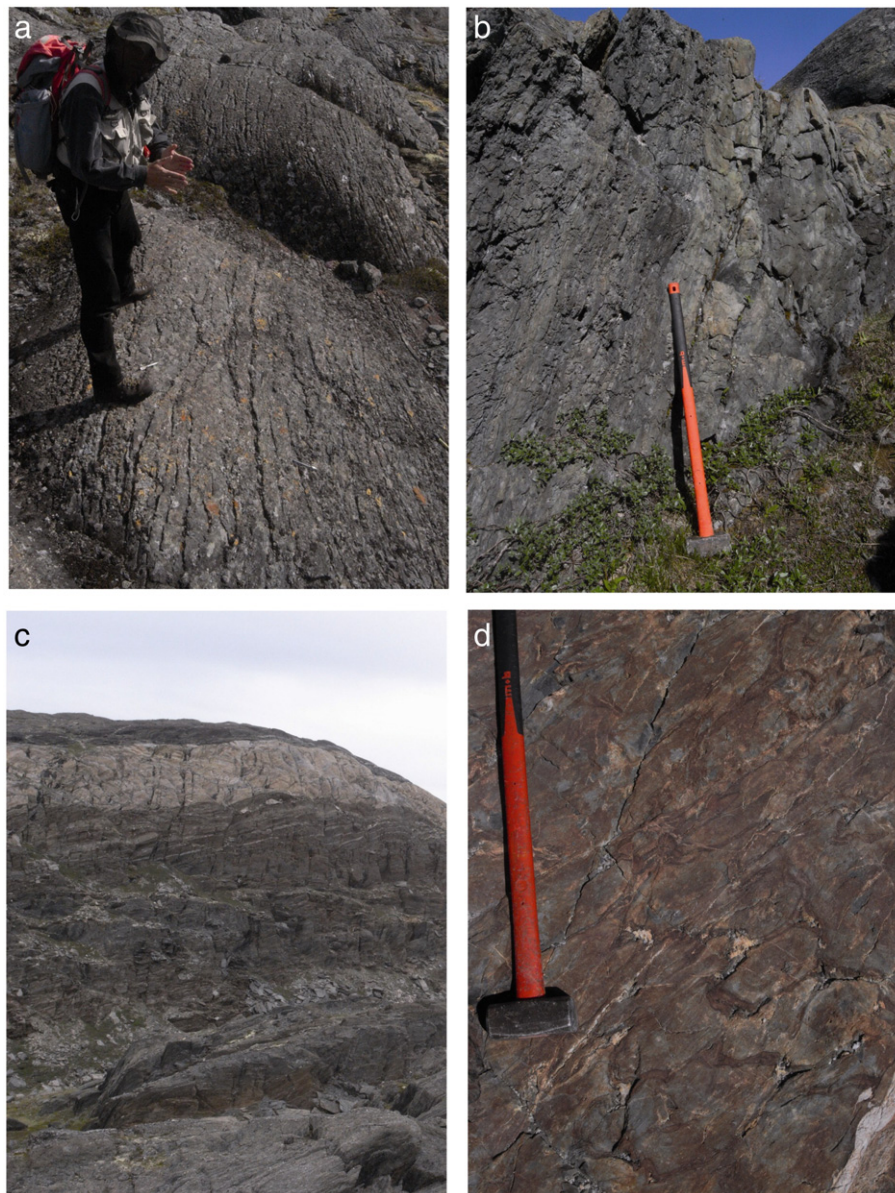


Fig. 3. (a) Subparallel primary layering in greenschists in the central Nuuluk block. (b) Coarse-grained greenstone sills or dykes in the south-eastern part of the Nuuluk block. (c) Felsic schist (the light coloured band in the cliff) is about 20 m in height sitting in variably carbonated greenschists in the central part of the Nuuluk block. (d) Pillow lava structures in amphibolites from the eastern part of the Nuna Qaqqortoq block.

formation are in excess of 6 kbar and temperatures may locally have reached 850 °C (Van Hinsberg et al., 2010).

The serpentinites consist of serpentine (lizardite) and disseminated magnetite; rarely the magnetite forms a network that outlines relict mineral textures (Fig. 2c). The serpentinite bodies are always enveloped by a margin of talc–carbonate–magnetite schist, which commonly has completely replaced the serpentinite bodies.

The felsic schists occur in high strain zones throughout the Tartog Group, particularly in the Nuuluk and Iterlak blocks, and often have strongly carbonated rocks in their vicinity. The felsic schists consist of quartz–plagioclase–muscovite \pm chlorite and usually have a mylonitic texture (Fig. 2d). In high-strain zones, the transposition of felsic schists and greenschists has given rise to an interlayered structure of the two, which results in intermediate finely laminated, ribbon mylonites.

The TTG gneisses enclosing the Tartog Group generally consist of medium-grained plagioclase–quartz–biotite with a distinct contact-parallel high-temperature foliation. Locally, TTG breccia zones occur near the margins of the Tartog Group, e.g. west of the Nuuluk and north of the Amitsuarsua blocks. Highly deformed TTG mylonites are

only different from the felsic schists by having large plagioclase relicts, which have survived deformation and indicate derivation from the TTG gneisses, whereas the felsic schists are usually too fine-grained to identify their protolith.

4. Methods

4.1. Whole-rock geochemical analyses

Samples, a few kilograms size, were collected from in-situ outcrops and weathered crusts were removed, if present. Crushing was performed at the ACME Labs in Vancouver, Canada, in a tungsten–carbide jaw crusher and material was subsequently pulverised in a ceramic box–mill to reduce trace element contamination of e.g. W, Co, Sc and Ta.

Whole-rock analyses were carried out at ACME Labs, following analytical procedures termed “Group 4A and 4B – lithogeochemical whole rock fusion”. A brief description of the procedure is summarised below based on that available on the homepage (www.acmelab.com) and on information obtained upon personal request from the company.

Prepared samples were mixed with $\text{LiBO}_2/\text{Li}_2\text{B}_4\text{O}_7$ flux and crucibles were fused in a furnace. The cooled bead was then dissolved in ACS-grade nitric acid. For “Group 4A” the total abundances of the major oxides and several minor elements were analysed for a 200 mg sample by ICP-emission spectrometry following a lithium metaborate/tetraborate fusion and dilute nitric digestion. Loss on ignition (LOI) was determined by igniting a sample split at 1000 °C then measuring the weight loss. “Group 4B” comprises two separate analyses for the total trace elements by ICP-MS. Rare earth and refractory elements were determined by ICP mass spectrometry following a lithium metaborate/tetraborate fusion and nitric acid digestion of a 200 mg sample. Additionally a separate 500 mg split is digested in Aqua Regia and analysed by ICP Mass Spectrometry to determine the precious and base metals. Sample splits of 500 mg were leached in hot (95 °C) Aqua Regia. Fe valence was not determined and Fe_2O_3 thus refers to total Fe. The geochemical data of the various lithological units is presented in Supplementary Data Table 1, where the detection limits of the ACME Labs data can also be found.

The GEUS in-house standard “Disko-1 basalt” was given a regular sample number and sent with each batch analysed at ACME Labs (21 runs over three years). The reported trace element contents for this standard were compared with data from GEUS’ ICP-MS lab (32 runs over eight years). The results from the two laboratories agree well and are within the analytical uncertainty (Supplementary Data Table 2).

4.2. Lu–Hf and Sm–Nd isotope analyses

Isotope dilution techniques were used to measure the ^{176}Lu – ^{176}Hf and ^{147}Sm – ^{143}Nd compositions and Lu, Hf, Sm, Nd concentrations of 10 representative samples from the Tartoq Group employing mixed ^{176}Lu – ^{180}Hf and ^{149}Sm – ^{150}Nd tracers following the procedures of Münker et al. (2001) and Weyer et al. (2002). Separation of Lu and Hf was achieved using Eichrom® Ln spec resin following Münker et al. (2001) and Weyer et al. (2002). Sm and Nd were separated from the remaining matrix following Pin and Zalduegui (1997).

Complete digestion of the samples was achieved by table-top digestion, followed by Parr® bomb digestion for three days. Lu, Hf, Sm and Nd were measured using the Finnigan® Neptune multicollector ICP-MS at Bonn. Mass-bias correction of the measured $^{176}\text{Hf}/^{177}\text{Hf}$ was conducted by correction to a $^{179}\text{Hf}/^{177}\text{Hf}$ of 0.7325. The Münster AMES standard, isotopically indistinguishable from the JMC-475 standard, yielded an average $^{176}\text{Hf}/^{177}\text{Hf}$ of 0.282160 with an external reproducibility of ± 40 ppm (2 σ). Reported data are given relative to a JMC-475 value of 0.282160. The typical external reproducibility of the $^{176}\text{Lu}/^{177}\text{Hf}$ is reported in Supplementary Data Table 3 and it is $\pm 0.2\%$ for ideally spiked samples and includes the effects of error magnification due to non-ideal spike-sample ratios and uncertainties imparted by corrections for Yb interferences (Blichert-Toft et al., 2002; Vervoort et al., 2004; Lagos et al., 2007). The calculated initial Hf isotope compositions include both the propagated external errors from the measured Hf isotope compositions and from the Lu/Hf ratios. For the calculation of initial ϵHf and ϵNd values, we used a ^{176}Lu decay constant of 1.867×10^{-11} (Scherer et al., 2001; Söderlund et al., 2004), a ^{147}Sm decay constant of 6.54×10^{-12} (Lugmair and Marti, 1978) and the CHUR values of Bouvier et al. (2008). All measured $^{143}\text{Nd}/^{144}\text{Nd}$ data were mass-bias corrected using a value of 0.7219 for $^{146}\text{Nd}/^{144}\text{Nd}$. During the course of this study the $^{143}\text{Nd}/^{144}\text{Nd}$ values measured for a 20 ppb LaJolla standard solution were 0.511818 and 0.511791, and all data reported here are given relative to a $^{143}\text{Nd}/^{144}\text{Nd}$ of 0.511859 for LaJolla. The external reproducibility for $^{143}\text{Nd}/^{144}\text{Nd}$ measurements was ± 30 ppm and $\pm 0.2\%$ for $^{147}\text{Sm}/^{144}\text{Nd}$. Total procedural blanks during the course of this study were <49 pg for Lu, <70 pg for Hf, and <50 pg for Sm and Nd.

4.3. U–Pb zircon analyses

Zircon analyses were conducted at the Department of Petrology and Economic Geology, Geological Survey of Denmark and Greenland

(GEUS). Hand-hammered chips from the rock samples were crushed directly in a tungsten–carbide disc mill. The crushed and sieved material was poured onto a Wilfley shaking table where the heavy mineral grains were separated. The heavy mineral fraction was transferred to disposable plastic Petri dishes using ethanol, and magnetic minerals were removed using a hand-magnet. Zircon grains were subsequently hand-picked from the final heavy mineral separate in the Petri dish. The hand-picked zircon grains were cast into epoxy and polished to expose a central cross-section of each grain. The mount was documented prior to ablation using backscattered electron imaging in a scanning electron microscope. The mount was subsequently cleaned in an ultrasonic bath with propanol, and then loaded into the sample cell of the laser ablation system for age dating.

Zircon ages were obtained using a Laser-Ablation Sector Field Inductively Coupled Plasma Mass Spectrometer (LA-SF-ICP-MS). The laser ablation unit uses a focused laser beam to ablate a small amount of a sample contained in an air-tight sample cell. Detailed analytical protocols are described by Gerdes and Zeh (2006) and Frei and Gerdes (2009), but a brief summary is given here.

Samples and standards were mounted in a low-volume ablation cell specially developed for U–Pb dating (Horstwood et al., 2003). Helium was used to flush the sample cell and was mixed downstream with the Ar sample gas of the mass-spectrometer. A NewWave Research®/Merchantek® UP213 laser ablation unit was used, which emits a beam wavelength of 213 nm and a 10 Hz repetition rate. For the spot diameter (30 μm) and ablation times (30 s) used in this study, the ablated mass of zircon was typically between 150 and 200 ng. The ablated material was transferred to the mass-spectrometer in an Ar–He carrier gas via Tygon® tubing into an Element2 (ThermoFinnigan®, Bremen) single-collector double focusing magnetic sector ICPMS. The total acquisition time for each analysis was 60 seconds of which the first 30 seconds were used to determine the gas blank. The instrument was tuned to give large, stable signals for the ^{206}Pb and ^{238}U peaks, low background count rates (typically around 150 counts per second for ^{207}Pb) and low oxide production rates ($^{238}\text{U}^{16}\text{O}/^{238}\text{U}$ generally below 2.5%). ^{202}Hg , $^{204}(\text{Pb} + \text{Hg})$, ^{206}Pb , ^{207}Pb , ^{208}Pb , ^{232}Th and ^{238}U intensities were determined through peak jumping using electrostatic scanning in low resolution mode and with the magnet resting at ^{202}Hg . Each peak was determined at four slightly different masses and integrated sampling and a settling time of 1 ms for each isotope. Mass ^{202}Hg was measured to monitor the ^{204}Hg interference on ^{204}Pb where the $^{202}\text{Hg}/^{204}\text{Hg} \equiv 4.36$, which can be used to correct significant common Pb contributions using the model by Stacey and Kramers (1975). $^{207}\text{Pb}/^{235}\text{U}$ was calculated from the $^{207}\text{Pb}/^{206}\text{Pb}$ and $^{206}\text{Pb}/^{238}\text{U}$ assuming $^{238}\text{U}/^{235}\text{U} \equiv 137.88$. The laser-induced elemental fractionation and the instrumental mass bias on measured isotopic ratios were corrected through standard-sample bracketing using the GJ-1 zircon (Jackson et al., 2004). Samples were analyzed in sequences where three standards bracket each set of ten samples. The Plešovice zircon standard (Aftalion et al., 1989) was used as an external reproducibility check, and yielded long-term 2 σ RSD precisions ($n = 109$) of 2%, 2.3% and 1.1% for the $^{206}\text{Pb}/^{238}\text{U}$, $^{207}\text{Pb}/^{235}\text{U}$ and $^{207}\text{Pb}/^{206}\text{Pb}$ ratios respectively (Frei et al., 2006). The raw data were corrected for instrumental mass-bias and laser-induced U–Pb fractionation through normalization to the GJ-1 zircon using in-house data reduction software. All isotope data were plotted and evaluated using ISOPLOT/EX 3.71 (Ludwig, 2003). Model age calculation and error propagation follow Sambridge and Lambert (1997).

5. Results

5.1. Field relationships

The Tartoq Group comprises of a series of supracrustal blocks (Fig. 1) with variable lithological units and metamorphic grades. Here we briefly outline the main features of the different blocks.

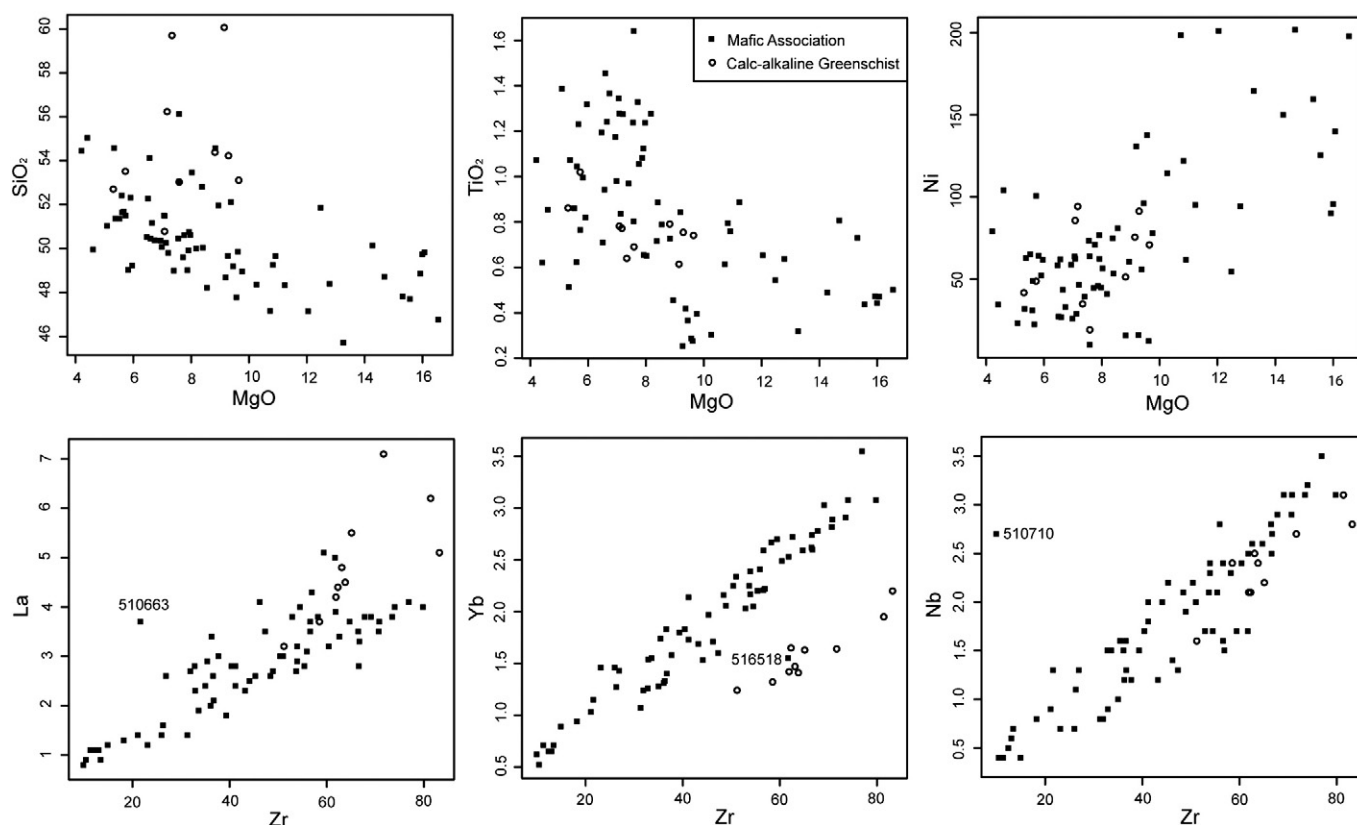


Fig. 4. Variation diagrams of SiO_2 , TiO_2 and Ni vs. MgO and La, Yb and Nb vs. Zr for the mafic association and the calc-alkaline greenschists. The mafic association shows trends that are expected for fractional crystallisation of particularly olivine. Although the calc-alkaline association generally follows a similar pattern they also display distinct enrichment in SiO_2 and La and a have lower Yb/Zr ratio.

The Nuuluk block is presently at greenschist facies conditions and foliated and sheared greenschists are the most common primary lithology. They occur together with minor greenstones with low strain and primary textures and with gabbros. Relict amphibolites with isolated amphibole grains are common, especially in the western part of the block. The centre of the block, especially, has a strong carbonate alteration overprint that locally results in almost pure ankerite, particularly in high strain zones. In the south-eastern part of the Nuuluk block greenstones are coarse-grained and less altered. They have preserved semi-ophitic textures (Fig. 2a) and occur as decimeter- to meter-scale sheets with parallel contact. In moderately altered rocks west of this locality the greenschists also appear to have a decimetre-scale sub-parallel layering (Fig. 3a and b). However, intense carbonation has left these rocks without relict textures, so it is only the weathered surfaces that give an impression of the primary layering in these rocks. There is a large thrust zone in the central part of the Nuuluk block, as mentioned above, in and surrounding a felsic schist band that is up to 40 m thick but pinches to a few metres in places (Fig. 3c). This felsic band is interpreted as a sliver of TTG gneiss that accommodated most of the over-trust shearing and essentially separates the Nuuluk block into two structurally overlying units (Kisters et al., 2011).

The Ilerlak block has both greenschist and amphibolite facies assemblages, but abundant amphibole relicts suggest that the greenschists in this block have invariably been retrogressed from amphibolite facies metamorphic assemblages. In many areas a relict gabbroic texture is observed (Fig. 2b), especially in the northern part of the block, and in plagioclase-rich amphibolites. There is an abrupt change in metamorphic grade across a set of closely spaced shear zones and generally the grade increases from west to east (Van Hinsberg et al., 2010). Large bodies, as well as extensive thin layers of talc-carbonate-magnetite schist

occur, particularly in the northern and eastern margins of the block, and in places these are in contact with a finely layered magnetite-amphibole rock that has previously been interpreted as a banded iron formation (Appel, 1984).

The Bikuben block mainly consists of amphibolites, only recording localized retrogression along its margins or along 10–30 meter-wide zones of chlorite schists. This block also contains large lenses of serpentinite up to 30 m wide, which can be traced for several 100 m along strike. These serpentinites are rimmed by talc-carbonate-magnetite schist, but they mostly consist of massive serpentinite-magnetite lenses locally with textures that resemble olivine-pseudomorphism by lizardite (Fig. 2c). They commonly display a talc-defined fabric that is at an angle to that in the surrounding amphibolites, and records a late stage of deformation. Locally, the amphibolites in the Bikuben block contain garnet and clinopyroxene, indicating a higher grade than found in the Ilerlak block; evidence of partial melting was observed in one locality. Structurally, the Bikuben block is similar to the Ilerlak and Nuuluk blocks in that it represents a klippe structure (Kisters et al., 2011). The Bikuben block is intruded by abundant syn- to late-tectonic pegmatites in an extensive stockwork.

The Amitsuaarsua and Naalagaaffik blocks contain both greenschists and amphibolites. In contrast to other blocks of the Tartoq Group, the rocks have mainly steep to subvertical dips. Abundant shear sense indicators point to dextral strike-slip kinematics along the steep layering and foliation, in marked contrast to the dip-slip-dominated kinematics (both top-to-the-SE thrusts and top-to-the-NW normal faults) of shear zones in the other blocks (Kisters et al., 2011). Most primary textures have been overprinted by a strong foliation and associated carbonate alteration, although pillow lavas have been reported in the western part of the Amitsuaarsua block (A. Polat, pers. Comm., 2010). Serpentinites

generally occur in contact with TTG sheets except in one locality in the central part of the Amitsuaarsua block, where a fairly well-preserved serpentinite body about 50×200 m large appears to be bounded by greenschist on all sides.

The Nuna Qaqortoq block marks the easternmost extent of the Tartog Group (Fig. 1) and has been metamorphosed under amphibolite facies conditions. As observed by Higgins (1968) these rocks were found to contain, well-preserved pillow structures (Fig. 3d). These rocks are massive, fine- to medium-grained, and free of vesicles. A network of felsic veins outlines pillow shapes that generally have coarser rims than centres. The Nuna Qaqortoq rocks are not affected by carbonate alteration, and furthermore show minimal deformation, and therefore contain some of the best preserved original magmatic structures in the Tartog Group, although they might have experienced some degree of pre-metamorphic seawater alteration.

The present contacts between the Tartog Group and the surrounding TTG gneisses are mostly tectonic, although they may originally have been intrusive and subsequently tectonized. There is a sharp thrust contact on the eastern margin of the Nuuluk block with a southeast-vergent fabric that indicates top-to-the-SE movement. However, most contacts are diffuse and consist of a gradation from slivers of supracrustal rocks in TTG gneiss to slivers of TTG gneiss in supracrustal rocks, which can be several hundreds of metres wide (Kisters et al., 2011).

There is an intrusive contact between TTG gneiss and the Tartog Group on the northern margin of the Amitsuaarsua block, where there are felsic sheets kilometres away from the northern TTG gneiss contact. These sheets increase in abundance towards the north until they are finally predominant. The felsic sheets in this entire zone have undergone intense brittle deformation and chloritization, which makes them hard to recognize in the field. U–Pb zircon age dating of a felsic sheet (sample 510772) in this zone provides a minimum age of the Tartog Group (Sections 5.4 and 6.4). A similarly intrusive relationship between TTG gneiss and the Tartog Group occurs in the southern part of the Iterlak block as also reported by Nutman and Kalsbeek (1994).

5.2. Major and trace element geochemistry

Major and trace elements were analyzed in 118 whole-rock samples (Section 4.1), which are presented in Supplementary Data Table 1. Figures in this section are produced in the GCDkit software (Janosek et al., 2006). Additional samples were analyzed, but where the loss on ignition (LOI) exceeded 6 wt.% for greenschists, they were rejected, because this indicates extensive late-stage carbonate alteration (Van Hinsberg et al., 2010). Such samples are therefore unlikely to retain the primary composition of the igneous rocks, which is the subject of this study. Similarly, serpentinites were discarded when they contained over 15 wt.% LOI.

The samples were grouped according to their recognizable field characteristics as described in Section 3: greenschist, greenstone, amphibolite, gabbro, pillow lava, serpentinite, felsic schist, TTG gneiss and TTG mylonite. In addition a group of calc-alkaline greenschists were defined by their distinctive geochemistry, which differs from that of the other mafic rocks in terms of their content of critical trace elements as described below.

In the following we briefly summarize the most important geochemical features of the different lithological units after the data were recalculated on a volatile-free basis:

The greenschists ($n=27$), the largest group of rocks, have a wide variation in major element contents with 46–55 wt.% SiO_2 , 7.4–17.3 wt.% Fe_2O_3 , 5.1–16.1 wt.% MgO and 0.29–1.39 wt.% TiO_2 . Their trace element content includes 23–202 ppm Ni, 14–1368 ppm Cr, 0.4–3.2 ppm Nb, 10–74 ppm Zr, Hf/Lu of 2.7–5.7 and Zr/TiO₂ of 36–74.

The calc-alkaline greenschists ($n=10$) are mainly from one outcrop in the Iterlak block and two samples are from the Nuuluk block. They have major element compositions of 51–60 wt.% SiO_2 , 8–13.78 wt.%

Fe_2O_3 , 5.3–9.7 wt.% MgO and 0.61–1.02 wt.% TiO_2 and trace elements compositions of 19–94 ppm Ni, 178–568 ppm Cr, 1.6–3.1 ppm Nb, 51–83 ppm Zr, Hf/Lu of 7.3–9.1 and Zr/TiO₂ of 79–94.

The greenstones ($n=9$), which are all from the Nuuluk block, form a tight group with 50–51 wt.% SiO_2 , 13.8–16.7 wt.% Fe_2O_3 , 6.6–8.0 wt.% MgO and 1.12–1.46 wt.% TiO_2 . Their trace element content is also fairly uniform with 27–77 ppm Ni, 82–246 ppm Cr, 2.3–3.5 ppm Nb and 54–80 ppm Zr, Hf/Lu of 4.8–5.6 and Zr/TiO₂ of 48–64.

The amphibolites ($n=15$), which are a fairly large group from several supracrustal blocks, have major element compositions of 48–52 wt.% SiO_2 , 10.9–14.8 wt.% Fe_2O_3 , 4.6–16.0 wt.% MgO and 0.44–1.28 wt.% TiO_2 . Their trace element content varies widely with 22–131 ppm Ni, 21–2518 ppm Cr, 0.8–2.8 ppm Nb and 22–62 ppm Zr.

The gabbros ($n=9$), which are from the Iterlak and Nuuluk blocks, have variable major element contents with 47–56 wt.% SiO_2 , 5.7–13.9 wt.% Fe_2O_3 , 7.1–16.5 wt.% MgO and 0.25–1.64 wt.% TiO_2 , and they have a large range in their trace element contents with 10–198 ppm Ni, 14–880 ppm Cr, 0.4–2.7 ppm Nb and 10–62 ppm Zr.

The pillow lavas ($n=7$) are spatially restricted to the Nuna Qaqortoq block. They only have little variation in terms of major elements with 49–55 wt.% SiO_2 , 8.7–12.7 wt.% Fe_2O_3 , 4.2–7.4 wt.% MgO and 0.62–1.07 wt.% TiO_2 . They also have rather tight trace element contents with 34–79 ppm Ni, 192–315 ppm Cr, 1.5–2.4 ppm Nb and 34–60 ppm Zr.

The mafic association (greenschists, greenstones, amphibolites, gabbros and pillow lavas, $n=67$) plot (not shown) as basalts using immobile ratios (Winchester and Floyd, 1977; Pearce, 1996) and they follow a typical tholeiitic magmatic trend on the Jensen (1976) and AFM (Irvine and Baragar, 1971) classification diagrams (not shown), although some samples plot in the komatiitic-basalt field in the latter diagram. They generally plot in the MORB and IAT fields in various tectonic discrimination diagrams (e.g. Rollinson, 1993 and references therein; not shown), which is a typical feature of Archaean tholeiites. As mentioned above, they have quite scattered major element compositions, but some positive correlation appears for e.g. Fe_2O_3 vs. TiO_2 and inverse correlation of SiO_2 vs. MgO . Fig. 4 shows selected variation diagrams, where the trends of the mafic association are compared with the calc-alkaline greenschist. The inverse correlation of SiO_2 vs. MgO is apparent in the mafic association, whereas the calc-alkaline greenschists show little variation in MgO , but a range of SiO_2 . The calc-alkaline greenschist appear to form a distinct trend on the Yb vs. Zr diagram together with one gabbro (516518). The mafic association has fairly uniform trace element patterns and strong correlations between most incompatible trace elements, whereas the compatible trace elements scatter widely. The samples have relatively flat chondrite-normalized (Boynton, 1984) REE patterns (Fig. 5) with a mean $\text{La}_{\text{CN}}/\text{Sm}_{\text{CN}}$ of 1.0 (± 0.2 1σ) and a total range from 0.67 to 1.96 and Eu/Eu^* from 0.71 to 1.94. The mafic association generally has flat primitive mantle-normalized (Sun and McDonough, 1989) multi-element patterns (Fig. 6) and distinct negative Nb-anomalies with Nb/Nb^* of 0.26–1.31, where $\text{Nb}/\text{Nb}^* = \text{Nb}_{\text{N}}/(\sqrt{(\text{Th}_{\text{N}}^* \text{La}_{\text{N}})})$ (Eisele et al., 2002). Where trace elements are below detection limits they have not been included in Fig. 6. The mafic association has $\text{Nb}_{\text{N}}/\text{La}_{\text{N}}$ of 0.3–0.9 (with sample 510710 being an outlier at 3.3). Th/Yb range from 0.06 to 0.47 and Nb/Yb is close to unity (Fig. 7). They have large, but variable enrichments or depletions in Cs, Rb, Ba, K₂O, Pb as well as Sr (not shown). Their Ti/V ratio has a mean value of ~19, their mean Zr/Y is ~2.6 and their Ti/Zr has a mean of ~112.

The serpentinites ($n=15$) are ultramafic rocks with 41–49 wt.% SiO_2 and 10.4–18.8 wt.% Fe_2O_3 and 34.4–40.4 wt.% MgO . They are very low in Al_2O_3 (1–5 wt.%), CaO (0–2.9 wt.%) and TiO_2 (0.05–0.25 wt.%), and most of the other major elements are close to their respective detection limits. They have variable trace element contents with 653–2262 ppm Ni, 855–5289 ppm Cr and low incompatible trace element content with 0.1–1.3 ppm Nb and 1.8–16 ppm Zr. Their chondrite-normalized $\text{La}_{\text{CN}}/\text{Sm}_{\text{CN}}$ of 0.7–3.7 and Eu/Eu^* of 0.4–1.6.

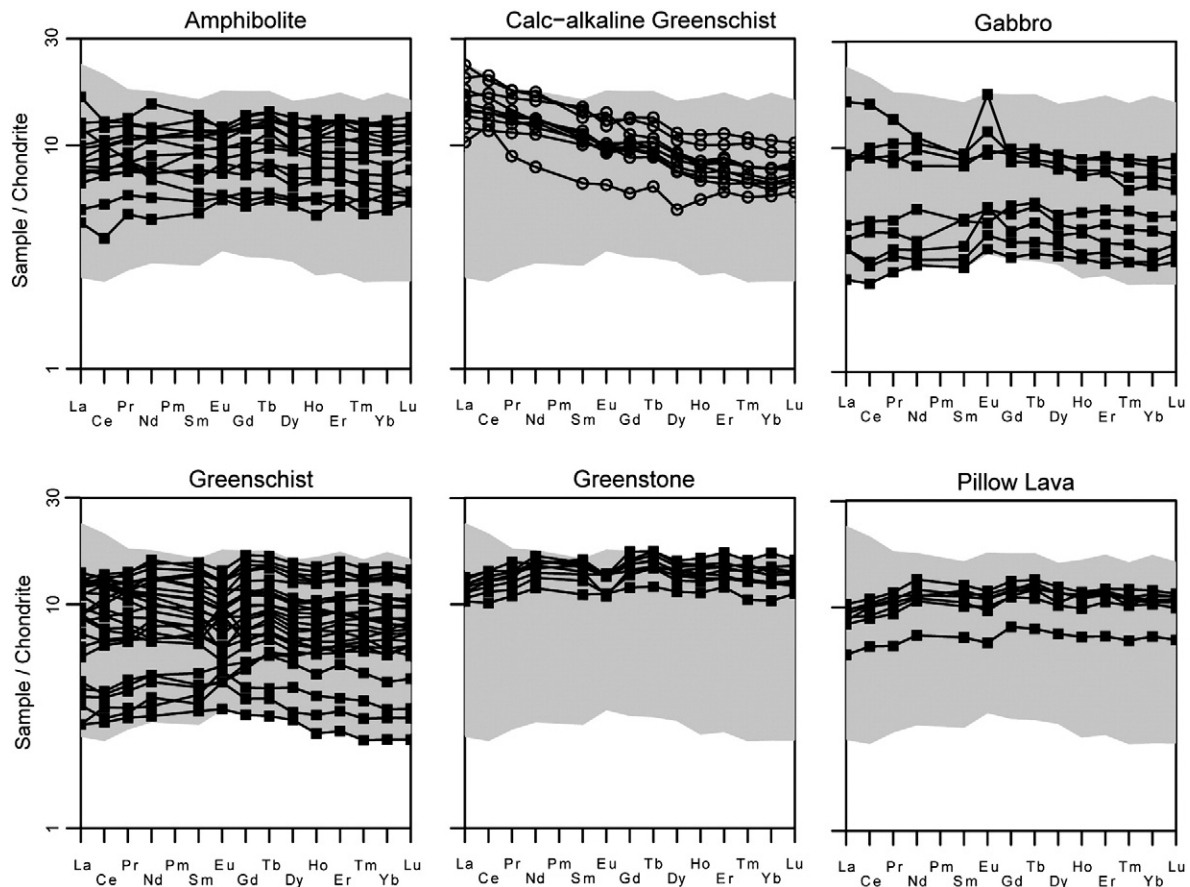


Fig. 5. Chondrite-normalized (Boynton, 1984) REE diagram for the mafic association. The shaded area outlines the total range. Note the scale of only 1 to 30 which makes the patterns appear slightly distorted. The mafic association has relatively flat patterns, whereas the calc-alkaline greenschist have slight LREE enrichment in comparison.

They have large positive Pb-anomalies and negative Sr-anomalies in a primitive mantle-normalized multi-element diagram (not shown). Applying the CIPW-norm calculation, assuming that all Fe originally occurred as FeO (McCammon, 2005), the serpentinites are dominantly olivine- and hypersthene-normative with their modal proportions ranging from 76% Ol and 23% Hy to 44% Ol and 54% Hy, respectively, and are thus harzburgitic in composition.

The felsic association (felsic schists, TTG mylonites and TTG gneisses) show largely overlapping major and trace element compositions, but the felsic schists ($n = 12$) generally have a wider range with 58–88 wt.% SiO₂, 7.4–19 wt.% Al₂O₃, 0.7–14.6 wt.% Fe₂O₃, 0.3–6.8 wt.% MgO and 0.2–1.7 wt.% TiO₂. Their trace element contents range from 2 to 96 ppm Ni, 14–322 ppm Cr, 1.6–12 ppm Nb, 66–168 ppm Zr, Hf/Lu of 11–63 and Zr/TiO₂ of 97–498.

The TTG mylonites ($n = 6$) vary almost as much as the felsic schists with 50–80 wt.% SiO₂, 6–17 wt.% Al₂O₃, 0.8–15.4 wt.% Fe₂O₃, 0.2–17 wt.% MgO and 0.06–1.03 wt.% TiO₂, 0.6–526 ppm Ni, 14–2258 ppm Cr, 2.8–6.3 ppm Nb and 51–155 ppm Zr.

The TTG gneisses ($n = 8$) show relatively tight major element variation with 62–78 wt.% SiO₂, 12–18 wt.% Al₂O₃, 0.9–6.4 wt.% Fe₂O₃, 0.2–3.8 wt.% MgO and 0.06–0.79 wt.% TiO₂ and variable trace element contents, which range from 1.1 to 75 ppm Ni, 14–103 ppm Cr, 0.9–6.5 ppm Nb and 70–253 ppm Zr.

The felsic association has steep negative chondrite-normalized REE patterns with La_{CN}/Sm_{CN} of 1.2–7.9 with the felsic schists and TTG mylonites extending to the lowest values and Eu/Eu* of 0.3–2.0. They have negative Nb-anomalies with Nb/Nb* of 0.05–0.59 (except one sample with a value of 1.05). Primitive mantle-normalized Nb_N/La_N ranges

from 0.1 to 1.1 and Th/Yb from 0.7 to 14.5 with the lowest values represented by felsic schists and TTG mylonites.

5.3. ¹⁷⁶Lu–¹⁷⁶Hf and ¹⁴⁷Sm–¹⁴³Nd isotope systematics

Ten whole-rock samples were analyzed for ¹⁷⁶Lu–¹⁷⁶Hf and ¹⁴⁷Sm–¹⁴³Nd isotope compositions using isotope dilution techniques by MC-ICP-MS (Section 4.2). The samples are representative of the different lithological units and supracrustal blocks and include: greenschist, greenstone, gabbro, pillow lava and serpentinite, as well as, one felsic schist sample. The results are presented in Supplementary Data Table 3 and Figs. 8 and 9 show Lu–Hf and Sm–Nd errorchron diagrams, respectively.

The initial epsilon values for both isotope systems were calculated using both the minimum age of c. 3000 Ma provided by an intrusive TTG gneiss (sample 510772 in Sections 5.4 and 6.4) and the age c. 3190 Ma determined by the best-fit ¹⁷⁶Lu–¹⁷⁶Hf isotope regression (see Section 6.3).

The initial εHf(3000) values of the mafic rocks range from +3.0 to +5.8 and εHf(3190) range from +3.7 to +6.7. The calculated initial εNd(3000 Ma) values range from +1.8 to +5.0 and εNd(3190 Ma) from +1.8 to +4.8.

The serpentinite sample is characterized by initial εHf(3000) of +0.4 and εHf(3190) of +2.1, whereas its εNd(3000) is +1.8 and εNd(3190) is +3.0. The felsic schist sample also has positive εHf(3000) of +3.4 and εHf(3190) of +6.3, but negative εNd(3000) of –0.6 and εNd(3190) of –2.1.

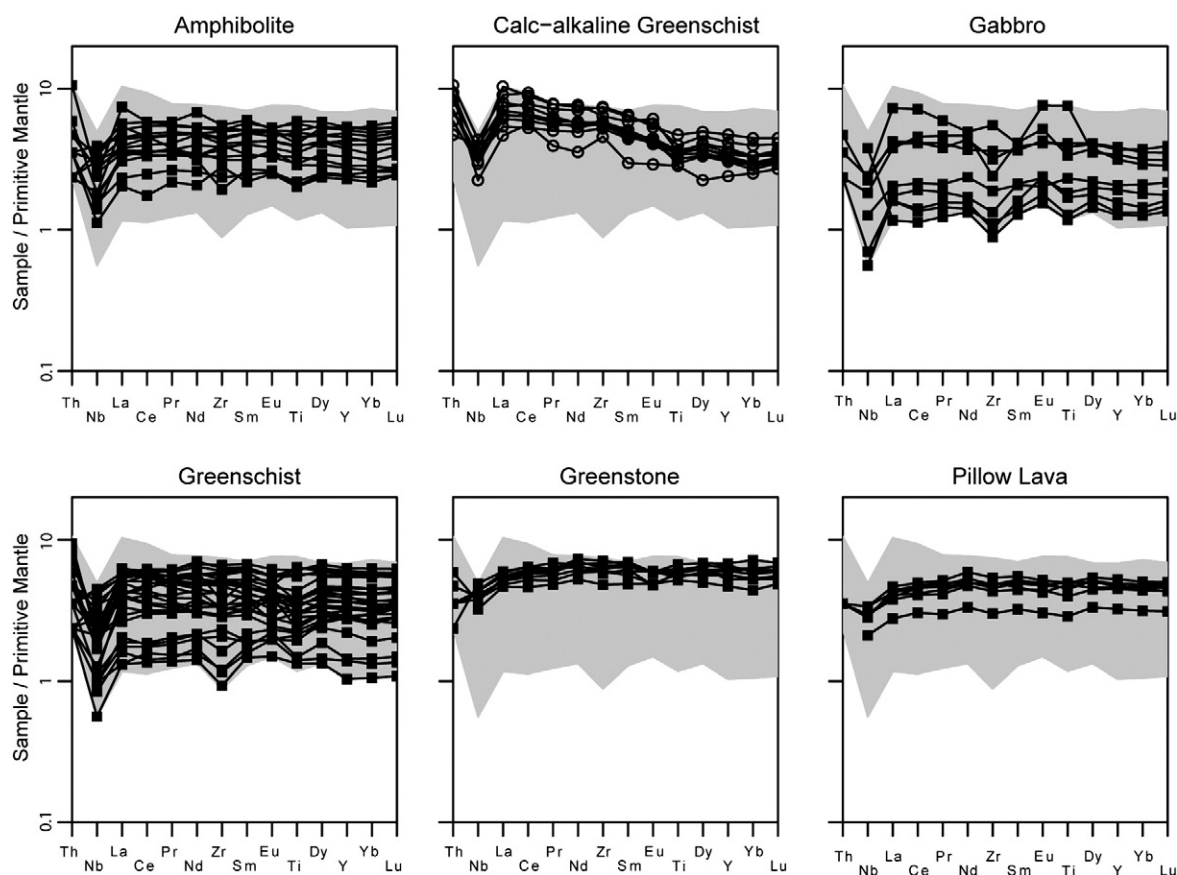


Fig. 6. Primitive mantle-normalized (Sun and McDonough, 1989) multi-element diagram for the mafic association. Only the relatively fluid immobile elements are shown. The shaded area outlines the total range. Certain elements have been left out from samples where the respective elemental concentration fall below the analytical detection limits (see Table 1 for detection limits).

5.4. U–Pb geochronology

Zircons separated from two TTG gneiss samples were analyzed by LA-ICP-MS (Section 4.3). The results are shown in Supplementary Data Table

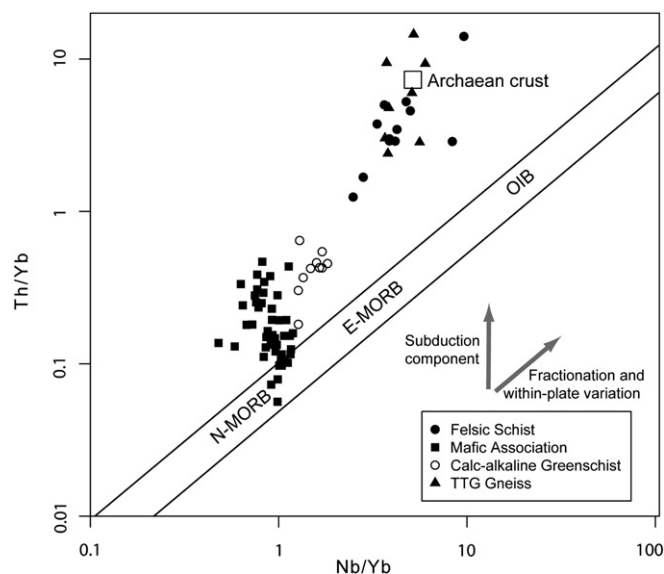


Fig. 7. Th/Yb vs. Nb/Yb diagram showing the vectors of a subduction component and a fractionation trend (Metcalfe and Shervais, 2008). The mafic association seems to follow a subduction trend going from the mantle array at a Nb/Yb of about unity, whereas the calc-alkaline greenschists follow a fractionation trend seen in modern arcs. The felsic schists and TTG gneisses plot near the field of Archaean crust (Rudnick and Fountain, 1995).

4 and are plotted in concordia diagrams in Figs. 10 and 11. The reported ages were calculated as weighted mean $^{207}\text{Pb}/^{206}\text{Pb}$ ages for analyses that are <5% discordant and filtered for outliers. The analyses are generally concordant with some evidence for ancient Pb-loss or metamorphic re-growth of zircon as seen in Figs. 10 and 11. The zircons are mostly prismatic and show oscillatory zoning with homogeneous rim domains. Generally only zircon cores were analysed, and where rims were analysed, they have not been included in the age calculations.

Sample 510772 (Fig. 10) is an intrusive TTG sheet on the northern contact of the Amitsua block, which yields an average $^{207}\text{Pb}/^{206}\text{Pb}$ age of 2986 ± 4 Ma ($n = 49/59$, MSWD = 0.99, probability = 0.49). The rejected analyses with lower $^{207}\text{Pb}/^{206}\text{Pb}$ ages were from rim domains on oscillatory-zoned zircons and from homogeneous zircons.

Sample 510657 (Fig. 11) is a TTG gneiss west of the Nuuluk block, where there is an entire zone marked by brittle deformation and chloritization. No intrusive relationship could be established with certainty; however, this sample was collected west of the deformation zone and is relatively fresh. This sample yields an average $^{207}\text{Pb}/^{206}\text{Pb}$ age of 2867 ± 17 Ma ($n = 14/18$, MSWD = 1.9, probability = 0.022).

6. Discussion

6.1. Field relationships

The strong deformation and variable metamorphism and alteration of the Tartuq Group supracrustal rocks have overprinted most primary textures. It is, therefore, difficult to assess the protoliths for these supracrustal rocks. This is especially true for the greenschists and fine-grained amphibolites, which are likely to represent pillow

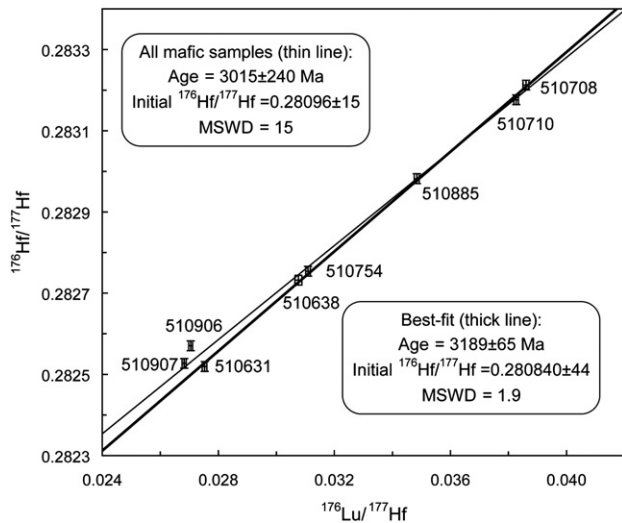


Fig. 8. ^{176}Lu – ^{176}Hf errorchron diagram showing one regression line for all samples with an age of 3015 ± 240 Ma and one best-fit regression line with an age of 3189 ± 65 Ma (after exclusion of samples 510906 and 510907). See Section 6.3 for explanation of the sample selection criteria).

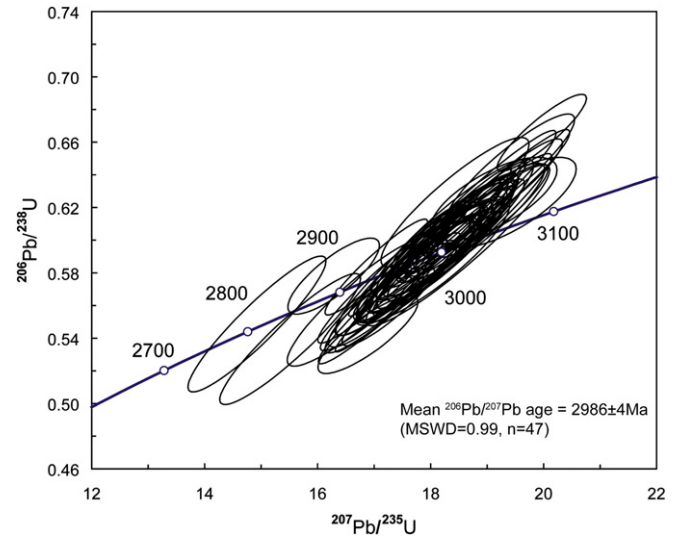


Fig. 10. Concordia diagram for TTG gneiss sample 510772 with an U–Pb zircon age of 2986 ± 4 Ma.

lavas, sills/dykes and gabbroic rocks, but they cannot be differentiated for lack of recognisable primary textures.

The most diagnostic field observation that indicates the primary environment of the Tartoq rocks is the well-preserved pillow structures, located on Nuna Qaqortoq (Fig. 3d). They indicate that at least part of the Tartoq Group was deposited as flows under subaqueous conditions. Such structures may also have been widely distributed in the other supracrustal blocks prior to the deformation and late carbonate alteration, and occasional pillow relicts have indeed been reported from elsewhere (e.g. Amitsuaarsua – A. Polat, pers. Comm., 2010).

The ophitic texture in the greenstones marks them as magmatic, but does not reveal whether their protoliths were intrusive sills/dykes or extrusive lava flows. However, we do not find it likely that they represent thin, extensive surface flows, because they have too low MgO to have had the required low viscosity (Section 5.2). Given that the greenstones are well preserved and that similarly preserved rocks on Nuna Qaqortoq contain distinct pillow structures, we would have expected similar structures if the more abundant greenstones were submarine

flows. Additionally, these units show regular, sub-parallel layering (Fig. 3a and b), which points to an origin as sills or dykes, rather than pillow lavas. Finally, the greenstones are commonly coarse-grained, approaching a gabbroic texture, and lack an internal fabric, which is consistent with them being intrusive rather than extrusive. Thus, we regard the greenstones as being sills or dykes, although we will maintain the term “greenstone”, because it is free of interpretation. The greenstones in Nuuluk grade into greenschists at their margins as a result of progressive deformation and retrogression. We therefore extend the interpretation of an intrusive origin to most of the Nuuluk greenschists. Such gradational contacts are rare in the other blocks, and we, therefore, do not rule out a lava flow or volcanoclastic origin for these. The greenstones are regarded as prograde greenschist facies rocks with well-preserved mineral compositions, whereas much of the greenschist rocks in the rest of the Tartoq Group probably represent a retrograde overprint of amphibolite facies rocks.

The gabbros are coarse-grained intrusives that mainly occur as lens-shaped bodies, commonly with only a minor fabric in their

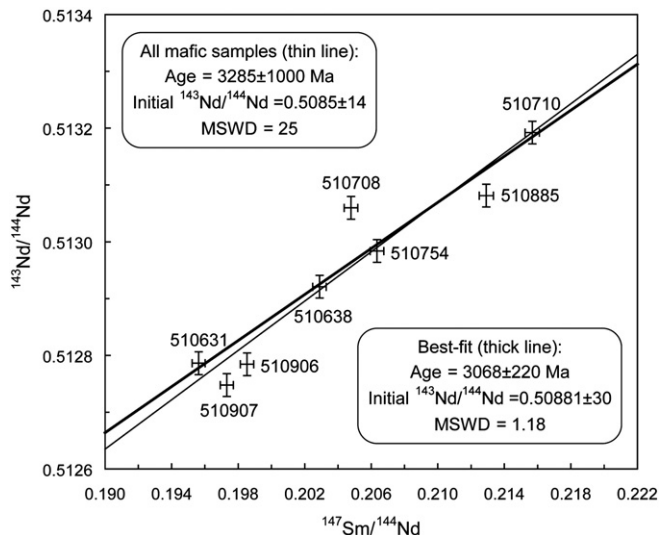


Fig. 9. ^{147}Sm – ^{143}Nd errorchron diagram showing one regression line for all samples with an age of 3285 ± 1000 Ma and one best-fit regression line with an age of 3068 ± 220 Ma (after exclusion of samples 510708, 510906, 510907 and 510885). See Section 6.3 for explanation of the sample selection criteria).

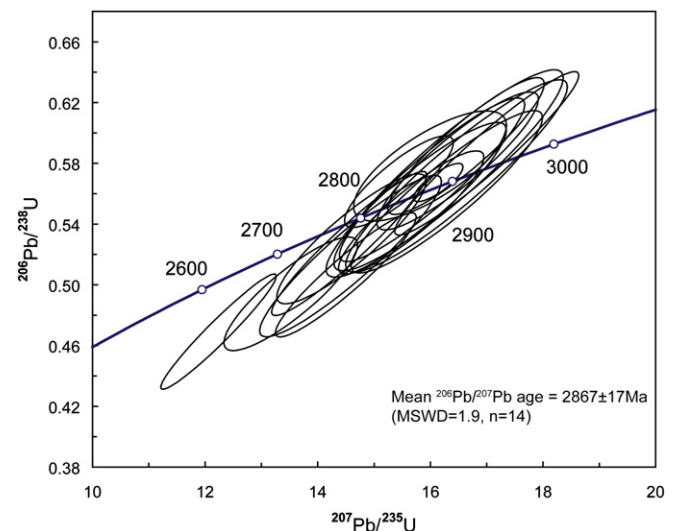


Fig. 11. Concordia diagram for TTG gneiss sample 510657 with an U–Pb zircon age of 2867 ± 17 Ma.

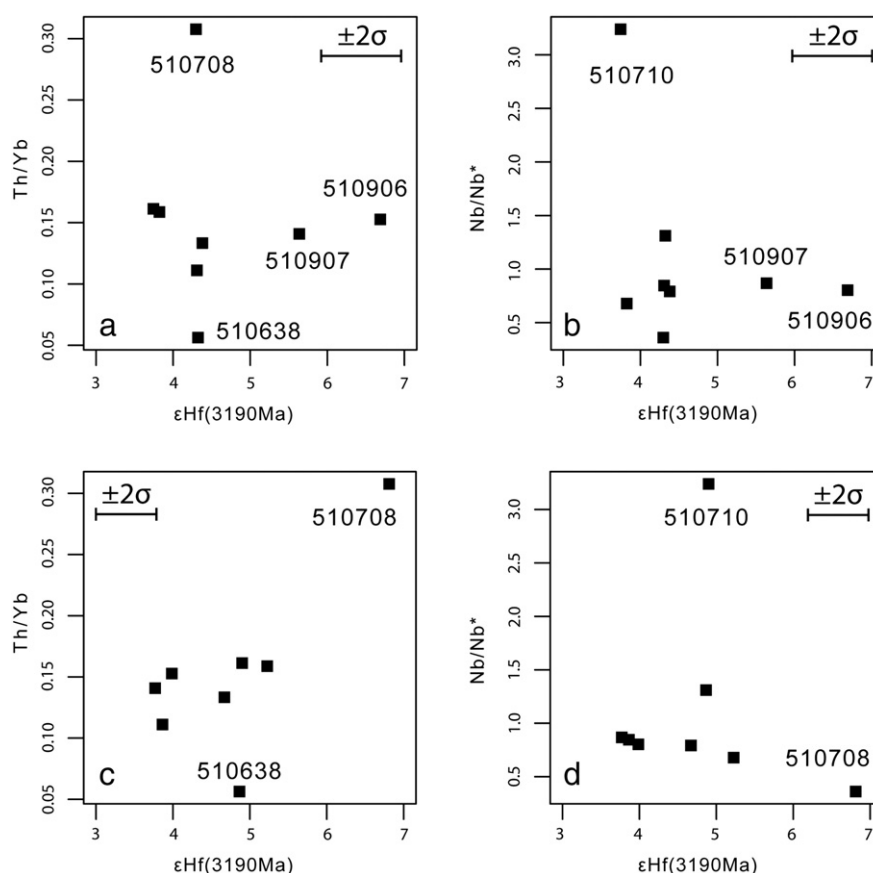


Fig. 12. Initial $\epsilon_{\text{Hf}}(3190 \text{ Ma})$ and $\epsilon_{\text{Nd}}(3190 \text{ Ma})$ versus the contamination-sensitive trace element ratios of Th/Yb and Nb/Nb*, which show no systematic variations. This argues against the possibility of crustal contamination of the mafic association of the Tartoq Group.

interiors. Intrusive contacts between different generations of gabbro can be observed in both Ilerlak and Amitsuaarsua, and these typically vary in composition from mafic, amphibole-dominated, to felsic, plagioclase-dominated gabbro. These observations indicate that the gabbros were intrusions at a deeper crustal level compared with the greenstones discussed above.

The serpentinites in the Bikuben block have previously been described as intrusive into the Tartoq Group, but this was based on their steeper-dipping fabric compared with the surrounding greenschists and amphibolites (Berthelsen and Henriksen, 1975). We did not observe any crosscutting relations that would lead us to believe that these rocks were later than the surrounding Tartoq Group, although they do occur in areas with intense thrusting adjacent to TTG sheets. Instead we interpret the fabrics in the serpentinites to be the result of strain localisation into the incompetent serpentinites, compared to the more competent enveloping greenschists and amphibolites, which can give them a discordant appearance. The highly sheared contacts of the serpentinites provide little information about their original contacts and protoliths. Thus, we do not support the view that they are intrusive rocks and the texture outlined by magnetite (Fig. 2c) is interpreted as a primary texture in olivine-rich cumulate or mantle rocks, although this could also have formed during breakdown of olivine to form serpentine and magnetite during metamorphic reactions.

The felsic schists, such as those in the central part of the Nuuluk block, were previously described as quartzitic or semipelitic sedimentary rocks (Higgins, 1968) or felsic volcanic rocks (Petersen, 1992). However, these schists contain abundant zircons with ages that are much younger (~2842 Ma according to Nutman et al., 2004) than

the oldest intrusive TTG gneisses (Section 6.4), which yield definite minimum ages for the Tartoq Group of 2944 Ma and 2986 Ma. This can be interpreted in two ways: 1) the Tartoq Group consists of supracrustal blocks of different age, or 2) the felsic sheets represent intrusive TTG gneisses or basement that have been sheared into the supracrustal blocks. The presence of supracrustal blocks of different age within the Tartoq Group is contradicted by the highly consistent errorchron ages of the mafic rocks (Section 6.3), as well as their uniform major and trace element compositions (Section 6.2). The felsic schists invariably display high strain and the surrounding rocks are often strongly carbonated (Kisters et al., 2011). Furthermore, the felsic schists have major and trace element contents that overlaps with those of the local TTG gneisses (Section 6.2). Supporting evidence for the second hypothesis is thus abundant. The broad age-population of the felsic schists is likely due to extensive transport over variable basement in large shear zones, because they contain zircons both younger and older than the surrounding TTG gneisses (Sections 5.4 and 6.4). We therefore conclude that the felsic schists and TTG mylonites represent fragments of TTG gneiss that were sheared into the Tartoq along thrust planes.

Collectively the lithological assemblage of the Tartoq Group consisting of pillow lavas, sill/dykes, gabbros and ultramafic cumulate/mantle is consistent with a section through oceanic crust.

6.2. Major and trace element geochemistry

The alteration observed in many of the Tartoq Group samples, as well as the potential for original seawater alteration and element

mobility during deformation and metamorphism highlight the need for care when interpreting the geochemical data. In general, elements with higher mobility, such as Sr, Rb, Ba, Cs and Pb should be given less significance than refractory elements when interpreting these Archaean supracrustal rocks, thus large ion lithophile elements (LILE) have not been included in multi-element diagrams (Fig. 6).

Some filtering was performed by discarding samples with high LOI as mentioned in Section 5.2 and thus most of the remaining samples are assumed to be reasonably unaltered. However, a few mafic samples with high K_2O (>1 wt.%) are clearly outliers and are considered to be either altered, contaminated or simply enriched in incompatible elements compared to the greenschists. These have been defined as calc-alkaline greenschists based on their geochemistry as discussed below.

The variable, but consistent, enrichments in the fluid mobile elements Cs, Rb, Ba, K_2O , Pb and Sr in most rocks of the Tartuq Group likely reflects a combination of metamorphic and hydrothermal fluids interacting with the mafic protoliths given that the least altered greenstones also show the smallest enrichment in these elements. Essentially only the HREE, HFSE and Al_2O_3 can be considered immobile in Archaean supracrustal rocks (e.g. Arndt, 1994; Polat and Hofmann, 2003) and although their concentration may change during dilution and leaching, their ratios will remain the same.

The basaltic composition of the mafic rocks was determined by the immobile ratios of Zr/Ti vs. Nb/Y (Pearce, 1996). Their tholeiitic affinity relies on less immobile elements in the AFM diagram ($Na_2O + K_2O$ vs. FeO^T vs. MgO) and the Jensen diagram (Al vs. $Fe^T + Ti$ vs. Mg), however the vast majority of the samples plot within the tholeiitic field in diagrams that distinguish between a tholeiitic and calc-alkaline fractionation trend for a suite of volcanic rocks (not shown).

The REE patterns of the rocks in the mafic association are generally flat, but some variation is seen especially within the group of greenschists. To some degree this can be accounted for by addition of late carbonate and quartz, which will tend to dilute the REE concentrations, and some mobility of LREE would be expected if the alteration were intense as seen in other Archaean supracrustal belts (e.g. Polat and Hofmann, 2003). However, fractional crystallisation will also change the absolute REE concentrations without affecting the patterns much.

The calc-alkaline greenschists are not distinguishable from the regular greenschists in the field, but chemically have higher Hf/Lu and Zr/TiO₂ and are distinct in terms of immobile trace element ratios such as La_{CN}/Yb_{CN} , Th/Yb and Nb/Yb, as well as their elevated LREE, K_2O and SiO_2 contents (Section 5.2) as also seen in Fig. 4. They are often located in high strain zones and the immediate interpretation of these would be as altered and possibly mechanically contaminated with TTGs, however, it is also a possibility that they simply represent evolved arc volcanics as suggested from Fig. 7.

The range in REE abundances in the amphibolites and gabbros is similar to that in the greenschists, but there is a gap in the gabbros that divides them into high and low REE groups, however, no other differences exist between the two groups of gabbros. One gabbro (sample 516518) from the Naalagaaffik block is distinctly enriched in LREE compared to the rest and has a large positive Eu-anomaly. This sample is extremely plagioclase-rich and coarser than the other gabbros. However, it is located adjacent to felsic schists in an intense deformation zone, and therefore possibly altered, but the positive Eu-anomaly is likely related to cumulate plagioclase.

The strong enrichments and depletions in fluid mobile elements such as Cs, Rb, Ba, K_2O , Pb and Sr, as generally observed for the Tartuq Group mafic rocks, is often related to fluid enrichment of a mantle wedge in an arc setting by slab-derived volatiles. However, the least altered greenstones also show less disturbance in these fluid mobile elements, which would lead to the conclusion that the addition was post-magmatic. This is reasonable considering that the supracrustal rocks are situated in a TTG gneiss terrain that is enriched in these particular elements, which in turn would be expected to be mobilised during

metamorphism. If we only consider the immobile elements in the primitive mantle-normalized multi-element diagrams, then the patterns of the greenstones and the pillow lavas are rather flat except for their negative Nb-anomalies.

The multi-element patterns for the gabbros, amphibolites and greenschists are also generally flat (Fig. 6), and in addition to their consistently negative Nb-anomalies, they have minor negative anomalies for Zr and Ti and positive Eu anomalies. A few samples show LREE enrichments (Fig. 5) and one gabbro sample has a large positive Ti-anomaly. These relations are likely due to the cumulate effects caused by fractionation of plagioclase (Eu) and amphibole (Zr), which would be expected for some of the coarser grained samples, while the negative Ti and Nb anomalies are likely controlled by ilmenite or rutile in the source (Baier et al., 2008).

The TiO₂ content in the mafic association of 0.3–1.6 wt.% suggests an arc-affinity rather than MORB-affinity, when compared with modern setting (e.g. Metcalf and Shervais, 2008). This is supported by the La, Y and Nb contents of the mafic association, which plot in the back-arc basin field in the discrimination diagram of Cabanis and Lecolle (1989) (not shown), indicating they are more La-rich than mid-ocean ridge basalts (MORB), but with higher Nb-concentrations than island arc tholeiites. Their Ti/V, Zr/Y and Ti/Zr values cannot be used to relate these rocks to a specific tectonic setting on various diagrams proposed in the literature (e.g. Pearce and Cann, 1973; Pearce and Norry, 1979; Wood, 1980; Rollinson, 1993 and references therein), because their range overlap with those of MORB and island arc tholeiites (IAT). However, the mafic association plots in the subduction zone field of the Nb/Th vs. Zr/Nb diagram of Kerrich et al. (2008), which effectively distinguishes between arc and MORB rocks (not shown).

Th/Yb vs. Nb/Yb (Fig. 7) has commonly been used to detect a crustal signature in volcanic rocks. Pearce (2008) concluded that essentially all Archaean tholeiitic suites contain evidence of a crustal input. However, the surrounding TTG gneisses contain an order of magnitude higher Th contents than the supracrustal rocks, and mobility of Th has been documented in Archaean supracrustal belts (Frei et al., 2002; Polat and Hofmann, 2003). In addition Yb and MgO are inversely correlated, and because MgO-rich samples are likely more prone to alteration, the Th/Yb ratio could possibly be disturbed relative to their primary magmatic ratio. This in turn suggests that the use of the Th/Yb–Nb/Yb diagram is perhaps less diagnostic than commonly assumed. However, our knowledge of the relative impact of metasomatism on the various samples provides a check on the observed trends and this does not suggest significant Th-mobility. There appears to be a general sub-vertical elevation in Th/Yb in the mafic association (Fig. 7), with the greenstones and pillow lavas having the most MORB-like ratios. This trend is similar to that seen in Cenozoic fore-arc lavas (Metcalf and Shervais, 2008), so a similar setting is possible for the Tartuq Group if we accept that post-magmatic Th-mobility was insignificant for the mafic association.

The calc-alkaline greenschists appear to plot towards the local TTG crust (Fig. 7) and thus would either reflect contamination or an internal island arc fractionation trend. The former is not supported by generally juvenile character of the Tartuq Group mafic association (Section 6.3), so we interpret the calc-alkaline greenschist to be primitive island arc rocks. However, we cannot rule out that they have been mechanically mixed with TTG during late deformation, because they generally have a sheared appearance in thin section. Both the mafic association and the calc-alkaline rocks appear to be derived from a source on the mantle array with a constant Nb/Yb of about unity as seen in Fig. 7. This is also seen for mafic rocks from the Isua, Ivisartoq and Fiskensæset supracrustal belts in SW Greenland as well as the subvertical trends of Th/Yb (Polat et al., 2011). This suggests a similar mantle source and tectonic environment of formation for these different supracrustal belts.

Some of the felsic schists plot from the TTG field towards the mafic association, which likely reflects mechanical mixing of the two end-members during deformation that resulted in the TTG mylonites and felsic schists. This must be a late feature given the presence of

zircon grains in the felsic schists that are younger than the minimum age of the Tartoq Group (Nutman et al., 2004 and Section 6.4). Although it is not entirely clear if the Th/Yb–Nb/Yb diagram is a diagnostic tool for detecting arc contributions to magmas, it can certainly trace crustal input during assimilation and also during post-magmatic alteration if Th was mobilised. However, following the line of reasoning of previous workers using the Th/Yb–Nb/Yb diagram (Pearce, 2008; Polat et al., 2011) together with the consistent negative Nb-anomalies and the occasional negative Ti-anomalies, which would be hard to produce via crustal contamination, the mafic association was likely affected by an arc-component during its formation. The mafic association essentially overlaps with data from mafic rocks of the Isua and Ivvisaartoq supracrustal belts in SW Greenland (not shown), which have been ascribed to a SSZ environment (Polat et al., 2011).

Our field interpretation that the serpentinites are cumulates or relict mantle related to the mafic association, rather than intrusive sills as previously proposed (Berthelsen and Henriksen, 1975), is supported by their high MgO (34.4–40.4 wt.%). A brief comparison with literature data of komatiites show no resembles and the serpentinites do also not show olivine fractionation trends in variation diagrams (not shown). They are rather rich in Fe_2O_3 (5.7–17.3 wt.%) compared with examples of Archaean mantle, but they are depleted in CaO, Al_2O_3 and incompatible elements as expected for mantle harzburgites. However, with the available data we are not able to confidently determine if the serpentinites are cumulates or tectonized mantle.

The felsic schist and TTG mylonite samples with the lowest $\text{La}_{\text{CN}}/\text{Sm}_{\text{CN}}$ (down to 1.2) and Th/Yb (down to 0.7) also have the highest Fe_2O_3 and MgO. This is interpreted as mechanical mixing with the mafic association rather than primary variation within the TTG magmas. The interpretation that the felsic schists formed by intrusion into the supracrustal sequence and were later preferentially sheared into mylonitic rocks that incorporated mafic wall-rocks, is consistent with the field occurrence of these rocks, but they may equally well represent sheared basement mixed with the mafic association (Section 6.1). They generally fall with the elemental range of Archaean TTG gneisses (Martin et al., 2005; Moyen, 2011).

Many Archaean supracrustal belts hosting tholeiites are ascribed to an oceanic plateau setting such as the modern Ontong Java. These are generally dominated by pillow lavas and komatiites and have no pronounced negative Nb-anomalies (e.g. Arndt et al., 1997). This is not the case for the Tartoq Group supracrustal rocks, which have a pronounced negative Nb-anomaly and is clearly not derived from an OIB mantle source as seen in Fig. 7. They form a range of different lithological units rather than a pile of monotonous pillow lava and, finally, no komatiites have been discovered in the Tartoq Group, so there is no support for an oceanic plateau setting.

Archaean tholeiites generally differ from modern MORB by having higher FeO^T , Ni, Cr and Co, and similarities between Archaean tholeiites and modern back-arc basin (BAB) and island arc tholeiites (IAT) have long been recognized (e.g. Hart et al., 1970; Glikson, 1971; Hart and Brooks, 1977; Gill, 1979; Condie, 1985; Manikyamba et al., 2009). These geochemical characteristics are also seen in rocks of the mafic association of the Tartoq Group, which suggests that they are intermediate between MORB and IAT with a possible relation to a BAB environment. It can be argued that rocks formed in a BAB setting are more likely to be preserved than true MORB, because the BAB crust will tend to be thinner and is already located in a collisional setting (Martinez and Taylor, 2003; Taylor and Martinez, 2003). Many of the best-preserved sections of oceanic crust formed in SSZ settings and show a shift from MORB to IAT geochemical signatures, as seen in fore-arcs and back-arcs (Dilek and Polat, 2008). The Izu-Bonin-Mariana arc-trench system is considered the best modern analogue for formation of SSZ oceanic crust and such small SSZ island arc complexes could be a modern analogue for many Archaean volcanic rocks of oceanic arc origin (Pearce, 2003; Dilek and Furnes, 2011).

The SSZ setting indicated by the geochemical data of the Tartoq Group is consistent with the subhorizontal structural data (Kisters et al., 2011), which suggests lateral accretion in an arc-trench environment. As Shervais (2001) emphasized, most characteristic SSZ oceanic crust, present and past, formed in a fore-arc, which is the main environment of accretion and imbrication of MORB and IAT rocks. This setting is consistent with the trend observed in the Th/Yb–Nb/Yb diagram (Fig. 7). Because it is widely accepted that subduction zones have been operating since around 3200 Ma (Condie, 1981; De Wit, 1998; Shervais, 2001; Smithies et al., 2005; Kerrich and Polat, 2006; Moyen et al., 2006; Van Kranendonk et al., 2007; Pease et al., 2008; Windley and Garde, 2009) and possibly even as early as 3800 Ma (Komiya et al., 1999; Polat et al., 2002; Dilek and Polat, 2008; Furnes et al., 2009; Friend and Nutman, 2010) it is reasonable to assume that the Tartoq Group represents oceanic crust, which formed in a modern-style SSZ environment. It is worth nothing that according to the geochemical classification of Dilek and Furnes (2011), the Tartoq Group qualifies as being a subduction-related ophiolite (Jenner et al., 2008), if the field relationships are accepted to represent a section through oceanic crust (Section 6.1), as previously proposed by Szilas et al. (2011).

6.3. ^{176}Lu – ^{176}Hf and ^{147}Sm – ^{143}Nd isotope systematics

The Lu–Hf and Sm–Nd isotope systems are used to constrain isochron diagrams. However, only a co-genetic suite of samples unaffected by metamorphic disturbance provides reliable age information. Therefore, the felsic schist sample (510839) was excluded from the errorchron regression, because it contains components originating from reworked younger TTG gneisses. In addition, the serpentinite sample (510766) was omitted from the Lu–Hf and Sm–Nd errorchrons, because its origin is unclear, as it could be either a co-genetic cumulate associated with the mafic rocks or a vestige of a mantle enclave. Figs. 8 and 9 show ^{176}Lu – ^{176}Hf and ^{147}Sm – ^{143}Nd errorchron diagrams, respectively. The samples defining the best-fit errorchrons are listed in Supplementary Data Table 3.

Plotting all mafic samples on the errorchron, yields a ^{176}Lu – ^{176}Hf errorchron age of 3015 ± 240 Ma (MSWD = 15). For the best-fit ^{176}Lu – ^{176}Hf errorchron two greenstones (510906 and 510907) were excluded from the array, because their Lu–Hf isotope compositions were likely disturbed either by alteration or by tectonic mixing with TTG. Sample 510907 has extensive carbonate alteration and sample 510906 was collected a few metres from the former, so both have likely been affected by hydrothermal alteration. This is supported by their relatively high $\text{Al}_2\text{O}_3/(\text{CaO} + \text{Na}_2\text{O} + \text{K}_2\text{O})$ compared with the other mafic samples. An alternative explanation for these two outliers is that they are not co-magmatic with the rest of the Tartoq Group. When excluding these two samples (510906 and 510907) the mafic samples define a best-fit six-point Lu–Hf errorchron at $3189 \text{ Ma} \pm 65 \text{ Ma}$ (MSWD = 1.9) with an initial $\varepsilon_{\text{Hf}}(3190 \text{ Ma})$ of $+4.1 \pm 1.6$. This age is taken as the best estimate for the formation of the mafic association of the Tartoq Group.

When plotting all mafic samples a ^{147}Sm – ^{143}Nd errorchron yields an age of 3285 ± 1000 Ma (MSWD = 25). For the best-fit ^{147}Sm – ^{143}Nd errorchron a greenschist (510885) and a gabbro (510708) sample were excluded, in addition to the two altered samples (510906 and 510907) mentioned above, because of likely disturbance as seen by deviation from the errorchron array (Fig. 9). However, no petrographic or geochemical evidence was found for this deviation, which suggests a significant disturbance of the Sm–Nd isotopic system compared with the Lu–Hf system. The best-fit four-point Sm–Nd errorchron yields an age of 3068 ± 220 Ma (MSWD = 1.18) with an initial $\varepsilon_{\text{Nd}}(3190 \text{ Ma})$ of $+3.1 \pm 0.6$.

Initial $\varepsilon_{\text{Hf}}(3190 \text{ Ma})$ value of $+4.1 \pm 1.6$ and $\varepsilon_{\text{Nd}}(3190 \text{ Ma})$ of $+3.1 \pm 0.6$ for the best-fit errorchrons, provide evidence for a juvenile mantle source. As there are no systematic variations of the initial $\varepsilon_{\text{Hf}}(3190 \text{ Ma})$ and $\varepsilon_{\text{Nd}}(3190 \text{ Ma})$ values with contamination-sensitive

trace element ratios such as Th/Yb and Nb/Nb* (Fig. 12) the mafic association likely represents pristine mantle-derived rocks with no evidence of contamination by older crustal components.

6.4. U–Pb geochronology

Nutman and Kalsbeek (1994) published a U–Pb zircon age of 2944 ± 7 Ma for an intrusive TTG sheet in the southern part of the Ilerlak block that provides a minimum age of the Tartoq Group. We here confirm the minimum Mesoarchaeon age of the Tartoq Group and extend this back to 2986 ± 4 Ma with sample 510772, which is an intrusive TTG sheet on the northern contact of the Amitsuaarsua block. Our Lu–Hf and Sm–Nd isotope data (Section 6.3), which suggest an age of c. 3190 Ma for the Tartoq Group, is consistent with the minimum ages provided by the intrusive TTG sheets.

Nutman et al. (2004) proposed that the Tartoq Group might be a composite supracrustal belt with different ages, because of young zircons (2842 ± 6 Ma) within the felsic schists, which are thus much younger than the above intrusive minimum ages. However, the felsic schists of the Tartoq Group were previously regarded as syn-volcanic metasediments (Higgins, 1968) or felsic volcanics (Petersen, 1992). This is inconsistent with field relationships in which the felsic schists commonly occur as mylonitised slivers within shear zones bounding prominent tectonostratigraphic packages that make up individual belts (Sections 5.1 and 6.1). This structural imbrication of gneisses with the greenschists may explain the younger ages, during which intrusive TTG gneisses and/or older basement were imbricated into the Tartoq Group during juxtaposition of the TTG–supracrustal sequence (Kisters et al., 2011). A composite supracrustal belt is also not supported by the Lu–Hf and Sm–Nd data (Section 6.3), which suggest the various blocks were coeval. The data from the TTG gneiss sample 510657 west of Nuuluk with an age of 2867 ± 17 Ma (interpreted as an intrusive age) clearly shows that the felsic schists could have incorporated young zircons during deformation and thrusting of the surrounding TTG gneisses under cataclastic to mylonitic conditions when they were intruded or sheared into the mafic supracrustal blocks. To sum up, the felsic schists are not metasediments and are not part of the primary Tartoq Group volcanic sequence due to their younger zircon ages and their elemental data (Sections 5.2 and 6.2) show that they have the exact same geochemistry as the TTG gneisses in this region.

7. Conclusions

Our detailed work on field relations, petrology, geochronology and geochemistry, combined with earlier work on the metamorphism and structure of the Tartoq Group, leads us to conclude that the Tartoq Group of SW Greenland represents a section through Archaean oceanic crust. In particular:

1. The rocks of the Tartoq Group range from subaqueous lava flows, to shallow mafic sills/dykes, to deeper level gabbroic intrusives, and to harzburgitic cumulates or mantle. This assemblage is consistent with the lithological units that are expected in a section through oceanic crust (Dilek, 2003; Dilek and Furnes, 2011).
2. Whole rock Lu–Hf and Sm–Nd isotope data from different blocks and various lithological units, indicate that the Tartoq Group is a coeval suite of rocks, with a formation age of c. 3190 Ma. This age is supported by a U–Pb zircon age of 2986 ± 4 Ma from TTG gneiss that was intrusive into the Tartoq Group and thus provides a minimum age. As reported above (Section 6.4) the minimum age of the felsic schists is too young for them to be part of the Tartoq Group, because convincing intrusive TTG gneisses are significantly older. Thus, the Tartoq Group is comprised exclusively of mafic and ultramafic rocks, which formed as a coeval suite and the felsic schists thus represent tectonic slivers of TTG gneiss consistent with field relationships (Section 6.1).

3. The mafic supracrustal rocks of the Tartoq Group are a geochemically consistent and co-magmatic suite with MgO contents of 4.2–16.5 wt.%, Fe_2O_3 of 5.7–17.3 wt.% and TiO_2 of 0.3–1.6 wt.%. They have relatively flat chondrite-normalized REE patterns with $\text{La}_{\text{CN}}/\text{Sm}_{\text{CN}}$ of 0.67–1.96 and flat primitive mantle-normalized multi-element patterns. The negative Nb-anomalies together with Th/Yb ratios of 0.06–0.47 are consistent with an arc affinity rather than a modern MORB setting and thus similar to other examples of arc-related Archaean supracrustal rocks (Dilek and Polat, 2008; Dilek and Furnes, 2011).

The co-magmatic and coeval nature of this lithological sequence, as pointed out above, suggests that the Tartoq Group represents a section through Archaean oceanic crust. Compositions are furthermore similar to those of the Isua and Ivsaartoq supracrustal belts of SW Greenland (Polat et al., 2011), for which a SSZ setting was viably demonstrated. A SSZ setting also agrees well with the style of subsequent deformation and metamorphism, for which the horizontal fabrics, shear zones with consistent sense of displacement, folds with consistent vergence, and exceptional range of metamorphic conditions are commensurate with those of a convergent margin that has undergone collision tectonics. As stated previously, a back-arc or preferably a fore-arc setting proposed here for the Tartoq Group is a favorable environment for accretion of such rocks.

Although different alternative tectonic settings have been proposed for Archaean mafic sequences (e.g. Zegers and Van Keken, 2001; Bédard, 2006; Van Kranendonk, 2011), the data from the Tartoq Group are entirely consistent with a modern-style SSZ environment, suggesting that some form of plate tectonics has been in operation since at least around 3200 Ma, in support of earlier work from Mesoarchaeon rocks (e.g. Condie, 1981; De Wit, 1998; Smithies et al., 2005; Kerrich and Polat, 2006; Moyen et al., 2006; Condie and Kröner, 2008; Pease et al., 2008).

We thus consider that the similar trace element geochemistry and isotopic compositions of the Mesoarchaeon Tartoq Group mafic association consisting of pillow lavas, sills/dykes and gabbros demonstrate a co-magmatic sequence, which we in turn interpret to have formed as oceanic crust in a suprasubduction zone geodynamic environment.

Supplementary materials related to this article can be found online at doi:10.1016/j.gr.2011.11.006.

Acknowledgements

We acknowledge the critical reviews by R. Kerrich and C.R.L. Friend, which greatly improved the present paper. We also acknowledge the editorial handling of the manuscript by M. Santosh and particularly guest editor A. Polat. We thank the Geological Survey of Denmark and Greenland (GEUS) for permission to publish this work. We acknowledge the Greenland Bureau of Minerals and Petroleum (BMP) for financial support of the field and analytical work. K. Szilas thanks Geocenter Denmark for funding his Ph.D. project with the title “Archaean supracrustal belts of SW Greenland”, which this work forms part. V.J. van Hinsberg acknowledges financial support from the European Union Seventh Framework Program (FP7/2007–2013) under grant agreement no. 254015. J.E. Hoffmann was supported by Grant Mu 1406/08 of the DFG (German Research Foundation). A. Scherstén acknowledges financial support from the Swedish Research Council through grant #2008-3447. Contribution to IGCP project 599.

References

- Aftalion, M., Bowes, D.R., Vřana, S., 1989. Early Carboniferous U–Pb zircon ages for garnetiferous perpotassic granulites, Blanský les massif, Czechoslovakia. *Neues Jahrbuch für Mineralogie, Monatshefte* 4, 145–152.
- Appel, P.W.U., 1984. An iron-formation in the Precambrian Tartoq Group, South-West Greenland. *Rapport Grønlands Geologiske Undersøgelse* 120, 74–78.
- Appel, P.W.U., Secher, K., 1984. On gold mineralization in the Precambrian Tartoq Group, SW Greenland. *Journal of the Geological Society of London* 141, 273–278.

- Arndt, N.T., 1994. Archean komatiites. In: Condie, K.C. (Ed.), *Archean crustal evolution*. Elsevier, Amsterdam, pp. 11–44.
- Arndt, N.T., Kerr, A.C., Tarney, J., 1997. Dynamic melting in plume heads: the formation of Gorgona komatiites and basalts. *Earth and Planetary Science Letters* 146, 289–301.
- Baier, J., Audébert, A., Keppler, H., 2008. The origin of the negative niobium tantalum anomaly in subduction zone magmas. *Earth and Planetary Science Letters* 267, 290–300.
- Bédard, J.H., 2006. A catalytic delamination-driven model for coupled genesis of Archean crust and sub-continental lithospheric mantle. *Geochimica et Cosmochimica Acta* 70, 1188–1214.
- Berthelsen, A., Henriksen, N., 1975. Geological map of Greenland, 1:100,000 Ivittuat 61 V.1 Syd (with description). Geological Survey of Greenland, Copenhagen. (169 pp).
- Blichert-Toft, J., Boyet, M., Télouk, P., Albarède, F., 2002. Sm–147Nd–143 and Lu–176Hf–176 in eucrites and the differentiation of the HED parent body. *Earth and Planetary Science Letters* 204, 167–181.
- Bouvier, A., Vervoort, J.D., Patchett, P.J., 2008. The Lu–Hf and Sm–Nd isotopic composition of CHUR: Constraints from unequilibrated chondrites and implications for the bulk composition of terrestrial planets. *Earth and Planetary Science Letters* 273, 48–57.
- Boynton, W.V., 1984. Cosmochemistry of the rare earth elements: meteorite studies. In: Henderson, P. (Ed.), *Rare Earth Element Geochemistry*. Elsevier, Amsterdam, pp. 63–114.
- Cabanis, B., Lecolle, M., 1989. Le diagramme La/10-Y/15-Nb/8: un outil pour la discrimination des séries volcaniques et la mise en évidence des processus de mélange et/ou de contamination crustale. *Compte Rendus Académie Science Séries II*, pp. 2023–2029.
- Condé, K.C., 1981. *Archean Greenstone Belts*. Elsevier, Amsterdam. (435 pp).
- Condé, K.C., 1985. Secular variation in the composition of basalts: an index to mantle evolution. *Journal of Petrology* 26, 545–563.
- Condé, K.C., Kröner, A., 2008. When did plate tectonics begin? Evidence from the geological record. In: Condé, K.C., Pease, V. (Eds.), *When did Plate Tectonics begin on Planet Earth? : Geological Society of America, Special Paper*, 440, pp. 281–294.
- Condé, K.C., Kröner, A., 2011. The building blocks of continental crust: Evidence for a major change in the tectonic setting of continental growth at the end of the Archean. *Gondwana Research*. doi:10.1016/j.gr.2011.09.011.
- Davies, G.F., 1999. *Dynamic Earth Plates, Plumes and Mantle Convection*. Cambridge University Press. (458 pp).
- De Wit, M.J., 1998. On Archean granites, greenstones, cratons, and tectonics: does the evidence demand a verdict? *Precambrian Research* 91, 181–226.
- De Wit, M.J., Hart, R.A., Hart, R.J., 1987. The Jamestown Ophiolite Complex, Barberton mountain belt: a section through 3.5 Ga oceanic crust. *Journal of African Earth Sciences* 6, 681–730.
- Dilek, Y., 2003. Ophiolite concept and its evolution. In: Dilek, Y., Newcomb, S. (Eds.), *Ophiolite concept and the evolution of geological thought: Geological Society of America, Special Paper*, 373, pp. 1–16.
- Dilek, Y., Furnes, H., 2011. Ophiolite genesis and global tectonics: geochemical and tectonic fingerprinting of ancient oceanic lithosphere. *Geological Society of America Bulletin* 123, 387–411.
- Dilek, Y., Polat, A., 2008. Suprasubduction zone ophiolites and Archean tectonics. *Geology* 36, 431–432.
- Eisele, J., Sharma, M., Galer, S.J.G., Blichert-Toft, J., Devey, C.W., Hofmann, A.W., 2002. The role of sediment recycling in EM-1 inferred from Os, Pb, Hf, Nb, Sr isotope and trace element systematics of the Pitcairn hotspot. *Earth and Planetary Science Letters* 196, 197–212.
- Evans, D.M., King, A.R., 1993. Sediment and shear-hosted gold mineralization of the Tartoq Group supracrustals, southwest Greenland. *Precambrian Research* 62, 61–82.
- Frei, D., Gerdes, A., 2009. Precise and accurate in situ U–Pb dating of zircon with high sample throughput by automated LA-SF-ICP-MS. *Chemical Geology* 261, 261–270.
- Frei, R., Rosing, M.T., Waight, T.E., Ulffbeck, D.G., 2002. Hydrothermal-metasomatic and tectono-metamorphic processes in the Isua supracrustal belt (West Greenland): a multi-isotopic investigation of their effects on the Earth's oldest oceanic crustal sequence. *Geochimica et Cosmochimica Acta* 66, 467–486.
- Frei, D., Hollis, J.A., Gerdes, A., Harlov, D., Karlsson, C., Vasquez, P., Franz, G., Johansson, L., Knudsen, C., 2006. Advanced in-situ trace element and geochronological microanalysis of geomaterials by laser ablation techniques. *Geological Survey of Denmark and Greenland Bulletin* 10, 25–28.
- Friend, C.R.L., Nutman, A.P., 2010. Eoarchean ophiolites? New evidence for the debate on the Isua supracrustal belt, southern West Greenland. *American Journal of Science* 310, 826–861.
- Furnes, H., de Wit, M., Staudigel, H., Rosing, M., Muehlenbachs, K., 2007. A vestige of Earth's oldest ophiolite. *Science* 315, 1704–1707.
- Furnes, H., Rosing, M., Dilek, Y., De Wit, M., 2009. Isua supracrustal belt (Greenland) – A vestige of a 3.8 Ga suprasubduction zone ophiolite, and the implications for Archean geology. *Lithos* 113, 115–132.
- Gerdes, A., Zeh, A., 2006. Combined U–Pb and Hf isotope LA–(MC)–ICP–MS analyses of detrital zircons: Comparison with SHRIMP and new constraints for the provenance and age of an Armerian metasediment in Central Germany. *Earth and Planetary Science Letters* 249, 47–61.
- Gill, R.C.O., 1979. Comparative petrogenesis of Archean and modern low-K tholeiites. A critical review of some geochemical aspects. In: Ahrens, L.H. (Ed.), *Origin and Distribution of the Elements*, 2nd ed. : Physics and Chemistry of the Earth, 11. Pergamon, Oxford, pp. 431–447.
- Glikson, A.Y., 1971. Primitive Archean element distribution patterns: chemical evidence and geotectonic significance. *Earth and Planetary Science Letters* 12, 309–320.
- Hamilton, W.B., 1998. Archean magmatism and deformation were not products of plate tectonics. *Precambrian Research* 91, 143–179.
- Hamilton, W.B., 2007. Comment on “A vestige of Earth's oldest ophiolite”. *Science* 318, 746d.
- Hamilton, W.B., 2011. Plate tectonics began in Neoproterozoic time, and plumes from deep mantle have never operated. *Lithos* 123, 1–20.
- Hart, S.R., Brooks, C., 1977. The geochemistry and evolution of Early Precambrian mantle. *Contributions to Mineralogy and Petrology* 61, 109–128.
- Hart, S.R., Brooks, C., Krogh, T.E., Davis, G.L., Nava, D., 1970. Ancient and modern volcanic rocks: A trace element model. *Earth and Planetary Science Letters* 10, 17–28.
- Higgins, A.K., 1968. The Tartoq Group on Nuna Qaqortoq and in the Ilerdlak area, South-West Greenland: Rapport Grønlands Geologiske Undersøgelse, 17 (17 pp).
- Higgins, A.K., 1990. Descriptive text to 1:100000 sheets Neria 61 V.1 N and Midternæs 61 V.2 N. Geological Survey of Greenland. (23 pp).
- Higgins, A.K., Bondesen, E., 1966. Supracrustals of pre-Ketilidian age (the Tartoq Group) and their relationships with Ketilidian supracrustals in the Ivigtut region, South-West Greenland: Rapport Grønlands Geologiske Undersøgelse, 8 (21 pp).
- Hoffmann, J.E., Münker, C., Polat, A., Rosing, M.T., Schulz, T., 2011. The origin of decoupled Hf–Nd isotope compositions in Eoarchean rocks from southern West Greenland. *Geochimica et Cosmochimica Acta* 75, 6610–6628.
- Horstwood, M.S.A., Foster, G.L., Parrish, R.R., Noble, S.R., Nowell, G.M., 2003. Common-Pb corrected in situ U–Pb accessory mineral geochronology by LA–MC–ICP–MS. *Journal of Analytical Atomic Spectrometry* 18, 837–846.
- Irvine, T.N., Baragar, W.R.A., 1971. A guide to the chemical classification of the common volcanic rocks. *Canadian Journal of Earth Sciences* 8, 523–548.
- Jackson, S., Pearson, N.J., Griffin, W.L., Belousova, E.A., 2004. The application of laser ablation – inductively coupled plasma – mass spectrometry to in situ U–Pb zircon geochronology. *Chemical Geology* 211, 47–69.
- Janosek, V., Farrow, C.M., Erban, V., 2006. Interpretation of whole-rock geochemical data in igneous geochemistry: introducing Geochemical Data Tool (GCDKit). *Journal of Petrology* 47, 1255–1259.
- Jenner, F.E., Bennett, V.C., Nutman, A.P., Friend, C.R.L., Norman, M.D., Yaxley, G., 2008. Evidence for subduction at 3.8 Ga: geochemistry of arc-like metabasalts from the southern edge of the Isua Supracrustal Belt. *Chemical Geology* 261, 83–98.
- Jensen, L.S., 1976. A New Cation Plot for Classifying Subalkalic Volcanic Rocks. *Ontario Geological Survey Miscellaneous Paper* 66.
- Kerrick, R., Polat, A., 2006. Archean greenstone-tonalite duality: thermodynamic mantle convection models or plate tectonics in the early Earth global dynamics. *Tectonophysics* 415, 141–165.
- Kerrick, R., Polat, A., Xie, Q., 2008. Geochemical systematics of 2.7 Ga Korojovis Group (Abitibi), and Manitouwadge and Winston Lake (Wawa) Fe-rich basalt-rhyolite associations: Barcarc rift oceanic crust? *Lithos* 101, 1–23.
- King, A.R., 1985. Greenex A/S Sermiligarsuk exploration concession. Report on geological field work carried out in the Sermiligarsuk Fjord area, South-west Greenland, July–August 1984. (Greenex A/S, 142 pp).
- Kisters, A.F.M., Szilas, K., Van Hinsberg, V.J., 2011. Structural geology and emplacement of the Tartoq Group, SW Greenland. In: Kolb, J. (Ed.), *Controls of Hydrothermal Quartz Vein Mineralisation and Wall-rock Alteration in the Paamiut and Tartoq Areas, South-West Greenland*. Danmarks og Grønlands Geologiske Undersøgelse Rapport, (in review).
- Komiya, T., Maruyama, S., Masuda, T., Nohda, S., Hayashi, M., Okamoto, K., 1999. Plate tectonics at 3.8–3.7 Ga: field evidence from the Isua accretionary complex, southern West Greenland. *Journal of Geology* 107, 515–554.
- Kusky, T.M., Li, J.-H., Tucker, R.D., 2001. The Archean Dongwanzi Ophiolite Complex, North China Craton: 2.505-billion-year-old oceanic crust and mantle. *Science* 292, 1142–1145.
- Kusky, T.M., Lu, W., Dilek, Y., Robinson, P., Peng, S., Huang, X., 2011. Application of the modern ophiolite concept with special reference to Precambrian ophiolites. *Science China Earth Science* 54, 315–341.
- Lagos, M., Scherer, E.E., Tomaschek, F., Münker, C., Keiter, M., Berndt, J., Ballhaus, C., 2007. High precision Lu–Hf geochronology of Eocene eclogite-facies rocks from Syros, Cyclades, Greece. *Chemical Geology* 243, 16–35.
- Lowe, D.R., Byerly, G.R., 2007. An overview of the geology of the Barberton Greenstone Belt and vicinity: implications for early crustal development. In: Van Kranendonk, M.J., Smithies, R.H., Bennett, V.C. (Eds.), *Earth's Oldest Rocks. : Developments in Precambrian Geology*, vol. 15. Elsevier, Amsterdam, pp. 481–526.
- Ludwig, K.R., 2003. *Isoplot/Ex 3.00. A Geochronological Toolkit for Microsoft Excel*. Special Publication 4. Berkeley Geochronological Center, Berkeley, CA.
- Lugmair, G.W., Marti, K., 1978. Lunar initial 143Nd/144Nd: differential evolution of the lunar crust and mantle. *Earth and Planetary Science Letters* 39, 349–357.
- Manikyamba, C., Kerrich, R., Khanna, T.C., Satyanarayanan, M., Krishna, A.K., 2009. Enriched and depleted arc basalts, with Mg-andesites and adakites: A potential paired arc-back-arc of the 2.6 Ga Huttu greenstone terrane, India. *Geochimica et Cosmochimica Acta* 73, 1711–1736.
- Martin, H., Smithies, R.H., Rapp, R., Moya, J.-F., Champion, D., 2005. An overview of adakite, tonalite-trondhjemite-granodiorite (TTG) and sanukitoid: relationships and some implications for crustal evolution. *Lithos* 79, 1–24.
- Martinez, F., Taylor, B., 2003. Controls on back-arc crustal accretion: insights from the Lau, Manus and Mariana basins. In: Larter, R.D., Leat, P.T. (Eds.), *Intra-Oceanic Subduction Systems: Tectonic and Magmatic Processes: Geological Society of London, Special Publications*, 219, pp. 19–54.
- McCall, G.J.H., 2003. A critique of the analogy between Archean and Phanerozoic tectonics based on regional mapping of the Mesozoic–Cenozoic plate convergent zone in the Makran, Iran. *Precambrian Research* 127, 5–17.
- McCammon, C., 2005. The paradox of mantle redox. *Science* 308, 807–808.
- Metcalfe, R.V., Shervais, J.W., 2008. Suprasubduction-zone ophiolites: Is there really an ophiolite conundrum? In: Wright, J.E., Shervais, J.W. (Eds.), *Ophiolites, Arcs, and Batholiths: A Tribute to Cliff Hopson: Geological Society of America, Special Paper*, 438, pp. 191–222.

- Moyen, J.-F., 2011. The composite Archaean grey gneisses: Petrological significance, and evidence for a non-unique tectonic setting for Archaean crustal growth. *Lithos* 123, 21–36.
- Moyen, J.-F., Stevens, G., Kisters, A.F.M., 2006. Record of mid-Archaean subduction from metamorphism in the Barberton terrain, South Africa. *Nature* 442, 559–562.
- Münker, C., Weyer, S., Scherer, E., Mezger, K., 2001. Separation of high field strength elements (Nb, Ta, Zr, Hf) and Lu from rock samples for MC-ICPMS measurements. *Geochemistry, Geophysics, Geosystems* 2 (G3). doi:10.1029/2001GC000183.
- Nutman, A.P., Friend, C.R.L., 2007. Comment on “A vestige of Earth's oldest ophiolite”. *Science* 318, 746c.
- Nutman, A.P., Kalsbeek, F., 1994. A minimum age of 2944 ± 7 Ma for the Tartoq Group, South-West Greenland. *Rapport Grønlands Geologiske Undersøgelse* 161, 35–38.
- Nutman, A.P., Friend, C.R.L., Barker, S.L.L., McGregor, V.R., 2004. Inventory and assessment of Palaeoarchaean gneiss terrains and detrital zircons in southern West Greenland. *Precambrian Research* 135, 281–314.
- Pearce, J.A., 1996. A user's guide to basalt discrimination diagrams. In: Wyman, D.A. (Ed.), *Trace Element Geochemistry of Volcanic Rocks: Applications for Massive Sulphide Exploration*: Geological Association of Canada, 12, pp. 79–113 (short course notes).
- Pearce, J.A., 2003. Supra-subduction zone ophiolites: The search for modern analogues. In: Dilek, Y., Newcomb, S. (Eds.), *Ophiolite Concept and the Evolution of Geological Thought*: Geological Society of America Special Paper, 373, pp. 269–293.
- Pearce, J.A., 2008. Geochemical fingerprinting of oceanic basalts with applications to ophiolite classification and the search for Archean oceanic crust. *Lithos* 100, 14–48.
- Pearce, J.A., Cann, J.R., 1973. Tectonic setting of basic volcanic rocks determined using trace element analyses. *Earth and Planetary Science Letters* 19, 290–300.
- Pearce, J.A., Norry, M.J., 1979. Petrogenetic implications of Ti, Zr, Y, and Nb variations in volcanic rocks. *Contributions to Mineralogy and Petrology* 69, 33–47.
- Pease, V., Percival, J., Smithies, H., Stevens, G., Van Kranendonk, M., 2008. When did plate tectonics begin? Evidence from the orogenic record. In: Condie, K.C., Pease, V. (Eds.), *When did Plate Tectonics Begin on Planet Earth?*: Geological Society of America, Special Paper, 440, pp. 199–208.
- Petersen, J.S., 1992. Nuuluk-Iterlak gold and massive-sulfide project, Taartoq Archaean greenstone belt, SW Greenland. (Field report, Nunaoil A/S, 164 pp).
- Pin, C., Zalduegui, J.F.S., 1997. Sequential separation of light rare-earth elements, thorium and uranium by miniaturized extraction chromatography: Application to isotopic analyses of silicate rocks. *Analytica Chimica Acta* 339, 79–89.
- Polat, A., 2010. Personal communication (conversation) at Sioralik/Bikuben during field work in the summer of 2010 in the Tartoq Group, SW Greenland.
- Polat, A., Hofmann, A.W., 2003. Alteration and geochemical patterns in the 3.7–3.8 Ga Isua greenstone belt, West Greenland. *Precambrian Research* 126, 197–218.
- Polat, A., Hofmann, A.W., Rosing, M.T., 2002. Boninite-like volcanic rocks in the 3.7–3.8 Ga Isua greenstone belt, West Greenland: geochemical evidence for intra-oceanic subduction zone processes in the early Earth. *Chemical Geology* 184, 231–254.
- Polat, A., Appel, P.W.U., Fryer, B.J., 2011. An overview of the geochemistry of Eoarchean to Mesoarchean ultramafic to mafic volcanic rocks, SW Greenland: Implication for mantle depletion and petrogenetic processes at subduction zones in the early Earth. *Gondwana Research* 20, 255–283.
- Rollinson, H.R., 1993. *Using Geochemical Data: Evaluation, Presentation, Interpretation*. Longman, UK (352 pp).
- Rudnick, R.L., Fountain, D.M., 1995. Nature and composition of the continental crust – a lower crustal perspective. *Reviews of Geophysics* 33, 267–309.
- Sambridge, M., Lambert, D.D., 1997. Propagating errors in decay equations: Examples from the Re–Os isotopic system. *Geochimica et Cosmochimica Acta* 61, 3019–3024.
- Scherer, E., Münker, C., Mezger, K., 2001. Calibration of the lutetium–hafnium clock. *Science* 293, 683–687.
- Servais, J.W., 2001. Birth, death, and resurrection: The life cycle of suprasubduction zone ophiolites. *Geochemistry, Geophysics, Geosystems* 2 (G3). doi:10.1029/2000GC000080.
- Smithies, R.H., Champion, D.C., Van Kranendonk, M.J., Howard, H.M., Hickman, A.H., 2005. Modern-style subduction processes in the Mesoarchaean: geochemical evidence from the 3.12 Ga Whundo intraoceanic arc. *Earth and Planetary Science Letters* 231, 221–237.
- Söderlund, U., Patchett, P.J., Vervoort, J.D., Isachsen, C.E., 2004. The ¹⁷⁶Lu decay constant determined by Lu–Hf and U–Pb isotope systematics of Precambrian mafic intrusions. *Earth and Planetary Science Letters* 219, 311–324.
- Stacey, J.S., Kramers, J.D., 1975. Approximation of terrestrial lead isotope evolution by a two-stage model. *Earth and Planetary Science Letters* 26, 207–221.
- Stern, R.J., 2005. Evidence from ophiolites, blueschists, and ultrahigh-pressure metamorphic terranes that the modern episode of subduction tectonics began in Neoproterozoic time. *Geology* 33, 557–560.
- Stern, R.J., 2008. Modern-style plate tectonics began in Neoproterozoic time: an alternative interpretation of Earth's tectonic history. In: Condie, K.C., Pease, V. (Eds.), *When did Plate Tectonics Begin on Planet Earth?*: Geological Society of America, Special Paper, 440, pp. 265–280.
- Sun, S., McDonough, W.F., 1989. Chemical and isotopic systematics of oceanic basalts: implications for mantle composition and processes. In: Saunders, A.D., Norry, M.J. (Eds.), *Magmatism in the Ocean Basins*: Geological Society London, Special Publications, 42, pp. 313–345.
- Szilas, K., Van Hinsberg, V.J., Kisters, A.F.M., Kokfelt, T.F., Scherstén, A., Windley, B.F., 2011. Remnants of Mesoarchaean oceanic crust in the Tartoq Group, South-West Greenland. *Geological Survey of Denmark and Greenland Bulletin* 23, 57–60.
- Taylor, B., Martinez, F., 2003. Back-arc basin basalt systematics. *Earth and Planetary Science Letters* 210, 481–497.
- Van Hinsberg, V.J., Szilas, K., Kisters, A.F.M., 2010. The Tartoq Group, SW Greenland: Mineralogy, textures and a preliminary metamorphic to hydrothermal history. *Danmarks og Grønlands Geologiske Undersøgelse Rapport 2010/120*. (52 pp).
- Van Kranendonk, M.J., 2011. Onset of plate tectonics. *Science* 333, 413–414.
- Van Kranendonk, M.J., Smithies, R.H., Hickman, A.H., Champion, D.C., 2007. Secular tectonic evolution of Archean continental crust: interplay between horizontal and vertical processes in the formation of the Pilbara Craton, Australia. *Terra Nova* 19, 1–38.
- Van Kranendonk, M.J., Kröner, A., Hegner, E., Connelly, J., 2009. Age, lithology and structural evolution of the c. 3.53 Ga Theespruit Formation in the Tjakastad area, southwestern Barberton Greenstone Belt, South Africa, with implications for Archean tectonics. *Chemical Geology* 261, 114–138.
- Vervoort, J.D., Patchett, P.J., Söderlund, U., Baker, M., 2004. Isotopic composition of Yb and the determination of Lu concentrations and Lu/Hf ratios by isotope dilution using MC-ICPMS. *Geochemistry, Geophysics, Geosystems* 5 (G3). doi:10.1029/2004GC000721.
- Weyer, S., Münker, C., Rehkämper, M., Mezger, K., 2002. Determination of ultra-low Nb, Ta, Zr and Hf concentrations and the chondritic Zr/Hf and Nb/Ta ratios by isotope dilution analyses with multiple collector ICP-MS. *Chemical Geology* 187, 295–313.
- Winchester, J.A., Floyd, P.A., 1977. Geochemical discrimination of different magma series and their differentiation products using immobile elements. *Chemical Geology* 20, 325–343.
- Windley, B.F., Garde, A.A., 2009. Arc-generated blocks with crustal sections in the North Atlantic craton of West Greenland: crustal growth in the Archean with modern analogues. *Earth-Science Reviews* 93, 1–30.
- Wood, D.A., 1980. The application of a Th–Hf–Ta diagram to problems of tectonomagmatic classification and to establishing the nature of crustal contamination of basaltic lavas of the British Tertiary volcanic province. *Earth and Planetary Science Letters* 50, 11–30.
- Zegers, T.E., Van Keken, P.E., 2001. Middle Archean continent formation by crustal delamination. *Geology* 29, 1083–1086.
- Zhai, M., Zhao, G., Zhang, Q., 2002. Is the Dongwanzi complex an Archean ophiolite? *Science* 295, 923a.
- Zhao, G., Wilde, S.A., Li, Sanzhong, L., Sun, M., Grant, M.L., Li, X., 2007. U–Pb zircon age constraints on the Dongwanzi ultramafic–mafic body, North China, confirm it is not an Archean ophiolite. *Earth and Planetary Science Letters* 255, 85–93.

Supplementary material for Paper I

Supplementary data table 1 (Paper I): Major and trace element data

Sample	Lithology	Locality	Latitude	Longitude
510601	Gabbro	Nuuluk	61.4387083	-48.7869783
510619	Greenschist	Nuuluk	61.4371533	-48.8011583
510624	Felsic Schist	Nuuluk	61.4376033	-48.7995867
510625	Felsic Schist	Nuuluk	61.4381400	-48.7994567
510626	Felsic Schist	Nuuluk	61.4399983	-48.7990450
510627	Greenschist	Nuuluk	61.4270717	-48.7997533
510631	Greenschist	Nuuluk	61.4260033	-48.7970417
510632	Greenschist	Nuuluk	61.4251783	-48.7959733
510633	Greenstone	Nuuluk	61.4250833	-48.7955600
510636	Greenstone	Nuuluk	61.4249167	-48.7952367
510637	Greenstone	Nuuluk	61.4249150	-48.7946983
510638	Greenstone	Nuuluk	61.4247417	-48.7941233
510657	TTG Gneiss	Nuuluk	61.4255883	-48.8738133
510662	Amphibolite	Nuuluk	61.4254833	-48.8466950
510663	Amphibolite	Nuuluk	61.4258200	-48.8467617
510664	Amphibolite	Nuuluk	61.4280683	-48.8472383
510665	Amphibolite	Nuuluk	61.4289983	-48.8445000
510670	Felsic Schist	Ilerlak	61.5725900	-48.5744483
510671	Amphibolite	Ilerlak	61.5715817	-48.5775717
510673	Amphibolite	Ilerlak	61.5781317	-48.5662667
510674	Felsic Schist	Ilerlak	61.5793807	-48.5778581
510684	Gabbro	Ilerlak	61.5824283	-48.5840883
510687	Amphibolite	Ilerlak	61.5831017	-48.5862983
510690	Gabbro	Ilerlak	61.5847000	-48.5868750
510707	Amphibolite	Ilerlak	61.5828500	-48.5868033
510708	Gabbro	Ilerlak	61.5825317	-48.5852383
510710	Gabbro	Ilerlak	61.5817217	-48.5860517
510711	Gabbro	Ilerlak	61.5824500	-48.5877817
510714	Amphibolite	Ilerlak	61.5779650	-48.5533067
510722	Greenschist	Ilerlak	61.5738750	-48.5482083
510740	Greenschist	Ilerlak	61.5713383	-48.5806150
510743	TTG Gneiss	Ilerlak	61.5338650	-48.5951467
510744	Amphibolite	Nuna Qaqortoq	61.7248117	-47.8671100
510746	Amphibolite	Nuna Qaqortoq	61.7259408	-47.8649253
510751	Pillow Lava	Nuna Qaqortoq	61.7232933	-47.8643317
510752	Pillow Lava	Nuna Qaqortoq	61.7233633	-47.8672467
510753	Pillow Lava	Nuna Qaqortoq	61.7233633	-47.8672467
510756	Serpentinite	Nuna Qaqortoq	61.7261150	-47.9412683
510760	Serpentinite	Amitsuarsua	61.6266033	-48.3466733
510762	Serpentinite	Amitsuarsua	61.6260300	-48.3381333
510763	Serpentinite	Amitsuarsua	61.6260300	-48.3381333
510765	Serpentinite	Amitsuarsua	61.6260300	-48.3381333
510766	Serpentinite	Amitsuarsua	61.6260300	-48.3381333
510767	Serpentinite	Amitsuarsua	61.6260300	-48.3381333
510768	Serpentinite	Amitsuarsua	61.6260300	-48.3381333
510771	TTG Gneiss	Amitsuarsua	61.6423840	-48.3070285
510772	TTG Gneiss	Amitsuarsua	61.6461717	-48.3084050
510780	Serpentinite	Bikuben	61.4988567	-48.3301817
510783	Amphibolite	Bikuben	61.5008050	-48.3316350
510784	Serpentinite	Bikuben	61.5020733	-48.3313483
510785	Serpentinite	Bikuben	61.5022650	-48.3322917
510789	Amphibolite	Bikuben	61.4893317	-48.3184617

Sample	Lithology	Locality	Latitude	Longitude
510790	Serpentinite	Bikuben	61.4887867	-48.3174533
510793	Serpentinite	Bikuben	61.4778367	-48.2986867
510798	Serpentinite	Bikuben	61.4850233	-48.3102817
510834	Calc-alkaline Greenschist	Iterlak	61.5382850	-48.5787670
510835	Calc-alkaline Greenschist	Iterlak	61.5382850	-48.5787670
510838	Calc-alkaline Greenschist	Iterlak	61.5376900	-48.5797370
510839	Felsic Schist	Iterlak	61.5376400	-48.5798330
510840	Greenschist	Iterlak	61.5373730	-48.5789320
510841	Calc-alkaline Greenschist	Iterlak	61.5369620	-48.5794730
510843	Felsic Schist	Iterlak	61.5364270	-48.5803170
510844	Calc-alkaline Greenschist	Iterlak	61.5363300	-48.5813130
510845	Calc-alkaline Greenschist	Iterlak	61.5362820	-48.5825450
510846	TTG Gneiss	Iterlak	61.5313280	-48.5926200
510860	Greenschist	Nuuluk	61.4235270	-48.8134700
510862	Greenschist	Nuuluk	61.4244800	-48.8116030
510868	Greenschist	Nuuluk	61.4338080	-48.8060870
510870	Greenschist	Nuuluk	61.4183450	-48.8120270
510872	Greenschist	Nuuluk	61.4337420	-48.8077080
510874	Greenschist	Nuuluk	61.4417080	-48.8149330
510878	Greenschist	Nuuluk	61.4371750	-48.8138780
510879	Calc-alkaline Greenschist	Nuuluk	61.4356320	-48.8107580
510885	Greenschist	Nuuluk	61.4308000	-48.8030370
510887	Felsic Schist	Nuuluk	61.4308950	-48.8029250
510891	TTG Gneiss	Nuuluk	61.4086350	-48.8114780
510892	Calc-alkaline Greenschist	Nuuluk	61.4089530	-48.8130750
510893	Greenschist	Nuuluk	61.4296280	-48.8020320
510901	Greenstone	Nuuluk	61.4311750	-48.7871767
510906	Greenschist	Nuuluk	61.4225617	-48.8008800
510947	Felsic Schist	Nuuluk	61.4360683	-48.8011700
510960	Gabbro	Nuuluk	61.4386900	-48.7862933
510961	Greenschist	Nuuluk	61.4376533	-48.7840500
510967	Greenschist	Nuuluk	61.4357050	-48.7806200
510969	TTG Mylonite	Nuuluk	61.4360767	-48.7789767
510970	Greenschist	Nuuluk	61.4365817	-48.7793300
510971	Greenschist	Nuuluk	61.4351683	-48.7801317
510983	Felsic Schist	Nuuluk	61.4446300	-48.7933967
510990	Greenschist	Nuuluk	61.4424533	-48.7842633
510992	Felsic Schist	Nuuluk	61.4424850	-48.7824383
510995	Gabbro	Nuuluk	61.4432550	-48.7762267
510999	Greenschist	Nuuluk	61.4383900	-48.7843367
512251	Calc-alkaline Greenschist	Iterlak	-	-
512252	Calc-alkaline Greenschist	Iterlak	-	-
512255	TTG Gneiss	Nuuluk	-	-
512262	Felsic Schist	Nuuluk	-	-
512263	Greenschist	Nuuluk	-	-
512268	Greenschist	Nuuluk	-	-
512270	TTG Gneiss	Nuuluk	-	-
512272	TTG Mylonite	Nuuluk	-	-
512273	TTG Mylonite	Nuuluk	-	-
512274	TTG Mylonite	Nuuluk	-	-
512275	Greenschist	Nuuluk	-	-
512282	Greenschist	Nuuluk	-	-
512283	Greenstone	Nuuluk	-	-
512284	Greenstone	Nuuluk	-	-

Sample	Lithology	Locality	Latitude	Longitude
512285	Greenstone	Nuuluk	-	-
512286	Greenstone	Nuuluk	-	-
516505	TTG Mylonite	Bikuben	61.4833367	-48.3551283
516509	Amphibolite	Bikuben	61.4930033	-48.3373533
516516	Serpentine	Naalagaaffik	61.5612750	-48.2370217
516518	Gabbro	Naalagaaffik	61.5606233	-48.2370733
516519	TTG Mylonite	Naalagaaffik	61.5601900	-48.2358700
516522	Amphibolite	Naalagaaffik	61.5604250	-48.2257350
510750-1	Pillow Lava	Nuna Qaqortoq	61.7242383	-47.8628983
510750-2	Pillow Lava	Nuna Qaqortoq	61.7242383	-47.8628983
510754-1	Pillow Lava	Nuna Qaqortoq	61.7259017	-47.8616500
510754-2	Pillow Lava	Nuna Qaqortoq	61.7259017	-47.8616500

Sample	SiO ₂	Al ₂ O ₃	Fe ₂ O ₃ *	MgO	CaO	Na ₂ O	K ₂ O	TiO ₂	P ₂ O ₅
Unit	%	%	%	%	%	%	%	%	%
MDL	0.01	0.01	0.04	0.01	0.01	0.01	0.01	0.01	0.01
510601	46.91	16.55	7.66	9.01	13.96	0.77	0.02	0.35	0.02
510619	50.20	13.78	11.37	7.96	8.55	1.99	0.30	0.68	0.06
510624	63.32	15.51	4.63	1.73	3.64	4.04	2.13	0.57	0.18
510625	66.78	15.41	4.62	1.71	1.39	4.31	2.00	0.56	0.18
510626	67.88	15.09	3.99	1.52	1.63	4.37	2.23	0.48	0.17
510627	46.06	17.94	7.05	9.77	12.58	1.39	0.01	0.29	<0.01
510631	44.57	17.21	10.47	10.14	10.40	0.92	0.02	0.58	0.05
510632	49.77	14.70	10.51	8.95	9.85	1.06	0.06	0.40	<0.01
510633	47.97	15.77	13.24	7.60	7.03	3.02	0.14	1.08	0.07
510636	48.74	13.55	13.91	6.70	8.06	2.04	0.17	1.21	0.08
510637	48.86	14.50	14.43	7.07	9.18	2.36	0.17	1.25	0.09
510638	49.59	12.98	16.43	6.48	8.40	2.41	0.24	1.43	0.10
510657	73.16	15.18	0.89	0.30	1.60	4.86	3.29	0.11	0.02
510662	47.44	9.57	10.99	15.46	11.44	1.11	0.42	0.46	0.03
510663	48.20	9.23	10.60	15.50	10.99	1.18	0.55	0.43	0.03
510664	45.86	9.05	11.06	14.96	12.66	1.10	0.81	0.42	0.02
510665	49.12	12.74	14.13	8.25	10.18	2.04	0.53	0.87	0.08
510670	62.77	18.43	4.55	2.50	2.78	1.43	3.37	0.67	0.15
510671	48.91	14.75	13.92	7.50	8.72	1.46	0.10	1.02	0.07
510673	50.00	13.98	13.47	5.48	9.68	2.54	0.10	1.19	0.08
510674	74.39	15.01	1.83	0.82	1.20	1.48	3.00	0.15	0.06
510684	52.49	14.73	5.72	8.49	8.99	4.02	0.86	0.70	0.06
510687	47.05	13.11	11.27	12.43	10.57	1.61	0.34	0.62	0.04
510690	48.67	15.25	10.09	6.90	11.65	2.55	0.70	0.81	0.05
510707	48.42	12.17	11.31	10.64	12.17	1.66	0.15	0.74	0.06
510708	48.84	15.81	7.89	9.42	13.39	1.66	0.50	0.27	0.02
510710	48.78	15.88	8.22	9.10	13.84	1.64	0.33	0.25	0.02
510711	44.72	10.91	13.25	15.82	9.34	0.73	0.12	0.48	0.04
510714	46.83	16.72	11.46	8.84	9.13	2.08	0.11	0.81	0.05
510722	51.13	13.80	13.98	6.20	8.19	0.03	<0.01	0.89	0.07
510740	49.46	14.23	14.25	6.33	10.56	1.52	0.08	1.17	0.09
510743	59.55	16.49	6.22	3.32	4.04	3.84	2.26	0.69	0.18
510744	49.54	15.84	11.50	6.91	11.14	2.66	0.12	0.97	0.07
510746	47.97	14.93	13.07	7.70	10.31	1.99	0.55	1.06	0.08
510751	47.79	14.54	12.41	5.67	13.25	2.48	0.11	0.97	0.07
510752	53.29	16.11	10.18	4.12	9.23	3.09	0.57	1.05	0.05
510753	48.53	16.11	12.05	7.33	11.53	2.11	0.16	0.96	0.07
510756	38.63	2.78	13.59	32.69	1.19	0.02	<0.01	0.12	0.07
510760	42.66	1.02	9.06	33.69	0.09	0.01	<0.01	0.11	0.01
510762	41.35	1.00	9.84	33.76	0.04	<0.01	<0.01	0.11	0.01
510763	38.02	1.23	13.55	30.93	0.12	<0.01	<0.01	0.13	0.02
510765	39.09	1.31	14.40	32.83	0.11	<0.01	0.01	0.18	0.03
510766	37.58	1.09	14.57	34.50	0.05	<0.01	<0.01	0.14	0.02
510767	38.66	1.21	10.36	34.72	0.64	<0.01	<0.01	0.13	0.01
510768	42.47	1.12	14.57	30.66	0.03	<0.01	<0.01	0.11	0.02
510771	61.83	16.47	5.31	1.99	5.78	4.49	0.74	0.77	0.18
510772	59.34	17.61	5.67	3.68	3.47	3.44	1.74	0.47	0.10
510780	40.73	0.83	9.86	33.87	0.85	<0.01	<0.01	0.06	0.01
510783	51.33	14.41	13.70	5.48	9.68	2.10	0.36	0.61	0.05
510784	40.24	2.92	12.06	32.33	0.16	<0.01	<0.01	0.12	<0.01
510785	37.91	1.66	12.94	33.83	0.58	<0.01	<0.01	0.12	<0.01

Sample	SiO ₂	Al ₂ O ₃	Fe ₂ O ₃ *	MgO	CaO	Na ₂ O	K ₂ O	TiO ₂	P ₂ O ₅
Unit	%	%	%	%	%	%	%	%	%
MDL	0.01	0.01	0.04	0.01	0.01	0.01	0.01	0.01	0.01
510789	51.53	14.02	13.73	6.41	7.63	3.65	0.63	0.70	0.06
510790	34.96	0.89	16.18	32.05	1.68	<0.01	<0.01	0.05	<0.01
510793	38.23	0.70	14.01	33.52	0.14	<0.01	<0.01	0.04	<0.01
510798	36.68	4.70	11.85	30.59	2.25	<0.01	<0.01	0.22	0.02
510834	58.75	12.41	7.91	7.22	7.74	3.06	0.48	0.63	0.07
510835	51.45	12.98	8.11	7.36	12.60	3.14	0.45	0.67	0.08
510838	52.47	14.00	9.63	8.99	6.86	3.02	0.82	0.73	0.08
510839	56.54	14.15	8.01	6.66	7.14	3.37	0.88	0.68	0.13
510840	50.52	11.41	11.65	12.15	9.12	1.33	0.41	0.53	0.05
510841	51.59	13.77	9.78	9.37	8.80	2.40	0.48	0.72	0.07
510843	58.62	15.67	7.66	4.95	6.62	2.98	0.69	0.75	0.18
510844	52.95	14.44	9.88	8.59	7.03	3.13	0.35	0.77	0.07
510845	54.61	14.70	9.13	6.96	5.75	4.00	0.98	0.75	0.09
510846	68.30	15.18	3.46	1.41	3.14	3.83	2.42	0.43	0.12
510860	45.81	15.54	12.36	8.12	10.01	1.98	0.18	0.75	0.08
510862	50.84	14.41	11.59	7.26	8.15	2.54	0.07	0.77	0.07
510868	49.71	15.69	12.40	5.61	9.14	1.03	0.40	0.78	0.08
510870	44.76	17.49	7.52	8.96	13.11	1.24	0.18	0.27	0.03
510872	51.65	14.57	11.22	7.75	7.59	2.61	0.35	0.63	0.06
510874	48.83	15.43	12.59	7.62	8.78	1.63	0.45	0.63	0.06
510878	48.10	11.42	11.49	13.69	8.91	1.30	0.32	0.47	0.05
510879	56.70	14.32	10.64	8.63	1.41	0.03	1.88	0.58	0.09
510885	48.47	14.30	11.24	5.39	13.68	0.07	0.01	0.72	0.06
510887	55.56	16.19	13.99	3.19	0.77	2.26	1.98	1.61	0.12
510891	76.71	12.57	1.03	0.39	0.12	3.39	4.95	0.13	0.05
510892	51.41	17.10	10.35	5.50	5.44	3.74	1.27	0.98	0.10
510893	50.04	12.03	16.92	4.99	10.02	2.19	0.19	1.36	0.10
510901	49.50	13.84	14.10	6.43	9.97	1.34	0.05	1.20	0.11
510906	44.72	15.79	11.81	11.42	8.86	1.37	0.04	0.62	0.05
510947	79.80	10.41	1.63	0.95	0.95	2.05	1.83	0.26	0.03
510960	46.97	16.28	6.84	9.36	14.48	1.44	0.02	0.38	0.03
510961	48.52	14.43	13.88	7.26	9.27	1.26	0.04	1.19	0.09
510967	48.17	15.13	15.28	5.83	9.14	2.39	0.32	1.29	0.09
510969	68.91	14.62	3.96	1.50	2.52	3.85	2.71	0.44	0.11
510970	46.50	10.88	13.22	14.89	9.19	0.98	0.63	0.71	0.04
510971	47.12	10.84	12.78	14.20	8.85	1.51	0.38	0.78	0.05
510983	72.23	13.65	2.27	0.62	2.34	1.85	3.07	0.38	0.03
510990	47.51	10.10	11.02	15.32	10.56	0.15	0.03	0.45	0.03
510992	69.46	14.66	4.88	1.76	1.20	3.49	1.38	0.37	0.11
510995	46.85	14.15	11.67	10.89	10.24	1.55	0.52	0.86	0.03
510999	49.04	13.81	14.26	6.72	9.57	0.23	<0.01	1.28	0.08
512251	51.37	16.68	11.04	5.17	8.00	2.32	1.73	0.84	0.12
512252	49.36	14.32	12.39	6.88	8.95	1.54	2.65	0.76	0.10
512255	75.29	12.86	2.82	0.55	1.11	3.88	1.93	0.29	0.06
512262	86.58	7.32	0.67	0.26	0.49	1.63	1.35	0.16	0.03
512263	43.00	16.97	9.85	12.47	10.87	0.42	<0.01	0.30	0.03
512268	47.64	14.19	11.34	10.47	9.48	2.43	0.20	0.77	0.02
512270	77.53	12.33	1.10	0.16	0.19	4.17	4.13	0.06	0.01
512272	56.96	16.66	7.47	4.20	7.17	3.28	1.44	0.71	0.20
512273	73.51	15.27	0.79	0.15	2.17	5.32	1.94	0.06	0.04
512274	54.40	17.08	8.34	4.75	7.95	3.23	0.86	0.74	0.23
512275	53.15	15.16	9.87	5.19	12.20	1.01	0.09	0.50	0.06

Sample	SiO ₂	Al ₂ O ₃	Fe ₂ O ₃ *	MgO	CaO	Na ₂ O	K ₂ O	TiO ₂	P ₂ O ₅
Unit	%	%	%	%	%	%	%	%	%
MDL	0.01	0.01	0.04	0.01	0.01	0.01	0.01	0.01	0.01
512282	49.00	14.46	10.67	8.43	9.42	1.62	0.07	0.43	0.03
512283	49.43	13.33	15.18	6.61	8.58	3.09	0.25	1.34	0.10
512284	49.09	13.70	13.92	7.73	7.93	3.04	0.10	1.20	0.08
512285	48.91	14.70	13.71	6.74	9.80	1.76	0.08	1.14	0.10
512286	48.14	14.37	14.90	7.49	8.36	2.08	0.11	1.29	0.10
516505	47.57	5.66	14.72	16.24	10.07	0.17	0.04	0.99	0.06
516509	49.07	16.25	11.35	4.52	13.25	2.13	0.58	0.84	0.05
516516	37.19	2.60	14.45	30.12	2.50	0.01	<0.01	0.20	0.02
516518	54.34	11.85	5.56	7.34	13.31	2.60	0.10	1.59	<0.01
516519	78.24	11.92	1.94	1.91	0.63	0.99	2.13	0.19	0.01
516522	48.55	13.58	14.41	7.94	8.41	2.39	0.29	1.24	0.08
510750-1	53.16	14.15	8.39	4.26	15.20	0.17	0.46	0.60	0.02
510750-2	49.57	14.36	10.87	5.33	14.82	0.27	0.21	0.83	0.05
510754-1	50.27	15.47	11.65	5.26	10.98	2.42	0.49	1.05	0.08
510754-2	50.43	15.43	10.88	5.48	11.08	2.68	0.37	1.02	0.08

Sample	MnO	Cr ₂ O ₃	LOI	Sum	Sc	Ba	Co	Cs	Ga	Hf
Unit	%	%	%	%	ppm	ppm	ppm	ppm	ppm	ppm
MDL	0.01	0.002	5.1	0.01	1	1	0.2	0.1	0.5	0.1
510601	0.12	0.055	4.4	99.82	37	4	35.3	0.1	13.1	0.4
510619	0.16	0.045	4.7	99.80	46	30	45.1	1.3	14.4	1.7
510624	0.07	0.003	4.1	99.89	10	473	9.2	1.5	15.8	3.9
510625	0.08	<0.002	2.8	99.86	9	486	11.5	1.2	17.7	4.5
510626	0.07	<0.002	2.4	99.87	8	537	9.9	1.4	17.0	4.4
510627	0.12	0.158	4.4	99.80	29	4	32.1	0.1	13.0	0.3
510631	0.15	0.044	5.2	99.79	22	5	42.8	<0.1	15.2	0.8
510632	0.17	0.062	4.2	99.79	48	13	44.2	0.1	12.8	0.9
510633	0.17	0.033	3.6	99.79	45	29	48.1	0.2	17.1	1.5
510636	0.20	0.033	5.1	99.80	46	12	37.7	0.8	18.2	2.2
510637	0.20	0.034	1.6	99.80	49	12	45.8	<0.1	18.2	2.2
510638	0.21	0.012	1.5	99.80	54	20	50.4	0.4	18.0	2.7
510657	0.01	<0.002	0.4	99.80	1	1508	1.2	0.7	17.7	2.5
510662	0.18	0.326	2.2	99.68	34	150	77.3	0.4	10.0	0.8
510663	0.20	0.289	2.4	99.69	33	97	66.5	1.0	9.7	0.7
510664	0.19	0.368	3.1	99.68	31	106	70.9	1.6	9.1	0.9
510665	0.21	0.112	1.4	99.75	42	137	57.9	0.5	15.7	2.0
510670	0.05	0.017	3.1	99.86	15	596	18.7	3.4	21.3	3.7
510671	0.20	0.022	3.1	99.81	46	9	51.5	0.2	17.4	1.7
510673	0.21	0.004	3.1	99.81	52	21	38.2	0.3	18.4	1.8
510674	0.02	<0.002	2.0	99.93	2	628	2.8	2.0	18.2	2.5
510684	0.11	0.007	3.6	99.76	38	409	32.0	0.9	17.9	0.7
510687	0.17	0.135	2.4	99.73	50	77	60.0	0.4	12.1	1.4
510690	0.18	0.014	2.9	99.79	54	195	34.9	1.8	16.0	1.3
510707	0.18	0.078	2.2	99.76	63	28	51.0	0.4	12.8	1.3
510708	0.15	0.015	1.9	99.82	35	131	41.9	0.5	12.7	0.5
510710	0.14	0.018	1.6	99.81	35	70	40.6	0.5	12.5	0.4
510711	0.22	0.114	3.9	99.70	41	30	81.0	0.3	9.8	0.7
510714	0.16	0.058	3.5	99.77	34	32	52.0	0.3	16.6	1.5
510722	0.16	0.011	5.3	99.80	52	2	50.3	<0.1	16.0	2.0
510740	0.20	0.021	1.9	99.78	46	8	54.8	0.1	18.0	2.1
510743	0.09	0.011	3.1	99.83	16	492	20.1	0.6	19.1	4.2
510744	0.19	0.039	0.8	99.82	43	13	42.5	0.4	18.1	1.6
510746	0.21	0.042	1.8	99.78	45	39	44.6	6.5	16.6	1.7
510751	0.20	0.040	2.3	99.82	45	26	47.5	0.8	18.7	1.8
510752	0.18	0.044	1.9	99.82	48	120	47.8	2.6	16.1	1.8
510753	0.20	0.040	0.7	99.79	42	27	46.9	0.8	17.2	1.7
510756	0.17	0.402	9.6	99.43	12	3	126.7	1.1	4.7	0.4
510760	0.08	0.427	11.9	99.44	6	12	141.6	0.2	1.5	0.2
510762	0.15	0.434	12.4	99.44	6	3	150.9	<0.1	1.7	0.3
510763	0.15	0.437	14.5	99.48	7	3	159.4	0.5	1.7	0.2
510765	0.19	0.401	10.5	99.44	8	4	158.0	0.3	2.2	0.3
510766	0.18	0.454	10.4	99.41	9	1	163.7	<0.1	1.6	0.3
510767	0.24	0.459	12.6	99.40	9	1	162.4	0.2	2.1	0.2
510768	0.21	0.508	9.4	99.44	8	<1	169.0	0.5	2.4	0.3
510771	0.07	0.003	2.2	99.87	9	235	13.8	0.2	18.5	5.4
510772	0.07	0.015	4.2	99.87	11	336	22.7	0.5	17.8	2.4
510780	0.12	0.575	12.3	99.43	9	<1	106.3	0.3	3.5	<0.1
510783	0.20	0.005	1.9	99.84	41	58	52.8	0.4	15.9	1.2
510784	0.10	0.664	10.5	99.43	13	<1	114.8	0.3	5.1	0.2
510785	0.11	0.125	11.8	99.42	10	1	126.4	0.2	2.6	<0.1

Sample	MnO	Cr ₂ O ₃	LOI	Sum	Sc	Ba	Co	Cs	Ga	Hf
Unit	%	%	%	%	ppm	ppm	ppm	ppm	ppm	ppm
MDL	0.01	0.002	5.1	0.01	1	1	0.2	0.1	0.5	0.1
510789	0.22	0.003	1.2	99.80	45	78	61.5	2.6	16.5	1.1
510790	0.09	0.773	12.5	99.43	6	2	114.5	<0.1	2.2	<0.1
510793	0.07	0.212	12.2	99.45	6	<1	100.8	0.5	1.2	<0.1
510798	0.16	0.657	12.0	99.44	14	2	132.7	0.1	6.1	0.4
510834	0.14	0.064	1.3	99.78	28	94	33.7	0.3	12.8	1.8
510835	0.18	0.072	2.7	99.76	30	90	34.5	0.3	13.2	1.8
510838	0.16	0.067	2.9	99.72	31	225	41.4	0.9	14.0	1.8
510839	0.13	0.047	2.0	99.76	25	237	30.3	0.7	15.2	2.8
510840	0.22	0.158	2.1	99.70	41	92	61.6	0.2	11.5	1.2
510841	0.15	0.069	2.5	99.73	31	116	46.9	0.3	13.4	2.0
510843	0.11	0.024	1.5	99.78	21	243	30.0	0.9	15.5	3.3
510844	0.15	0.043	2.3	99.75	35	60	41.8	0.4	13.9	2.0
510845	0.14	0.066	2.5	99.73	32	168	40.5	0.4	16.1	2.2
510846	0.05	0.004	1.5	99.81	8	496	9.6	0.3	16.2	4.2
510860	0.18	0.051	4.7	99.74	51	17	47.9	1.0	14.6	1.8
510862	0.15	0.036	3.9	99.76	48	10	44.8	0.2	14.4	1.8
510868	0.17	0.008	4.8	99.78	45	39	43.4	2.1	17.1	1.7
510870	0.12	0.153	5.9	99.78	27	21	49.3	0.7	12.4	0.4
510872	0.17	0.043	3.1	99.76	43	63	45.0	1.2	13.4	1.3
510874	0.18	0.042	3.5	99.74	43	85	48.8	0.6	14.4	1.4
510878	0.18	0.191	3.5	99.68	36	99	66.0	0.2	10.5	1.2
510879	0.11	0.051	5.3	99.73	37	483	35.3	0.8	15.3	1.6
510885	0.16	0.047	5.6	99.78	40	4	41.4	<0.1	14.6	1.2
510887	0.09	0.015	4.0	99.79	29	243	44.0	1.3	22.1	4.4
510891	0.02	<0.002	0.5	99.88	2	550	2.0	0.4	13.1	4.1
510892	0.17	0.026	3.7	99.77	33	125	34.0	1.9	18.3	3.0
510893	0.22	<0.002	1.7	99.75	45	34	56.4	2.8	16.6	2.1
510901	0.18	0.036	3.0	99.75	49	3	46.0	<0.1	16.6	2.3
510906	0.16	0.124	4.7	99.73	25	8	53.2	0.1	13.0	1.0
510947	0.03	0.015	2.0	99.92	6	431	8.3	1.0	11.5	3.3
510960	0.13	0.043	3.8	99.81	47	7	28.4	0.1	13.3	0.6
510961	0.20	0.032	3.6	99.78	47	5	38.9	<0.1	18.1	2.0
510967	0.21	0.025	1.9	99.79	47	36	55.2	0.3	20.1	2.4
510969	0.06	<0.002	1.2	99.86	9	616	12.9	0.7	17.6	4.5
510970	0.20	0.200	2.2	99.67	38	67	78.0	1.4	13.5	1.2
510971	0.20	0.181	2.7	99.69	40	48	66.2	0.4	11.9	0.9
510983	0.03	0.015	3.4	99.90	8	645	10.0	1.7	14.3	2.4
510990	0.17	0.048	4.3	99.69	51	5	76.3	<0.1	9.7	0.6
510992	0.02	0.003	2.6	99.92	6	315	8.2	0.7	17.6	3.4
510995	0.18	0.092	2.7	99.72	46	74	57.7	0.7	17.5	1.2
510999	0.20	0.035	4.5	99.77	48	6	42.4	0.1	17.6	2.0
512251	0.19	0.035	2.2	99.74	23	532	32.8	1.0	18.2	2.2
512252	0.24	0.083	2.4	99.69	29	692	45.5	0.7	14.2	2.0
512255	0.04	<0.002	1.0	99.81	9	458	3.1	1.6	14.0	6.9
512262	<0.01	0.004	1.4	99.92	3	343	3.0	0.8	7.4	2.1
512263	0.13	0.182	5.5	99.73	35	2	62.2	<0.1	12.0	0.3
512268	0.17	0.113	2.9	99.72	28	24	50.5	0.7	13.1	1.4
512270	0.02	<0.002	0.2	99.90	9	563	1.3	0.7	14.1	4.0
512272	0.12	0.014	1.6	99.77	19	238	24.0	4.8	19.1	2.6
512273	0.01	<0.002	0.6	99.88	1	415	0.9	0.4	19.4	2.0
512274	0.12	0.014	2.0	99.75	21	285	28.0	0.6	19.5	2.4
512275	0.14	0.037	2.4	99.82	38	22	29.5	<0.1	18.5	1.0

Sample	MnO	Cr ₂ O ₃	LOI	Sum	Sc	Ba	Co	Cs	Ga	Hf
Unit	%	%	%	%	ppm	ppm	ppm	ppm	ppm	ppm
MDL	0.01	0.002	5.1	0.01	1	1	0.2	0.1	0.5	0.1
512282	0.16	0.056	5.4	99.78	48	13	42.1	0.1	12.4	0.8
512283	0.20	0.032	1.6	99.75	52	42	45.8	0.6	17.9	2.2
512284	0.19	0.033	2.7	99.75	49	13	44.0	<0.1	16.4	2.2
512285	0.18	0.031	2.6	99.75	45	10	42.0	0.1	17.5	1.9
512286	0.21	0.035	2.6	99.75	52	12	44.4	0.2	17.4	2.5
516505	0.23	0.330	3.5	99.68	21	3	95.7	0.1	8.1	1.7
516509	0.18	0.053	1.5	99.79	48	63	55.5	0.3	16.6	1.6
516516	0.15	0.535	11.4	99.41	17	13	101.3	0.5	4.3	0.2
516518	0.12	<0.002	3.0	99.84	47	19	27.0	0.3	11.4	2.0
516519	0.03	<0.002	1.9	99.94	6	325	4.2	5.6	14.5	3.7
516522	0.21	0.034	2.6	99.78	49	32	37.1	0.4	16.7	2.0
510750-1	0.17	0.028	3.2	99.86	27	75	31.5	2.8	15.3	1.1
510750-2	0.20	0.036	3.3	99.82	37	34	43.7	1.3	16.8	1.6
510754-1	0.19	0.046	1.9	99.82	47	90	49.5	1.3	15.9	1.7
510754-2	0.21	0.041	2.1	99.83	46	60	45.3	1.6	16.6	1.6

Sample	Nb	Rb	Sr	Ta	Th	U	V	W	Zr	Y	La	Ce
Unit	ppm	ppm	ppm	ppm	ppm	ppm	ppm	ppm	ppm	ppm	ppm	ppm
MDL	0.1	0.1	0.5	0.1	0.2	0.1	8	0.5	0.1	0.1	0.1	0.1
510601	0.4	0.5	127.7	0.1	<0.2	<0.1	151	<0.5	11.3	7.1	1.1	2.5
510619	1.7	10.3	98.1	<0.1	0.7	0.1	270	<0.5	52.9	18.7	3.8	9.8
510624	5.3	61.8	182.3	0.3	4.1	0.9	74	1.1	143.6	14.5	24.8	53.8
510625	6.6	61.6	164.6	0.4	4.6	0.9	79	0.9	167.7	15.8	29.0	60.6
510626	6.0	64.7	89.7	0.4	4.5	1.1	67	0.7	161.4	17.0	34.5	70.5
510627	0.6	0.3	148.2	<0.1	<0.2	<0.1	126	<0.5	13.0	6.3	1.1	2.5
510631	1.5	0.4	153.6	<0.1	0.2	<0.1	164	<0.5	32.8	12.5	2.8	6.3
510632	0.7	0.9	68.6	<0.1	<0.2	<0.1	243	<0.5	26.0	12.7	1.4	3.2
510633	2.3	2.5	108.6	0.1	<0.2	<0.1	325	<0.5	53.9	21.3	3.2	8.2
510636	2.6	4.8	103.5	0.1	0.5	0.1	353	<0.5	64.7	23.9	3.7	10.3
510637	3.1	1.7	107.0	0.2	0.3	<0.1	356	<0.5	69.1	27.7	3.8	10.7
510638	3.5	4.2	103.5	0.2	0.2	0.1	412	<0.5	76.9	31.0	4.1	11.4
510657	0.9	50.8	359.9	<0.1	1.4	1.0	9	<0.5	70.1	1.4	4.6	16.1
510662	1.1	13.1	76.5	<0.1	<0.2	<0.1	196	<0.5	26.3	11.1	1.6	4.4
510663	1.3	16.4	59.7	0.1	0.5	0.2	173	1.0	21.6	10.9	3.7	8.1
510664	0.8	25.1	122.6	<0.1	0.3	<0.1	188	<0.5	31.3	10.4	1.4	3.1
510665	1.7	13.6	93.4	<0.1	0.9	0.1	319	<0.5	59.4	23.3	5.1	10.3
510670	5.9	100.6	123.9	0.4	4.8	1.2	109	<0.5	152.8	12.7	23.1	49.2
510671	2.2	0.8	99.5	0.2	0.3	<0.1	303	<0.5	50.4	21.9	3.0	8.1
510673	2.4	2.0	99.7	0.1	0.4	<0.1	321	<0.5	56.6	24.4	3.5	9.7
510674	2.6	88.7	117.8	0.2	3.8	0.4	9	1.4	76.3	3.4	17.8	29.9
510684	1.3	19.1	193.2	<0.1	0.2	<0.1	244	1.7	26.9	14.3	2.6	8.1
510687	2.0	7.2	82.0	0.2	<0.2	<0.1	225	<0.5	44.1	15.0	2.5	6.4
510690	1.7	32.8	125.7	0.1	<0.2	0.1	283	<0.5	40.4	16.9	2.8	7.3
510707	1.2	3.0	97.1	<0.1	<0.2	<0.1	307	<0.5	43.2	17.1	2.3	6.3
510708	0.5	16.9	180.5	<0.1	0.2	<0.1	154	<0.5	12.4	6.0	1.1	2.4
510710	2.7	11.7	174.3	0.3	<0.2	<0.1	140	<0.5	9.9	5.8	0.8	2.0
510711	0.9	2.3	21.8	<0.1	<0.2	<0.1	170	<0.5	21.1	9.4	1.4	3.8
510714	2.2	2.7	160.7	0.1	0.2	<0.1	247	<0.5	45.3	18.2	2.6	7.1
510722	2.3	0.3	224.4	0.2	0.4	0.1	326	<0.5	58.2	24.9	3.8	10.3
510740	2.9	0.7	127.7	0.2	<0.2	0.1	329	<0.5	67.8	26.8	3.8	10.7
510743	5.7	44.5	338.4	0.3	3.6	0.8	109	<0.5	157.8	15.0	23.6	52.5
510744	1.9	5.0	103.5	0.1	0.4	<0.1	273	<0.5	48.9	20.5	2.7	7.9
510746	2.8	160.8	71.7	0.1	0.3	0.1	293	6.1	55.9	22.9	3.1	8.5
510751	2.0	7.7	75.5	0.2	0.3	0.2	290	<0.5	51.0	21.0	3.0	8.4
510752	2.4	55.7	134.4	0.2	0.3	<0.1	321	<0.5	60.4	23.9	3.2	8.8
510753	2.4	6.9	103.5	0.2	<0.2	0.3	289	<0.5	53.9	22.2	2.9	8.2
510756	0.8	1.0	1.2	<0.1	0.4	<0.1	76	<0.5	13.5	3.7	1.6	3.6
510760	0.5	0.7	1.1	<0.1	<0.2	<0.1	30	<0.5	9.0	1.7	0.5	1.7
510762	0.6	0.7	1.0	<0.1	<0.2	<0.1	27	<0.5	8.0	1.2	0.5	1.2
510763	0.6	0.6	2.8	<0.1	<0.2	<0.1	32	<0.5	8.4	1.3	0.9	2.1
510765	0.7	1.2	2.8	<0.1	<0.2	<0.1	40	<0.5	16.0	2.1	1.0	2.3
510766	0.7	0.4	0.9	0.1	<0.2	<0.1	38	<0.5	10.2	1.8	0.7	2.2
510767	0.9	0.3	9.1	<0.1	<0.2	<0.1	31	<0.5	6.8	1.6	0.8	2.2
510768	0.7	0.3	0.6	<0.1	0.2	<0.1	38	<0.5	9.0	3.2	0.5	1.7
510771	6.5	17.2	317.1	0.5	3.3	0.7	68	0.9	235.3	11.5	15.5	32.0
510772	4.0	54.1	188.3	0.4	3.3	0.8	72	<0.5	85.2	11.7	18.0	36.0
510780	1.3	0.9	5.4	<0.1	<0.2	<0.1	37	3.9	2.1	0.9	0.5	0.9
510783	1.0	15.0	172.8	<0.1	0.3	<0.1	234	<0.5	35.0	12.5	2.4	6.0
510784	0.3	0.6	1.2	<0.1	<0.2	<0.1	109	1.0	4.8	2.0	0.2	0.6
510785	0.2	0.4	3.0	<0.1	<0.2	<0.1	60	0.8	1.8	1.6	0.2	0.5

Sample	Nb	Rb	Sr	Ta	Th	U	V	W	Zr	Y	La	Ce
Unit	ppm	ppm	ppm	ppm	ppm	ppm	ppm	ppm	ppm	ppm	ppm	ppm
MDL	0.1	0.1	0.5	0.1	0.2	0.1	8	0.5	0.1	0.1	0.1	0.1
510789	1.3	29.6	87.1	<0.1	0.2	<0.1	301	<0.5	36.7	12.9	2.1	5.9
510790	0.1	0.3	10.4	<0.1	<0.2	<0.1	35	1.4	2.4	1.4	0.4	0.8
510793	<0.1	0.3	1.1	<0.1	<0.2	<0.1	21	0.9	2.4	1.1	1.1	2.5
510798	0.6	0.4	20.0	<0.1	<0.2	<0.1	90	0.6	11.9	4.0	0.9	2.5
510834	2.4	11.3	128.7	0.1	0.6	0.2	185	2.5	58.5	13.8	3.7	9.4
510835	2.4	11.6	186.1	0.1	0.6	0.1	188	3.3	63.8	14.0	4.5	11.3
510838	2.5	26.2	195.8	0.1	0.8	0.2	190	2.5	63.1	15.0	4.8	11.7
510839	3.8	30.0	250.6	0.3	1.9	0.5	158	2.3	99.6	15.7	12.2	26.5
510840	1.2	10.2	67.1	<0.1	0.5	<0.1	211	2.4	36.3	12.5	3.4	7.7
510841	2.1	13.6	161.4	0.2	0.6	0.2	194	2.2	61.9	14.6	4.2	10.5
510843	4.7	18.7	353.8	0.3	2.8	0.5	146	3.8	121.9	17.1	18.5	41.5
510844	2.1	9.7	115.0	0.2	0.5	0.2	223	2.9	62.3	16.2	4.4	11.3
510845	2.7	21.6	265.2	0.2	0.7	0.2	201	3.1	71.7	17.2	7.1	15.8
510846	5.1	62.5	285.3	0.5	6.0	1.0	53	8.9	155.8	11.3	27.5	56.0
510860	1.7	8.8	185.8	<0.1	0.6	0.1	298	0.9	54.5	19.7	4.0	10.1
510862	1.6	2.2	168.8	<0.1	0.4	<0.1	281	1.8	56.6	20.7	3.7	10.0
510868	1.5	14.8	172.8	<0.1	0.4	0.2	290	1.0	56.9	21.1	4.3	10.6
510870	0.4	4.9	108.9	<0.1	<0.2	<0.1	117	3.4	10.4	4.7	0.9	2.4
510872	1.4	8.0	87.7	0.1	0.8	0.1	248	0.7	46.2	16.5	4.1	9.5
510874	1.3	12.3	127.0	<0.1	0.4	0.1	253	1.9	47.3	15.2	3.5	9.0
510878	0.8	6.7	78.9	0.1	0.3	<0.1	197	0.6	31.9	12.6	2.7	6.2
510879	1.6	49.1	7.3	0.1	0.8	0.2	208	1.4	51.2	10.9	3.2	9.9
510885	1.5	0.2	280.3	<0.1	0.2	<0.1	242	1.5	39.3	16.5	1.8	5.3
510887	12.2	53.8	46.4	0.8	4.2	1.0	201	1.3	162.6	15.8	19.0	44.8
510891	6.3	105.6	98.0	0.5	17.6	1.5	8	2.9	115.0	12.5	26.1	60.0
510892	2.8	55.6	223.5	0.2	0.4	0.2	217	2.4	83.2	21.5	5.1	13.8
510893	2.5	9.2	64.1	0.2	<0.2	<0.1	417	4.4	66.6	25.5	2.8	8.1
510901	3.1	0.5	109.1	0.2	0.3	<0.1	335	3.1	79.8	28.5	4.0	11.4
510906	1.5	0.6	139.4	0.1	0.2	<0.1	176	1.4	36.1	13.0	2.0	5.6
510947	3.2	45.5	50.6	0.3	4.4	1.4	33	0.5	116.2	9.2	18.0	36.5
510960	0.4	0.1	148.9	<0.1	<0.2	<0.1	178	<0.5	14.9	8.7	1.2	3.4
510961	2.6	0.3	131.6	0.2	0.4	<0.1	333	<0.5	62.6	24.7	3.4	9.9
510967	3.2	7.4	99.7	0.2	0.3	0.1	352	<0.5	74.0	28.6	4.0	11.0
510969	6.2	81.3	203.1	0.5	6.8	1.0	53	1.2	155.2	13.4	24.3	48.1
510970	1.6	20.7	38.5	<0.1	0.3	<0.1	253	<0.5	36.6	17.6	2.6	7.1
510971	0.9	11.8	29.4	0.1	0.2	0.1	297	0.7	32.9	14.6	2.3	5.5
510983	3.8	84.0	123.6	0.4	4.2	1.0	49	0.8	86.0	9.5	18.5	38.4
510990	0.8	0.4	64.4	<0.1	<0.2	<0.1	195	<0.5	18.2	10.0	1.3	3.3
510992	3.5	37.9	45.2	0.2	3.2	0.8	37	0.5	130.6	7.4	20.9	40.9
510995	1.6	13.7	138.5	<0.1	0.4	<0.1	392	0.7	35.4	17.5	2.9	7.4
510999	3.1	0.3	203.6	0.2	0.3	<0.1	342	<0.5	70.8	27.4	3.7	10.4
512251	3.1	51.2	267.9	0.2	0.9	0.2	156	3.1	81.4	19.0	6.2	16.6
512252	2.2	74.8	155.6	0.2	0.6	0.2	169	2.3	65.1	15.6	5.5	13.2
512255	5.5	56.5	197.8	0.3	13.9	1.1	<8	5.7	253.4	15.5	93.4	183.9
512262	1.6	36.1	78.1	0.1	1.8	0.4	19	2.9	66.0	3.6	8.4	17.9
512263	0.7	0.1	130.5	<0.1	<0.2	<0.1	140	1.2	13.4	6.5	0.9	2.8
512268	2.0	4.6	107.9	0.2	0.2	<0.1	242	3.5	41.2	18.2	2.8	8.6
512270	6.2	75.9	33.8	0.5	7.7	1.3	<8	11.0	110.7	16.1	17.3	46.1
512272	4.9	137.1	429.5	0.7	1.5	0.7	152	2.1	87.3	14.9	13.6	32.3
512273	2.8	47.9	301.3	0.2	0.8	0.3	<8	5.4	51.1	1.9	3.2	5.2
512274	3.0	30.4	510.4	0.2	0.8	0.2	160	2.4	91.3	12.9	12.9	31.5
512275	1.2	1.4	155.7	<0.1	0.4	0.1	226	3.5	37.7	14.4	3.0	7.2

Sample	Nb	Rb	Sr	Ta	Th	U	V	W	Zr	Y	La	Ce
Unit	ppm	ppm	ppm	ppm	ppm	ppm	ppm	ppm	ppm	ppm	ppm	ppm
MDL	0.1	0.1	0.5	0.1	0.2	0.1	8	0.5	0.1	0.1	0.1	0.1
512282	0.7	1.8	97.5	<0.1	<0.2	<0.1	236	1.8	23.1	13.1	1.2	3.1
512283	2.9	5.2	75.3	0.2	0.3	<0.1	381	3.6	70.7	27.3	3.5	10.3
512284	2.7	0.6	68.1	0.2	0.3	<0.1	350	4.7	66.7	25.5	3.3	9.2
512285	2.8	1.0	114.7	0.1	0.4	<0.1	331	4.1	66.5	25.6	3.5	9.7
512286	3.1	1.5	96.1	0.2	0.3	<0.1	393	1.4	73.5	30.0	3.8	10.9
516505	4.9	0.7	4.3	0.4	0.6	0.2	195	<0.5	57.1	8.2	4.2	13.3
516509	1.8	24.2	220.3	<0.1	<0.2	0.1	285	0.9	41.2	19.5	2.4	6.2
516516	0.1	0.8	7.4	<0.1	<0.2	<0.1	124	<0.5	8.1	3.0	0.4	1.2
516518	1.7	3.3	78.5	0.2	0.3	0.1	260	<0.5	61.7	15.5	5.0	12.7
516519	6.3	71.7	86.0	0.5	5.8	1.3	21	0.6	83.9	10.3	7.7	22.4
516522	2.5	8.0	56.1	0.1	0.2	<0.1	336	0.7	61.8	24.2	3.9	10.3
510750-1	1.5	49.7	101.1	<0.1	<0.2	0.2	207	0.8	33.6	14.7	1.9	5.4
510750-2	2.1	18.5	95.7	<0.1	<0.2	0.1	265	0.9	48.4	20.4	2.6	7.2
510754-1	2.1	41.5	103.2	0.1	0.3	<0.1	284	<0.5	53.7	21.5	2.7	8.1
510754-2	2.1	40.2	97.3	0.1	<0.2	<0.1	282	0.7	55.4	20.9	2.8	7.4

Sample	Pr	Nd	Sm	Eu	Gd	Tb	Dy	Ho	Er	Tm	Yb
Unit	ppm	ppm	ppm	ppm	ppm	ppm	ppm	ppm	ppm	ppm	ppm
MDL	0.02	0.3	0.05	0.02	0.05	0.01	0.05	0.02	0.03	0.01	0.05
510601	0.43	2.1	0.71	0.40	1.10	0.22	1.31	0.30	0.79	0.12	0.71
510619	1.34	6.5	1.82	0.64	2.54	0.47	3.03	0.69	1.91	0.30	2.03
510624	6.09	23.4	3.80	0.99	2.99	0.47	2.56	0.52	1.42	0.25	1.37
510625	6.99	26.3	4.21	1.07	3.21	0.51	2.81	0.54	1.60	0.25	1.59
510626	8.31	31.9	5.09	1.13	3.95	0.55	2.81	0.53	1.60	0.24	1.55
510627	0.40	2.3	0.70	0.33	0.98	0.18	1.06	0.23	0.70	0.10	0.65
510631	0.96	4.2	1.41	0.73	1.89	0.35	2.12	0.46	1.29	0.20	1.26
510632	0.53	2.9	0.85	0.33	1.40	0.28	1.89	0.44	1.39	0.22	1.46
510633	1.33	7.1	2.16	0.82	3.08	0.57	3.67	0.81	2.51	0.34	2.17
510636	1.65	9.0	2.73	0.80	3.70	0.70	4.55	0.99	2.82	0.41	2.59
510637	1.72	8.7	2.92	0.99	3.93	0.74	4.54	1.04	3.08	0.45	3.03
510638	1.89	9.1	3.10	0.99	4.47	0.82	5.04	1.16	3.58	0.51	3.55
510657	1.24	4.2	0.73	0.29	0.47	0.06	0.27	0.05	0.11	0.02	0.15
510662	0.73	3.5	1.09	0.43	1.59	0.29	1.87	0.42	1.26	0.18	1.27
510663	1.05	4.2	1.19	0.44	1.46	0.28	1.82	0.41	1.12	0.19	1.15
510664	0.60	2.8	0.97	0.42	1.38	0.27	1.73	0.35	1.20	0.16	1.07
510665	1.54	7.2	2.23	0.84	3.13	0.61	3.89	0.86	2.72	0.40	2.70
510670	5.92	23.0	3.82	1.03	3.12	0.45	2.31	0.50	1.51	0.21	1.39
510671	1.30	6.5	2.16	0.77	3.07	0.59	3.45	0.78	2.48	0.37	2.25
510673	1.50	7.2	2.54	0.89	3.48	0.66	3.83	0.89	2.74	0.41	2.59
510674	3.38	11.2	1.49	0.33	1.04	0.13	0.64	0.11	0.28	0.04	0.27
510684	1.28	6.3	1.84	0.87	2.43	0.42	2.77	0.54	1.64	0.21	1.43
510687	0.99	4.5	1.52	0.55	2.18	0.39	2.52	0.57	1.66	0.24	1.53
510690	1.13	5.0	1.62	0.72	2.43	0.46	2.98	0.64	1.87	0.29	1.83
510707	1.02	5.4	1.79	0.64	2.37	0.46	3.04	0.63	1.82	0.28	1.69
510708	0.40	1.9	0.62	0.30	0.98	0.18	1.19	0.24	0.72	0.10	0.65
510710	0.34	1.8	0.57	0.26	0.84	0.16	1.06	0.23	0.64	0.10	0.62
510711	0.58	3.2	0.92	0.34	1.43	0.27	1.62	0.37	1.11	0.17	1.03
510714	1.13	6.4	1.87	0.71	2.68	0.48	3.13	0.67	1.95	0.30	1.97
510722	1.53	7.9	2.30	0.78	3.29	0.61	4.03	0.89	2.75	0.41	2.67
510740	1.63	8.7	2.76	0.92	3.88	0.71	4.43	0.96	2.95	0.42	2.78
510743	5.79	21.9	3.63	1.06	3.08	0.46	2.50	0.51	1.52	0.22	1.50
510744	1.29	6.5	2.14	0.83	3.08	0.57	3.45	0.78	2.27	0.33	2.06
510746	1.36	6.5	2.27	0.85	3.32	0.62	4.04	0.81	2.68	0.37	2.41
510751	1.37	6.8	2.18	0.80	3.05	0.57	3.76	0.80	2.44	0.33	2.34
510752	1.42	8.0	2.45	0.87	3.39	0.63	3.98	0.84	2.54	0.39	2.49
510753	1.32	7.2	2.22	0.84	3.18	0.58	3.76	0.79	2.38	0.36	2.39
510756	0.57	2.6	0.60	0.17	0.77	0.13	0.73	0.15	0.45	0.05	0.35
510760	0.27	1.0	0.33	0.06	0.34	0.07	0.36	0.08	0.22	0.03	0.21
510762	0.19	0.9	0.21	0.04	0.23	0.04	0.22	0.05	0.18	0.03	0.15
510763	0.27	1.3	0.22	0.07	0.24	0.04	0.23	0.05	0.15	0.03	0.19
510765	0.44	2.3	0.44	0.10	0.42	0.08	0.39	0.09	0.26	0.05	0.25
510766	0.30	1.3	0.38	0.07	0.39	0.06	0.35	0.07	0.20	0.03	0.21
510767	0.30	1.5	0.34	0.08	0.35	0.06	0.33	0.07	0.20	0.02	0.21
510768	0.25	1.3	0.36	<0.02	0.50	0.08	0.50	0.11	0.36	0.05	0.31
510771	3.64	13.9	2.53	1.22	2.49	0.37	1.80	0.41	1.19	0.19	1.16
510772	4.02	15.2	3.04	1.32	3.01	0.47	2.41	0.49	1.16	0.18	1.09
510780	0.14	0.4	0.11	0.04	0.17	0.04	0.14	0.04	0.10	0.02	0.14
510783	0.93	4.8	1.38	0.61	2.04	0.36	2.11	0.50	1.49	0.21	1.28
510784	0.09	0.4	0.18	0.06	0.31	0.06	0.37	0.08	0.25	0.04	0.25
510785	0.09	0.4	0.15	0.07	0.24	0.04	0.28	0.06	0.21	0.03	0.19

Sample	Pr	Nd	Sm	Eu	Gd	Tb	Dy	Ho	Er	Tm	Yb
Unit	ppm	ppm	ppm	ppm	ppm	ppm	ppm	ppm	ppm	ppm	ppm
MDL	0.02	0.3	0.05	0.02	0.05	0.01	0.05	0.02	0.03	0.01	0.05
510789	0.93	4.5	1.50	0.56	1.91	0.39	2.30	0.51	1.45	0.22	1.40
510790	0.11	0.7	0.16	0.09	0.19	0.04	0.19	0.05	0.16	0.03	0.16
510793	0.29	0.9	0.19	0.05	0.20	0.04	0.21	0.05	0.11	0.02	0.09
510798	0.36	1.9	0.44	0.07	0.63	0.11	0.68	0.15	0.41	0.06	0.40
510834	1.39	6.7	1.96	0.73	2.28	0.42	2.45	0.50	1.41	0.22	1.32
510835	1.59	7.2	2.08	0.68	2.48	0.43	2.47	0.52	1.50	0.22	1.41
510838	1.66	7.9	2.18	0.71	2.56	0.46	2.77	0.58	1.59	0.24	1.47
510839	3.34	14.1	2.87	0.86	2.96	0.51	3.03	0.59	1.69	0.25	1.53
510840	1.07	5.2	1.42	0.47	1.81	0.35	2.21	0.46	1.36	0.21	1.33
510841	1.52	7.6	2.03	0.69	2.51	0.44	2.57	0.54	1.62	0.23	1.42
510843	5.26	19.9	3.67	0.97	3.51	0.56	2.84	0.62	1.91	0.28	1.67
510844	1.62	7.9	2.10	0.75	2.66	0.49	2.92	0.59	1.75	0.26	1.65
510845	2.14	10.4	2.59	1.03	2.90	0.51	2.99	0.61	1.85	0.26	1.64
510846	5.93	19.5	3.11	0.72	2.38	0.38	2.07	0.38	1.09	0.17	1.00
510860	1.41	6.7	2.03	0.69	2.85	0.52	3.27	0.73	2.19	0.34	2.05
510862	1.36	6.7	2.06	0.70	2.86	0.54	3.31	0.75	2.28	0.36	2.21
510868	1.50	7.1	2.18	0.72	2.91	0.56	3.45	0.72	2.25	0.36	2.22
510870	0.38	1.9	0.65	0.25	0.83	0.15	0.98	0.19	0.57	0.08	0.52
510872	1.35	6.1	1.74	0.54	2.30	0.44	2.68	0.58	1.78	0.28	1.71
510874	1.27	5.6	1.67	0.45	2.22	0.43	2.53	0.55	1.72	0.26	1.60
510878	0.90	4.1	1.30	0.41	1.68	0.33	1.98	0.43	1.28	0.21	1.24
510879	1.09	4.8	1.32	0.49	1.58	0.31	1.66	0.41	1.30	0.19	1.24
510885	0.83	4.8	1.57	0.65	2.28	0.45	2.81	0.63	1.96	0.28	1.80
510887	5.29	22.3	4.53	1.45	4.14	0.67	3.28	0.58	1.57	0.22	1.46
510891	5.80	19.5	3.68	0.38	3.10	0.43	2.40	0.42	1.22	0.19	1.21
510892	1.98	9.5	2.89	0.90	3.45	0.63	3.65	0.80	2.37	0.35	2.20
510893	1.40	7.6	2.61	0.80	3.68	0.71	4.40	0.91	2.66	0.42	2.74
510901	1.72	9.9	2.99	0.99	4.10	0.82	4.91	1.08	3.22	0.47	3.08
510906	0.87	5.1	1.55	0.60	1.99	0.39	2.31	0.49	1.43	0.23	1.31
510947	3.93	14.9	2.38	0.59	2.05	0.30	1.68	0.32	0.88	0.14	0.88
510960	0.51	2.3	0.94	0.39	1.31	0.26	1.47	0.31	0.96	0.14	0.89
510961	1.52	7.8	2.68	0.93	3.66	0.69	4.18	0.91	2.73	0.41	2.72
510967	1.70	9.1	3.00	1.04	4.31	0.78	4.94	1.06	3.27	0.47	3.08
510969	5.35	19.1	3.05	0.73	2.73	0.41	2.26	0.46	1.39	0.21	1.41
510970	1.12	5.9	1.87	0.62	2.58	0.47	2.97	0.65	1.95	0.28	1.83
510971	0.85	4.2	1.44	0.48	1.98	0.41	2.43	0.55	1.58	0.25	1.54
510983	4.13	15.8	2.46	0.65	2.02	0.31	1.59	0.30	0.86	0.13	0.80
510990	0.56	2.9	0.96	0.39	1.43	0.28	1.75	0.35	1.13	0.16	0.94
510992	4.69	16.6	2.54	0.89	2.04	0.26	1.33	0.25	0.67	0.10	0.70
510995	1.05	5.9	1.72	0.69	2.57	0.47	3.01	0.64	1.93	0.28	1.74
510999	1.68	9.5	2.84	0.93	4.08	0.73	4.64	1.01	2.95	0.43	2.89
512251	2.15	10.0	2.80	0.95	3.39	0.58	3.39	0.72	2.11	0.33	1.95
512252	1.75	7.7	2.26	0.72	2.69	0.46	2.75	0.59	1.82	0.26	1.63
512255	17.90	57.8	7.46	1.13	5.00	0.62	3.06	0.55	1.68	0.24	1.47
512262	1.84	6.0	1.17	0.34	0.87	0.14	0.76	0.16	0.37	0.07	0.48
512263	0.42	2.1	0.77	0.37	1.10	0.20	1.37	0.28	0.80	0.12	0.71
512268	1.43	8.0	2.34	0.86	3.01	0.53	3.21	0.68	1.90	0.28	1.73
512270	5.93	24.5	4.54	0.53	3.51	0.53	2.85	0.55	1.50	0.25	1.61
512272	4.12	18.0	3.45	1.01	3.06	0.49	2.47	0.54	1.45	0.22	1.47
512273	0.65	2.3	0.49	0.29	0.42	0.07	0.30	0.06	0.15	0.03	0.16
512274	4.00	17.9	3.35	1.10	2.86	0.45	2.34	0.45	1.25	0.19	1.12
512275	0.99	4.5	1.34	0.66	1.76	0.36	2.18	0.51	1.58	0.23	1.58

Sample	Pr	Nd	Sm	Eu	Gd	Tb	Dy	Ho	Er	Tm	Yb
Unit	ppm	ppm	ppm	ppm	ppm	ppm	ppm	ppm	ppm	ppm	ppm
MDL	0.02	0.3	0.05	0.02	0.05	0.01	0.05	0.02	0.03	0.01	0.05
512282	0.50	2.7	0.83	0.33	1.33	0.29	1.91	0.44	1.38	0.22	1.46
512283	1.60	9.5	2.86	0.98	3.90	0.75	4.41	0.97	2.99	0.46	2.82
512284	1.42	7.9	2.49	0.82	3.51	0.69	4.11	0.91	2.75	0.41	2.60
512285	1.54	8.3	2.66	1.00	3.66	0.69	4.33	0.94	2.75	0.42	2.62
512286	1.69	9.3	2.95	1.01	4.02	0.79	4.76	1.07	3.10	0.49	2.91
516505	2.05	9.4	2.28	0.21	2.12	0.32	1.61	0.34	0.89	0.13	0.83
516509	1.04	4.6	1.85	0.72	2.55	0.54	3.03	0.74	2.19	0.35	2.14
516516	0.20	0.8	0.25	0.09	0.40	0.10	0.43	0.12	0.39	0.07	0.37
516518	1.64	6.7	1.80	1.28	2.25	0.41	2.60	0.57	1.67	0.24	1.55
516519	2.51	9.6	2.37	0.44	2.29	0.40	2.34	0.44	1.19	0.18	1.10
516522	1.61	9.2	2.66	0.87	3.53	0.67	4.28	0.93	2.70	0.40	2.53
510750-1	0.82	4.5	1.43	0.51	2.12	0.38	2.45	0.53	1.56	0.23	1.55
510750-2	1.14	6.4	1.97	0.74	2.88	0.52	3.28	0.71	2.22	0.33	2.16
510754-1	1.28	6.7	2.32	0.81	3.08	0.61	3.71	0.82	2.48	0.36	2.25
510754-2	1.22	6.6	2.05	0.71	2.91	0.57	3.37	0.83	2.42	0.35	2.20

Sample	Lu	Cu	Pb	Zn	Ni	As	Au
Unit	ppm	ppm	ppm	ppm	ppm	ppm	ppb
MDL	0.01	0.1	0.1	1	0.1	0.5	0.5
510601	0.12	44.0	0.8	14	96.2	51.8	<0.5
510619	0.31	91.7	1.0	44	74.9	6.3	2.0
510624	0.23	17.2	7.8	55	11.0	0.9	<0.5
510625	0.25	5.3	1.4	57	9.3	0.9	<0.5
510626	0.25	4.8	2.5	26	6.0	9.8	3.3
510627	0.10	4.9	0.9	20	114.5	5.2	0.5
510631	0.21	11.3	0.5	44	198.4	6.3	<0.5
510632	0.24	46.0	0.5	36	56.0	1.5	0.6
510633	0.36	70.6	0.5	61	76.7	1.6	2.7
510636	0.39	55.3	0.3	65	62.4	<0.5	1.2
510637	0.45	57.0	0.4	39	46.6	0.8	1.3
510638	0.51	100.2	0.4	38	26.9	2.3	0.7
510657	0.02	13.3	4.3	24	1.4	<0.5	<0.5
510662	0.19	27.6	0.8	16	90.1	<0.5	<0.5
510663	0.18	7.0	0.5	18	95.7	<0.5	<0.5
510664	0.18	6.4	2.1	25	125.4	<0.5	<0.5
510665	0.43	19.4	0.5	24	53.4	<0.5	<0.5
510670	0.21	1.7	5.7	66	95.9	50.6	<0.5
510671	0.36	84.3	5.5	63	70.8	3.8	0.6
510673	0.39	181.5	0.7	48	22.4	4.1	1.2
510674	0.04	2.6	1.5	12	2.0	2.2	<0.5
510684	0.21	7.8	1.1	8	15.7	<0.5	<0.5
510687	0.25	39.2	0.7	24	94.3	2.8	1.8
510690	0.29	94.2	1.0	33	28.8	2.7	2.0
510707	0.29	104.8	0.6	17	61.8	7.1	1.3
510708	0.11	19.5	1.2	7	12.2	0.6	<0.5
510710	0.10	10.1	1.1	8	15.9	<0.5	0.6
510711	0.16	84.6	2.7	44	197.8	12.2	1.5
510714	0.30	59.6	1.9	47	130.8	2.9	<0.5
510722	0.42	10.3	1.8	84	62.1	1.3	1.4
510740	0.43	169.1	0.5	42	58.5	2.6	1.4
510743	0.23	19.3	3.8	61	44.7	<0.5	0.5
510744	0.34	68.6	0.3	13	26.0	<0.5	<0.5
510746	0.37	59.0	3.9	33	45.8	6.3	<0.5
510751	0.36	141.9	0.6	51	64.3	0.9	<0.5
510752	0.37	94.7	1.4	31	79.0	9.4	0.9
510753	0.36	91.2	0.5	14	39.2	0.8	<0.5
510756	0.06	0.9	0.2	33	899.9	1.3	<0.5
510760	0.04	1.2	8.3	30	1693.9	1.0	<0.5
510762	0.03	1.4	7.3	14	1586.2	<0.5	<0.5
510763	0.04	2.8	3.6	38	2157.1	27.4	<0.5
510765	0.04	0.1	0.1	6	1337.7	<0.5	<0.5
510766	0.03	0.8	0.3	10	1905.3	1.0	<0.5
510767	0.03	1.4	0.3	20	1314.8	0.7	<0.5
510768	0.05	142.6	0.6	55	2262.4	0.7	11.2
510771	0.20	84.9	3.3	35	26.1	2.5	<0.5
510772	0.18	7.3	2.2	45	75.0	1.5	<0.5
510780	0.02	<0.1	0.2	7	653.0	8.4	<0.5
510783	0.20	32.7	4.0	42	30.9	<0.5	<0.5
510784	0.04	3.5	2.1	16	1336.5	16.8	1.3
510785	0.03	9.8	0.6	28	1880.2	10.2	1.9

Sample	Lu	Cu	Pb	Zn	Ni	As	Au
Unit	ppm	ppm	ppm	ppm	ppm	ppm	ppb
MDL	0.01	0.1	0.1	1	0.1	0.5	0.5
510789	0.20	205.0	0.8	32	27.2	<0.5	3.5
510790	0.03	8.1	1.3	24	1581.1	5.5	1.8
510793	0.02	3.6	0.4	12	1829.9	4.6	<0.5
510798	0.06	22.4	1.5	36	1645.7	5.4	1.6
510834	0.22	35.2	0.6	20	34.9	<0.5	0.7
510835	0.22	49.7	0.7	13	19.1	<0.5	3.9
510838	0.24	12.6	0.3	44	91.3	0.5	<0.5
510839	0.25	19.5	0.7	37	52.9	0.6	1.6
510840	0.21	33.5	<0.1	22	54.6	<0.5	1.7
510841	0.23	32.1	0.6	32	70.8	<0.5	1.8
510843	0.26	39.5	2.6	39	39.7	<0.5	0.6
510844	0.27	43.2	1.1	37	51.3	<0.5	<0.5
510845	0.25	113.9	1.2	49	94.2	<0.5	7.6
510846	0.16	10.7	6.1	44	14.9	<0.5	0.7
510860	0.32	46.5	1.2	53	80.9	5.4	0.6
510862	0.33	56.0	1.6	47	63.8	1.3	1.8
510868	0.34	123.2	0.9	56	52.2	2.9	3.9
510870	0.08	15.2	0.6	9	137.6	2.7	5.5
510872	0.26	97.3	6.2	48	56.5	1.8	1.0
510874	0.27	138.4	0.5	49	62.3	7.1	1.9
510878	0.21	52.8	2.4	27	150.0	1.1	<0.5
510879	0.20	36.7	1.2	53	75.5	8.0	<0.5
510885	0.28	114.1	1.6	39	100.7	20.0	1.2
510887	0.22	101.5	29.4	123	61.8	3.7	1.2
510891	0.17	6.3	18.0	16	1.8	<0.5	0.6
510892	0.33	35.3	0.8	94	48.7	<0.5	1.4
510893	0.40	187.8	0.8	29	23.3	9.8	9.4
510901	0.48	150.0	0.6	50	43.5	1.9	1.6
510906	0.19	14.2	0.5	49	201.2	29.3	4.7
510947	0.13	19.7	4.0	22	34.9	24.8	<0.5
510960	0.13	19.2	1.0	12	78.0	10.6	0.7
510961	0.43	101.6	0.6	76	73.3	17.2	2.4
510967	0.46	74.1	0.4	54	61.8	1.1	<0.5
510969	0.21	26.8	4.9	40	11.7	1.4	<0.5
510970	0.27	59.3	0.7	17	159.5	1.2	2.8
510971	0.24	102.8	0.4	30	201.7	<0.5	<0.5
510983	0.14	33.3	4.4	22	37.8	138.0	<0.5
510990	0.15	83.6	0.5	27	139.8	12.7	0.6
510992	0.10	21.5	0.9	54	24.0	8.5	<0.5
510995	0.26	17.6	0.5	29	95.1	2.1	0.6
510999	0.43	107.1	1.2	97	63.7	22.7	8.5
512251	0.30	72.1	3.8	87	41.7	<0.5	2.0
512252	0.26	106.1	3.1	85	85.7	0.7	0.9
512255	0.23	6.5	5.5	38	1.1	<0.5	1.4
512262	0.06	10.8	1.9	6	10.5	20.0	<0.5
512263	0.11	4.9	0.4	29	164.4	2.9	<0.5
512268	0.25	23.7	0.2	27	122.0	0.6	0.8
512270	0.24	8.9	8.8	23	1.4	<0.5	<0.5
512272	0.21	29.5	3.5	63	46.0	<0.5	<0.5
512273	0.03	2.1	6.2	19	0.6	<0.5	<0.5
512274	0.19	34.3	1.4	50	43.0	<0.5	1.1
512275	0.25	50.7	0.9	23	31.9	1.5	<0.5

Sample	Lu	Cu	Pb	Zn	Ni	As	Au
Unit	ppm	ppm	ppm	ppm	ppm	ppm	ppb
MDL	0.01	0.1	0.1	1	0.1	0.5	0.5
512282	0.22	52.6	0.5	37	60.6	1.0	2.4
512283	0.44	98.9	0.3	27	33.0	1.1	1.1
512284	0.40	64.7	0.3	43	44.8	0.7	3.1
512285	0.41	115.5	0.8	50	58.7	<0.5	2.4
512286	0.45	38.8	0.2	50	44.6	<0.5	<0.5
516505	0.12	103.1	1.4	37	526.2	2.5	<0.5
516509	0.34	218.3	3.2	29	104.1	2.1	2.1
516516	0.07	12.2	2.7	42	1481.3	304.0	4.1
516518	0.23	5.9	1.2	2	9.9	<0.5	<0.5
516519	0.14	1.7	1.0	57	14.9	<0.5	<0.5
516522	0.40	58.7	1.2	73	41.0	1.5	1.1
510750-1	0.23	55.6	3.3	15	34.4	0.9	<0.5
510750-2	0.32	132.3	1.6	28	65.1	1.2	<0.5
510754-1	0.35	121.7	0.4	28	62.8	1.2	<0.5
510754-2	0.34	61.4	0.8	38	49.0	2.6	<0.5

Supplementary data table 2 (Paper I): Interlab standard comparison

GEUS (2003-2010) ¹					ACME lab (2008-2010) ²				ACME/GEUS	
Element	Avg	±1σ (abs.)	±1σ (%)	n	Avg	±1σ (abs.)	±1σ (%)	n	(% diff.)	Isotope
Sc	40.9	1.3	3.3	32	41.8	0.9	2.2	21	2.1	45
V	412	12	2.9	32	434	17	3.9	21	5.5	51
Cr	126	3	2.5	32	129	5	3.7	21	2.7	
Co	56.7	1.0	1.7	32	51.9	4.9	9.4	21	-8.5	59
Ni	60.1	2.1	3.5	32	61.0	7.1	11.7	19	1.6	
Cu	226	3	1.5	32	222	10	4.4	21	-1.8	63
Zn	106	2	2.2	32	62.2	5.1	8.1	21	-41.1	66
Ga	20.8	0.2	1.0	32	20.1	1.0	5.0	21	-3.4	71
Rb	3.30	0.05	1.6	32	3.57	0.51	14.4	21	8.1	85
Sr	213	3	1.4	32	224	7	3.1	21	5.4	88
Y	33.8	0.6	1.7	32	30.6	1.2	3.8	21	-9.5	89
Zr	122	3	2.3	32	111	5	4.3	21	-8.7	90
Nb	4.46	0.09	1.9	32	4.16	0.35	8.3	21	-6.8	93
Cs	0.059	0.003	4.5	32	0.121	0.043	35.1	14	106.2	133
Ba	46.5	1.1	2.4	31	47.9	4.4	9.2	21	3.0	137
La	6.58	0.08	1.2	32	6.41	0.32	5.0	21	-2.6	139
Ce	17.4	0.3	1.7	32	17.9	1.0	5.5	21	2.8	140
Pr	2.87	0.07	2.4	32	2.78	0.11	4.1	21	-3.2	141
Nd	14.7	0.3	2.0	32	14.4	0.8	5.4	21	-2.1	143
Sm	4.67	0.09	1.9	32	4.43	0.20	4.4	21	-5.1	147
Eu	1.67	0.04	2.5	32	1.64	0.06	3.8	21	-2.0	153
Gd	5.54	0.32	5.8	32	5.55	0.26	4.7	21	0.1	157
Tb	0.963	0.019	2.0	32	0.991	0.040	4.0	21	2.9	159
Dy	5.86	0.10	1.6	32	5.73	0.20	3.6	21	-2.1	161
Ho	1.23	0.03	2.3	32	1.16	0.05	4.0	21	-5.9	165
Er	3.19	0.06	1.8	32	3.26	0.16	4.9	21	2.0	166
Tm	0.479	0.009	1.8	32	0.469	0.030	6.4	21	-2.0	169
Yb	2.89	0.04	1.5	32	2.81	0.14	5.1	21	-2.6	174
Lu	0.425	0.012	2.9	32	0.419	0.029	7.0	21	-1.6	175
Hf	3.26	0.06	1.8	32	3.27	0.31	9.5	21	0.3	177
Ta	0.305	0.017	5.4	32	0.276	0.089	32.2	21	-9.4	181
W	n.a.				83.3	5.2	6.2	9		
Pb	1.24	0.08	6.5	32	1.17	1.57	134.9	21	-5.9	208
Th	0.594	0.024	4.0	32	0.790	0.232	29.4	21	33.0	232
U	0.147	0.005	3.1	32	0.186	0.096	51.9	21	26.2	238

¹Based on total digestion solution ICP-MS

²Based on total fusion ICP-MS

Sample	Lithology	Locality	Lu (ppm)	Hf (ppm)	Sm (ppm)	Nd (ppm)	Best-fit Hf	Best-fit Nd
510631	Greenschist	Nuuluk	0.2002	1.032	1.448	4.476	Yes	Yes
510638	Greenstone	Nuuluk	0.5637	2.601	3.399	10.13	Yes	Yes
510708	Gabbro	Ilerlak	0.09431	0.3468	0.6137	1.812	Yes	No
510710	Gabbro	Ilerlak	0.08760	0.3250	0.4865	1.364	Yes	Yes
510754	Pillow lava	Nuna Qaqortoq	0.3893	1.777	2.338	6.851	Yes	Yes
510766	Serpentine	Amitsuarsua	0.03288	0.2256	0.3163	1.295	No	No
510839	Felsic schist	Ilerlak	0.2429	2.843	2.784	12.44	No	No
510885	Greenschist	Nuuluk	0.2928	1.193	1.585	4.502	Yes	No
510906	Greenschist	Nuuluk	0.0209	0.1098	1.535	4.676	No	No
510907	Greenschist	Nuuluk	0.2082	1.102	1.590	4.871	No	No

Sample	$^{176}\text{Lu}/^{144}\text{Hf}$	2 σ error	$^{176}\text{Hf}/^{177}\text{Hf}$	2 σ error	$^{147}\text{Sm}/^{144}\text{Nd}$	2 σ error	$^{143}\text{Nd}/^{144}\text{Nd}$	2 σ error
510631	0.02752	±8	0.282520	±8	0.1956	±4	0.512786	±6
510638	0.03076	±12	0.282732	±6	0.2029	±4	0.512921	±5
510708	0.03860	±10	0.283213	±9	0.2048	±4	0.513060	±10
510710	0.03826	±8	0.283176	±9	0.2157	±4	0.513192	±6
510754	0.03109	±8	0.282754	±6	0.2063	±4	0.512984	±6
510766	0.02068	±8	0.282052	±9	0.1476	±3	0.511762	±8
510839	0.01213	±4	0.281644	±5	0.1353	±3	0.511459	±11
510885	0.03484	±9	0.282982	±6	0.2129	±4	0.513081	±10
510906	0.02704	±7	0.282570	±5	0.1985	±4	0.512784	±10
510907	0.02682	±7	0.282527	±5	0.1973	±4	0.512748	±8

Sample	$\epsilon\text{Hf}_{(3000\text{Ma})}$	2 σ error	$\epsilon\text{Hf}_{(3190\text{Ma})}$	2 σ error	$\epsilon\text{Nd}_{(3000\text{Ma})}$	2 σ error	$\epsilon\text{Nd}_{(3190\text{Ma})}$	2 σ error
510631	+3.0	±0.5	+3.8	0.5	+3.2	±0.4	+3.2	0.4
510638	+3.9	±0.5	+4.3	0.5	+3.0	±0.4	+2.9	0.4
510708	+5.0	±0.5	+4.3	0.5	+5.0	±0.4	+4.8	0.4
510710	+4.4	±0.5	+3.7	0.5	+3.4	±0.4	+2.9	0.4
510754	+4.0	±0.5	+4.4	0.5	+2.9	±0.4	+2.7	0.4
510766	+0.4	±0.5	+2.1	0.5	+1.8	±0.4	+3.0	0.4
510839	+3.4	±0.5	+6.3	0.4	-0.6	±0.4	-2.1	0.4
510885	+4.5	±0.5	+4.3	0.5	+2.3	±0.4	+1.9	0.4
510906	+5.8	±0.5	+6.7	0.5	+2.0	±0.4	+2.0	0.4
510907	+4.7	±0.5	+5.6	0.5	+1.8	±0.4	+1.8	0.4

$^{176}\text{Lu}/^{144}\text{Hf}$ and $^{147}\text{Sm}/^{144}\text{Nd}$ errors are 2 σ on the 5th digit and $^{176}\text{Hf}/^{177}\text{Hf}$ and $^{143}\text{Nd}/^{144}\text{Nd}$ errors are 2 σ internal errors on the 6th digit

Supplementary data table 4 (Paper I): U-Pb isotope data

Sample	Analysis	U (ppm) ^a	Th/U ^a
510772	Zircon_sample-007	201	0.74
510772	Zircon_sample-008	157	1.03
510772	Zircon_sample-009	119	0.95
510772	Zircon_sample-010	194	0.95
510772	Zircon_sample-011	104	0.92
510772	Zircon_sample-012	85	0.99
510772	Zircon_sample-013	70	0.63
510772	Zircon_sample-014	77	0.63
510772	Zircon_sample-015	107	0.91
510772	Zircon_sample-020	159	0.92
510772	Zircon_sample-021	192	1.13
510772	Zircon_sample-022	226	1.33
510772	Zircon_sample-023	265	1.31
510772	Zircon_sample-024	68	0.76
510772	Zircon_sample-025	145	0.86
510772	Zircon_sample-028	97	0.80
510772	Zircon_sample-033	178	0.94
510772	Zircon_sample-034	302	1.22
510772	Zircon_sample-035	88	0.96
510772	Zircon_sample-037	57	0.65
510772	Zircon_sample-038	209	1.16
510772	Zircon_sample-039	187	1.04
510772	Zircon_sample-040	201	1.11
510772	Zircon_sample-041	124	0.79
510772	Zircon_sample-046	159	0.49
510772	Zircon_Sample-047	370	0.64
510772	Zircon_Sample-048	101	0.64
510772	Zircon_Sample-049	145	0.94
510772	Zircon_Sample-050	85	0.78
510772	Zircon_Sample-051	194	1.14
510772	Zircon_Sample-052	183	0.84
510772	Zircon_Sample-053	56	0.70
510772	Zircon_Sample-054	119	0.72
510772	Zircon_Sample-059	96	0.88
510772	Zircon_Sample-060	55	0.90
510772	Zircon_Sample-061	82	0.91
510772	Zircon_Sample-062	195	0.82
510772	Zircon_Sample-063	88	0.79
510772	Zircon_Sample-064	174	1.20
510772	Zircon_Sample-065	196	1.06
510772	Zircon_Sample-066	211	0.69
510772	Zircon_Sample-067	97	0.43
510772	Zircon_Sample-072	149	1.15
510772	Zircon_Sample-073	245	0.45
510772	Zircon_Sample-074	222	0.43
510772	Zircon_Sample-075	65	0.88
510772	Zircon_Sample-076	151	0.98
510772	Zircon_Sample-077	178	1.04
510772	Zircon_Sample-078	430	0.42
510772	Zircon_Sample-079	88	0.91
510772	Zircon_Sample-080	253	0.18

^aU and Pb concentrations and Th/U ratios are calculated relative to GJ-1 reference zircon

^bCorrected for background and within-run Pb/U frac. and norm. to ref. zircon GJ-1 (ID-TIMS values/meas. value); $^{207}\text{Pb}/^{235}\text{U}$ calculated using $(^{207}\text{Pb}/^{206}\text{Pb})/(^{238}\text{U}/^{206}\text{Pb} * 1/137.88)$

^cRho is the error correlation defined as the quotient of the propagated errors of the $^{206}\text{Pb}/^{238}\text{U}$ and the $^{207}\text{Pb}/^{235}\text{U}$ ratio

^dQuadratic addition of within-run errors (2σ) and daily reproducibility of GJ-1 (2σ)

^eCorrected for mass-bias by normalising to GJ-1 reference zircon (~0.6 per atomic mass unit) and common Pb using the model Pb composition of Stacey & Kramers (1975)

Sample	Analysis	U (ppm) ^a	Th/U ^a
510772	Zircon_Sample-085	201	0.83
510772	Zircon_Sample-086	122	0.85
510772	Zircon_Sample-087	95	0.94
510772	Zircon_Sample-088	172	0.97
510772	Zircon_Sample-089	33	0.46
510772	Zircon_Sample-090	90	0.65
510772	Zircon_Sample-091	253	1.07
510772	Zircon_Sample-092	124	0.68
510657	Zircon_sample-008	136	0.71
510657	Zircon_sample-009	191	0.20
510657	Zircon_sample-010	144	0.26
510657	Zircon_sample-011	592	0.23
510657	Zircon_sample-012	630	0.15
510657	Zircon_sample-013	262	0.28
510657	Zircon_sample-014	554	0.23
510657	Zircon_sample-015	656	0.48
510657	Zircon_sample-020	261	0.29
510657	Zircon_sample-022	182	0.13
510657	Zircon_sample-023	476	0.13
510657	Zircon_sample-024	145	0.26
510657	Zircon_sample-027	506	0.29
510657	Zircon_sample-035	185	0.15
510657	Zircon_sample-037	679	0.21
510657	Zircon_sample-038	654	0.06
510657	Zircon_sample-039	398	0.44
510657	Zircon_sample-040	174	0.36

RATIOS

Analysis	$^{207}\text{Pb}/^{235}\text{U}^b$	$2\sigma^d$	$^{206}\text{Pb}/^{238}\text{U}^b$	$2\sigma^d$	ρ^c	$^{207}\text{Pb}/^{206}\text{Pb}^e$	$2\sigma^d$
Zircon_sample-007	18.61	0.89	0.61	0.03	0.97	0.220	0.003
Zircon_sample-008	18.04	1.11	0.59	0.03	0.87	0.223	0.007
Zircon_sample-009	18.38	1.18	0.61	0.04	0.92	0.220	0.006
Zircon_sample-010	18.37	0.36	0.60	0.01	0.84	0.221	0.002
Zircon_sample-011	19.42	0.95	0.62	0.02	0.74	0.226	0.007
Zircon_sample-012	19.12	0.92	0.63	0.02	0.70	0.222	0.008
Zircon_sample-013	19.97	0.64	0.67	0.02	0.90	0.218	0.003
Zircon_sample-014	17.92	1.31	0.58	0.04	0.98	0.223	0.003
Zircon_sample-015	18.06	0.72	0.60	0.02	0.90	0.219	0.004
Zircon_sample-020	17.47	1.19	0.57	0.04	0.97	0.222	0.004
Zircon_sample-021	17.89	0.83	0.59	0.02	0.91	0.221	0.004
Zircon_sample-022	19.41	0.93	0.64	0.03	0.90	0.219	0.005
Zircon_sample-023	17.84	1.25	0.59	0.04	0.94	0.220	0.005
Zircon_sample-024	17.77	0.84	0.58	0.03	0.93	0.222	0.004
Zircon_sample-025	17.47	0.64	0.57	0.02	0.94	0.221	0.003
Zircon_sample-028	18.48	1.33	0.60	0.04	0.94	0.225	0.006
Zircon_sample-033	18.25	0.90	0.60	0.03	0.91	0.221	0.005
Zircon_sample-034	17.90	1.29	0.59	0.04	0.94	0.220	0.005
Zircon_sample-035	18.07	0.96	0.59	0.03	0.90	0.222	0.005
Zircon_sample-037	17.12	0.91	0.57	0.03	0.95	0.217	0.004
Zircon_sample-038	17.62	1.21	0.58	0.04	0.95	0.221	0.005
Zircon_sample-039	17.22	0.48	0.57	0.01	0.79	0.221	0.004
Zircon_sample-040	18.80	1.16	0.62	0.04	0.96	0.219	0.004
Zircon_sample-041	18.45	0.99	0.60	0.03	0.94	0.223	0.004
Zircon_sample-046	19.33	0.93	0.63	0.03	0.95	0.222	0.003
Zircon_Sample-047	15.51	1.02	0.54	0.03	0.93	0.209	0.005
Zircon_Sample-048	18.56	1.30	0.60	0.04	0.96	0.223	0.004
Zircon_Sample-049	18.25	1.01	0.60	0.03	0.89	0.221	0.006
Zircon_Sample-050	18.81	0.99	0.61	0.03	0.89	0.223	0.005
Zircon_Sample-051	17.99	0.77	0.59	0.02	0.94	0.220	0.003
Zircon_Sample-052	18.17	0.92	0.60	0.03	0.96	0.220	0.003
Zircon_Sample-053	18.10	0.85	0.59	0.03	0.90	0.223	0.005
Zircon_Sample-054	16.89	0.72	0.54	0.02	0.84	0.226	0.005
Zircon_Sample-059	17.57	0.73	0.57	0.02	0.87	0.222	0.005
Zircon_Sample-060	19.46	0.71	0.64	0.02	0.91	0.222	0.003
Zircon_Sample-061	16.99	0.65	0.56	0.02	0.88	0.221	0.004
Zircon_Sample-062	18.67	0.53	0.61	0.01	0.77	0.222	0.004
Zircon_Sample-063	16.77	1.07	0.56	0.03	0.91	0.216	0.006
Zircon_Sample-064	17.42	0.53	0.57	0.02	0.90	0.221	0.003
Zircon_Sample-065	17.03	0.80	0.56	0.02	0.94	0.219	0.004
Zircon_Sample-066	17.62	0.88	0.59	0.03	0.97	0.217	0.002
Zircon_Sample-067	17.25	0.67	0.56	0.02	0.90	0.224	0.004
Zircon_Sample-072	18.21	0.65	0.60	0.02	0.90	0.221	0.003
Zircon_Sample-073	18.43	1.07	0.62	0.03	0.89	0.214	0.006
Zircon_Sample-074	16.28	0.66	0.58	0.02	0.81	0.204	0.005
Zircon_Sample-075	17.73	0.66	0.58	0.02	0.91	0.221	0.003
Zircon_Sample-076	18.21	0.42	0.60	0.01	0.90	0.221	0.002
Zircon_Sample-077	18.74	0.65	0.62	0.02	0.89	0.220	0.003
Zircon_Sample-078	17.04	0.74	0.58	0.02	0.94	0.212	0.003
Zircon_Sample-079	17.97	0.77	0.59	0.02	0.93	0.222	0.004
Zircon_Sample-080	14.93	1.00	0.55	0.03	0.93	0.197	0.005

RATIOS

Analysis	$^{207}\text{Pb}/^{235}\text{U}^b$	$2\sigma^d$	$^{206}\text{Pb}/^{238}\text{U}^b$	$2\sigma^d$	ρ^c	$^{207}\text{Pb}/^{206}\text{Pb}^e$	$2\sigma^d$
Zircon_Sample-085	18.48	0.49	0.61	0.01	0.90	0.221	0.003
Zircon_Sample-086	18.15	0.58	0.59	0.02	0.80	0.222	0.004
Zircon_Sample-087	18.50	0.76	0.60	0.02	0.89	0.222	0.004
Zircon_Sample-088	18.60	0.78	0.61	0.02	0.92	0.221	0.004
Zircon_Sample-089	19.09	0.81	0.62	0.02	0.90	0.224	0.004
Zircon_Sample-090	18.09	0.65	0.60	0.02	0.86	0.218	0.004
Zircon_Sample-091	18.55	0.72	0.62	0.02	0.96	0.218	0.002
Zircon_Sample-092	18.68	0.82	0.62	0.03	0.98	0.219	0.002
Zircon_sample-008	14.50	1.02	0.51	0.03	0.93	0.208	0.005
Zircon_sample-009	15.66	1.05	0.55	0.03	0.90	0.207	0.006
Zircon_sample-010	16.48	1.17	0.58	0.04	0.90	0.206	0.006
Zircon_sample-011	16.03	1.34	0.57	0.04	0.92	0.204	0.007
Zircon_sample-012	16.14	0.36	0.57	0.01	0.81	0.206	0.003
Zircon_sample-013	15.75	1.31	0.56	0.04	0.90	0.205	0.007
Zircon_sample-014	14.56	1.13	0.53	0.04	0.95	0.200	0.005
Zircon_sample-015	12.24	0.84	0.47	0.03	0.96	0.189	0.003
Zircon_sample-020	16.63	1.14	0.59	0.04	0.91	0.204	0.006
Zircon_sample-022	16.47	1.61	0.57	0.05	0.93	0.209	0.008
Zircon_sample-023	14.60	1.08	0.53	0.03	0.89	0.200	0.007
Zircon_sample-024	16.29	1.39	0.56	0.04	0.91	0.211	0.007
Zircon_sample-027	16.32	1.66	0.58	0.05	0.92	0.206	0.008
Zircon_sample-035	17.00	1.34	0.59	0.04	0.95	0.210	0.005
Zircon_sample-037	13.52	0.97	0.49	0.03	0.86	0.198	0.007
Zircon_sample-038	15.99	1.11	0.58	0.03	0.74	0.201	0.009
Zircon_sample-039	15.44	0.79	0.57	0.02	0.85	0.197	0.005
Zircon_sample-040	14.58	1.32	0.52	0.04	0.93	0.204	0.007

AGES (Ma)							
Analysis	$^{207}\text{Pb}/^{235}\text{U}$	2 σ	$^{206}\text{Pb}/^{238}\text{U}$	2 σ	$^{207}\text{Pb}/^{206}\text{Pb}$	2 σ	Conc. %
Zircon_sample-007	3022	46	3086	113	2980	20	104
Zircon_sample-008	2992	59	2981	129	3000	48	99
Zircon_sample-009	3010	62	3054	143	2981	42	102
Zircon_sample-010	3009	19	3038	39	2991	17	102
Zircon_sample-011	3063	47	3122	90	3024	52	103
Zircon_sample-012	3048	46	3131	83	2993	55	105
Zircon_sample-013	3090	31	3290	74	2962	23	111
Zircon_sample-014	2985	71	2960	171	3002	22	99
Zircon_sample-015	2993	38	3019	87	2976	28	101
Zircon_sample-020	2961	65	2909	154	2996	27	97
Zircon_sample-021	2984	45	2973	101	2991	31	99
Zircon_sample-022	3063	46	3203	108	2972	34	108
Zircon_sample-023	2981	68	2987	158	2977	38	100
Zircon_sample-024	2977	45	2952	104	2994	28	99
Zircon_sample-025	2961	35	2924	81	2987	20	98
Zircon_sample-028	3015	69	3017	163	3014	40	100
Zircon_sample-033	3003	47	3023	108	2990	33	101
Zircon_sample-034	2984	69	2991	162	2980	40	100
Zircon_sample-035	2994	51	2988	114	2997	38	100
Zircon_sample-037	2941	51	2917	118	2958	26	99
Zircon_sample-038	2969	66	2937	154	2991	35	98
Zircon_sample-039	2947	27	2890	51	2987	28	97
Zircon_sample-040	3032	60	3117	147	2975	27	105
Zircon_sample-041	3013	52	3030	123	3002	29	101
Zircon_sample-046	3058	46	3159	114	2992	25	106
Zircon_Sample-047	2847	63	2781	137	2894	40	96
Zircon_Sample-048	3019	67	3044	163	3003	31	101
Zircon_Sample-049	3003	53	3028	119	2986	40	101
Zircon_Sample-050	3032	51	3077	115	3002	38	102
Zircon_Sample-051	2989	41	3001	97	2981	23	101
Zircon_Sample-052	2999	49	3030	117	2978	23	102
Zircon_Sample-053	2995	45	2983	102	3003	32	99
Zircon_Sample-054	2929	41	2792	81	3024	38	92
Zircon_Sample-059	2966	40	2921	85	2997	33	97
Zircon_Sample-060	3065	35	3174	83	2994	25	106
Zircon_Sample-061	2934	37	2857	78	2987	29	96
Zircon_Sample-062	3025	27	3066	53	2998	29	102
Zircon_Sample-063	2922	61	2878	134	2953	44	97
Zircon_Sample-064	2958	29	2910	64	2991	21	97
Zircon_Sample-065	2937	45	2878	102	2977	27	97
Zircon_Sample-066	2969	48	2983	116	2960	18	101
Zircon_Sample-067	2949	37	2864	81	3007	27	95
Zircon_Sample-072	3001	34	3021	78	2987	25	101
Zircon_Sample-073	3013	56	3123	129	2940	42	106
Zircon_Sample-074	2894	39	2941	78	2861	39	103
Zircon_Sample-075	2975	36	2950	80	2992	25	99
Zircon_Sample-076	3001	22	3020	50	2988	16	101
Zircon_Sample-077	3029	34	3100	77	2981	25	104
Zircon_Sample-078	2937	42	2963	98	2919	23	102
Zircon_Sample-079	2988	41	2976	94	2997	26	99
Zircon_Sample-080	2811	64	2820	142	2804	41	101

AGES (Ma)

Analysis	$^{207}\text{Pb}/^{235}\text{U}$	2 σ	$^{206}\text{Pb}/^{238}\text{U}$	2 σ	$^{207}\text{Pb}/^{206}\text{Pb}$	2 σ	Conc. %
Zircon_Sample-085	3015	25	3058	58	2987	18	102
Zircon_Sample-086	2998	31	3003	61	2995	31	100
Zircon_Sample-087	3016	39	3050	89	2994	30	102
Zircon_Sample-088	3021	41	3075	95	2985	27	103
Zircon_Sample-089	3047	41	3103	93	3010	30	103
Zircon_Sample-090	2995	34	3039	75	2965	29	103
Zircon_Sample-091	3019	37	3096	92	2968	17	104
Zircon_Sample-092	3025	42	3101	105	2976	15	104
Zircon_sample-008	2783	67	2642	143	2887	41	92
Zircon_sample-009	2856	64	2816	138	2885	48	98
Zircon_sample-010	2905	68	2955	151	2871	51	103
Zircon_sample-011	2879	80	2904	181	2861	53	102
Zircon_sample-012	2885	21	2897	42	2877	21	101
Zircon_sample-013	2862	79	2850	172	2870	59	99
Zircon_sample-014	2787	74	2730	164	2829	39	97
Zircon_sample-015	2623	64	2480	136	2735	30	91
Zircon_sample-020	2914	65	2995	149	2858	46	105
Zircon_sample-022	2904	94	2915	212	2897	59	101
Zircon_sample-023	2790	71	2743	147	2824	56	97
Zircon_sample-024	2894	82	2872	180	2910	57	99
Zircon_sample-027	2896	98	2930	221	2872	65	102
Zircon_sample-035	2935	75	2975	179	2907	38	102
Zircon_sample-037	2717	68	2588	132	2814	60	92
Zircon_sample-038	2876	66	2942	121	2831	76	104
Zircon_sample-039	2843	49	2899	101	2803	44	103
Zircon_sample-040	2788	86	2695	184	2857	56	94

Paper II:

Complex calc-alkaline volcanism
recorded in Mesoarchaeoan
supracrustal belts north of
Frederikshåb Isblink, southern West
Greenland: implications for
subduction zone processes in the
early Earth

Precambrian Research (in press)
DOI: 10.1016/j.precamres.2012.03.013

Complex calc-alkaline volcanism recorded in Mesoarchaeoan supracrustal belts north of Frederikshåb Isblink, southern West Greenland: implications for subduction zone processes in the early Earth

Kristoffer Szilas^{a,b,c,*}, J. Elis Hoffmann^{d,e}, Anders Scherstén^f, Minik T. Rosing^{c,g}, Brian F. Windley^h, Thomas F. Kokfelt^a, Nynke Keulen^a, Vincent J. van Hinsbergⁱ, Tomas Næraa^a, Robert Frei^{b,g}, Carsten Münker^e

^aGeological Survey of Denmark and Greenland - GEUS, Øster Voldgade 10, 1350 Copenhagen K, Denmark (ksz@geus.dk)

^bDepartment of Geography and Geology, University of Copenhagen, Øster Voldgade 10, 1350 Copenhagen K, Denmark

^cNatural History Museum of Denmark, Øster Voldgade 5-7, 1350 Copenhagen K, Denmark

^dSteinmann Institut, Abt. Endogene Prozesse, Universität zu Bonn, Poppelsdorfer Schloss, 53115 Bonn, Germany

^eInstitut für Geologie und Mineralogie, Universität zu Köln, Zùlpicher Str. 49b, 50674 Köln, Germany

^fDepartment of Earth and Ecosystem Sciences Division of Geology, Lund University, Sölvegatan 12, 223 62 Lund, Sweden

^gNordic Center for Earth Evolution, NordCEE, Denmark

^hDepartment of Geology, University of Leicester, Leicester LE1 7RH, UK

ⁱDepartment of Earth Sciences, University of Oxford, South Parks Road, Oxford OX1 3AN, UK

ABSTRACT

We present new geochemical data for three Mesoarchaeoan supracrustal belts (Ravns Storø, Bjørnesund and Perserajorsuaq) situated north of Frederikshåb Isblink in southern West Greenland for which we propose the collective name ‘The Ikkattup Nunaa Supracrustal Association’. They comprise mainly amphibolites of tholeiitic basalt composition and leucoamphibolites of calc-alkaline andesite composition. Both lithological units are cut by aplite sheets of tonalite-trondhjemite-granodiorite (TTG) composition with U-Pb zircon ages of c. 2900 Ma. Lu-Hf and Sm-Nd isochrons based on whole rock amphibolite and leucoamphibolite samples yield ages of 2990 ± 41 Ma and 3020 ± 78 Ma, respectively, which are within error of the age of the Fiskenset Complex situated 5–25 km to the north.

Leucoamphibolites from the three supracrustal belts show apparent geochemical mixing trends between tholeiitic amphibolites and TTG gneisses, as the end-members. By assimilation-fractional-crystallisation (AFC) modelling we can show that one group of leucoamphibolites can indeed be explained by contamination of the parental melts by a TTG-like end-member and another group of high P_2O_5 , La and Nb leucoamphibolites can be explained by contamination involving a hypothetical low-silica adakite end-member. However, the leucoamphibolites are juvenile with $\epsilon Nd_{(2970Ma)}$ from +2.1 to +3.5 and $\epsilon Hf_{(2970Ma)}$ of +3.5 to +4.3. Thus, the mafic source of the felsic contaminant melts must have been derived from a depleted mantle source more or less at the same time (<60 Ma) as the volcanism took place.

Our preferred interpretation of the geochemical and isotopic data is that the protoliths of the supracrustal rocks formed in an island arc setting, where early tholeiitic volcanism gave way to calc-alkaline volcanism in a maturing arc. The apparent AFC trends are thus explained by *in situ* partial melting of basaltic arc crust to form juvenile TTG- and adakite-melts that mixed with mafic magmas or contaminated their mantle source to produce the calc-alkaline leucoamphibolite protolith.

This model has important implications for the general interpretation of other Archaeoan supracrustal belts, because AFC and geochemical mixing trends towards a TTG end-member are not uniquely diagnostic of crustal contamination, but may rather reflect processes operating at source levels in arcs, such as melting-assimilation-storage-homogenisation (MASH) or slab-melt (low-silica adakite) metasomatism of their mantle source.

Keywords: *Archeoan; Supracrustal belt; Calc-alkaline volcanism; The Ikkattup Nunaa Supracrustal Association; southern West Greenland*

1. Introduction

The detailed petrogenesis of volcanic arc-related calc-alkaline andesitic rocks is still much debated (e.g. Kelemen et al., 2003; and references therein). The observation of disequilibrium textures in modern calc-alkaline arc rocks suggests the operation of complex processes for their formation that have been ascribed to both differentiation of water-rich magmas (Green and Ringwood, 1967; Grove et al., 2003; Sisson and Grove, 1993), degassing-induced crystallisation (Frey and Lange, 2010), and mixing of felsic and mafic magmas (Anderson, 1975; Eichelberger, 1978; Tatsumi and Suzuki, 2009). Although all of these effects could contribute to the documented disequilibrium features in arc magmas, mixing is strongly supported by recent work on melt inclusions and quenched glasses from volcanic arcs, which show a strong bimodal distribution and suggests that andesites are the product of mixing between two end-members (Kovalenko et al., 2010; Reubi and Blundy, 2009). This conclusion is also supported by mineral-scale isotope and trace element variations (e.g. Davidson et al., 2005, 2007).

Calc-alkaline andesitic rocks of Archaeoan age are rare, but they are indeed sometimes present within supracrustal belts (Barley et al., 1998; Klausen et al., 2011; Leclerc et al., 2011; Mtoro et al., 2009; Polat and Münker, 2004; Wang et al., 2004). Such intermediate volcanic rocks always carry a geochemical signature that is characteristic of modern arc rocks (e.g. LILE and LREE enrichment

and Nb-Ta-Ti depletions relative to MORB). However, controversy still exists regarding the initiation of modern-style subduction volcanism in the Archaeoan (e.g. Condie and Pease, 2008; Hamilton, 1998; Stern, 2008; van Kranendonk, 2004; van Kranendonk, 2011). The origin of calc-alkaline rocks through Archaeoan subduction is complicated by the possibility that their parental melts assimilated continental crust. Such a scenario must be tested prior to making conclusions about possible arc affinities. Accordingly, a combined geochemical and isotopic study of calc-alkaline andesitic rocks from the Archaeoan rock record might give important constraints, as to when and how modern-style subduction tectonics began in the early Earth.

In this study we investigate the petrogenesis of Mesoarchaeoan calc-alkaline volcanic rocks in the Ravns Storø, Bjørnesund and Perserajorsuaq supracrustal belts north of Frederikshåb Isblink in SW Greenland in order to elucidate the origin of such calc-alkaline volcanism.

2. Geological setting

The study area is located north of Frederikshåb Isblink in southern West Greenland (Fig. 1). Rocks from the Ravns Storø, Bjørnesund and Perserajorsuaq supracrustal belts were collected with the purpose of investigating the geological environment in which these volcanic rocks formed.

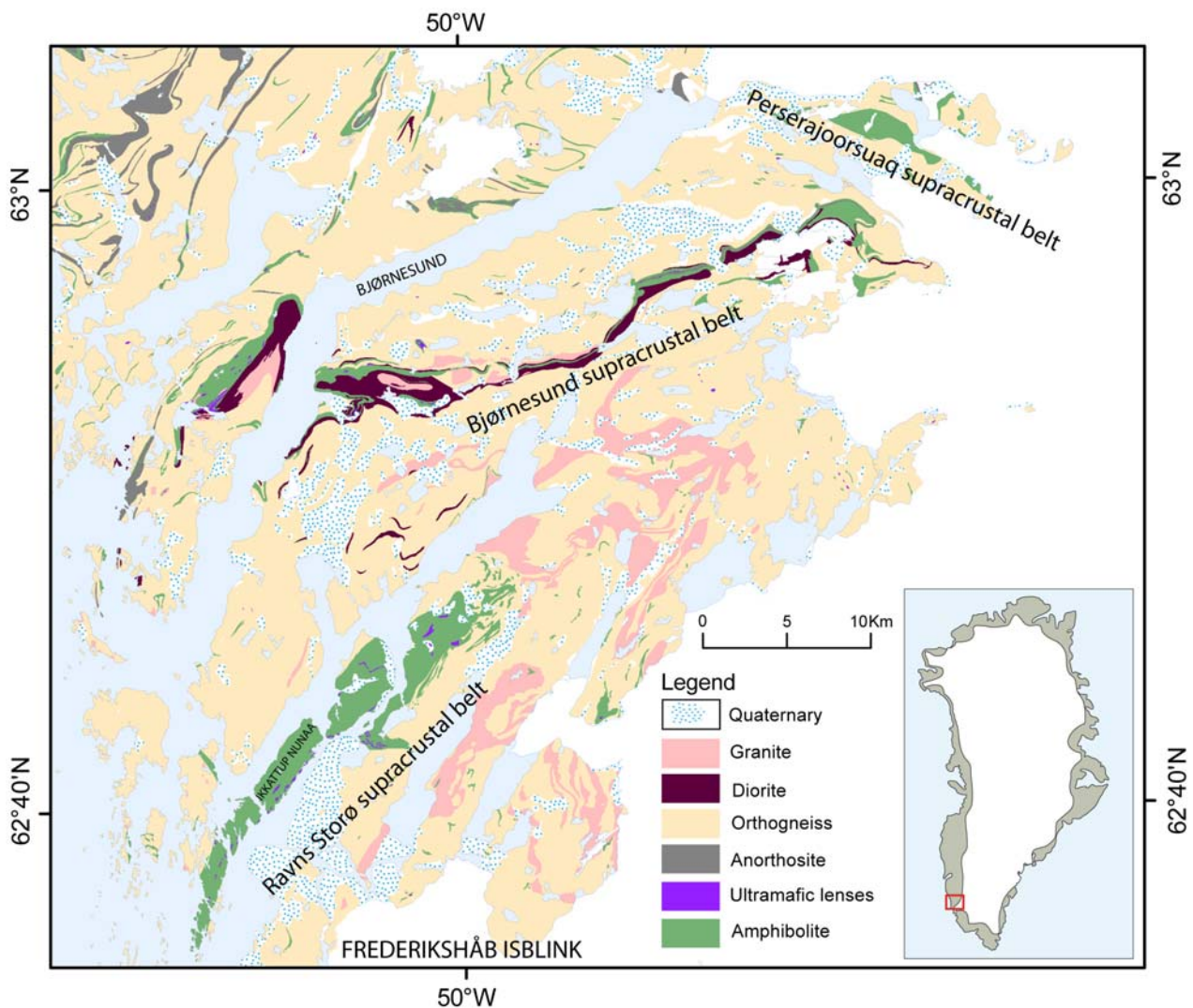


Figure 1. Map of the Ravns Storø, Bjørnesund and Perserajoorsuaq supracrustal belts (collectively referred to as ‘The Ikkattup Nunaa Supracrustal Association’) located north of Frederikshåb Isblink. The Archaean TTG orthogneisses are intrusive into the ‘The Ikkattup Nunaa Supracrustal Association’.

The three supracrustal belts are up to 5 x 20 km in size and crop out within intrusive Mesoproterozoic TTG orthogneisses. The existence of a genetic link between the three supracrustal belts has been speculated since the area was mapped in the 1960’s, due to their spatial proximity and because they contain similar lithological units and field relationships. We here propose that the three belts should be collectively named ‘The Ikkattup Nunaa Supracrustal Association’, after the island where the best preserved lithological units are found in the Ravns Storø supracrustal belt.

The Ravns Storø supracrustal belt is also referred to as Ikkattup Nunaa in the literature (e.g. Windley and Garde, 2009), but the former name is preferred here as it was used in most of the earlier published works about this area (Andersen and Friend, 1973; Dawes, 1969; Friend, 1975; Windley et al., 1966; Windley, 1966, 1968). The lithological units include amphibolites, amphibolite dykes, pillow lavas, gabbros, lithic tuffs, leucoamphibolites, ultramafic rocks and their altered derivatives. An age of 2908 ± 13 Ma from a volcano-sedimentary rock was previously interpreted as the age of deposition of the supracrustal belt (Nutman et al., 2004). However, aplite dykes with an age of c. 2900 Ma cut the amphibolites and this age is thus taken as the minimum age of the supracrustal rocks (Section 4.4; Szilas et al., 2011a). Additionally, we suggest that the volcano-sedimentary rocks dated by Nutman et al. (2004) are actually fine-grained volcanic rocks similar to the leucoamphibolites we have dated in this study and that they mainly record metamorphic ages (Section 5.5). The end of the low-grade amphibolite-facies overprint

in the area is indicated by a zircon U-Pb measurement of an intrusive granitic sheet with a relict amphibolite-facies mineral assemblage yielding an age of 2660 ± 20 Ma (Pidgeon and Kalsbeek, 1978). Samples for the present study were collected by the Geological Survey of Denmark and Greenland (GEUS) during field work in 2008 and 2009.

The Bjørnesund supracrustal belt has only seen very limited scientific study (Keulen et al., 2011; McGregor and Friend, 1992; Pulvertaft, 1972) and some Au exploration (Appel, 1992; Schlatter and Steensgaard, 2011). This belt is characterised by amphibolites, amphibolite dykes, gabbros, calc-silicate-rich amphibolites, leucoamphibolites, lithic tuffs, as well as anorthosites and associated layered gabbros. The supracrustal rocks have been intruded by aplite sheets of tonalitic composition, providing a minimum age c. 2900 Ma (Section 4.4). The lithological units and their field relations are very similar to those in the Ravns Storø supracrustal belt, but a higher degree of deformation in the Bjørnesund supracrustal belt has obscured many primary features. The samples from this area were collected by GEUS in 2009.

The Bjørnesund supracrustal belt is in direct contact with a large (c. 50 x 5000 m) anorthosite sheet along its northern margin; however, the nature of the contact is not clear. On the basis of similar lithological units and field relations in the Fiskensæset Complex (located 5–25 km to the north; Fig. 1), a link between the Fiskensæset Complex and the Bjørnesund supracrustal belt has previously been suggested (Keulen et al., 2011; Myers, 1985). However, it has been

noted that the contact between the anorthosite and the supracrustal rocks is intrusive (Bridgewater et al., 1976; Kalsbeek and Myers, 1973). Similarities in age and geochemistry between the Ravns Størø and Bjørnesund supracrustal belts extend this interpolation even farther southwards (Szilas et al., 2011a).

The Perserajorsuaq supracrustal belt has never been studied in detail and no previous geological data have been published from this area. To our knowledge, this locality has not been visited since it was first mapped by H. R. Williams in the beginning of the 1970s, except for a brief reconnaissance by GEUS in 2009 during which the present samples were collected. The two main lithological units are amphibolites and leucoamphibolites in a repeated succession that is cut by aplite and granite sheets. The rocks in the Perserajorsuaq supracrustal belt record high strain, preventing a proper recognition of primary igneous structures.

The well-studied Fiskenæsset Complex is located immediately to the north of the Ravns Størø, Bjørnesund and Perserajorsuaq supracrustal belts (Fig. 1); its formation age was recently determined as c. 2970 Ma (Polat et al., 2010). Roof pendants of foliated amphibolite have been observed within the anorthosite of the Fiskenæsset Complex (B.F. Windley and V.J. van Hinsberg pers. comm., 2010), suggesting an intrusive contact relationship with the adjacent supracrustal belts. This implies that the anorthosites of the Fiskenæsset Complex postdates the amphibolites, as previously suggested (Bridgewater et al., 1976; Kalsbeek and Myers, 1973). However, the age difference is marginal, because the anorthosites and the supracrustal rocks fall on the same isochron (Polat et al.,

2010). The geochemical characteristics of the supracrustal rocks in the Fiskenæsset Complex show forearc affinity (Polat et al., 2009b, 2011a), and thus overall show similarities to 'The Ikkattup Nunaa Supracrustal Association' described in the present study (Section 4.2). Accordingly, the supracrustal belts in this region might have formed at the same time and in a similar tectonic setting as suggested by Szilas et al. (2011a).

The entire area was reworked through amphibolite-facies metamorphism (Friend, 1975, 1976a, 1976b; McGregor and Friend, 1992; Schumacher et al., 2011; Windley and Garde, 2009), so the prefix 'meta' will be taken as implicit for all lithological units in the following sections.

In this paper we treat the Ravns Størø, Bjørnesund and Perserajorsuaq supracrustal belts as being coeval and co-genetic for the following reasons: (1) the belts are spatially associated and appear to have formed a linear belt that was disrupted by TTG intrusion (Fig. 1), (2) the lithological units and their field relationships within the belts are similar (Section 4.1), (3) the major and trace element geochemical data of the belts essentially overlap (Section 4.2; Szilas et al., 2011a), (4) Lu-Hf and Sm-Nd isotopic data show that the Ravns Størø and Bjørnesund supracrustal belts fall on the same isochron (Section 4.3; Szilas et al., 2011a) and (5) the U-Pb zircon ages for felsic lithological units are similar for all three supracrustal belts (see Section 4.4). The above justifies naming the three supracrustal belts collectively as 'The Ikkattup Nunaa Supracrustal Association'.

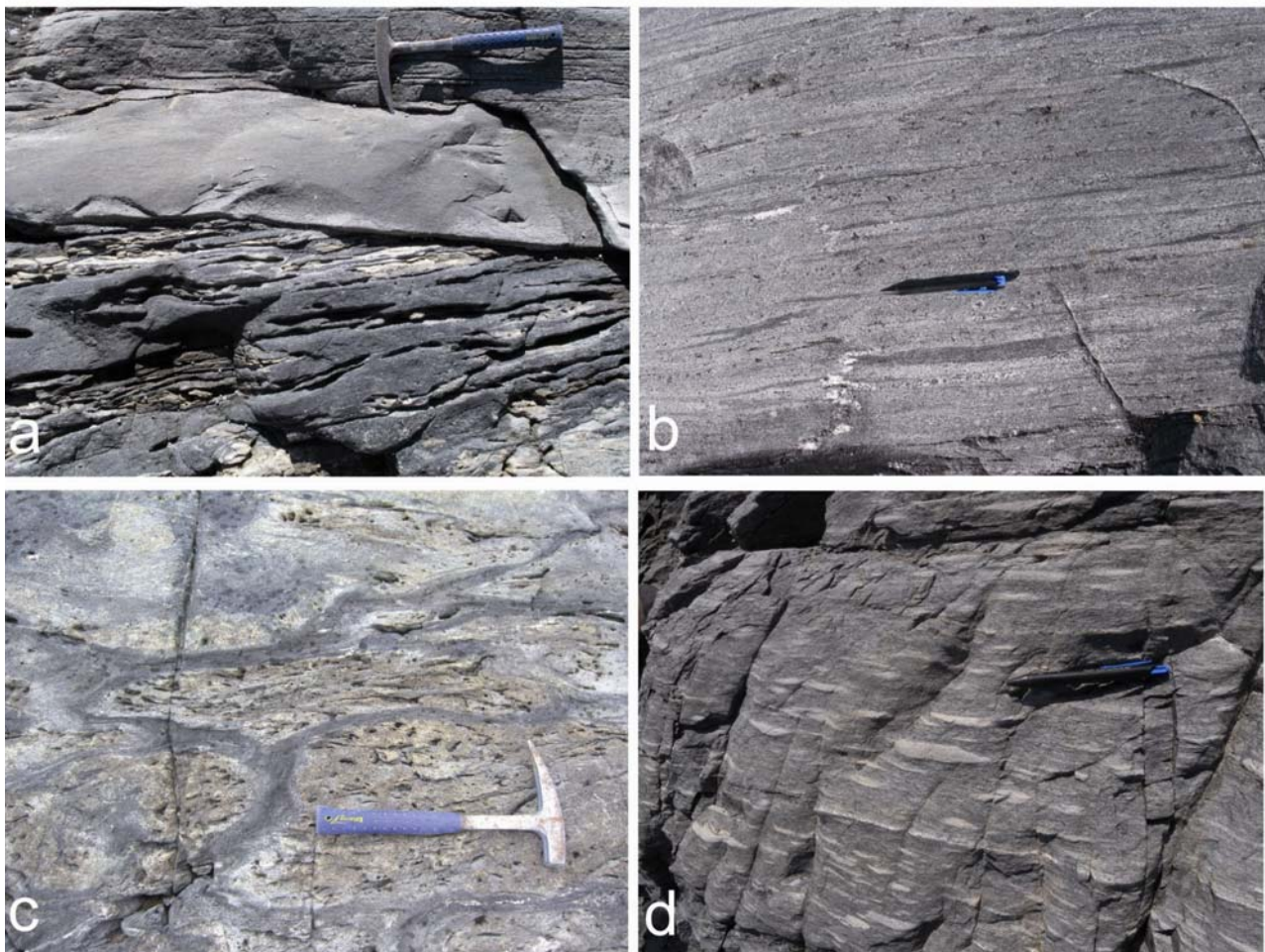


Figure 2. (a) Aplite sheet (468793) with clear intrusive relationship to the main amphibolite unit at the Ravns Størø supracrustal belt. The light coloured aplite sheet cuts the foliation of the amphibolite. Hammer for scale. (b) Leucoamphibolite (510813) with felsic and mafic patches at the Bjørnesund supracrustal belt. The composite nature of this deformed rock suggests a volcanoclastic protolith. Pen for scale. (c) Pillow lava (510913) at the Ravns Størø supracrustal belt. The pillow cores are light coloured and epidote-rich, whereas the rims consist of homogeneous dark amphibolite. Hammer for scale. (d) Tuff (510914) with lithic clasts at the Ravns Størø supracrustal belt. Pen for scale.

3. Samples and petrography

During detailed sampling of 'The Ikkattup Nunaa Supracrustal Association' in 2008 and 2009 the authors collected about 500 rock samples, of which the 149 best preserved and least altered samples were analysed for major and trace elements. The samples were divided into nine lithological groups according to their mineral assemblage and field appearance into the following lithological units that were distinguishable in the field: anorthosite, amphibolite, amphibolite dyke, aplite, gabbro, leucoamphibolite, pillow lava, tuff and ultramafic rocks. A brief description is outlined below:

Anorthosite ($n = 1$) consists almost exclusively of plagioclase, but sometimes with quartz (likely metamorphic), amphibole, garnet and biotite. In some cases the anorthosite is finely banded with hornblende and diopside and often displays a mylonitic texture. This unit is only found along the northern margin of the Bjørnesund supracrustal belt.

Amphibolite ($n = 45$) occurs as the main lithological unit in all three supracrustal belts and consists of dark, medium- to coarse-grained hornblende-, plagioclase- and quartz-bearing rocks of basaltic composition. They are always well foliated. They sometimes contain abundant carbonate, diopside, biotite and garnet, but such samples have generally been avoided for the geochemical analyses.

Amphibolite dykes ($n = 16$) are generally more leucocratic than the above mentioned main group of amphibolites, which they clearly crosscut (Section 4.1). They are plagioclase-rich and sometimes have isolated porphyroblasts of plagioclase. Their discordant relationship to the main amphibolites and leucoamphibolites is mainly recognisable in the Ravns Storø supracrustal belt, but this is possibly due to the lower strain in that area compared with the higher strain and transposition in the Bjørnesund and Perserajoorsuaq supracrustal belts. However, some good examples are also found in the Bjørnesund supracrustal belt.

Aplites ($n = 16$) occur as decimetre- to meter-wide dykes throughout the three supracrustal belts. They often occur as mutually sub-parallel sets, and clearly crosscut the main amphibolites (Fig. 2a), amphibolite dykes and the leucoamphibolites; although they commonly occur as conformable dykes (Section 4.1). The aplites consist of fine- to medium-grained plagioclase- and quartz-bearing rocks of tonalitic composition and contain biotite. Their fine grain size has often made them difficult to interpret in the field and previously they have been described as quartzites or volcano-sedimentary rocks (e.g. Nutman et al, 2004). However, in thin section they are clearly of igneous plutonic origin. They commonly contain large (cm-sized) garnet porphyroblasts that are rimmed by plagioclase, which distinguish them from the adjacent orthogneisses terrain.

Gabbros ($n = 5$), where best preserved, are coarse grained hornblende gabbros with a relict igneous texture marked by plagioclase megacrysts. Locally the hornblende gabbros are well layered. Deformed equivalents are coarse-grained amphibolites with segregations of plagioclase giving the rock a spotted appearance. They form prominent lithological units in the Ravns Storø supracrustal belt, but they have been found only in the easternmost, well-preserved part of the Bjørnesund belt. Their apparent absence elsewhere may be due to higher degree of deformation and metamorphism.

Leucoamphibolites ($n = 42$) occur throughout the three supracrustal belts and together with the main amphibolites they make up the major part of the volcanic stratigraphy. They are leucocratic plagioclase-rich amphibolites, which can contain filled amygdalae, carbonates and calc-silicates such as diopside and garnet. A pyroclastic origin has commonly been ascribed to some of these rocks in the field because they contain elongated felsic and mafic, tuff-like lenses (Fig. 2b).

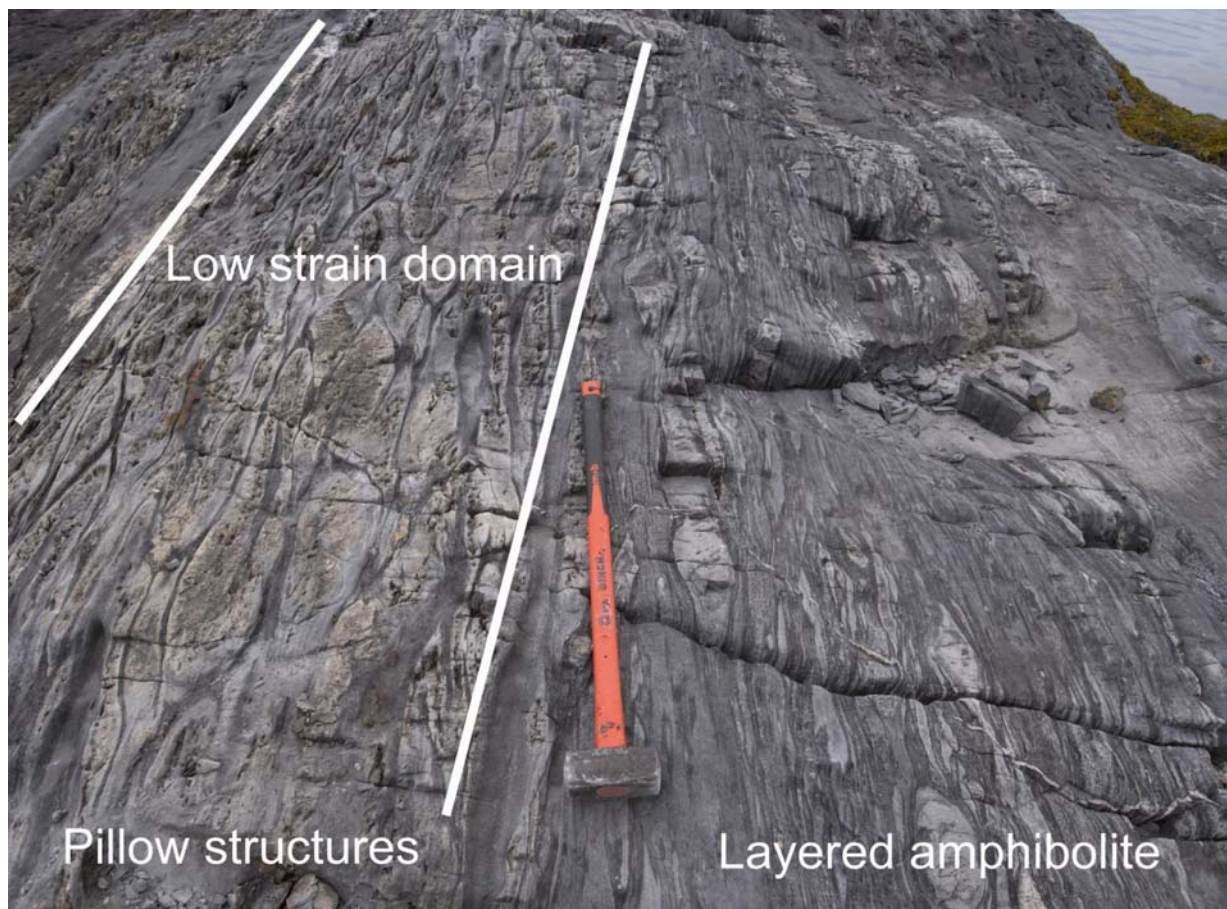


Figure 3. Pillow structures (left) in a low strain domain being progressively transposed to a layered amphibolite (right) in the Ravns Storø supracrustal belt. Hammer with 1 m long shaft for scale.

Pillow lavas ($n = 14$) are only recognisable as well-preserved structures in the areas of least strain in the Ravns Storø supracrustal belt and in the westernmost part of the Bjørnesund supracrustal belt (Fig. 2c). However they show clear progression into a layered/banded amphibolite with increasing strain (Fig. 3). This rock type is found throughout the three supracrustal belts. Thus pillow lavas likely formed the protolith for most of the amphibolites before they were metamorphosed and deformed. Examples of pillow structures have been found in both the main amphibolites and in some leucoamphibolites. The individual pillows appear to have altered cores, which are now fine grained and epidote-rich, whereas the better preserved rims consist of homogenous amphibolite. Comparable deformation of pillow lavas into banded amphibolites was described by Myers (1978) from the Grædefjord region in SW Greenland.

Tuffs ($n = 7$) are only found in the well-preserved parts of the Ravns Storø supracrustal belt. They occur as fine- to medium-grained leucoamphibolites and often contain leucocratic lenses that resemble pyroclastic fragments (Fig. 2d). They often contain some carbonate or biotite. Locally well-preserved stratigraphic sections of pillow lavas face upwards towards overlying beds of lithic tuff. It is likely that deformation of the tuffs gave rise to many of the leucoamphibolites, because they have a similar appearance and have complete overlap in their major and trace element geochemical characteristics (Section 4.2).

Ultramafic rocks ($n = 3$) are magnetite-bearing serpentinites, pyroxenites, and actinolite-anthophyllite rocks that mainly occur as lenses, tens of metres long, in the amphibolites. They occur in particular abundances along the southern margin of the island of Ikkattup Nunaa in the Ravns Storø supracrustal belt and on the mainland south of the islands, although there are some lenses in the Bjørnesund supracrustal belt. The serpentinites are commonly traversed by veins of talc and asbestos. In rare cases metamorphic olivine is observed in thin section.

4. Results

A detailed description of the methods and analytical techniques can be found in Appendix A.

4.1. Field relationships

Below we briefly describe key observations of the field relationships of the different lithological units in the three components of 'The Ikkattup Nunaa Supracrustal Association'. Further details of the field relationship of the rocks in the Ravns Storø supracrustal belt can be found in a comprehensive PhD-thesis covering this area (Friend, 1975).

4.1.1. The Ravns Storø supracrustal belt

The Ravns Storø supracrustal belt mainly comprises amphibolites and leucoamphibolites. The degree of preservation of primary features in this belt is high compared to those of the Bjørnesund and the Perserajorsuaq belts due to lower strain. Thus lithic tuff and pillow lavas are well preserved in this area (Friend, 1975). Well-preserved pillow structures are present in the western part of the island of Ikkattup Nunaa and on the islands to the south and north of it. Lithic tuffs (Fig. 2d) form important stratigraphic units, and provide convincing evidence of a volcanoclastic origin for some parts of the sequence.

The Ravns Storø supracrustal belt contains leucocratic amphibolite dykes (e.g. 468769), mafic amphibolite (468779) and mafic plagioclase-phyric amphibolite dykes (e.g. 510942), which cut the foliation in the main amphibolite and leucoamphibolite sequence.

Aplite dykes (e.g. 468789, 468793 and 468799) that were previously described as quartzites or volcano-sedimentary rocks are clearly intrusive into the main amphibolites (Fig. 2a). On the northern side of the belt these aplite dykes with their distinctive garnet rimmed by plagioclase cut the regional orthogneisses.

Ultramafic lenses are prominent along the south-eastern part of the belt and sometimes associated with unusual aluminous schists

that contain cordierite, staurolite, garnet and anthophyllite (Friend, 1976b). The schists have been interpreted as metamorphosed volcanic rocks that were hydrothermally-altered prior to metamorphism and they are not included in the geochemical data set (Schumacher et al., 2011).

4.1.2. The Bjørnesund supracrustal belt

This supracrustal belt is characterised by amphibolites and leucoamphibolites that occur as alternating bands several metres wide. On its northern side it is bordered by a sheet of layered anorthosite and associated layered gabbroic rocks. This is interpreted as sheet of the Fiskensæset Complex by Myers (1985). These gabbroic rock were thus not analysed in the present study. Aplite sheets intrude the gabbros. The supracrustal rocks are in direct contact with a large anorthosite body along the northern margin of the belt, but the high strain prevents interpretation of the nature of the contact, which may be tectonic or intrusive. The rocks have been intensively stained/deformed, and along the north-eastern margin the anorthosite has been transposed to anorthosite mylonite. No primary structures have been observed in the belt.

The leucoamphibolites often contain calc-silicate minerals and are generally banded and resemble lithic tuffs (Fig. 2b). Some banded mafic amphibolites contain calc-silicate rich domains and ocelli/amygdales. A few discordant dark plagioclase-phyric amphibolite dykes (e.g. 510804), similar to those observed at Ravns Storø, cut the aplite dykes (e.g. 510803) and thus must be later than both the main amphibolites, leucoamphibolites and the aplites.

4.1.3. The Perserajorsuaq supracrustal belt

Alternating bands of mafic and leucocratic amphibolite comprises this relatively small supracrustal belt. Generally these rocks have experienced high strain preventing recognition of primary structures. The main lithological units are mafic amphibolites and leucoamphibolites that appear to be intruded by sub-parallel aplite and late pale granite sheets. The leucoamphibolites often have felsic patches and layers that give them an appearance that resembles felsic tuff beds.

4.2. Major and trace element geochemistry

The raw geochemical data for 149 samples from 'The Ikkattup Nunaa Supracrustal Association' are presented in Supplementary Table 1. For the reasons outlined at the end of Section 2 we treat the geochemical data from the three belts collectively.

Amphibolite samples with significant amounts of garnet (>25%) or carbonate have not been included in the data set, nor have the anthophyllite-bearing felsic schists described by Friend (1976a), because they are likely metamorphosed alteration products. Below we summarise the main geochemical features of the various lithological units.

Anorthosite ($n = 1$) contains mainly plagioclase, which is evident from its major element composition of 48 wt.% SiO_2 , 32 wt.% Al_2O_3 , 16 wt.% CaO and 2 wt.% Na_2O , which adds up to 98 wt.% of the bulk rock. Mg\# is 0.55, Ni is 9.7 ppm and Cr 445 ppm. The anorthosite has close to chondritic REE abundance with Eu/Eu^* of 1.6.

Amphibolites ($n = 45$) have SiO_2 that ranges from 44 to 54 wt.%, TiO_2 from 0.5 to 2.2 wt.%, MgO from 3.6 to 17 wt.%, Fe_2O_3 from 9.1 to 21 wt.% and Mg\# from 0.29 to 0.74. They plot as basalts in the classification diagrams of Winchester and Floyd (1977) and Pearce (1996). The REE patterns are flat at about 10x chondritic abundance and $\text{La}_{\text{CN}}/\text{Sm}_{\text{CN}}$ range from 0.9 to 1.8. Nb/Nb^* is from 0.36 to 1.45, $\text{Nb}_\text{N}/\text{La}_\text{N}$ is from 0.4 to 1.3. They generally have flat primitive-mantle normalised multi-element distributions, except for negative Nb-anomalies (Fig. 4). The amphibolites plot mainly in the Fe-tholeiitic field on the Jensen (1976) and AFM (Irvine and Barager, 1971) diagrams and they plot in the MORB to IAT fields in various tectonic discrimination diagrams (e.g. Pearce and Cann, 1973; Pearce and Norry, 1979; Wood, 1980).

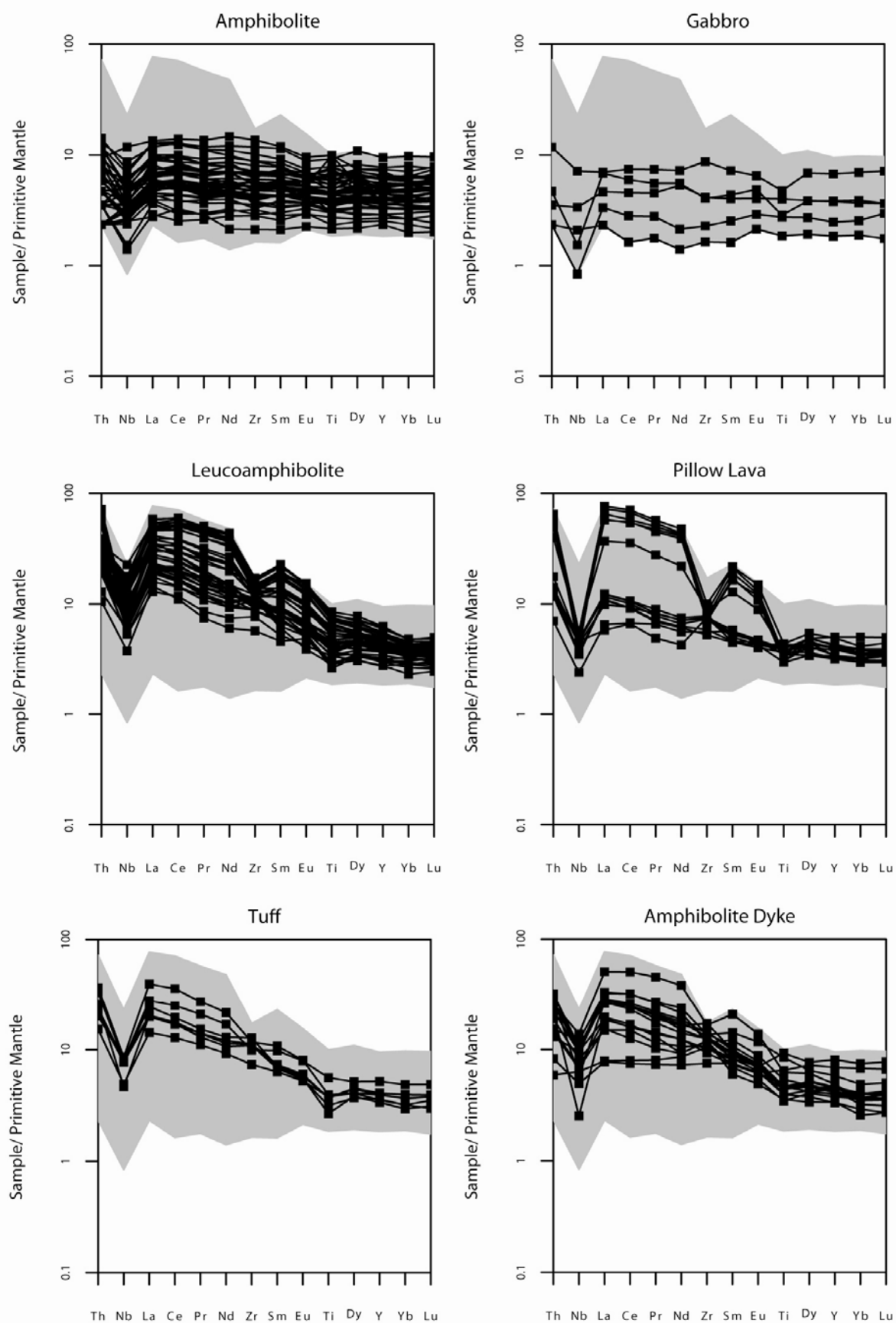


Figure 4. Primitive-mantle-normalised multi-element diagrams with HFSE, Y and REE for the different supracrustal rock groups. Note the consistent negative Nb-anomaly for all the lithological units. The pillow lavas from two distinct groups as discussed in Section 5.2.2.

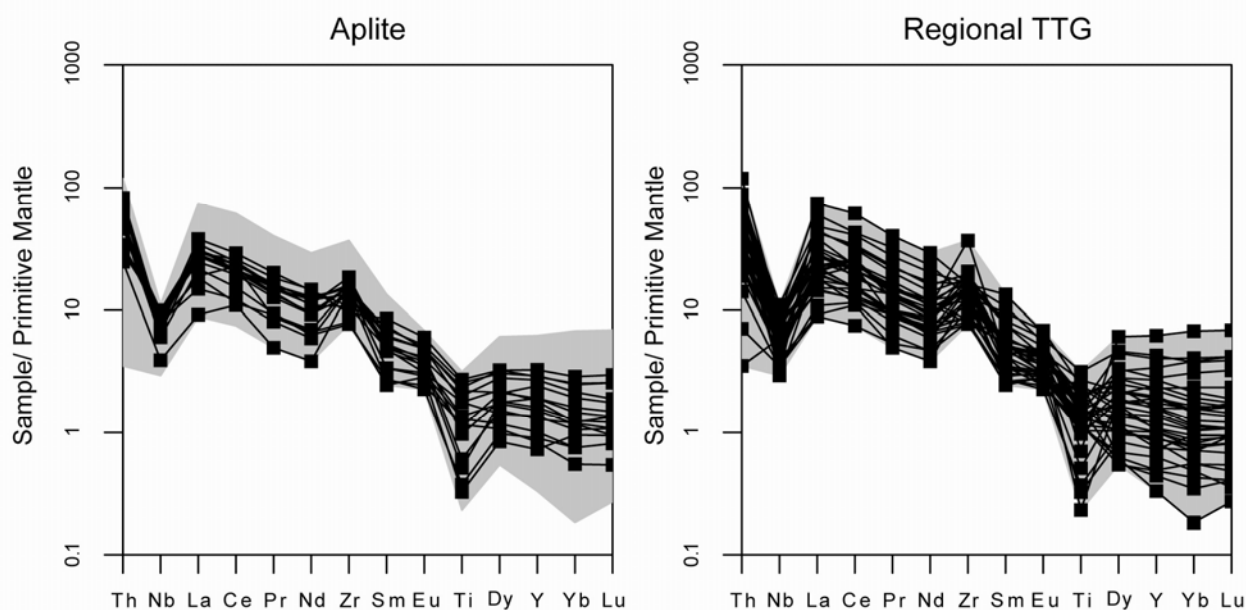


Figure 5. Primitive-mantle-normalised multi-element diagrams for the aplites and regional TTG crust in comparison. TTG data from Szilas et al. (2011c).

Amphibolite dykes ($n = 16$) have SiO_2 that ranges from 49 to 64 wt.%, TiO_2 from 0.8 to 2.0 wt.%, MgO from 2.1 to 7.8 wt.% and Fe_2O_3 from 6.6 to 20 wt.% and Mg\# from 0.38 to 0.61. The REE patterns are elevated up to about 100x chondritic abundance with $\text{La}_{\text{CN}}/\text{Sm}_{\text{CN}}$ from 2 to 3.1 except for two samples from the Ravns Storø supracrustal belt (468770 and 510942), which have flat REE with $\text{La}_{\text{CN}}/\text{Sm}_{\text{CN}} \sim 0.9$. Nb_N/La_N is from 0.1 to 0.8 and they have enriched multi-element patterns except for negative Nb- and Zr-anomalies (Fig. 4).

Aplites ($n = 16$) have SiO_2 that ranges from 64 to 76 wt.%, TiO_2 from 0.1 to 0.6 wt.%, MgO from 0.3 to 2.7 wt.%, Fe_2O_3 from 1.8 to 5.6 wt.%, Mg\# from 0.2 to 0.5, K_2O from 0.4 to 2.6 wt.%, CaO from 2.4 to 5.1 wt.% and Na_2O from 3.6 to 5.5 wt.%. The REE patterns are enriched with La up to c. 100x chondritic abundance and $\text{La}_{\text{CN}}/\text{Sm}_{\text{CN}}$ ranges from 3.3 to 7.7 and they have a wide range of the HREE from about 1 to 10x chondritic abundance. Nb/Nb^* ranges from 0.15 to 0.33, Nb_N/La_N is from 0.2 to 0.5. It is worth noting on Fig. 5 that the aplites show complete overlap in terms of both major and trace elements with TTGs from elsewhere in SW Greenland (TTG data from Szilas et al., 2011c).

Gabbros ($n = 5$) have SiO_2 that ranges from 46 to 52 wt.%, TiO_2 from 0.4 to 1.0 wt.%, MgO from 4.8 to 8.9 wt.%, Fe_2O_3 from 7.6 to 16 wt.% and Mg\# from 0.55 to 0.66. The REE patterns are flat although there is some spread in the actual concentrations with $\text{La}_{\text{CN}}/\text{Sm}_{\text{CN}}$ from 0.9 to 1.5. They have flat multi-element patterns and Nb_N/La_N is from 0.2 to 1.0 (Fig. 4).

Leucoamphibolites ($n = 42$) have SiO_2 that ranges from 45 to 66 wt.%, TiO_2 from 0.6 to 1.9 wt.%, MgO from 1.8 to 9.2 wt.%, Fe_2O_3 from 5.1 to 13 wt.% and Mg\# 0.42 to 0.63. The REE patterns are enriched with La up to about 100x chondritic abundance and $\text{La}_{\text{CN}}/\text{Sm}_{\text{CN}}$ ranges from 2.2 to 4.4, but there is a narrow range of the HREE at about 10x chondritic values. Nb/Nb^* ranges from 0.17 to 0.59, Nb_N/La_N is from 0.2 to 0.5. They have enriched multi-element patterns (Fig. 4) with negative Nb and Zr-anomalies. The leucoamphibolites mainly plot in the calc-alkaline fields of the Jensen (1976) and AFM (Irvine and Barager, 1971) diagrams. They show a broad enriched pattern that overlaps with the enriched pillow lavas, the tuffs and the amphibolite dykes. However, one group of leucoamphibolites from the Bjørnesund supracrustal belt has a range of elevated elements when compared to leucoamphibolites from the Ravns Storø and the Perserajorsuaq supracrustal belts. The following elements are generally enriched in the Bjørnesund leucoamphibolites at a given SiO_2 value: P_2O_5 , TiO_2 , CaO , Sr , Zr , Nb , La and Ce . These enriched leucoamphibolites resemble low-

silica adakites to some degree.

Pillow lavas ($n = 14$) have SiO_2 that ranges from 49 to 63 wt.%, TiO_2 from 0.6 to 1.0 wt.%, MgO from 1.0 to 9.4 wt.%, Fe_2O_3 from 4.5 to 13 wt.% and Mg\# from 0.27 to 0.63. The HREE form a tight cluster at about 10x chondritic abundance, but the LREEs form two distinct groups that are either fairly flat ($\text{La}_{\text{CN}}/\text{Yb}_{\text{CN}}$ from 1.2 to 3.46) or distinctly enriched ($\text{La}_{\text{CN}}/\text{Yb}_{\text{CN}}$ from 8.8 to 19) with La up to about 100x chondritic abundance. Nb_N/La_N is from 0.1 to 0.8 and they form two distinct groups on a multi-element diagram (Fig. 4). The pillow lavas form two distinct groups that are clearly distinguished by their Th/Nb ratio being above or below unity.

Tuffs ($n = 7$) have SiO_2 that ranges from 52 to 59 wt.%, TiO_2 from 0.6 to 1.2 wt.%, MgO from 2.2 to 6.8 wt.%, Fe_2O_3 from 6.3 to 10 wt.% and Mg\# from 0.44 to 0.59. The REE patterns are enriched with La up to about 100x chondritic abundance with $\text{La}_{\text{CN}}/\text{Sm}_{\text{CN}}$ from 2.2 to 3.6, but with a narrow range of the HREE at about 10x the chondritic value. They have enriched multi-element patterns and negative Nb-anomalies with Nb_N/La_N is from 0.2 to 0.4 (Fig. 4).

Ultramafic rocks ($n = 3$) have SiO_2 that ranges from 33 to 45 wt.%, TiO_2 from 0.2 to 1.2 wt.%, MgO from 32 to 35 wt.%, Fe_2O_3 from 13 to 16 wt.% and Mg\# from 0.82 to 0.85. Ni ranges from 136 to 840 ppm and Cr from 137 to 4071 ppm. The REE pattern is variable, but generally flat with $\text{La}_{\text{CN}}/\text{Sm}_{\text{CN}}$ from 0.7 to 3.1, Nb_N/La_N is from 0.4 to 4.7 and Eu/Eu^* from 0.33 to 0.70.

4.3. ^{176}Lu , ^{176}Hf and ^{147}Sm - ^{143}Nd isotope systematics

17 whole rock samples were analysed for Lu-Hf isotope compositions and 15 samples were also analysed for Sm-Nd isotope compositions using isotope dilution techniques by MC-ICP-MS at the University of Bonn (see method details in Appendix A). The results are presented in Supplementary Table 3. The samples are from the Ravns Storø and Bjørnesund supracrustal belts and represent a range of lithological units. Unfortunately no isotopic data are available for the Perserajorsuaq supracrustal belt.

The amphibolites and leucoamphibolites define a Sm-Nd isochron age of 3014 ± 73 Ma (MSWD = 6.5) (Fig. 6a) and Lu-Hf isochron age of 3007 ± 54 Ma (MSWD = 4.9) (Fig. 6b). These ages overlap within error with the c. 2970 Ma age of the Fiskensæset Complex (Polat et al., 2010). However, one amphibolite clearly plots off the Lu-Hf isochron (510942) and this is consistent with it being a late dyke similar to the ones observed in the Bjørnesund supracrustal belt that cuts the aplite sheets (Section 4.1.2). When excluding this sample the Lu-Hf isochron yields an age of 2990 ± 41 Ma (MSWD = 2.6) and the Sm-Nd isochron yields an age of 3020 ± 78 Ma (MSWD = 6.8).

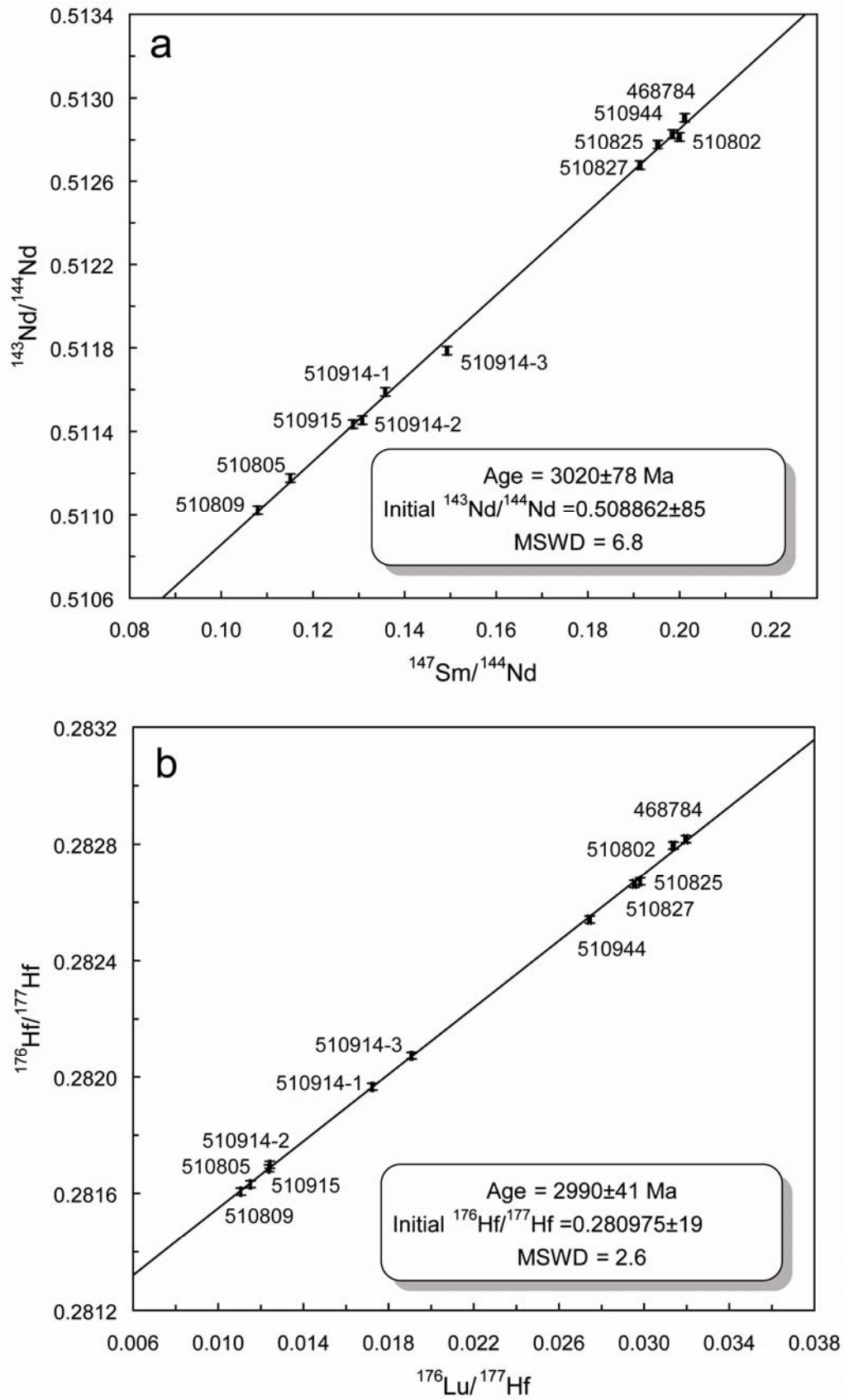


Figure 6. (a) Sm-Nd isochron for the leucoamphibolites and amphibolites (excluding sample 510942) from the Ravns Stø and Bjørnesund supracrustal belts yielding and isochron age of 3020 ± 85 Ma. (b) Lu-Hf isochron for the leucoamphibolites and amphibolites (excluding sample 510942) from the Ravns Stø and Bjørnesund supracrustal belts yielding and isochron age of 2990 ± 41 Ma.

The Sm-Nd data show some scatter around the isochron. Accepting the well-defined age for the Fiskensæset Complex as the likely age of the Ravns Storø, Bjørnesund and Perserajoorsuaq supracrustal belts, the $\epsilon\text{Hf}_{(2970\text{Ma})}$ of the amphibolites from +3.7 to +4.9 and the leucoamphibolites ranges from +3.5 to +4.3, when excluding the late amphibolite dyke (510942). The $\epsilon\text{Nd}_{(2970\text{Ma})}$ of the amphibolites ranges from +1.4 to +2.4 and of the leucoamphibolites from +2.1 to +3.5.

The ultramafic sample plots close to a chondritic $\epsilon\text{Hf}_{(2970\text{Ma})}$ value of +0.13, but with a DM-like $\epsilon\text{Nd}_{(2970\text{Ma})}$ value of +2.1.

The anorthosite samples yield high $\epsilon\text{Hf}_{(2970\text{Ma})}$ of +14.7 and +6.5 and $\epsilon\text{Nd}_{(2970\text{Ma})}$ of +5.9.

4.4. U-Pb geochronology

Zircons separated from aplites, leucoamphibolites and anorthosites were analysed for their U-Pb isotope compositions by LA-ICP-MS at the Geological Survey of Denmark and Greenland (GEUS). Measurements were mainly done on zircon cores, although some rims were also included in the analysis.

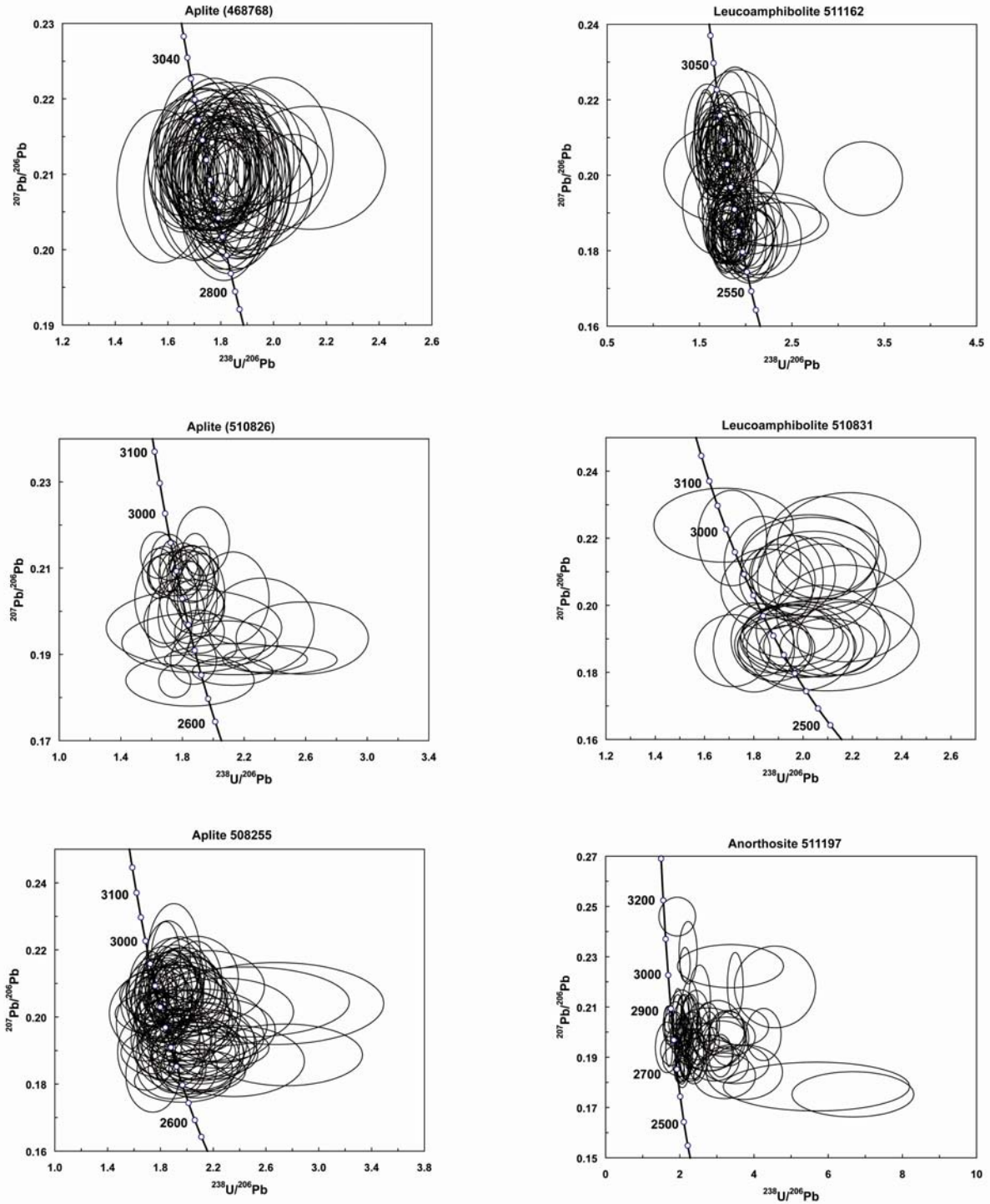


Figure 7. Tera-Wasserburg concordia diagrams for aplite sheets (468768, 510826 and 508255), leucoamphibolites (510831 and 511162) and one anorthosite (511197). All data is included.

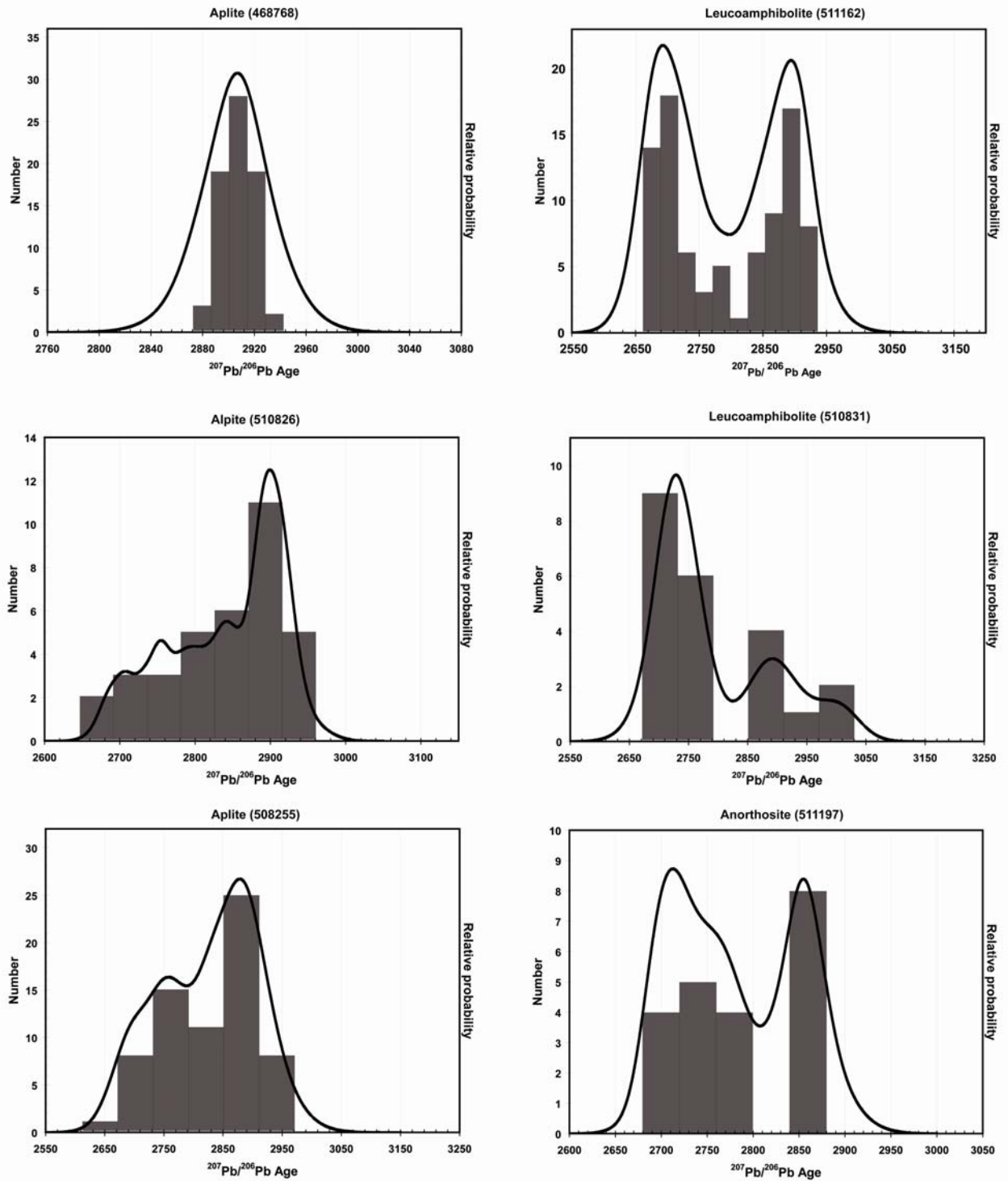


Figure 8. Probability density plots for aplite sheets (468768, 510826 and 508255), leucoamphibolites (510831 and 511162) and one anorthosite (511197). Only data that are within 10% concordant are included in the histograms. The calculated ‘unmixed’ ages are presented in Section 4.4.

The U-Pb data are presented in Supplementary Table 4. Tera-Wasserburg concordia diagrams are presented in Fig. 7 and probability density plots are presented in Fig. 8. We present data from three aplite sheets and two leucoamphibolites. Unfortunately no zircons were found in the leucoamphibolites or tuffs from the Ravns Storø supracrustal belt despite separation of heavy minerals from over ten samples. We additionally report data from the anorthosite at the Bjørnesund supracrustal belt.

The aplite sheet from the Ravns Storø supracrustal belt (468768) has a single age population that yields an average age of 2905 ± 5 Ma. The zircon grains are mostly euhedral prismatic crystals and show oscillatory zoning.

The aplite sheet (510826) from the Bjørnesund supracrustal belt yields three component ‘unmixed’ ages of 2727 ± 11 Ma ($F = 0.23$), 2820 ± 18 Ma ($F = 0.25$) and 2903 ± 9 Ma ($F = 0.52$). The zircon grains are mostly euhedral prismatic crystals with oscillatory zoning

with homogeneous rim domains. The leucoamphibolite (510831) gave three component 'unmixed' ages of 2731 ± 18 Ma ($F = 0.68$), 2895 ± 38 Ma ($F = 0.23$) and 2996 ± 60 Ma ($F = 0.08$). The zircon grains are small rounded and homogenous. The anorthosite (511197) yields two component ages of 2776 ± 13 Ma ($F = 0.6$) and 2853 ± 17 Ma ($F = 0.4$), however on the concordia diagram it is seen that there are a few grains with ages up to c. 3150 Ma. These zircon grains have many different shapes ranging from thin needles to euhedral oscillatory zoned crystals.

The aplite sheet (508255) from the Perserajorsuaq supracrustal belt has a bimodal age population that yields 'unmixed' ages of 2729 ± 14 Ma ($F = 0.36$) and 2873 ± 10 Ma ($F = 0.64$). The zircon grains are mostly euhedral prismatic to rounded crystals with oscillatory zoning with homogenous rims. The leucoamphibolite (511162) gives 'unmixed' ages of 2707 ± 9 Ma ($F = 0.53$) and 2885 ± 10 Ma ($F = 0.47$). These zircon grains are generally small, rounded and homogeneous, but some display oscillatory zoning.

Most of the samples (except 468768 and 511197) show a good correlation between age and the Th/U, so that older grains have ratios of about 0.6 and younger grains have values of about 0.02.

5. Discussion

5.1. Field relationships

The Ikkattup Nunaa Supracrustal Association' mainly consists of amphibolite and leucoamphibolite, which are intimately inter-layered in bands generally a few meters thick. A common feature for all three supracrustal belts is that they are cut by aplite sheets, with distinctive garnets rimmed by plagioclase, are of tonalitic composition. The aplites have previously been described as quartzites or volcano-sedimentary rocks, because the field interpretation can be difficult due to the fine grain size and their common conformity with the amphibolites. However, clear intrusive relationships have been established with the main amphibolite unit (Fig. 2a) and given the fact that the aplites have U-Pb zircon ages similar to the surrounding TTG gneisses, which they locally cut (Section 4.4), they cannot be regarded as part of the supracrustal sequence. This demonstrates that the supracrustal belts formed prior to the TTG-forming event, which is also observed in many other supracrustal belts throughout southern West Greenland, e.g. the Isua supracrustal belt (Friend and Nutman, 2010), the Ivisartaq supracrustal belt (Polat et al., 2008), the Tartoq Group (Szilas et al., 2011b), and the Qussuk and Bjørneøen supracrustal belts (Garde, 2007, 2012).

The main difference within 'The Ikkattup Nunaa Supracrustal Association' appears to be the degree of deformation, which on a regional scale seems to increase towards the NE. In turn this means that the Ravns Størø belt provides the best opportunity to study the primary lithological units in this region. The lithic tuffs in the Ravns Størø belt point to a volcanic arc environment and the very well-preserved pillow structures indicate that at least some parts of the volcanic sequence formed in a subaqueous environment. The clear transition from well-preserved pillow lavas to deformed pillow lavas to layered amphibolites observed at Ravns Størø suggests that deformation has obliterated many of the primary features in these three supracrustal belts (Fig. 3). When the layered amphibolites are found without a direct relation to undeformed pillow lavas their origin will be speculative as alternating felsic and mafic ash layers might produce the same appearance. Thus, the main lithological units appear to have comprised mafic pillow lava and felsic tuff than were sheared out to become the mafic amphibolite and leucoamphibolite units respectively. These were later intruded by the amphibolite dykes, which cut the foliation in the main amphibolite and leucoamphibolite sequence. Even later, these were cut by tonalitic aplite sheets associated with the regional TTG formation event. A similar relative chronology is likely for the Bjørnesund and Perserajorsuaq supracrustal belts, and although they have been strongly overprinted and transposed by deformation, clear crosscutting relationships are still preserved between the amphibolites and aplite sheets.

5.2. Major and trace element geochemistry

5.2.1. Alteration and element mobility

Element mobility during hydrothermal alteration and metamorphism can affect the primary inventory of major and trace elements in supracrustal rock, and has been documented in other supracrustal belts in SW Greenland (e.g. Polat et al., 2002, 2008).

Well-preserved pillow structures are present in the Ravns Størø supracrustal belt, indicating that at least some of these volcanic rocks formed in a subaqueous environment. Consequently, caution must be exercised regarding the use of the more fluid-mobile elements for the petrological interpretations, as they might have been remobilised shortly after extrusion under water and possibly also later during amphibolite-facies metamorphism.

A good example of local hydrothermal alteration is sample 510934, which is a leucoamphibolite that contains mm-sized quartz-rich spheres. We interpret these spheres as replaced amygdaloids, which is supported by the fact that this sample has a weathering index (W) of 17%, which lies off the igneous fractionation curve (Ohta and Arai, 2007). It also agrees with an isocon mass balance calculation following Grant (1986) by comparing this sample with an adjacent less altered leucoamphibolite (510935). The isocon modelling indicates a significant enrichment in Ca and less so in Mn, as well as depletions in Na, K, Ba, Rb, Mg and Fe, which is consistent with leaching and carbonation during extrusion in seawater.

Two core-rim pairs were collected from the pillow lavas and isocon modelling suggests similar mass change as for the amygdale-bearing leucoamphibolite. Ca, Sr, P, La and Sm were added and Mg, Fe, Na, K, Mn, Rb and Ba were lost (core: 5109131 and rim: 510932). The other sample-pair records addition of Ca, Si and Sr and depletion of Mg, Fe, Na, K, Ba and Rb (core: 5158071 and rim: 5158072). These changes are consistent with the altered appearance of the pillow cores, which contain abundant epidote and the unaltered and homogeneous appearance of the pillow rims. Thus the large ion lithophile elements (LILE) and the light rare earth elements (LREE) are likely to have been disturbed in some of the samples, particularly the ones associated with pillow lavas or their deformed derivatives. However, the MFW weathering index shows that the samples generally follow the igneous fractionation trend and only few samples are significantly altered.

5.2.2 Geochemical fingerprints

The geochemical signature of subduction zones includes enrichment in large ion lithophile elements (LILE), such as Rb, Ba, K, Pb, Sr and Th, U and LREE compared to MORB, as well as depletions in TiO_2 , Nb and Ta (Kelemen et al., 2003; König et al., 2010; Pearce and Peate, 1995). The elements enriched through subduction zone processes are partly the same ones, which we have just mentioned as potentially mobilised during alteration and metamorphism. This implies that an enriched trace element pattern cannot readily be linked with a subduction zone environment. However, some elements can still be of importance, such as Th, Ti, Nb and the heavy rare earth elements (HREE), which are usually taken to be immobile in hydrothermal fluids (Grant, 2005 and references therein). In the following we will thus mainly focus on the immobile elements and have therefore only included these in the multi-element diagrams and the discussion on the petrogenesis of supracrustal rocks.

The intrusive field relations of the aplites mentioned in Section 5.1 together with their younger ages (c. 2873–2905 Ma; Section 4.4) implies that they are unrelated to the primary volcanism that formed the supracrustal belts. Furthermore they plot within the same range of major and trace element compositions as the TTG orthogneisses from SW Greenland (Fig. 5) and their multi-element patterns also overlap with the high-silica adakite average of Martin et al. (2005). Thus, the aplites likely represent TTG apophyses that were injected into the supracrustal belts during the early stages of the regional TTG forming event, which post-dates the volcanism by at least 70 Ma (Section 5.5). High-silica adakites are thought to be formed by melting of hydrated basalt, which has also been proposed to be the origin of TTGs (e.g. Hoffmann et al., 2011a). This model also appears to apply for the aplites, because they post-date the

supracrustal belts and could have formed by partial melting of such supracrustal rocks during accretion and crustal thickening (Nagel et al., 2012).

The anorthosite sample is similar to rocks from the Fiskensæset Complex (Polat et al., 2011a). It has Mg# of 0.55 compared to around 0.7 for the Fiskensæset Complex. The La_{CN}/Sm_{CN} is also lower at 1.1 compared to values of up to 5.8. Ni is low at 9.7 ppm compared to between 79 and 157 ppm and Cr is high at 445 ppm compared to values up to 317 ppm for the Fiskensæset Complex. However, there is nothing that lead us to believe that the Bjørnesund anorthosite is significantly different the anorthosites in the Fiskensæset Complex. Much of the variation can simply be explained by variable contents of chromite and/or contamination with a LREE-rich felsic component.

The ultramafic rocks have major and trace element compositions consistent with them being cumulate rocks such as high MgO, Ni and Cr, but one sample has unusually high P_2O_5 , TiO_2 and Zr (468765), which could reflect accumulation of apatite, rutile and zircon. The two other ultramafic samples, however, define end-members for a few amphibolites that show enriched trends in MgO, Cr and Ni and are thus consistent with the ultramafic rocks being olivine and orthopyroxene cumulates.

Various tectonic discrimination diagrams can be found in the literature and several of the most commonly used were summarised by Rollinson (1993). The principle behind these types of diagrams is to use the chemical fingerprint in rock suites of known tectonic affinity as a 'predictive' tool to determine the tectonic setting of rocks of unknown petrogenetic affinity. Going back in the rock record to Archaean times, a main caveat in applying such tectonic discrimination methods lies in the assumption of 'uniformitarianism', i.e. the idea that rocks formed by the same processes during Archaean times as they do today. There is generally a consensus that subduction zones were in operation by at least 3000 Ma (e.g. Dhuime et al., 2012; Kerrich and Polat, 2006; Moyen et al., 2006; Næraa et al., 2012; Pease et al., 2008; Shirey and Richardson, 2011; Smithies et al. 2005) and some authors even suggest extending this event back to about 3800 Ma (e.g. Dilek and Furnes, 2011; Friend and Nutman, 2010; Furnes et al., 2009; Polat et al., 2002). Thus, it seems likely that tectonic discrimination diagrams relying on immobile elements could indeed be used for these Mesoarchaean supracrustal rocks if allowing for subtle differences due to the likely higher degree of partial melting of the mantle, given that its temperature was hotter in the Archaean (Herzberg et al., 2010).

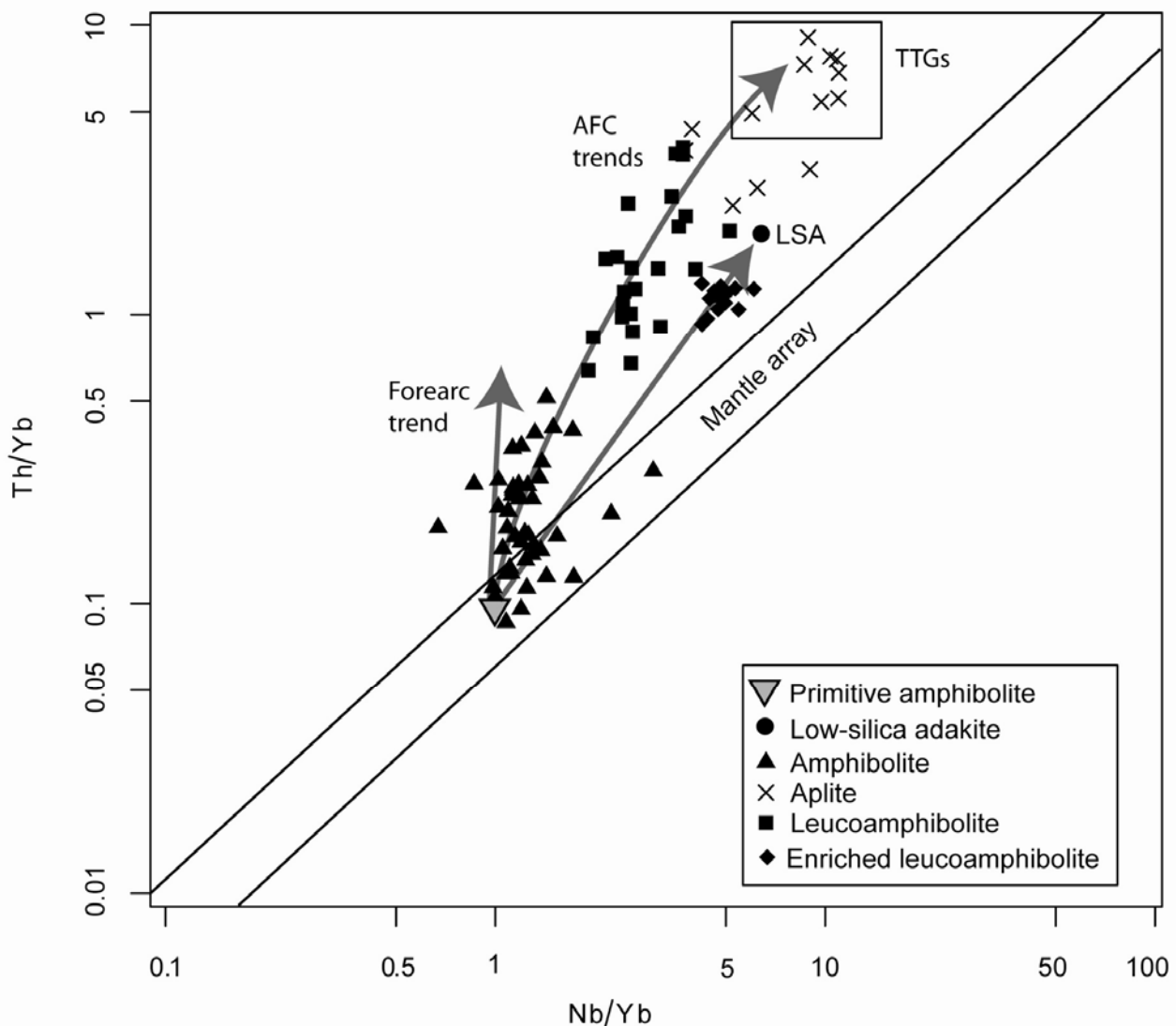


Figure 9. Th/Yb versus Nb/Yb diagram with the amphibolites, leucoamphibolites and aplite sheets forming a trend above the mantle array. The amphibolites generally plot in the area of TTGs and the amphibolites form a trend that is seen in forearc ophiolites. The leucoamphibolites plot on trends that resemble trends of assimilation-fractional-crystallisation (AFC) with either a TTG or low-silica adakite end-member. TTG field from Szilas et al. (2011c) and forearc trend from Metcalf and Shervais (2008). Low-silica adakite average from Martin et al. (2005) with Th and Hf values from Yagodinski et al. (1995).

The main group of amphibolites is of tholeiitic basalt composition with flat trace element patterns and have MORB-like major element compositions, which at first hand would suggest an ocean floor environment. However, the distinct negative Nb-anomaly and undepleted character of the LREE combined with the IAT-affinity on the discrimination diagrams suggest that it differs from N-MORB. A backarc basin (BAB) affinity is suggested from such diagrams (e.g. Cabanis and Lecolle, 1989), which is in agreement with the arc-flavour that was suggested from the IAT affinity. A BAB environment similar to the Lau and Mariana basins (Taylor and Martinez, 2003) is therefore considered as a more plausible setting than a MOR. A comparison of the main amphibolites with similar Archaean tholeiitic rocks from Canada (e.g. Hollings et al., 2000; Sandeman et al., 2006), that were interpreted to have formed in a backarc environment; show good overlap with our data. However, because there is practically no geochemical difference between backarc and forearc tholeiites (Metcalfe and Shervais, 2008), it could be one or the other based on the geochemical data.

Another environment for Archaean tholeiites in the literature is an oceanic plateau (e.g. Arndt et al., 1997; Campbell et al., 1989; Kerr et al., 1996), but such rocks are generally associated with abundant komatiites in all of the Archaean examples, which is a feature that is generally lacking in the supracrustal belts of SW Greenland. Oceanic plateau rocks generally have positive Nb-anomalies, whereas the supracrustal rocks reported here have negative anomalies. A backarc to forearc environment is also more likely to be preserved over time rather than actual MORB or oceanic plateaus since the crust is generally thinner and more prone to obduction as it is already present in a collisional setting (Martinez and Taylor, 2003). On the Th/Yb vs. Nb/Yb diagram (Pearce, 2008) on Fig. 9, the amphibolites plot in the same field as forearc ophiolites (Metcalfe and Shervais, 2008). Additionally, these mafic supracrustal rocks overlap in terms of major and trace elements with data from the Tartuq Group (Szilas et al., 2011b) and the Ivisartoq supracrustal belts in SW Greenland, which were both interpreted to have a suprasubduction zone origin (Polat et al., 2008).

The gabbros show broadly overlapping major and trace element geochemical data with the main amphibolites and are of tholeiitic basalt composition. Except for one sample that is plagioclase-rich and slightly calc-alkaline (468783), the gabbros do not appear to be cumulate rocks. These rocks are thus likely to be mafic intrusives that have crystallised to a coarse grain size without much crystal segregation.

The pillow lavas have been affected by some degree of alteration, but even when considering this, two distinct groups emerge; one has fairly flat REE patterns (La_{CN}/Yb_{CN} of 1.2-3.5) and a Th/Nb ratio of about 0.4 and the other is distinctly LREE enriched (La_{CN}/Yb_{CN} of 8.9-19) and has a high Th/Nb ratio of >1. The flat group is similar to the main amphibolites, but the enriched group has some characteristics that resemble the leucoamphibolites by having high Th and LREE concentrations in combination with depletion in TiO_2 , Nb, Ta, Hf and Zr. This suggests either crustal contamination, involvement of an enriched mantle source or that they formed by arc processes. Interestingly they resemble the low-silica adakite average (Martin et al., 2005) on multi-element diagrams, except they do not have fractionated HREE.

The amphibolite dykes generally also show overlap with the leucoamphibolites in terms of major and trace elements, except for two samples (468779 and 510942), which have flat REE patterns and resemble the main amphibolites.

The tuffs overlap chemically with parts of the leucoamphibolites and it is likely from the field relations that some leucoamphibolites simply represent deformed tuffs.

The leucoamphibolites are calc-alkaline volcanic rocks that resemble arc andesites with characteristic negative Nb-, Ta- and Ti-anomalies and they consistently plot in the calc-alkaline basalt (CAB) field in discrimination diagrams. They appear to form an array in terms of both major and trace elements that is intermediate between the main amphibolites and the aplite sheets, which is also seen on Fig. 9. This might at first appear as crustal contamination, as suggested for other Archaean supracrustal rocks by Pearce (2008) and this will be discussed further in Section 5.3.

Polat et al. (2011b) have shown that the many well-studied supracrustal belts in SW Greenland show characteristics of arc volcanism and in this study we see similar characteristics in the Ravns Størø, Bjørnesund and Perserajoorsuaq supracrustal belts. A similar origin is possibly also responsible for the incompatible element enrichments observed in the enriched pillow lavas, amphibolite dykes, tuffs and leucoamphibolites, however the LILE- and LREE-enriched nature of these lithological units could have developed in several ways: (1) enrichment by hydrothermal alteration, (2) tectonic mixing, (3) primary enriched mantle source, (4) magma mixing, (5) crustal contamination or (6) metasomatism of their mantle source. The first case can be rejected, since we have already shown that although LILE and LREE can be mobilised during alteration this would be associated with a strong enrichment in Ca and depletions in Mg, Fe, K and Na, which is not seen. The fact that we observe both calc-alkaline and tholeiitic pillow lavas, each with altered cores and well preserved rims also argues against general alteration to explain the calc-alkaline leucoamphibolites, amphibolite dykes and tuffs. The case for tectonic mixing can also be rejected, because we have observed leucoamphibolites with well-preserved pillow lava structures and lithic tuffs, which have enriched geochemical characteristics (Section 5.2). A primary enriched mantle source would first of all be difficult to reconcile with the interlayering of the two fundamentally different types of volcanic rocks, but because andesites are not primary mantle melts some kind of felsic enrichment would still be required to explain the calc-alkaline andesites. Thus, it appears unlikely that the difference of the amphibolites and the leucoamphibolites can be explained by invoking different source regions.

Below we will examine the whole rock geochemical data and see if the evidence argues for magma mixing, crustal contamination or mantle metasomatism. To simplify the modelling we chose to look only at the main tholeiitic amphibolites ($n = 46$), the calc-alkaline leucoamphibolites ($n = 42$) and the aplites/TTG sheets ($n = 16$), which cover the entire observed range seen in the various lithological units. Given that the TTG-like aplite sheets are younger than the supracrustal rocks (Section 4.3 and 4.4) and thus cannot be co-magmatic, we simply use their geochemical composition as a hypothetical end-member, which approximates the local continental crust

5.3 Test of mixing and AFC processes

On the major and trace element variation diagrams, it appears that the tholeiitic amphibolites and the aplite/TTG sheets form compositional end-members, while the calc-alkaline leucoamphibolites plot with intermediate compositions (Fig. 10). Thus, much of the compositional range observed in the calc-alkaline leucoamphibolites could possibly be explained as the result of mixing processes involving mafic and felsic compositional end-members.

The bimodal distribution of the supracrustal rocks is especially evident from the REE patterns that show two distinct groups. The tholeiitic group of rocks has flat patterns (La_{CN}/Sm_{CN} of 0.8-1.8) and the calc-alkaline rocks have steeper patterns (La_{CN}/Sm_{CN} 2.2-4.4). No transitional samples have been found, indicating that these rocks formed by two fundamentally different processes. The sharp contrast between the REE-patterns in the main tholeiitic amphibolites and the calc-alkaline leucoamphibolites (including the enriched pillow lavas, tuffs and amphibolite dykes) cannot be explained by fractional crystallisation, because the slopes are very different and the two groups do not show a corresponding change in SiO_2 or MgO as expected during such processes. Rather the differences in LREE enrichment are likely to reflect either different sources, different degrees of partial melting or some form of magma mixing or mantle source metasomatism. Alternatively the relative enrichment in the leucoamphibolites could reflect crustal contamination of a basaltic magma. However, as we mentioned above different sources appears to be an unrealistic solution to this problem. Different degrees of partial melting is also not a viable explanation, because andesitic rocks are not primary melts (Kolavenko et al., 2010). In Section 5.3.1 below we investigate if magma mixing or mantle source metasomatism could explain our data.

Fractional crystallisation could on the other hand be a possible mechanism to explain part of the variations found within each of the two rock groups, such as the anomalies seen in the multi-element diagrams. The fractionation (removal/addition) of plagioclase could explain the negative or positive Eu-anomalies, and the negative Nb-Ta-Ti anomalies could be explained by fractionation of phases such as rutile or ilmenite. However, it could equally well be explained as the result of partial melting in the presence of a residual phase retaining Nb in the mantle source region, such as rutile or cpx (Baier

et al., 2008), Ti-chondrodite and titanoclinohumite (López Sánchez-Vizaino et al., 2005) or alternatively a previously depleted source (Ryerson and Watson, 1987).

It is worth noting that the bimodal distribution of rocks from Bjørnesund was observed very early on by Williams (1976), who showed that poorly banded gneisses and amphibolites were connected by a linear array of transitional rocks (leucoamphibolites). However, this idea was not pursued by later workers, likely because they worked with smaller and more focused data-sets.

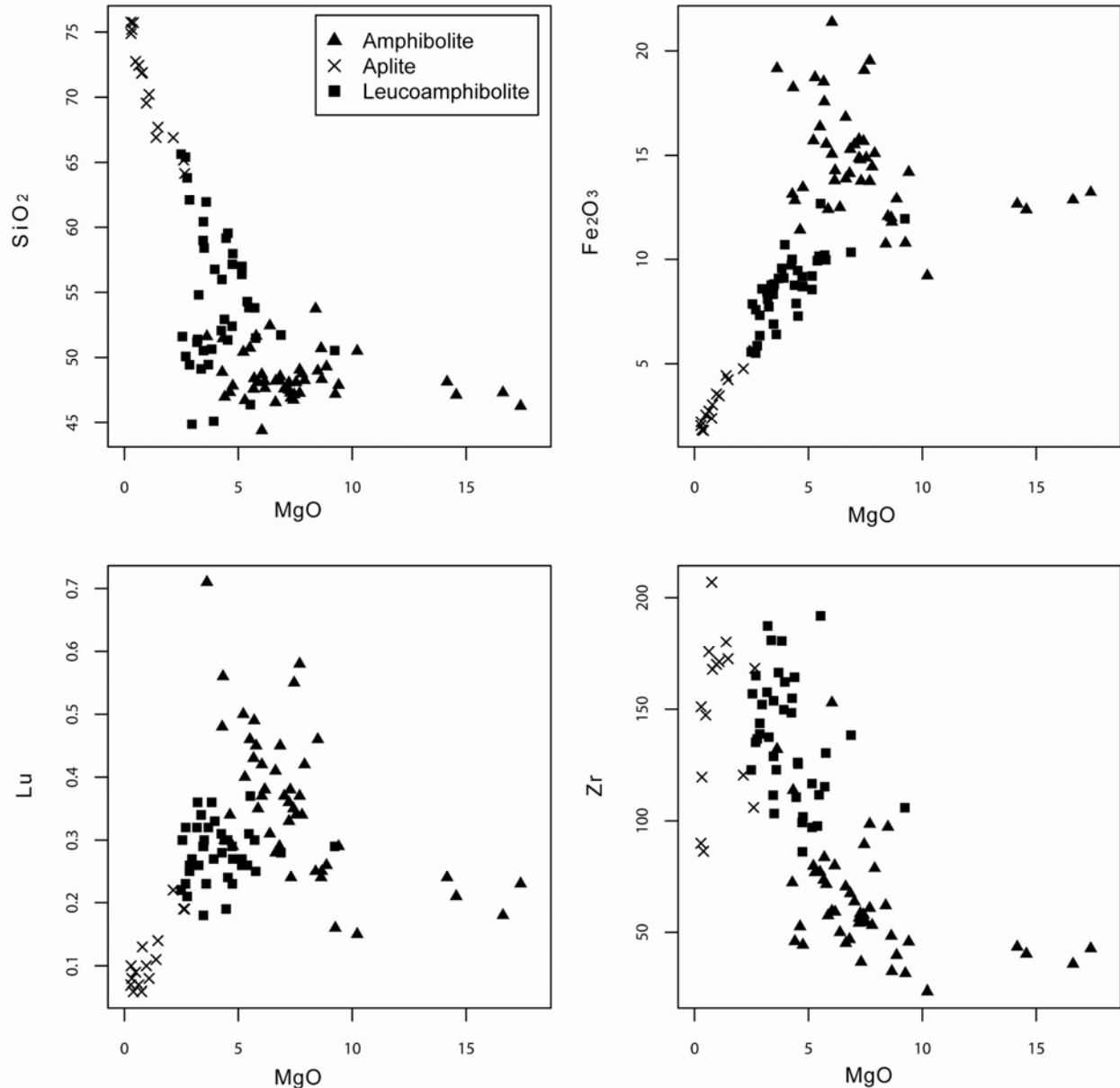


Figure 10. Variation diagrams with MgO versus SiO₂, Fe₂O₃, Lu and Zr. These elements have been selected because they display the possible mixing trends well and the leucoamphibolites all show the same trends for these elements. Other elements such as Nb, P₂O₅, CaO do not adhere to such a simply mixing relationship, but requires an additional low-silica adakite end-member to explain the trends for the enriched leucoamphibolites as explained in Section 5.3.2 or in the case of CaO possibly also contamination by carbonate sediments.

5.3.1 Magma mixing model

Testing of the apparent mixing trends shows that such a process alone cannot explain all of the data. First of all we do not find samples with an intermediate LREE enrichment between the two groups. When plotting major and trace element data against Mg# the main amphibolites and the leucoamphibolites form two separate trends rather than a continuum. Additional testing of the data with the relations outlined by Langmuir et al. (1978) does not support magma

mixing as the only process responsible for the distinctly different groups of mafic and andesitic rocks. From the trends in incompatible element plots and incompatible ratio plots it is possible to distinguish between mixing of magmas and mixing of sources (Langmuir et al., 1978). Incompatible element plots of Zr, Y, Nb, Th and REE show that the amphibolites and the leucoamphibolites form two sub-parallel trends, which do not have the aplites as an end-member and thus they could not be related by mixing of magmas alone. However,

when plotting incompatible ratios, slightly compatible to incompatible ratios or normalised ratios possible mixing trends appear. Ratio-ratio plots such as Nb/Th vs. Lu/Hf (Fig. 11) for the leucoamphibolites show trends towards a TTG-like or a low-silica adakite end-member, as also noted by Hoffmann et al. (2011b) for similar rocks from the Isua supracrustal belt. Hoffmann et al. (2011b) interpreted these trends as resulting from a mantle source overprint by a subduction-derived melt/fluid component.

A similar interpretation is also in agreement with the trace element compositions of the leucoamphibolites in the present study

and their trends could thus be interpreted as mixing within the mantle source region prior to formation of the parental magmas for some of the leucoamphibolites. Thus, in the following we will keep source contamination open as a possibility for the observed trends. However, this does not rule out that magma mixing occurred in combination with fractionation in a magma chamber prior to extrusion of the andesitic leucoamphibolite protolith, which we will test further with a combined AFC model in the following.

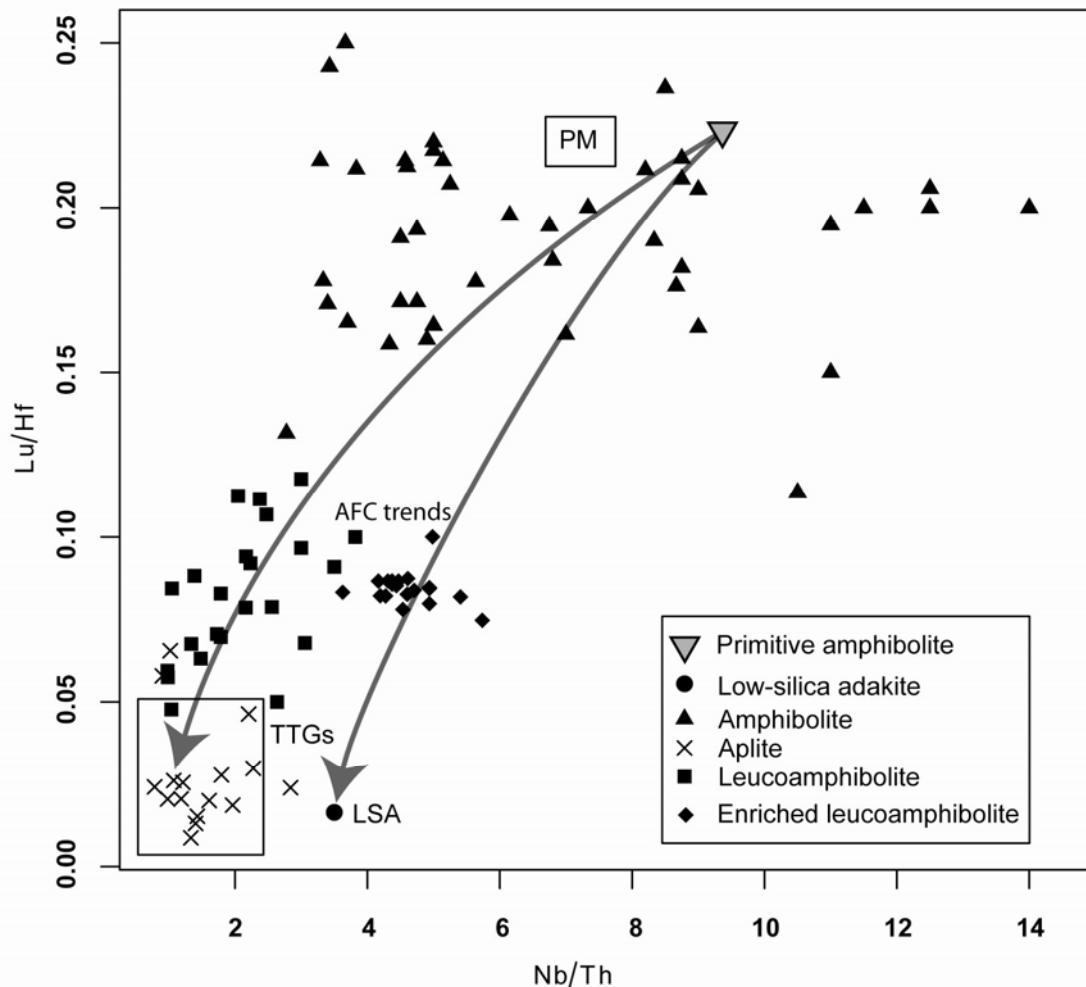


Figure 11. Lu/Hf versus Nb/Th diagram showing that the leucoamphibolites plot on AFC trends intermediate between the amphibolites and either TTGs or a low-silica adakite end-member. Similar trends have been noted from the Isua supracrustal belt and interpreted as being caused by a melt-like subduction component (Hoffmann et al., 2011b). TTG field from Szilas et al. (2011c) and low-silica adakite average from Martin et al. (2005) with Th and Hf values from Yogodzinski et al. (1995). PM field from Sun and McDonough (1989).

5.3.2 AFC model

On the Th/Yb vs. Nb/Yb diagram (Fig. 9) the leucoamphibolites plot towards the aplites/TTG, which could be interpreted as the result of crustal contamination of basaltic magmas. We have therefore tested this scenario by assimilation-fractional-crystallisation (AFC) modelling (c.f. DePaolo, 1981). We applied the AFC model of Ersoy and Helvacı (2010) in an attempt to reproduce the characteristics of the calc-alkaline leucoamphibolites. We divided the rocks into one group of main leucoamphibolites and another group of enriched leucoamphibolites from the Bjørnesund supracrustal belt; the latter being characterised by enrichment in P_2O_5 , TiO_2 , CaO, Sr, Zr, Nb and LREE. We have approximated the composition of the parental magma by using the most primitive of the tholeiitic amphibolites (510802). As contaminants we have used the median value of the aplites, which broadly overlaps with the high-silica adakite average

of Martin et al. (2005). We also tested the low-silica adakite average of Martin et al. (2005). Th and Hf are not included in those estimates and therefore we adopted average values of 3.1 and 4.4 ppm, respectively, from the adakite data by Yogodzinski et al. (1995).

Our modelling shows that the main leucoamphibolites can be reproduced by AFC processes involving the TTG-like aplite median composition as a contaminant and a 'R-value' of 0.8 and 16% fractionation (60% plagioclase, 20% clinopyroxene and 20% olivine). At first this would appear to confirm the hypothesis that the calc-alkaline signature of the main leucoamphibolites is an artefact of contamination of tholeiitic magmas by older continental crust of TTG composition. However, as the initial ϵ_{Hf} and ϵ_{Nd} in these samples show no trends when plotted against contamination-sensitive trace elements it is clear that the contaminant must have been juvenile (Fig. 12; Section 5.4).

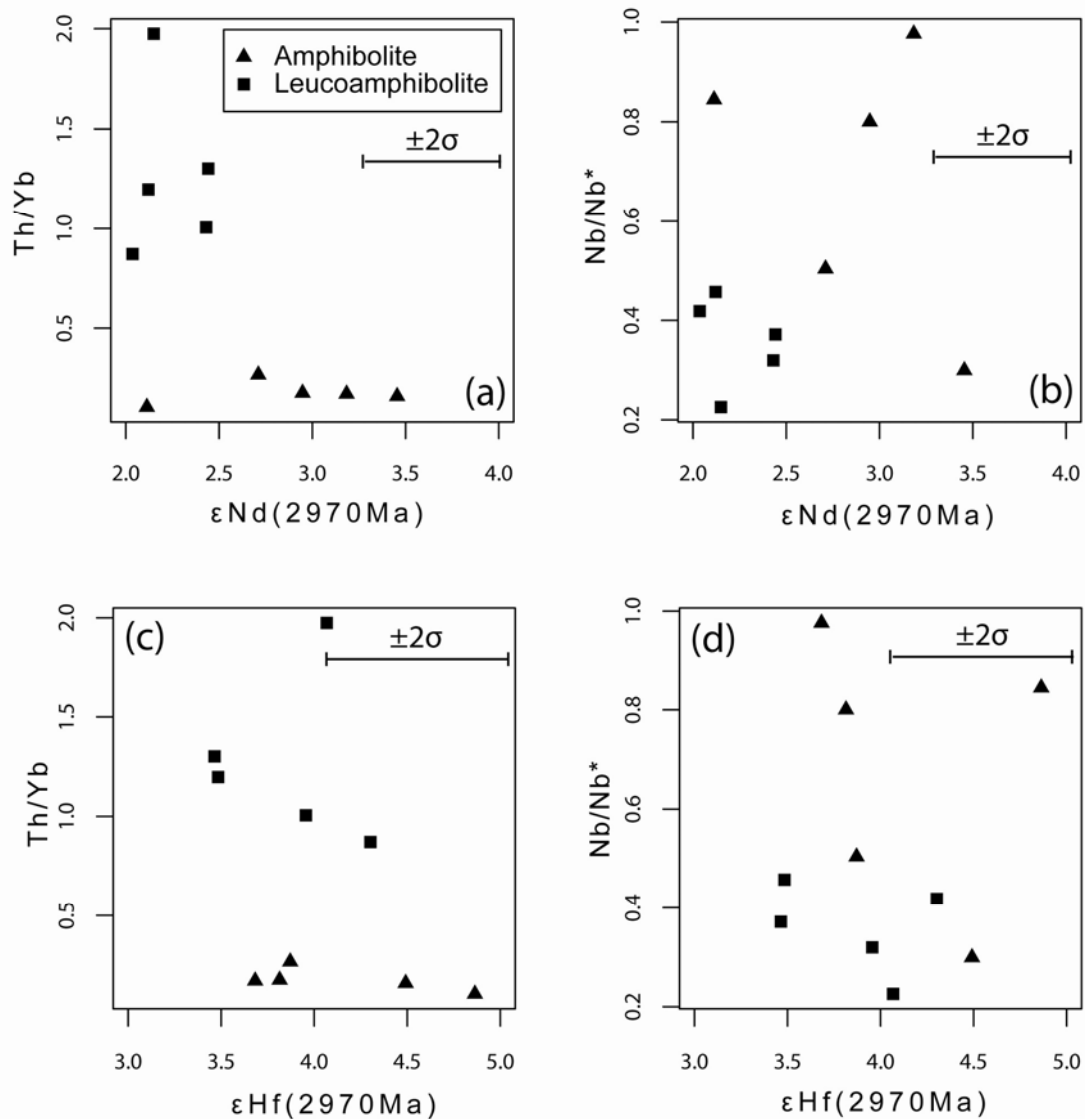


Figure 12. $\epsilon Hf(2970 Ma)$ and $\epsilon Nd(2970 Ma)$ versus Nb/Nb* and Th/Yb. There are no systematic correlations, which suggest that the amphibolites and leucoamphibolites are both juvenile. We show the conservative standard error of ± 0.5 ϵ -units.

We interpret this as melting-assimilation-storage-homogenisation (MASH) processes (Hildreth and Moorbath, 1988), where mafic crust partially melted at the base of a volcanic arc to form high-silica adakite or TTG-like melts, which then mixed with juvenile basaltic melts in a magma chamber to form the calc-alkaline magmas that were the protolith of the main leucoamphibolites. This is in agreement with models for modern andesites, which show evidence of mixing between mafic and felsic end-members (Kovalenko et al., 2010; Reubi and Blundy, 2009; Tatsumi and Suzuki, 2009).

The enriched group of leucoamphibolites can be modelled satisfactorily by AFC processes involving the hypothetical low-silica adakite component and using a ‘R-value’ of 0.8 and 12% fractionation (60% plagioclase, 20% clinopyroxene and 20% olivine). Because these rocks are also juvenile as seen by their isotopic compositions (Section 5.4), we interpret this as a felsic slab-melt (low-silica adakite) that metasomatised the mantle source, which later produced the enriched calc-alkaline leucoamphibolites that are found in the Bjørnesund supracrustal belt. If the Archaean mantle was indeed hotter than at present (Herzberg et al., 2010), then it is reasonable to assume that slab melts (low-silica adakite) were more common then than they are today. It is however also possible that ridge subduction was the cause of the locally hotter conditions

that resulted in slab melts in the Bjørnesund supracrustal belt. This model is also invoked for modern high-Mg andesites (Castillo, 2012 and references therein), but alternatively the adakitic melts could be the product of high-pressure crystallisation (Macpherson et al., 2006). However, given that the Archaean was hotter, we find it entirely plausible that slab-melts may have been more common.

It is interesting to note that the main leucoamphibolites form a large range along the AFC trends (Figs. 8 and 10), whereas the enriched leucoamphibolites form a tight clustering at a level on the AFC line. Given that they may be affected by slab-melts (low-silica adakite) is possible that this corresponds to a distinct pressure or temperature interval where the melts entered the mantle wedge. These enriched leucoamphibolites resemble high-magnesium andesites for which a similar petrogenesis has been invoked (Kelemen, 1995).

There is no reported TTG crust in the region with components older than c. 2900 Ma, except for a few grains at 3200 Ma (Polat et al., 2010). Additionally, such crust would have much too low initial Nd and Hf isotopic compositions to yield the observed initial isotopic compositions of the leucoamphibolites. We have modelled how AFC processes would affect the initial Hf and Nd compositions of the amphibolites with a TTG gneiss end-member contaminant using a 3033 Ma old sample (477678) from Hoffmann et al. (2011a). From

this model (Fig. 13) it is clear that even TTG formed immediately prior (c. 60 Ma) to the volcanism would be have too low initial isotopic compositions to provide a viable contaminant. We have also considered if the contaminant could have been subducted sediment, but given the juvenile isotopic compositions of the volcanic rocks we assume this to have been an island-arc environment with limited continental input. Sediment derived from a TTG source would also yield the problem of lower initial isotopic compositions as shown in Fig. 13 due to the long residence time for such material to develop and differentiate from a mantle-derived rock. Melts of juvenile pelite would likely have a granitic composition and this is also not compatible in our AFC model as a contaminant. However, the slab melt model fails to explain the elevated CaO contents of the enriched leucoamphibolites found at the Bjørnesund supracrustal belt. This is not due to alteration, because the main amphibolites in this area do not show elevated CaO and it is thus likely a primary feature. One

possible explanation could be contribution of CaO-rich sediments in the slab melt-contaminated source region.

We have additionally considered if selective contamination could have overprinted a potential TTG-derived isotopic signature, as proposed by Blichert-Toft et al. (1992) for other mafic rocks, however, the high 'R-value' in the AFC-model clearly requires a significant degree of contamination, which would be seen in the isotopic compositions. This also shows that the enrichment is not simply caused by assimilation, but rather by a significant felsic melt contribution.

All of the above supports that the TTG-like and adakitic end-members must have been derived by partial melting of nearly juvenile mafic volcanic rocks within the arc itself and then mix into the mantle source or directly with mafic melts in a magma chamber to produce the two distinct types of andesitic leucoamphibolites.

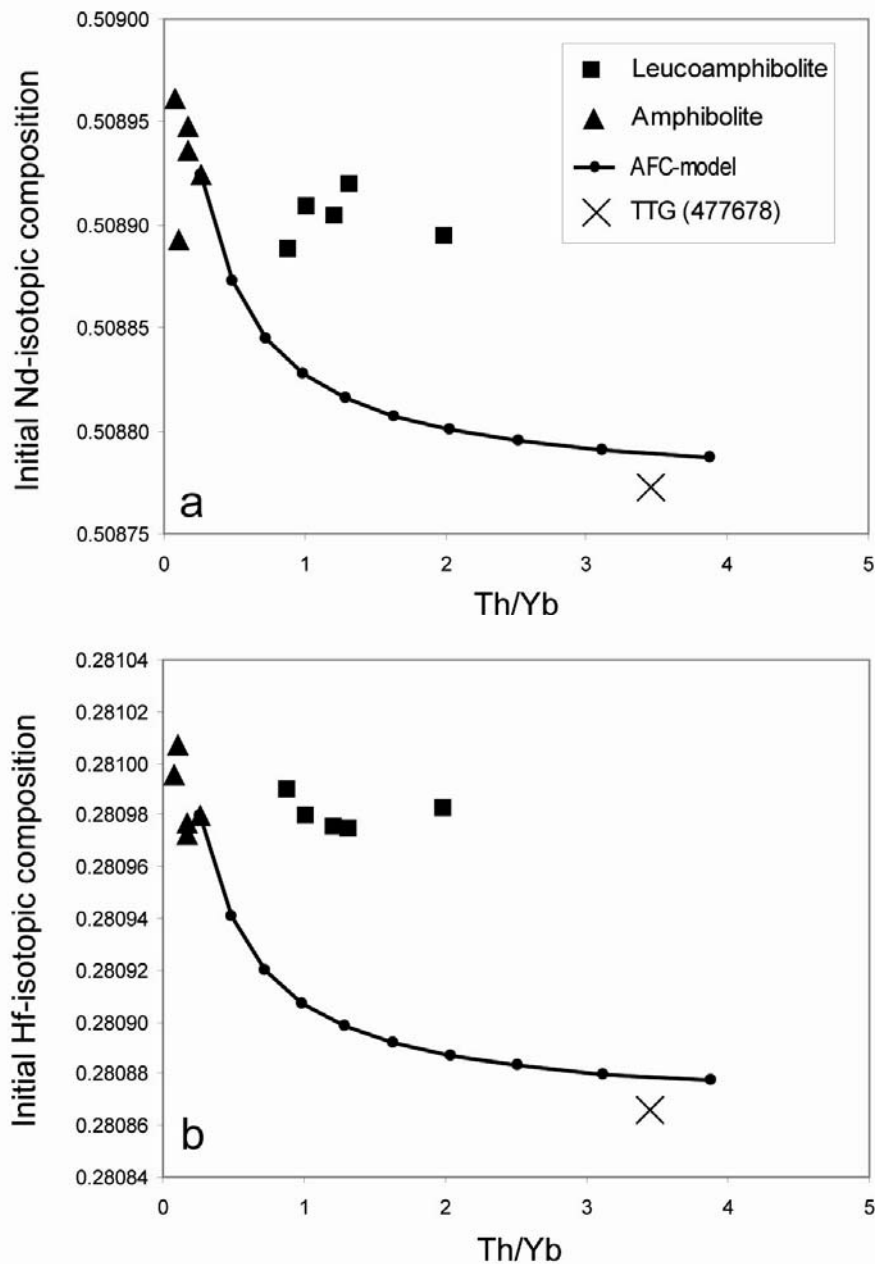


Figure 13. Assimilation-fractional-crystallisation (AFC) trend versus initial Hf and Nd isotopic compositions using a 3033 Ma old TTG sample (477678) from Hoffmann et al. (2011a) as a hypothetical TTG gneiss contaminant. The model starts at 100% melt fraction remaining and decreases to 37% in steps of 7%.

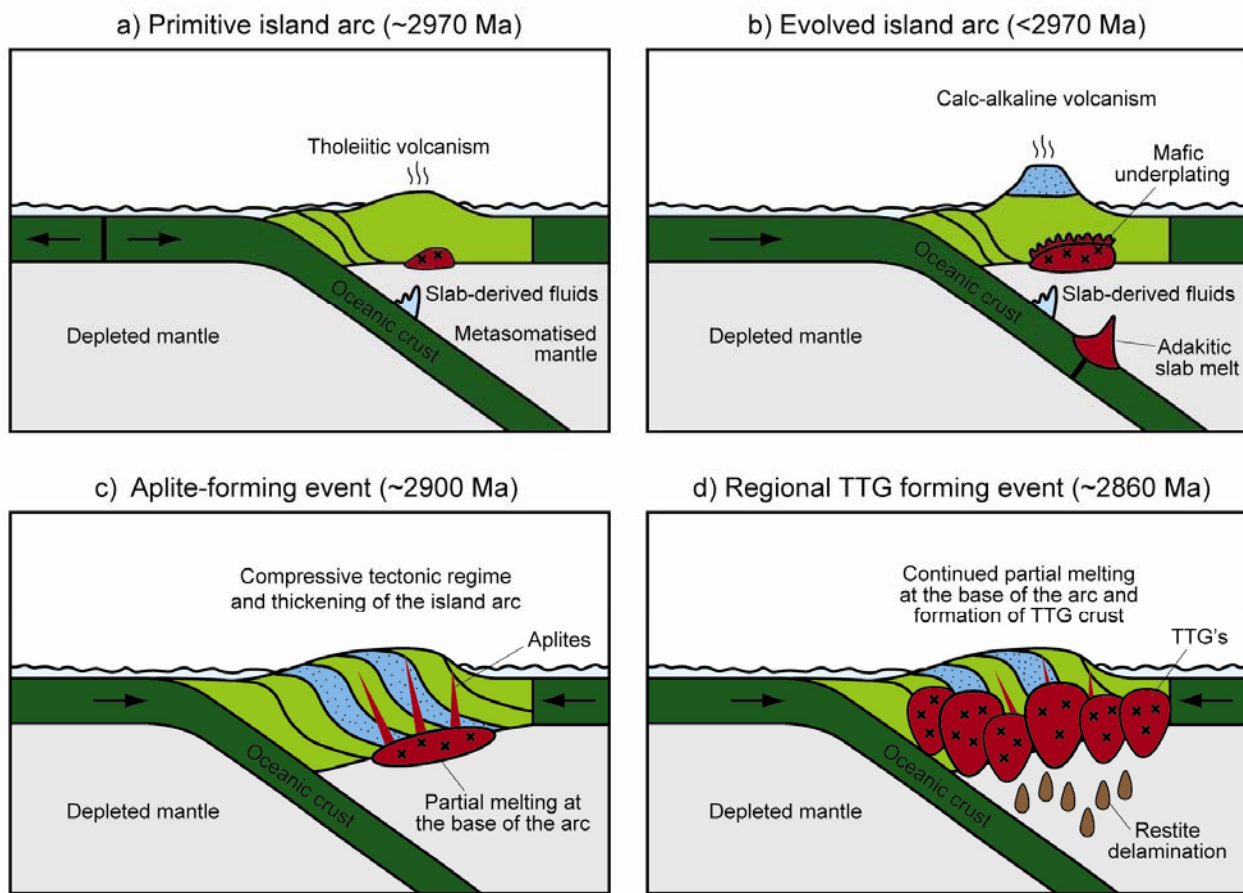


Figure 14. Model of the geodynamic setting for the Ikkattup Nunaa Supracrustal Association. a) Primitive island arc with tholeiitic basalts derived by fluid flux-melting of depleted mantle at c. 2970 Ma. b) Evolved island arc with two types of calc-alkaline volcanism occurring shortly after 2970 Ma. (1) Mafic underplating due to the thickened island arc crust formed partial melts of TTG-like composition, which could mix with new batches of mafic melts in shallow magma chambers and lead to the main andesitic leucoamphibolites. (2) Direct melting of the subducting slab in locally hot areas (perhaps aided by subduction or a spreading ridge), would lead to melts of low-silica adakite composition. These melts would metasomatise the mantle wedge and yield the enriched andesitic leucoamphibolites. c) Aplite-forming event at c. 2900 Ma, which intruded both the mafic and the andesitic volcanic sequence. The apolites formed by partial melting of the island arc volcanic rocks either during further underplating or by tectonic thickening of the island arc into deep levels of granulite facies metamorphism. d) Regional TTG forming event from c. 2920–2830 Ma (Friend and Nutman, 2001, 2005) likely caused by the tectonic thickening of the island arc crust in a compressional setting. This would cause the entire base of the island arc to partially melt and form TTG batholiths that intruded the above supracrustal sequence, whereas the residues would like delaminate and disappear into the mantle.

Fig. 14 outlines a tectonic model, which we consider to be a viable explanation of the data. Such a model is consistent with the regional development of other supracrustal belts in SW Greenland, as well as the regional TTG crust formation (e.g. Appel et al., 2009; Garde, 2007; Polat et al., 2008, 2009a; Windley and Garde, 2009; Friend and Nutman, 2010; Dilek and Furnes, 2011; Hoffmann et al., 2011b; Polat et al., 2011a; 2011b; Szilas et al., 2011b).

A model in which the regional TTG crust formed by tectonic thickening of mafic island arc crust rather than by direct melting of subducting oceanic crust is supported by periodic crust production and the long residence times for the mafic source rocks of the TTGs in SW Greenland as documented by *in situ* Hf isotopic studies (Næraa, 2011; Næraa et al., 2012; Hoffmann et al., 2011a), as well as based on combined petrological and geochemical modelling (Nagel et al., 2012). Such a model of cyclic crust formation is also compatible with work in younger orogens (Collins, 2002; DeCelles et al., 2009; Kemp et al., 2009).

The major implication of this petrogenetic model for the leucoamphibolites is that although some Archaean supracrustal rocks display apparent AFC trends towards TTG crust this is not necessarily evidence of crustal contamination as suggested by Pearce (2008). MASH and adakitic slab-melt processes operating in modern volcanic arc settings can also produce such trends (Castillo, 2012; Kovalenko et al., 2010; Price et al., 2005; Reubi and Blundy, 2009; Tatsumi and Suzuki, 2009). The calc-alkaline rocks described in this study of 'The Ikkattup Nunaa Supracrustal Association' are not unique to the Archaean rock record and comparable associations of Archaean calc-alkaline volcanic rocks are described in the literature

(e.g. Barley et al., 1998; Polat and Münker, 2004; Wang et al., 2004; Mtoro et al., 2009; Leclerc et al., 2011; Klausen et al., 2011). Thus similar interpretations may be applicable to the other examples and accordingly careful examination of isotopic data is crucial in order to evaluate the effects of crustal contamination versus modern-style arc processes.

5.4. ^{176}Lu - ^{176}Hf and ^{147}Sm - ^{143}Nd isotope systematics

The consistent isochron ages of the Ravns Storø and Bjørnesund supracrustal belts support the idea that they were contemporaneous within analytical resolution and thus possibly co-magmatic. The initial ϵ -values at 2970 Ma suggest that the protoliths of the amphibolites and the leucoamphibolites were derived from a mildly depleted mantle source.

When plotting initial ϵHf and ϵNd at 2970 Ma for the amphibolites and leucoamphibolites versus contamination-sensitive trace element ratios such as Nb/Nb* and Th/Yb there is no systematic correlation (Fig. 12). It is possible that small degrees of contamination of the leucoamphibolites with slab-derived melts could give a slightly lower ϵ -value, but within error they still lie on the same isochron as the juvenile tholeiitic amphibolites. This suggests that they represent juvenile magmas extracted from the depleted mantle at that time.

The anorthosite samples are clearly not derived from a DM source at 2970 Ma and their high initial ϵHf and ϵNd suggests derivation from a very depleted mantle source with an unusually high degree of early mantle depletion similar to the sources tapped by Eoarchaean boninite-like metabasalts from the Isua supracrustal belt

(Hoffmann et al., 2010b) or alternatively they display altered isotopic compositions, possibly resulting from element mobility during metamorphic overprint. However, more data is needed to conclude anything about the origin of the anorthosites.

The ultramafic sample shows $\epsilon\text{Nd}(t)$ that is consistent with the volcanic rocks, but the $\epsilon\text{Hf}(t)$ is chondritic. This suggests disturbance and perhaps overprinting of Nd, which is likely, given that these rocks would not have any phases in which Lu, Hf, Sm and Nd would be compatible.

It appears that the Sm-Nd system has been disturbed compared with the Lu-Hf system. The amphibolites and leucoamphibolites yield a Sm-Nd isochron that is indistinguishable from the Lu-Hf isochron within analytical error, but in detail the tholeiitic amphibolites show scatter and the calc-alkaline leucoamphibolites yield an isochron with an age of 2789 ± 92 Ma. This age is within error of the aplite/TTG sheets, as well as of later metamorphism (Section 4.4). This suggests that the disturbance happened during the intrusion of the TTG sheets into the supracrustal belt or during regional metamorphism and was likely caused by fluids capable of mobilising Sm and Nd, but not Lu and Hf. Metamorphic disturbance of the Sm-Nd system was treated theoretically by Rosing (1990) and has been described for similar rocks in the Isua supracrustal belt (Gruau et al., 1996). Because the Sm/Nd ratio is higher for the tholeiitic amphibolites than for the leucoamphibolites the former are less affected by the disturbance, whereas the latter records the time of disturbance. However, although the disturbance occurred c. 200 Ma after the mantle extraction event, it was not sufficiently severe to alter the overall isochron age of the volcanic sequence.

One final observation worth noting is that $\epsilon\text{Hf}(t)$ and $\epsilon\text{Nd}(t)$ in the amphibolites and leucoamphibolites are decoupled relative to the MORB-array, which is a feature that is seen in modern arc systems as well, where Nd is readily mobilised in the slab-derived component, whereas Hf is less mobile (König et al., 2010). Similar observations are seen for rocks in the Isua supracrustal belt (Hoffman et al., 2011b).

The isochron ages are essentially overlapping the age of the Fiskensæset Complex within error (Polat et al., 2010). Given that these rocks also show an arc-affinity, we propose that the whole region formed at the same time and in a similar geodynamic setting.

5.5. U-Pb geochronology

The similar U-Pb zircon ages (c. 2900 Ma) recorded in aplite sheets from the Ravns Storø, Bjørnesund and Perserajoorsuaq supracrustal belts suggest that the aplite sheets of ‘The Ikkattup Nunaa Supracrustal Association’ formed during the same regional event of TTG formation, which spans 2920–2830 Ma (Friend and Nutman, 2001, 2005). Two of the samples additionally record a known metamorphic event at c. 2720 Ma (Næraa and Scherstén, 2008), which is likely due to analysis of zircon rims that represent metamorphic overgrowth of magmatic zircon, whereas the analyses for sample 468768 were exclusively of zircon cores.

The leucoamphibolites from the Bjørnesund and the Perserajoorsuaq supracrustal belts also record two events at c. 2900 and c. 2720 Ma, respectively. We interpret the 2900 event in the leucoamphibolites as being related to the collision and amalgamation of island arcs, which were subsequently intruded by TTGs and then later metamorphosed under amphibolite-facies condition at c. 2720 Ma. Interestingly the leucoamphibolite from the Bjørnesund (510831) records an age that is within error of the supposed volcanic age of c. 2970 Ma. This is interpreted as rare volcanic zircon grains that survived metamorphic recrystallisation. It is not entirely clear, why we were unable to find zircon grains in the leucoamphibolites from the Ravns Storø supracrustal belt, but given that the zircons we found in the other two localities are mainly metamorphic it is reasonable to assume that the generally higher degree of deformation also lead to higher fluid content, which would be conducive for zircon growth under metamorphic conditions. Additionally, the Ravns Storø supracrustal belt experienced slightly lower metamorphic conditions than the Bjørnesund supracrustal belt (Schumacher et al., 2011), although the difference is not large enough to explain a difference in zircon-saturation without additional fluids. We propose that the so-called volcano-sedimentary rocks

dated by Nutman et al. (2004) are actually fine-grained rock similar to the leucoamphibolites that we have dated in this study.

The anorthosite appears to record two events at c. 2850 Ma and c. 2720 Ma, which are likely both metamorphic events. A few older grains support the findings from their Hf- and Nd-isotope systematics that this rock is derived from an ancient source, but we do not have enough data to make conclusions on the origin of the anorthosite.

6. Conclusions

We suggest that the reported isotopic and whole rock geochemical data combined with the comparable field relations, lithological units and U-Pb zircon ages for the Ravns Storø, Bjørnesund and Perserajoorsuaq supracrustal belt are best explained by a single co-magmatic volcanic sequence that formed in an island arc setting, by processes similar to modern-day arc volcanism at about 2970 Ma. We propose the collective name of ‘The Ikkattup Nunaa Supracrustal Association’ for these three supracrustal belts. This assemblage of supracrustal rocks is likely related to the Fiskensæset Complex immediately to the north and could possibly represent higher crustal levels (pillow lavas and tuffs), whereas the Fiskensæset could represent plutonic levels (cumulates, layered gabbros and anorthosite).

Trends on major and trace element diagrams show apparent mixing between the aplite sheets and amphibolites to produce the leucoamphibolites. The Th/Yb vs. Nb/Yb and the AFC trends support this model. However, the initial ϵHf and ϵNd of the calc-alkaline leucoamphibolites versus contamination sensitive trace elements show that the contaminating felsic magma was juvenile and thus that these trends are not due to contamination with pre-existing crust, but rather due to intra-arc differentiation and melting processes.

Using the sum of all available geochemical and isotopic data it is likely that the two groups of andesitic leucoamphibolites formed by two different processes, involving a similar mantle source. It cannot be established unambiguously whether mixing of mantle- and crust-derived magmas was predominant or whether felsic melt metasomatism of the mantle source prior to melt generation was responsible for the trends. However, in our preferred model (Fig. 14) the following could reasonably well explain the geochemical data: (1) mixing of juvenile island arc basaltic magmas with partial melts of slightly older (0–60 Ma) hydrated mafic island arc crust through underplating and MASH-processes to form the regular leucoamphibolites, and (2) by metasomatism of the mantle source with slab-derived melts of low-silica adakite composition to form the enriched leucoamphibolites found in the Bjørnesund supracrustal belt.

The implication of this study is that other Archaean calc-alkaline supracrustal rocks that have previously been interpreted as being contaminated by felsic crust during transit from the mantle (Pearce, 2008), may simply owe their enrichments in incompatible trace elements to a short lived complex melting regime, which record juvenile isotopic compositions. This would support operation of the two above mentioned processes and accordingly be consistent with Archaean subduction zone volcanism. Similar interpretations may be applicable to the other examples of Archaean calc-alkaline supracrustal rocks and accordingly careful examination of isotopic data is crucial in order to evaluate the effects of crustal contamination versus modern-style arc processes.

Appendix A. Methods

Detailed descriptions of the employed analytical methods can be found in the online version.

Appendix B. Supplementary data

Supplementary data can be found in the online version.

Table 1: Major and trace element data for the 149 samples presented in this study.

Table 2: ACME and GEUS Disko-1 standard interlab comparison.

Table 3: Lu-Hf and Sm-Nd isotopic data.

Table 4: LA-ICP-MS U-Pb zircon data.

Acknowledgements

We acknowledge the Greenland Bureau of Minerals and Petroleum (BMP) for financial support of the field and analytical work and thank the Geological Survey of Denmark and Greenland (GEUS) for permission to publish this work. We thank Fiorella Fabra Aguilera and Mojagan Alaei for help with the zircon separation at GEUS. We are grateful for the help provided by Susanne Rømer at GEUS with preparation of the tectonic sketch figure. K. Szilas would like to thank Geocenter Danmark for funding his Ph.D. project at GEUS with the title 'Archaean supracrustal belts of SW Greenland', which this work will form a part of. J.E. Hoffmann was supported by Grant Mu 1406/08 of the DFG (German Research Foundation). A. Scherstén acknowledges financial support from the Swedish Research council through grant #2008-3447. V.J. van Hinsberg acknowledges financial support from the European Union Seventh Framework Program (FP7/2007-2013) under grant agreement no. 254015. This study is a contribution to IGCP project 599.

We are thankful for the critical reviews by Hugh Rollinson and one anonymous reviewer, which improved the manuscript. We thank Guochun Zao for the editorial handling of this paper.

References

- Arndt, N.T., Kerr, A.C., Tarney, J., 1997. Dynamic melting in plume heads: the formation of Gorgona komatiites and basalts. *Earth and Planetary Science Letters* 146, 289–301.
- Andersen, L.S., Friend, C., 1973. Structure of the Ravns Storø amphibolite belt in the Fiskenaeset region. *Geological Survey of Greenland report* 51, 37–40.
- Anderson, A.T., 1975. Magma mixing: petrological process and volcanological tool. *Journal of Volcanology and Geothermal Research* 1, 3–33.
- Appel, P.W.U., 1992. Bjørnesund Project, West Greenland. *Rapport Grønlands Geologiske Undersøgelse* 155, 24–27.
- Appel, P.W.U., Polat, A., Frei, R., 2009. Dacitic ocelli in mafic lavas, 3.8–3.7 Ga Isua greenstone belt, West Greenland: Geochemical evidence for partial melting of oceanic crust and magma mixing. *Chemical Geology* 258, 105–124.
- Baier, J., Audéata, A., Keppler, H., 2008. The origin of the negative niobium tantalum anomaly in subduction zone magmas. *Earth and Planetary Science Letters* 267, 290–300.
- Barker, F., Peterman, A.E., 1974. Bimodal tholeiitic-dacitic magmatism and the early Precambrian crust. *Precambrian Research* 1, 1–12.
- Barley, M.E., Loader, S.E., McNaughton, N.J., 1998. 3430 to 3417 Ma calc-alkaline volcanism in the McPhee Dome and Kelly Belt, and growth of the eastern Pilbara Craton. *Precambrian research* 88, 3–23.
- Blichert-Toft, J., Leshner, C.E., Rosing, M.T., 1992. Selectively contaminated magmas of the Tertiary East Greenland macrodike complex. *Contributions to Mineralogy and Petrology* 110, 154–172.
- Boynton, W.V., 1984. Cosmochemistry of the rare earth elements: meteorite studies. In: Henderson, P. (ed.), *Rare Earth Element Geochemistry*, Elsevier, Amsterdam (1984), 63–114.
- Bridgwater, D., Keto, L., McGregor, V.R., Myers, J.S., 1976. Archaean gneiss complex of Greenland. In: Escher, A., Watt, W.S. (eds.), *Geology of Greenland, Grønlands Geologiske Undersøgelse*, Copenhagen, 18–75.
- Cabanis, B., Lecolle, M., 1989. Le diagramme La/10-Y/15-Nb/8: un outil pour la discrimination des séries volcaniques et la mise en évidence des processus de mélange et/ou de contamination crustale. *C.R. Acad. Sci. Ser. II*, 2023–2029.
- Campbell, I.H., Griffiths, R.W., Hill, R.I., 1989. Melting in an Archean mantle plume: heads it's basalts, tails it's komatiites. *Nature* 369, 697–699.
- Klausen, M.B., Kokfelt, T.F., Keulen, N., Berger, A., Schumacher, J.C., 2011. Geochemistry of Archaean serpentinites, tholeiitic amphibolites and calc-alkaline schists across the Nigellikassik section in the Kvanefjord Terrane, South-West Greenland, ~62°S. *Geological Survey of Denmark and Greenland, report 2011/XX* (in press).
- Castillo, P.R., 2012. Adakite petrogenesis. *Lithos* 134–135, 304–316.
- Collins, W.J., 2002. Hot orogens, tectonic switching and the creation of continental crust. *Geology* 30, 535–538.
- Condie K.C., Pease V. (eds.), 2008. When did Plate Tectonics Begin on Planet Earth? Geological Society of America, Special Paper 440.
- Davidson, J.P., Hora, J.M., Garrison, J.M., Dungan, M.A., 2005. Crustal forensics in arc magmas. *Journal of Volcanology and Geothermal Research* 140, 157–170.
- Davidson, J.P., Morgan, D.J., Charlier, B.L.A., Harlou, R., Hora, J.M., 2007. Microsampling and isotopic analysis of igneous rocks: implications for the study of magmatic systems. *Annual Reviews of Earth and Planetary Sciences* 35, 273–311.
- Dawes, P.R., 1969. Age and correlation of supracrustal rocks in the Frederikshåb Isblink area. *Rapport Grønlands Geologiske Undersøgelse* 19, 31–33.
- DeCelles, P.G., Ducea, M.N., Kapp, P., Zandt, G., 2009. Cyclicity in Cordilleran orogenic systems. *Nature Geoscience* 2, 251–257.
- DePaolo, D.J., 1981. Trace element and isotopic effects of combined wallrock assimilation and fractional crystallization. *Earth and Planetary Science Letters* 53, 189–202.
- Dilek, Y., Furnes, H., 2011. Ophiolite genesis and global tectonics: geochemical and tectonic fingerprinting of ancient oceanic lithosphere. *Geological Society of America Bulletin* 123, 387–411.
- Dhuime, B., Hawkesworth, C.J., Cawood, P.A., Storey, C.D., 2012. A Change in the Geodynamics of Continental Growth 3 Billion Years Ago. *Science* 335, 1334–1336.
- Eichelberger, J.C., 1978. Andesitic volcanism and crustal evolution. *Nature* 275, 21–27.
- Ersoy, Y., Helvacı, C., 2010. FC-AFC-FCA and mixing modeler: A Microsoft® Excel® spreadsheet program for modeling geochemical differentiation of magma by crystal fractionation, crustal assimilation and mixing. *Computer and Geoscience* 36, 383–390.
- Frey, H.M., Lange, R.A., 2010. Phenocryst complexity in andesites and dacites from the Tequila volcanic field, Mexico: resolving the effects of degassing vs. magma mixing. *Contributions to Mineralogy and Petrology* 162, 415–445.
- Friend, C.R.L., 1975. The geology and geochemistry of the Preketilidian basement complex in the Ravns Storø area, Fiskenaeset region, southern West Greenland. Unpublished Ph.D. thesis, University London, 233 pp.
- Friend, C.R.L., 1976a. Field relationships and petrology of leucocratic schists from the Ravns Storø Group near Fiskenaeset. *Rapport Grønlands Geologiske Undersøgelse* 73, 81–85.
- Friend, C.R.L., 1976b. A metamorphosed basic dyke swarm in the vicinity of Sarqarigsup Nunå (Ravns Storø area) Fiskenaeset, southern West Greenland. *Rapport Grønlands Geologiske Undersøgelse* 73, 22–30.
- Friend, C.R.L., Nutman, A.P., 2001. U-Pb zircon study of tectonically bounded blocks of 2940–2840 Ma crust with different metamorphic histories, Paamiut region, South-West Greenland: implications for the tectonic assembly of the North Atlantic craton. *Precambrian Research* 105, 143–164.
- Friend, C.R.L., Nutman, A.P., 2005. New pieces to the Archaean jigsaw puzzle in the Nuuk region, southern West Greenland: steps in transforming a simple insight into a complex regional tectonothermal model. *Journal of the Geological Society of London* 162, 147–162.
- Friend, C.R.L., Nutman, A.P., 2010. Eoarchean ophiolites? New evidence for the debate on the Isua supracrustal belt, southern West Greenland. *American Journal of Science* 310, 826–861.
- Furnes, H., Rosing, M., Dilek, Y., De Wit, M., 2009. Isua supracrustal belt (Greenland) – A vestige of a 3.8 Ga suprasubduction zone ophiolite, and the implications for Archean geology. *Lithos* 113, 115–132.
- Garde, A.A., 2007. A mid-Archaean island arc complex in the eastern Akia terrane, Godthåbsfjord, southern West Greenland. *Journal of the Geological Society (London)* 164, 565–579.
- Garde, A.A., Whitehouse, M., Christensen, R., 2012. Mesoarchean epithermal gold mineralization preserved at upper amphibolite facies grade, Qussuk, southern West Greenland. *The Society of Economic Geology* (in press).
- Grant, J.A., 1986. The isocon diagram - a simple solution to Gresens' equation for metasomatic alteration. *Economic Geology* 81, 1976–1982.
- Grant, J.A., 2005. Isocon analysis: A brief review of the method and applications. *Physics and Chemistry of the Earth* 30, 997–1004.
- Green, T.H., Ringwood, A.E., 1967. Crystallization of basalt and andesite under high pressure hydrous conditions. *Earth and Planetary Science Letters* 3, 481–489.
- Grove, T.L., Elkins-Tanton, L.T., Parman, S.W., Chatterjee, N., Müntener, O., Gaetani, G.A., 2003. Fractional crystallization and mantle-melting controls on calc-alkaline differentiation trends. *Contributions to Mineralogy and Petrology* 145, 515–533.
- Gruau, G., Rosing, M., Bridgwater, D., Gill, R.O.C., 1996. Resetting of Sm-Nd systematics during metamorphism of > 3.7-Ga rocks: implications for isotopic models of early Earth differentiation. *Chemical Geology* 133, 225–240.
- Hamilton, W.B., 1998. Archean magmatism and deformation were not products of plate tectonics. *Precambrian Research* 91, 143–179.
- Herzberg, C., Condie, K., Korenaga, J., 2010. Thermal history of the Earth and its petrological expression. *Earth and Planetary Science Letters* 292, 79–88.
- Hildreth, W., Moorath, S., 1988. Crustal contributions to arc magmatism in the Andes of Central Chile. *Contributions to Mineralogy and Petrology* 98, 455–489.
- Hoffmann, J.E., Münker, C., Næraa, T., Rosing, M.T., Herwartz, D., Garbe-Schönberg, D., Svahnberg, H., 2011a. Mechanisms of Archean crust formation inferred from high-precision HFSE systematics in TTGs. *Geochimica et Cosmochimica Acta* 75, 4157–4178.
- Hoffmann, J.E., Münker, C., Polat, A., Rosing, M.T., Schulz, T., 2011b. The origin of decoupled Hf-Nd isotope compositions in Eoarchean rocks from southern West Greenland. *Geochimica et Cosmochimica Acta* 75, 6610–6628.
- Hollings, P., Stott, G., Wyman, D., 2000. Trace element geochemistry of the Meen-Dempster greenstone belt, Uchi subprovince, Superior Province, Canada: backarc development on the margins of an Archean protocontinent. *Canadian Journal of Earth Science* 37, 1021–1038.
- Hunter, D.R., Barker, F., Millard, H.T., 1984. Geochemical investigation of Archaean bimodal and Dwalile metamorphic suites, Ancient Gneiss Complex, Swaziland. *Precambrian Research* 24, 131–155.
- Irvine, T.N., Baragar, W.R.A., 1971. A guide to the chemical classification of the common volcanic rocks. *Canadian Journal of Earth Sciences* 8, 523–548.
- Jensen, L.S., 1976. A New Cation Plot for Classifying Subalkalic Volcanic Rocks. *Ontario Geological Survey Miscellaneous Paper* 66.
- Kalsbeek, F., Myers, J.S., 1973. The geology of the Fiskenaeset region. *Rapport Grønlands Geologiske Undersøgelse* 51, 5–18.
- Kelemen, P.B., 1995. Genesis of high Mg# andesites and the continental crust. *Contributions to Mineralogy and Petrology* 120, 1–19.
- Kelemen, P.B., Hanghøj, K., Greene, A., 2003. One view of the geochemistry of subduction-related magmatic arcs, with an emphasis on primitive andesite and lower crust. In: Rudnick R.L. (ed.), *The Crust*, Vol. 3, Treatise on Geochemistry. Holland, H.D., Turekian, K.K., (eds.) Oxford, UK, Elsevier-Perigamon, 593–659.
- Kemp, A.I.S., Hawkesworth, C.J., Collins, W.J., Gray, C.M., Blevin, P.L., Edinburgh Ion Microprobe Facility, 2009. Nd, Hf and O isotope evidence for rapid continental growth during accretionary orogenesis in the Tasmanides, eastern Australia. *Earth and Planetary Science Letters* 284, 455–466.
- Kerr, A.C., Marriner, G.F., Arndt, N.T., Tarney, J., Nivia, A., Saunders, A.D., Duncan, R.A., 1996. The petrogenesis of Gorgona komatiites, picrites and basalts: new field, petrographic and geochemical constraints. *Lithos* 37, 245–260.
- Kerrick, R., Polat, A., 2006. Archean greenstone-tonalite duality: thermodynamic mantle convection models or plate tectonics in the early Earth global dynamics. *Tectonophysics* 415, 141–165.
- Keulen, N., Schumacher, J.C., van Hinsberg, V.J., Szilas, K., Windley, B.F., Kokfelt, T.F., Schlatter, D.M., Scherstén, A., 2011. The Bjørnesund anorthositic-greenstone belt – a link between the Fiskenaeset Complex and the Ravns Storø metavolcanic belt, southern West Greenland. *Geophysical Research Abstracts*, vol. 13, EGU2011-8525-1.
- Kovalenko, V.I., Naumov, V.B., Girmis, A.V., Dorofeeva, V.A., Yarmolyuk, V.V., 2010. Average composition of basic magmas and mantle sources of island arcs and active continental margins estimated from the data on melt inclusions and quenched rock glasses. *Petrology* 18, 1–26.
- König, S., Münker, C., Schuth, S., Luguet, A., Hoffmann, J.E., Kuduon, J., 2010. Boninites as windows into trace element mobility in subduction zones. *Geochimica et Cosmochimica Acta* 74, 684–704.
- Langmuir, C.H., Vocke Jr., R.D., Hanson, G.N., Hart, S.R., 1978. A general mixing equation with applications to Icelandic basalts. *Earth and Planetary Science Letters* 37, 380–392.

- Leclerc, F., Bédard, J.H., Harris, L.B., McNicoll, V.J., Goulet, N., Roy, P., Houle, P., 2011. Tholeiitic to calc-alkaline cyclic volcanism in the Roy Group, Chibougamau area, Abitibi Greenstone Belt – revised stratigraphy and implications for VHMS exploration. *Canadian Journal of Earth Sciences* 48, 661-694.
- López Sánchez-Vizcaino, V., Trommsdorff, V., Gómez-Pugnaire, M.T., Garrido, C.J., Müntener, O., 2005. Petrology of titanian clinohumite and olivine at the high-pressure breakdown of antigorite serpentinite to chlorite harzburgite (Almirez Massif, S. Spain). *Contributions to Mineralogy and Petrology* 149, 627-646.
- Macpherson, C.G., Dreher, S.T., Thirwall, M.F., 2006. Adakites without slab melting: high pressure differentiation of island arc magma, Mindanao, the Philippines. *Earth and Planetary Science Letters* 243, 581-593.
- Martin, H., Smithies, R.H., Rapp, R., Moya, J.-F., Champion, D., 2005. An overview of adakite, tonalite-trondhjemite-granodiorite (TTG), and sanukitoid: relationships and some implications for crustal evolution. *Lithos* 79, 1-24.
- Martinez, F., Taylor, B., 2003. Controls on backarc crustal accretion: insights from the Lau, Manus and Mariana basins. In: Larter, R.D. and Leat, P.T. (eds.). *Intra-oceanic subduction systems: tectonic and magmatic processes*. Geological Society of London, Special Publications 219, 19-54.
- McGregor, V.R., Friend, C.R.L., 1992. Late Archean prograde amphibolite- to granulite-facies relations in the Fiskeneset region, southern West Greenland. *Journal of Geology* 100, 207-219.
- Metcalfe, R.V., Shervais, J.W., 2008. Supra-Subduction Zone (SSZ) Ophiolites: Is There Really An "Ophiolite Conundrum"? In: Wright, J.E., Shervais, J.W. (eds.). *Ophiolites, Arcs, and Batholiths: A Tribute to Cliff Hopson*. GSA Special Paper 438, p. 191-222.
- Moya, J.-F., Stevens, G., Kisters, A.F.M., 2006. Record of mid-Archean subduction from metamorphism in the Barberton terrain, South Africa. *Nature* 442, 559-562.
- Myers, J.S., 1978. Formation of banded gneisses by deformation of igneous rocks. *Precambrian Research* 6, 43-64.
- Myers, J.S., 1985. Stratigraphy and structure of the Fiskeneset Complex, southern West Greenland. *Grønlands Geologiske Undersøgelse Bulletin* 150, 72.
- Mtoro, M., Maboko, M.A.H., Many, S., 2009. Geochemistry and geochronology of the bimodal volcanic rocks of the Suguti area in the southern part of the Musoma-Mara Greenstone Belt, Northern Tanzania. *Precambrian Research* 174, 241-257.
- Nagel, T., Hoffmann, J.E., Münker, C., 2012. Generation of Eoarchean TTGs from thickened mafic arc crust. *Geology*. DOI: 10.1130/G32729.1.
- Næraa, T., 2011. Zircon U/Pb, Hf and O isotopic systematics from the Archean basement in the Nuuk region southern West Greenland – Constraints on the early evolution of the continental crust. Unpublished Ph.D. thesis, University of Copenhagen, pp. 195.
- Næraa, T., Scherstén, A., 2008. New zircon ages from the Tasiusarsuaq terrane, southern West Greenland. *Geological Survey of Denmark and Greenland Bulletin* 15, 73-76.
- Næraa, T., Scherstén, A., Rosing, M.T., Kemp, A.I.S., Hoffmann, J.E., Kokfelt, T.F., Whitehouse, M., 2012. Hafnium isotope evidence for a transition in the geodynamics of continental growth after 3.2 Ga. *Nature* (accepted).
- Nutman, A.P., Friend, C.R.L., Barker, S.L.L., McGregor, V.R., 2004. Inventory and assessment of Palaeoarchean gneiss terranes and detrital zircons in southern West Greenland. *Precambrian Research* 135, 281-314.
- Ohta, T., Arai, H., 2007. Statistical empirical index of chemical weathering in igneous rocks: A new tool for evaluating the degree of weathering. *Chemical Geology* 240, 280-297.
- Pearce, J.A., Cann, J.R., 1973. Tectonic setting of basic volcanic rocks determined using trace element analyses. *Earth and Planetary Science Letters* 19, 290-300.
- Pearce, J.A., Norry, M.J., 1979. Petrogenetic implications of Ti, Zr, Y, and Nb variations in volcanic rocks. *Contributions to Mineralogy and Petrology* 69, 33-47.
- Pearce, J.A., Peate, D.W., 1995. Tectonic implications of the composition of volcanic arc magmas. *Annual Reviews of Earth and Planetary Sciences* 23, 251-285.
- Pearce, J.A., 1996. A user's guide to basalt discrimination diagrams. In: Wyman, D. A. (editor) *Trace element geochemistry of volcanic rocks: applications for massive sulphide exploration*. Geological Association of Canada, short course notes 12, 79-113.
- Pearce, J.A., 2008. Geochemical fingerprinting of oceanic basalts with applications to ophiolite classification and the search for Archean oceanic crust. *Lithos* 100, 14-48.
- Pease, V., Percival, J., Smithies, R.H., Stevens, G., van Kranendonk, M., 2008. When did plate tectonics begin? Evidence from the orogenic record. In: Condie K.C., Pease V. (eds.). *When did Plate Tectonics Begin on Planet Earth?* Geological Society of America, Special Paper 440, 199-208.
- Pidgeon, R.T., Kalsbeek, F., 1978. Dating of igneous and metamorphic events in the Fiskeneset region of southern West Greenland. *Canadian Journal of Earth Science* 15, 2021-2025.
- Polat, A., Hofmann, A.W., Rosing, M.T., 2002. Boninite-like volcanic rocks in the 3.7–3.8 Ga Isua greenstone belt, West Greenland: geochemical evidence for intra-oceanic subduction zone processes in the early Earth. *Chemical Geology* Volume 184, 231-254.
- Polat, A., Münker, C., 2004. Hf-Nd isotope evidence for contemporaneous subduction processes in the source of late Archean arc lavas from the Superior Province, Canada. *Chemical Geology* 213, 403-429.
- Polat, A., Frei, R., Appel, P.W.U., Dilek, Y., Fryer, B., Ordóñez-Calderón, J.C., Yang, Z., 2008. The origin and compositions of Mesoproterozoic oceanic crust: Evidence from the 3075 Ma Ivisartoq greenstone belt, SW Greenland. *Lithos* 100, 293-321.
- Polat, A., Frei, R., Fryer, B., Appel, P.W.U., 2009a. The origin of geochemical trends and Eoarchean (ca. 3700 Ma) zircons in Mesoproterozoic (ca. 3075 Ma) ocelli-hosting pillow basalts, Ivisartoq greenstone belt, SW Greenland: Evidence for crustal contamination versus crustal recycling. *Chemical Geology* 268, 248-271.
- Polat, A., Appel, P.W.U., Fryer, B., Windley, B.F., Frei, R., Samson, I.M., Huang, H., 2009b. Trace element systematics of the Neoproterozoic Fiskeneset anorthosite complex and associated meta-volcanic rocks, SW Greenland: evidence for a magmatic arc origin. *Precambrian Research*, 175, 87-115.
- Polat, A., Frei, R., Scherstén, A., Appel, P.W.U., 2010. New age (ca. 2970 Ma), mantle source composition and geodynamic constraints on the Archean Fiskeneset anorthosite complex, SW Greenland. *Chemical Geology*, 277, 1-20.
- Polat, A., Fryer, B.J., Appel, P.W.U., Kalvig, P., Kerrich, R., Dilek, Y., Yang, Z., 2011a. Geochemistry of anorthositic differentiated sills in the Archean (~2970 Ma) Fiskeneset Complex, SW Greenland: Implication for parental magma compositions, geodynamic setting, and secular heat flow in arcs. *Lithos* 123, 50-72.
- Polat, A., Appel, P.W.U., Fryer, B.J., 2011b. An overview of the geochemistry of Eoarchean to Mesoproterozoic ultramafic to mafic volcanic rocks, SW Greenland: Implication for mantle depletion and petrogenetic processes at subduction zones in the early Earth. *Gondwana Research*.
- Price, R.C., Gamble, J.A., Smith, I.E.M., Stewart, R.B., Eggs, S., Wright, I.C., 2005. An integrated model for the temporal evolution of andesites and rhyolites and crustal development in New Zealand's North Island. *Journal of Volcanology and Geothermal Research* 140, 1-24.
- Pulvertaft, T.C.R. 1972. Preliminary report on the geology of the area between Kigutilik and Bjørnsund (62° V 1). Geological Survey of Greenland achieve.
- Reubi, O., Blundy, J., 2009. A dearth of intermediate melts at subduction zone volcanoes and the petrogenesis of arc andesites. *Nature Letters* 461, 1269-1274.
- Rollinson, H.R., 1993. *Using geochemical data: evaluation, presentation, interpretation*. Longman, UK. 352 pp.
- Rosing, M.T., 1990. The theoretical effect of metasomatism on Sm-Nd isotopic systems. *Geochimica et Cosmochimica Acta* 54, 1337-1341.
- Ryerson, F.J., Watson, E.B., 1987. Rutile saturation in magmas: implications for Ti-Nb-Ta depletion in island-arc basalts. *Earth and Planetary Science Letters* 86, 225-239.
- Sandeman, H.A., Hanmer, S., Tella, S., Armitage, A.A., Davis, W.J., Ryan, J.J., 2006. Petrogenesis of Neoproterozoic volcanic rocks of the MacQuoid supracrustal belt: a backarc setting for the northwestern Hearne subdomain, western Churchill Province, Canada. *Precambrian Research* 144, 140-165.
- Schlatter, D., Möller Steensgaard, B., 2011. Evaluation of the mineral potential in the Bjørnesund Greenstone belt combining multivariate studies, field work and lithogeochemistry. *Danmarks og Grønlands Geologiske Undersøgelse Rapport* 2011 (in prep).
- Schumacher, J.C., van Hinsberg, V.J., Keulen, N., 2011. Metamorphism in supracrustal and ultramafic rocks in southern West Greenland and South-West Greenland 64-61.5°N. Geological Survey of Denmark and Greenland Report 2011/6.
- Shirey, S.B., Richardson, S.H., 2011. Start of the Wilson Cycle at 3 Ga Shown by Diamonds from Subcontinental Mantle. *Science* 333, 434-436.
- Sisson, T.W., Grove, T.L., 1993. Experimental investigations of the role of H₂O in calc-alkaline differentiation and subduction zone magmatism. *Contributions to Mineralogy and Petrology* 113, 143-166.
- Smithies, R.H., Champion, D.C., van Kranendonk, M.J., Howard, H.M., Hickman, A.H., 2005. Modern-style subduction processes in the Mesoproterozoic: geochemical evidence from the 3.12 Ga Whundo intraoceanic arc. *Earth and Planetary Science Letters* 231, 221-237.
- Stern, R.J., 2008. Modern-style plate tectonics began in Neoproterozoic time: an alternative interpretation of Earth's tectonic history. In: Condie K.C., Pease V. (eds.). *When did Plate Tectonics Begin on Planet Earth?* Geological Society of America, Special Paper 440, 265-280.
- Sun, S., McDonough, W.F., 1989. Chemical and isotopic systematics of oceanic basalts: implications for mantle composition and processes. In: Saunders, A.D., Norry, M.J. (eds.) *Magmatism in the Ocean Basins*. Geological Society of London, Special Publications 42, 313-345.
- Szilas, K., Scherstén, A., Hoffmann, J.E., Kokfelt, T.F., van Hinsberg, V.J., Windley, B.F., Münker, C., 2011a. Linking the Ravns Storo and Bjørnesund supracrustal belts (SW Greenland) using Lu-Hf and Sm-Nd isotopic data and whole-rock geochemistry. *Geophysical Research Abstracts*, vol. 13, EGU2011-11114-1.
- Szilas, K., van Hinsberg, J., Kisters, A.F.M., Hoffmann, E.J., Kokfelt, T.F., Scherstén, A., Windley, B.F., Frei, R., Rosing, M.T., Münker, C., 2011b. Remnants of arc-related oceanic crust in the Tartoq Group, SW Greenland. *Gondwana Research* (in press).
- Szilas, K., Kokfelt, T.F., Næraa, T., Scherstén, A., 2011c. Geochemistry of Archean felsic crust in SW Greenland. In: Kokfelt, T.F. (ed.) *Geochemistry of supracrustal rocks and associated intrusive TTG suites of the Archean craton in South-West Greenland and southern West Greenland, 61°30' - 64°N*. Geological Survey of Denmark and Greenland report 2011/10 (in press).
- Tatsumi, Y., Suzuki, T., 2009. Tholeiitic vs calc-alkaline differentiation and evolution of arc crust: constraints from melting experiments on a basalt from the Izu-Bonin-Mariana arc. *Journal of Petrology* 50, 1575-1603.
- Taylor, B., Martinez, F., 2003. Backarc basin basalt systematics. *Earth and Planetary Science Letters* 210, 481-497.
- van Kranendonk, M.J., 2004. Archean tectonics 2004: a review. *Precambrian Research* 131, 143-151.
- van Kranendonk, M.J., 2011. Onset of Plate Tectonics. *Science*, 333, 413-414.
- Wang, Z., Wilde, S.A., Wang, K., Yu, L., 2004. A MORB-arc basalt-adakite association in the 2.5 Ga Wutai greenstone belt: late Archean magmatism and crustal growth in the North China Craton. *Precambrian Research* 131, 323-343.
- Williams, H.R., 1976. Granitisation of basic rocks in the Bjørnsund area, near Fiskeneset, West Greenland. *Rapport Grønlands Geologiske Undersøgelse* 73, 47-54.
- Winchester, J.A., Floyd, P.A., 1977. Geochemical discrimination of different magma series and their differentiation products using immobile elements. *Chemical Geology* 20, 325-343.
- Windley, B.F., 1966. Anorthosites and polymetamorphism between Ravns Storo and Sukkertoppen, West Greenland. *Rapport Grønlands Geologiske Undersøgelse* 11, 27-29.
- Windley, B.F., 1968. New field relations from the early Precambrian of west Greenland. *Rapport Grønlands Geologiske Undersøgelse* 15, 27-31.
- Windley, B.F., Henriksen, H., Higgins, A.K., Bondesen, E., Jensen, S.B., 1966. Some border relations between supracrustal and infracrustal rocks in South-West Greenland. *Rapport Grønlands Geologiske Undersøgelse* 9, 43 pp.
- Windley, B., Garde, A.A., 2009. Arc-generated blocks with sections in the North Atlantic craton of West Greenland: Crustal growth in the Archean with modern analogues. *Earth-Science Reviews* 93, 1-30.
- Wood, D.A., 1980. The application of a Th-Hf-Ta diagram to problems of tectonomagmatic classification and to establishing the nature of crustal contamination of basaltic lavas of the British Tertiary volcanic province. *Earth and Planetary Science Letters* 50, 11-30.
- Yogodzinski, G.M., Kay, R.W., Volynets, O.N., Koloskov, A.V., Kay, S.M., 1995. Magnesian andesite in the western Aleutian Komandorsky region: Implications for slab melting and processes in the mantle wedge. *Geological Society of America Bulletin* 107, 505-519.

Supplementary material for Paper II

Appendix A (Paper II): Methods

We have employed various methods to investigate rocks from the three supracrustal belts. First of all we have acquired major and trace element analyses by ICP methods. Secondly, we have analysed key samples for their Lu-Hf and Sm-Nd isotopic compositions by MC-ICP-MS and finally we have measured U-Pb isotopic compositions in zircons to get absolute age constraints.

Whole rock analyses

Samples of a few kilograms in size were collected in the field and weathered crusts if present were removed. Crushing was performed at ACMELabs in Vancouver, Canada, in a tungsten-carbide jaw crusher and material was subsequently pulverised in a ceramic box-mill to reduce trace element contamination of W, Co, Sc and Ta. However, samples in the series 5158XX and 4687XX, were pulverised at GEUS in a tungsten-carbide swing-mill and accordingly the above contamination-sensitive trace elements were not used for petrogenetic interpretations for these two series.

Whole rock analyses were carried out at ACMELabs in Vancouver, Canada, following the analytical procedures termed “Group 4A & 4B - lithogeochemical whole rock fusion”. A brief description of the procedure is summarised below based on the description available on the homepage (www.acmelab.com) and on information obtained upon personal request from the company: “Prepared samples are mixed with $\text{LiBO}_2/\text{Li}_2\text{B}_4\text{O}_7$ flux in crucibles and fused in a furnace. The cooled bead is then dissolved in ACS grade nitric acid. For “Group 4A” the total abundances of the major oxides and several minor elements are analysed for a 200 mg sample by ICP-emission spectrometry following a lithium metaborate/tetraborate fusion and dilute nitric digestion. Loss on ignition (LOI) is determined by igniting a sample split at 1000°C then measuring the weight loss. “Group 4B” comprises two separate analyses for the total trace elements by ICP-MS. Rare earth and refractory elements are determined by ICP mass spectrometry following a lithium metaborate/tetraborate fusion and nitric acid digestion of a 200 mg sample. Additionally a separate 500 mg split is digested in Aqua Regia and analysed by ICP Mass Spectrometry to determine the precious and base metals”. Fe valence was not determined and Fe_2O_3 thus refers to total Fe. The geochemical data are presented in Supplementary Table 1.

The GEUS in-house standard “Disko-1 basalt” was given a regular sample number and sent with each batch analysed at ACMELabs (21 runs over 3 year). The reported rare earth element (REE) contents for this standard were compared with data from GEUS’ ICP-MS lab (32 runs over 8 years). The results from the two laboratories agree well and are within analytical uncertainty (Supplementary Table 2).

The raw data were treated by converting Cr_2O_3 in wt.% to Cr in ppm and then recalculating the remaining major elements on a volatile-free basis. Fe_2O_3 in the following refers to total Fe, because Fe^{2+} was not determined. The Mg-number was calculated as the molecular ratio of $\text{Mg}/(\text{Mg}+0.9\text{xFe})$. Additionally, the MFW weathering indexes were calculated (Ohta and Arai, 2007) and Nb/Nb^* was calculated as $\text{Nb}/\text{Nb}^* = \text{Nb}_\text{N}/(\text{Th}_\text{N}\text{xLa}_\text{N})^{0.5}$ (Eisele et al., 2002). The REE diagrams were normalised to the chondrite-values of Boynton (1984) and in the text the normalised values are given the subscript ‘CN’. The primitive-mantle-values of Sun and McDonough (1989) were used to normalise multi-element diagrams and the normalised values are given the subscript ‘N’ in the text. Only relatively immobile elements have been included in the multi-element diagrams (Fig. 4). The freeware GCDkit (Janoušek et al., 2006) was used to make all the geochemical diagrams.

Sm-Nd and Lu-Hf

Isotope dilution techniques were applied to measure the ^{176}Lu - ^{176}Hf compositions for 17 samples and ^{147}Sm - ^{143}Nd compositions for 15 samples from the Ravns Storø and the Bjørnesund supracrustal belts. Isotope compositions and Lu, Hf, Sm, Nd concentrations of the representative samples were measured employing mixed ^{176}Lu - ^{180}Hf and ^{149}Sm - ^{150}Nd tracers following the protocols of Münker et al. (2001) and Weyer et al. (2002), including the separation of Lu and Hf using Ln spec resin. Sm and Nd were separated from the remaining matrix following the method of Pin and Zaldegui (1997).

Complete digestion of the samples was achieved by table-top digestion, followed by Parr® bomb digestion for three days. Lu, Hf, Sm and Nd were measured using the Finnigan® Neptune multicollector ICP-MS at the University of Bonn, Germany. Measured $^{176}\text{Hf}/^{177}\text{Hf}$ were mass-bias corrected to a $^{179}\text{Hf}/^{177}\text{Hf}$ of 0.7325. The Münster AMES standard, isotopically indistinguishable from the JMC-475 standard, yielded an average $^{176}\text{Hf}/^{177}\text{Hf}$ of 0.282160 with an external reproducibility of ± 40 ppm (2σ). Reported data are given relative to a JMC-475 value of 0.282160. The typical external reproducibility of the $^{176}\text{Lu}/^{177}\text{Hf}$ is reported in Table 2 and it is $\pm 0.2\%$ for ideally spiked samples and includes the effects of error magnification due to non-ideal spike-sample ratios and uncertainties imparted by corrections for Yb interferences (Blichert-Toft et al., 2002; Lagos et al., 2007; Vervoort et al., 2004). The calculated initial Hf isotope compositions include both the propagated external errors from the measured Hf isotope compositions and from the Lu/Hf ratios. For the calculation of initial ϵHf and ϵNd values, we used the ^{176}Lu decay constant of 1.867×10^{-11} (Scherer et al., 2001; Söderlund et al., 2004), a ^{147}Sm decay constant of 6.54×10^{-12} (Lugmair and Marti, 1978) and the CHUR values of Bouvier et al. (2008). All measured $^{143}\text{Nd}/^{144}\text{Nd}$ data were mass-bias corrected using a value of 0.7219 for $^{146}\text{Nd}/^{144}\text{Nd}$. During the course of this study the $^{143}\text{Nd}/^{144}\text{Nd}$ values measured for a 20 ppb LaJolla standard solution

were 0.511818 and 0.511791, and all data reported here are given relative to a $^{143}\text{Nd}/^{144}\text{Nd}$ of 0.511859 for LaJolla. The external reproducibility for $^{143}\text{Nd}/^{144}\text{Nd}$ measurements was ± 30 ppm and $\pm 0.2\%$ for $^{147}\text{Sm}/^{144}\text{Nd}$. Total procedural blanks during the course of this study were <49 pg for Lu, <70 pg for Hf, and <50 pg for Sm and Nd.

Zircon U-Pb analyses

Zircon analyses were conducted at the Department of Petrology and Economic Geology, Geological Survey of Denmark and Greenland (GEUS). Hand-hammered chips from the rock samples were crushed directly in a tungsten-carbide disc mill. The crushed material was poured onto a Wilfrey shaking table where the heavy mineral grains were separated. The heavy mineral fraction was transferred to disposable plastic Petri dishes using ethanol, and magnetic minerals were removed using a hand magnet. Zircon grains were subsequently hand-picked from the final heavy mineral concentrate in the Petri dish. The hand-picked zircon grains were cast into epoxy and polished to expose a central cross-section of each grain. The mount was documented prior to ablation using backscattered electron imaging in a scanning electron microscope. The mount was subsequently cleaned in an ultrasonic bath with propanol, and then loaded into the sample cell of the laser ablation system for age dating.

Zircon ages were obtained using a Laser-Ablation Sector Field Inductively Coupled Plasma Mass Spectrometer (LA-SF-ICP-MS). The laser ablation unit uses a focused laser beam to ablate a small amount of a sample contained in an air-tight sample cell. Detailed analytical protocols were described by Frei and Gerdes (2009) and Gerdes and Zeh (2006), but a brief summary is given here.

Samples and standards were mounted in a low-volume ablation cell specially developed for U-Pb dating (Horstwood et al., 2003). Helium was used to flush the sample cell and was mixed downstream with the Ar sample gas of the mass spectrometer. A NewWave Research®/Merchantek® UP213 laser ablation unit was used, which emits a beam wavelength of 213 nm at a 10 Hz repetition rate. For the spot diameter (30 μm) and ablation times (30s) used in this study, the ablated mass of zircon was typically between 150-200 ng. The ablated material was transferred to the mass spectrometer in an Ar-He carrier gas via Tygon® tubing into an Element2 (ThermoFinnigan®, Bremen) single-collector double focusing magnetic sector ICP-MS. The total acquisition time for each analysis was 60 seconds of which the first 30 seconds were used to determine the gas blank. The instrument was tuned to give large, stable signals for the ^{206}Pb and ^{238}U peaks, low background count rates (typically around 150 counts per second for ^{207}Pb) and low oxide production rates ($^{238}\text{U}^{16}\text{O}/^{238}\text{U}$ generally below 2.5 %). ^{202}Hg , $^{204}(\text{Pb} + \text{Hg})$, ^{206}Pb , ^{207}Pb , ^{208}Pb , ^{232}Th and ^{238}U intensities were determined through peak jumping using electrostatic scanning in low resolution mode and with the magnet resting at ^{202}Hg . Each peak was determined at four slightly different masses and integrated sampling and a settling time of 1 ms for each isotope. Mass ^{202}Hg was measured to monitor the ^{204}Hg interference on ^{204}Pb where the $^{202}\text{Hg}/^{204}\text{Hg} \approx 4.36$, which can be used to correct significant common Pb contributions using the model by Stacey and Kramers (1975). $^{207}\text{Pb}/^{235}\text{U}$ was calculated from the $^{207}\text{Pb}/^{206}\text{Pb}$ and $^{206}\text{Pb}/^{238}\text{U}$ assuming $^{238}\text{U}/^{235}\text{U} \equiv 137.88$. The elemental fractionation induced by the laser ablation and the instrumental mass bias on measured isotopic ratios were corrected through standard-sample bracketing using the GJ-1 zircon (Jackson et al., 2004). Samples were analyzed in sequences where three standards bracket each set of ten samples. The Plesovice zircon standard (Aftalion et al., 1989) was used as an external reproducibility check, and yielded long-term 2σ RSD precisions ($n=109$) of 2%, 2.3% and 1.1% for the $^{206}\text{Pb}/^{238}\text{U}$, $^{207}\text{Pb}/^{235}\text{U}$ and $^{207}\text{Pb}/^{206}\text{Pb}$ ratios respectively (Frei et al., 2006). The raw data were corrected for instrumental mass bias and laser-induced U-Pb fractionation through normalization to the GJ-1 zircon using in-house data reduction software. All isotope data were plotted and evaluated using ISOPLOT/EX 3.71 (Ludwig, 2003). Model age calculation and error propagation follow Sambridge and Lambert (1997).

The reported ‘unmixed’ ages and the probability diagrams (PDD) are based on data after filtering out samples that are more than 10% discordant, whereas the concordia diagrams show all the data. All reported ages are $^{207}\text{Pb}/^{206}\text{Pb}$ ages as these are considered to be more robust ages as compared to $^{238}\text{U}/^{206}\text{Pb}$ based ages that may be more susceptible to post-formation alteration and weathering processes. The ‘unmixed’ ages are calculated by Isoplot/EX 3.71 after the number of components was estimated by the user and the simplest model that yielded the geologically meaningful ages was chosen.

References for Appendix A

- Aftalion, M., Bowes, D.R., Vřana, S., 1989. Early Carboniferous U–Pb zircon ages for garnetiferous potassic granulites, Blanský les massif, Czechoslovakia. *Neues Jahrbuch für Mineralogie, Monatshefte* 4, 145–152.
- Blichert-Toft J., Boyet M., Télouk P., Albarède F., 2002. Sm-147-Nd-143 and Lu-176-Hf-176 in eucrites and the differentiation of the HED parent body. *Earth and Planetary Science Letters* 204, 167–181.
- Bouvier A., Vervoort J.D., Patchett P.J., 2008. The Lu–Hf and Sm–Nd isotopic composition of CHUR: Constraints from unequilibrated chondrites and implications for the bulk composition of terrestrial planets. *Earth and Planetary Science Letters* 273, 48–57.
- Boynton, W.V., 1984. Cosmochemistry of the rare earth elements: meteorite studies. In: Henderson, P. (ed.), *Rare Earth Element Geochemistry*, Elsevier, Amsterdam (1984), 63–114.
- Eisele, J., Sharma, M., Galer, S.J.G., Blichert-Toft, J., Devey, C.W., Hofmann, A.W., 2002 The role of sediment recycling in EM-1 inferred from Os, Pb, Hf, Nb, Sr isotope and trace element systematics of the Pitcairn hotspot. *Earth and Planetary Science Letters* 196, 197–212.

- Frei D., Hollis J.A., Gerdes A., Harlov D., Karlsson C., Vasquez P., Franz G., Johansson L., Knudsen C., 2006. Advanced in-situ trace element and geochronological microanalysis of geomaterials by laser ablation techniques. *Geological Survey of Denmark and Greenland Bulletin* 10, 25-28.
- Frei, D., Gerdes, A., 2009. Precise and accurate in situ U–Pb dating of zircon with high sample throughput by automated LA-SF-ICP-MS. *Chemical Geology* 261, 261-270.
- Gerdes, A., Zeh, A., 2006. Combined U-Pb and Hf isotope LA-(MC)-ICP-MS analyses of detrital zircons: Comparison with SHRIMP and new constraints for the provenance and age of an Armorican metasediment in Central Germany. *Earth and Planetary Science Letters* 249, 47-61.
- Horstwood, M.S.A., Foster, G.L., Parrish, R.R., Noble, S.R., Nowell, G.M., 2003. Common-Pb corrected in situ U–Pb accessory mineral geochronology by LA-MC-ICP-MS. *Journal of Analytical Atomic Spectrometry* 18, 837-846.
- Jackson, S., Pearson, N.J., Griffin, W.L., Belousova, E.A., 2004. The application of laser ablation - inductively coupled plasma - mass spectrometry to in situ U-Pb zircon geochronology. *Chemical Geology* 211, 47-69.
- Janoušek, V., Farrow, C. M., Erban, V., 2006. Interpretation of whole-rock geochemical data in igneous geochemistry: introducing geochemical data toolkit (GCDkit). *Journal of Petrology* 47, 1255-1259.
- Lagos M., Scherer E.E., Tomaschek F., Münker C., Keiter M., Berndt J., Ballhaus C., 2007. High precision Lu–Hf geochronology of Eocene eclogite-facies rocks from Syros, Cyclades, Greece. *Chemical Geology* 243, 16-35.
- Ludwig, K.R., 2003. Isoplot/Ex 3.00. A geochronological toolkit for Microsoft Excel. Special Publication 4. Berkeley Geochronological Center, Berkeley, CA.
- Lugmair G.W., Marti K., 1978. Lunar initial $^{143}\text{Nd}/^{144}\text{Nd}$: differential evolution of the lunar crust and mantle. *Earth and Planetary Science Letters* 39, 349-357.
- Münker C., Weyer S., Scherer E., Mezger K., 2001. Separation of high field strength elements (Nb, Ta, Zr, Hf) and Lu from rock samples for MC-ICPMS measurements. *Geochemistry Geophysics Geosystems* (G3) 2, DOI: 10.1029/2001GC000183.
- Ohta, T., Arai, H., 2007. Stastical empirical index of chemical weathering in igneous rocks: A new tool for evaluating the degree of weathering. *Chemical Geology* 240, 280-297.
- Pin C., Zaldugui J.F.S., 1997. Sequential separation of light rare-earth elements, thorium and uranium by miniaturized extraction chromatography: Application to isotopic analyzes of silicate rocks. *Analytica Chimica Acta* 339, 79-89.
- Sambridge, M., Lambert, D.D., 1997. Propagating errors in decay equations: Examples from the Re-Os isotopic system. *Geochimica et Cosmochimica Acta*, 61, 3019-3024.
- Scherer E., Münker C., Mezger K., 2001. Calibration of the lutetium-hafnium clock. *Science* 293, 683-687.
- Söderlund U., Patchett P.J., Vervoort J.D., Isachsen C.E., 2004. The ^{176}Lu decay constant determined by Lu-Hf and U-Pb isotope systematics of Precambrian mafic intrusions. *Earth and Planetary Science Letters* 219, 311-324.
- Stacey, J.S., Kramers, J.D., 1975. Approximation of terrestrial lead isotope evolution by a two-stage model. *Earth and Planetary Science Letters* 26, 207-221.
- Sun, S., McDonough, W.F., 1989. Chemical and isotopic systematics of oceanic basalts: implications for mantle composition and processes. In: Saunders, A.D., Norry, M.J. (eds.) *Magmatism in the Ocean Basins*. Geological Society of London, Special Publications 42, 313-345.
- Vervoort J.D., Patchett P.J., Söderlund U., Baker M., 2004. Isotopic composition of Yb and the determination of Lu concentrations and Lu/Hf ratios by isotope dilution using MC-ICPMS. *Geochemistry Geophysics Geosystems* (G3) 5, Q11002, DOI: 10.1029/2004GC000721.
- Weyer, S., Münker C., Rehkämper M., Mezger K., 2002. Determination of ultra-low Nb, Ta, Zr and Hf concentrations and the chondritic Zr/Hf and Nb/Ta ratios by isotope dilution analyses with multiple collector ICP-MS. *Chemical Geology* 187, 295-313.

Supplementary data table 1 (Paper II): Major and trace element data

Sample	Lithology	Locality	Longitude	Latitude
468758	Amphibolite Dyke	Ravns Storø	62.72501000	-50.14944333
468759	Aplite	Ravns Storø	62.72216874	-50.15437855
468761	Aplite	Ravns Storø	62.72103000	-50.15605000
468763	Tuff	Ravns Storø	62.72053500	-50.15735833
468764	Ultramafic	Ravns Storø	62.72923333	-50.14598667
468765	Ultramafic	Ravns Storø	62.72923333	-50.14598667
468767	Aplite	Ravns Storø	62.73601833	-50.14935500
468769	Amphibolite Dyke	Ravns Storø	62.73601833	-50.14935500
468770	Aplite	Ravns Storø	62.73601833	-50.14935500
468771	Aplite	Ravns Storø	62.73601833	-50.14935500
468774	Amphibolite	Ravns Storø	62.71703500	-50.18660333
468775	Amphibolite	Ravns Storø	62.71692333	-50.18628667
468777	Amphibolite	Ravns Storø	62.71684000	-50.18552167
468778	Amphibolite Dyke	Ravns Storø	62.71691333	-50.18479333
468779	Amphibolite Dyke	Ravns Storø	62.71691333	-50.18479333
468780	Leucoamphibolite	Ravns Storø	62.71668500	-50.18342667
468781	Gabbro	Ravns Storø	62.71675833	-50.18247500
468783	Gabbro	Ravns Storø	62.71737833	-50.17938000
468784	Gabbro	Ravns Storø	62.71737833	-50.17938000
468787	Aplite	Ravns Storø	62.71577167	-50.17662167
468788	Tuff	Ravns Storø	62.71510167	-50.17708333
468791	Pillow Lava	Ravns Storø	62.71376167	-50.17620667
468792	Pillow Lava	Ravns Storø	62.71362000	-50.17588667
468793	Aplite	Ravns Storø	62.71362000	-50.17588667
468794	Amphibolite	Ravns Storø	62.71301167	-50.17541500
468795	Amphibolite	Ravns Storø	62.71276907	-50.17472077
468796	Amphibolite	Ravns Storø	62.71281000	-50.17325667
468797	Leucoamphibolite	Ravns Storø	62.71300833	-50.17092333
468798	Leucoamphibolite	Ravns Storø	62.71241667	-50.17047000
508252	Leucoamphibolite	Perserajorsuaq	63.03789333	-49.50047167
508253	Amphibolite	Perserajorsuaq	63.03799500	-49.49949000
508254	Amphibolite	Perserajorsuaq	63.03799500	-49.49949000
508255	Aplite	Perserajorsuaq	63.03681667	-49.49863667
508256	Amphibolite	Perserajorsuaq	63.03681667	-49.49863667
508257	Amphibolite	Perserajorsuaq	63.03425167	-49.50263833
508258	Amphibolite	Perserajorsuaq	63.03425167	-49.50263833
508259	Amphibolite	Perserajorsuaq	63.03425167	-49.50263833
510802	Amphibolite	Bjørnesund	62.98622667	-49.55140167
510803	Aplite	Bjørnesund	62.98622667	-49.55140167
510804	Amphibolite Dyke	Bjørnesund	62.98622667	-49.55140167
510805	Leucoamphibolite	Bjørnesund	62.98622667	-49.55140167
510806	Leucoamphibolite	Bjørnesund	62.98622667	-49.55140167
510807	Aplite	Bjørnesund	62.98622667	-49.55140167
510808	Leucoamphibolite	Bjørnesund	62.98622667	-49.55140167
510809	Leucoamphibolite	Bjørnesund	62.98622667	-49.55140167
510810	Amphibolite	Bjørnesund	62.98622667	-49.55140167
510811	Amphibolite	Bjørnesund	62.98622667	-49.55140167
510812	Amphibolite	Bjørnesund	62.98622667	-49.55140167
510813	Leucoamphibolite	Bjørnesund	62.98622667	-49.55140167
510816	Leucoamphibolite	Bjørnesund	62.98622667	-49.55140167
510817	Leucoamphibolite	Bjørnesund	62.98622667	-49.55140167
510818	Amphibolite	Bjørnesund	62.98622667	-49.55140167

Sample	Lithology	Locality	Longitude	Latitude
510819	Leucoamphibolite	Bjørnesund	62.98622667	-49.55140167
510820	Leucoamphibolite	Bjørnesund	62.98622667	-49.55140167
510822	Leucoamphibolite	Bjørnesund	62.98622667	-49.55140167
510823	Amphibolite	Bjørnesund	62.98622667	-49.55140167
510824	Leucoamphibolite	Bjørnesund	62.98622667	-49.55140167
510825	Amphibolite	Bjørnesund	62.98622667	-49.55140167
510826	Aplite	Bjørnesund	62.98622667	-49.55140167
510827	Amphibolite	Bjørnesund	62.98622667	-49.55140167
510828	Leucoamphibolite	Bjørnesund	62.98622667	-49.55140167
510829	Leucoamphibolite	Bjørnesund	62.98622667	-49.55140167
510830	Leucoamphibolite	Bjørnesund	62.98622667	-49.55140167
510831	Leucoamphibolite	Bjørnesund	62.98622667	-49.55140167
510832	Leucoamphibolite	Bjørnesund	62.98622667	-49.55140167
510912	Aplite	Ravns Storø	62.66926167	-50.26473500
510913	Pillow Lava	Ravns Storø	62.66822333	-50.26444833
510915	Leucoamphibolite	Ravns Storø	62.65162167	-50.28159833
510917	Amphibolite	Ravns Storø	62.68072000	-50.20223667
510922	Amphibolite	Ravns Storø	62.68072000	-50.20223667
510924	Amphibolite	Ravns Storø	62.68072000	-50.20223667
510928	Amphibolite	Ravns Storø	62.68072000	-50.20223667
510929	Amphibolite	Ravns Storø	62.68072000	-50.20223667
510931	Pillow Lava	Ravns Storø	62.72498000	-50.14934833
510932	Pillow Lava	Ravns Storø	62.72498000	-50.14934833
510933	Pillow Lava	Ravns Storø	62.72498000	-50.14934833
510934	Leucoamphibolite	Ravns Storø	62.72498000	-50.14934833
510935	Leucoamphibolite	Ravns Storø	62.72498000	-50.14934833
510936	Pillow Lava	Ravns Storø	62.72498000	-50.14934833
510937	Pillow Lava	Ravns Storø	62.72498000	-50.14934833
510938	Amphibolite	Ravns Storø	62.72498000	-50.14934833
510939	Amphibolite	Ravns Storø	62.72498000	-50.14934833
510940	Leucoamphibolite	Ravns Storø	62.72498000	-50.14934833
510941	Aplite	Ravns Storø	62.72407833	-50.15079000
510942	Amphibolite Dyke	Ravns Storø	62.73572333	-50.14905500
510943	Aplite	Ravns Storø	62.74703167	-50.14311000
510944	Amphibolite	Ravns Storø	62.71183500	-50.16929000
511152	Amphibolite	Perserajorsuaq	63.03157667	-49.49298167
511155	Amphibolite	Perserajorsuaq	63.03088167	-49.49346000
511156	Aplite	Perserajorsuaq	63.03090333	-49.49375500
511157	Leucoamphibolite	Perserajorsuaq	63.03090333	-49.49375500
511158	Amphibolite	Perserajorsuaq	63.03090333	-49.49375500
511159	Leucoamphibolite	Perserajorsuaq	63.03090333	-49.49375500
511160	Leucoamphibolite	Perserajorsuaq	63.03090333	-49.49375500
511162	Leucoamphibolite	Perserajorsuaq	63.03090333	-49.49375500
511163	Amphibolite	Perserajorsuaq	63.03090333	-49.49375500
511164	Leucoamphibolite	Perserajorsuaq	63.03090333	-49.49375500
511165	Leucoamphibolite	Perserajorsuaq	63.03090333	-49.49375500
511166	Amphibolite	Perserajorsuaq	63.03063667	-49.49431667
511169	Leucoamphibolite	Perserajorsuaq	63.03063667	-49.49431667
511172	Amphibolite	Bjørnesund	62.98779667	-49.56053333
511173	Anorthosite	Bjørnesund	62.98852167	-49.56208833
511174	Leucoamphibolite	Bjørnesund	62.98925167	-49.56386833
511175	Amphibolite	Bjørnesund	62.98927500	-49.56613000
511176	Amphibolite	Bjørnesund	62.98937167	-49.56586500
511180	Amphibolite	Bjørnesund	62.98770167	-49.56042667

Sample	Lithology	Locality	Longitude	Latitude
511181	Amphibolite	Bjørnesund	62.98750333	-49.55983167
511182	Amphibolite	Bjørnesund	62.98750333	-49.55983167
511183	Amphibolite	Bjørnesund	62.98709167	-49.55311833
511184	Amphibolite	Bjørnesund	62.98709167	-49.55311833
511185	Amphibolite	Bjørnesund	62.98709167	-49.55311833
511186	Leucoamphibolite	Bjørnesund	62.98864833	-49.54141333
511188	Leucoamphibolite	Bjørnesund	62.98849167	-49.54215000
511189	Leucoamphibolite	Bjørnesund	62.98817833	-49.54316667
511190	Leucoamphibolite	Bjørnesund	62.98771333	-49.54679500
511192	Leucoamphibolite	Bjørnesund	62.98758500	-49.54691167
511193	Leucoamphibolite	Bjørnesund	62.98758500	-49.54691167
511194	Leucoamphibolite	Bjørnesund	62.98754833	-49.54681333
512148	Amphibolite	Bjørnesund	62.98387833	-49.53734833
512149	Amphibolite	Bjørnesund	62.98361000	-49.53997500
512150	Amphibolite	Bjørnesund	62.98361000	-49.53997500
512151	Leucoamphibolite	Bjørnesund	62.98423667	-49.54071000
515802	Gabbro	Ravns Storø	62.71049667	-50.16856833
515803	Gabbro	Ravns Storø	62.70985000	-50.16804333
515804	Pillow Lava	Ravns Storø	62.70864333	-50.16657833
515806	Pillow Lava	Ravns Storø	62.66828000	-50.26430667
515808	Amphibolite Dyke	Ravns Storø	62.66828000	-50.26430667
515809	Tuff	Ravns Storø	62.66396833	-50.26837000
515810	Amphibolite Dyke	Ravns Storø	62.66349000	-50.27332167
515811	Amphibolite Dyke	Ravns Storø	62.66349000	-50.27332167
515813	Amphibolite Dyke	Ravns Storø	62.66349000	-50.27332167
515814	Amphibolite Dyke	Ravns Storø	62.66349000	-50.27332167
515815	Amphibolite Dyke	Ravns Storø	62.66308667	-50.27212667
515816	Tuff	Ravns Storø	62.66308667	-50.27212667
515817	Amphibolite Dyke	Ravns Storø	62.66245500	-50.27391333
515818	Amphibolite Dyke	Ravns Storø	62.66245500	-50.27391333
515819	Amphibolite Dyke	Ravns Storø	62.66215167	-50.27475667
515820	Aplite	Ravns Storø	62.65992833	-50.28880000
515824	Ultramafic	Ravns Storø	62.65552167	-50.28886167
515825	Tuff	Ravns Storø	62.65155500	-50.28150833
515826	Amphibolite Dyke	Ravns Storø	62.65155500	-50.28150833
5108211	Leucoamphibolite	Bjørnesund	62.98622667	-49.55140167
5108212	Leucoamphibolite	Bjørnesund	62.98622667	-49.55140167
5109131	Pillow Lava	Ravns Storø	62.66822333	-50.26444833
5109132	Pillow Lava	Ravns Storø	62.66822333	-50.26444833
5109141	Tuff	Ravns Storø	62.65162167	-50.28159833
5109142	Tuff	Ravns Storø	62.65162167	-50.28159833
5158071	Pillow Lava	Ravns Storø	62.66828000	-50.26430667
5158072	Pillow Lava	Ravns Storø	62.66828000	-50.26430667

Sample	SiO ₂	Al ₂ O ₃	Fe ₂ O ₃ *	MgO	CaO	Na ₂ O	K ₂ O	TiO ₂
Unit	%	%	%	%	%	%	%	%
MDL	0.01	0.01	0.04	0.01	0.01	0.01	0.01	0.01
468758	52.84	16.16	10.43	5.97	9.24	2.80	0.09	1.02
468759	69.43	15.66	3.42	1.07	2.93	4.32	1.51	0.38
468761	63.50	16.39	5.56	2.62	4.47	4.20	1.48	0.55
468763	55.79	15.59	5.96	2.12	11.65	2.40	0.69	0.55
468764	37.23	3.71	12.27	31.01	4.05	0.01	<0.01	0.21
468765	29.25	17.36	11.81	28.00	0.22	<0.01	<0.01	1.06
468767	74.40	14.00	2.19	0.29	2.73	4.92	0.60	0.11
468769	59.01	16.78	7.62	3.24	7.06	4.42	0.08	0.84
468770	75.06	13.92	1.77	0.39	2.74	4.65	0.44	0.08
468771	75.47	13.72	2.02	0.28	2.37	4.41	1.21	0.07
468774	46.32	16.45	13.60	7.22	10.78	2.71	0.63	0.78
468775	46.60	17.22	10.65	9.14	12.66	1.60	0.14	0.50
468777	48.28	14.40	14.93	5.98	9.76	2.89	0.33	2.14
468778	56.04	17.18	7.81	4.31	8.08	3.98	0.12	0.76
468779	49.11	11.73	19.53	5.51	9.25	1.55	0.27	1.99
468780	58.72	15.71	7.83	4.43	7.41	3.31	0.75	0.80
468781	45.62	15.53	15.73	8.77	10.14	1.91	0.22	0.86
468783	47.03	23.96	7.52	4.80	12.58	2.71	0.05	0.40
468784	48.54	17.00	11.01	7.46	12.33	1.77	0.09	0.59
468787	71.20	15.14	3.00	0.78	3.33	4.67	0.55	0.24
468788	50.71	17.85	9.12	3.42	12.68	2.35	0.31	1.19
468791	53.77	19.09	5.56	0.95	15.13	1.84	0.03	0.74
468792	48.31	17.41	12.72	6.06	10.33	2.69	0.11	0.92
468793	71.20	15.63	2.35	0.75	3.19	4.67	0.92	0.28
468794	49.71	15.34	9.07	10.06	12.16	1.47	<0.01	0.46
468795	45.91	13.91	12.06	14.19	9.05	1.38	0.03	0.65
468796	44.62	11.87	12.74	16.77	8.47	0.93	0.09	0.66
468797	61.43	13.96	8.28	2.69	6.66	2.53	0.64	0.86
468798	56.14	15.70	10.58	3.92	6.39	4.33	0.20	1.25
508252	59.93	16.81	6.84	3.44	5.93	4.89	0.35	0.73
508253	47.16	16.18	13.27	4.69	13.96	1.69	0.54	0.79
508254	47.17	15.18	14.13	6.11	12.55	2.28	0.19	1.10
508255	64.00	15.86	5.52	2.55	5.05	3.62	0.81	0.58
508256	46.71	15.16	14.61	7.19	10.56	2.21	0.58	1.39
508257	47.46	15.91	13.59	6.06	11.45	1.91	0.51	1.28
508258	48.05	16.82	12.91	4.22	12.53	1.88	0.20	1.40
508259	47.33	15.86	12.20	5.77	14.15	1.58	0.24	0.97
510802	47.31	15.29	14.02	9.29	9.24	2.39	0.15	0.85
510803	65.55	15.95	4.34	1.36	4.00	4.54	1.51	0.47
510804	49.43	14.69	10.46	7.55	8.49	2.90	2.27	1.13
510805	50.22	15.51	9.73	5.62	12.23	2.09	0.56	1.10
510806	50.56	14.92	9.32	4.46	14.03	2.87	0.53	1.17
510807	74.52	13.55	1.80	0.32	2.53	3.61	2.56	0.13
510808	53.46	14.49	7.54	3.18	14.71	2.27	0.16	1.17
510809	51.13	15.08	10.22	6.79	10.42	2.85	0.50	1.27
510810	47.61	15.16	13.71	6.56	11.99	2.21	0.48	0.80
510811	47.65	15.15	14.74	7.16	10.35	2.67	0.16	0.96
510812	46.38	15.04	15.55	7.36	10.43	2.24	0.93	0.98
510813	41.35	13.78	7.91	2.73	22.01	2.03	0.28	1.31
510816	47.69	15.81	8.51	3.27	15.75	3.02	0.53	1.69
510817	46.47	14.32	6.88	2.69	18.58	2.31	0.64	1.36
510818	47.17	13.29	18.36	5.62	9.76	2.58	0.51	1.50

Sample	SiO ₂	Al ₂ O ₃	Fe ₂ O ₃ *	MgO	CaO	Na ₂ O	K ₂ O	TiO ₂
Unit	%	%	%	%	%	%	%	%
MDL	0.01	0.01	0.04	0.01	0.01	0.01	0.01	0.01
510819	51.86	15.57	8.58	4.30	10.64	4.02	0.69	1.57
510820	42.34	12.94	8.55	3.68	22.43	1.68	0.12	1.32
510822	50.58	16.11	7.97	3.16	14.68	3.17	0.23	1.69
510823	47.79	14.84	14.00	6.74	11.67	2.44	0.46	0.82
510824	51.18	16.12	9.57	4.18	11.30	3.74	0.44	1.23
510825	47.07	14.95	15.34	6.94	11.28	1.57	0.48	0.98
510826	68.54	15.61	3.50	0.95	3.58	4.26	1.58	0.38
510827	47.13	15.04	15.63	7.16	10.64	2.18	0.11	1.00
510828	48.20	15.86	7.30	2.59	16.09	3.22	0.59	1.57
510829	47.91	14.56	8.80	3.57	16.21	3.06	0.45	1.53
510830	49.44	15.60	9.34	3.74	12.54	3.22	1.24	1.69
510831	49.83	14.82	8.20	3.10	15.65	3.08	0.35	1.53
510832	48.93	14.18	8.46	3.36	16.04	3.01	0.59	1.48
510912	72.43	15.09	2.53	0.49	2.69	5.47	0.54	0.21
510913	50.54	15.00	9.05	7.04	13.45	2.58	0.29	0.75
510915	55.90	16.43	8.48	5.11	8.48	2.85	0.88	0.74
510917	44.14	13.12	21.26	6.00	9.73	2.66	0.17	2.12
510922	51.24	12.36	18.17	4.31	8.97	2.24	0.19	1.70
510924	48.58	15.40	11.96	8.42	10.84	2.60	0.12	1.03
510928	47.71	12.90	12.54	14.04	9.44	1.48	0.11	0.65
510929	53.34	14.48	10.66	8.33	10.34	1.00	0.12	0.74
510931	56.79	17.43	5.82	1.66	14.59	0.88	0.06	0.75
510932	54.17	17.18	8.86	5.26	8.75	3.65	0.13	0.79
510933	60.04	14.00	4.27	0.92	15.33	0.43	0.04	0.62
510934	54.06	16.71	4.93	1.76	18.63	0.05	0.03	0.60
510935	56.73	16.49	8.63	4.70	8.29	3.27	0.19	0.73
510936	55.07	18.06	8.12	3.08	10.66	2.25	0.53	0.82
510937	53.36	16.89	10.39	4.85	10.19	2.24	0.26	0.84
510938	49.73	15.14	11.76	8.47	9.86	2.01	0.11	0.77
510939	46.27	11.17	12.57	16.25	9.67	0.97	0.07	0.58
510940	53.58	16.39	10.16	5.69	9.78	2.46	0.16	1.03
510941	71.23	15.11	2.69	0.62	2.54	3.68	2.02	0.29
510942	48.00	14.23	17.42	5.65	9.77	2.09	0.27	1.39
510943	67.19	16.07	4.20	1.46	4.03	4.08	1.58	0.43
510944	47.78	14.65	14.95	7.83	9.56	2.49	0.18	1.30
511152	47.32	15.39	11.54	8.48	11.75	2.05	0.52	0.64
511155	50.64	13.57	15.24	5.67	8.05	2.66	0.23	1.64
511156	65.89	15.70	4.69	2.11	3.64	4.00	1.76	0.50
511157	58.09	15.95	8.20	3.40	6.55	3.88	1.29	0.82
511158	47.77	14.41	13.40	7.49	9.36	2.77	0.85	1.05
511159	64.41	15.07	5.46	2.44	5.05	3.64	1.20	0.63
511160	62.62	15.81	5.75	2.70	5.13	3.79	1.49	0.61
511162	57.44	15.83	8.67	3.44	7.36	3.22	1.15	0.91
511163	51.02	12.27	18.94	3.58	8.07	1.98	0.58	1.97
511164	56.79	15.24	8.52	4.66	6.44	3.97	1.22	0.81
511165	60.78	16.33	6.21	2.80	4.97	4.31	1.37	0.77
511166	50.21	13.03	16.20	5.45	8.86	2.75	0.40	1.67
511169	64.59	15.52	5.44	2.65	4.83	3.84	1.09	0.56
511172	46.41	13.86	12.67	4.35	18.70	1.38	0.19	0.84
511173	46.42	31.15	0.88	0.49	15.66	2.18	0.10	0.10
511174	58.07	16.23	7.10	4.43	6.63	3.69	0.52	0.61
511175	48.23	14.99	15.19	6.79	9.54	2.85	0.30	1.18

Sample	SiO ₂	Al ₂ O ₃	Fe ₂ O ₃ *	MgO	CaO	Na ₂ O	K ₂ O	TiO ₂
Unit	%	%	%	%	%	%	%	%
MDL	0.01	0.01	0.04	0.01	0.01	0.01	0.01	0.01
511176	50.05	14.71	15.59	5.18	9.03	2.48	0.52	1.39
511180	48.03	15.17	14.24	7.68	10.27	1.82	0.12	0.93
511181	47.68	15.32	14.75	7.47	10.68	1.90	0.15	0.94
511182	46.60	13.33	11.23	4.56	20.54	0.96	0.05	0.85
511183	47.15	12.99	19.48	7.67	8.53	1.85	0.30	1.40
511184	51.85	14.92	12.34	6.31	10.69	1.64	0.08	0.80
511185	48.90	15.37	12.80	8.80	9.64	2.47	0.30	0.69
511186	59.18	15.71	6.12	3.43	4.87	4.54	0.92	0.59
511188	53.24	16.00	9.74	5.29	9.22	3.04	0.39	0.89
511189	51.35	15.98	8.98	4.63	12.24	2.89	0.78	0.86
511190	56.13	15.11	9.06	5.08	8.86	2.70	0.38	0.89
511192	52.98	16.01	9.99	5.38	8.85	3.61	0.34	0.98
511193	53.35	18.53	8.33	3.72	9.39	3.40	0.19	1.10
511194	49.65	14.26	11.73	9.07	9.26	2.81	0.22	0.94
512148	46.85	13.76	18.95	7.40	8.65	1.82	0.30	1.27
512149	46.37	14.86	18.59	5.25	9.72	2.31	0.27	1.57
512150	46.40	16.18	16.77	6.61	9.30	2.72	0.27	1.15
512151	55.20	15.64	9.86	4.22	6.93	4.07	0.84	1.32
515802	49.20	18.54	8.26	7.20	13.00	1.33	0.06	0.61
515803	50.81	15.05	10.80	7.82	10.21	2.51	0.13	1.02
515804	48.55	15.09	12.66	9.29	9.71	2.38	0.10	0.85
515806	50.02	14.17	7.50	4.38	19.23	0.95	0.09	0.70
515808	56.54	16.26	8.98	3.82	7.08	4.11	0.82	0.99
515809	52.79	15.08	10.28	6.71	9.59	2.55	0.46	0.81
515810	55.53	15.74	9.26	4.63	10.87	1.34	0.20	0.94
515811	55.84	15.06	10.09	2.95	10.75	1.65	0.22	1.81
515813	62.85	15.57	6.54	2.04	7.04	3.12	0.36	0.84
515814	57.29	16.03	8.72	4.04	8.03	3.40	0.22	1.00
515815	58.37	15.81	8.15	4.13	7.72	3.45	0.19	0.94
515816	56.83	16.46	7.86	4.61	6.97	3.46	0.97	0.67
515817	55.66	15.69	7.90	4.89	7.76	3.52	0.07	0.72
515818	53.68	15.35	9.42	4.43	13.21	0.64	0.17	0.94
515819	58.61	15.61	8.16	3.67	7.90	3.22	0.19	0.94
515820	70.80	15.92	2.18	0.68	2.85	5.35	1.03	0.25
515824	42.05	4.59	14.76	31.08	1.29	0.03	<0.01	0.29
515825	54.76	15.79	9.34	4.87	9.05	3.33	0.31	0.79
515826	52.54	14.61	10.69	4.91	11.78	2.11	0.08	1.33
5108211	49.70	14.85	7.57	2.45	17.49	1.85	0.12	1.53
5108212	45.71	15.96	12.48	5.45	13.29	2.68	0.27	1.82
5109131	54.76	14.23	5.05	2.39	18.24	0.87	0.04	0.64
5109132	54.72	16.02	8.60	5.54	9.46	3.41	0.44	0.80
5109141	52.41	15.37	6.47	3.49	15.23	1.86	0.17	0.82
5109142	54.80	16.66	9.63	5.22	6.00	3.75	1.71	0.79
5158071	52.32	15.68	5.98	2.57	17.23	1.31	0.04	0.64
5158072	48.03	17.04	9.27	5.99	10.09	3.00	0.90	0.91

Sample	P ₂ O ₅	MnO	Cr ₂ O ₃	LOI	Sum	Sc	Ba	Co
Unit	%	%	%	%	%	ppm	ppm	ppm
MDL	0.01	0.01	0.002	5.1	0.01	1	1	0.2
468758	0.20	0.13	0.015	0.9	99.79	25	23	47.9
468759	0.13	0.03	<0.002	1.0	99.89	5	312	18.1
468761	0.14	0.08	0.007	0.8	99.84	10	453	26.8
468763	0.14	0.14	0.009	4.8	99.86	12	253	16.4
468764	0.02	0.20	0.489	10.1	99.45	14	5	120.6
468765	0.16	0.05	0.020	11.5	99.47	25	<1	193.0
468767	0.07	0.04	<0.002	0.6	99.91	1	300	24.8
468769	0.25	0.11	0.004	0.4	99.82	13	89	39.6
468770	0.03	0.04	0.004	0.8	99.96	<1	325	2.5
468771	0.05	0.02	0.004	0.3	99.95	<1	373	1.4
468774	0.05	0.20	0.032	1.1	99.85	33	56	54.0
468775	0.06	0.17	0.066	0.9	99.76	37	34	63.2
468777	0.23	0.19	0.020	0.6	99.76	29	106	65.3
468778	0.10	0.12	0.004	1.3	99.83	18	71	48.5
468779	0.17	0.27	<0.002	0.4	99.78	47	41	67.1
468780	0.19	0.11	0.023	0.5	99.82	17	149	26.8
468781	0.05	0.21	0.028	0.7	99.79	32	39	68.0
468783	<0.01	0.11	0.016	0.7	99.85	21	35	29.1
468784	0.03	0.17	0.060	0.7	99.80	37	20	46.7
468787	0.08	0.04	0.002	0.8	99.85	4	808	4.7
468788	0.17	0.11	0.013	1.9	99.82	30	124	36.5
468791	0.11	0.09	0.029	2.5	99.89	28	33	47.1
468792	0.10	0.19	0.053	0.9	99.79	33	29	72.6
468793	0.10	0.03	<0.002	0.7	99.86	3	539	21.4
468794	0.01	0.15	0.122	1.2	99.78	40	11	40.9
468795	0.07	0.16	0.136	2.1	99.71	29	12	66.9
468796	0.09	0.18	0.169	3.0	99.66	25	3	77.2
468797	0.22	0.51	0.007	2.1	99.85	16	355	19.8
468798	0.27	0.11	0.004	0.9	99.81	23	186	29.6
508252	0.17	0.09	0.009	0.6	99.83	15	67	20.8
508253	0.06	0.26	0.023	1.2	99.80	37	52	51.0
508254	0.10	0.20	0.025	0.7	99.76	38	28	49.3
508255	0.13	0.07	0.006	1.6	99.79	13	254	16.5
508256	0.12	0.22	0.037	0.9	99.72	44	98	40.9
508257	0.15	0.20	0.037	1.2	99.76	37	102	44.4
508258	0.11	0.19	0.037	1.4	99.79	41	28	47.2
508259	0.07	0.23	0.045	1.3	99.78	38	40	52.2
510802	0.06	0.19	0.034	0.9	99.77	40	56	61.0
510803	0.18	0.06	0.003	1.9	99.87	6	291	11.8
510804	0.31	0.15	0.051	2.3	99.74	23	138	42.8
510805	0.29	0.18	0.031	2.2	99.79	23	93	40.5
510806	0.35	0.25	0.040	1.3	99.80	25	180	36.7
510807	0.05	0.03	<0.002	0.8	99.91	1	472	6.2
510808	0.39	0.16	0.041	2.2	99.80	22	52	39.4
510809	0.43	0.15	0.049	0.8	99.72	24	168	42.2
510810	0.05	0.20	0.021	1.0	99.79	39	45	61.1
510811	0.07	0.21	0.035	0.6	99.78	40	51	62.7
510812	0.07	0.23	0.035	0.5	99.77	40	84	61.9
510813	0.49	0.26	0.032	7.6	99.79	21	141	33.7
510816	0.60	0.21	0.041	2.7	99.81	25	81	45.6
510817	0.49	0.23	0.033	5.8	99.80	20	409	31.3
510818	0.10	0.23	0.013	0.6	99.75	45	29	61.5

Sample	P ₂ O ₅	MnO	Cr ₂ O ₃	LOI	Sum	Sc	Ba	Co
Unit	%	%	%	%	%	ppm	ppm	ppm
MDL	0.01	0.01	0.002	5.1	0.01	1	1	0.2
510819	0.56	0.18	0.038	1.7	99.77	24	290	41.7
510820	0.48	0.35	0.035	5.9	99.79	21	101	29.7
510822	0.64	0.18	0.043	1.3	99.76	26	60	44.1
510823	0.06	0.21	0.022	0.7	99.77	40	45	60.6
510824	0.33	0.20	0.057	1.4	99.79	26	142	45.2
510825	0.06	0.20	0.034	0.8	99.73	40	85	65.2
510826	0.12	0.03	<0.002	1.3	99.84	5	375	10.7
510827	0.07	0.22	0.035	0.5	99.74	40	44	60.1
510828	0.60	0.21	0.038	3.5	99.78	23	195	39.8
510829	0.53	0.24	0.038	2.9	99.77	23	129	45.9
510830	0.61	0.21	0.041	2.0	99.72	26	443	46.5
510831	0.58	0.22	0.037	2.4	99.79	23	38	41.1
510832	0.56	0.21	0.036	2.9	99.77	22	204	42.0
510912	0.07	0.04	<0.002	0.3	99.87	2	402	5.7
510913	0.33	0.16	0.047	0.5	99.73	30	78	41.8
510915	0.16	0.11	0.016	0.6	99.78	22	206	33.3
510917	0.07	0.19	<0.002	0.2	99.67	63	26	72.5
510922	0.15	0.24	<0.002	0.2	99.76	49	90	58.0
510924	0.10	0.13	0.049	0.5	99.75	36	26	48.9
510928	0.07	0.18	0.131	0.4	99.71	35	8	71.2
510929	0.08	0.16	0.061	0.4	99.77	35	11	49.3
510931	0.07	0.11	0.024	1.7	99.91	26	25	29.3
510932	0.09	0.12	0.033	0.8	99.86	27	26	39.3
510933	0.08	0.12	0.017	4.1	99.93	22	21	15.4
510934	0.08	0.16	0.026	2.9	99.93	21	13	19.5
510935	0.10	0.12	0.031	0.5	99.83	26	73	46.9
510936	0.09	0.11	0.031	1.0	99.80	30	365	51.5
510937	0.09	0.15	0.031	0.5	99.82	29	172	46.7
510938	0.06	0.17	0.053	1.6	99.78	43	33	57.2
510939	0.05	0.20	0.208	1.6	99.68	33	7	87.7
510940	0.19	0.13	0.017	0.2	99.80	27	27	39.0
510941	0.10	0.04	<0.002	1.6	99.87	3	650	7.8
510942	0.12	0.23	0.013	0.6	99.79	47	42	61.7
510943	0.14	0.07	0.003	0.6	99.87	8	370	12.9
510944	0.09	0.19	0.035	0.7	99.76	46	51	57.3
511152	0.03	0.18	0.033	1.8	99.75	36	55	53.7
511155	0.12	0.23	0.008	1.7	99.75	48	64	48.3
511156	0.12	0.08	0.004	1.3	99.81	9	484	13.6
511157	0.17	0.14	0.007	1.3	99.77	18	375	24.0
511158	0.07	0.21	0.030	2.3	99.71	38	186	53.5
511159	0.14	0.09	0.006	1.7	99.81	14	377	17.5
511160	0.14	0.09	0.007	1.7	99.81	13	387	18.4
511162	0.18	0.14	0.007	1.4	99.77	22	366	26.8
511163	0.18	0.26	<0.002	0.9	99.76	41	146	44.5
511164	0.17	0.14	0.019	1.8	99.78	22	360	29.1
511165	0.24	0.09	0.003	1.9	99.80	13	356	21.8
511166	0.13	0.26	0.008	0.8	99.76	49	78	51.7
511169	0.14	0.09	0.004	1.0	99.79	12	532	17.4
511172	0.06	0.32	0.032	1.0	99.80	36	28	59.3
511173	<0.01	0.02	0.065	2.9	99.97	3	17	6.9
511174	0.14	0.11	0.019	2.3	99.82	15	43	27.9
511175	0.09	0.18	0.018	0.4	99.78	40	34	54.8

Sample	P ₂ O ₅	MnO	Cr ₂ O ₃	LOI	Sum	Sc	Ba	Co
Unit	%	%	%	%	%	ppm	ppm	ppm
MDL	0.01	0.01	0.002	5.1	0.01	1	1	0.2
511176	0.09	0.21	0.014	0.5	99.76	41	67	55.5
511180	0.06	0.19	0.034	1.2	99.78	38	20	56.2
511181	0.06	0.18	0.035	0.6	99.77	39	33	58.2
511182	0.06	0.28	0.030	1.3	99.84	35	27	56.9
511183	0.12	0.24	0.005	0.0	99.74	38	24	88.9
511184	0.06	0.17	0.036	0.9	99.80	46	27	51.4
511185	0.04	0.18	0.042	0.5	99.78	35	23	67.3
511186	0.11	0.08	0.008	4.3	99.88	15	125	27.0
511188	0.13	0.13	0.027	1.7	99.82	23	157	41.2
511189	0.14	0.14	0.020	1.8	99.82	26	143	38.8
511190	0.15	0.12	0.023	1.3	99.82	26	100	35.5
511192	0.16	0.13	0.024	1.3	99.79	30	84	37.1
511193	0.20	0.08	0.012	1.5	99.82	23	43	33.8
511194	0.15	0.15	0.072	1.4	99.75	26	34	59.1
512148	0.11	0.23	0.005	0.4	99.76	33	28	65.2
512149	0.11	0.21	0.011	0.5	99.77	39	29	59.3
512150	0.08	0.18	0.004	0.1	99.77	30	54	70.7
512151	0.36	0.14	0.019	1.2	99.81	18	67	28.5
515802	0.05	0.15	0.071	1.3	99.80	29	27	34.4
515803	0.11	0.18	0.030	1.1	99.78	40	32	46.7
515804	0.07	0.17	0.047	0.8	99.76	42	31	48.5
515806	0.36	0.16	0.043	2.2	99.77	27	38	41.7
515808	0.26	0.11	0.007	0.8	99.80	17	343	29.7
515809	0.14	0.15	0.048	1.1	99.78	28	104	47.3
515810	0.19	0.12	0.008	1.0	99.80	23	31	53.0
515811	0.36	0.11	<0.002	1.0	99.83	20	39	30.0
515813	0.19	0.08	<0.002	1.2	99.88	12	125	13.6
515814	0.26	0.12	0.009	0.7	99.81	19	64	40.4
515815	0.23	0.11	0.009	0.7	99.80	17	54	42.1
515816	0.12	0.11	0.021	1.7	99.83	18	182	26.5
515817	0.18	0.12	0.030	3.3	99.81	19	41	28.6
515818	0.17	0.12	0.008	1.7	99.83	22	81	33.1
515819	0.23	0.11	0.008	1.2	99.84	17	33	26.1
515820	0.09	0.03	<0.002	0.7	99.90	3	172	23.4
515824	<0.01	0.20	0.595	4.3	99.41	16	3	138.8
515825	0.18	0.13	0.024	1.2	99.83	21	120	33.7
515826	0.47	0.11	0.021	1.1	99.74	21	37	58.7
5108211	0.57	0.17	0.037	3.4	99.80	23	20	43.3
5108212	0.64	0.23	0.045	1.1	99.72	27	49	52.0
5109131	0.27	0.09	0.038	3.2	99.78	26	33	20.3
5109132	0.21	0.16	0.037	0.4	99.80	27	130	37.9
5109141	0.27	0.14	0.013	3.6	99.82	15	53	28.3
5109142	0.18	0.13	0.023	0.8	99.75	22	464	36.7
5158071	0.28	0.11	0.040	3.6	99.82	25	38	21.0
5158072	0.36	0.14	0.052	3.9	99.72	36	338	42.7

Sample	Cs	Ga	Hf	Nb	Rb	Sr	Ta	Th
Unit	ppm	ppm	ppm	ppm	ppm	ppm	ppm	ppm
MDL	0.1	0.5	0.1	0.1	0.1	0.5	0.1	0.2
468758	<0.1	19.9	3.3	5.8	0.6	356.1	0.4	1.6
468759	0.6	18.6	4.3	5.7	58.4	160.3	0.5	2.9
468761	2.9	20.0	4.1	6.4	49.6	178.4	0.5	2.9
468763	1.0	18.2	3.8	5.7	22.7	345.5	0.4	2.8
468764	<0.1	4.9	0.4	0.8	0.2	50.7	<0.1	<0.2
468765	<0.1	18.4	3.1	4.9	<0.1	2.5	0.3	<0.2
468767	1.4	21.5	3.6	7.0	38.3	230.6	0.7	3.9
468769	<0.1	23.5	4.1	7.7	1.3	409.4	0.5	2.1
468770	0.6	15.4	2.3	4.3	17.0	236.4	0.4	4.0
468771	0.7	15.5	2.9	5.5	39.5	182.1	0.4	7.0
468774	0.2	17.0	1.2	2.3	5.1	162.8	0.2	0.2
468775	<0.1	15.4	0.9	1.0	1.6	107.7	<0.1	0.3
468777	<0.1	25.2	3.7	8.4	10.2	188.4	0.5	0.8
468778	<0.1	22.0	3.3	4.8	1.9	208.3	0.4	1.2
468779	<0.1	22.9	3.0	4.5	6.8	50.0	0.3	0.5
468780	0.3	18.0	2.8	5.5	17.6	465.6	0.3	1.8
468781	0.1	15.8	1.5	2.4	2.9	120.2	0.1	0.3
468783	<0.1	14.5	0.7	1.5	0.7	224.3	<0.1	0.2
468784	<0.1	14.2	0.9	0.6	0.6	163.8	<0.1	<0.2
468787	0.2	18.9	5.1	5.7	24.6	136.0	0.6	4.7
468788	<0.1	23.9	2.9	5.7	2.8	410.2	0.4	2.0
468791	<0.1	25.0	2.3	3.4	0.7	154.0	0.2	1.1
468792	<0.1	17.8	2.4	3.1	1.7	124.8	0.2	1.1
468793	0.5	22.2	4.6	5.9	39.4	252.8	0.6	4.2
468794	<0.1	11.9	1.0	2.2	0.1	88.7	<0.1	<0.2
468795	<0.1	11.0	1.1	1.8	0.6	113.4	<0.1	0.4
468796	<0.1	10.7	1.4	2.0	0.6	7.2	<0.1	0.4
468797	1.0	13.6	3.8	4.0	26.9	84.2	0.4	2.7
468798	0.7	16.9	4.2	6.7	10.2	119.2	0.5	3.1
508252	0.2	18.1	3.6	5.8	12.1	295.5	0.4	2.2
508253	0.2	15.7	1.5	1.9	31.5	212.6	0.1	0.4
508254	0.4	17.7	2.0	2.5	10.2	262.0	0.2	0.3
508255	1.4	18.7	2.9	4.7	19.5	383.4	0.4	4.6
508256	0.3	17.9	1.9	4.2	6.1	277.3	0.2	0.3
508257	0.3	18.4	2.3	3.7	15.8	204.9	0.3	1.0
508258	0.2	17.8	2.3	3.5	5.2	186.4	0.4	0.4
508259	0.2	16.7	1.7	2.5	6.3	172.9	0.2	0.2
510802	<0.1	15.3	1.3	1.9	3.2	83.8	0.1	0.2
510803	1.7	19.3	4.6	7.1	44.7	296.8	0.6	2.5
510804	1.7	17.4	3.3	8.5	49.5	456.0	0.5	1.3
510805	0.2	17.8	3.3	7.4	6.8	281.2	0.4	2.2
510806	<0.1	17.0	3.1	8.6	3.4	363.3	0.5	1.7
510807	1.1	16.9	3.9	5.1	67.4	159.7	0.2	4.3
510808	<0.1	20.6	3.3	8.6	1.7	549.0	0.5	2.0
510809	<0.1	18.1	3.5	9.7	7.6	498.3	0.6	2.3
510810	<0.1	16.8	1.4	2.2	1.8	238.4	0.1	0.3
510811	<0.1	18.5	1.5	2.5	1.1	250.6	0.2	0.5
510812	0.1	17.1	1.8	2.7	7.2	185.1	0.2	0.4
510813	<0.1	20.2	3.9	9.9	4.9	395.8	0.6	2.2
510816	<0.1	19.1	4.2	12.4	5.1	297.6	0.8	2.7
510817	0.5	20.0	3.4	9.9	14.7	376.3	0.6	2.1
510818	<0.1	16.6	2.0	3.5	4.5	555.9	0.3	0.4

Sample	Cs	Ga	Hf	Nb	Rb	Sr	Ta	Th
Unit	ppm	ppm	ppm	ppm	ppm	ppm	ppm	ppm
MDL	0.1	0.5	0.1	0.1	0.1	0.5	0.1	0.2
510819	0.1	18.6	4.2	10.5	6.0	353.0	0.5	2.1
510820	<0.1	16.1	3.5	9.5	1.1	448.5	0.5	1.9
510822	<0.1	20.4	4.6	12.7	1.0	585.6	0.8	2.9
510823	<0.1	16.6	1.4	2.1	5.9	252.3	0.2	0.4
510824	<0.1	17.7	4.0	9.0	4.2	308.6	0.5	1.8
510825	<0.1	18.2	1.8	3.6	12.4	382.7	0.4	0.4
510826	1.1	19.3	5.0	6.6	47.6	197.6	0.7	4.1
510827	<0.1	16.1	1.7	2.3	1.3	218.4	0.2	0.6
510828	0.5	19.8	4.3	11.0	13.8	325.3	0.6	2.7
510829	<0.1	15.1	4.0	10.5	5.8	287.4	0.5	2.6
510830	0.9	16.3	4.5	11.6	26.9	286.8	0.6	2.7
510831	<0.1	15.4	4.0	10.6	3.2	364.5	0.5	2.4
510832	0.3	15.5	3.9	9.6	9.6	325.9	0.5	2.3
510912	1.6	16.8	4.4	5.5	35.5	192.4	0.6	5.6
510913	<0.1	15.9	2.5	4.0	1.1	554.3	0.3	5.5
510915	0.7	16.1	3.3	4.6	28.5	285.8	0.3	1.8
510917	<0.1	20.1	1.9	3.3	0.6	66.2	0.2	0.3
510922	<0.1	18.9	3.5	4.9	2.5	76.1	0.3	1.0
510924	<0.1	16.6	2.9	5.2	<0.1	128.7	0.4	1.2
510928	<0.1	14.5	1.4	1.8	0.2	22.4	0.1	0.4
510929	<0.1	14.2	1.9	2.5	<0.1	161.9	0.2	0.9
510931	<0.1	20.7	1.9	2.5	1.0	261.9	0.2	1.0
510932	<0.1	16.9	2.4	3.3	0.3	147.4	0.3	1.2
510933	<0.1	18.9	1.7	2.6	1.6	235.7	0.2	1.1
510934	<0.1	27.2	1.7	2.7	1.2	197.7	0.2	0.9
510935	0.1	17.8	2.5	3.8	4.1	240.4	0.4	1.7
510936	0.6	19.3	2.6	3.3	27.8	215.1	0.3	1.5
510937	<0.1	20.4	2.6	3.3	3.7	193.7	0.3	1.5
510938	<0.1	17.4	1.4	1.9	0.7	133.5	0.1	0.4
510939	<0.1	13.2	1.1	1.8	0.7	15.0	0.2	0.2
510940	<0.1	20.7	3.3	6.3	0.8	324.7	0.4	1.8
510941	0.5	19.8	4.6	6.3	70.6	112.5	0.5	4.4
510942	<0.1	19.4	2.5	3.5	2.1	113.3	0.2	0.7
510943	2.0	21.1	4.7	6.6	81.7	247.0	0.7	2.9
510944	<0.1	20.6	2.6	3.5	1.1	130.9	0.3	0.5
511152	0.3	14.9	1.0	1.1	18.3	167.6	<0.1	0.3
511155	0.3	16.2	2.1	3.6	4.0	137.0	0.3	0.7
511156	1.7	17.5	3.8	5.6	61.3	198.4	0.4	6.2
511157	0.6	18.5	3.5	5.0	32.3	274.7	0.3	2.8
511158	0.3	16.8	2.1	2.6	16.3	261.4	0.2	0.3
511159	0.7	16.4	3.7	5.0	36.8	326.2	0.4	5.1
511160	0.7	16.9	4.4	5.4	46.4	300.2	0.4	5.2
511162	0.4	17.8	3.4	4.3	30.0	278.9	0.3	3.1
511163	0.4	18.3	4.0	6.2	11.5	154.1	0.4	1.1
511164	0.5	16.3	3.2	4.5	42.1	187.2	0.3	4.3
511165	0.3	15.3	3.7	6.3	22.5	305.7	0.4	4.7
511166	0.2	16.2	2.5	3.4	10.7	87.3	0.3	0.5
511169	0.4	17.5	4.0	6.0	34.1	297.7	0.4	6.1
511172	<0.1	14.5	1.4	2.3	2.6	211.4	0.2	0.7
511173	0.6	17.5	0.2	0.3	3.6	130.4	<0.1	<0.2
511174	2.8	15.3	3.4	5.7	15.8	450.9	0.4	3.3
511175	0.3	16.5	2.1	3.2	5.3	251.0	0.2	0.7

Sample	Cs	Ga	Hf	Nb	Rb	Sr	Ta	Th
Unit	ppm	ppm	ppm	ppm	ppm	ppm	ppm	ppm
MDL	0.1	0.5	0.1	0.1	0.1	0.5	0.1	0.2
511176	0.6	17.7	2.3	4.0	7.2	187.4	0.4	0.8
511180	<0.1	16.6	1.4	2.4	2.6	171.9	0.2	0.7
511181	<0.1	15.3	1.7	2.5	2.1	164.2	0.1	0.2
511182	<0.1	16.8	1.6	2.3	0.9	176.1	0.2	0.5
511183	<0.1	20.9	2.9	4.4	3.0	155.6	0.3	0.6
511184	0.2	18.5	1.4	1.9	2.5	156.3	0.2	<0.2
511185	<0.1	16.7	1.1	1.7	5.3	101.9	0.1	0.2
511186	1.6	16.8	3.3	5.0	54.8	118.0	0.4	2.8
511188	0.2	18.0	2.6	4.2	4.9	216.0	0.3	1.1
511189	0.2	17.1	2.6	3.8	12.9	229.9	0.3	1.6
511190	0.2	16.7	2.4	4.3	5.2	128.2	0.3	2.1
511192	0.5	18.4	2.9	4.7	9.1	265.1	0.4	1.9
511193	<0.1	17.9	3.4	5.2	0.9	269.2	0.4	2.4
511194	<0.1	16.6	3.0	4.8	1.1	175.9	0.3	1.6
512148	<0.1	16.0	2.6	4.1	2.0	126.6	0.3	0.5
512149	<0.1	19.1	2.2	3.5	4.7	118.0	0.2	0.4
512150	<0.1	17.7	2.4	3.4	2.4	301.6	0.2	1.0
512151	1.3	16.8	4.3	11.4	31.2	423.6	0.6	1.9
515802	<0.1	14.3	1.7	1.1	0.5	153.4	0.1	0.4
515803	<0.1	15.3	3.1	5.1	0.8	128.1	0.2	1.0
515804	<0.1	16.0	2.0	1.7	0.5	126.6	<0.1	0.6
515806	0.1	18.4	2.5	3.8	0.8	735.0	<0.1	4.5
515808	3.5	16.8	4.0	6.7	27.1	388.9	0.3	1.9
515809	0.6	16.7	2.3	3.5	14.7	244.0	0.2	1.3
515810	0.2	21.0	3.1	6.8	1.0	226.2	0.5	1.1
515811	<0.1	20.4	4.2	6.9	1.6	272.1	0.4	2.2
515813	0.4	16.6	3.7	4.1	12.4	267.0	0.3	2.5
515814	<0.1	21.1	4.1	7.5	2.1	323.9	0.5	2.3
515815	<0.1	20.0	4.4	7.5	2.4	342.2	0.6	2.7
515816	10.0	15.3	3.3	3.3	84.3	264.4	0.4	2.2
515817	<0.1	16.8	3.5	1.8	0.5	282.9	0.4	1.8
515818	<0.1	21.0	2.8	4.9	2.1	251.2	0.3	1.3
515819	<0.1	19.4	4.0	7.1	0.7	328.9	0.4	2.7
515820	1.2	22.5	4.6	2.8	62.3	234.0	0.3	2.1
515824	<0.1	5.7	0.7	1.0	0.1	6.9	0.2	0.4
515825	<0.1	18.5	3.5	5.5	1.8	180.9	0.5	1.8
515826	<0.1	24.2	4.5	9.8	0.9	531.4	0.6	2.2
5108211	<0.1	22.7	4.0	11.0	1.6	589.1	0.6	2.4
5108212	<0.1	17.4	5.0	16.2	2.2	494.5	1.0	2.9
5109131	0.4	17.4	1.8	3.7	0.2	649.8	0.2	4.2
5109132	1.1	14.9	2.8	4.1	5.3	371.0	0.3	3.4
5109141	<0.1	16.6	3.2	6.1	1.0	255.5	0.3	3.1
5109142	2.6	17.0	3.5	6.0	43.1	201.1	0.5	1.7
5158071	0.2	20.7	2.2	3.5	1.1	621.4	0.2	4.4
5158072	3.3	18.6	3.4	2.8	23.4	446.2	0.2	5.3

Sample	U	V	W	Zr	Y	La	Ce	Pr
Unit	ppm	ppm	ppm	ppm	ppm	ppm	ppm	ppm
MDL	0.1	8	0.5	0.1	0.1	0.1	0.1	0.02
468758	0.2	197	97.7	119.9	20.3	10.2	26.4	3.15
468759	0.7	40	89.4	171.3	6.2	12.6	20.3	2.51
468761	0.7	87	78.6	168.3	13.3	19.1	37.8	4.40
468763	0.7	83	<0.5	143.1	15.3	16.8	34.6	4.23
468764	<0.1	80	<0.5	10.6	4.7	0.8	2.3	0.35
468765	0.1	160	1.2	132.8	6.1	1.0	3.1	0.54
468767	0.8	<8	177.5	151.1	8.7	21.4	37.8	4.16
468769	0.4	133	85.2	191.8	19.4	17.8	43.6	5.20
468770	0.8	<8	<0.5	86.4	4.1	14.9	27.2	2.60
468771	0.7	<8	<0.5	90.0	3.3	13.0	40.2	2.42
468774	<0.1	206	<0.5	36.8	15.3	3.0	6.7	1.08
468775	<0.1	187	49.2	31.7	11.6	2.0	4.5	0.72
468777	0.2	290	51.1	152.9	32.4	9.2	24.7	3.75
468778	0.3	164	98.1	134.3	15.3	10.5	22.2	2.82
468779	0.2	413	73.4	117.0	36.7	5.4	14.1	2.21
468780	0.5	120	<0.5	110.6	13.6	16.2	34.7	4.64
468781	0.1	218	<0.5	46.4	17.3	3.2	8.1	1.25
468783	<0.1	135	0.8	18.4	8.4	1.6	2.9	0.49
468784	<0.1	217	<0.5	25.6	11.3	2.3	5.0	0.77
468787	1.0	26	<0.5	167.9	11.0	10.2	21.8	2.23
468788	0.4	208	<0.5	110.7	23.6	19.1	44.3	5.76
468791	0.4	223	66.0	87.3	17.7	8.5	19.0	2.48
468792	0.2	219	41.5	84.4	18.8	6.8	16.6	2.26
468793	0.7	30	135.7	206.9	4.6	18.1	43.2	4.10
468794	<0.1	186	0.7	23.8	10.7	2.7	5.5	0.80
468795	<0.1	152	<0.5	40.4	13.1	3.6	9.9	1.33
468796	0.1	139	19.9	42.8	13.2	3.3	9.1	1.22
468797	0.6	121	0.7	126.0	16.7	18.1	42.5	5.12
468798	0.7	174	<0.5	162.2	22.9	23.2	53.3	6.92
508252	0.8	94	3.9	128.9	12.5	14.8	33.8	3.91
508253	0.2	220	3.4	44.4	16.4	3.3	9.0	1.17
508254	<0.1	257	2.7	59.1	21.1	3.5	10.5	1.45
508255	0.7	93	5.6	106.0	13.1	20.0	46.0	5.05
508256	0.1	304	3.4	58.5	20.7	3.2	9.7	1.39
508257	0.2	241	3.8	80.0	21.6	6.1	17.3	2.29
508258	0.2	307	4.9	72.2	29.8	6.7	16.7	2.31
508259	0.1	248	4.7	57.5	21.6	3.4	10.1	1.52
510802	<0.1	261	6.2	45.8	18.6	2.9	7.7	1.11
510803	0.6	46	6.1	180.2	8.7	21.3	41.7	4.53
510804	0.4	149	3.5	129.6	19.5	22.0	56.5	7.22
510805	0.5	146	7.5	130.4	17.5	20.7	52.9	6.46
510806	0.5	148	4.3	126.2	21.5	23.9	58.6	7.71
510807	0.5	<8	30.3	119.6	5.9	23.7	44.0	4.37
510808	0.5	142	10.4	137.5	19.8	28.5	67.4	8.40
510809	0.6	151	3.6	138.4	21.1	26.7	68.9	8.79
510810	0.2	257	3.1	45.2	17.8	3.6	8.6	1.27
510811	<0.1	272	3.4	56.4	20.1	4.1	9.8	1.42
510812	0.2	268	2.7	57.9	22.7	4.6	12.0	1.67
510813	0.5	151	2.2	152.1	21.9	33.0	83.5	10.96
510816	0.7	155	2.4	181.0	24.8	40.2	105.3	13.16
510817	0.5	134	1.9	143.7	21.0	31.7	82.9	10.97
510818	0.2	382	1.3	73.4	27.3	4.5	12.3	1.82

Sample	U	V	W	Zr	Y	La	Ce	Pr
Unit	ppm	ppm	ppm	ppm	ppm	ppm	ppm	ppm
MDL	0.1	8	0.5	0.1	0.1	0.1	0.1	0.02
510819	0.6	150	2.6	164.3	24.5	32.6	89.7	12.01
510820	0.5	136	4.0	149.8	21.5	32.2	84.4	10.89
510822	0.8	163	4.4	187.4	28.0	39.6	106.4	13.82
510823	0.1	262	5.0	46.9	17.5	3.5	9.0	1.25
510824	0.5	163	8.7	148.4	21.2	23.4	60.6	7.53
510825	0.2	289	6.3	63.7	20.7	3.9	10.6	1.50
510826	0.8	62	23.6	170.1	8.2	20.5	41.3	4.42
510827	<0.1	269	7.2	54.2	20.8	4.0	9.4	1.53
510828	0.7	161	3.6	165.0	25.5	36.3	97.0	12.84
510829	0.7	154	2.4	166.4	24.7	33.5	92.7	12.41
510830	0.6	163	4.0	180.7	27.2	34.2	97.9	13.34
510831	0.6	151	5.3	157.6	24.3	34.5	91.6	12.14
510832	0.6	149	1.9	153.8	22.8	32.2	89.5	11.84
510912	1.4	21	19.4	147.4	7.3	19.6	38.2	3.85
510913	1.0	171	10.8	94.4	19.2	49.8	119.6	14.86
510915	0.5	142	10.9	116.7	16.9	13.2	29.7	3.61
510917	0.1	1068	4.1	59.5	22.9	4.7	12.5	1.83
510922	0.3	494	9.8	113.7	35.1	8.7	21.9	3.08
510924	0.3	227	7.3	97.3	28.2	8.8	23.2	3.05
510928	<0.1	216	4.5	43.5	15.0	3.2	9.7	1.23
510929	0.2	213	9.2	62.0	16.2	6.2	15.1	1.98
510931	0.3	184	21.2	66.1	15.6	7.4	16.5	1.96
510932	0.2	160	5.0	85.2	14.7	4.0	11.8	1.36
510933	0.2	164	7.8	59.0	14.5	7.6	16.3	1.91
510934	0.3	141	13.4	64.4	12.6	10.0	19.7	2.07
510935	0.4	182	15.7	86.2	15.7	8.9	20.9	2.37
510936	0.4	226	11.6	83.7	18.1	8.4	18.8	2.29
510937	0.2	215	5.9	82.1	17.5	8.0	17.9	2.16
510938	<0.1	267	4.9	48.4	16.9	3.9	9.2	1.33
510939	<0.1	201	2.2	35.9	12.3	1.9	5.8	0.79
510940	0.3	208	6.6	115.3	21.5	13.4	35.8	4.20
510941	1.1	23	26.0	175.8	6.9	18.9	36.4	3.71
510942	0.2	378	11.2	83.7	31.3	5.3	13.2	2.02
510943	0.5	58	16.3	172.6	12.3	16.9	34.5	3.50
510944	0.1	335	6.6	78.7	27.6	4.4	11.7	1.81
511152	<0.1	232	4.2	32.6	14.9	2.5	5.2	0.82
511155	0.1	396	3.3	71.5	28.1	4.7	13.2	1.93
511156	0.7	74	3.1	120.5	14.9	26.1	51.6	5.56
511157	0.7	165	5.8	111.5	18.8	15.1	38.5	4.74
511158	0.2	275	2.4	60.8	23.4	5.6	12.1	1.77
511159	1.3	113	4.1	122.8	13.9	18.5	40.8	4.44
511160	0.6	101	5.2	136.7	13.9	22.2	48.6	5.26
511162	0.7	186	6.5	103.3	18.7	15.2	34.8	4.32
511163	0.3	304	3.8	132.1	43.1	8.1	22.6	3.26
511164	0.8	164	5.5	101.8	17.8	19.3	44.3	5.16
511165	0.8	98	7.1	138.9	16.6	26.4	61.4	6.95
511166	<0.1	397	8.1	77.1	27.8	5.0	14.3	1.99
511169	0.9	93	6.9	135.2	14.5	24.9	49.0	5.57
511172	0.3	235	3.0	46.0	17.6	3.7	9.3	1.26
511173	<0.1	32	8.0	4.6	1.9	0.4	0.8	0.12
511174	0.6	94	12.2	125.4	13.9	13.8	30.4	3.40
511175	0.1	274	6.6	67.4	24.1	4.3	12.1	1.67

Sample	U	V	W	Zr	Y	La	Ce	Pr
Unit	ppm	ppm	ppm	ppm	ppm	ppm	ppm	ppm
MDL	0.1	8	0.5	0.1	0.1	0.1	0.1	0.02
511176	0.3	312	14.4	79.8	27.9	6.9	17.8	2.25
511180	<0.1	238	9.8	53.2	18.9	3.2	9.6	1.28
511181	0.1	249	4.6	54.4	18.5	3.2	9.5	1.33
511182	0.2	240	6.3	52.6	20.3	3.8	9.6	1.41
511183	0.2	334	8.1	98.6	33.8	6.5	17.4	2.53
511184	0.1	283	7.4	50.0	18.3	3.1	7.8	1.15
511185	0.2	223	3.3	39.8	15.6	2.7	6.9	1.01
511186	0.7	106	11.8	122.9	14.9	13.7	29.1	3.26
511188	0.3	168	9.9	97.7	17.5	12.2	25.5	3.22
511189	0.4	175	15.2	99.3	18.0	10.9	25.5	2.99
511190	0.5	173	9.6	97.1	17.6	13.1	28.2	3.58
511192	0.6	176	7.4	111.7	19.9	14.5	31.9	3.93
511193	0.8	161	9.7	124.4	20.8	15.9	36.3	4.55
511194	0.4	167	5.3	105.9	19.3	16.2	35.7	4.29
512148	0.2	258	8.2	89.5	29.0	6.6	15.4	2.30
512149	0.1	426	3.2	76.8	25.4	5.1	13.8	1.97
512150	0.2	242	3.0	70.4	24.3	5.1	13.3	1.95
512151	1.1	126	7.7	154.9	19.8	22.8	60.5	7.20
515802	0.1	153	<0.5	45.6	17.5	4.7	10.6	1.53
515803	0.4	262	58.8	97.6	30.7	4.8	13.2	2.04
515804	0.1	249	<0.5	62.7	23.0	4.5	12.0	1.82
515806	1.0	169	75.3	84.9	17.8	44.7	102.2	13.85
515808	0.5	130	50.1	139.1	18.0	19.2	44.3	5.59
515809	0.3	175	55.9	82.3	17.9	9.8	22.8	3.05
515810	0.5	166	160.4	112.9	20.8	12.9	28.1	3.94
515811	0.7	203	0.6	152.1	26.4	22.7	56.1	7.38
515813	0.7	90	<0.5	139.6	15.1	18.3	40.9	4.78
515814	0.7	141	84.7	155.0	20.4	19.7	46.2	6.04
515815	0.7	133	113.5	160.2	20.8	19.0	43.6	5.55
515816	0.5	118	<0.5	122.4	16.4	14.0	30.3	3.59
515817	0.5	122	<0.5	132.7	17.0	13.4	29.7	3.60
515818	0.4	156	<0.5	103.7	18.6	12.7	28.2	3.78
515819	0.7	123	<0.5	145.6	19.2	18.9	43.8	5.79
515820	1.2	25	164.0	156.0	3.8	6.3	19.5	1.37
515824	<0.1	98	20.4	17.8	4.3	2.7	3.3	0.49
515825	0.5	133	<0.5	126.4	17.9	13.6	29.9	3.87
515826	0.7	163	83.4	184.5	22.1	34.7	89.3	12.49
5108211	0.6	150	4.2	156.9	23.8	33.8	90.0	11.82
5108212	0.8	162	2.7	191.9	28.6	36.9	102.9	13.91
5109131	0.8	160	15.9	79.0	15.7	39.3	97.9	12.43
5109132	0.6	161	11.0	99.1	19.6	25.4	63.3	7.67
5109141	0.8	121	10.6	131.4	16.1	27.1	63.5	7.50
5109142	0.5	140	7.2	125.8	18.5	13.9	31.4	3.86
5158071	1.0	169	<0.5	79.0	15.5	40.0	96.1	13.03
5158072	1.1	207	<0.5	112.1	22.5	52.7	125.4	15.79

Sample	Nd	Sm	Eu	Gd	Tb	Dy	Ho	Er
Unit	ppm	ppm	ppm	ppm	ppm	ppm	ppm	ppm
MDL	0.3	0.05	0.02	0.05	0.01	0.05	0.02	0.03
468758	14.4	3.23	1.03	3.41	0.59	3.42	0.68	2.14
468759	9.4	1.50	0.52	1.30	0.20	1.05	0.21	0.59
468761	17.4	3.12	0.87	2.63	0.41	2.26	0.44	1.34
468763	17.5	3.13	0.93	2.91	0.48	2.81	0.50	1.48
468764	2.1	0.49	0.13	0.67	0.13	0.83	0.17	0.54
468765	2.9	0.87	0.10	0.99	0.17	0.96	0.19	0.56
468767	16.3	2.36	0.58	1.76	0.26	1.30	0.26	0.72
468769	22.1	4.36	1.19	3.86	0.58	3.15	0.59	1.72
468770	8.5	1.22	0.38	0.91	0.14	0.72	0.12	0.32
468771	9.0	1.09	0.48	0.69	0.10	0.62	0.10	0.35
468774	5.4	1.73	0.62	2.41	0.43	2.73	0.56	1.83
468775	3.8	1.14	0.50	1.52	0.25	1.84	0.36	1.11
468777	19.9	5.27	1.60	5.52	0.96	5.50	1.08	3.16
468778	12.4	2.66	0.82	2.65	0.46	2.48	0.50	1.50
468779	11.6	3.69	1.17	4.57	0.89	5.64	1.22	3.73
468780	20.5	3.62	1.03	2.96	0.47	2.54	0.49	1.28
468781	7.2	1.79	0.68	2.47	0.47	2.86	0.64	1.92
468783	1.9	0.72	0.36	1.02	0.22	1.42	0.28	0.92
468784	2.9	1.13	0.49	1.52	0.36	2.01	0.39	1.25
468787	8.0	1.50	0.49	1.64	0.29	1.54	0.35	0.89
468788	22.9	4.35	1.33	4.18	0.75	3.80	0.81	2.50
468791	10.2	2.40	0.80	2.56	0.38	2.92	0.57	1.72
468792	9.7	2.59	0.73	2.72	0.41	3.19	0.63	1.83
468793	15.1	2.15	0.52	1.40	0.18	0.87	0.15	0.41
468794	2.9	0.94	0.38	1.36	0.28	1.61	0.32	0.97
468795	6.9	1.47	0.60	1.96	0.36	2.19	0.46	1.41
468796	6.3	1.53	0.60	1.82	0.35	2.12	0.46	1.53
468797	18.2	3.65	1.01	3.32	0.57	3.25	0.59	1.79
468798	27.3	5.63	1.41	4.77	0.78	4.04	0.80	2.24
508252	15.6	3.07	0.95	2.91	0.45	2.28	0.46	1.35
508253	5.8	1.93	0.64	2.50	0.46	2.79	0.64	1.99
508254	7.0	2.43	0.87	3.24	0.63	3.83	0.85	2.53
508255	19.9	3.78	1.01	3.11	0.46	2.40	0.48	1.33
508256	7.5	2.38	0.97	3.23	0.62	3.67	0.85	2.40
508257	10.6	3.04	1.06	3.87	0.69	4.22	0.91	2.60
508258	11.5	3.32	1.15	4.64	0.85	5.21	1.10	3.28
508259	7.5	2.29	0.83	3.25	0.60	3.69	0.76	2.24
510802	5.8	1.93	0.72	2.61	0.50	3.07	0.66	2.00
510803	16.3	2.76	0.82	2.14	0.32	1.57	0.29	0.85
510804	28.8	5.38	1.48	4.30	0.69	3.51	0.68	1.91
510805	27.4	5.23	1.51	4.43	0.67	3.60	0.66	1.95
510806	31.9	5.77	1.60	4.83	0.74	3.87	0.73	2.09
510807	14.8	2.18	0.64	1.53	0.22	1.12	0.18	0.50
510808	34.1	5.91	1.69	4.58	0.71	3.68	0.70	1.90
510809	36.2	6.34	1.73	5.23	0.78	4.04	0.74	2.05
510810	5.9	1.94	0.69	2.56	0.49	3.01	0.64	1.97
510811	7.4	2.23	0.78	2.94	0.54	3.36	0.75	2.27
510812	7.7	2.52	0.87	3.25	0.61	3.83	0.81	2.42
510813	46.3	8.01	2.13	5.90	0.83	4.07	0.76	2.02
510816	53.1	9.77	2.59	7.39	1.07	5.17	0.91	2.73
510817	44.3	7.65	2.01	5.54	0.82	4.17	0.76	2.01
510818	9.6	2.84	0.96	3.74	0.74	4.69	1.01	3.07

Sample	Nd	Sm	Eu	Gd	Tb	Dy	Ho	Er
Unit	ppm	ppm	ppm	ppm	ppm	ppm	ppm	ppm
MDL	0.3	0.05	0.02	0.05	0.01	0.05	0.02	0.03
510819	51.7	8.58	2.24	6.29	0.93	4.69	0.89	2.28
510820	45.7	7.45	2.08	5.72	0.82	4.02	0.74	2.00
510822	57.6	9.67	2.59	7.60	1.07	5.35	0.97	2.71
510823	6.1	1.88	0.68	2.57	0.49	3.12	0.66	1.95
510824	31.0	5.77	1.64	4.82	0.76	4.11	0.75	2.13
510825	7.4	2.40	0.87	3.18	0.61	3.97	0.82	2.44
510826	16.8	2.67	0.82	2.33	0.33	1.65	0.27	0.74
510827	8.0	2.32	0.81	3.07	0.58	3.51	0.76	2.26
510828	53.4	8.63	2.50	6.95	0.98	4.93	0.88	2.39
510829	51.6	8.86	2.33	6.98	0.96	4.65	0.86	2.36
510830	56.6	9.67	2.53	7.59	1.04	5.33	0.90	2.58
510831	51.3	8.57	2.32	6.58	0.94	4.55	0.83	2.28
510832	49.2	8.46	2.29	6.42	0.89	4.48	0.81	2.26
510912	12.6	2.23	0.70	1.84	0.28	1.33	0.24	0.63
510913	58.6	9.51	2.20	5.49	0.76	3.63	0.68	1.77
510915	14.8	3.06	0.94	3.08	0.52	2.84	0.58	1.77
510917	9.6	2.61	0.89	3.51	0.64	4.06	0.85	2.48
510922	14.9	4.06	1.25	5.06	0.96	6.05	1.30	3.66
510924	13.4	3.53	1.05	4.17	0.78	4.83	1.04	3.16
510928	5.7	1.94	0.76	2.37	0.43	2.54	0.56	1.63
510929	9.3	2.18	0.70	2.50	0.46	2.84	0.61	1.90
510931	8.5	2.04	0.77	2.54	0.46	2.53	0.58	1.65
510932	5.8	2.02	0.68	2.52	0.45	2.71	0.55	1.67
510933	8.3	2.00	0.72	2.38	0.41	2.54	0.52	1.57
510934	8.2	2.05	0.82	2.22	0.38	2.31	0.50	1.44
510935	10.1	2.32	0.71	2.49	0.43	2.63	0.53	1.64
510936	9.7	2.35	0.78	2.72	0.50	3.24	0.65	1.88
510937	9.0	2.24	0.72	2.67	0.47	2.99	0.61	1.89
510938	6.5	1.89	0.68	2.50	0.46	2.95	0.60	1.75
510939	4.2	1.26	0.49	1.77	0.31	1.94	0.42	1.35
510940	17.3	3.83	1.18	3.78	0.67	3.65	0.76	2.16
510941	12.9	2.06	0.60	1.42	0.21	1.27	0.21	0.61
510942	9.8	3.32	1.04	4.47	0.84	5.31	1.13	3.36
510943	12.5	2.36	0.67	2.15	0.35	2.07	0.36	1.11
510944	9.5	3.02	1.03	4.08	0.78	4.68	1.01	2.95
511152	4.4	1.34	0.55	2.04	0.36	2.45	0.54	1.66
511155	9.6	3.30	1.08	4.08	0.75	4.68	1.02	3.02
511156	19.4	3.30	0.81	2.67	0.45	2.39	0.51	1.33
511157	19.8	4.17	1.18	3.74	0.59	3.30	0.66	1.88
511158	9.3	2.55	0.88	3.42	0.65	4.30	0.90	2.48
511159	16.6	3.18	0.86	2.74	0.45	2.48	0.53	1.38
511160	19.9	3.61	0.90	3.01	0.47	2.55	0.53	1.43
511162	17.0	3.86	1.09	3.64	0.61	3.40	0.69	1.95
511163	16.3	5.06	1.48	6.68	1.23	8.02	1.64	4.80
511164	20.6	4.19	1.10	3.67	0.60	3.21	0.68	1.87
511165	26.9	5.05	1.28	3.94	0.60	3.22	0.60	1.61
511166	9.4	3.02	1.03	4.30	0.78	4.87	1.05	3.07
511169	20.3	3.59	0.90	2.92	0.47	2.51	0.54	1.49
511172	6.3	1.87	0.72	2.70	0.49	3.17	0.72	2.01
511173	0.9	0.23	0.12	0.23	0.05	0.32	0.08	0.24
511174	13.7	2.81	0.86	2.91	0.47	2.62	0.52	1.49
511175	8.3	2.62	0.96	3.79	0.73	4.64	0.95	2.89

Sample	Nd	Sm	Eu	Gd	Tb	Dy	Ho	Er
Unit	ppm	ppm	ppm	ppm	ppm	ppm	ppm	ppm
MDL	0.3	0.05	0.02	0.05	0.01	0.05	0.02	0.03
511176	10.6	3.07	1.06	4.27	0.78	4.94	1.07	3.14
511180	7.0	2.09	0.79	2.96	0.53	3.12	0.70	2.00
511181	6.0	2.20	0.76	2.98	0.57	3.51	0.77	2.32
511182	6.8	2.23	0.70	2.87	0.55	3.25	0.73	2.20
511183	12.8	3.77	1.16	4.88	0.93	5.48	1.24	3.61
511184	5.8	1.90	0.69	2.43	0.50	3.02	0.66	2.08
511185	5.0	1.66	0.62	2.23	0.43	2.48	0.56	1.69
511186	12.6	2.71	0.66	2.64	0.48	2.54	0.54	1.52
511188	13.5	3.04	0.95	3.20	0.54	2.91	0.61	1.78
511189	12.7	3.04	0.96	3.20	0.59	3.30	0.72	2.08
511190	15.1	3.27	0.89	3.11	0.54	3.14	0.61	1.81
511192	16.7	3.59	1.07	3.69	0.61	3.46	0.70	2.12
511193	18.5	3.94	1.16	3.97	0.66	3.65	0.74	2.17
511194	18.2	3.61	1.03	3.54	0.59	3.34	0.70	1.99
512148	11.7	3.46	1.04	4.39	0.84	5.29	1.17	3.30
512149	10.7	2.91	1.11	4.01	0.76	4.34	0.99	2.90
512150	9.6	3.24	1.08	4.01	0.76	4.61	0.92	2.95
512151	30.7	6.18	1.64	5.36	0.77	3.84	0.75	2.09
515802	7.5	1.93	0.82	2.52	0.49	2.83	0.61	1.76
515803	9.8	3.21	1.09	4.04	0.81	5.06	1.14	3.40
515804	7.6	2.54	0.80	3.24	0.63	3.59	0.81	2.38
515806	57.0	8.52	2.06	5.76	0.69	3.42	0.61	1.69
515808	20.3	3.95	1.15	3.66	0.59	3.09	0.61	1.87
515809	12.5	2.81	0.88	2.89	0.52	3.01	0.67	1.89
515810	16.6	3.56	1.22	3.69	0.62	3.76	0.71	2.14
515811	31.9	6.27	1.96	5.71	0.93	4.76	0.92	2.68
515813	18.9	3.68	1.07	3.13	0.54	2.77	0.55	1.47
515814	25.1	4.74	1.31	4.15	0.68	3.76	0.72	2.02
515815	22.7	4.37	1.24	4.11	0.67	3.84	0.71	2.11
515816	14.5	3.01	0.91	2.97	0.51	2.73	0.54	1.74
515817	12.4	3.08	0.91	2.91	0.52	2.98	0.62	1.81
515818	16.8	3.22	1.02	3.41	0.58	3.38	0.67	1.93
515819	23.8	4.13	1.20	3.88	0.64	3.54	0.68	1.91
515820	5.2	1.19	0.41	1.02	0.16	0.79	0.12	0.30
515824	2.4	0.54	0.13	0.76	0.12	0.62	0.18	0.41
515825	16.3	3.11	0.98	3.14	0.54	3.25	0.65	1.80
515826	51.4	9.17	2.31	6.73	0.93	4.49	0.78	1.96
5108211	48.9	8.24	2.37	6.09	0.91	4.70	0.82	2.27
5108212	59.1	10.14	2.52	7.77	1.13	5.76	1.04	2.84
5109131	52.6	7.60	1.82	5.19	0.62	3.07	0.53	1.56
5109132	29.8	5.72	1.50	4.35	0.67	3.60	0.68	1.94
5109141	29.2	4.79	1.35	4.07	0.57	3.00	0.55	1.63
5109142	15.4	3.25	1.01	3.37	0.56	3.32	0.64	1.94
5158071	55.1	7.30	2.00	5.21	0.62	3.31	0.56	1.54
5158072	64.6	9.67	2.51	6.35	0.87	4.01	0.73	2.05

Sample	Tm	Yb	Lu	TOT/C	TOT/S	Cu	Pb	Zn
Unit	ppm	ppm	ppm	-	-	ppm	ppm	ppm
MDL	0.01	0.05	0.01	0.02	0.02	0.1	0.1	1
468758	0.31	1.96	0.31	0.03	<0.02	52.6	0.5	7
468759	0.09	0.52	0.08	<0.02	<0.02	13.1	0.7	55
468761	0.20	1.22	0.19	0.04	<0.02	2.2	0.8	70
468763	0.22	1.45	0.23	0.92	<0.02	20.1	2.2	31
468764	0.08	0.52	0.09	1.76	<0.02	2.8	0.8	31
468765	0.08	0.51	0.09	0.04	<0.02	1.7	0.3	14
468767	0.11	0.72	0.10	<0.02	0.02	4.4	1.0	47
468769	0.25	1.58	0.23	<0.02	0.02	20.4	0.7	9
468770	0.05	0.37	0.06	0.03	<0.02	3.7	3.0	42
468771	0.05	0.47	0.07	<0.02	0.08	3.1	6.4	50
468774	0.26	1.61	0.24	<0.02	0.02	4.6	0.6	27
468775	0.17	1.16	0.16	0.05	0.05	148.5	0.6	4
468777	0.45	2.79	0.42	0.03	<0.02	42.1	0.4	11
468778	0.22	1.26	0.20	<0.02	<0.02	28.0	0.8	4
468779	0.56	3.66	0.57	<0.02	<0.02	15.9	0.2	12
468780	0.18	1.31	0.19	0.07	<0.02	47.2	1.1	35
468781	0.29	1.82	0.27	0.02	<0.02	131.5	0.5	23
468783	0.13	0.93	0.13	<0.02	0.03	83.4	20.4	13
468784	0.23	1.26	0.22	0.04	0.02	109.4	0.7	12
468787	0.13	0.95	0.13	0.04	<0.02	10.8	1.8	43
468788	0.34	2.39	0.36	0.32	<0.02	73.8	1.0	30
468791	0.25	1.81	0.26	0.39	<0.02	21.6	0.5	3
468792	0.27	1.91	0.28	0.04	<0.02	32.4	0.5	8
468793	0.06	0.37	0.06	0.04	<0.02	1.6	1.5	42
468794	0.16	0.98	0.15	0.09	<0.02	72.7	0.7	8
468795	0.20	1.30	0.21	0.04	<0.02	41.9	1.3	15
468796	0.24	1.47	0.23	0.02	<0.02	1.8	0.3	6
468797	0.25	1.71	0.24	0.33	<0.02	15.3	1.8	81
468798	0.35	2.15	0.33	0.03	<0.02	48.1	1.0	33
508252	0.20	1.13	0.18	<0.02	<0.02	14.3	1.3	27
508253	0.29	1.86	0.29	0.03	0.06	102.2	0.4	23
508254	0.37	2.26	0.38	0.05	<0.02	16.3	0.3	15
508255	0.20	1.25	0.19	0.04	0.11	65.3	2.2	34
508256	0.38	2.43	0.38	<0.02	0.18	53.2	1.8	19
508257	0.39	2.47	0.38	<0.02	0.42	75.5	0.8	23
508258	0.48	3.14	0.48	0.04	0.08	121.4	0.7	31
508259	0.36	2.32	0.35	0.11	0.04	31.8	1.8	25
510802	0.31	1.91	0.29	0.03	<0.02	29.2	0.5	10
510803	0.11	0.79	0.11	0.12	<0.02	9.8	0.8	74
510804	0.29	1.71	0.26	0.38	<0.02	2.0	1.1	67
510805	0.28	1.69	0.25	0.36	0.07	74.3	2.1	32
510806	0.32	1.96	0.30	0.26	0.02	18.0	0.6	17
510807	0.07	0.59	0.08	0.17	0.12	56.8	2.0	29
510808	0.28	1.66	0.26	0.35	0.05	77.7	1.6	11
510809	0.31	1.92	0.28	0.06	<0.02	39.7	0.5	18
510810	0.30	1.84	0.28	0.09	0.03	90.3	1.1	16
510811	0.33	2.12	0.33	0.03	<0.02	44.6	0.3	17
510812	0.36	2.35	0.35	<0.02	0.02	74.1	0.7	24
510813	0.29	1.83	0.27	1.92	0.06	121.2	1.8	14
510816	0.38	2.27	0.34	0.60	0.02	38.3	1.0	23
510817	0.28	1.69	0.26	1.40	<0.02	32.9	0.7	11
510818	0.44	2.83	0.43	0.09	0.04	35.9	0.7	23

Sample	Tm	Yb	Lu	TOT/C	TOT/S	Cu	Pb	Zn
Unit	ppm	ppm	ppm	-	-	ppm	ppm	ppm
MDL	0.01	0.05	0.01	0.02	0.02	0.1	0.1	1
510819	0.33	2.08	0.30	0.30	<0.02	25.3	0.5	32
510820	0.27	1.77	0.27	1.47	<0.02	70.5	1.5	12
510822	0.38	2.39	0.36	0.37	0.16	97.6	1.0	16
510823	0.30	1.92	0.29	0.11	0.11	118.7	1.1	18
510824	0.32	1.96	0.31	0.09	<0.02	7.9	0.7	29
510825	0.37	2.34	0.37	0.04	0.10	203.6	1.8	17
510826	0.11	0.60	0.10	0.15	<0.02	20.3	1.4	69
510827	0.38	2.25	0.36	0.03	0.04	93.4	0.4	14
510828	0.34	2.13	0.32	0.91	0.02	41.0	0.8	16
510829	0.34	2.15	0.32	0.74	0.03	66.3	1.9	20
510830	0.38	2.37	0.36	0.38	<0.02	38.3	0.8	30
510831	0.33	2.03	0.32	0.57	0.02	29.9	0.8	12
510832	0.31	2.05	0.29	0.70	<0.02	21.1	0.8	14
510912	0.10	0.62	0.09	<0.02	<0.02	9.3	1.6	51
510913	0.24	1.74	0.25	0.11	<0.02	52.6	0.8	5
510915	0.26	1.79	0.26	0.04	<0.02	49.6	0.9	25
510917	0.38	2.65	0.37	0.03	<0.02	34.7	0.2	6
510922	0.58	3.91	0.56	<0.02	<0.02	35.5	0.8	23
510924	0.46	3.03	0.46	<0.02	<0.02	1.1	0.4	4
510928	0.23	1.59	0.24	<0.02	<0.02	26.3	<0.1	3
510929	0.27	1.75	0.25	<0.02	<0.02	4.8	2.0	7
510931	0.22	1.61	0.25	0.14	<0.02	7.2	0.7	6
510932	0.23	1.59	0.25	<0.02	<0.02	68.2	0.8	13
510933	0.20	1.48	0.23	0.91	<0.02	6.2	0.7	4
510934	0.19	1.41	0.20	0.44	<0.02	20.5	0.3	<1
510935	0.24	1.56	0.23	0.03	<0.02	61.3	0.6	12
510936	0.28	1.92	0.26	0.05	0.04	111.3	0.5	20
510937	0.28	1.92	0.27	<0.02	<0.02	28.3	0.6	11
510938	0.27	1.69	0.24	0.14	0.04	94.0	0.4	10
510939	0.19	1.31	0.18	<0.02	<0.02	42.2	<0.1	10
510940	0.32	1.99	0.30	<0.02	<0.02	51.0	0.9	11
510941	0.07	0.58	0.07	0.08	0.04	11.5	1.2	53
510942	0.51	3.32	0.49	<0.02	0.03	27.3	0.4	19
510943	0.17	1.06	0.14	<0.02	<0.02	0.8	1.0	68
510944	0.46	2.85	0.42	<0.02	0.06	56.9	0.3	14
511152	0.24	1.64	0.25	<0.02	<0.02	44.0	0.6	19
511155	0.48	3.05	0.45	<0.02	<0.02	34.0	0.8	55
511156	0.22	1.42	0.22	0.04	<0.02	97.7	3.7	61
511157	0.30	1.93	0.29	<0.02	0.03	47.3	3.9	45
511158	0.40	2.64	0.37	0.02	<0.02	120.9	3.3	54
511159	0.23	1.42	0.22	0.05	<0.02	27.4	3.4	40
511160	0.23	1.46	0.21	0.03	<0.02	13.3	4.7	45
511162	0.30	1.99	0.30	0.05	0.04	47.4	2.6	38
511163	0.75	4.79	0.71	<0.02	0.03	44.0	1.1	51
511164	0.29	1.78	0.27	0.08	<0.02	25.8	2.0	42
511165	0.27	1.84	0.25	<0.02	<0.02	3.1	2.7	119
511166	0.49	3.23	0.46	0.05	0.04	50.3	0.9	44
511169	0.25	1.62	0.23	0.03	<0.02	2.6	3.4	45
511172	0.31	2.04	0.30	0.45	0.04	118.9	1.3	14
511173	0.04	0.24	0.05	0.34	0.08	35.4	1.7	2
511174	0.24	1.51	0.24	0.24	<0.02	24.9	1.0	47
511175	0.46	2.72	0.45	<0.02	<0.02	43.7	0.6	17

Sample	Tm	Yb	Lu	TOT/C	TOT/S	Cu	Pb	Zn
Unit	ppm	ppm	ppm	-	-	ppm	ppm	ppm
MDL	0.01	0.05	0.01	0.02	0.02	0.1	0.1	1
511176	0.47	2.95	0.50	<0.02	0.23	285.2	1.1	37
511180	0.34	2.00	0.34	0.04	0.02	101.3	0.8	12
511181	0.34	2.09	0.34	<0.02	0.05	168.5	0.4	14
511182	0.34	2.03	0.34	0.46	0.02	30.8	1.4	8
511183	0.60	3.49	0.58	<0.02	0.06	151.9	1.2	25
511184	0.32	1.90	0.31	0.02	0.06	140.1	1.0	15
511185	0.27	1.58	0.26	<0.02	<0.02	82.4	0.4	15
511186	0.23	1.39	0.23	0.58	<0.02	3.6	5.9	69
511188	0.28	1.63	0.26	0.16	<0.02	31.9	0.7	22
511189	0.31	1.92	0.29	0.20	<0.02	22.9	0.8	20
511190	0.27	1.75	0.27	0.12	0.07	128.4	0.7	18
511192	0.31	1.94	0.31	0.19	<0.02	172.7	0.4	21
511193	0.32	1.96	0.32	0.02	1.37	288.6	0.8	13
511194	0.30	1.84	0.29	0.05	0.02	67.1	0.6	10
512148	0.53	3.14	0.55	0.02	<0.02	123.2	1.8	15
512149	0.46	2.71	0.40	0.02	0.04	184.9	0.6	24
512150	0.46	2.58	0.41	<0.02	<0.02	132.5	0.5	17
512151	0.32	1.89	0.28	0.16	<0.02	37.5	1.4	26
515802	0.26	1.92	0.27	0.14	<0.02	147.9	2.6	16
515803	0.53	3.43	0.53	0.07	<0.02	0.5	0.3	4
515804	0.38	2.49	0.37	<0.02	<0.02	67.8	0.3	17
515806	0.27	1.70	0.25	0.44	<0.02	36.0	2.1	4
515808	0.28	1.73	0.26	<0.02	<0.02	32.0	0.9	21
515809	0.30	1.81	0.28	0.04	<0.02	51.1	0.4	10
515810	0.34	1.99	0.30	<0.02	0.05	78.9	1.4	4
515811	0.36	2.39	0.37	<0.02	<0.02	171.8	1.3	26
515813	0.22	1.43	0.20	<0.02	<0.02	47.3	1.7	31
515814	0.31	1.82	0.29	0.02	<0.02	29.9	0.9	9
515815	0.30	1.83	0.27	<0.02	<0.02	29.5	0.7	9
515816	0.25	1.57	0.26	0.02	<0.02	12.6	0.8	37
515817	0.28	1.78	0.27	<0.02	0.03	13.4	1.1	18
515818	0.30	1.96	0.29	<0.02	<0.02	26.6	6.6	31
515819	0.28	1.81	0.26	<0.02	<0.02	11.0	1.3	25
515820	0.05	0.27	0.04	0.03	0.02	0.4	1.0	60
515824	0.07	0.51	0.07	0.08	0.07	38.6	0.4	52
515825	0.28	1.80	0.28	<0.02	<0.02	82.9	0.8	27
515826	0.29	1.75	0.26	0.03	0.03	143.4	0.9	13
5108211	0.33	2.05	0.30	0.82	0.05	26.1	1.2	10
5108212	0.39	2.35	0.37	0.19	0.15	77.7	1.4	32
5109131	0.24	1.46	0.22	0.80	<0.02	60.8	2.0	3
5109132	0.26	1.93	0.29	0.02	<0.02	20.9	0.4	12
5109141	0.24	1.57	0.22	1.08	<0.02	15.1	3.2	13
5109142	0.29	1.95	0.29	0.04	0.06	98.0	0.8	57
5158071	0.23	1.55	0.23	0.73	<0.02	34.4	4.3	6
5158072	0.29	2.05	0.33	<0.02	<0.02	12.0	1.7	32

Sample	Ni	M-index	F-index	W-index	Nb/Nb*	Mg#
Unit	ppm	-	-	-	-	-
MDL	0.1	-	-	-	-	-
468758	5.1	93.99	1.75	4.27	0.49	0.56
468759	8.1	31.08	55.92	13.00	0.32	0.41
468761	26.7	54.72	32.26	13.01	0.29	0.51
468763	21.8	75.42	16.52	8.06	0.28	0.44
468764	738.2	83.51	0.03	16.46	0.68	0.85
468765	135.8	17.43	0.01	82.56	3.71	0.84
468767	0.7	15.17	78.79	6.05	0.26	0.23
468769	5.6	91.31	3.82	4.87	0.43	0.48
468770	7.0	16.11	78.41	5.48	0.19	0.33
468771	2.2	7.52	87.89	4.59	0.20	0.23
468774	36.7	88.45	5.05	6.50	1.01	0.54
468775	17.2	93.39	2.08	4.53	0.44	0.65
468777	8.7	92.49	1.98	5.53	1.05	0.47
468778	7.5	91.03	4.12	4.85	0.46	0.55
468779	2.8	91.81	1.27	6.92	0.93	0.38
468780	35.0	79.24	11.49	9.27	0.35	0.55
468781	60.3	92.73	1.81	5.45	0.83	0.55
468783	12.4	93.91	2.66	3.43	0.90	0.58
468784	23.5	94.32	1.63	4.06	0.30	0.60
468787	5.8	36.17	53.95	9.87	0.28	0.36
468788	18.7	89.36	4.34	6.30	0.31	0.45
468791	41.9	93.14	2.76	4.10	0.38	0.27
468792	16.9	93.96	1.77	4.27	0.38	0.51
468793	3.9	27.66	62.88	9.46	0.23	0.41
468794	20.6	97.70	0.39	1.91	1.02	0.71
468795	105.7	96.50	0.47	3.03	0.51	0.72
468796	49.9	94.41	0.72	4.87	0.59	0.74
468797	21.9	77.29	11.10	11.61	0.19	0.42
468798	7.1	89.48	4.04	6.48	0.27	0.45
508252	13.7	80.89	11.27	7.84	0.34	0.53
508253	39.5	88.35	4.53	7.12	0.56	0.44
508254	19.2	93.78	1.83	4.38	0.83	0.49
508255	26.1	64.85	23.03	12.12	0.17	0.50
508256	25.0	90.02	3.05	6.93	1.45	0.52
508257	81.2	89.62	3.16	7.22	0.51	0.50
508258	66.2	92.29	2.00	5.70	0.72	0.42
508259	60.5	92.41	2.22	5.37	1.03	0.51
510802	24.1	93.74	1.66	4.59	0.84	0.59
510803	12.9	41.63	46.17	12.20	0.33	0.41
510804	82.6	79.35	10.60	10.04	0.54	0.61
510805	60.3	88.52	4.68	6.80	0.37	0.56
510806	21.0	89.44	5.30	5.26	0.46	0.51
510807	0.4	7.20	87.12	5.67	0.17	0.28
510808	41.9	92.70	3.03	4.27	0.39	0.48
510809	25.8	89.79	4.14	6.07	0.42	0.59
510810	30.2	89.98	3.95	6.08	0.72	0.51
510811	25.1	93.90	1.80	4.31	0.59	0.52
510812	34.4	87.29	4.80	7.90	0.67	0.51
510813	21.9	93.37	3.17	3.46	0.39	0.43
510816	37.6	89.94	5.05	5.01	0.40	0.46
510817	18.7	88.29	6.60	5.11	0.41	0.46
510818	14.6	90.69	2.78	6.54	0.88	0.40

Sample	Ni	M-index	F-index	W-index	Nb/Nb*	Mg#
Unit	ppm	-	-	-	-	-
MDL	0.1	-	-	-	-	-
510819	41.1	87.06	6.82	6.12	0.43	0.52
510820	9.5	95.97	1.41	2.62	0.41	0.49
510822	64.6	92.47	3.36	4.17	0.40	0.47
510823	35.9	90.43	3.83	5.74	0.60	0.51
510824	25.6	89.05	5.50	5.45	0.47	0.49
510825	32.0	89.67	2.88	7.45	0.98	0.50
510826	4.7	31.62	56.67	11.71	0.24	0.37
510827	23.7	94.66	1.22	4.12	0.50	0.50
510828	32.4	87.98	6.90	5.12	0.38	0.44
510829	38.9	91.20	4.45	4.35	0.38	0.47
510830	45.6	84.44	8.31	7.25	0.41	0.47
510831	26.8	91.27	4.36	4.37	0.39	0.45
510832	22.2	89.54	5.64	4.83	0.38	0.47
510912	1.4	26.42	64.80	8.78	0.18	0.30
510913	8.3	91.91	3.77	4.32	0.08	0.63
510915	29.8	79.83	10.92	9.25	0.32	0.57
510917	10.2	94.72	0.97	4.31	0.94	0.38
510922	6.6	92.60	1.55	5.85	0.56	0.34
510924	12.5	94.80	1.47	3.73	0.54	0.61
510928	22.6	94.57	1.12	4.31	0.54	0.71
510929	17.0	92.15	1.44	6.41	0.36	0.63
510931	17.8	90.71	2.58	6.72	0.31	0.39
510932	14.8	91.91	3.42	4.67	0.51	0.57
510933	17.2	89.11	2.56	8.34	0.31	0.32
510934	3.0	82.40	0.64	16.96	0.31	0.44
510935	48.6	89.29	4.80	5.92	0.33	0.55
510936	41.7	82.32	8.75	8.93	0.32	0.46
510937	14.7	89.36	3.95	6.70	0.32	0.51
510938	30.7	93.96	1.57	4.47	0.51	0.61
510939	59.5	95.36	0.68	3.97	0.99	0.74
510940	6.5	92.10	2.51	5.39	0.43	0.55
510941	1.4	18.51	69.69	11.80	0.23	0.34
510942	13.0	91.87	1.90	6.23	0.62	0.42
510943	18.8	40.37	46.96	12.67	0.32	0.43
510944	29.9	93.73	1.52	4.75	0.80	0.54
511152	56.0	89.34	4.50	6.16	0.43	0.62
511155	20.9	92.05	1.92	6.02	0.67	0.45
511156	25.8	45.00	40.63	14.38	0.15	0.50
511157	21.6	71.30	17.75	10.95	0.26	0.48
511158	64.9	87.51	5.17	7.32	0.68	0.55
511159	19.5	60.34	27.00	12.66	0.17	0.50
511160	22.5	58.50	28.82	12.68	0.17	0.51
511162	17.0	74.91	14.12	10.97	0.21	0.47
511163	4.7	87.16	3.00	9.85	0.70	0.29
511164	23.9	74.98	14.96	10.06	0.17	0.55
511165	20.4	62.56	24.92	12.53	0.19	0.50
511166	15.1	90.95	2.60	6.45	0.73	0.43
511169	16.1	60.38	27.27	12.36	0.17	0.52
511172	50.0	93.81	1.97	4.22	0.48	0.43
511173	9.7	49.16	46.83	4.01	0.36	0.55
511174	70.3	79.49	11.99	8.52	0.29	0.58
511175	18.6	91.99	2.51	5.50	0.63	0.50

Sample	Ni	M-index	F-index	W-index	Nb/Nb*	Mg#
Unit	ppm	-	-	-	-	-
MDL	0.1	-	-	-	-	-
511176	33.2	88.65	3.54	7.81	0.58	0.42
511180	25.1	93.92	1.32	4.76	0.54	0.54
511181	35.7	93.58	1.52	4.90	1.06	0.53
511182	14.8	96.34	0.73	2.93	0.57	0.47
511183	41.6	91.71	1.58	6.71	0.75	0.46
511184	18.2	94.12	1.30	4.58	0.82	0.53
511185	40.1	91.19	3.22	5.59	0.78	0.60
511186	74.4	67.47	21.88	10.65	0.27	0.55
511188	32.4	87.97	5.45	6.59	0.39	0.54
511189	27.0	84.88	8.47	6.65	0.31	0.53
511190	31.4	87.30	5.55	7.15	0.28	0.55
511192	19.4	89.10	4.95	5.96	0.30	0.54
511193	44.8	90.03	4.23	5.74	0.29	0.50
511194	56.0	92.96	2.37	4.68	0.32	0.63
512148	33.0	91.32	1.73	6.94	0.76	0.46
512149	12.6	92.08	1.82	6.10	0.83	0.38
512150	34.2	91.97	2.28	5.75	0.51	0.46
512151	26.8	81.84	8.99	9.17	0.59	0.49
515802	11.7	94.50	1.35	4.15	0.27	0.66
515803	2.8	94.11	1.73	4.16	0.79	0.61
515804	19.6	94.80	1.34	3.87	0.35	0.62
515806	13.2	94.40	1.60	3.99	0.09	0.56
515808	16.4	79.28	11.54	9.18	0.38	0.48
515809	22.3	88.11	5.12	6.77	0.33	0.59
515810	4.6	89.71	2.79	7.50	0.61	0.52
515811	4.7	89.84	2.53	7.63	0.33	0.39
515813	8.3	79.28	11.20	9.51	0.21	0.41
515814	7.0	88.93	4.72	6.35	0.38	0.50
515815	13.0	89.17	4.67	6.17	0.35	0.53
515816	44.3	75.47	14.64	9.90	0.20	0.56
515817	27.9	93.26	2.61	4.12	0.12	0.58
515818	15.3	89.42	1.82	8.76	0.41	0.51
515819	24.6	88.83	4.77	6.40	0.34	0.50
515820	3.5	22.37	69.27	8.36	0.26	0.41
515824	840.1	74.68	0.06	25.26	0.33	0.82
515825	29.9	88.38	5.57	6.05	0.38	0.53
515826	24.8	94.90	1.23	3.86	0.38	0.50
5108211	52.3	93.99	2.10	3.92	0.41	0.42
5108212	78.8	93.56	2.00	4.44	0.53	0.49
5109131	6.3	94.28	1.73	3.99	0.10	0.51
5109132	25.1	86.93	6.81	6.26	0.15	0.59
5109141	10.4	91.60	3.75	4.65	0.23	0.54
5109142	75.3	71.69	16.35	11.97	0.42	0.54
5158071	17.6	94.86	1.73	3.41	0.09	0.49
5158072	37.2	84.34	8.17	7.49	0.06	0.59

Supplementary data table 2 (Paper II): Interlab standard comparison

GEUS (2003-2010) ¹					ACME lab (2008-2010) ²				ACME/GEUS	
Element	Avg	$\pm 1\sigma$ (abs.)	$\pm 1\sigma$ (%)	n	Avg	$\pm 1\sigma$ (abs.)	$\pm 1\sigma$ (%)	n	(% diff.)	Isotope
Sc	40.9	1.3	3.3	32	41.8	0.9	2.2	21	2.1	45
V	412	12	2.9	32	434	17	3.9	21	5.5	51
Cr	126	3	2.5	32	129	5	3.7	21	2.7	
Co	56.7	1.0	1.7	32	51.9	4.9	9.4	21	-8.5	59
Ni	60.1	2.1	3.5	32	61.0	7.1	11.7	19	1.6	
Cu	226	3	1.5	32	222	10	4.4	21	-1.8	63
Zn	106	2	2.2	32	62.2	5.1	8.1	21	-41.1	66
Ga	20.8	0.2	1.0	32	20.1	1.0	5.0	21	-3.4	71
Rb	3.30	0.05	1.6	32	3.57	0.51	14.4	21	8.1	85
Sr	213	3	1.4	32	224	7	3.1	21	5.4	88
Y	33.8	0.6	1.7	32	30.6	1.2	3.8	21	-9.5	89
Zr	122	3	2.3	32	111	5	4.3	21	-8.7	90
Nb	4.46	0.09	1.9	32	4.16	0.35	8.3	21	-6.8	93
Cs	0.059	0.003	4.5	32	0.121	0.043	35.1	14	106.2	133
Ba	46.5	1.1	2.4	31	47.9	4.4	9.2	21	3.0	137
La	6.58	0.08	1.2	32	6.41	0.32	5.0	21	-2.6	139
Ce	17.4	0.3	1.7	32	17.9	1.0	5.5	21	2.8	140
Pr	2.87	0.07	2.4	32	2.78	0.11	4.1	21	-3.2	141
Nd	14.7	0.3	2.0	32	14.4	0.8	5.4	21	-2.1	143
Sm	4.67	0.09	1.9	32	4.43	0.20	4.4	21	-5.1	147
Eu	1.67	0.04	2.5	32	1.64	0.06	3.8	21	-2.0	153
Gd	5.54	0.32	5.8	32	5.55	0.26	4.7	21	0.1	157
Tb	0.963	0.019	2.0	32	0.991	0.040	4.0	21	2.9	159
Dy	5.86	0.10	1.6	32	5.73	0.20	3.6	21	-2.1	161
Ho	1.23	0.03	2.3	32	1.16	0.05	4.0	21	-5.9	165
Er	3.19	0.06	1.8	32	3.26	0.16	4.9	21	2.0	166
Tm	0.479	0.009	1.8	32	0.469	0.030	6.4	21	-2.0	169
Yb	2.89	0.04	1.5	32	2.81	0.14	5.1	21	-2.6	174
Lu	0.425	0.012	2.9	32	0.419	0.029	7.0	21	-1.6	175
Hf	3.26	0.06	1.8	32	3.27	0.31	9.5	21	0.3	177
Ta	0.305	0.017	5.4	32	0.276	0.089	32.2	21	-9.4	181
W	n.a.				83.3	5.2	6.2	9		
Pb	1.24	0.08	6.5	32	1.17	1.57	134.9	21	-5.9	208
Th	0.594	0.024	4.0	32	0.790	0.232	29.4	21	33.0	232
U	0.147	0.005	3.1	32	0.186	0.096	51.9	21	26.2	238

¹Based on total digestion solution ICP-MS

²Based on total fusion ICP-MS

Supplementary data table 3 (Paper II): Lu-Hf and Sm-Nd isotope data

Sample	Locality	Rock-type	Lu (ppm)	Hf (ppm)	$^{176}\text{Lu}/^{177}\text{Hf}$	Error	$^{176}\text{Hf}/^{177}\text{Hf}$	2 σ int.	$\epsilon\text{Hf}_{(2970)}$	error 2 σ
468764	Ravns Storø	Ultramafic	0.0992	0.2876	0.04897	±12	0.283665	±8	0.1	±0.5
468784	Ravns Storø	Gabbro	0.1832	0.8134	0.03196	±8	0.282818	±9	4.5	±0.5
510802	Bjørnesund	Amphibolite	0.2998	1.357	0.03137	±8	0.282795	±5	4.9	±0.5
510805	Bjørnesund	Leucoamphibolite	0.2672	3.293	0.01152	±3	0.281632	±6	3.5	±0.4
510807	Bjørnesund	Aplite	0.08931	3.745	0.003384	±2	0.281205	±7	4.7	±0.4
510809	Bjørnesund	Leucoamphibolite	0.2845	3.650	0.01106	±3	0.281607	±6	3.5	±0.4
510825	Bjørnesund	Amphibolite	0.3478	1.656	0.02981	±5	0.282672	±7	3.7	±0.4
510827	Bjørnesund	Amphibolite	0.3551	1.706	0.02954	±8	0.282664	±5	3.9	±0.5
510915	Ravns Storø	Leucoamphibolite	0.2669	3.058	0.01239	±4	0.281687	±6	4.0	±0.4
510941	Ravns Storø	Aplite	0.09417	4.388	0.003045	±2	0.281173	±5	4.6	±0.4
510942	Ravns Storø	Amphibolite	0.4843	2.324	0.02958	±8	0.282709	±4	5.4	±0.5
510944	Ravns Storø	Amphibolite	0.4375	2.263	0.027437	±7	0.282541	±8	3.8	±0.5
511173	Bjørnesund	Anorthosite	0.04307	0.1706	0.03585	±9	0.283325	±6	14.7	±0.5
511179	Bjørnesund	Anorthosite	0.05698	0.1865	0.04336	±11	0.283524	±10	6.5	±0.5
510914-1	Ravns Storø	Tuff	0.2211	1.821	0.01723	±5	0.281966	±5	4.1	±0.4
510914-2	Ravns Storø	Tuff	0.2891	3.302	0.01243	±4	0.281699	±3	4.3	±0.4
510914-3	Ravns Storø	Tuff	0.2778	2.067	0.01908	±5	0.282073	±6	4.1	±0.4
Sample	Locality	Rock-type	Sm (ppm)	Nd (ppm)	$^{147}\text{Sm}/^{144}\text{Nd}$	Error	$^{143}\text{Nd}/^{144}\text{Nd}$	2 σ int.	$\epsilon\text{Nd}_{(2970)}$	error 2 σ
468764	Ravns Storø	Ultramafic	0.5377	1.714	0.1896	±4	0.512614	±10	2.1	±0.4
468784	Ravns Storø	Gabbro	1.098	3.300	0.2011	±4	0.512906	±7	3.5	±0.4
510802	Bjørnesund	Amphibolite	1.782	5.388	0.2000	±4	0.512814	±10	2.1	±0.4
510805	Bjørnesund	Leucoamphibolite	5.093	26.75	0.1150	±2	0.511177	±8	2.4	±0.4
510807	Bjørnesund	Aplite	2.017	12.87	0.09473	±2	0.510794	±10	2.7	±0.4
510809	Bjørnesund	Leucoamphibolite	6.046	33.85	0.1079	±2	0.511023	±12	2.1	±0.4
510825	Bjørnesund	Amphibolite	2.176	6.739	0.1952	±4	0.512777	±6	3.2	±0.4
510827	Bjørnesund	Amphibolite	2.249	7.105	0.1913	±4	0.512677	±10	2.7	±0.4
510915	Ravns Storø	Leucoamphibolite	2.954	13.87	0.1287	±3	0.511434	±6	2.4	±0.4
510941	Ravns Storø	Aplite	n.a.	n.a.	n.a.	n.a.	n.a.	n.a.	n.a.	n.a.
510942	Ravns Storø	Amphibolite	3.104	9.838	0.1907	±4	0.512645	±10	2.3	±0.4
510944	Ravns Storø	Amphibolite	2.860	8.715	0.1984	±4	0.512828	±8	2.9	±0.4
511173	Bjørnesund	Anorthosite	0.163	0.540	0.1823	±4	0.512662	±15	5.9	±0.4
511179	Bjørnesund	Anorthosite	n.a.	n.a.	n.a.	n.a.	n.a.	n.a.	n.a.	n.a.
510914-1	Ravns Storø	Tuff	1.917	8.534	0.1358	±3	0.511589	±10	2.1	±0.4
510914-2	Ravns Storø	Tuff	3.213	14.85	0.1307	±3	0.511454	±11	2.0	±0.4
510914-3	Ravns Storø	Tuff	2.062	8.352	0.1493	±3	0.511786	±8	1.4	±0.4

Supplementary data table 4 (Paper II): U-Pb isotope data

Sample	Analysis	U (ppm) ^a	Th/U ^a
468768	Zircon_sample-010	74	0.30
468768	Zircon_sample-011	78	0.28
468768	Zircon_sample-012	132	0.32
468768	Zircon_sample-013	173	0.34
468768	Zircon_sample-014	111	0.38
468768	Zircon_sample-015	57	0.35
468768	Zircon_sample-016	108	0.34
468768	Zircon_sample-021	20	0.32
468768	Zircon_sample-022	30	0.32
468768	Zircon_sample-023	65	0.31
468768	Zircon_sample-024	115	0.33
468768	Zircon_sample-025	91	0.36
468768	Zircon_sample-026	99	0.32
468768	Zircon_sample-027	87	0.38
468768	Zircon_sample-028	175	0.37
468768	Zircon_sample-029	124	0.34
468768	Zircon_sample-034	162	0.46
468768	Zircon_sample-035	85	0.37
468768	Zircon_sample-036	75	0.32
468768	Zircon_sample-037	98	0.37
468768	Zircon_sample-038	90	0.34
468768	Zircon_sample-039	194	0.49
468768	Zircon_sample-040	75	0.28
468768	Zircon_sample-041	876	0.70
468768	Zircon_sample-042	129	0.41
468768	Zircon_sample-046	94	0.31
468768	Zircon_Sample-047	94	0.31
468768	Zircon_Sample-048	99	0.49
468768	Zircon_Sample-049	104	0.33
468768	Zircon_Sample-050	86	0.30
468768	Zircon_Sample-051	124	0.37
468768	Zircon_Sample-052	97	0.35
468768	Zircon_Sample-053	84	0.48
468768	Zircon_Sample-054	136	0.39
468768	Zircon_Sample-055	144	0.38
468768	Zircon_Sample-060	46	0.29
468768	Zircon_Sample-061	57	0.33
468768	Zircon_Sample-062	156	0.39
468768	Zircon_Sample-063	136	0.40
468768	Zircon_Sample-064	100	0.35
468768	Zircon_Sample-065	71	0.30
468768	Zircon_Sample-066	114	0.40
468768	Zircon_Sample-067	72	0.31
468768	Zircon_Sample-068	105	0.38
468768	Zircon_Sample-072	112	0.34
468768	Zircon_Sample-073	47	0.27
468768	Zircon_Sample-074	98	0.36
468768	Zircon_Sample-075	83	0.38
468768	Zircon_Sample-076	183	0.54
468768	Zircon_Sample-077	109	0.35
468768	Zircon_Sample-078	64	0.38
468768	Zircon_Sample-079	129	0.44
468768	Zircon_Sample-080	76	0.39
468768	Zircon_Sample-086	122	0.35
468768	Zircon_Sample-087	77	0.34
468768	Zircon_Sample-088	95	0.34

^aMeasured Th/U ratios^bCorrected for background and within-run Pb/U frac. and norm. to reference zircon GJ-1 (ID-TIMS values/meas. value); $^{207}\text{Pb}/^{235}\text{U}$ calc. using $(^{207}\text{Pb}/^{206}\text{Pb})/(^{238}\text{U}/^{206}\text{Pb} * 1/137.88)$ ^cRho is the error correlation defined as the quotient of the propagated errors of the $^{206}\text{Pb}/^{238}\text{U}$ and the $^{207}\text{Pb}/^{235}\text{U}$ ratio^dQuadratic addition of within-run errors (2σ) and daily reproducibility of GJ-1 (2σ)^eCorrected for mass-bias by normalising to GJ-1 reference zircon (~0.6 per atomic mass unit) and common Pb using the model Pb composition of Stacey & Kramers (1975)

Sample	Analysis	U (ppm) ^a	Th/U ^a
468768	Zircon_Sample-089	159	0.40
468768	Zircon_Sample-090	368	0.44
468768	Zircon_Sample-091	84	0.30
468768	Zircon_Sample-093	63	0.32
468768	Zircon_Sample-094	83	0.28
468768	Zircon_Sample-099	113	0.32
468768	Zircon_Sample-100	41	0.27
468768	Zircon_Sample-101	70	0.36
468768	Zircon_Sample-102	55	0.24
468768	Zircon_Sample-103	133	0.33
468768	Zircon_Sample-104	55	0.27
468768	Zircon_Sample-105	122	0.29
468768	Zircon_Sample-106	66	0.27
468768	Zircon_Sample-113	102	0.31
468768	Zircon_Sample-115	61	0.31
508255	Zircon_sample-007	338	0.08
508255	Zircon_sample-009	262	0.37
508255	Zircon_sample-010	185	0.67
508255	Zircon_sample-011	249	0.66
508255	Zircon_sample-015	492	0.21
508255	Zircon_sample-020	169	0.65
508255	Zircon_sample-021	610	0.15
508255	Zircon_sample-023	245	0.71
508255	Zircon_sample-024	95	0.59
508255	Zircon_sample-025	947	0.20
508255	Zircon_sample-026	105	0.67
508255	Zircon_sample-027	166	0.51
508255	Zircon_sample-028	384	0.37
508255	Zircon_sample-033	303	0.34
508255	Zircon_sample-034	67	0.56
508255	Zircon_sample-036	296	0.53
508255	Zircon_sample-037	257	0.35
508255	Zircon_sample-038	170	0.57
508255	Zircon_sample-040	214	0.14
508255	Zircon_sample-046	157	0.27
508255	Zircon_Sample-047	457	0.27
508255	Zircon_Sample-048	167	0.65
508255	Zircon_Sample-050	183	0.54
508255	Zircon_Sample-052	144	0.60
508255	Zircon_Sample-053	597	0.19
508255	Zircon_Sample-054	549	0.04
508255	Zircon_Sample-059	87	0.66
508255	Zircon_Sample-060	156	0.53
508255	Zircon_Sample-061	121	0.53
508255	Zircon_Sample-062	154	0.56
508255	Zircon_Sample-063	96	0.56
508255	Zircon_Sample-064	347	0.34
508255	Zircon_Sample-065	301	0.17
508255	Zircon_Sample-066	574	0.13
508255	Zircon_Sample-067	924	0.02
508255	Zircon_Sample-072	179	0.42
508255	Zircon_Sample-074	1425	0.03
508255	Zircon_Sample-075	178	0.63
508255	Zircon_Sample-077	174	0.60
508255	Zircon_Sample-079	75	0.61
508255	Zircon_Sample-080	142	0.36
508255	Zircon_Sample-085	186	0.96
508255	Zircon_Sample-086	395	0.20

Sample	Analysis	U (ppm) ^a	Th/U ^a
508255	Zircon_Sample-087	1144	0.02
508255	Zircon_Sample-088	121	0.38
508255	Zircon_Sample-089	255	0.38
508255	Zircon_Sample-093	169	0.14
508255	Zircon_Sample-098	130	0.52
508255	Zircon_Sample-099	337	0.18
508255	Zircon_Sample-100	156	0.64
508255	Zircon_Sample-101	466	0.05
508255	Zircon_Sample-103	263	0.72
508255	Zircon_Sample-104	173	0.67
508255	Zircon_Sample-105	104	0.47
508255	Zircon_Sample-106	405	0.13
508255	Zircon_Sample-111	898	0.01
508255	Zircon_Sample-112	210	0.54
508255	Zircon_Sample-113	722	0.92
508255	Zircon_Sample-114	177	0.47
508255	Zircon_Sample-115	1189	0.01
508255	Zircon_Sample-116	726	0.04
508255	Zircon_Sample-117	139	0.52
508255	Zircon_Sample-118	94	0.62
508255	Zircon_Sample-119	228	0.35
508255	Zircon_Sample-124	169	0.60
508255	Zircon_Sample-125	208	0.45
508255	Zircon_Sample-126	156	0.62
508255	Zircon_Sample-127	516	0.12
508255	Zircon_Sample-128	111	0.67
508255	Zircon_Sample-130	139	0.59
508255	Zircon_Sample-131	169	0.64
508255	Zircon_Sample-132	299	0.27
508255	Zircon_Sample-137	173	0.67
508255	Zircon_Sample-138	73	0.70
508255	Zircon_Sample-140	97	0.60
508255	Zircon_Sample-141	360	0.25
508255	Zircon_Sample-142	355	0.22
508255	Zircon_Sample-143	561	0.35
508255	Zircon_Sample-144	447	0.15
508255	Zircon_Sample-145	77	0.78
508255	Zircon_Sample-150	310	0.41
508255	Zircon_Sample-151	126	0.53
508255	Zircon_Sample-152	127	0.61
508255	Zircon_Sample-156	158	0.51
508255	Zircon_Sample-157	415	0.12
508255	Zircon_Sample-158	242	0.66
510826	Zircon_Sample-047	121	0.40
510826	Zircon_Sample-048	103	0.34
510826	Zircon_Sample-049	101	0.26
510826	Zircon_Sample-050	158	0.41
510826	Zircon_Sample-051	136	0.40
510826	Zircon_Sample-053	186	0.23
510826	Zircon_Sample-054	765	0.03
510826	Zircon_Sample-059	188	0.21
510826	Zircon_Sample-060	45	0.32
510826	Zircon_Sample-062	225	0.19
510826	Zircon_Sample-063	457	0.05
510826	Zircon_Sample-064	330	0.10
510826	Zircon_Sample-065	148	0.15
510826	Zircon_Sample-066	560	0.01
510826	Zircon_Sample-067	115	0.23

Sample	Analysis	U (ppm) ^a	Th/U ^a
510826	Zircon_Sample-072	85	0.32
510826	Zircon_Sample-073	118	0.20
510826	Zircon_Sample-074	229	0.47
510826	Zircon_Sample-075	102	0.34
510826	Zircon_Sample-076	369	0.16
510826	Zircon_Sample-078	592	0.05
510826	Zircon_Sample-079	160	0.11
510826	Zircon_Sample-080	200	0.11
510826	Zircon_Sample-085	271	0.11
510826	Zircon_Sample-086	278	0.17
510826	Zircon_Sample-087	357	0.04
510826	Zircon_Sample-089	145	0.27
510826	Zircon_Sample-090	153	0.26
510826	Zircon_Sample-091	161	0.15
510826	Zircon_Sample-092	64	0.37
510826	Zircon_Sample-093	84	0.41
510826	Zircon_Sample-098	189	0.32
510826	Zircon_Sample-099	132	0.35
510826	Zircon_Sample-100	126	0.44
510826	Zircon_Sample-101	98	0.36
510826	Zircon_Sample-102	81	0.33
510826	Zircon_Sample-103	29	0.27
510826	Zircon_Sample-105	102	0.39
510826	Zircon_Sample-106	84	0.32
510831	Zircon_Sample-112	14	1.51
510831	Zircon_Sample-113	55	0.07
510831	Zircon_Sample-114	26	0.01
510831	Zircon_Sample-117	9	1.47
510831	Zircon_Sample-119	31	0.05
510831	Zircon_Sample-124	14	2.30
510831	Zircon_Sample-125	17	2.81
510831	Zircon_Sample-129	10	1.22
510831	Zircon_Sample-130	10	1.97
510831	Zircon_Sample-138	49	0.14
510831	Zircon_Sample-140	19	0.52
510831	Zircon_Sample-141	46	0.05
510831	Zircon_Sample-142	23	0.28
510831	Zircon_Sample-145	22	0.37
510831	Zircon_Sample-150	10	1.15
510831	Zircon_Sample-151	13	1.75
510831	Zircon_Sample-152	27	0.05
510831	Zircon_Sample-153	11	4.05
510831	Zircon_Sample-154	56	0.05
510831	Zircon_Sample-157	12	2.84
510831	Zircon_Sample-164	16	3.53
510831	Zircon_Sample-165	11	2.46
510831	Zircon_Sample-167	30	0.10
510831	Zircon_Sample-168	16	0.49
510831	Zircon_Sample-169	6	3.77
510831	Zircon_Sample-170	37	0.04
510831	Zircon_Sample-171	11	1.26
510831	Zircon_Sample-180	16	1.71
510831	Zircon_Sample-181	24	0.06
510831	Zircon_Sample-182	29	0.22
511162	Zircon_sample-008	297	0.57
511162	Zircon_sample-010	476	0.32
511162	Zircon_sample-011	1002	0.03
511162	Zircon_sample-012	845	0.29

Sample	Analysis	U (ppm) ^a	Th/U ^a
511162	Zircon_sample-013	435	0.25
511162	Zircon_sample-014	110	0.66
511162	Zircon_sample-015	98	0.62
511162	Zircon_sample-020	770	0.01
511162	Zircon_sample-021	469	0.58
511162	Zircon_sample-022	235	0.44
511162	Zircon_sample-025	381	0.02
511162	Zircon_sample-026	414	0.46
511162	Zircon_sample-027	1211	0.01
511162	Zircon_sample-028	1160	0.42
511162	Zircon_sample-033	478	0.78
511162	Zircon_sample-034	498	0.39
511162	Zircon_sample-035	505	0.44
511162	Zircon_sample-036	1241	0.02
511162	Zircon_sample-037	299	0.29
511162	Zircon_sample-038	392	0.75
511162	Zircon_sample-040	1176	0.03
511162	Zircon_sample-041	477	0.56
511162	Zircon_sample-046	652	0.65
511162	Zircon_Sample-047	586	0.11
511162	Zircon_Sample-048	531	0.27
511162	Zircon_Sample-049	797	0.05
511162	Zircon_Sample-050	540	0.31
511162	Zircon_Sample-051	161	0.53
511162	Zircon_Sample-052	833	1.00
511162	Zircon_Sample-053	1002	0.83
511162	Zircon_Sample-054	922	0.02
511162	Zircon_Sample-059	333	0.40
511162	Zircon_Sample-060	273	0.68
511162	Zircon_Sample-061	1165	0.02
511162	Zircon_Sample-062	813	0.97
511162	Zircon_Sample-063	973	0.02
511162	Zircon_Sample-064	599	0.13
511162	Zircon_Sample-065	993	0.04
511162	Zircon_Sample-066	1035	0.03
511162	Zircon_Sample-067	829	0.03
511162	Zircon_Sample-072	834	0.04
511162	Zircon_Sample-074	679	0.22
511162	Zircon_Sample-075	946	0.03
511162	Zircon_Sample-076	360	0.80
511162	Zircon_Sample-077	362	0.34
511162	Zircon_Sample-078	689	0.07
511162	Zircon_Sample-079	877	0.04
511162	Zircon_Sample-080	437	0.19
511162	Zircon_Sample-086	126	0.51
511162	Zircon_Sample-087	785	0.03
511162	Zircon_Sample-088	495	0.60
511162	Zircon_Sample-089	390	0.46
511162	Zircon_Sample-099	717	0.57
511162	Zircon_Sample-100	480	0.28
511162	Zircon_Sample-101	506	0.46
511162	Zircon_Sample-102	729	0.67
511162	Zircon_Sample-104	708	0.08
511162	Zircon_Sample-105	573	1.78
511162	Zircon_Sample-111	322	0.46
511162	Zircon_Sample-112	1050	0.03
511162	Zircon_Sample-113	1026	0.01
511162	Zircon_Sample-115	700	0.05

Sample	Analysis	U (ppm) ^a	Th/U ^a
511162	Zircon_Sample-116	864	0.09
511162	Zircon_Sample-117	230	0.67
511162	Zircon_Sample-118	610	0.41
511162	Zircon_Sample-119	1156	0.02
511162	Zircon_Sample-124	296	0.53
511162	Zircon_Sample-127	512	0.17
511162	Zircon_Sample-129	375	0.42
511162	Zircon_Sample-130	276	0.65
511162	Zircon_Sample-131	1427	0.02
511162	Zircon_Sample-132	318	0.49
511162	Zircon_Sample-137	1202	0.03
511162	Zircon_Sample-138	1165	0.02
511162	Zircon_Sample-139	1318	0.03
511162	Zircon_Sample-140	551	0.04
511162	Zircon_Sample-141	1411	0.02
511162	Zircon_Sample-142	1090	0.02
511162	Zircon_Sample-143	266	0.40
511162	Zircon_Sample-144	170	0.72
511162	Zircon_Sample-145	439	0.01
511162	Zircon_Sample-150	896	0.02
511162	Zircon_Sample-151	714	0.01
511162	Zircon_Sample-152	444	0.47
511162	Zircon_Sample-153	1124	0.03
511162	Zircon_Sample-154	774	0.03
511162	Zircon_Sample-155	809	0.03
511162	Zircon_Sample-156	928	0.04
511162	Zircon_Sample-157	515	0.33
511162	Zircon_Sample-158	552	0.55
511162	Zircon_Sample-159	625	0.84
511197	Zircon_sample-008	248	0.73
511197	Zircon_sample-009	375	0.36
511197	Zircon_sample-011	148	1.20
511197	Zircon_sample-013	421	0.13
511197	Zircon_sample-014	341	0.16
511197	Zircon_sample-020	191	1.51
511197	Zircon_sample-021	815	0.11
511197	Zircon_sample-023	891	0.03
511197	Zircon_sample-024	834	0.18
511197	Zircon_sample-025	78	1.20
511197	Zircon_sample-033	204	0.94
511197	Zircon_sample-034	553	0.51
511197	Zircon_sample-035	900	0.39
511197	Zircon_sample-036	228	0.72
511197	Zircon_sample-037	548	0.31
511197	Zircon_sample-038	801	0.28
511197	Zircon_sample-046	349	0.77
511197	Zircon_Sample-047	138	0.60
511197	Zircon_Sample-048	68	0.68
511197	Zircon_Sample-049	400	0.45
511197	Zircon_Sample-052	510	0.30
511197	Zircon_Sample-053	377	0.51
511197	Zircon_Sample-054	363	0.44
511197	Zircon_Sample-059	812	0.05
511197	Zircon_Sample-060	699	0.18
511197	Zircon_Sample-061	373	0.31
511197	Zircon_Sample-062	104	0.97
511197	Zircon_Sample-064	159	0.28
511197	Zircon_Sample-065	857	0.54

Sample	Analysis	U (ppm) ^a	Th/U ^a
511197	Zircon_Sample-066	1203	0.26
511197	Zircon_Sample-067	340	0.77
511197	Zircon_Sample-073	390	0.66
511197	Zircon_Sample-074	776	0.22
511197	Zircon_Sample-077	506	0.14
511197	Zircon_Sample-078	345	0.49
511197	Zircon_Sample-085	860	0.21
511197	Zircon_Sample-087	165	0.64
511197	Zircon_Sample-088	1112	0.11
511197	Zircon_Sample-089	914	0.17
511197	Zircon_Sample-091	1091	0.13
511197	Zircon_Sample-092	86	0.42
511197	Zircon_Sample-099	463	0.89
511197	Zircon_Sample-100	317	0.46
511197	Zircon_Sample-101	177	0.32
511197	Zircon_Sample-102	359	0.90
511197	Zircon_Sample-103	704	0.20
511197	Zircon_Sample-104	201	0.43
511197	Zircon_Sample-105	410	0.99
511197	Zircon_Sample-106	478	0.40
511197	Zircon_Sample-112	586	0.40
511197	Zircon_Sample-115	1513	0.11
511197	Zircon_Sample-117	590	0.21
511197	Zircon_Sample-125	822	0.04
511197	Zircon_Sample-126	470	0.25
511197	Zircon_Sample-129	283	0.53
511197	Zircon_Sample-137	646	0.06
511197	Zircon_Sample-140	743	0.22
511197	Zircon_Sample-143	703	0.07
511197	Zircon_Sample-145	561	0.42
511197	Zircon_Sample-150	557	0.38
511197	Zircon_Sample-151	1471	0.06
511197	Zircon_Sample-153	97	0.96
511197	Zircon_Sample-154	375	0.29
511197	Zircon_Sample-155	186	0.75
511197	Zircon_Sample-156	315	0.72
511197	Zircon_Sample-163	1018	0.43
511197	Zircon_Sample-165	1071	0.09
511197	Zircon_Sample-167	299	0.55
511197	Zircon_Sample-168	634	0.43
511197	Zircon_Sample-169	550	0.18
511197	Zircon_Sample-171	463	0.47

	RATIOS						
Sample	$^{207}\text{Pb}/^{235}\text{U}^b$	$2\sigma^d$	$^{206}\text{Pb}/^{238}\text{U}^b$	$2\sigma^d$	ρ^c	$^{207}\text{Pb}/^{206}\text{Pb}^e$	$2\sigma^d$
468768	15.34	1.27	0.53	0.04	0.90	0.212	0.008
468768	15.46	1.09	0.53	0.03	0.78	0.210	0.009
468768	16.21	1.22	0.56	0.04	0.97	0.210	0.004
468768	15.21	1.59	0.52	0.05	0.97	0.213	0.005
468768	15.41	1.18	0.53	0.03	0.80	0.209	0.010
468768	15.34	1.40	0.53	0.04	0.91	0.208	0.008
468768	15.08	1.65	0.53	0.05	0.96	0.208	0.007
468768	16.08	2.05	0.55	0.07	0.97	0.213	0.007
468768	16.87	1.40	0.59	0.04	0.88	0.208	0.008
468768	16.14	1.63	0.55	0.05	0.95	0.212	0.006
468768	15.84	1.42	0.55	0.04	0.88	0.208	0.009
468768	14.65	1.46	0.50	0.05	0.92	0.213	0.008
468768	15.73	1.35	0.55	0.04	0.87	0.207	0.009
468768	13.59	1.54	0.47	0.05	0.96	0.211	0.007
468768	14.78	1.31	0.51	0.04	0.95	0.209	0.006
468768	15.76	1.43	0.55	0.04	0.85	0.209	0.010
468768	16.79	1.38	0.57	0.04	0.90	0.212	0.008
468768	15.35	1.20	0.54	0.04	0.93	0.208	0.006
468768	16.21	1.36	0.56	0.04	0.92	0.209	0.007
468768	15.62	1.17	0.54	0.04	0.89	0.208	0.007
468768	16.52	1.45	0.56	0.04	0.90	0.213	0.008
468768	15.20	1.06	0.53	0.03	0.94	0.208	0.005
468768	15.53	1.75	0.54	0.06	0.93	0.210	0.009
468768	16.04	0.95	0.56	0.03	0.92	0.209	0.005
468768	15.46	1.30	0.53	0.04	0.92	0.211	0.007
468768	15.30	0.96	0.53	0.03	0.94	0.210	0.004
468768	16.36	1.30	0.56	0.04	0.91	0.210	0.007
468768	15.96	1.49	0.55	0.05	0.94	0.209	0.007
468768	16.75	1.35	0.58	0.04	0.87	0.209	0.008
468768	16.60	1.37	0.57	0.04	0.95	0.209	0.006
468768	16.04	1.02	0.55	0.03	0.92	0.210	0.005
468768	18.24	1.75	0.63	0.06	0.91	0.208	0.008
468768	16.36	1.44	0.56	0.05	0.92	0.211	0.007
468768	17.47	1.32	0.61	0.04	0.88	0.208	0.008
468768	16.06	0.91	0.56	0.03	0.92	0.209	0.005
468768	16.69	0.85	0.58	0.02	0.85	0.210	0.006
468768	16.92	1.13	0.59	0.04	0.94	0.209	0.005
468768	17.30	1.24	0.59	0.04	0.92	0.212	0.006
468768	15.88	0.79	0.55	0.03	0.93	0.210	0.004
468768	15.51	0.87	0.54	0.02	0.72	0.210	0.008
468768	16.10	1.12	0.56	0.03	0.79	0.209	0.009
468768	15.69	1.06	0.54	0.03	0.92	0.210	0.005
468768	16.48	1.34	0.57	0.04	0.91	0.210	0.007
468768	17.24	1.35	0.59	0.04	0.88	0.214	0.008
468768	15.74	1.08	0.54	0.04	0.95	0.211	0.005
468768	16.43	1.34	0.56	0.04	0.87	0.212	0.008
468768	16.93	1.58	0.58	0.05	0.94	0.213	0.007
468768	16.53	1.38	0.57	0.05	0.96	0.209	0.005
468768	17.58	1.28	0.60	0.04	0.88	0.211	0.007
468768	15.46	1.49	0.54	0.05	0.93	0.209	0.007
468768	17.57	1.26	0.60	0.04	0.93	0.211	0.006
468768	16.11	1.46	0.55	0.05	0.97	0.211	0.005
468768	16.57	1.22	0.57	0.04	0.88	0.210	0.007
468768	16.39	1.67	0.56	0.05	0.94	0.212	0.007
468768	15.87	0.96	0.55	0.03	0.88	0.210	0.006
468768	15.62	1.58	0.54	0.05	0.90	0.209	0.009

Sample	$^{207}\text{Pb}/^{235}\text{U}^b$	$2\sigma^d$	$^{206}\text{Pb}/^{238}\text{U}^b$	$2\sigma^d$	ρ^c	$^{207}\text{Pb}/^{206}\text{Pb}^e$	$2\sigma^d$
468768	15.08	1.12	0.52	0.03	0.86	0.209	0.008
468768	16.20	0.85	0.55	0.03	0.92	0.212	0.004
468768	15.96	0.70	0.55	0.02	0.78	0.210	0.006
468768	15.77	0.73	0.54	0.02	0.94	0.211	0.003
468768	15.76	0.63	0.55	0.02	0.92	0.206	0.003
468768	17.22	0.47	0.60	0.01	0.87	0.210	0.003
468768	16.30	0.67	0.57	0.02	0.77	0.207	0.005
468768	15.65	1.33	0.54	0.04	0.94	0.211	0.006
468768	14.03	0.77	0.48	0.02	0.95	0.211	0.004
468768	17.09	0.70	0.59	0.02	0.89	0.209	0.004
468768	16.06	1.00	0.55	0.03	0.87	0.212	0.006
468768	17.32	1.14	0.60	0.04	0.93	0.209	0.005
468768	16.88	1.13	0.58	0.04	0.95	0.212	0.005
468768	17.62	0.52	0.61	0.02	0.88	0.211	0.003
468768	15.37	0.53	0.53	0.02	0.86	0.210	0.004
508255	12.34	1.89	0.48	0.07	0.96	0.188	0.008
508255	13.56	1.89	0.50	0.07	0.96	0.198	0.008
508255	16.22	1.87	0.59	0.06	0.92	0.198	0.009
508255	13.93	1.26	0.48	0.04	0.83	0.210	0.010
508255	12.53	1.77	0.48	0.06	0.93	0.188	0.010
508255	14.09	1.91	0.48	0.06	0.93	0.212	0.010
508255	15.08	1.19	0.57	0.04	0.91	0.191	0.006
508255	13.30	2.18	0.46	0.07	0.97	0.209	0.009
508255	15.38	1.66	0.53	0.05	0.91	0.212	0.009
508255	9.46	1.68	0.36	0.06	0.97	0.189	0.008
508255	16.80	1.39	0.58	0.04	0.84	0.208	0.009
508255	15.32	1.18	0.54	0.03	0.83	0.206	0.009
508255	12.59	2.09	0.47	0.07	0.95	0.192	0.010
508255	15.74	1.16	0.57	0.04	0.92	0.200	0.006
508255	15.14	1.48	0.52	0.05	0.88	0.210	0.010
508255	15.28	1.50	0.54	0.05	0.89	0.204	0.009
508255	12.88	2.53	0.47	0.09	0.97	0.198	0.009
508255	16.20	1.33	0.57	0.04	0.89	0.208	0.008
508255	12.39	1.64	0.47	0.06	0.96	0.189	0.007
508255	14.05	2.08	0.53	0.07	0.93	0.193	0.010
508255	14.80	1.34	0.56	0.04	0.83	0.193	0.010
508255	14.24	1.93	0.50	0.06	0.95	0.206	0.009
508255	14.99	1.34	0.52	0.04	0.91	0.211	0.008
508255	14.06	1.59	0.49	0.05	0.92	0.207	0.009
508255	12.87	2.21	0.49	0.08	0.96	0.189	0.010
508255	14.46	1.55	0.57	0.05	0.89	0.183	0.009
508255	15.12	1.37	0.53	0.04	0.87	0.208	0.009
508255	14.86	1.96	0.52	0.06	0.95	0.209	0.009
508255	16.29	1.10	0.57	0.03	0.78	0.207	0.009
508255	14.83	1.36	0.52	0.04	0.92	0.207	0.007
508255	13.69	1.73	0.49	0.06	0.96	0.203	0.007
508255	14.42	1.50	0.53	0.05	0.90	0.198	0.009
508255	13.99	1.77	0.53	0.06	0.95	0.193	0.008
508255	12.03	1.61	0.47	0.06	0.98	0.184	0.005
508255	12.67	1.95	0.51	0.08	0.98	0.181	0.005
508255	11.50	3.02	0.41	0.11	0.99	0.204	0.009
508255	13.51	1.62	0.53	0.06	0.94	0.185	0.007
508255	12.18	2.35	0.44	0.08	0.98	0.202	0.008
508255	10.51	2.66	0.37	0.09	0.98	0.204	0.010
508255	15.79	1.65	0.53	0.05	0.82	0.218	0.013
508255	12.10	1.98	0.45	0.07	0.97	0.196	0.008
508255	15.14	2.61	0.53	0.09	0.98	0.207	0.007
508255	11.72	1.40	0.45	0.05	0.97	0.189	0.005

Sample	$^{207}\text{Pb}/^{235}\text{U}^b$	$2\sigma^d$	$^{206}\text{Pb}/^{238}\text{U}^b$	$2\sigma^d$	ρ^c	$^{207}\text{Pb}/^{206}\text{Pb}^e$	$2\sigma^d$
508255	12.63	1.19	0.50	0.04	0.92	0.185	0.007
508255	14.51	3.20	0.52	0.11	0.96	0.201	0.012
508255	13.79	1.97	0.50	0.06	0.91	0.200	0.012
508255	13.49	2.52	0.52	0.09	0.98	0.189	0.007
508255	15.59	1.58	0.56	0.05	0.96	0.200	0.006
508255	11.68	1.59	0.44	0.06	0.98	0.191	0.005
508255	15.45	2.19	0.55	0.07	0.92	0.205	0.011
508255	12.08	1.18	0.47	0.04	0.96	0.184	0.005
508255	15.79	1.55	0.56	0.05	0.92	0.204	0.008
508255	16.10	1.37	0.54	0.04	0.86	0.217	0.009
508255	13.32	1.62	0.48	0.05	0.93	0.203	0.009
508255	13.02	1.99	0.49	0.07	0.97	0.192	0.007
508255	10.92	2.08	0.42	0.08	0.97	0.187	0.009
508255	16.84	1.54	0.60	0.05	0.92	0.204	0.007
508255	11.96	1.53	0.45	0.05	0.94	0.191	0.008
508255	16.48	1.61	0.58	0.05	0.93	0.207	0.008
508255	13.30	1.25	0.52	0.05	0.94	0.185	0.006
508255	13.55	1.30	0.52	0.04	0.87	0.190	0.009
508255	13.86	1.61	0.49	0.05	0.89	0.205	0.011
508255	15.38	1.58	0.53	0.05	0.94	0.209	0.007
508255	13.35	1.97	0.49	0.07	0.97	0.197	0.007
508255	16.18	1.03	0.58	0.03	0.83	0.204	0.007
508255	15.58	1.05	0.54	0.03	0.87	0.209	0.007
508255	14.40	1.13	0.50	0.04	0.94	0.209	0.006
508255	13.51	0.93	0.51	0.03	0.80	0.193	0.008
508255	15.09	1.05	0.51	0.03	0.90	0.213	0.006
508255	15.16	1.48	0.53	0.04	0.87	0.207	0.010
508255	14.60	1.48	0.50	0.05	0.92	0.211	0.008
508255	11.85	1.45	0.44	0.05	0.96	0.194	0.006
508255	15.63	1.77	0.55	0.05	0.87	0.207	0.012
508255	16.21	1.10	0.54	0.03	0.74	0.216	0.010
508255	15.77	1.86	0.56	0.06	0.96	0.206	0.007
508255	15.36	1.41	0.56	0.05	0.91	0.199	0.007
508255	13.53	1.29	0.51	0.04	0.93	0.194	0.007
508255	12.70	1.93	0.48	0.07	0.95	0.192	0.009
508255	15.42	1.80	0.59	0.06	0.91	0.190	0.009
508255	15.20	1.40	0.51	0.04	0.92	0.215	0.008
508255	15.16	1.48	0.55	0.05	0.95	0.200	0.006
508255	14.92	1.43	0.52	0.05	0.92	0.206	0.008
508255	16.12	1.40	0.57	0.05	0.93	0.205	0.006
508255	14.76	0.77	0.52	0.02	0.81	0.205	0.006
508255	13.26	1.92	0.50	0.07	0.98	0.192	0.006
508255	14.63	2.79	0.53	0.10	0.99	0.201	0.006
510826	17.57	0.63	0.61	0.02	0.90	0.209	0.003
510826	15.63	0.76	0.55	0.03	0.95	0.208	0.003
510826	14.69	1.25	0.53	0.04	0.95	0.201	0.005
510826	15.30	1.19	0.56	0.04	0.89	0.199	0.007
510826	17.16	0.90	0.59	0.03	0.90	0.209	0.005
510826	16.26	1.06	0.60	0.04	0.93	0.197	0.005
510826	14.47	0.74	0.57	0.03	0.95	0.184	0.003
510826	15.25	1.07	0.53	0.04	0.95	0.208	0.005
510826	15.42	1.21	0.52	0.04	0.92	0.216	0.007
510826	14.43	3.62	0.53	0.13	0.99	0.196	0.007
510826	13.71	2.55	0.54	0.10	0.99	0.184	0.005
510826	12.13	2.15	0.47	0.08	1.00	0.189	0.003
510826	15.82	1.26	0.58	0.04	0.86	0.197	0.008
510826	12.07	1.23	0.47	0.05	0.99	0.186	0.003
510826	13.16	1.31	0.47	0.04	0.90	0.203	0.009

Sample	$^{207}\text{Pb}/^{235}\text{U}^b$	$2\sigma^d$	$^{206}\text{Pb}/^{238}\text{U}^b$	$2\sigma^d$	ρ^c	$^{207}\text{Pb}/^{206}\text{Pb}^e$	$2\sigma^d$
510826	15.52	0.75	0.53	0.02	0.87	0.212	0.005
510826	16.52	1.75	0.59	0.06	0.92	0.203	0.008
510826	17.13	0.99	0.58	0.03	0.93	0.213	0.004
510826	15.07	0.69	0.52	0.02	0.94	0.211	0.003
510826	10.36	1.46	0.39	0.05	0.97	0.194	0.007
510826	13.90	0.97	0.53	0.03	0.94	0.189	0.005
510826	11.73	1.52	0.43	0.05	0.94	0.197	0.009
510826	13.24	0.89	0.50	0.03	0.98	0.191	0.003
510826	12.75	1.70	0.48	0.06	0.99	0.193	0.004
510826	14.09	1.02	0.52	0.04	0.96	0.195	0.004
510826	10.70	1.34	0.41	0.05	0.99	0.189	0.003
510826	15.25	1.43	0.54	0.05	0.89	0.203	0.009
510826	14.43	0.87	0.52	0.03	0.96	0.202	0.003
510826	14.18	2.92	0.53	0.11	0.99	0.193	0.006
510826	15.47	1.06	0.54	0.03	0.93	0.209	0.005
510826	17.87	1.09	0.61	0.03	0.94	0.213	0.004
510826	14.62	1.11	0.52	0.03	0.86	0.204	0.008
510826	15.17	0.86	0.54	0.03	0.86	0.204	0.006
510826	16.13	0.75	0.55	0.02	0.93	0.211	0.004
510826	15.39	1.17	0.54	0.04	0.90	0.207	0.007
510826	16.12	1.07	0.56	0.03	0.94	0.208	0.005
510826	16.82	0.70	0.58	0.02	0.83	0.210	0.005
510826	17.46	1.02	0.61	0.03	0.92	0.209	0.005
510826	16.53	1.33	0.57	0.04	0.97	0.209	0.004
510831	12.55	1.52	0.46	0.05	0.87	0.198	0.012
510831	12.30	1.04	0.48	0.04	0.90	0.188	0.007
510831	12.11	1.03	0.46	0.03	0.83	0.190	0.009
510831	14.62	1.75	0.49	0.05	0.92	0.215	0.010
510831	13.46	1.28	0.51	0.04	0.91	0.191	0.007
510831	13.59	1.32	0.48	0.04	0.85	0.206	0.010
510831	15.24	1.45	0.54	0.04	0.86	0.205	0.010
510831	14.13	1.06	0.49	0.03	0.87	0.211	0.008
510831	13.80	1.68	0.46	0.05	0.89	0.219	0.012
510831	13.20	1.27	0.51	0.05	0.93	0.189	0.007
510831	15.01	1.30	0.58	0.04	0.84	0.186	0.009
510831	13.66	1.15	0.52	0.04	0.92	0.192	0.007
510831	12.80	1.51	0.48	0.05	0.87	0.192	0.011
510831	12.38	1.95	0.48	0.07	0.93	0.188	0.011
510831	17.72	1.51	0.58	0.04	0.78	0.220	0.012
510831	14.70	1.24	0.51	0.04	0.84	0.209	0.010
510831	13.34	0.75	0.52	0.02	0.85	0.187	0.006
510831	15.08	1.18	0.53	0.03	0.84	0.207	0.009
510831	14.26	1.04	0.55	0.03	0.77	0.190	0.009
510831	14.41	1.54	0.48	0.04	0.84	0.217	0.012
510831	14.73	1.11	0.51	0.03	0.74	0.208	0.010
510831	14.34	1.85	0.49	0.06	0.91	0.212	0.011
510831	12.77	1.08	0.49	0.04	0.89	0.188	0.007
510831	13.78	1.01	0.53	0.03	0.87	0.188	0.007
510831	18.40	2.64	0.60	0.08	0.96	0.224	0.009
510831	13.11	1.49	0.50	0.05	0.90	0.190	0.009
510831	14.11	1.64	0.49	0.05	0.90	0.209	0.010
510831	15.98	1.39	0.54	0.04	0.79	0.213	0.011
510831	14.35	1.36	0.56	0.04	0.79	0.187	0.011
510831	12.99	1.37	0.50	0.04	0.85	0.187	0.011
511162	16.91	2.23	0.58	0.07	0.97	0.210	0.007
511162	14.58	1.75	0.54	0.06	0.93	0.194	0.009
511162	14.11	1.25	0.55	0.04	0.90	0.186	0.007
511162	17.69	1.90	0.63	0.06	0.96	0.205	0.006

Sample	$^{207}\text{Pb}/^{235}\text{U}^b$	$2\sigma^d$	$^{206}\text{Pb}/^{238}\text{U}^b$	$2\sigma^d$	ρ^c	$^{207}\text{Pb}/^{206}\text{Pb}^e$	$2\sigma^d$
511162	15.01	1.77	0.55	0.06	0.90	0.198	0.010
511162	15.35	1.77	0.53	0.06	0.97	0.209	0.006
511162	17.30	1.37	0.61	0.04	0.89	0.207	0.008
511162	13.87	1.08	0.56	0.04	0.93	0.181	0.005
511162	16.53	1.60	0.60	0.06	0.96	0.201	0.006
511162	16.13	1.64	0.57	0.05	0.88	0.207	0.010
511162	13.20	1.43	0.51	0.05	0.97	0.189	0.005
511162	16.62	1.75	0.58	0.06	0.92	0.207	0.008
511162	14.22	1.18	0.56	0.04	0.93	0.185	0.006
511162	17.33	1.63	0.61	0.05	0.92	0.206	0.007
511162	15.80	0.87	0.55	0.03	0.87	0.207	0.006
511162	17.00	1.63	0.60	0.05	0.90	0.207	0.009
511162	16.58	1.39	0.58	0.04	0.90	0.208	0.008
511162	13.98	1.33	0.55	0.05	0.92	0.185	0.007
511162	14.21	1.64	0.53	0.05	0.89	0.196	0.010
511162	14.54	1.32	0.53	0.04	0.92	0.200	0.007
511162	12.43	1.18	0.50	0.04	0.92	0.181	0.007
511162	18.41	1.47	0.64	0.04	0.76	0.210	0.011
511162	17.80	1.08	0.61	0.03	0.88	0.210	0.006
511162	13.86	0.89	0.54	0.03	0.87	0.188	0.006
511162	14.95	1.02	0.57	0.03	0.76	0.189	0.008
511162	13.96	1.34	0.54	0.05	0.91	0.189	0.007
511162	14.91	1.01	0.55	0.04	0.94	0.195	0.004
511162	16.46	0.90	0.57	0.03	0.83	0.210	0.006
511162	15.53	1.14	0.54	0.04	0.94	0.209	0.005
511162	13.32	1.61	0.47	0.05	0.92	0.205	0.010
511162	14.14	0.92	0.55	0.03	0.94	0.185	0.004
511162	16.18	1.44	0.58	0.05	0.89	0.204	0.008
511162	15.75	1.27	0.54	0.04	0.95	0.210	0.005
511162	13.77	1.09	0.55	0.04	0.94	0.182	0.005
511162	16.11	0.95	0.58	0.03	0.84	0.202	0.006
511162	14.19	1.16	0.55	0.04	0.92	0.186	0.006
511162	12.97	1.95	0.50	0.07	0.98	0.189	0.005
511162	14.52	1.25	0.57	0.05	0.94	0.184	0.006
511162	13.31	1.22	0.53	0.05	0.94	0.181	0.006
511162	13.35	0.95	0.53	0.04	0.93	0.183	0.005
511162	13.07	1.02	0.52	0.04	0.95	0.183	0.004
511162	16.33	1.76	0.58	0.06	0.93	0.204	0.008
511162	14.37	0.86	0.57	0.03	0.93	0.182	0.004
511162	17.67	1.43	0.61	0.05	0.96	0.211	0.005
511162	14.18	1.32	0.53	0.04	0.91	0.195	0.008
511162	14.02	1.18	0.54	0.04	0.96	0.189	0.004
511162	14.60	1.38	0.57	0.05	0.91	0.186	0.007
511162	14.97	1.94	0.57	0.07	0.98	0.191	0.005
511162	15.58	2.13	0.53	0.07	0.90	0.213	0.013
511162	14.77	1.55	0.57	0.05	0.91	0.187	0.008
511162	18.33	2.50	0.63	0.08	0.93	0.211	0.011
511162	17.67	1.90	0.62	0.06	0.88	0.206	0.011
511162	17.11	1.42	0.61	0.04	0.86	0.205	0.009
511162	15.80	2.14	0.57	0.07	0.90	0.201	0.012
511162	15.68	1.92	0.55	0.06	0.94	0.207	0.009
511162	15.44	2.92	0.52	0.09	0.96	0.213	0.012
511162	15.86	2.88	0.60	0.10	0.95	0.192	0.011
511162	8.39	0.95	0.31	0.03	0.94	0.199	0.008
511162	16.72	2.15	0.58	0.07	0.93	0.210	0.010
511162	12.15	1.27	0.48	0.05	0.91	0.182	0.008
511162	13.48	1.15	0.53	0.04	0.88	0.185	0.007
511162	14.32	1.18	0.56	0.04	0.81	0.185	0.009

Sample	$^{207}\text{Pb}/^{235}\text{U}^b$	$2\sigma^d$	$^{206}\text{Pb}/^{238}\text{U}^b$	$2\sigma^d$	ρ^c	$^{207}\text{Pb}/^{206}\text{Pb}^e$	$2\sigma^d$
511162	15.30	1.62	0.58	0.05	0.86	0.191	0.010
511162	18.69	1.37	0.64	0.04	0.84	0.212	0.008
511162	15.23	1.34	0.53	0.04	0.94	0.210	0.007
511162	13.76	1.41	0.54	0.05	0.94	0.184	0.006
511162	15.80	1.89	0.55	0.06	0.92	0.207	0.010
511162	14.82	1.57	0.56	0.05	0.90	0.193	0.009
511162	16.44	1.32	0.58	0.04	0.93	0.207	0.006
511162	15.82	1.72	0.54	0.05	0.84	0.212	0.013
511162	13.27	1.27	0.52	0.04	0.86	0.186	0.009
511162	16.64	1.38	0.57	0.04	0.88	0.211	0.008
511162	13.73	1.76	0.54	0.06	0.90	0.185	0.010
511162	10.82	1.92	0.42	0.07	0.99	0.187	0.005
511162	12.26	1.59	0.49	0.06	0.94	0.182	0.008
511162	11.77	2.67	0.45	0.10	0.99	0.188	0.006
511162	12.21	1.60	0.48	0.06	0.91	0.186	0.010
511162	12.34	1.29	0.48	0.05	0.97	0.185	0.005
511162	14.77	1.21	0.52	0.04	0.88	0.204	0.008
511162	16.38	1.29	0.56	0.04	0.89	0.212	0.008
511162	12.68	1.20	0.49	0.04	0.87	0.187	0.009
511162	12.86	1.87	0.50	0.07	0.94	0.185	0.009
511162	11.93	1.64	0.47	0.06	0.95	0.183	0.008
511162	15.93	4.73	0.58	0.17	0.98	0.201	0.010
511162	14.08	1.52	0.55	0.06	0.94	0.185	0.007
511162	12.25	1.20	0.49	0.04	0.93	0.183	0.006
511162	14.04	1.19	0.56	0.04	0.91	0.183	0.006
511162	13.79	1.66	0.54	0.06	0.95	0.186	0.007
511162	15.78	1.61	0.57	0.05	0.93	0.202	0.008
511162	11.65	1.96	0.46	0.07	0.96	0.184	0.009
511162	14.84	1.94	0.51	0.06	0.94	0.210	0.010
511197	14.37	1.43	0.45	0.04	0.90	0.232	0.010
511197	17.56	3.70	0.52	0.11	0.99	0.246	0.006
511197	13.02	1.08	0.47	0.04	0.97	0.200	0.004
511197	8.87	1.68	0.34	0.06	0.98	0.189	0.007
511197	9.27	3.23	0.30	0.10	1.00	0.226	0.007
511197	14.59	1.10	0.51	0.03	0.88	0.206	0.007
511197	12.38	0.99	0.48	0.04	0.91	0.186	0.006
511197	12.76	0.76	0.50	0.03	0.95	0.184	0.004
511197	14.56	1.13	0.51	0.03	0.82	0.206	0.009
511197	13.18	1.12	0.48	0.04	0.93	0.200	0.006
511197	12.39	1.21	0.47	0.04	0.92	0.190	0.007
511197	13.08	0.83	0.48	0.03	0.84	0.199	0.007
511197	6.58	1.35	0.22	0.04	0.95	0.218	0.013
511197	15.23	1.95	0.55	0.07	0.98	0.202	0.005
511197	14.97	2.05	0.56	0.08	0.98	0.193	0.005
511197	6.45	0.65	0.23	0.02	0.91	0.199	0.009
511197	12.97	1.11	0.47	0.04	0.92	0.198	0.006
511197	11.97	0.98	0.43	0.03	0.98	0.204	0.004
511197	14.89	1.89	0.53	0.06	0.95	0.203	0.008
511197	12.12	1.35	0.44	0.04	0.86	0.201	0.011
511197	16.44	1.26	0.59	0.04	0.92	0.203	0.006
511197	15.14	1.06	0.54	0.04	0.97	0.203	0.004
511197	16.79	1.00	0.59	0.03	0.94	0.205	0.004
511197	11.85	1.09	0.44	0.04	0.90	0.196	0.008
511197	6.78	1.56	0.27	0.06	0.98	0.184	0.009
511197	7.56	1.21	0.27	0.04	0.98	0.202	0.006
511197	11.60	1.58	0.41	0.05	0.94	0.205	0.010
511197	8.43	1.02	0.30	0.04	0.97	0.201	0.006
511197	11.59	1.25	0.39	0.04	0.88	0.213	0.011

Sample	$^{207}\text{Pb}/^{235}\text{U}^b$	$2\sigma^d$	$^{206}\text{Pb}/^{238}\text{U}^b$	$2\sigma^d$	ρ^c	$^{207}\text{Pb}/^{206}\text{Pb}^e$	$2\sigma^d$
511197	9.10	1.83	0.33	0.06	0.96	0.199	0.011
511197	8.63	0.59	0.29	0.01	0.72	0.219	0.011
511197	14.62	0.85	0.47	0.02	0.91	0.227	0.006
511197	8.78	1.58	0.32	0.06	0.99	0.198	0.005
511197	9.49	0.61	0.35	0.02	0.93	0.196	0.005
511197	12.76	2.57	0.49	0.10	0.99	0.189	0.005
511197	10.95	1.40	0.42	0.05	0.95	0.189	0.007
511197	16.13	2.61	0.60	0.09	0.96	0.194	0.008
511197	10.90	0.95	0.41	0.03	0.81	0.193	0.010
511197	12.61	1.26	0.44	0.04	0.87	0.208	0.010
511197	10.23	0.98	0.38	0.03	0.96	0.197	0.006
511197	13.95	1.96	0.49	0.07	0.97	0.208	0.007
511197	12.46	1.26	0.48	0.05	0.98	0.187	0.003
511197	12.67	1.07	0.49	0.04	0.87	0.189	0.008
511197	9.44	1.82	0.36	0.07	0.99	0.192	0.006
511197	13.08	1.19	0.49	0.04	0.95	0.195	0.005
511197	8.20	1.15	0.30	0.04	0.95	0.197	0.009
511197	13.18	1.33	0.47	0.04	0.89	0.204	0.009
511197	12.14	0.84	0.47	0.03	0.88	0.189	0.006
511197	7.84	1.12	0.30	0.04	0.98	0.187	0.006
511197	11.44	1.51	0.44	0.05	0.94	0.191	0.008
511197	3.63	0.74	0.15	0.03	0.98	0.175	0.007
511197	4.33	1.57	0.18	0.06	0.99	0.178	0.008
511197	15.56	0.80	0.58	0.03	0.83	0.193	0.006
511197	11.33	1.58	0.43	0.06	0.95	0.191	0.008
511197	12.38	0.80	0.49	0.03	0.95	0.185	0.004
511197	11.06	1.35	0.41	0.05	0.96	0.198	0.007
511197	11.02	1.26	0.40	0.04	0.90	0.199	0.010
511197	7.41	1.60	0.29	0.06	0.99	0.187	0.006
511197	10.80	1.08	0.41	0.04	0.95	0.193	0.006
511197	9.97	0.67	0.36	0.02	0.93	0.202	0.005
511197	7.85	1.69	0.31	0.07	0.98	0.183	0.007
511197	13.99	1.15	0.50	0.04	0.90	0.202	0.007
511197	10.17	1.00	0.36	0.03	0.94	0.203	0.007
511197	13.70	1.00	0.48	0.03	0.89	0.206	0.007
511197	8.37	1.64	0.31	0.06	0.99	0.198	0.006
511197	12.53	1.04	0.44	0.03	0.93	0.206	0.006
511197	12.93	0.70	0.50	0.02	0.89	0.188	0.005
511197	9.86	3.01	0.36	0.11	0.99	0.197	0.010
511197	8.48	0.77	0.32	0.03	0.92	0.191	0.007
511197	12.05	0.35	0.46	0.01	0.56	0.191	0.005
511197	12.41	1.22	0.44	0.04	0.87	0.203	0.010

Sample	AGES [Ma]						Conc. %
	$^{207}\text{Pb}/^{235}\text{U}$	2 σ	$^{206}\text{Pb}/^{238}\text{U}$	2 σ	$^{207}\text{Pb}/^{206}\text{Pb}$	2 σ	
468768	2837	79	2721	165	2920	60	96
468768	2844	68	2754	124	2909	71	97
468768	2889	72	2868	168	2904	32	99
468768	2829	100	2693	224	2926	42	95
468768	2841	73	2758	136	2901	75	97
468768	2836	87	2759	187	2892	60	97
468768	2820	105	2722	232	2891	53	97
468768	2882	123	2811	281	2932	54	98
468768	2928	80	2977	175	2894	63	102
468768	2885	97	2839	222	2918	49	98
468768	2867	86	2833	181	2892	69	99
468768	2793	95	2613	197	2926	63	94
468768	2861	82	2834	172	2879	69	99
468768	2722	107	2472	223	2912	51	91
468768	2801	85	2672	184	2895	45	95
468768	2862	87	2811	176	2898	78	98
468768	2923	79	2926	173	2921	59	100
468768	2837	75	2769	163	2886	47	98
468768	2889	80	2873	179	2900	53	99
468768	2854	72	2803	151	2890	56	98
468768	2908	84	2882	183	2925	63	99
468768	2828	66	2746	146	2887	39	97
468768	2848	108	2770	234	2904	69	97
468768	2879	57	2856	126	2896	38	99
468768	2844	80	2749	172	2912	54	97
468768	2834	60	2731	131	2908	34	96
468768	2898	76	2884	168	2908	52	100
468768	2874	90	2836	201	2901	53	99
468768	2921	78	2957	167	2896	64	101
468768	2912	79	2928	184	2901	43	101
468768	2879	61	2839	134	2907	41	99
468768	3002	93	3168	219	2893	64	106
468768	2898	84	2871	188	2917	55	99
468768	2961	73	3066	162	2890	59	104
468768	2880	54	2850	120	2901	36	99
468768	2917	49	2933	102	2907	43	101
468768	2930	64	2982	149	2895	38	102
468768	2952	69	2991	157	2925	46	101
468768	2870	47	2822	105	2903	30	98
468768	2847	54	2769	91	2903	64	97
468768	2883	67	2857	127	2901	69	99
468768	2858	64	2792	141	2905	42	98
468768	2905	78	2909	174	2903	55	100
468768	2948	75	2970	165	2933	59	101
468768	2861	66	2792	148	2910	36	98
468768	2902	78	2876	166	2920	64	99
468768	2931	89	2938	206	2927	53	100
468768	2908	80	2927	189	2895	38	101
468768	2967	70	3046	156	2914	55	103
468768	2844	92	2770	202	2897	58	97
468768	2966	69	3042	161	2916	43	103
468768	2883	87	2837	201	2916	38	98
468768	2910	70	2912	151	2909	57	100
468768	2900	98	2870	222	2921	57	99
468768	2869	58	2813	122	2908	46	98
468768	2854	97	2794	206	2896	73	98

Sample	$^{207}\text{Pb}/^{235}\text{U}$	2 σ	$^{206}\text{Pb}/^{238}\text{U}$	2 σ	$^{207}\text{Pb}/^{206}\text{Pb}$	2 σ	Conc. %
468768	2820	71	2712	142	2898	62	96
468768	2889	50	2845	111	2919	34	98
468768	2874	42	2825	79	2909	44	98
468768	2863	44	2789	98	2915	26	97
468768	2862	38	2843	85	2876	25	99
468768	2947	26	3011	57	2903	22	102
468768	2895	39	2914	74	2881	42	101
468768	2856	81	2773	180	2915	47	97
468768	2752	52	2540	109	2911	29	92
468768	2940	39	2998	88	2900	30	102
468768	2880	60	2819	124	2923	49	98
468768	2953	63	3035	148	2897	39	103
468768	2928	64	2937	150	2922	34	100
468768	2969	28	3056	63	2911	23	103
468768	2838	33	2742	66	2908	29	97
508255	2630	145	2508	304	2726	73	92
508255	2719	133	2595	286	2813	64	92
508255	2890	111	3005	254	2810	75	107
508255	2745	86	2534	157	2904	81	87
508255	2645	134	2544	277	2723	85	93
508255	2756	129	2541	266	2918	78	87
508255	2821	75	2921	167	2749	55	106
508255	2701	156	2445	323	2898	68	84
508255	2839	103	2725	219	2921	72	93
508255	2384	164	1999	297	2731	66	73
508255	2923	80	2968	167	2893	72	103
508255	2835	74	2779	145	2876	69	97
508255	2649	158	2504	328	2762	85	91
508255	2861	71	2911	158	2826	48	103
508255	2824	94	2716	191	2902	75	94
508255	2833	94	2800	198	2857	73	98
508255	2671	187	2497	396	2806	73	89
508255	2889	79	2889	170	2888	60	100
508255	2634	125	2505	266	2735	58	92
508255	2753	141	2728	307	2771	88	98
508255	2803	86	2851	173	2768	82	103
508255	2766	129	2620	277	2874	67	91
508255	2815	86	2681	178	2912	61	92
508255	2754	108	2583	222	2881	73	90
508255	2670	163	2589	350	2732	84	95
508255	2781	102	2925	224	2677	82	109
508255	2823	86	2727	175	2893	73	94
508255	2806	126	2681	273	2898	69	93
508255	2894	64	2913	123	2881	68	101
508255	2805	88	2693	187	2886	57	93
508255	2728	120	2565	258	2851	56	90
508255	2778	99	2732	210	2811	73	97
508255	2749	120	2725	266	2766	66	99
508255	2607	126	2504	272	2688	46	93
508255	2655	146	2648	329	2661	47	100
508255	2564	251	2205	486	2862	68	77
508255	2716	114	2744	252	2695	66	102
508255	2618	183	2343	371	2839	66	83
508255	2480	239	2046	437	2859	80	72
508255	2864	100	2723	191	2965	97	92
508255	2612	155	2384	317	2794	64	85
508255	2824	165	2748	379	2879	53	95
508255	2583	113	2396	233	2733	47	88

Sample	$^{207}\text{Pb}/^{235}\text{U}$	2 σ	$^{206}\text{Pb}/^{238}\text{U}$	2 σ	$^{207}\text{Pb}/^{206}\text{Pb}$	2 σ	Conc. %
508255	2653	89	2597	185	2696	62	96
508255	2784	213	2713	472	2835	95	96
508255	2736	136	2611	279	2829	97	92
508255	2715	178	2685	403	2737	59	98
508255	2852	97	2884	226	2830	45	102
508255	2579	128	2367	265	2750	43	86
508255	2844	136	2809	297	2868	91	98
508255	2610	92	2505	194	2693	45	93
508255	2864	94	2878	211	2855	61	101
508255	2883	82	2774	166	2960	70	94
508255	2703	115	2512	235	2849	75	88
508255	2681	145	2582	316	2757	61	94
508255	2516	179	2278	354	2715	76	84
508255	2926	88	3022	203	2860	58	106
508255	2602	120	2411	242	2754	70	88
508255	2905	94	2939	214	2881	60	102
508255	2701	89	2709	195	2695	54	101
508255	2719	91	2685	184	2744	77	98
508255	2740	111	2574	221	2865	85	90
508255	2839	98	2752	217	2902	56	95
508255	2705	140	2581	306	2799	54	92
508255	2888	61	2932	124	2857	57	103
508255	2851	64	2784	133	2899	53	96
508255	2777	75	2617	159	2895	44	90
508255	2716	65	2651	120	2764	68	96
508255	2821	66	2674	138	2927	48	91
508255	2826	94	2743	190	2885	79	95
508255	2790	97	2626	202	2910	63	90
508255	2593	115	2363	234	2778	54	85
508255	2855	109	2819	224	2880	92	98
508255	2889	65	2797	113	2954	74	95
508255	2863	113	2851	261	2871	54	99
508255	2838	88	2871	194	2814	61	102
508255	2718	90	2638	191	2777	59	95
508255	2658	144	2526	303	2760	74	92
508255	2842	112	2989	253	2739	81	109
508255	2828	88	2674	185	2940	58	91
508255	2825	94	2823	213	2827	49	100
508255	2810	92	2718	196	2876	61	95
508255	2884	83	2911	190	2865	50	102
508255	2800	49	2708	92	2867	50	94
508255	2699	137	2620	306	2758	47	95
508255	2791	183	2733	420	2834	47	96
510826	2966	35	3073	79	2895	25	106
510826	2855	46	2807	105	2888	26	97
510826	2795	81	2742	182	2835	42	97
510826	2834	74	2857	159	2818	58	101
510826	2944	51	3009	114	2900	37	104
510826	2892	62	3018	146	2805	39	108
510826	2781	49	2913	114	2687	27	108
510826	2831	67	2747	148	2891	37	95
510826	2842	75	2687	159	2953	49	91
510826	2778	243	2756	558	2794	61	99
510826	2730	178	2786	417	2689	44	104
510826	2614	167	2464	361	2732	26	90
510826	2866	76	2958	162	2802	67	106
510826	2610	95	2486	207	2708	23	92
510826	2691	94	2483	185	2851	70	87

Sample	$^{207}\text{Pb}/^{235}\text{U}$	2 σ	$^{206}\text{Pb}/^{238}\text{U}$	2 σ	$^{207}\text{Pb}/^{206}\text{Pb}$	2 σ	Conc. %
510826	2848	46	2746	95	2920	38	94
510826	2907	102	2991	233	2849	68	105
510826	2942	55	2968	128	2925	33	101
510826	2820	44	2690	95	2914	25	92
510826	2468	131	2113	245	2775	58	76
510826	2743	66	2760	147	2731	40	101
510826	2583	122	2317	236	2800	74	83
510826	2697	63	2622	141	2754	21	95
510826	2661	126	2527	275	2765	36	91
510826	2756	69	2714	153	2787	34	97
510826	2497	117	2220	235	2731	23	81
510826	2831	90	2800	189	2853	71	98
510826	2778	58	2692	128	2842	27	95
510826	2762	198	2758	457	2765	48	100
510826	2844	65	2774	143	2894	42	96
510826	2983	59	3064	140	2929	33	105
510826	2791	72	2701	145	2857	63	95
510826	2826	54	2778	110	2861	47	97
510826	2884	44	2839	99	2916	28	97
510826	2840	72	2779	155	2883	53	96
510826	2884	64	2872	144	2892	38	99
510826	2924	40	2947	82	2909	38	101
510826	2961	56	3057	132	2896	37	106
510826	2908	77	2926	183	2895	32	101
510831	2647	114	2443	213	2807	98	87
510831	2628	80	2508	159	2721	61	92
510831	2613	80	2449	145	2743	77	89
510831	2791	114	2588	235	2940	76	88
510831	2713	90	2663	189	2750	63	97
510831	2722	92	2525	174	2871	82	88
510831	2830	91	2782	186	2865	78	97
510831	2759	71	2557	137	2910	60	88
510831	2736	116	2428	219	2972	89	82
510831	2694	91	2646	194	2731	59	97
510831	2816	83	2963	174	2711	77	109
510831	2726	80	2678	170	2762	55	97
510831	2665	112	2540	216	2762	95	92
510831	2634	149	2514	304	2727	98	92
510831	2975	82	2965	159	2981	85	99
510831	2796	81	2656	154	2898	75	92
510831	2704	53	2685	104	2717	49	99
510831	2821	75	2730	147	2886	68	95
510831	2767	70	2804	129	2740	76	102
510831	2777	102	2532	189	2960	93	86
510831	2798	71	2670	122	2891	81	92
510831	2772	123	2569	250	2924	86	88
510831	2663	80	2585	161	2722	64	95
510831	2735	69	2748	143	2725	59	101
510831	3011	139	3014	332	3009	65	100
510831	2688	107	2619	220	2740	80	96
510831	2757	111	2565	223	2901	81	88
510831	2875	83	2803	157	2926	86	96
510831	2773	90	2848	172	2720	95	105
510831	2679	100	2625	193	2720	93	97
511162	2930	127	2963	304	2907	53	102
511162	2788	115	2800	254	2780	73	101
511162	2757	84	2825	182	2707	65	104
511162	2973	104	3132	255	2867	51	109

Sample	$^{207}\text{Pb}/^{235}\text{U}$	2 σ	$^{206}\text{Pb}/^{238}\text{U}$	2 σ	$^{207}\text{Pb}/^{206}\text{Pb}$	2 σ	Conc. %
511162	2816	113	2826	242	2809	85	101
511162	2837	111	2757	251	2895	48	95
511162	2952	76	3051	171	2885	59	106
511162	2741	74	2850	166	2662	49	107
511162	2908	93	3011	223	2837	47	106
511162	2885	98	2890	208	2881	79	100
511162	2694	102	2647	227	2730	47	97
511162	2913	101	2958	230	2882	66	103
511162	2765	79	2854	179	2700	50	106
511162	2953	91	3067	212	2876	59	107
511162	2865	53	2837	110	2884	44	98
511162	2935	92	3016	209	2879	67	105
511162	2911	80	2941	179	2890	59	102
511162	2748	91	2817	200	2698	62	104
511162	2764	110	2727	229	2790	86	98
511162	2785	87	2725	185	2830	59	96
511162	2638	89	2608	188	2661	60	98
511162	3011	77	3178	153	2902	83	109
511162	2979	58	3090	130	2905	47	106
511162	2740	61	2764	126	2723	51	101
511162	2812	65	2921	121	2735	73	107
511162	2747	91	2765	196	2733	65	101
511162	2810	64	2842	147	2787	37	102
511162	2904	52	2899	105	2907	50	100
511162	2848	70	2773	155	2901	41	96
511162	2703	115	2494	229	2863	79	87
511162	2759	62	2843	141	2698	36	105
511162	2887	85	2931	185	2857	67	103
511162	2862	77	2804	174	2903	40	97
511162	2734	75	2817	171	2673	44	105
511162	2883	56	2946	118	2840	51	104
511162	2762	78	2840	173	2706	53	105
511162	2678	143	2601	316	2736	48	95
511162	2784	82	2922	190	2686	50	109
511162	2702	87	2756	192	2662	53	104
511162	2705	67	2738	148	2679	43	102
511162	2685	74	2697	164	2676	39	101
511162	2896	103	2956	237	2855	65	104
511162	2775	57	2918	131	2672	36	109
511162	2972	78	3059	189	2914	36	105
511162	2762	89	2732	189	2783	64	98
511162	2751	80	2779	182	2730	39	102
511162	2790	90	2909	201	2704	66	108
511162	2813	124	2903	296	2750	47	106
511162	2851	131	2744	274	2928	98	94
511162	2800	100	2924	225	2712	70	108
511162	3007	132	3150	315	2913	83	108
511162	2972	104	3112	233	2878	83	108
511162	2941	80	3053	173	2866	70	107
511162	2865	130	2911	285	2833	98	103
511162	2857	117	2828	263	2878	68	98
511162	2843	182	2719	402	2932	90	93
511162	2868	175	3025	418	2760	91	110
511162	2274	103	1719	160	2819	65	61
511162	2919	124	2939	281	2905	79	101
511162	2616	99	2548	200	2669	73	95
511162	2714	81	2731	167	2701	66	101
511162	2771	78	2874	155	2697	79	107

Sample	$^{207}\text{Pb}/^{235}\text{U}$	2 σ	$^{206}\text{Pb}/^{238}\text{U}$	2 σ	$^{207}\text{Pb}/^{206}\text{Pb}$	2 σ	Conc. %
511162	2834	101	2952	215	2752	89	107
511162	3026	71	3190	156	2919	64	109
511162	2830	84	2727	183	2904	50	94
511162	2733	97	2789	218	2692	56	104
511162	2865	115	2837	252	2885	77	98
511162	2804	101	2849	221	2771	74	103
511162	2903	77	2935	177	2881	47	102
511162	2866	104	2789	206	2921	96	95
511162	2699	91	2691	181	2705	82	99
511162	2914	80	2913	171	2915	64	100
511162	2731	122	2772	260	2701	93	103
511162	2508	166	2259	334	2716	42	83
511162	2625	122	2570	257	2667	75	96
511162	2586	216	2409	453	2728	50	88
511162	2621	124	2509	248	2708	91	93
511162	2631	98	2544	212	2699	43	94
511162	2800	78	2718	161	2860	62	95
511162	2899	76	2867	163	2922	58	98
511162	2656	89	2582	174	2713	78	95
511162	2669	138	2626	294	2702	84	97
511162	2599	129	2493	270	2683	71	93
511162	2872	291	2933	691	2830	85	104
511162	2755	103	2834	233	2698	60	105
511162	2624	92	2549	192	2682	58	95
511162	2753	80	2853	177	2680	58	106
511162	2735	114	2774	256	2706	65	103
511162	2864	98	2890	221	2845	62	102
511162	2577	159	2441	328	2685	79	91
511162	2805	125	2666	267	2907	75	92
511197	2774	95	2395	179	3063	70	78
511197	2966	205	2689	461	3159	41	85
511197	2681	79	2490	166	2829	35	88
511197	2325	174	1891	304	2731	58	69
511197	2365	330	1676	513	3026	50	55
511197	2789	72	2672	145	2875	57	93
511197	2634	76	2544	153	2704	56	94
511197	2662	56	2624	121	2691	31	98
511197	2787	74	2669	139	2874	73	93
511197	2692	81	2523	165	2822	52	89
511197	2634	92	2499	185	2740	64	91
511197	2685	60	2512	110	2819	56	89
511197	2057	183	1276	227	2966	98	43
511197	2829	123	2811	287	2843	41	99
511197	2813	131	2883	313	2764	41	104
511197	2039	89	1360	112	2818	70	48
511197	2677	81	2504	164	2810	53	89
511197	2602	77	2290	155	2855	28	80
511197	2808	122	2754	272	2847	62	97
511197	2614	105	2336	189	2836	92	82
511197	2903	74	2983	169	2847	49	105
511197	2824	66	2784	152	2853	29	98
511197	2923	57	3003	135	2868	34	105
511197	2592	86	2344	162	2793	65	84
511197	2083	206	1527	305	2690	79	57
511197	2181	145	1548	217	2843	49	54
511197	2573	128	2219	240	2864	77	77
511197	2279	110	1713	175	2834	51	60
511197	2572	101	2144	173	2929	85	73

Sample	$^{207}\text{Pb}/^{235}\text{U}$	2 σ	$^{206}\text{Pb}/^{238}\text{U}$	2 σ	$^{207}\text{Pb}/^{206}\text{Pb}$	2 σ	Conc. %
511197	2348	186	1844	311	2820	89	65
511197	2300	63	1622	71	2972	77	55
511197	2791	55	2471	109	3031	39	82
511197	2316	166	1795	279	2813	41	64
511197	2386	59	1936	100	2796	38	69
511197	2662	192	2570	424	2732	46	94
511197	2519	120	2266	233	2729	65	83
511197	2885	156	3043	379	2776	70	110
511197	2515	81	2216	132	2766	84	80
511197	2651	94	2352	170	2887	81	81
511197	2456	89	2062	161	2800	46	74
511197	2746	134	2556	287	2889	57	88
511197	2640	95	2547	209	2712	31	94
511197	2655	80	2554	155	2733	68	93
511197	2382	179	1969	323	2757	50	71
511197	2686	86	2554	183	2786	46	92
511197	2254	128	1698	199	2805	73	61
511197	2693	95	2481	185	2856	74	87
511197	2615	65	2466	124	2733	55	90
511197	2213	129	1712	210	2716	51	63
511197	2560	124	2328	243	2749	72	85
511197	1555	165	901	169	2608	70	35
511197	1698	309	1045	349	2638	74	40
511197	2850	49	2968	102	2768	47	107
511197	2551	131	2303	257	2754	71	84
511197	2634	60	2553	129	2697	33	95
511197	2529	114	2197	218	2806	58	78
511197	2525	107	2174	190	2820	82	77
511197	2162	196	1626	307	2718	56	60
511197	2506	93	2199	176	2766	50	79
511197	2432	62	1971	106	2844	39	69
511197	2214	197	1749	325	2677	67	65
511197	2749	78	2625	159	2842	60	92
511197	2450	91	1995	159	2853	55	70
511197	2729	69	2534	136	2877	55	88
511197	2272	180	1724	293	2811	53	61
511197	2645	78	2354	153	2875	48	82
511197	2674	51	2613	104	2721	40	96
511197	2422	289	1995	517	2803	85	71
511197	2284	82	1802	130	2747	60	66
511197	2608	28	2425	33	2754	40	88
511197	2636	93	2369	169	2848	80	83

Paper III:

Origin of Mesoarchaeoan arc related
rocks with boninite/komatiite
affinities from southern West
Greenland

Lithos (in press)

DOI: 10.1016/j.lithos.2012.03.023

Origin of Mesoarchaeoan arc related rocks with boninite/komatiite affinities from southern West Greenland

Kristoffer Szilas^{a,b,c,*}, Tomas Næraa^a, Anders Scherstén^d, Henrik Stendal^e, Robert Frei^{b,f}, Vincent J. van Hinsberg^g, Thomas F. Kokfelt^a, Minik T. Rosing^{c,f}

^aGeological Survey of Denmark and Greenland - GEUS, Øster Voldgade 10, 1350, Copenhagen K, Denmark (ksz@geus.dk)

^bDepartment of Geography and Geology, University of Copenhagen, Øster Voldgade 10, 1350, Copenhagen K, Denmark

^cNatural History Museum of Denmark, Øster Voldgade 5-7, 1350, Copenhagen K, Denmark

^dDepartment of Geology, Lund University Sölvegatan 12, 223 62 Lund, Sweden

^eBureau of Mineral and Petroleum, Geology Department, Imaneq 29, P.O. Box 930, 3900 Nuuk, Greenland

^fNordic Center for Earth Evolution, NordCEE, Denmark

^gDepartment of Earth Sciences, University of Oxford, South Parks Road, Oxford, United Kingdom

ABSTRACT

We report whole-rock elemental and Sm-Nd isotope geochemical data from mafic-ultramafic supracrustal rocks from the Nunatak 1390 area in southern West Greenland. Additionally, we report the metamorphic temperature history for these rocks as derived from tourmaline thermometry on a tourmalinite inlier, as well as *in situ* U-Pb, Hf and O isotopic data from zircons extracted from tonalite-trondhjemite-granodiorite (TTG) gneisses that intruded the mafic-ultramafic sequence.

The supracrustal rocks from the Nunatak 1390 area have a minimum age of c. 2900 Ma defined by U-Pb zircon ages of cross-cutting aplite sheets of TTG composition. The supracrustal sequence comprise mafic rocks with pillow structures and ultramafic rocks with no evidence of their protolith. They all have amphibolite-facies mineral assemblages and a peak metamorphic temperature of approximately 550°C. The mafic sequence has relatively flat trace element patterns (La_N/Sm_N of 0.70-2.4) and mostly negative Nb-anomalies (Nb/Nb^* of 0.30-1.0) and resembles modern island arc tholeiites. The mafic sequence can be divided into a high- and low-Ti group, where the former group has lower MgO, and significantly higher contents of incompatible elements such as TiO_2 , P_2O_5 , Zr, Nb and Th. The ultramafic rocks have major and trace element compositions similar to Ti-enriched/Karasjok-type komatiites described in the literature. However, there are no textural indications that the ultramafic rocks from Nunatak 1390 are komatiites *sensu stricto*.

The low-Ti group of the mafic sequence appears to have been derived from a N-MORB source, whereas the high-Ti group and the ultramafic rocks appear to have been derived from a mantle source that is more enriched than the N-MORB source. However, there is no difference in the initial ϵ_{Nd} of the mafic and ultramafic rocks. Additionally, assimilation-fractional-crystallisation (AFC) modelling is consistent with this enrichment being caused by introduction of juvenile low-silica adakite (slab-melt) into the mantle source region. Accordingly, we propose that the mafic and ultramafic rocks were derived from a similar type of mantle source, but that the ultramafic rocks were derived from a previously depleted mantle source that was refertilised by slab melts in a subduction zone setting. The high MgO contents of the ultramafic rocks could thus reflect a second stage of partial melting of a refractory mantle in a process similar to that which is suggested for the formation of modern boninites.

We propose that the mafic-ultramafic sequence represents an island arc that evolved initially as a juvenile complex (c. 3000 Ma). However, inherited zircon grains in aplites and Hf isotope data recorded by the second intrusive TTG phase (c. 2850-2870 Ma), show that mixing with older pre-existing crust occurred during this event. Because the regional crust is dominated by TTGs of this younger age, our data suggests that it likely formed by accretion and melting of arcs of different ages and/or contamination of juvenile arcs by pre-existing continental crust rather than entirely by juvenile arc differentiation or melting. Our data thus supports melting of thickened mafic crust in an accretionary setting, rather than direct slab melting, as a mechanism for Archaeoan crust formation.

Keywords: Archaeoan; Greenland; Nunatak 1390; supracrustal belts; ultramafic rocks

1. Introduction

The interpretations of the geodynamic formation environment of Archaeoan supracrustal belts in southern West Greenland have thus far exclusively pointed to an arc-related setting (e.g. Dilek and Furnes, 2011; Friend and Nutman, 2010; Furnes et al., 2009; Garde, 2007; Hoffmann et al., 2011; Polat et al., 2002; Polat et al., 2008; Polat et al., 2010; Polat et al., 2011a; Szilas et al., 2011a, 2012; Windley and Garde, 2009). None of these studies have demonstrated the presence of komatiites in the Archaeoan supracrustal belts of southern West Greenland. Although abundant ultramafic lenses are observed within the supracrustal belts and within the TTG orthogneiss terrain, they are generally interpreted as either cumulates (Polat et al., 2011b), mantle restites (Bennett et al., 2002; Friend et al., 2002) or volcanic rocks of boninitic origin (Polat et al., 2002).

In this paper we present new data from the supracrustal rocks located on Nunatak 1390 (Fig. 1) with a focus on the geochemistry of ultramafic rocks for which a komatiite origin has previously been suggested (Scherstén and Stendal, 2008). Given that komatiites are commonly regarded as having formed in a plume-related geodynamic environment (e.g. Arndt et al., 2008; Arndt and Nisbet, 1982), their identification would apparently be in conflict with the current arc models, which is the predominate setting proposed for the origin of Archaeoan supracrustal rocks in southern West Greenland as mentioned above.

We explore different possible origins for the ultramafic rocks found on Nunatak 1390 and assess the implications of our

interpretation for the general geodynamic environment of the Archaeoan supracrustal belts of southern West Greenland.

2. Regional geology

Nunatak 1390 is part of the Tasiusarsuaq terrane (Friend and Nutman 2001, 2005; Hollis et al., 2006; Kolb and Stendal, 2007; Næraa and Scherstén, 2008; Stendal, 2007; Stendal and Scherstén, 2007). This area is located southeast of Kangerdluarssenguup in southern West Greenland and is part of the North Atlantic craton (Fig. 1). The Tasiusarsuaq terrane is dominated by tonalitic gneiss and granodiorite yielding ages of 2920-2860 Ma, but mafic rocks are also present as supracrustal belts and as inclusions in the orthogneisses (Fig. 1; Crowley, 2002; Friend and Nutman, 2001; Næraa and Scherstén, 2008; Schiøtte et al., 1989). The metamorphic grade ranges from amphibolite to granulite facies conditions, with peak metamorphism dated at c. 2790 Ma (Pidgeon and Kalsbeek, 1978). The supracrustal rocks comprise pillow lavas, layered amphibolites, gabbros and ultramafic pods. The thicknesses of the mafic to ultramafic sequences vary from 5 m up to more than 1000 m.

Alteration is common within the amphibolites with calc-silicate formation within pillow lava sequences, and the presence of intercalations of 1-2 m wide rusty, sulfide-bearing layers interpreted as exhalative rocks (Stendal, 2007). Occurrences of garnet-sillimanite-biotite rocks are relatively common and likely formed by metasomatic alteration followed by metamorphism. Tourmalinite

beds have also been observed and such an occurrence is described from Nunatak 1390. The Tasiusarsuaq terrane rocks are cross-cut by brown-weathering E–W-trending dolerite dykes (up to 30 m wide) with well-developed chilled margins.

Nunatak 1390 is located at 63°42.96'N - 49°16.89' W within the Tasiusarsuaq terrane (Fig. 1) and has previously been referred to as 'Nunatak 1390 m East of Alangordlia' by Escher and Pidgeon (1976). It comprises tonalite-trondhjemite-granodiorite (TTG) gneiss to the SE and mafic to ultramafic supracrustal rocks to the NW (Fig. 2). According to Escher and Myers (1975):

'Ultramafic sills with rhythmic igneous layering also occur within the pillow lava sequence and some pass laterally into ultramafic pillows. The pillow lavas are cut by a large number of thin, fine grained, grey dykes of intermediate composition. The dykes are irregular in thickness and in some cases interfinger with individual pillows. This relationship probably indicates that these dykes were intruded soon after eruption of the pillow lavas, and before the lava pile had consolidated.'

We provide new field observations and new geochemical and geochronological data that does not support the latter observation (Section 5.1).

In the following we regard the mafic-ultramafic sequence found on Nunatak 1390 as an outcrop of supracrustal rocks rather than a supracrustal belt, because the areal extent is rather small at around 6 km². These rocks have not been correlated with other supracrustal belts in the region so far, although Windley and Garde (2009) suggest that these rocks can be correlated with the Grædefjord supracrustal belt. On a regional scale, however, it should be noted that western and southern parts of the Tasiusarsuaq terrane preserve remnants of volcanic rocks at several localities, which resemble the rock assemblages observed on Nunatak 1390 (Escher and Myers, 1975). The term 'Nunatak' itself refers to an island of rock situated on the ice cap.

Because the rocks on Nunatak 1390 have experienced amphibolite-facies metamorphism we will take the prefix 'meta' as being implicit for all lithological units throughout this paper. Additionally, we use the term 'pillow lava' for amphibolites, which preserves pillow lava structures, to distinguish them from banded or homogeneous amphibolites.

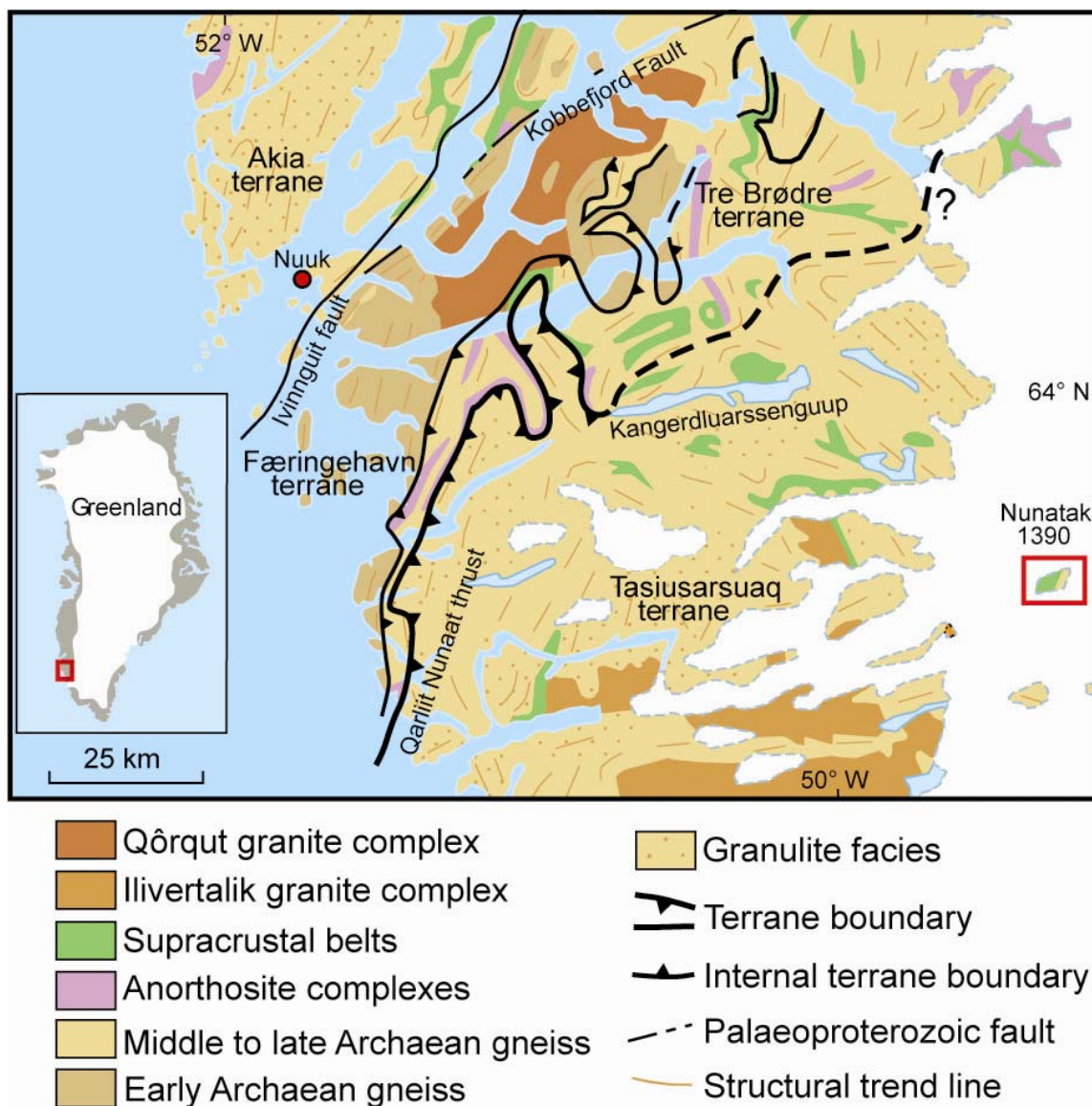


Figure 1. Map of the Nuuk region and the Tasiusarsuaq terrane with Nunatak 1390 marked with a red box in the east. The structural trends on the map refers to the foliation in the gneisses.

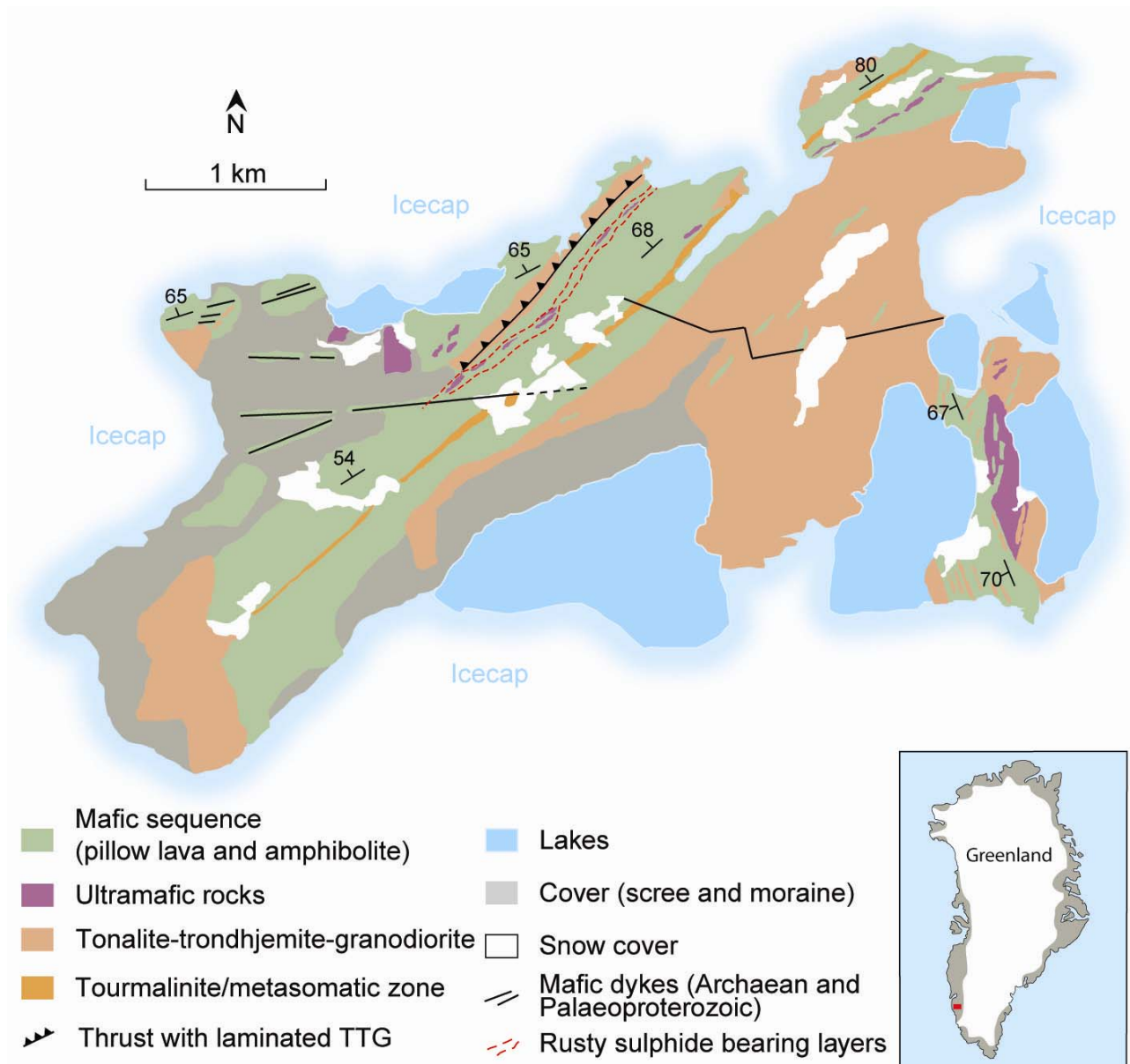


Figure 2. Map of Nunatak 1390, showing outcrops of the amphibolites (undifferentiated) and the ultramafic rocks, which comprise the supracrustal sequence, and then zone of tourmaline alteration. Intrusive TTG have been sheared along the thrust zone, which has associated alteration in the foot wall.

3. Samples and petrography

About 100 samples were collected on Nunatak 1390 by GEUS in 2006 and 2007. Preliminary geochemical data were reported by Scherstén and Stendal (2008) and some field descriptions have been presented by Stendal (2007). The Nunatak 1390 supracrustal sequence comprises several different lithological units (Section 5.1) and samples were divided into six groups according to their mineral assemblage and their field appearance: (1) pillow lava, (2) amphibolite, (3) ultramafic rock, (4) aplite, (5) TTG and (6) tourmalinite/metasomatic rock.

Pillow lava structures in amphibolites (Fig. 3a) are well-preserved in many parts of Nunatak 1390, but are generally restricted to the north-western part. The pillow cores range from fine-grained and homogeneous to medium-grained with a spotted appearance owing to quartz- and plagioclase-rich domains, which could represent ocelli of primary origin. The pillow lavas commonly contain epidote, diopside and carbonate. Calc-silicates and carbonate comprise up to 20 vol.% of the pillowed amphibolites and light coloured rims outline the pillow structures. As already mentioned, we simply refer to these rocks as pillow lavas due to their preservation

of pillow structures in contrast to the homogeneous or banded amphibolites described below, even though their mineralogy is the same.

Amphibolites make up the vast majority of the Nunatak 1390 supracrustal rocks. These mostly consist of fine- to medium-grained amphibole, plagioclase and quartz, but occasionally they are coarse-grained and have more plagioclase. The latter have been termed gabbros in the field. However, based on their spatial occurrence and geochemical similarity with the amphibolites, they have been grouped together in this study.

Ultramafic rocks mainly occur as lenses within the amphibolites. They are fine-grained and consist of amphibole (possibly anthophyllite) or serpentine and always contain abundant magnetite. In some cases they have been completely replaced by talc and develop a laminated appearance.

Aplites form intrusive felsic sheets within the supracrustal sequence (Fig. 3b). They are composed of fine- to medium-grained quartz, plagioclase and biotite. They commonly have a well-developed foliation and are finely laminated with biotite defining a cleavage. They commonly have a sheared appearance in thin section

with some carbonate veining. However, they can also be more homogenous with a spotted or porphyritic appearance and have relict plagioclase in a fine-grained matrix. They have previously been interpreted as being felsic tuffs with phenocrysts (Stendal and Scherstén, 2007), however, new field evidence clearly shows that the aplite sheets are intrusive into the supracrustal sequence and that the lamination they sometimes display is due to shearing (Section 5.1).

TTG occur mainly as a large undeformed plutonic body in the south-eastern part of the Nunatak 1390 area (Fig. 2). These rocks

consists of quartz, plagioclase and biotite and commonly has plagioclase macrocrysts up to several cm in size. Along the contacts with the supracrustal sequence, mylonites and deformed apophyses are commonly present.

Tourmalinites consist of quartz and tourmaline, where the latter form black euhedral crystals up to several cm in length and up to 1-2 cm in width. They are found as horizons within the layered mafic sequence in the footwall of a thrust and follow structural lineaments (Fig. 2). They are commonly associated with sulfides.



Figure 3. (a) Pillow lava structures observed within the amphibolites on Nunatak 1390. (b) Aplite dyke intruding the pillowed amphibolite sequence.

4. Methods

We have employed various methods to investigate the samples from Nunatak 1390. Major and trace element analyses were obtained by Inductively Coupled Plasma (ICP) methods, as well as fire-assay platinum group trace element analyses. A subset of mafic and ultramafic samples were analysed for their Sm-Nd isotopic compositions by Thermal Ionisation Mass Spectrometry (TIMS). We have measured U-Pb isotopic compositions in zircon to get absolute age constraints on the aplites and TTGs and some of these zircon have also been measured for their Hf and O isotopic compositions. Finally, we have made electron microprobe analyses on tourmaline in order to establish the temperature conditions of the supracrustal rocks.

Detailed descriptions of the analytical procedures can be found in Appendix A and all of the data can be found in Appendix B in the online supplementary material.

5. Results

5.1. Field relationships

The Nunatak 1390 area contains well-preserved pillow lava structures, which have way-up criteria that consistently point to top to the southeast. Accordingly, we give a brief overview of the tectonostratigraphy starting from the NW going towards the SE (Fig. 2).

The lower mafic pillow sequence consists of slightly deformed pillows about 10-100 cm in size (Fig. 3a), as well as pillow breccia

with calc-silicate alteration in the matrix between the pillows and in their centre. The least deformed pillow lavas contain felsic patches that consist of plagioclase and quartz, which could represent ocelli that preserves immiscible melt droplets. The pillowed sequence is cut by a slightly deformed mafic dyke swarm (1-5 m in thickness) striking more or less E-W. The dykes are fine- to medium-grained basaltic rocks.

Ultramafic rocks are present between the lower and upper pillow lava sequences, as well as within the latter. These magnetite-bearing rocks were interpreted as sills in the field, but they predominantly form discontinuous lenses within the mafic sequence. It is worth noting that pillow structures have been observed in similar ultramafic rocks at a locality about 30 km NW of Nunatak 1390 (Scherstén et al., 2008). They may thus originally have been of volcanic origin. However, no such evidence has been observed in the ultramafic rocks on the Nunatak 1390 area and it remains unclear if they represent intrusive or extrusive igneous rocks.

The upper pillow sequence is overlain by a c. 80 m thick biotite-rich laminated felsic rock consisting of quartz and plagioclase with a composition and U-Pb zircon age similar to regional TTGs (Section 5.2, 5.4). This unit was previously described as an ignimbrite (Stendal and Scherstén, 2007) and the fine grained, grey to light-coloured porphyritic aplite sheets (0.3-0.8 m wide) that cut the thick felsic unit were interpreted as feeder dykes to this 'ignimbrite'. Escher and Myers (1975) argued that these dykes likely intruded the pillow lavas shortly after eruption. However, this interpretation is not consistent with the geochronological data (Section 5.4).

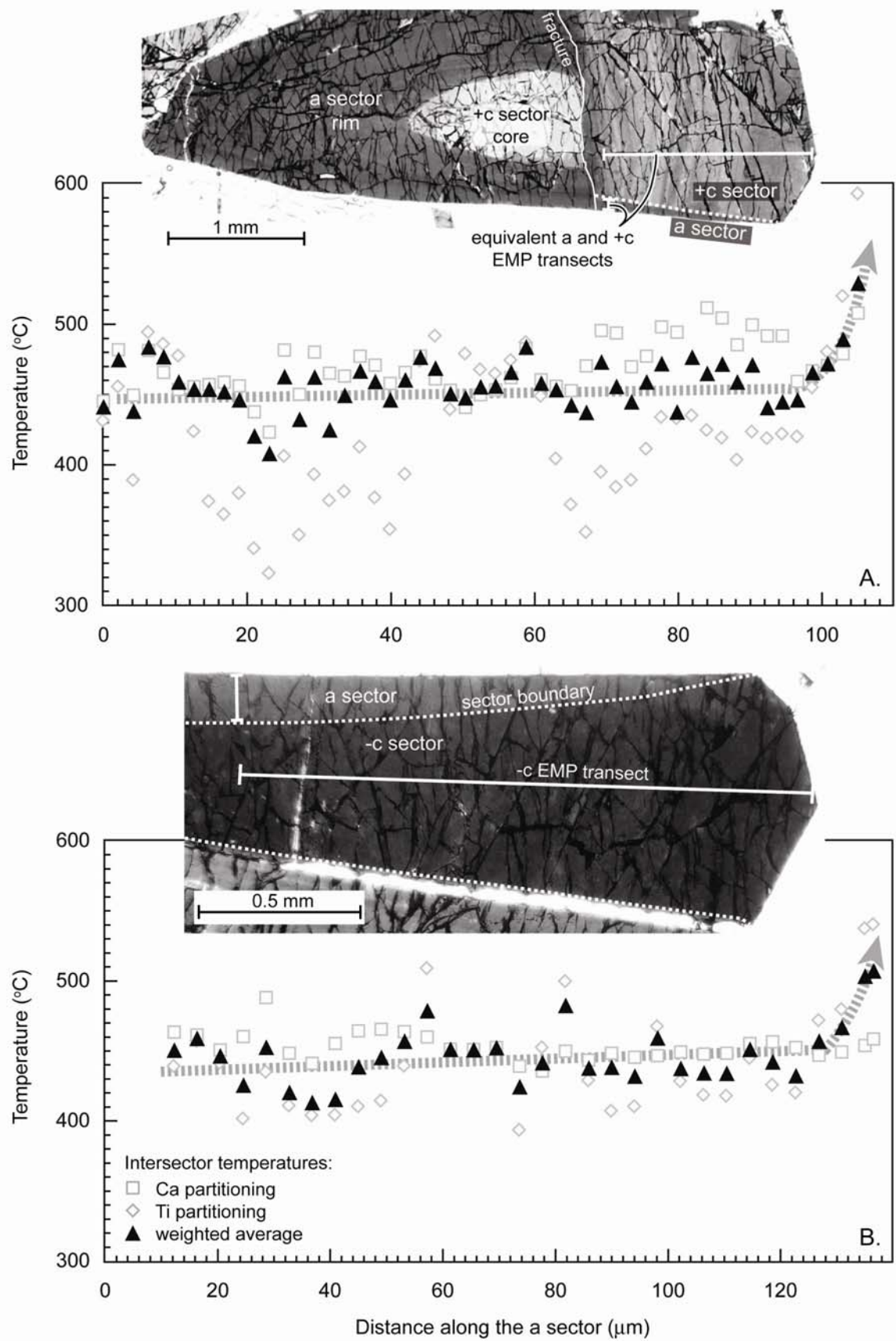


Figure 4. Examples of tourmaline thin sections and probe transects. The diagrams show the calculated temperature along the two transects.

Above the 80 m thick laminated felsic unit a c. 700 m sequence of layered amphibolites follow. These range from massive, homogeneous amphibolites to gabbroic amphibolites to finely layered amphibolites with apparent modal variation of plagioclase and amphibole. Along the contact between the felsic unit and these amphibolites there is an extensive metasomatic zone with tourmalinites and sulfide mineralisation. Another metasomatic zone is found in the middle of the layered amphibolite sequence and here tourmalinites form an up to one metre thick horizon. This central, prominent metasomatic zone is 50 m wide and strongly silicified and epidotised and has a hornfels-like appearance. It strikes parallel with the layering in the amphibolite sequence and follows a fault lineament, which is recognised from the light brownish surface colour of the altered rocks. The sulfides recorded include pyrite, pyrrhotite, chalcopyrite and arsenopyrite. Here we will only discuss the tourmalinites, because they are used to constrain temperature conditions (Section 6.7). The tourmalinite horizon consists of black tourmaline crystals up to several cm in length within a matrix of quartz and a (minor) oxide phase that has been altered beyond identification. In thin section, the tourmaline grains are idiomorphic and display intense oscillatory growth zoning, as well as hourglass sector zoning with a dark brown –c sector, yellow-brown a sector and bright blue +c sector. Grains are ubiquitously fractured, with quartz infill in these fractures. An older brittle deformation event is evident within the tourmaline grains with discordant overgrowths of tourmaline on fractured grains (Fig. 4).

Aplites within the layered amphibolites increase in abundance towards the SE of Nunatak 1390 and grade into porphyritic TTG containing amphibolite xenoliths. The felsic plutonic body in the south-eastern part of the Nunatak 1390 area (Fig. 2) was previously

described as a granite (Stendal and Scherstén, 2007); however, it is in fact granodioritic in composition. As will be shown later (Section 5.2) the composition of this intrusion is overlapping with that of other Archaean TTG gneisses in the region, so we simply refer to this large intrusive body as undeformed TTG. Some areas of the TTG body, especially in the western part of the outcrop, are altered and have a distinct pink coloration due to hematite formation and they can locally have mylonites along the margins of the intrusive bodies. Two types of TTG occur: (1) one is coarse grained and porphyritic with plagioclase macrocrysts up to several cm in length and has only minimal foliation (e.g. sample 468653); (2) the other is fine- to medium-grained, slightly foliated, muscovite-bearing and can have a slight porphyritic appearance (e.g. sample 499161). Thin sheets of the latter type of TTG have previously been mistaken for rhyolitic tuffs with phenocrysts (Stendal and Scherstén, 2007) and the group of felsic sheets that we simply term aplites is transitional to this type of TTG. New field evidence clearly shows that these sheets are intrusive into the supracrustal sequence (Fig. 3b), as also noted by Næraa and Scherstén (2008).

5.2. Major and trace element geochemistry

Pillow lavas ($n = 12$) have SiO_2 of 40-54 wt.%, MgO of 4.3-9.7 wt.%, Fe_2O_3^* of 11-21 wt.% and TiO_2 of 0.58-2.2. Their trace element contents range from 0.60-7.2 ppm Nb, 0.20-1.2 ppm Th, 56-143 ppm Zr, 11-33 ppm Y, 5.9-60 ppm Ni and 14-465 ppm Cr. They have flat chondrite-normalised (Boynton, 1984) rare earth element patterns with La_N/Sm_N of 0.85-1.3 and flat primitive mantle-normalised (Sun and McDonough, 1989) incompatible element diagrams (Fig. 5). They have negative Nb-anomalies with Nb/Nb^* of 0.30-0.86 calculated as $\text{Nb}_N/(\text{Th}_N \cdot \text{La}_N)^{1/2}$.

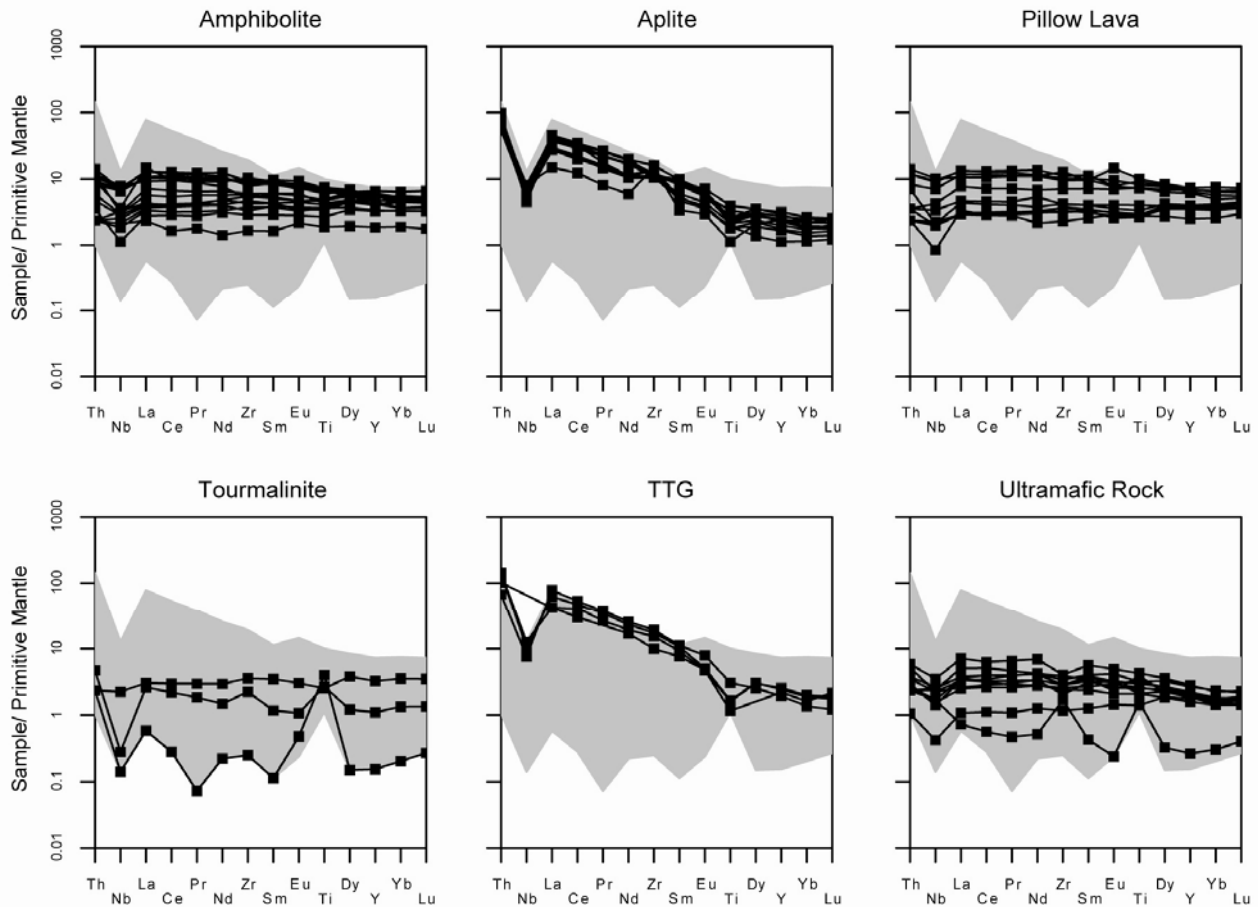


Figure 5. Primitive mantle normalised trace element diagram for the different lithological units found on Nunatak 1390. The supracrustal rocks (amphibolites, pillow lavas and ultramafic rocks) have relatively flat patterns and significant negative Nb-anomalies. The tourmalinites have similar flat patterns as the supracrustal sequence, but one sample is close to the detection limit and has an irregular pattern as a result of this. The aplites and TTGs have similar steeply negative patterns with distinctly negative Nb- and Ti-anomalies.

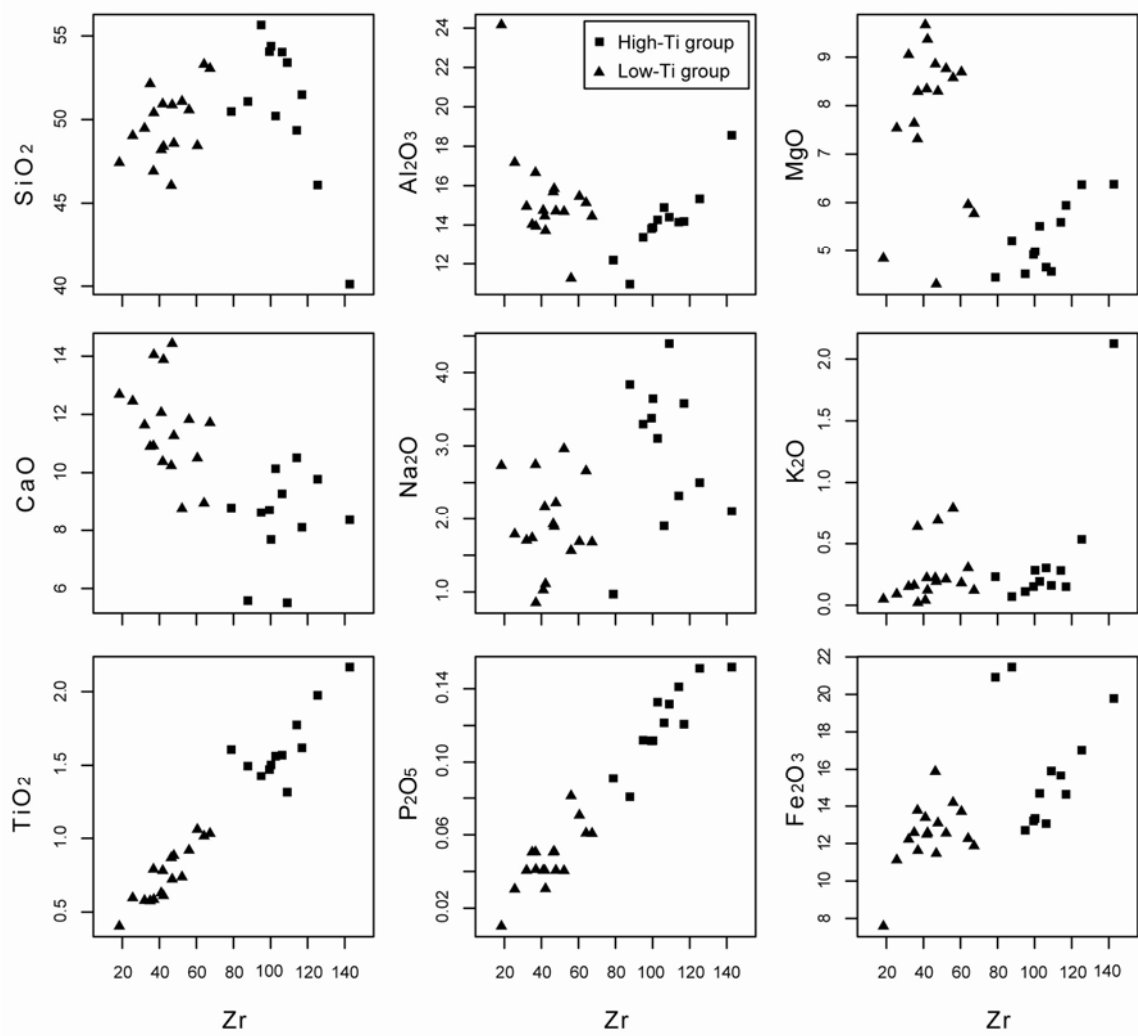


Figure 6. Major elements versus Zr for the high- and low-Ti groups of the mafic sequence.

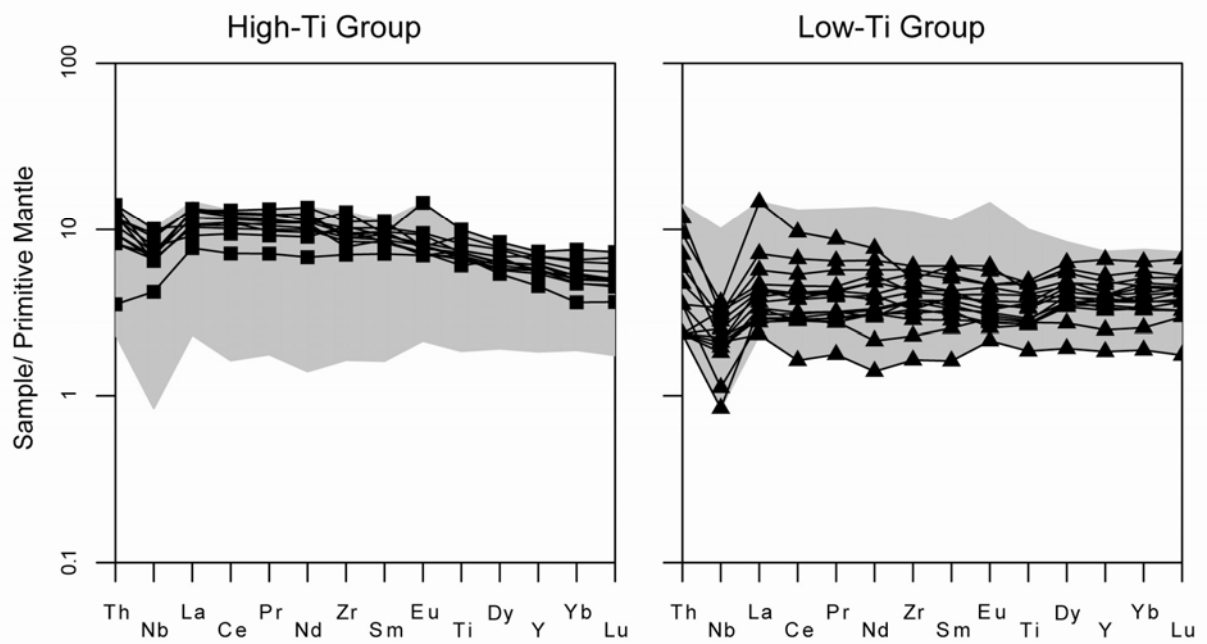


Figure 7. Primitive mantle normalised trace element diagrams for high- and low-Ti groups of the mafic sequence. The former group is significantly more enriched in incompatible trace elements.

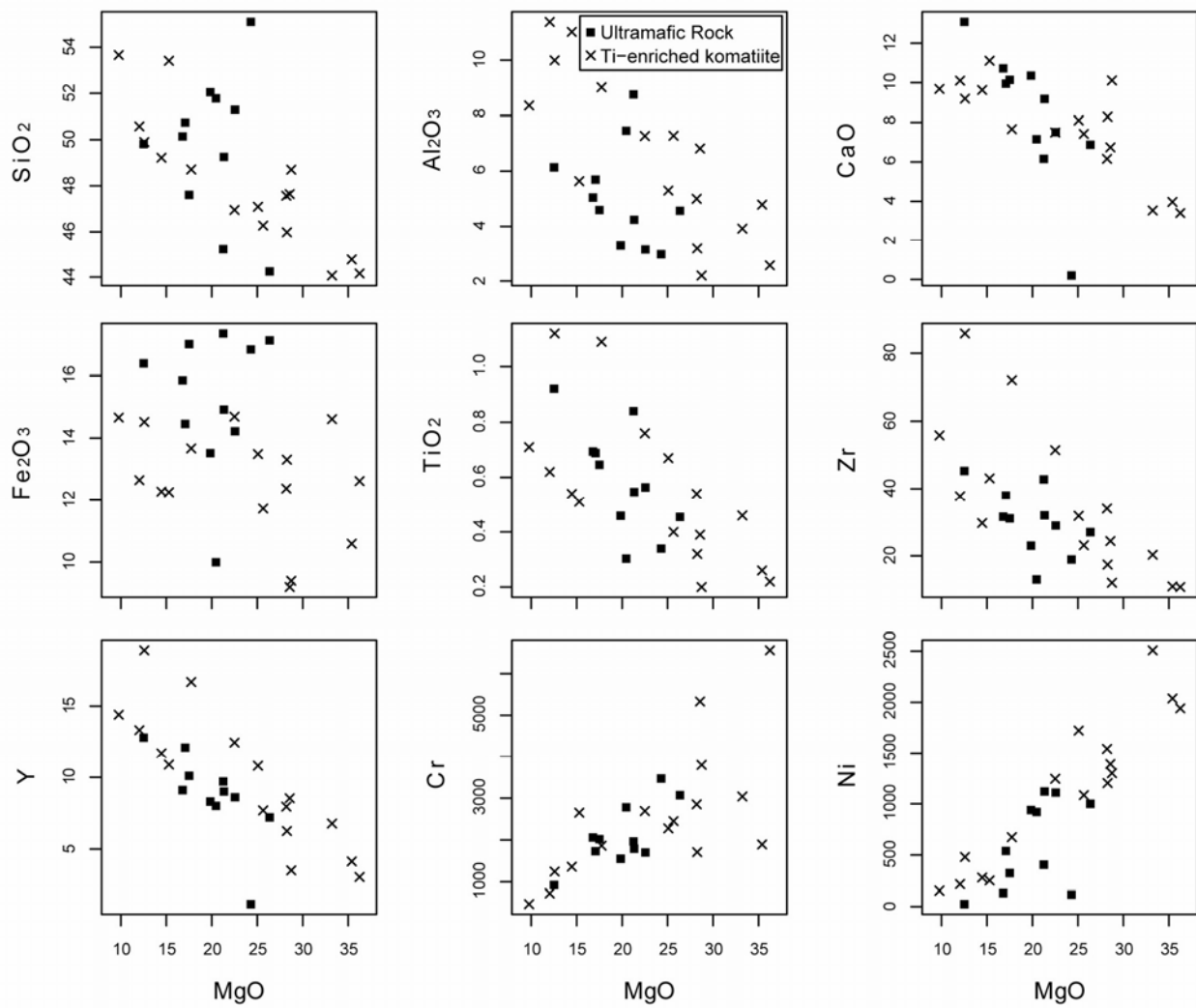


Figure 8. Major and trace element variation versus MgO for the ultramafic rocks. Ti-enriched komatiites from the Murchinson Terrane (Barley et al., 2000) have been plotted for comparison and show almost complete overlap of the Nunatak 1390 ultramafic rocks.

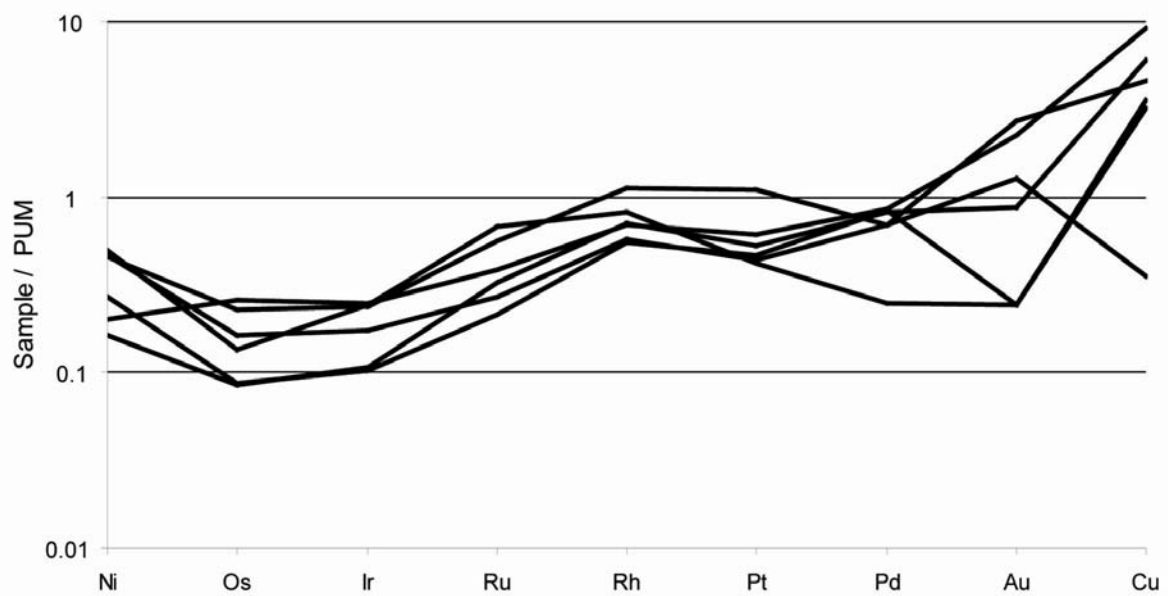


Figure 9. Primitive upper mantle normalised platinum group element (PGE) and Ni, Au, Cu diagram for six ultramafic rocks from Nunatak 1390. The patterns are similar to global data for komatiites reported by Fiorentini et al. (2011a).

Amphibolites (n = 17) have SiO₂ of 47-56 wt.%, MgO of 4.5-9.1 wt.%, Fe₂O₃* of 7.6-21 wt.% and TiO₂ of 0.40-1.6. Their trace element contents range from 0.80-5.6 ppm Nb, 0.20-1.2 ppm Th, 18-117 ppm Zr, 8.4-30 ppm Y, 12-130 ppm Ni and 14-490 ppm Cr. They have flat chondrite-normalised rare earth element patterns with La_N/Sm_N of 0.70-2.4 and flat primitive mantle-normalised incompatible element diagrams with a negative Nb-anomaly with Nb/Nb* of 0.31-1.0.

Collectively the pillow lavas and the amphibolites contain two distinct geochemical groups, which can be distinguished in terms of their TiO₂ contents. It is thus possible to classify the mafic rocks into a high-Ti group (>1.3 wt.% TiO₂) and a low-Ti group (<1.3 wt.% TiO₂) as seen in Figs. 6 and 7. The high-Ti group of mafic rocks are particularly rich in TiO₂, P₂O₅, Hf, Nb, Th, La and REEs.

Ultramafic rocks (n = 11) have SiO₂ of 44-55 wt.%, MgO of 13-26 wt.%, Fe₂O₃* of 10-17 wt.% and TiO₂ of 0.30-0.92 (Fig. 8). Their trace element contents range from 0.30-2.5 ppm Nb, 0.09-0.50 ppm Th, 13-45 ppm Zr, 1.2-13 ppm Y, 25-1120 ppm Ni and 924-3470 ppm Cr. They have flat chondrite-normalised rare earth element patterns with La_N/Sm_N of 0.78-1.7 and flat primitive mantle-normalised incompatible element diagrams with a negative Nb-anomaly with Nb/Nb* of 0.40-1.3. One sample (468669) has generally low incompatible element contents, except for distinct positive Zr- and Ti-anomalies. Six of the ultramafic samples were additionally analysed for their platinum group element (PGE) contents by fire-assay (Supplementary Table 2). They show coherent primitive upper mantle-normalised (Becker et al., 2006) patterns with low Os and Ir contents compared with the other PGEs (Fig. 9). According to the classification of high-Mg volcanic rocks by Le Bas (2000) the ultramafic rocks from the Nunatak 1390 area should be classified as picrites or komatiites due to their high MgO and low TiO₂ contents. However, according to the suggestions for classification of high-Mg volcanic rocks by Kerr and Arndt (2001), they cannot be termed komatiites, because these rocks do not display spinifex textures. Therefore, we simply term them ultramafic rocks, because there is no textural evidence of a possible komatiite protolith (Section 5.1) or of possible olivine crystals as in the case of picrites. However, it is a possibility that the lack of spinifex textures is simply caused by metamorphic recrystallisation and/or deformation, because these ultramafic rocks share many geochemical characteristics with Ti-enriched komatiites (Section 6.2.1).

Aplites (n = 13) have SiO₂ of 57-72 wt.%, MgO of 0.79-3.5 wt.%, Fe₂O₃* of 3.0-7.5 wt.% and TiO₂ of 0.24-0.86. Their trace

element contents range from 3.2-5.8 ppm Nb, 4.6-8.4 ppm Th, 117-179 ppm Zr, 5.1-14 ppm Y, 4.7-36 ppm Ni and 14-62 ppm Cr. They have steep chondrite-normalised rare earth element patterns with La_N/Sm_N of 4.1-8.0 and steep primitive mantle-normalised incompatible element diagrams with highly negative Nb-anomalies with Nb/Nb* of 0.071-0.28 and negative Ti-anomalies. One sample (499187) has a positive Zr-anomaly.

Tonalite-trondhjemite-granodiorites (TTGs) (n = 4) have SiO₂ of 67-73 wt.%, MgO of 0.70-1.6 wt.%, Fe₂O₃* of 2.4-4.4 wt.% and TiO₂ of 0.25-0.67. Their trace element contents range from 5.4-9.0 ppm Nb, 5.7-12 ppm Th, 111-215 ppm Zr, 8.8-12 ppm Y, 6.1-20 ppm Ni and 21-40 ppm Cr. They have steep chondrite-normalised rare earth element patterns with La_N/Sm_N of 4.5-6.8 and steep primitive mantle-normalised incompatible element diagrams with highly negative Nb-anomalies with Nb/Nb* of 0.10-0.16, as well as negative Ti-anomalies.

Tourmalinites (n = 3) have SiO₂ of 47-60 wt.%, MgO of 5.8-13 wt.%, Fe₂O₃* of 5.8-14 wt.% and TiO₂ of 0.55-0.87. Their trace element contents range from 0.10-1.6 ppm Nb, 0.20-0.40 ppm Th, 2.8-40 ppm Zr, 0.7-15 ppm Y, 4.2-78 ppm Ni and 130-513 ppm Cr. They have chondrite-normalised rare earth element patterns with La_N/Sm_N of 0.85-5.0, but one sample is close to the detection limit and has a somewhat irregular pattern. The same is seen for the primitive mantle-normalised incompatible element diagrams, which have negative Nb-anomalies with Nb/Nb* of 0.08-0.84. One sample (499190) has a large positive Ti-anomaly.

The whole-rock geochemical data can be found in Supplementary Table 1 and the PGE data can be found in Supplementary Table 2.

5.3. Sm-Nd isotopic compositions

Nine samples were analysed for their Sm-Nd isotope compositions by Thermal Ionisation Mass Spectrometry (TIMS). Unfortunately we were not able to obtain a meaningful isochron for these samples, which could be due to metamorphic disturbance. However, because the supracrustal rocks are cut by aplite sheets (Section 5.1) that have been dated by U-Pb zircon ages (Section 5.4) we know that the volcanic rocks must be older than about 2900 Ma (Section 5.4). Although we cannot determine their true mantle extraction age we estimate this to be around 3000 Ma, because many of the samples plot close to the depleted mantle (DM) at that time (Fig. 10).

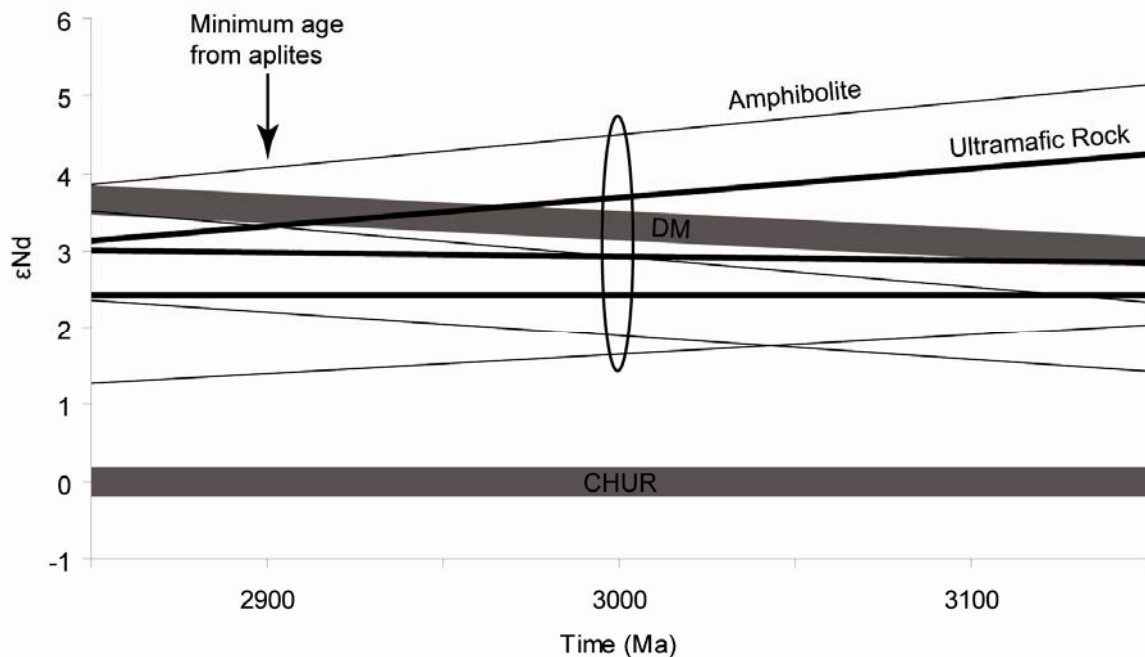


Figure 10. Calculated ϵ_{Nd} versus time. The DM-like values at 3000 Ma show that the amphibolites and the ultramafic rocks have likely been derived from a similar mantle source. The pillow lava (sample 468661) have not been shown as we interpret this sample to have been disturbed by alteration processes.

This age is supported by the similar age of 2970 Ma for the Fiskensæset anorthosite complex (Polat et al., 2010), which is located 25 km south of the Nunatak 1390 area. Accordingly, we report initial ϵ_{Nd} (with an error of ± 0.5 ϵ -values) at 3000 Ma as follows: One pillow lava sample has $\epsilon_{\text{Nd}} = +7.6$, four amphibolites have ϵ_{Nd} between +1.6 and +4.5 and three ultramafic rocks have ϵ_{Nd} between +2.4 and +3.7. The aplite sample has ϵ_{Nd} of +3.9 at 2900 Ma, which is a likely intrusion age of this sample as seen from U-Pb zircon ages of similar apolites (Section 5.4). The Sm-Nd isotopic data can be found in Supplementary Table 4.

5.4. U-Pb zircon ages

Only apolites and TTGs were analysed for U-Pb in this study. Fig. 11 show concordia diagrams for all of these samples. Sample 499161 was previously U-Pb dated by LA-ICP-MS in zircon yielding a crystallisation age of 2873 ± 5 Ma (Næraa and Scherstén, 2008). Additional data for this sample have been obtained in this study, which have confirmed the published age. An inherited zircon with an age of 3201 ± 22 Ma is also documented from this sample. The zircon grains are relatively rich common lead with $^{206}\text{Pb}/^{204}\text{Pb}$ ratios down to 200.

Sample 468653 has zircon grains that are prismatic with aspect ratios around 0.3. Most zircons are composed of back-scattered electron (BSE) bright and dark domains. Altered domains that are generally aligned parallel with the crystal shape are also present, but spot analyses have focused on the least altered domains. The 41 spot analyses are 83-109% concordant and have $^{207}\text{Pb}/^{206}\text{Pb}$ ages ranging from 2579 ± 27 to 2893 ± 37 Ma. The data show no correlation between age and Th/U. Concordant grains ($\pm 10\%$) show evidence for ancient Pb-loss, which texturally correlates with the altered domains. By selecting the 21 oldest grains we obtain a $^{207}\text{Pb}/^{206}\text{Pb}$ age of 2871 ± 7 Ma (MSWD = 1.5, probability = 0.083) which is interpreted as the crystallisation age for this rock.

Sample 468657 has zircon grains that are prismatic with aspect ratios around 0.3. Most grains display internal growth zoning that is variously overprinted by homogeneous BSE dark or bright alteration domains. Analyses were focused into the growth zoned domains and the 15 spot analyses are 90-101% concordant with ages ranging from 2834 ± 16 to 2868 ± 13 Ma. One inherited grain has been documented with an age of 3180 ± 27 Ma. The mean $^{207}\text{Pb}/^{206}\text{Pb}$ age of the main population yield 2853 ± 7 Ma (MSWD = 1.6, probability = 0.081), which is interpreted as the crystallization age for this sample.

Sample 468646 has zircon grains that are euhedral and prismatic with aspect ratios around 0.2-0.3. Most zircons are BSE grey and are growth zoned; few grains show irregular BSE dark alteration domains, which have been avoided during the U-Pb analyses. The 122 spot analyses are 93-110% concordant with $^{207}\text{Pb}/^{206}\text{Pb}$ ages ranging from 2870 ± 17 to 2961 ± 38 Ma. The data show no correlation between age and their Th/U ratio. The average $^{207}\text{Pb}/^{206}\text{Pb}$ age of all analyses is 2912 ± 2 Ma (MSWD = 1.01, probability = 0.46), which is interpreted as the crystallisation age.

Sample 484631 has zircon grains that are euhedral with aspect ratios from 0.3-0.5. Zircon grains are BSE grey and most are growth zoned with few alteration textures. The 34 spot analyses are 80-108% concordant with $^{207}\text{Pb}/^{206}\text{Pb}$ ages ranging from 2716 ± 63 to 2948 ± 42 Ma. By selecting the 28 oldest analyses we obtain a $^{207}\text{Pb}/^{206}\text{Pb}$ age 2914 ± 5 Ma (MSWD = 1.2, probability = 0.18), which is interpreted as the crystallisation age of this rock.

Sample 484633 has zircon grains that are euhedral with aspect ratios from 0.5-1. The 47 spot analyses are 90-110% concordant with $^{207}\text{Pb}/^{206}\text{Pb}$ ages ranging from 2837 ± 47 to 2938 ± 24 Ma. The five youngest analyses have the lowest Th/U ratios, suggesting Pb-loss affected these grains. By selecting the 42 oldest grains we obtain a $^{207}\text{Pb}/^{206}\text{Pb}$ age 2910 ± 4 Ma (MSWD = 0.70, probability = 0.92) interpreted as the crystallisation age.

The U-Pb zircon data can be found in Supplementary Table 5.

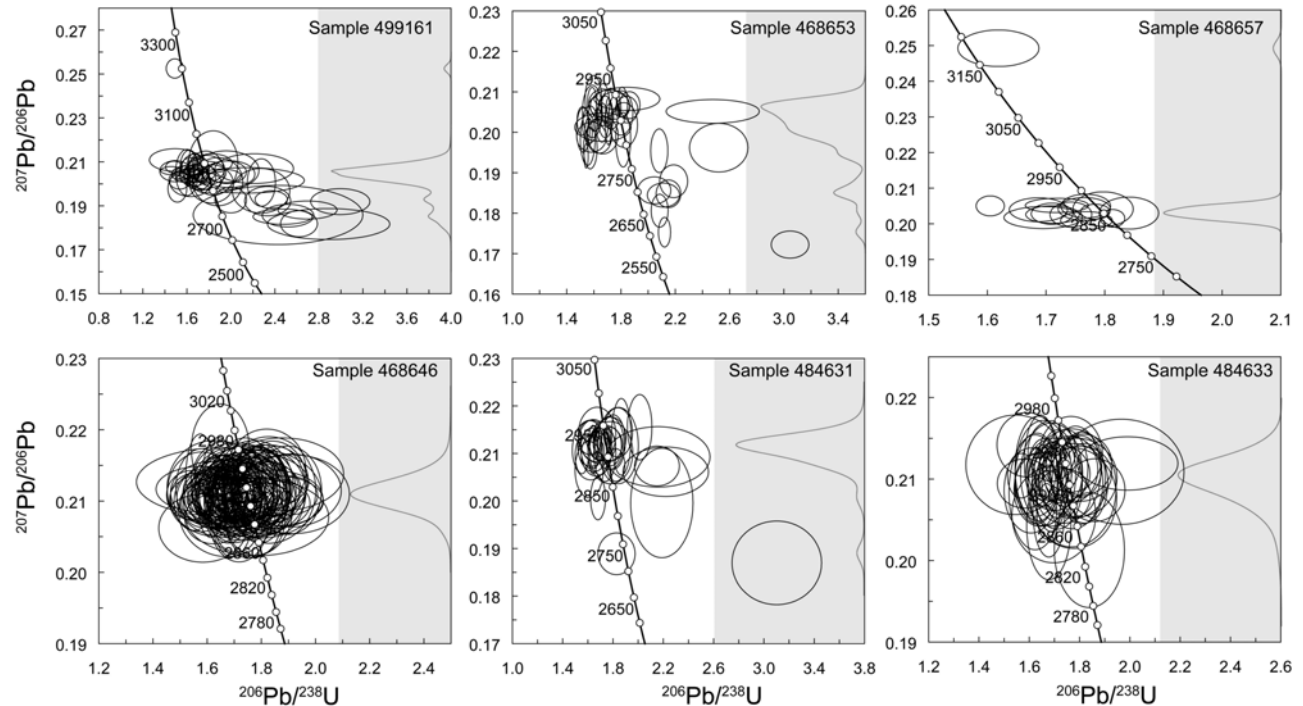


Figure 11. Plot with zircon U-Pb analyses in Tera-Wasserburg diagrams. Relative probability of $^{207}\text{Pb}/^{206}\text{Pb}$ ratios are shown in the right side of each diagram. Error ellipses are 2σ standard deviations.

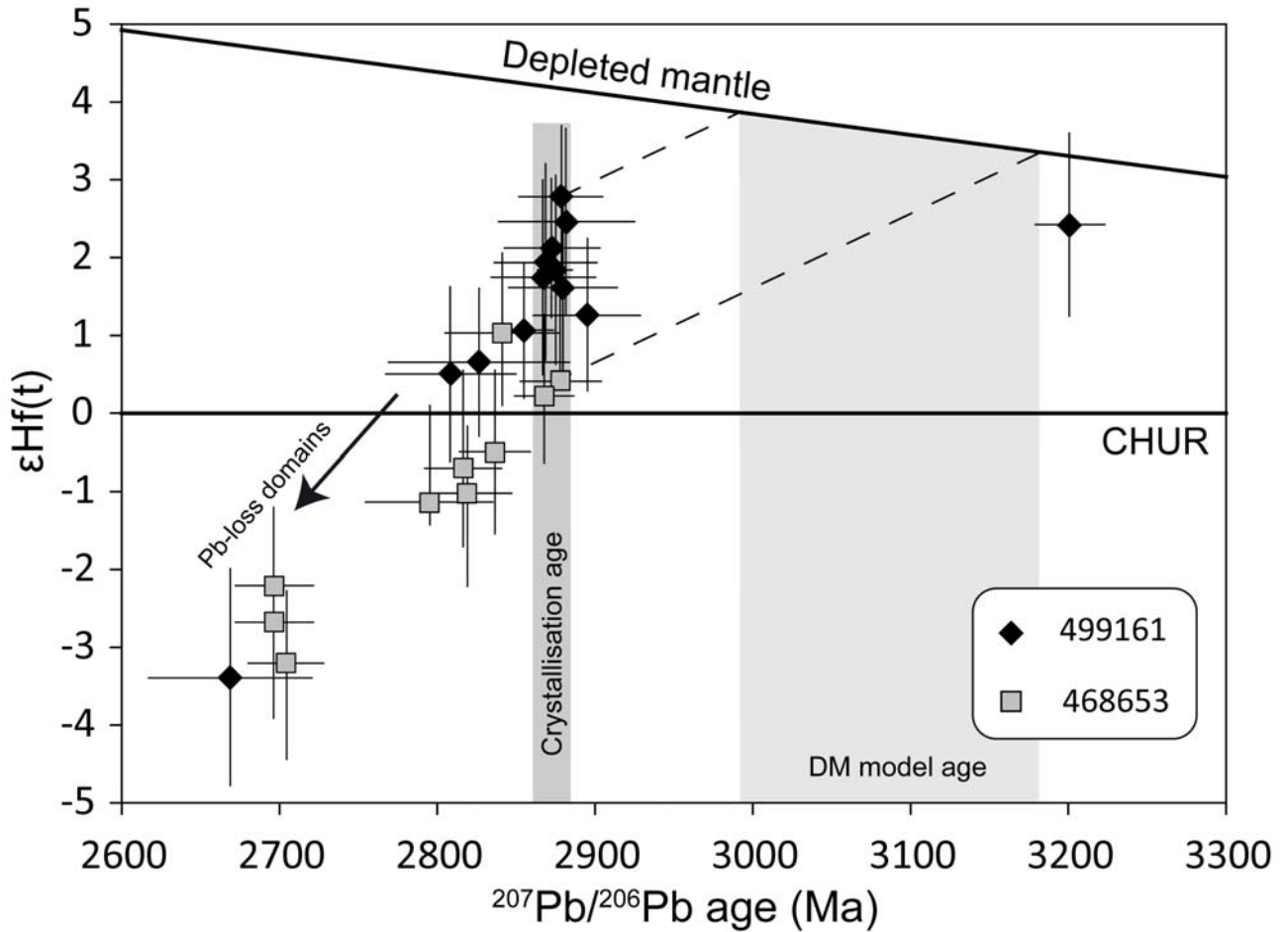


Figure 12. Plot of ϵ_{Hf} versus zircon age for one aplite (sample 499161) and the TTG intrusion (sample 468653), both with a crystallisation age of ca. 2.87 Ga. Depleted mantle slightly modified according to Næraa (2011), which have present day $^{176}\text{Lu}/^{177}\text{Hf} = 0.0375$ and $^{176}\text{Hf}/^{177}\text{Hf} = 0.283120$ and is modelled from detrital grains thought to have formed during TTG formations. Chondritic Uniform Reservoir (CHUR) after Bouvier et al. (2008). DM model ages are calculated with source region evolving with $^{176}\text{Lu}/^{177}\text{Hf} = 0.022$. Error bars are 2σ standard deviations

5.5. *In situ* zircon Hf isotope data

Fig. 12 shows the initial ϵ_{Hf} versus time for the two samples that we have analysed in this study.

Sample 499161 was analysed for its Hf isotope composition in zircon from the main igneous population and from one inherited zircon grain with an age of 3201 ± 22 Ma. $^{176}\text{Hf}/^{177}\text{Hf}(t)$ values from the main igneous population range from 0.280995 ± 28 to 0.281009 ± 26 and form a coherent group with an average of 0.280984 ± 8 corresponding to $\epsilon_{\text{Hf}}(2873\text{Ma}) = +1.8 \pm 0.3$. The inherited zircon grain has $\epsilon_{\text{Hf}}(3201\text{Ma}) = +2.4 \pm 1.2$.

Sample 468653 was analysed for Hf isotope compositions from both the unaltered and altered part of the grains, however, the Hf isotope composition define a coherent group regardless of the textures of the zircon. The obtained data have $^{176}\text{Hf}/^{177}\text{Hf}(t)$ values from 0.280941 ± 24 to 0.280988 ± 29 and a mean of 0.280958 ± 9 corresponding to $\epsilon_{\text{Hf}}(2871\text{Ma}) = +0.8 \pm 0.3$.

The Hf isotopic zircon data can be found in Supplementary Table 6.

5.6. *In situ* zircon O isotope data

Oxygen isotope data have been obtained from the TTG (sample 468653) that intrudes the supracrustal rocks in the SE part of Nunatak 1390 (Fig. 2). The isotope data have been measured from both the unaltered and altered domains. In unaltered domains $\delta^{18}\text{O}$ values range from $+4.79 \pm 0.28\text{‰}$ to $+6.68 \pm 0.24\text{‰}$ and the mean is $+6.1 \pm 0.3\text{‰}$. The altered domains have lower $\delta^{18}\text{O}$ values from $+2.06 \pm 0.26\text{‰}$ to $+3.08 \pm 0.22\text{‰}$.

The O isotopic data can be found in Supplementary Table 7.

5.7. Tourmaline electron microprobe data

The tourmalines are dravitic to schorlitic in composition with a high uvite component (up to 40% for the $-c$ sector). There is minimal substitution towards the olenite endmember (less than 6%, highest in the $+c$ sector) and Mn, K and F contents are insignificant. The average a sector composition is $\text{Na}_{0.6}\text{Ca}_{0.3}\text{Mg}_{2.0}\text{Fe}_{1.0}\text{Ti}_{0.15}\text{Al}_{5.9}(\text{BO}_3)_3\text{Si}_6\text{O}_{18}(\text{O},\text{OH})_4$. Compositional differences among sectors are large and exceed the core to rim growth zoning variations (Fig. 4). Within-sector transects from core to rim show a decreasing Ca contents, and corresponding increase in Na towards the rim. The X_{Mg} transects are absolutely flat at 0.67.

The microprobe data can be found in Supplementary Table 8.

6. Discussion

6.1. Field relationships

The Nunatak 1390 supracrustal rocks were previously described as a bimodal volcanic sequence (Stendal and Scherstén, 2007). However, from the observation of cross-cutting aplite sheets (Fig. 3b) we propose that the felsic component, the so-called rhyolite beds of Stendal and Scherstén (2007), are in fact deformed TTG sheets that were originally intrusive into the mafic-ultramafic sequence. This is also consistent with their U-Pb zircon ages (Section 5.4) and their geochemistry (Section 5.2), which overlap with those of regional TTG gneisses. Thus, the lamination displayed by some of these aplite sheets is due to deformation and shearing rather than representing primary volcanic bedding. The required tectonic activity is evidenced by the presence of mylonites within the TTG pluton

along the contact with the supracrustal rocks in the SE part of Nunatak 1390. Similarly, we interpret the 'laminated felsic volcanic unit' in the central part of the amphibolite sequence (see Stendal and Scherstén, 2007) to also represent a sheet of highly sheared TTG gneiss. This interpretation is supported by the geochemistry and the U-Pb zircon ages, which are essentially indistinguishable from those of the TTG intrusion to the SE (Section 5.4, 5.2). Evidence for such tectonic activity (i.e. thrusting) comes from the large metasomatic zone in the immediate footwall of this thrust, which led to silicification, epidotisation and tourmalinisation, and the introduction of sulfides. In the same way, much of the lamination and layering observed in the amphibolites in the central part of Nunatak 1390 could also have been introduced during deformation and shearing, rather than representing primary volcanic bedding. However, the presence of pillow structures in the NW part of Nunatak 1390, suggests that at least some have escaped significant deformation. Thus, the rocks that were previously considered to be of felsic volcanic origin are all shown to actually be intrusive and therefore post-dates the mafic-ultramafic sequence. Our interpretation is that the least stained rocks are found in the NW of the Nunatak 1390 area and that deformation generally increases to the SE.

There is no structural or textural evidence regarding the origin of the protolith of the ultramafic rocks on Nunatak 1390. However, the occurrence of pillow structures in similar ultramafic rocks found in outcrops about 30 km to the NW (Fig. 1; Scherstén et al., 2008), suggests that the ultramafic rocks on Nunatak 1390 could also have been of originally extrusive origin, but simply deformed and re-crystallised during metamorphism.

6.2. Major and trace element geochemistry

The pillow lavas and the amphibolites have overlapping major and trace elemental compositions. They have tholeiitic basaltic compositions and have relatively flat trace element patterns ($L_{\text{a}}/\text{Sm}_{\text{N}}$ of 0.70-2.4) and have negative Nb-anomalies (Nb/Nb^* of 0.30-1.09). They are similar to other Archaean tholeiitic basaltic rocks found in the supracrustal belts of southern West Greenland (e.g. Polat et al., 2008; Szilas et al., 2011a). These and other studies from this region propose that such rocks formed in primitive island arcs, consistent with their geochemical characteristics that are intermediate between mid-ocean ridge basalts (MORB) and island arc tholeiites (IAT). The Nb/Yb versus Th/Yb diagram of Pearce (2008) in Fig. 13 classifies the rocks from the Nunatak 1390 area as having formed in an island arc-related setting, because they plot above the mantle array. The distinction between a high- and low-Ti group of mafic rocks suggests two different origins for the mafic sequence. However, because the rocks are similar isotopically (Section 5.3), a variably enriched mantle source is needed to explain the trend that occurs above, but parallel to the mantle array in Fig. 13. It is interesting to note that assimilation-fractional-crystallisation (AFC) modelling (cf. DePaolo, 1981) suggests, that the variation in incompatible trace elements seen in the high-Ti group can be explained, by contaminating the most mafic low-Ti group with melts of a low-silica adakite (LSA) composition (Fig. 13). However, because the trend is not continuous this relationship likely reflects source contamination, rather than assimilation or mixing with the low-Ti group magmas (Figs. 6, 7). We propose that this can be explained by juvenile slab melts infiltrating the mantle wedge in a subduction zone setting. This could indeed cause the trace element variation observed in the high-Ti group without changing the isotopic composition of the mantle source.

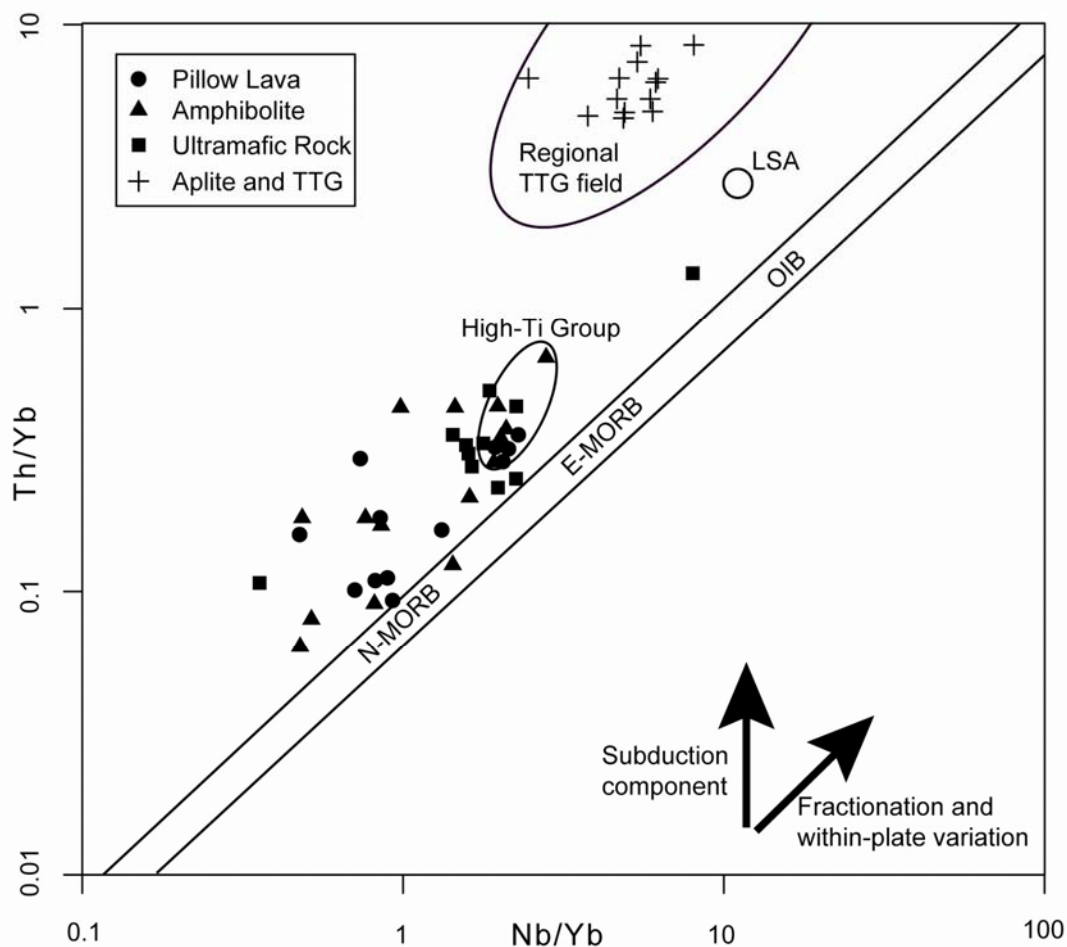


Figure 13. Th/Yb versus Nb/Yb diagram of Pearce (2008) showing all of the samples from Nunatak 1390. The TTG field is based on regional TTG data (Szilas et al., 2011b), the low-silica adakite (LSA) field is based on data from Martin et al. (2005) and Yogodzinski et al. (1995).

The ultramafic rocks do not show significant olivine fractionation trends on variation diagrams and they also have too high incompatible trace element contents to represent cumulate rocks (Fig. 8). In addition, the ultramafic rocks are not MgO-rich enough to represent typical mantle peridotites. The trace element patterns of the ultramafic rocks are similar to the mafic sequence (Fig. 5), which suggests a common origin, but they are distinctly enriched in MgO, Ni and Cr in comparison to the mafic sequence. The ultramafic rocks lack significant alteration as evident by the reasonable good correlation between MgO and immobile elements such as TiO₂, Zr, Y and Cr and, hence, likely preserve most of their primary composition (Fig. 8). The coherent PGE patterns (Fig. 9) suggests that these ultramafic rocks represent igneous rocks and we therefore compared them with literature data on komatiites from other Archaean terranes (Section 6.2.1).

The major and trace element compositions of the aplites generally overlap with the coarse-grained TTG plutons, which support the field interpretation that they represent apophyses of the same intrusive TTGs (Section 6.1). The aplites have slightly higher concentrations of compatible elements (e.g. MgO, Ni and Cr), indicating that they have assimilated small degrees of the mafic volcanic rocks during intrusion or that such material was mechanically mixed into the thin aplitic sheets during late-stage deformation and shearing. We have compared the aplites and the TTG gneisses from the Nunatak 1390 area with more regional geochemical data for TTG gneisses (e.g. Szilas et al., 2011b) and they are essentially indistinguishable in terms of major element contents and trace element patterns. We therefore interpret the aplites as early stages of TTG crust formation caused by partial melting of mafic supracrustal rocks of similar elemental and isotopic composition as the rocks reported here from the Nunatak 1390 area. This is consistent with the Sm-Nd and U-Pb isotopic data discussed below (Section 6.3, 6.4). However, an additional component of older crust is also needed to explain the data (Section 6.5).

The tourmalinites have previously been suggested to represent volcanic-exhalative rocks based on their 'interbedded' nature within the proposed bimodal volcanic sequence (Stendal and Scherstén, 2007). However, we have re-interpreted the felsic component as TTG sheets, that were sheared or tectonically emplaced within the mafic sequence (Section 6.1). Thus, the discordant nature of the metasomatic zone in the foot-wall of a thrust, leads us to conclude that the tourmalinites are related to late infiltration of fluids along thrust planes, and associated introduction of significant amounts of boron. This is supported by the temperatures recorded by the tourmaline, which are significantly higher than that expected for normal seafloor hydrothermal processes (Fig. 4). Despite the fact that these rocks essentially only consist of tourmaline and quartz, their trace element compositions are not dissimilar to that of the pillow lavas and amphibolites, except for enrichment in Al₂O₃. Al-mobility is confirmed by isocon modelling (cf. Grant, 1986, 2005), which show a distinct enrichment in this particular element. This indicates that the tourmalinite horizons represent replacement of an original mafic rock with metasomatic introduction of B and Al, which is strikingly similar to tourmalinisation of amphibolites around the Tanco pegmatite (Morgan and London, 1989). Aluminium is not normally regarded as fluid-mobile, but recent experimental work by Tagirov et al. (2004) indicates that borate complexes can significantly enhance the mobility of Al in aqueous fluids, which is consistent with our observations from the Nunatak 1390 area.

6.2.1. Komatiite data comparison of the ultramafic rocks

Unfortunately, the preservation of primary textures is non-existing for the ultramafic rocks on Nunatak 1390, because of amphibolite-facies metamorphism and high degree of deformation. Although there is some evidence that these rocks could potentially be of volcanic origin (Section 5.1), we have not been able to identify spinifex-textures or other textures characteristic of komatiites and according to Kerr and Arndt (2001) the ultramafic rocks of the Nunatak 1390 area cannot be classified as komatiites *sensu stricto*. However, we have nevertheless compared these ultramafic rocks with the komatiite database of Fiorentini et al. (2011a).

The major and trace element contents of our ultramafic rocks fall well within the range of the komatiite compositions in the database.

However, the ultramafic rocks have slightly higher average Fe₂O₃* and SiO₂. The PGE patterns of the ultramafic rocks from the Nunatak 1390 area are within the range of the komatiite data and have a similar shape (Fig. 9). These komatiite-like PGE patterns are to some degree diagnostic of komatiites, because these trace elements are normally immobile during alteration processes. The coherent PGE patterns confirms that the ultramafic rocks on Nunatak 1390 cannot be cumulate rocks, because such rocks would have widely scattered PGE patterns due to variable sulfide contents. These ultramafic rocks are not mantle peridotites, because such rocks usually have negative Pt and Pd anomalies. Additionally, the ultramafic rocks from Nunatak 1390 are not Mg-rich enough to represent peridotites. In contrast the ultramafic rocks show particular good resemblance to the Ti-enriched/Karasjok-type komatiites and they have similar ranges in their TiO₂, CaO, Zr, Hf, Nb and REE contents, which are elements characteristic of this type of komatiite. In detail the Nunatak 1390 ultramafic rocks have almost identical major and trace element compositions when compared to the Ti-enriched komatiites reported by Barley et al. (2000) from the Murchinson Terrane of Western Australia (Fig. 8). The only discrepancy is the marginally higher SiO₂ (44-55 wt.%) and Fe₂O₃* (10-17 wt.%) observed in the samples from the Nunatak 1390 area.

We find that the most straight forward interpretation of the ultramafic rocks from the Nunatak 1390 area is, that they are indeed igneous rocks, which are geochemically similar to komatiites of the Ti-enriched/Karasjok-type, and that the geochemical data is not compatible with them representing cumulate or mantle rocks.

6.2.2. Geodynamic setting

Accepting the above interpretation, that the ultramafic rocks on Nunatak 1390 have geochemical compositions similar with those of Ti-enriched/Karasjok-type komatiites, could obviously have major implications for the geodynamic model of these supracrustal rocks. This could perhaps also be the case for the interpretation for other coeval Archaean rocks in southern West Greenland, because komatiites are generally believed to be related to deep mantle plumes (e.g. Nisbet et al., 1993; Arndt et al., 2008).

As already mentioned, all previous work on Archaean supracrustal belts in southern West Greenland have proposed a subduction zone geodynamic environment of formation (e.g. Dilek and Furnes, 2011; Friend and Nutman, 2010; Furnes et al., 2009; Garde, 2007; Hoffmann et al., 2011; Polat et al., 2002; Polat et al., 2008; Polat et al., 2010; Polat et al., 2011a; Szilas et al., 2011a, 2012; Windley and Garde, 2009). Therefore, a deep mantle plume origin for the komatiite-like rocks in the Nunatak 1390 area seems to be at odds with the other observations in this region, where an arc origin is the generally preferred interpretation for the supracrustal rocks.

However, in a competing model, komatiites are suggested to be derived from shallow hydrous melting of a previously depleted mantle source that was fluxed by fluids from a descending slab in a subduction zone setting (Allège, 1982; Parman et al., 2001, 2004). In this model, komatiites are considered to be similar to modern boninites, which are believed to form by flux-melting of highly depleted mantle typically found in a forearc setting (König et al., 2010). Interestingly, there are remarkable similarities between the ultramafic rocks on Nunatak 1390 and low-Ca boninites from Papua New Guinea reported by König et al. (2010), for which a significant low-silica adakite (slab melt) contribution is responsible for their trace element geochemistry. It is noteworthy that we also invoke a low-silica adakite (slab melt) component to explain the variability in the high-Ti mafic sequence of the Nunatak 1390 area, as observed by AFC modelling, to explain the trace element enrichment. Additionally, this component is uncorrelated with initial εNd and must therefore have been derived from a juvenile mafic source.

Boninite-like rocks have also been reported from the 3800 Ma old Isua supracrustal belt in southern West Greenland (Polat et al., 2002). In this case a juvenile slab melt contribution was also involved to explain the trace element patterns of the boninite-like rocks, and was used to argue for an intra-oceanic subduction environment. One piece of independent evidence for a subduction-related geodynamic setting comes from eclogitic kimberlite xenoliths collected from a boulder on Nunatak 1390. The compositions of these eclogites were interpreted as evidence of crustal growth by

stacking of oceanic lithosphere in this region during the Mesoproterozoic (Tappe et al., 2011).

It is debatable whether or not modern mantle plumes exist (Fitton, 2007; Fougler, 2010, 2012; Koppers, 2011), despite the considerable geochemical and geophysical effort put into this problem for the last four decades. Therefore, it is probably too simplistic to assume that rocks of komatiitic composition always point to a plume-related geodynamic setting in the Archaean rock record, as commonly proposed. As mentioned previously there is growing evidence that komatiites were hydrous and thus a two stage boninitic origin is possible for at least the Ti-enriched type of komatiites.

If we allow ourselves to do a bit of speculation on why it would be reasonable to assume that komatiites were hydrous rather than dry magmas, it is obvious that the spinifex textures observed in komatiites globally is essentially the same as the bladed texture that is seen when water is cooled rapidly. Such cooling will make the crystallising water grow along the c-axis faster than the a- and b-axis (Hallet, J., 1964). The same would be true during olivine crystallisation, which would also grow rapidly along the c-axis in the case on fast cooling. This kind of texture would therefore be expected to form in komatiite flows during volatile release, which will remove significant amounts of heat from the magma, whereas deeper sills could be at pressures where the volatiles would not degas and the melt might retain its volatile contents during crystallisation. This idea is supported by the fact that most komatiites where spinifex textures are observed represents thin flows, whereas deep sills often contain hydromagmatic amphibole (Fiorentini et al., 2011b) and thus suggests a significant primary volatile contents in such magmas.

A subduction-related geodynamic environment for komatiites has mainly been promoted by Grove and Parman (e.g. Grove et al., 1999; Parman et al., 2001, 2004). These workers proposed that the Mg-rich komatiitic magmas were formed by fluid fluxed melting of previously depleted mantle and, thus, that komatiites essentially represent Archaean equivalents of modern boninites. This model is supported by the presence of high-Ca pyroxene in komatiites, which can be produced by hydrous melts (Parman et al., 1997; Parman and Grove, 2004). Another piece of evidence for the primary volatile contents of komatiites is the presence of volcanoclastic textures in komatiites from the Barberton Greenstone Belt (Stiegler et al., 2010). Even stronger evidence for an elevated water content of komatiites comes from magmatic amphibole, which has textures and compositions that are primary (Stone et al., 1997). Moreover, *in situ* trace element and B isotopic data suggests that these volatiles were not mantle-derived (Gurenko and Kamenetsky, 2011; Fiorentini et al., 2008, 2011b). Finally, water-rich melt inclusions in olivine have been reported in late Cretaceous komatiites on Gorgona Island (Kamenetsky et al., 2010). Thus, there seems to be growing evidence for an alternative explanation for the origin of komatiites that is markedly different from the deep mantle plume model, which has been the consensus view for three decades (Arndt and Nisbet, 1982).

Until the issue of whether or not komatiites were hydrous is resolved we can only speculate that at least Ti-enriched/Karasjok-type komatiites, could represent Archaean equivalents of modern boninitic rocks. Regardless of the komatiite controversy, the ultramafic rocks on Nunatak 1390 are sufficiently similar in composition to komatiites of the Ti-enriched/Karasjok-type (e.g. Barley et al., 2000) that we can term these rocks as ultramafic rocks of komatiitic-affinity, although a boninitic-affinity may prove to be a more appropriate term.

6.3. Sm-Nd isotopic compositions

The mafic-ultramafic rocks on Nunatak 1390 do not appear to have been crustally contaminated, because they lack systematic correlations between their initial ϵ_{Nd} and contamination sensitive trace element ratios such as Nb/Nb* and Th/Yb. However, the pillow lava (468661) have much higher $\epsilon_{\text{Nd}}(3000\text{Ma})$ (+7.6) than the rest of the mafic-ultramafic samples and we therefore interpret the Sm-Nd isotopic systematics of this sample to have been disturbed, possibly during seafloor alteration. The amphibolites plot close to the depleted mantle (DM) evolution line at about 3000 Ma and have thus likely been derived from such a mantle source (Fig. 10). It is interesting to note that the ultramafic rocks, which we interpret to represent melts

from a highly depleted mantle source (Section 6.2.2), appear to have been derived from a mantle source with a similar initial ϵ_{Nd} as the mafic sequence. This suggests, that the amphibolites and the ultramafic rocks formed in a similar geodynamic setting and were derived from an isotopically similar mantle source, but in the case of the ultramafic rocks this source was previously depleted to yield high-Mg melts. This supports the idea that the ultramafic rocks did not form from a distinct deep mantle plume source, but simply represent MgO-rich melts from a highly depleted mantle source, that was fluxed by fluids and/or melts. A depleted mantle source for komatiites was also proposed by Anderson (1994).

The aplite (sample 484641) has ϵ_{Nd} of +3.9 at 2900 Ma, which is within the range of the supracrustal rocks at that time. This value is compatible with the aplites, and in turn also the TTGs, having formed by partial melting of volcanic rocks similar to the ones found in the Nunatak 1390 mafic-ultramafic sequence.

6.4. U-Pb zircon ages

The age dated samples are from felsic dykes and a relatively undeformed intrusive TTG unit. The data have distinguished two intrusive phases where three aplite dykes with ages at 2914 ± 5 , 2912 ± 2 and 2910 ± 4 Ma, represents an early intrusive phase. The aplite sample 468646 is representing this early phase and is intrusive into the pillow lava sequence (Fig. 3b). This aplite is lineated and has been deformed together with the pillow lava sequence at a late stage. The aplite sample 484633 is from within an alteration zone (quartz-tourmaline rocks) at the boundary of a pillow lava sequence and a layered amphibolite sequence. Sample 484631 is from a c. 80 m wide biotite foliated felsic unit. The 'early phase' aplites apparently intruded the mafic sequence after initial amphibolite-facies metamorphism. However, the rocks were subsequently deformed together as seen by folded aplites. Tourmalinite formation occurred either during the early intrusive phase or possibly during later deformation and related fluid infiltration.

The second intrusive phase is represented by the main TTG unit in the SE part of Nunatak 1390 and the two aplite dykes, which have ages of 2871 ± 7 , 2873 ± 5 and 2853 ± 7 Ma, respectively. Their ages are within a well-known regional TTG-forming event (Næraa and Scherstén, 2008). Both aplites contain inherited grains with ages around 3200 Ma, suggesting assimilation of older felsic crust as discussed further in Section 6.5. A mylonite zone on the northern contact of the main TTG unit show that the late aplites intruded prior to this deformation event.

A so-called ignimbrite (sample 499161) was previously dated at 2873 ± 5 Ma (Næraa and Scherstén, 2008). However, this age is within the error of the main TTG on Nunatak 1390 (sample 468653) and this is also clearly intrusive into the pillow lava sequence (Fig. 3b). From the geochemistry, which shows overlap of aplites and TTGs (Section 5.2), together with the new field evidence of an intrusive relationship (Section 5.1), it is now clear that the neither the early or later aplite sheets within the mafic sequence represent felsic volcanic rocks, but are sheets of two distinct TTG forming events that have been preferentially sheared in contrast to the more competent mafic rocks during deformation.

6.5. *In situ* Hf isotopes in zircon

Combined U-Pb and Hf isotopic data have been obtained from the main TTG unit and one of the related intrusive dykes (c. 2870 Ma). The units have a mean $\epsilon_{\text{Hf}}(t)$ value at $+0.8 \pm 0.3$ and $+1.8 \pm 0.3$, respectively. In each sample the $\epsilon_{\text{Hf}}(t)$ -time arrays suggest that metamorphic overprinting has caused Pb-loss without affecting the Hf isotope composition (Fig. 12). Both of the mean $\epsilon_{\text{Hf}}(t)$ values are relatively juvenile, however, the variation between the samples is so large that mixing of different source regions seems likely. DM model ages calculated by using the suggested regional depleted mantle model (Næraa, 2011) range from c. 3000-3200 Ma, suggesting that the extraction age of the source region occurred during this time period. It is worth noting that the Tartuq Group, which is located at the southern margin of the North Atlantic craton, has an age of c. 3200 Ma (Szilas et al., 2011a) and could thus represent the mafic source for the low ϵ_{Hf} component that is seen in the data. Evidence for assimilation of older crust during the TTG intrusion is evident from the c. 3200 Ma inherited zircon grains observed in both aplite

dyke units. Whereas most of the documented basement in the Tasiarsuaq terrane have ages between 2880–2840 Ma, older TTG crust with ages ranging from 3200–3100 Ma are present SW of the Nunatak 1390 area in the Fiskensætt region (Kokfelt et al., 2011). The latter TTGs represent obvious older crustal source regions that could have mixed with TTG melts derived from mafic rocks from the Nunatak 1390 during the second phase of TTG intrusion. However, as the mafic-ultramafic sequence does not show evidence of crustal contamination (Fig. 10) it seems likely that this juvenile arc crust accreted with older crustal units prior to the second TTG forming event. However, it is not clear if this older component was exclusively represented by continental crust or if older mafic crust was also involved and melted during this event. Either way, our data supports the requirement of a certain residence time for mafic crust, prior to the formation of TTG crust. This observation argues against a direct slab melt derivation of TTGs and thus supports recent work by Nagel et al. (2012).

6.6. *In situ* O isotopes in zircon

Oxygen isotope data from the intrusive TTG plot in two groups, where the population of igneous grain domains varies from $4.8 \pm 0.3\%$ to $6.7 \pm 0.2\%$ and altered domains varies from $2.1 \pm 0.3\%$ to $3.1 \pm 0.2\%$. The variation in igneous domains seems mainly to be caused by late stage alteration bringing in lighter O isotopes. The mean value of $6.1 \pm 0.3\%$ is slightly elevated compared with mantle derived melts and might indicate that some supracrustal material was mixed into the TTG, which would fit well with input from subducted sediments. The light O isotope composition in the altered domains, suggest that grains were altered by late stage fluid infiltrations during a metamorphic event. Age constraints on this event are not obtained, but Pb-loss observed in the zircons suggest that the alteration could have occurred at 2700 Ma or later.

6.7. Metamorphic-metasomatic history of Nunatak 1390

The mineral parageneses of the least altered amphibolites and pillow lavas exposed on Nunatak 1390 point to peak metamorphism at mid-amphibolite facies conditions. Unfortunately, this event appears to have mostly obliterated evidence of the earlier history. However, a chronology and P-T history can still be partially reconstructed. The tourmalinite horizons are of particular help in this respect, because the hourglass sector zoning in the tourmaline grains allows for the temperature of their formation to be constrained using intersector thermometry (Van Hinsberg and Schumacher, 2007). However, this record is restricted to events following the intrusion and possible thrusting of the TTG sheets.

Extrusion of the mafic rocks in a submarine environment, as evidenced by pillow structures is followed by interaction with seawater, metasomatically altering their primary composition (sample 468661). Conditions for this alteration can be estimated to be at greenschist facies, from equivalent modern settings. This sequence must subsequently have been heated significantly to produce the aplite partial melts (see Section 6.3). However, the lack of evidence for *in situ* partial melting in the mafic sequence on Nunatak 1390 suggests that melting may have taken place in a deeper, but compositionally and chronologically equivalent mafic suite. A subduction zone setting, as proposed here, would be able to tear apart a rock package and subduct fragments to different depths and associated conditions, and melts released by deeper fragments could well interact with their overlying equivalents.

The development of tourmalinites is associated with the thrusting of the felsic sheets and is found in the footwall. Intersector thermometry on sector boundaries between the blue +c sector and yellow-brown a sector in the innermost core indicates a temperature of approximately $350 \pm 40^\circ\text{C}$ based on Ca and Ti partitioning for this event. A brittle deformation event follows this initial nucleation and growth, resulting in fracturing of tourmaline grains. Subsequent growth is continuous and displays a superposition of growth and sector zoning that allows for temperatures to be reconstructed for this full growth (Fig. 4). Data were obtained for both a +c-a and a -c-a sector boundary, and temperatures show good agreement. There is some discrepancy between Ca and Ti derived temperatures, but they display the same trend. Ti concentrations are remarkably variable along the electron microprobe transects, whereas Ca concentrations

vary smoothly, suggesting that the Ca-based temperatures may be more reliable. The weighted average takes this variability into account.

Fig. 4 shows that growth of the tourmaline rim essentially takes place at 450°C , followed by minor growth at conditions up to 550°C , which we attribute to prograde metamorphism. This suggests peak metamorphic conditions of at least 550°C , which is in good agreement with the paragenesis of the associated amphibolites. In conclusion, the tourmalines record two-stage growth, and hence at least a two-stage history for the thrust zone: (1) Initiation of thrusting and nucleation of tourmaline at 350°C . (2) Brittle deformation of these tourmalines without growth; A major growth pulse at 450°C with a tail showing prograde metamorphism up to 550°C . The break in growth could either reflect a change in fluid composition to one not suitable for tourmaline formation, or two discrete stages of thrust activity. A final stage of brittle deformation follows at a later unspecified time, with fracturing of the fully formed tourmaline grains and quartz infill in the fractures.

7. Conclusions

The Nunatak 1390 mafic-ultramafic rocks have a minimum age of c. 2900 Ma defined by U-Pb zircon ages of cross-cutting aplite sheets of TTG composition. Aplites within the supracrustal sequence represent intrusive TTG sheets that have been variably deformed and sheared, rather than ignimbrites as previously proposed (Stendal and Scherstén, 2007). Thus, the Nunatak 1390 supracrustal rocks do not represent a bimodal volcanic sequence, but rather a mafic-ultramafic supracrustal sequence. The supracrustal rocks comprise pillowed and layered amphibolites and ultramafic rocks with amphibolite facies mineral assemblages and a peak metamorphic temperature of approximately 550°C .

The ultramafic rocks have almost identical major and trace element compositions as Ti-enriched/Karasjok-type komatiites from the Murchison Terrane (Barley et al., 2000) and also have PGE patterns that are similar to komatiites from the database of Fiorentini et al. (2011a). However, because there is no evidence of spinifex textures, the ultramafic rocks found on Nunatak 1390 cannot be termed komatiites *sensu stricto* and thus such rocks have yet to be reported from the North Atlantic craton of southern West Greenland.

A low-Ti group of mafic rocks were likely derived from a N-MORB source, whereas a high-Ti group and the ultramafic rocks appear to have been derived from a mantle source that was more enriched than the N-MORB source. There is no difference in the initial Nd isotopic compositions between the mafic and ultramafic rocks. Additionally, AFC modelling suggests that the enrichment was caused by introduction of juvenile low-silica adakite melts into the mantle source region. Therefore, we propose that the mafic and ultramafic rocks were derived from a similar mantle source that was variably re-enriched by a slab-derived melt component.

Thus, the high MgO contents of the ultramafic rocks could reflect second-stage melting of a refractory mantle source in a process similar to that, which is proposed for the formation of modern boninites. The implication of this model is that rocks with a composition similar to Ti-enriched komatiites, may not be derived from deep mantle plumes, as has otherwise been the consensus view. They could instead reflect shallow melting of refractory mantle that was fluxed by melts and fluids, and thus represent Archaean equivalents of modern boninites. This scenario is likely for at least the ultramafic rocks that we have identified on Nunatak 1390 and such a model is supported by the recent literature that is continuously providing new evidence for a hydrous origin for at least some types of komatiites.

The arc rocks of the Nunatak 1390 evolved initially as a juvenile complex (c. 3000 Ma). However, inherited zircon grains in aplites and Hf isotope data recorded by the second intrusive TTG phase (c. 2850–2870 Ma), show that mixing with older pre-existing crust occurred during this late event. Because the regional crust is dominated by TTGs of this younger age, our data suggests that the regional crust likely formed by accretion and melting of island arc complexes of different ages and/or contamination of juvenile arcs by pre-existing continental crust rather than entirely by juvenile arc differentiation or melting.

Appendix A. Methods

Detailed descriptions of the employed analytical methods can be found in the online version.

Appendix B. Supplementary data

Supplementary data can be found in the online version.

Table 1: Whole rock geochemical data for 60 samples from Nunatak 1390 analysed for this study.

Table 2: Platinum group element (PGE) fire-assay for six ultramafic samples from Nunatak 1390.

Table 3: Interlab comparison of ACME Labs and GEUS for the Disko-1 standard.

Table 4: TIMS Sm-Nd isotopic data for nine samples from Nunatak 1390.

Table 5 LA-ICP-MS U-Pb zircon data for six samples from Nunatak 1390.

Table 6: *In situ* zircon Hf isotopic data for two samples from Nunatak 1390.

Table 7: *In situ* zircon O isotopic data for one sample from Nunatak 1390.

Table 8: Electron microprobe data for tourmalines from Nunatak 1390.

Acknowledgements

We acknowledge the Greenland Bureau of Minerals and Petroleum (BMP) for financial support of the field and analytical work and thank the Geological Survey of Denmark and Greenland (GEUS) for permission to publish this work. We thank two anonymous reviewers for constructive critique of the manuscript and in particular Andrew Kerr for comments and editorial work. K. Szilas would like to thank Geocenter Danmark for funding his Ph.D. project with the title 'Archean supracrustal belts of SW Greenland', which this work forms part of. A. Scherstén acknowledges financial support from the Swedish Research council through grant #2008-3447. V.J. van Hinsberg acknowledges financial support from the European Union Seventh Framework Program (FP7/2007-2013) under grant agreement no. 254015. This study is a contribution to IGCP project 599.

References

- Allègre, C.J., 1982. Genesis of Archean komatiites in a wet ultramafic subducted plate. In: Arndt, N.T., Nisbet, E.G. (eds.), *Komatiites*. London, Allen and Unwin, 495-500.
- Arndt, N.T., Nisbet, E.G., 1982. *Komatiites*. Allen and Unwin (London) 526 pp.
- Arndt, N.T., Lesher, C.M., Barnes, S.J., 2008. *Komatiites*. Cambridge University Press, pp. 488.
- Anderson, D.L., 1994. Komatiites and picrites: evidence that the 'plume' source is depleted. *Earth and Planetary Science Letters* 128, 303-311.
- Barley, M.E., Kerrich, R., Reudav, I., Xie, Q., 2000. Late Archean Ti-rich Al-depleted komatiites and komatiitic volcanoclastic rocks from the Murchison Terrane in Western Australia. *Australian Journal of Earth Sciences* 47, 873-883.
- Becker, H., Horan, M.F., Walker, R.J., Gao, S., Lorand, J.-P., Rudnick, R.L., 2006. Highly siderophile element composition of the Earth's primitive upper mantle: Constraints from new data on peridotites massifs and xenoliths. *Geochimica Cosmochimica Acta* 70, 4528-4550.
- Bennett, V.C., Nutman, A.P., Esat, T.M., 2002. Constraints on mantle evolution from ¹⁸⁷Os/¹⁸⁸Os isotopic compositions of Archean ultramafic rocks from southern West Greenland (3.8 Ga) and Western Australia (3.46 Ga). *Geochimica Cosmochimica Acta* 66, 2615-2630.
- Bouvier, A., Vervoort, J.D., Patchett, P.J., 2008. The Lu-Hf and Sm-Nd isotopic composition of CHUR: Constraints from unequilibrated chondrites and implications for the bulk composition of terrestrial planets. *Earth and Planetary Science Letters* 273, 48-57.
- Boynton, W.V., 1984. Cosmochemistry of the rare earth elements: meteorite studies. In: Henderson, P. (ed.), *Rare Earth Element Geochemistry*, Elsevier (Amsterdam), 63-114.
- Crowley, J.L., 2002. Testing the model of late Archean terrane accretion in southern West Greenland: a comparison of the timing of geological events across the Qarliit nunaat fault, Buksefjorden region. *Precambrian Research* 116, 57-79.
- DePaolo, D.J., 1981. Trace element and isotopic effects of combined wallrock assimilation and fractional crystallization. *Earth and Planetary Science Letters* 53, 189-202.
- Dilek, Y., Furnes, H., 2011. Ophiolite genesis and global tectonics: geochemical and tectonic fingerprinting of ancient oceanic lithosphere. *Geological Society of America, Bulletin* 123, 387-411.
- Escher, J.C., Myers, J.S., 1975. New evidence concerning the original relationships of early Precambrian volcanics and anorthosites in the Fiskefjorden region, southern West Greenland. *Rapport Grønlands Geologiske Undersøgelse* 75, 72-76.
- Escher, J.C., Pidgeon, R.T., 1976. Field mapping of nunatak 1390 m, east of Alángordlia, southern West Greenland. *Rapport Grønlands Geologiske Undersøgelse* 80, 84-87.
- Fiorentini, M.L., Beresford, S.W., Deloule, E., Hanski, E., Stone, W.E., Pearson, N., 2008. The role of mantle-derived volatiles in the petrogenesis of Palaeoproterozoic ferro picrites in the Pechenga Greenstone Belt, northwestern Russia: insights from in-situ microbeam and nanobeam analysis of hydromagmatic amphibole. *Earth and Planetary Science Letters* 268, 2-14.
- Fiorentini, M.L., Barnes, S.J., Maier, W.D., Brunham, O.M., Heggge, G., 2011a. Global variability in the platinum-group element contents of komatiites. *Journal of Petrology* 52, 83-112.
- Fiorentini, M.L., Beresford, S.W., Stone, W.E., Deloule, E., 2011b. Evidence of water degassing in Archean komatiites. *Goldschmidt Conference Abstract* 2011.
- Fitton, J.G., 2007. The OIB paradox. *Geological Society of America, Special Paper* 430, 387-412.
- Fouglér, G.R., 2010. *Plates vs. Plumes: a Geological Controversy*. Wiley-Blackwell, Chichester, UK, pp. 364.
- Fouglér, G.R., 2012. Are 'hot spots' hot spots? *Journal of Geodynamics* 58, 1-28.
- Friend, C.R.L., Nutman, A.P., 2001. U-Pb zircon study of tectonically bounded blocks of 2940-2840 Ma crust with different metamorphic histories, Paamiut region, South-West Greenland: implications for the tectonic assembly of the North Atlantic craton. *Precambrian Research* 105, 143-164.
- Friend, C.R.L., Bennett, V.C., Nutman, A.P., 2002. Abyssal peridotites >3,800 Ma from southern West Greenland: field relationships, petrography, geochronology, whole-rock and mineral chemistry of dunit and harzburgite inclusions in the Itsaq Gneiss Complex. *Contributions to Mineralogy and Petrology* 143, 71-92.
- Friend, C.R.L., Nutman, A.P., 2005. New pieces to the Archean jigsaw puzzle in the Nuuk region, southern West Greenland: steps in transforming a simple insight into a complex regional tectonothermal model. *Journal of the Geological Society (London)* 162, 147-162.
- Friend, C.R.L., Nutman, A.P., 2010. Eoarchean ophiolites? New evidence for the debate on the Isua supracrustal belt, southern West Greenland. *American Journal of Science* 310, 826-861.
- Furnes, H., Rosing, M., Dilek, Y., De Wit, M., 2009. Isua supracrustal belt (Greenland) – A vestige of a 3.8 Ga suprasubduction zone ophiolite, and the implications for Archean geology. *Lithos* 113, 115-132.
- Garde, A.A., 2007. A mid-Archean island arc complex in the eastern Akia terrane, Godthåbsfjord, southern West Greenland. *Journal of the Geological Society (London)* 164, 565-579.
- Grant, J.A., 1986. The isocon diagram - a simple solution to Gresens' equation for metasomatic alteration. *Economic Geology* 81, 1976-1982.
- Grant, J.A., 2005. Isocon analysis: A brief review of the method and applications. *Physics and Chemistry of the Earth* 30, 997-1004.
- Grove, T.L., Parman, S.W., Dann, J.C., 1999. Conditions of magma generation for Archean komatiites from the Barberton Mountainland, South Africa. In: Fei, Y., Bertka, C.M., Mysen, B.O. (eds.), *Mantle Petrology: Field Observations and High-Pressure Experimentation; a Tribute to Francis R. (Joe) Boyd*, Vol. 6, Geochemical Society, Houston, 155-167.
- Gurenko, A.A., Kamenetsky, V.S., 2011. Boron isotopic composition of olivine-hosted melt inclusions from Gorgona komatiites, Colombia: New evidence supporting wet komatiite origin. *Earth and Planetary Science Letters* 312, 201-212.
- Hallett, J., 1964. Experimental studies of the crystallization of supercooled water. *Journal of the Atmospheric Sciences* 21, 671-682.
- Hoffmann, J.E., Münker, C., Polat, A., Rosing, M.T., Schulz, T., 2011. The origin of decoupled Hf-Nd isotope compositions in Eoarchean rocks from southern West Greenland. *Geochimica et Cosmochimica Acta* 75, 6610-6628.
- Hollis, J.A., Schmid, S., Stendal, H., van Gool, J.A.M., Weng, W.L., 2006. Supracrustal belts in Godthåbsfjord region, southern West Greenland. Progress report on 2005 field work: geological mapping, regional hydrothermal alteration and tectonic sections. *Danmarks og Grønlands Geologiske Undersøgelse Rapport* 2006/7, pp. 171.
- Kamenetsky, V.S., Gurenko, A.A., Kerr, A.C., 2010. Composition and temperature of komatiites melts from Gorgona Island, Colombia, constrained from olivine-hosted melt inclusions. *Geology* 38, 1003-1006.
- Kerr, A.C., Arndt, N.T., 2001. A note on the IUGS reclassification of the high-Mg and picritic volcanic rocks. *Journal of Petrology* 42, 2169-2171.
- Kokfelt, T.F., Keulen, N., Næraa, T., Nilsson, M., Scherstén, A., Szilas, K., Heijboer, T., 2011. Geochronological characterisation of the felsic rocks of the Archean craton in South-West Greenland and southern West Greenland, 61°30' - 64°N. *Danmarks og Grønlands Geologiske Undersøgelse Rapport* 2011/12 (in press).
- Kolb, J., Stendal, H., 2007. Geological environments and hydrothermal mineralisation in Nunataarsuk, Qarliit Nunaat and Ameralik, Nuuk region, SW Greenland – a field report 2007. *Danmarks og Grønlands Geologiske Undersøgelse Rapport* 2007/58, pp. 44.
- König, S., Münker, C., Schuth, S., Luguét, A., Hoffmann, J.E., Kuduon, J., 2010. Boninites as windows into trace element mobility in subduction zones. *Geochimica et Cosmochimica Acta* 74, 684-704.
- Koppers, A.A.P., 2011. Mantle plumes persevere. *Nature Geoscience* 4, 816-817.
- Le Bas, M.J., 2000. IUGS reclassification of the high-Mg and picritic volcanic rocks. *Journal of Petrology* 41, 1467-1470.
- Martin, H., Smithies, R.H., Rapp, R., Moyen, J.-F., Champion, D., 2005. An overview of adakite, tonalite-trondhjemite-granodiorite (TTG), and sanukitoid: relationships and some implications for crustal evolution. *Lithos* 79, 1-24.
- Morgan, I.V., G.B., London, D., 1989. Experimental reactions of amphibolite with boron-bearing aqueous fluids at 200 MPa: implications for tourmaline stability and partial melting in mafic rocks. *Contributions to Mineralogy and Petrology* 102, 281-297.
- Nagel, T.J., Hoffmann, J.E., Münker, C., 2012. Generation of Eoarchean TTGs from thickened mafic arc crust. *Geology* (in press). DOI: 10.1130/G32729.1
- Næraa, T., 2011. Zircon U/Pb, Hf and O isotope systematics from the Archean basement in the Nuuk region, southern West Greenland - Constrains on the early evolution of the continental crust. Unpublished Ph.D. thesis, University of Copenhagen, pp. 195.
- Næraa, T., Scherstén, A., 2008. New zircon ages from the Tasiusarsuaq terrane, southern West Greenland. *Geological Survey of Denmark and Greenland Bulletin* 15, 73-76.
- Nisbet, E.G., Cheadle, M., Arndt, N., Bickle, M.J., 1993. Constraining the potential temperature of the Archean mantle: A review of the evidence from komatiites. *Lithos* 30, 291-307.
- Parman, S.W., Dann, J.C., Grove, T.L., de Wit, M.J., 1997. Emplacement conditions of komatiite magmas from the 3.49 Ga Komati formation, Barberton Greenstone Belt, South Africa. *Earth and Planetary Science Letters* 150, 303-323.
- Parman, S.W., Grove, T.L., Dann, J.C., 2001. The production of Barberton komatiites in an Archean subduction zone. *Geophysical Research Letters* 38, 2513-2516.
- Parman, S.W., Grove, T.L., Dann, J.C., De Wit, M.J., 2004. A subduction origin for komatiites and cratonic lithospheric mantle. *South African Journal of Geology* 107, 107-118.

- Parman, S.W., Grove, T.L., 2004. Harzburgite melting with and without H₂O : experimental data and predictive modeling. *Journal of Geophysical Research, Solid Earth* 109, B02201.
- Pearce, J.A., 2008. Geochemical fingerprinting of oceanic basalts with applications to ophiolite classification and the search for Archean oceanic crust. *Lithos* 100, 14-48.
- Pidgeon, R.T., Kalsbeek, F., 1978. Dating of igneous and metamorphic events in the Fiskensæset region of southern West Greenland. *Canadian Journal of Earth Science* 15, 2021-2025.
- Polat, A., Hofmann, A.W., Rosing, M.T., 2002. Boninite-like volcanic rocks in the 3.7–3.8 Ga Isua greenstone belt, West Greenland: geochemical evidence for intra-oceanic subduction zone processes in the early Earth. *Chemical Geology* 184, 231-254.
- Polat, A., Frei, R., Appel, P.W.U., Dilek, Y., Fryer, B., Ordóñez-Calderón, J.C., Yang, Z., 2008. The origin and compositions of Mesoarchean oceanic crust: Evidence from the 3075 Ma Ivisartoq greenstone belt, SW Greenland. *Lithos* 100, 293-321.
- Polat, A., Frei, R., Scherstén, A., Appel, P.W.U., 2010. New age (ca. 2970 Ma), mantle source composition and geodynamic constraints on the Archean Fiskensæset anorthositic complex, SW Greenland. *Chemical Geology* 277, 1-20.
- Polat, A., Appel, P.W.U., Fryer, B.J., 2011a. An overview of the geochemistry of Eoarchean to Mesarchean ultramafic to mafic volcanic rocks, SW Greenland: Implication for mantle depletion and petrogenetic processes at subduction zones in the early Earth. *Gondwana Research* 20, 255-283.
- Polat, A., Fryer, B.J., Appel, P.W.U., Kalvig, P., Kerrich, R., Dilek, Y., Yang, Z., 2011b. Geochemistry of anorthositic differentiated sills in the Archean (~2970 Ma) Fiskensæset Complex, SW Greenland: Implication for parental magma compositions, geodynamic setting, and secular heat flow in arcs. *Lithos* 123, 50-72.
- Schiøtte, L., Compston, W., Bridgwater, D., 1989. U-Pb single-zircon age for the Tinissaq gneiss of southern West Greenland: a controversy resolved. *Chemical Geology (Isotope Geoscience Section)* 79, 21-30.
- Scherstén, A., Stendal, H., 2008. Geochemistry of the Tasiarsuaq 'greenstone-granite' terrane, southern West Greenland. *Danmarks og Grønlands Geologiske Undersøgelse Rapport 2008/15*, pp. 40.
- Scherstén, A., Stendal, H., Næraa, T., 2008. Geochemistry of greenstones in the Tasiarsuaq terrane, southern West Greenland. *Geological Survey of Denmark and Greenland Bulletin* 15, 69-72.
- Stendal, H. (ed.), 2007. Characterisation of selected geological environments. Mineral resource assessment of the Archaean Craton (66° to 63°30'N) SW Greenland contribution no. 1. *Danmarks og Grønlands Geologiske Undersøgelse Rapport 2007/20*, pp. 90.
- Stendal, H., Scherstén, A., 2007. A well-preserved bimodal volcanic succession in the Tasiarsuaq terrane, South-West Greenland. *Geological Survey of Denmark and Greenland Bulletin* 13, 53-56.
- Stiegler, M.T., Lowe, D.R., Byerly, G.R., 2010. The petrogenesis of volcanoclastic komatiites in the Barberton Greenstone Belt, South Africa; a textural and geochemical study. *Journal of Petrology* 51, 947-972.
- Stone, W.E., Deloule, E., Larson, M.S., Leshner, C.M., 1997. Evidence for hydrous high-MgO melts in the Precambrian. *Geology* 25, 143-146.
- Sun, S., McDonough, W.F., 1989. Chemical and isotopic systematics of oceanic basalts: implications for mantle composition and processes. In: Saunders, A.D., Norry, M.J. (eds.), *Magmatism in the Ocean Basins*. Geological Society (London), Special Publications 42, 313-345.
- Szilas, K., Van Hinsberg, J., Kisters, A.F.M., Hoffmann, E.J., Kokfelt, T.F., Scherstén, A., Windley, B.F., Frei, R., Rosing, M.T., Münker, C., 2011a. Remnants of arc-related Mesarchean oceanic crust in the Tartoq Group, SW Greenland. *Gondwana Research*. (in press)
- Szilas, K., Kokfelt, T.F., Næraa, T., Scherstén, A., 2011b. Geochemistry of Archaean felsic crust in SW Greenland. In: Kokfelt, T.F. (ed.), *Geochemistry of supracrustal rocks and associated intrusive TTG suites of the Archaean craton in South-West Greenland and southern West Greenland, 61°30' - 64°N*. *Danmarks og Grønlands Geologiske Undersøgelse Rapport 2011/10* (in press).
- Szilas, K., Hoffmann, J.E., Scherstén, A., Rosing, M.T., Windley, B.F., Kokfelt, T.F., Keulen, N., Van Hinsberg, V.J., Næraa, T., Frei, R., Münker, C., 2012. Complex calc-alkaline volcanism recorded in Mesarchean supracrustal belts north of Frederikshåbs Isblink, southern West Greenland: implications for subduction zone processes in the early Earth. *Precambrian Research* (in press). DOI: 10.1016/j.precamres.2012.03.013.
- Tagirov, B., Schott, J., Harrichoury, J.-C., Escalier, J., 2004. Experimental study of the stability of aluminate-borate complexes in hydrothermal solutions. *Geochimica Cosmochimica Acta* 68, 1333-1345.
- Tappe, S., Smart, K.A., Pearson, D.G., Steenfelt, A., Simonetti, A., 2011. Craton formation in Late Archean subduction zones revealed by first Greenland eclogites. *Geology* 39, 1103-1106.
- Van Hinsberg, V.J., Schumacher, J.C., 2007. Intersector element partitioning in tourmaline: a potentially powerful single crystal thermometer. *Contributions to Mineralogy and Petrology* 153, 289-301.
- Windley, B., Garde, A.A., 2009. Arc-generated blocks with sections in the North Atlantic craton of West Greenland: Crustal growth in the Archean with modern analogues. *Earth-Science Reviews* 93, 1-30.
- Yogodzinski, G.M., Kay, R.W., Volynets, O.N., Koloskov, A.V., Kay, S.M., 1995. Magnesian andesite in the western Aleutian Komandorsky region: Implications for slab melting and processes in the mantle wedge. *Geological Society of America Bulletin* 107, 505-519.

Supplementary material for Paper III

Appendix A (Paper III): Methods

Major and trace element analyses

Samples, a few kilograms in size, were collected in the field and, where present, weathered crusts were removed. Crushing was performed at GEUS in a tungsten-carbide swing-mill. Whole rock analyses were mainly carried out at ACMELabs in Vancouver, Canada, although some samples were analysed at Actlabs, Canada (Supplementary Table 1).

At ACMELabs the analytical procedures termed “Group 4A and 4B - lithogeochemical whole rock fusion” were followed. A brief description of the procedure is summarised below based on the description available on the homepage (www.acmelab.com) and on information obtained upon personal request from the company: “Prepared samples are mixed with $\text{LiBO}_2/\text{Li}_2\text{B}_4\text{O}_7$ flux in crucibles and fused in a furnace. The cooled bead is then dissolved in ACS grade nitric acid. For “Group 4A” the total abundances of the major oxides and several minor elements are analysed for a 200 mg sample by ICP-emission spectrometry following a lithium metaborate/tetraborate fusion and dilute nitric digestion. Loss on ignition (LOI) is determined by igniting a sample split at 1000°C then measuring the weight loss. “Group 4B” comprises two separate analyses for the total trace elements by ICP-MS. Rare earth and refractory elements are determined by ICP mass spectrometry following a lithium metaborate/tetraborate fusion and nitric acid digestion of a 200 mg sample. Additionally a separate 500 mg split is digested in Aqua Regia and analysed by ICP Mass Spectrometry to determine the precious and base metals”. Fe valence was not determined and Fe_2O_3 thus refers to total Fe. The geochemical data are presented in Supplementary Table 1.

At Actlabs the analytical procedures of the “Research Package 4E”, were followed which are similar to those at ACMELabs. Although there are certain differences we will not give a detailed description here, but simply note that the detection limits are slightly lower than at ACMELabs, however, overall we did not find any systematic differences in the data from the two laboratories.

Platinum group elemental (PGE) analyses were conducted by fire-assay according to the protocols of Savard et al. (2010) at Université du Québec à Chicoutimi, Canada. The PGE data are reported in Supplementary Table 2.

The GEUS in-house standard “Disko-1 basalt” was given a regular sample number and sent with each batch analysed at ACMELabs (21 runs over three years). The reported rare earth element (REE) contents for this standard were compared with data from GEUS’ ICP-MS lab (32 runs over 8 years). The results from the two laboratories agree well and are within analytical uncertainty (Supplementary Table 3).

Variation and multi-element diagrams were produced with the GCDKit software (Janoušek et al., 2006) and we used the assimilation-fractional-crystallisation Excel® spreadsheet of Ersoy and Helvacı (2010).

Sm-Nd isotope analyses

Whole-rock Sm-Nd isotope analyses were carried out on a VG Sector 54-IT TIMS in the Geological Institute, University of Copenhagen, Denmark. Rock powders were spiked with a ^{149}Sm - ^{150}Nd mixed spike and the dissolution of the sample powders was achieved in the following steps: First a strong 8 N HBr attack was applied, that has been shown to effectively dissolve accessory phosphates (Frei et al., 1997; Schaller et al., 1997). This was followed by dissolution in a concentrated HF-14 N HNO_3 mixture. Finally, the samples were dissolved in strong 9 N HCl. The bulk rare earth elements (REEs) were separated over 15 ml glass-stem columns charged with AG 50W cation resin. REEs were further separated in 20 ml plastic columns (BioRad™) loaded with 6 ml of LN resin (Trischem™). During analysis both static and multi-dynamic routines were used for the collection of the isotopic ratios. Nd isotope ratios were normalised to $^{146}\text{Nd}/^{144}\text{Nd} = 0.7219$. The

mean value of $^{143}\text{Nd}/^{144}\text{Nd}$ for the JNdi-1 standard (Tanaka et al., 2000) during the period of measurement was 0.512109 ± 9 (2σ , $n = 5$). Procedural blanks run with unknowns show insignificant blank levels of c. 5 pg Sm and c. 12 pg Nd. Precisions for concentration analysis are approximately 0.5 % for Sm and Nd. Initial ϵNd values were calculated at 3000 Ma obtained from the minimum age from intrusive aplites (section 5.4). Uncertainties in calculated ϵ -values are ± 0.5 ϵ -units, based on results of duplicate runs. The Sm-Nd isotope data is present in Supplementary Table 4.

U-Pb zircon analyses

Zircon analyses were conducted at the Department of Petrology and Economic Geology, Geological Survey of Denmark and Greenland (GEUS). Hand-hammered chips from the rock samples were crushed directly in a tungsten-carbide disc-mill. The crushed material was poured onto a shaking table where the heavy mineral grains were separated. The heavy mineral fraction was transferred to disposable plastic Petri® dishes using ethanol, and magnetic minerals were removed using a hand magnet. Zircon grains were subsequently hand-picked from the final heavy mineral concentrate in the Petri® dish. The hand-picked zircon grains were cast into epoxy and polished to expose a central cross-section of each grain. The mount was documented prior to ablation using backscattered electron imaging in a scanning electron microscope. The mount was subsequently cleaned in an ultrasonic bath with propanol, and then loaded into the sample cell of the laser ablation system for age dating.

Zircon ages were obtained using a Laser-Ablation Sector Field Inductively Coupled Plasma Mass Spectrometer (LA-SF-ICP-MS). The laser ablation uses a focused laser beam to ablate a small amount of a sample contained in an air-tight sample cell. Detailed analytical protocols were described by Gerdes and Zeh (2006) and Frei and Gerdes (2009), but a brief summary is given here.

Samples and standards were mounted in a low-volume ablation cell specially developed for U-Pb dating (Horstwood et al., 2003). Helium was used to flush the sample cell and was mixed downstream with the Ar sample gas of the mass-spectrometer. A NewWave Research®/Merchantek® UP213 laser ablation unit was used, which emits a beam wavelength of 213nm and a 10Hz repetition rate. For the spot diameter (30 μm) and ablation times (30s) used in this study, the ablated mass of zircon was typically between 150-200 ng. The ablated material was transferred to the mass-spectrometer in an Ar-He carrier gas via Tygon® tubing into an Element2 (ThermoFinnigan®, Bremen) single-collector double focusing magnetic sector ICP-MS. The total acquisition time for each analysis was 60 seconds of which the first 30 seconds were used to determine the gas blank. The instrument was tuned to give large, stable signals for the ^{206}Pb and ^{238}U peaks, low background count rates (typically around 150 counts per second for ^{207}Pb) and low oxide production rates ($^{238}\text{U}^{16}\text{O}/^{238}\text{U}$ generally below 2.5 %). ^{202}Hg , $^{204}(\text{Pb} + \text{Hg})$, ^{206}Pb , ^{207}Pb , ^{208}Pb , ^{232}Th and ^{238}U intensities were determined through peak jumping using electrostatic scanning in low resolution mode and with the magnet resting at ^{202}Hg . Each peak was determined at four slightly different masses and integrated sampling and a settling time of 1ms for each isotope. Mass ^{202}Hg was measured to monitor the ^{204}Hg interference on ^{204}Pb where the $^{202}\text{Hg}/^{204}\text{Hg} \equiv 4.36$, which can be used to correct significant common Pb contributions using the model by Stacey and Kramers (1975). $^{207}\text{Pb}/^{235}\text{U}$ was calculated from the $^{207}\text{Pb}/^{206}\text{Pb}$ and $^{206}\text{Pb}/^{238}\text{U}$ assuming $^{238}\text{U}/^{235}\text{U} \equiv 137.88$. The elemental fractionation induced by the laser ablation and the instrumental mass bias on measured isotopic ratios were corrected through standard-sample bracketing using the GJ-1 zircon (Jackson et al., 2004). Samples were analyzed in sequences where three standards bracket each set of ten samples. The Plesovice zircon standard (Aftalion et al., 1989) was used as an external reproducibility check, and yielded long-term 2σ RSD precisions ($n = 109$) of 2%, 2.3% and 1.1% for the $^{206}\text{Pb}/^{238}\text{U}$, $^{207}\text{Pb}/^{235}\text{U}$ and $^{207}\text{Pb}/^{206}\text{Pb}$ ratios respectively (Frei et al., 2006). The raw data

were corrected for instrumental mass bias and laser-induced U-Pb fractionation through normalization to the GJ-1 zircon using in-house data reduction software. All isotope data were plotted and evaluated using ISOPLOT/EX 3.71 (Ludwig, 2003). Model age calculation and error propagation follow Sambridge and Lambert (1997). The U-Pb isotope data is presented in Supplementary Table 5.

In-situ Hf and O isotopic zircon analyses

Hf isotope analyses Laser ablation Lu-Hf isotope analyses were done at the Department of Earth Sciences at James Cook University, Townsville, Australia, using a 193 nm ArF laser and Finnigan Neptune mass spectrometer, with the same Faraday cup configuration employed by Woodhead et al. (2004). The method is outlined by Hawkesworth and Kemp (2006). Spot size were 31, 42 and 58 μm (only very few 31 μm spots) and with 4Hz laser pulse repetition rate. To counteract ArF degradation the power density at the sample was maintained at around 6-7 J/cm², which translated into an estimated ablation rate of c. 0.5 $\mu\text{m}/\text{sec}$. Ablation was conducted in He (flow rate c. 1.3 l/min, optimised daily). The isotope data were derived from a 60 second ablation period, comprising 60 cycles of 1s integration time. In the case of isotopic zoning or with intersecting cracks/inclusions, only the flattest, most stable portions of the time-resolved signal were selected for integration, performed off-line using a customised Excel spreadsheet. The correction for the isobaric interference of Lu and Yb on ^{176}Hf was performed in 'real time' as advocated by Woodhead et al. (2004). For Yb, this involved monitoring the interference-free ^{171}Yb during the analysis and then calculating the magnitude of the ^{176}Yb interference using the $^{176}\text{Yb}/^{171}\text{Yb}$ ratio determined by Segal et al. (2003) ($^{176}\text{Yb}/^{171}\text{Yb} = 0.897145$). The much smaller Lu correction is performed in the same way by measuring ^{175}Lu , and using $^{176}\text{Lu}/^{175}\text{Lu} = 0.02669$ (De Bièvre and Taylor, 1993). To correct for instrumental mass fractionation, Yb isotope ratios were normalised to $^{173}\text{Yb}/^{171}\text{Yb} = 1.130172$ (Segal et al., 2003) and Hf isotope ratios to $^{179}\text{Hf}/^{177}\text{Hf} = 0.7325$. The mass bias behaviour of Lu was assumed to follow that of Yb. The veracity of this protocol was checked by replicate analysis of a solution of known Hf isotope composition (JMC 475) that was spiked with variable amounts of pure Yb solution. The $^{176}\text{Hf}/^{177}\text{Hf}$ normalisation factor has been obtained from analyses of the Mud Tank zircon (MTZ) standard where the measured average during the entire analytical sessions was 0.282499 ± 18 and the 'true' (solution) value is taken as 0.282507 ± 6 (Woodhead and Herget, 2005). For CHUR we use the isotope ratios $^{176}\text{Lu}/^{177}\text{Hf} = 0.0336$ and $^{176}\text{Hf}/^{177}\text{Hf} = 0.282785$ as reported by Bouvier et al. (2008) and for the ^{176}Lu decay constant we use the value reported by Scherer et al. (2001) and Söderlund et al. (2004). The Hf isotope data is presented in Supplementary Table 6.

In-situ zircon oxygen isotope analyses

Oxygen isotope analyses Oxygen isotope ratios were measured using a CAMECA IMS1270 ion microprobe (NordSIMS Facility, Swedish Museum of Natural History) using a method similar to that described by Nemchin et al. (2006) with the exception that, for this study, only ^{16}O and ^{18}O were measured. Briefly, a 20keV Cs⁺ primary beam (+10kV primary, -10 kV secondary) of c. 5nA was used in aperture illumination mode to sputter a c. 15 μm diameter sample area, with a normal incidence electron gun providing charge compensation. Fully automated runs comprised a 20-s pre-sputter period with a raster of 25 μm , field aperture, entrance slit and mass centering, using the ^{16}O signal, followed by 240s of data acquisition using two Faraday detectors in the multicollector system operating at a common mass resolution of c. 2500. Data were normalised to measurements of the Geo-standard zircon 91500, assuming a $\delta^{18}\text{O}$ value of +9.86‰ determined by laser fluorination (reported in Wiedenbeck et al., 2004). The O isotope data is presented in Supplementary Table 7.

Tourmaline electron microprobe analyses

In-situ major element analyses of tourmaline from a tourmalinite horizon were obtained using the JEOL JXA 8900 electron microprobe at the Department of Earth and Planetary Sciences, McGill University. Operating conditions were a 15kV acceleration voltage, 20 nA beam current and focused beam. Element standards and on peak count times are as follows; albite (Na 30s), olivine (Si 20s, Fe 30s), orthoclase (Al 20s, K 50s), chromite (Cr 50s), diopside (Mg 30s, Ca 40s), apatite (F 60s), spessartine (Mn 50s) and rutile (Ti 40 s). Primary standards were regularly analyzed to allow for drift correction (only observed for K), and biotite, andradite and olivine secondary standards were analyzed throughout the run to check precision (better than 2% relative for major elements, and 10% for minor elements) and accuracy (better than 10% relative for major elements, and up to 21% relative for minor elements). The electron microprobe data are presented in Supplementary Table 8.

References

- Aftalion, M., Bowes, D.R., Vřana, S., 1989. Early Carboniferous U–Pb zircon ages for garnetiferous potassic granulites, Blanský les massif, Czechoslovakia. *Neues Jahrbuch für Mineralogie, Monatshefte* 4, 145–152.
- Bouvier A., Vervoort J.D., Patchett P.J., 2008. The Lu–Hf and Sm–Nd isotopic composition of CHUR: Constraints from unequilibrated chondrites and implications for the bulk composition of terrestrial planets. *Earth and Planetary Science Letters* 273, 48–57.
- De Bièvre P., Taylor, P.D.P., 1993. Table of the isotopic composition of the elements. *Int. J. Mass Spectrom. Ion Processes* 123, 149.
- Ersoy, Y., Helvacı, C., 2010. FC–AFC–FCA and mixing modeler: A Microsoft® Excel® spreadsheet program for modeling geochemical differentiation of magma by crystal fractionation, crustal assimilation and mixing. *Computer and Geoscience* 36, 383–390.
- Frei, R., Villa, I.M. Nägler, Th.F. Kramers, J.D., Pryzbyłowicz, W.J., Prozesky, V.M., Hofmann, B.A., Kamber, B.S., 1997. Single mineral dating by Pb–Pb step-leaching method; assessing the mechanisms. *Geochimica Cosmochimica Acta* 61, 393–414.
- Frei D., Hollis J.A., Gerdes A., Harlov D., Karlsson C., Vasquez P., Franz G., Johansson L., Knudsen C., 2006. Advanced in-situ trace element and geochronological microanalysis of geomaterials by laser ablation techniques. *Geological Survey of Denmark and Greenland Bulletin* 10, 25–28.
- Frei, D., Gerdes, A., 2009. Precise and accurate in situ U–Pb dating of zircon with high sample throughput by automated LA-SF-ICP-MS. *Chemical Geology* 261, 261–270.
- Gerdes, A., Zeh, A., 2006. Combined U–Pb and Hf isotope LA-(MC)-ICP-MS analyses of detrital zircons: Comparison with SHRIMP and new constraints for the provenance and age of an Armorican metasediment in Central Germany. *Earth and Planetary Science Letters* 249, 47–61.
- Hawkesworth, C.J., Kemp, A.I.S., 2006. Using hafnium and oxygen isotopes in zircons to unravel the record of crustal evolution. *Chemical Geology* 226, 144–162.
- Horstwood, M.S.A., Foster, G.L., Parrish, R.R., Noble, S.R., Nowell, G.M., 2003. Common-Pb corrected in situ U–Pb accessory mineral geochronology by LA-MC-ICP-MS. *Journal of Analytical Atomic Spectrometry* 18, 837–846.
- Jackson, S., Pearson, N.J., Griffin, W.L., Belousova, E.A., 2004. The application of laser ablation - inductively coupled plasma - mass spectrometry to in situ U–Pb zircon geochronology. *Chemical Geology* 211, 47–69.
- Janoušek, V., Farrow, C. M., Erban, V., 2006. Interpretation of whole-rock geochemical data in igneous geochemistry: introducing geochemical data toolkit (GCDkit). *Journal of Petrology* 47, 1255–1259.
- Ludwig, K.R., 2003. Isoplot/Ex 3.00. A geochronological toolkit for Microsoft Excel. Special Publication 4. Berkeley Geochronological Center, Berkeley, CA.
- Nemchin, A.A., Whitehouse, M.J., Pidgeon, R.T., Meyer, C., 2006. Oxygen isotopic signature of 4.4–3.9 Ga zircons as a monitor of differentiation processes on the Moon. *Geochimica Cosmochimica Acta* 70, 1864–1872.
- Sambridge, M., Lambert, D.D., 1997. Propagating errors in decay equations: Examples from the Re–Os isotopic system. *Geochimica Cosmochimica Acta* 61, 3019–3024.
- Savard, D., Barnes, S.-J., Meisel, T., 2010. Comparison between nickel-sulfur-fire-assay Te-coprecipitation and isotope-dilution with high pressure asher acid digestion for the determination of platinum-group elements, rhenium and gold concentrations. *Geostandards and Geoanalytical Research* 34, 281–291.
- Schaller, M., Steiner, O., Suder, I., Frei, R., Kramers, J.D., 1997. Pb stepwise leaching (PbSL) dating of garnet—addressing the inclusion problem. *Schweiz. Min. Pet. Mitt.* 77, 113–121.
- Scherer E., Münker C., Mezger K., 2001. Calibration of the lutetium-hafnium clock. *Science* 293, 683–687.
- Segal, I., Halicz, L. and Platzner, I.T., 2003. Accurate isotope ratio measurements of ytterbium by multi-collector inductively coupled plasma mass spectrometry applying erbium and hafnium in an improved double external normalisation procedure. *J. Anal. At. Spectrom.* 18, 1217–1223.
- Söderlund U., Patchett P.J., Vervoort J.D., Isachsen C.E., 2004. The ¹⁷⁶Lu decay constant determined by Lu–Hf and U–Pb isotope systematics of Precambrian mafic intrusions. *Earth and Planetary Science Letters* 219, 311–324.
- Stacey, J.S., Kramers, J.D., 1975. Approximation of terrestrial lead isotope evolution by a two-stage model. *Earth and Planetary Science Letters* 26, 207–221.
- Tanaka, T., Togashi, S., Kamioka, H., Amakawa, H., Kagami, H., Hamamoto, T., Yuhara, M., Orihashi, Y., Yoneda, S., Shimizu, H., Kunimaru, T., Takahashi, K., Yanagi, T., Nakano, T., Fujimaki, H., Shinjo, R., Asahara, Y., Tanimizu, M., Dragusanu, G., 2000. JNdi-1: a neodymium isotope reference in consistency with LaJolla neodymium. *Chemical Geology* 168, 279–281.
- Wiedenbeck, M., Hanchar, J. M., Peck, W. H., Sylvester, P., Valley, J., Whitehouse, M., Kronz, A., Morishita, Y., Nasdala, L., Fiebig, J., Franchi, I., Girard, J.-P., Greenwood, R.C., Hinton, R., Kita, N., Mason, P.R.D., Norman, M., Ogasawara, M., Piccoli, P.M., Rhede, D., Satoh, H., Schulz-Dobrick, B., Skår, O., Spicuzza, M.J., Terada, K., Tindle, A., Togashi, S., Vennemann, T., Xie, Q., Zheng, Y.-F., 2004. Further Characterisation of the 91500 Zircon Crystal. *Geostandards and Geoanalytical Research* 28, 9–39.
- Woodhead, J., Hergt, J., Shelley, M., Eggins, S., Kemp, R., 2004. Zircon Hf-isotope analysis with an excimer laser, depth profiling, ablation of complex geometries, and concomitant age estimation. *Chemical Geology* 209, 121–135.
- Woodhead, J., Hergt, J., 2005. A Preliminary Appraisal of Seven Natural Zircon Reference Materials for In Situ Hf Isotope Determination. *Geostandards and Geological Research* 29, 183–195.

Supplementary data table 1 (Paper III): Major and trace element data

ACME-labs	Lithology	Latitude	Longitude
468646	Aplite	63.71601195	-49.27854969
468647	Pillow Lava	63.71601195	-49.27854969
468648	Aplite	63.71601195	-49.27854969
468651	Amphibolite	63.71418595	-49.26752346
468653	Granite	63.70784479	-49.25146491
468654	Granite	63.70935772	-49.24545911
468660	Pillow Lava	63.71582470	-49.28264031
468661	Pillow Lava	63.71582470	-49.28264031
468662	Pillow Lava	63.71582470	-49.28264031
468665	Amphibolite	63.71556092	-49.28682413
468666	Ultramafic Rock	63.71556092	-49.28682413
468667	Ultramafic Rock	63.71598521	-49.29327962
468668	Ultramafic Rock	63.71544600	-49.29698199
468669	Ultramafic Rock	63.71544600	-49.29698199
468670	Amphibolite	63.71814347	-49.30232663
468672	Amphibolite	63.71749546	-49.31024904
468673	Amphibolite	63.71749546	-49.31024904
468674	Granite	63.71687713	-49.31359090
468676	Pillow Lava	63.71642023	-49.31298531
468677	Amphibolite	63.71642023	-49.31298531
468678	Aplite	63.71475860	-49.28339510
484630	Aplite	63.71645049	-49.27946055
484631	Aplite	63.71528054	-49.28021299
484632	Tourmalinite	63.71585152	-49.27828289
484633	Aplite	63.71585152	-49.27828289
484634	Pillow Lava	63.71585152	-49.27828289
484635	Amphibolite	63.71585152	-49.27828289
484636	Tourmalinite	63.71591488	-49.27773329
484638	Amphibolite	63.71540996	-49.27619395
484639	Pillow Lava	63.71590650	-49.27817409
484640	Aplite	63.71543351	-49.28175208
484641	Aplite	63.71543351	-49.28175208
499168	Ultramafic Rock	63.71582000	-49.29176000
499174	Amphibolite	63.70938000	-49.22555800
499181	Pillow Lava	63.71540000	-49.28505400
499182	Pillow Lava	63.71526000	-49.28453900
499183	Amphibolite	63.71597000	-49.28656200
499184	Pillow Lava	63.71501000	-49.28426600
499187	Aplite	63.71443000	-49.28301000
499190	Tourmalinite	63.71410000	-49.28234500
4686641	Pillow Lava	63.71580768	-49.28430437
4686642	Pillow Lava	63.71580768	-49.28430437
4846371	Amphibolite	63.71588530	-49.27720506
4846372	Amphibolite	63.71588530	-49.27720506
4846373	Amphibolite	63.71588530	-49.27720506
4846374	Amphibolite	63.71588530	-49.27720506
4846375	Amphibolite	63.71588530	-49.27720506
499161	Aplite	63.7222200	-49.2453680
499169	Ultramafic Rock	63.7157400	-49.2928490
499171	Ultramafic Rock	63.7194000	-49.2609570
499172	Ultramafic Rock	63.7218100	-49.2577390
499173	Granite	63.7179500	-49.2562310
499175	Ultramafic Rock	63.7093800	-49.2255580
499176	Amphibolite	63.7115300	-49.2757040
499185	Aplite	63.7148600	-49.2838040
499186	Aplite	63.7144300	-49.2830100
499188	Ultramafic Rock	63.7142400	-49.2825600
499189	Amphibolite	63.7142400	-49.2825600
499191	Ultramafic Rock	63.7141000	-49.2823450
499192	Aplite	63.7148900	-49.2838530

ACME-labs	SiO ₂	Al ₂ O ₃	Fe ₂ O ₃ *	MgO	CaO	Na ₂ O	K ₂ O	TiO ₂	P ₂ O ₅	MnO
Unit	%	%	%	%	%	%	%	%	%	%
MDL	0.01	0.01	0.04	0.01	0.01	0.01	0.01	0.01	0.01	0.01
468646	65.85	16.38	4.43	1.94	4.89	3.64	1.31	0.56	0.17	0.07
468647	51.62	13.89	12.46	7.56	10.79	1.72	0.16	0.57	0.05	0.19
468648	65.64	16.46	4.45	2.04	4.13	3.67	1.79	0.51	0.13	0.07
468651	50.24	14.26	12.32	8.23	10.24	2.14	0.22	0.77	0.04	0.19
468653	70.24	15.10	2.76	0.78	2.75	4.11	2.77	0.36	0.10	0.03
468654	71.46	14.55	2.61	0.77	2.50	3.91	2.87	0.35	0.12	0.04
468660	48.97	14.04	15.53	5.55	10.43	2.30	0.28	1.76	0.14	0.22
468661	45.73	15.21	16.89	6.32	9.70	2.48	0.53	1.96	0.15	0.25
468662	39.63	18.33	19.54	6.30	8.26	2.08	2.10	2.14	0.15	0.24
468665	50.58	10.86	21.25	5.16	5.53	3.80	0.07	1.48	0.08	0.21
468666	49.17	6.06	16.17	12.35	12.91	0.82	0.06	0.91	0.04	0.22
468667	46.43	4.48	16.58	17.07	9.89	0.43	1.77	0.63	0.03	0.22
468668	48.40	4.87	15.30	16.20	10.35	0.49	<0.01	0.67	0.02	0.21
468669	51.93	2.80	15.86	22.90	0.19	0.01	<0.01	0.32	0.02	0.21
468670	48.77	14.73	12.05	8.92	11.47	1.68	0.15	0.57	0.04	0.19
468672	52.52	14.91	12.09	5.87	8.82	2.62	0.30	1.00	0.06	0.35
468673	52.41	14.27	11.73	5.70	11.57	1.66	0.12	1.02	0.06	0.25
468674	70.28	14.22	3.49	1.38	1.95	5.15	1.57	0.41	0.09	0.04
468676	49.99	15.57	11.27	4.23	14.18	1.86	0.19	0.71	0.05	0.21
468677	47.85	14.49	12.90	8.17	11.10	2.19	0.68	0.87	0.04	0.21
468678	64.92	16.65	3.63	1.12	3.09	4.90	2.04	0.54	0.17	0.07
484630	62.65	15.32	4.78	2.06	5.56	4.43	1.71	0.45	0.08	0.06
484631	67.54	16.26	3.76	1.61	3.02	3.85	2.20	0.38	0.09	0.05
484632	55.93	19.12	5.41	5.43	6.33	1.10	<0.01	0.55	0.02	0.02
484633	65.08	16.53	4.97	1.96	4.15	4.70	0.73	0.46	0.14	0.05
484634	47.53	13.47	12.35	9.20	13.63	1.09	0.12	0.60	0.03	0.20
484635	50.55	14.53	12.42	8.67	8.67	2.93	0.21	0.73	0.04	0.20
484636	45.54	14.30	13.50	12.67	8.37	1.13	0.24	0.53	0.02	0.19
484638	47.98	15.31	13.58	8.61	10.40	1.67	0.18	1.05	0.07	0.20
484639	53.39	14.71	12.91	4.60	9.16	1.88	0.30	1.55	0.12	0.18
484640	65.76	15.53	4.29	1.40	3.95	3.52	2.24	0.52	0.15	0.06
484641	56.26	16.09	7.14	3.35	5.59	3.40	3.27	0.69	0.16	0.10
499168	41.96	8.13	16.09	19.72	5.72	0.17	<0.01	0.78	0.05	0.17
499174	46.32	16.45	13.60	7.22	10.78	2.71	0.63	0.78	0.05	0.20
499181	45.62	15.53	15.73	8.77	10.14	1.91	0.22	0.86	0.05	0.21
499182	49.95	12.06	20.70	4.40	8.69	0.96	0.23	1.59	0.09	0.28
499183	47.03	23.96	7.52	4.80	12.58	2.71	0.05	0.40	<0.01	0.11
499184	48.54	17.00	11.01	7.46	12.33	1.77	0.09	0.59	0.03	0.17
499187	71.20	15.14	3.00	0.78	3.33	4.67	0.55	0.24	0.08	0.04
499190	49.99	28.39	7.07	7.70	1.70	1.56	<0.01	0.85	<0.01	0.02
4686641	49.12	13.58	11.33	8.08	13.69	0.83	0.02	0.57	0.04	0.20
4686642	47.47	14.52	13.19	9.52	11.88	1.01	0.04	0.62	0.04	0.21
4846371	51.20	14.10	14.55	5.91	8.06	3.56	0.15	1.61	0.12	0.18
4846372	54.69	13.15	12.49	4.44	8.47	3.24	0.11	1.40	0.11	0.16
4846373	53.57	13.67	13.14	4.91	7.57	3.59	0.28	1.48	0.11	0.18
4846374	53.29	13.62	13.02	4.85	8.58	3.33	0.15	1.45	0.11	0.17
4846375	49.19	13.97	14.38	5.40	9.93	3.04	0.19	1.53	0.13	0.20
Actlabs	%	%	%	%	%	%	%	%	%	%
MDL	0.01	0.01	0.04	0.01	0.01	0.01	0.01	0.01	0.01	0.01
499161	72.76	13.98	2.39	0.7	1.19	3.81	3.86	0.25	0.1	0.06
499169	47.39	4.08	14.35	20.52	8.83	0.17	0.1	0.526	0.03	0.22
499171	48.2	5.41	13.73	16.22	9.45	0.43	0.6	0.654	0.05	0.24
499172	50.36	3.18	13.08	19.19	10.02	0.27	< 0.01	0.444	0.01	0.19
499173	66.3	15.87	4.35	1.56	2.95	4.88	1.58	0.655	0.23	0.05
499175	50.1	7.22	9.67	19.79	6.92	0.4	2.17	0.293	0.03	0.16
499176	49.8	11.09	13.97	8.44	11.64	1.54	0.78	0.905	0.08	0.22
499185	66.37	15.3	4.06	1.34	3.79	3.99	2.06	0.53	0.16	0.07
499186	69.01	15.59	3.5	1.47	3.06	4.02	1.87	0.387	0.1	0.05
499188	47.96	2.94	13.3	21.09	7.02	0.34	0.1	0.527	0.04	0.2
499189	52.73	14.22	15.71	4.51	5.44	4.34	0.16	1.297	0.13	0.19
499191	38.44	3.97	14.87	22.9	5.97	0.05	< 0.01	0.395	0.03	0.24
499192	55.12	17.66	7.27	3.19	5.19	4.13	3.03	0.827	0.19	0.09

ACME-labs	Cr ₂ O ₃	LOI	Sum	Sc	Ba	Co	Cs	Ga	Hf
Unit	%	%	%	ppm	ppm	ppm	ppm	ppm	ppm
MDL	0.002	0.005	0.01	1	1	0.2	0.1	0.5	0.1
468646	0.005	0.6	99.85	7	340	11.3	7.4	18.2	3.6
468647	0.066	0.7	99.81	43	30	53.3	0.2	13.8	0.9
468648	0.005	0.9	99.84	9	513	12.9	4.5	18.6	3.5
468651	0.029	1.1	99.77	51	51	48.4	4.1	14.5	1.3
468653	0.003	0.8	99.81	3	660	5.3	1.0	19.2	5.3
468654	0.004	0.7	99.84	6	493	5.4	1.3	18.2	5.1
468660	0.008	0.6	99.80	26	25	41.7	0.1	18.5	3.5
468661	0.007	0.5	99.76	29	87	46.6	0.7	16.8	3.6
468662	0.009	0.9	99.68	34	712	47.4	4.4	24.0	4.0
468665	<0.002	0.7	99.76	21	11	76.2	<0.1	19.7	2.7
468666	0.135	0.8	99.71	38	23	79.8	<0.1	10.8	1.4
468667	0.295	1.7	99.60	30	283	104.1	15.3	7.2	0.9
468668	0.301	2.8	99.66	28	14	106.9	0.2	7.6	1.0
468669	0.507	4.7	99.59	16	3	113.7	<0.1	4.6	0.7
468670	0.065	1.1	99.77	42	53	53.5	0.7	15.5	1.0
468672	0.008	1.3	99.81	48	68	47.2	1.1	15.4	1.9
468673	0.017	1.0	99.82	45	43	41.8	0.3	17.2	1.8
468674	0.003	1.3	99.89	6	463	8.3	0.7	9.6	4.0
468676	0.041	1.5	99.85	44	57	53.0	<0.1	16.5	1.7
468677	0.035	1.2	99.77	38	107	54.6	0.5	16.6	1.4
468678	<0.002	2.7	99.86	6	414	8.7	1.5	17.8	4.7
484630	0.003	2.7	99.84	10	746	14.9	2.3	17.7	3.4
484631	0.005	1.1	99.86	6	450	10.9	1.8	19.2	4.4
484632	0.019	6.0	99.86	13	10	23.5	1.4	15.4	0.8
484633	0.004	1.1	99.86	8	293	12.9	6.9	19.3	3.6
484634	0.068	1.5	99.78	44	19	54.1	2.1	13.9	1.4
484635	0.037	0.8	99.79	44	39	50.2	1.6	15.8	1.7
484636	0.075	3.1	99.71	36	29	68.6	83.5	14.6	1.2
484638	0.036	0.7	99.77	50	21	56.3	0.9	17.3	1.8
484639	0.018	0.9	99.79	29	117	37.8	8.6	18.6	3.1
484640	<0.002	2.4	99.86	7	380	8.3	2.4	17.5	3.7
484641	0.009	3.8	99.82	16	373	8.2	2.6	17.2	3.6
499168	0.287	6.4	99.58	34	8	122.7	0.3	10.9	1.7
499174	0.032	1.1	99.85	33	56	54.0	0.2	17.0	1.2
499181	0.028	0.7	99.79	32	39	68.0	0.1	15.8	1.5
499182	<0.002	0.8	99.78	43	11	56.1	<0.1	19.5	2.1
499183	0.016	0.7	99.85	21	35	29.1	<0.1	14.5	0.7
499184	0.060	0.7	99.80	37	20	46.7	<0.1	14.2	0.9
499187	0.002	0.8	99.85	4	808	4.7	0.2	18.9	5.1
499190	0.029	2.5	99.80	21	6	18.9	0.1	19.7	0.2
4686641	0.063	2.3	99.80	42	32	49.7	0.2	12.6	1.3
4686642	0.068	1.2	99.76	45	38	59.5	0.4	14.3	1.3
4846371	0.017	0.3	99.78	25	45	41.2	0.8	21.8	3.2
4846372	0.017	1.5	99.82	27	47	36.0	0.4	20.4	3.1
4846373	0.017	1.3	99.81	28	123	37.2	1.4	19.8	3.1
4846374	0.016	1.2	99.81	28	32	40.5	0.4	19.6	3.2
4846375	0.018	1.8	99.78	29	30	41.9	0.5	23.2	3.4
Actlabs	-	%	%	-	ppm	ppm	ppm	ppm	ppm
MDL	-	0.005	0.01	-	1	0.2	0.1	0.5	0.1
499161	-	1.12	100.2	-	880	6	6.7	-	3
499169	-	3.39	99.63	-	17	102	0.2	7	0.9
499171	-	4.44	99.42	-	71	81	53.8	8	1.1
499172	-	2.63	99.37	-	4	86	1	5	0.6
499173	-	1.79	100.2	-	627	9	1.3	20	5.1
499175	-	3.26	100	-	112	80	37.3	8	0.4
499176	-	1.42	99.89	-	136	56	1	14	1.7
499185	-	2.43	100.1	-	503	9	2.8	18	3.7
499186	-	1.28	100.3	-	381	9	1.7	18	3.1
499188	-	5.65	99.15	-	9	93	11.3	6	0.8
499189	-	0.49	99.22	-	14	51	1.8	18	2.9
499191	-	12.05	98.91	-	4	128	1.3	6	0.8
499192	-	3.59	100.3	-	527	21	5.4	20	3.1

ACME-labs	Nb	Rb	Sr	Ta	Th	U	V	W	ACME-labs
Unit	ppm	ppm	ppm	ppm	ppm	ppm	ppm	ppm	Unit
MDL	0.1	0.1	0.5	0.1	0.2	0.1	8	0.5	MDL
468646	5.6	65.2	317.3	0.5	5.2	1.7	71	<0.5	468646
468647	1.4	0.9	82.0	<0.1	0.3	<0.1	224	<0.5	468647
468648	5.8	58.6	240.2	0.4	6.0	1.6	78	<0.5	468648
468651	1.3	23.7	59.3	<0.1	0.2	0.1	308	1.0	468651
468653	7.5	88.0	289.7	0.8	11.8	0.9	30	<0.5	468653
468654	9.0	96.9	297.1	1.1	12.2	0.9	28	<0.5	468654
468660	6.4	1.8	194.2	0.4	1.0	0.2	269	<0.5	468660
468661	6.7	13.2	124.8	0.4	1.0	0.3	287	<0.5	468661
468662	7.2	90.8	120.7	0.5	1.2	0.3	340	<0.5	468662
468665	5.0	0.3	154.1	0.3	1.2	0.3	288	<0.5	468665
468666	2.5	0.6	43.2	0.2	0.5	0.2	238	<0.5	468666
468667	1.6	75.1	126.1	0.2	0.3	<0.1	171	<0.5	468667
468668	1.8	0.4	18.1	0.2	<0.2	<0.1	177	0.5	468668
468669	1.2	0.4	0.9	<0.1	<0.2	<0.1	79	<0.5	468669
468670	0.8	5.3	65.9	<0.1	0.3	<0.1	251	<0.5	468670
468672	2.1	17.0	66.9	0.2	0.5	0.1	321	1.0	468672
468673	2.2	6.2	54.2	0.2	1.0	0.2	294	<0.5	468673
468674	3.2	40.6	66.3	0.2	6.2	0.6	43	0.7	468674
468676	1.5	3.2	54.9	0.1	0.6	0.1	295	<0.5	468676
468677	1.8	21.6	121.4	0.1	0.2	<0.1	270	<0.5	468677
468678	5.1	42.1	311.6	0.4	7.0	1.0	46	2.9	468678
484630	3.9	49.9	143.9	0.3	4.6	0.9	81	<0.5	484630
484631	4.6	67.2	284.3	0.4	4.7	0.7	53	0.8	484631
484632	0.2	0.4	221.0	<0.1	0.4	<0.1	164	<0.5	484632
484633	4.9	23.1	327.3	0.4	7.5	1.5	76	<0.5	484633
484634	1.4	1.7	89.1	0.1	0.2	<0.1	261	<0.5	484634
484635	2.0	5.3	91.0	0.1	0.4	<0.1	279	<0.5	484635
484636	1.6	15.2	61.8	0.1	<0.2	<0.1	218	0.5	484636
484638	1.5	2.4	59.7	<0.1	0.2	<0.1	329	<0.5	484638
484639	5.0	10.1	258.2	0.4	0.7	0.3	261	<0.5	484639
484640	5.4	49.5	357.9	0.4	5.2	1.0	43	1.6	484640
484641	5.3	48.4	354.3	0.4	5.3	1.0	43	1.4	484641
499168	1.7	0.8	19.0	<0.1	0.2	0.1	196	<0.5	499168
499174	2.3	5.1	162.8	0.2	0.2	<0.1	206	<0.5	499174
499181	2.4	2.9	120.2	0.1	0.3	0.1	218	<0.5	499181
499182	3.0	0.7	9.0	0.1	0.3	0.2	413	<0.5	499182
499183	1.5	0.7	224.3	<0.1	0.2	<0.1	135	0.8	499183
499184	0.6	0.6	163.8	<0.1	<0.2	<0.1	217	<0.5	499184
499187	5.7	24.6	136.0	0.6	4.7	1.0	26	<0.5	499187
499190	<0.1	0.1	160.2	<0.1	<0.2	<0.1	295	<0.5	499190
4686641	1.6	1.1	99.2	<0.1	0.2	<0.1	236	<0.5	4686641
4686642	1.5	1.4	76.7	<0.1	<0.2	<0.1	256	<0.5	4686642
4846371	5.6	1.2	213.5	0.4	1.0	0.2	267	<0.5	4846371
4846372	4.7	0.6	228.1	0.3	0.8	0.2	232	<0.5	4846372
4846373	4.7	8.6	179.8	0.4	0.7	0.3	243	<0.5	4846373
4846374	4.9	1.4	193.2	0.4	0.8	0.3	237	<0.5	4846374
4846375	5.2	1.5	246.9	0.5	0.9	0.2	273	<0.5	4846375
Actlabs	ppm	ppm	ppm	ppm	ppm	ppm	ppm	ppm	Actlabs
MDL	0.1	1	0.5	0.01	0.2	0.1	8	0.5	MDL
499161	-	100	241	< 0.01	8.7	1.5	28	< 0.5	499161
499169	1.6	3	41	0.13	0.44	0.12	135	< 0.5	499169
499171	1.9	42	58	0.14	0.32	0.09	188	< 0.5	499171
499172	1.2	1	98	0.09	0.23	0.12	128	< 0.5	499172
499173	5.4	50	364	0.57	5.68	1.12	58	< 0.5	499173
499175	0.3	126	13	0.01	0.09	0.05	165	< 0.5	499175
499176	2.6	17	209	0.22	0.8	0.2	241	< 0.5	499176
499185	4.6	53	350	0.42	5.82	0.74	52	1.2	499185
499186	3.6	62	270	0.43	4.95	0.66	46	1	499186
499188	1.1	4	48	0.09	0.23	0.1	133	< 0.5	499188
499189	4.6	< 1	117	0.38	1.05	0.24	215	< 0.5	499189
499191	1	< 1	75	0.08	0.25	0.07	111	< 0.5	499191
499192	3.2	102	374	0.27	8.42	1.39	123	0.7	499192

Zr	Y	La	Ce	Pr	Nd	Sm	Eu	Gd	Tb	Dy
ppm	ppm	ppm	ppm	ppm	ppm	ppm	ppm	ppm	ppm	ppm
0.1	0.1	0.1	0.1	0.02	0.3	0.05	0.02	0.05	0.01	0.05
123.5	10.9	28.5	59.4	7.20	26.9	4.38	1.08	3.14	0.41	2.01
35.0	15.9	2.0	5.0	0.81	4.2	1.44	0.43	1.96	0.38	2.58
131.8	11.2	29.3	60.2	7.09	25.9	4.07	0.93	3.08	0.40	2.07
41.8	21.1	2.3	5.6	0.88	4.5	1.65	0.55	2.47	0.50	3.50
193.5	11.1	42.4	84.0	9.49	31.4	4.74	0.85	3.22	0.45	2.26
170.9	11.6	29.0	72.7	7.31	26.1	4.08	0.79	3.02	0.44	2.23
114.1	29.1	9.2	22.5	3.43	15.4	4.54	1.60	5.35	0.93	5.59
125.4	31.2	9.0	23.2	3.67	18.4	5.00	1.32	5.56	0.97	5.73
142.7	33.4	7.3	18.8	3.03	14.9	4.19	2.44	5.42	0.98	6.18
87.7	20.7	8.9	21.2	3.19	14.8	3.83	1.17	4.16	0.72	3.97
45.3	12.8	4.9	11.2	1.82	9.4	2.50	0.83	2.96	0.46	2.64
31.1	10.1	2.3	6.1	1.10	5.6	1.73	0.54	2.01	0.33	1.97
31.6	9.1	2.6	7.0	1.08	5.7	1.60	0.51	1.92	0.33	1.94
18.9	1.2	0.5	1.0	0.13	0.7	0.19	0.04	0.27	0.04	0.24
32.0	14.8	1.9	5.0	0.76	4.2	1.26	0.47	1.84	0.39	2.52
64.1	23.9	3.9	9.5	1.57	7.7	2.35	0.78	3.29	0.66	4.26
67.3	22.0	4.9	11.8	1.78	8.8	2.67	0.94	3.28	0.62	4.03
148.3	5.1	26.4	56.9	4.90	15.0	2.07	0.60	1.56	0.21	1.00
46.9	18.2	3.0	7.3	1.11	5.1	1.78	0.60	2.41	0.50	3.08
47.8	18.1	2.7	7.4	1.18	6.5	1.90	0.75	2.70	0.51	3.31
178.9	13.2	31.6	60.3	7.38	26.5	4.27	1.10	3.45	0.47	2.61
121.8	9.0	18.7	35.3	4.16	15.1	2.65	0.74	2.14	0.32	1.73
154.4	7.9	20.7	39.6	4.37	15.5	2.35	0.62	1.97	0.29	1.64
25.2	5.0	1.8	3.9	0.51	2.0	0.52	0.18	0.68	0.12	0.89
126.1	10.3	31.4	61.7	7.29	27.0	4.14	1.05	3.12	0.43	2.10
42.2	16.4	2.1	5.5	0.88	4.0	1.55	0.51	2.41	0.44	2.93
52.2	18.3	2.9	7.2	1.17	5.5	1.89	0.58	2.64	0.52	3.29
40.2	14.8	2.1	5.3	0.82	4.0	1.55	0.51	2.26	0.42	2.81
60.5	29.9	2.5	6.8	1.16	6.5	2.25	0.78	3.50	0.71	4.64
106.2	27.8	8.1	20.6	3.10	15.1	4.29	1.29	4.66	0.85	4.67
133.2	11.0	26.0	50.7	6.06	22.4	3.57	0.92	2.92	0.42	2.13
135.5	10.7	25.8	51.1	6.03	23.5	3.58	0.95	2.73	0.43	2.14
42.8	9.7	3.5	9.1	1.28	5.7	1.55	0.39	1.77	0.31	1.62
36.8	15.3	3.0	6.7	1.08	5.4	1.73	0.62	2.41	0.43	2.73
46.4	17.3	3.2	8.1	1.25	7.2	1.79	0.68	2.47	0.47	2.86
78.8	31.3	5.3	12.7	1.97	9.2	3.16	1.17	4.12	0.83	5.05
18.4	8.4	1.6	2.9	0.49	1.9	0.72	0.36	1.02	0.22	1.42
25.6	11.3	2.3	5.0	0.77	2.9	1.13	0.49	1.52	0.36	2.01
167.9	11.0	10.2	21.8	2.23	8.0	1.50	0.49	1.64	0.29	1.54
2.8	0.7	0.4	0.5	<0.02	<0.3	<0.05	0.08	0.07	0.02	0.11
37.0	16.7	2.0	5.1	0.80	4.1	1.37	0.46	2.05	0.41	2.66
41.0	16.9	2.0	5.2	0.86	4.4	1.47	0.53	2.13	0.43	2.68
116.9	24.7	6.3	16.7	2.54	12.2	4.05	1.39	5.09	0.86	5.03
94.9	24.6	7.1	18.0	2.76	13.5	3.69	1.21	4.41	0.77	4.19
100.2	26.0	7.2	19.7	2.92	13.8	3.84	1.34	4.44	0.80	4.46
99.4	25.7	9.0	22.0	3.37	16.7	4.13	1.33	4.58	0.82	4.27
102.7	27.8	8.9	22.4	3.39	16.8	4.30	1.56	4.83	0.84	4.62
ppm	ppm	ppm	ppm	ppm	ppm	ppm	ppm	ppm	ppm	ppm
0.1	0.1	0.1	0.1	0.02	0.3	0.05	0.02	0.05	0.01	0.05
111	10	28.8	53	-	23	3.4	0.8	-	< 0.01	-
32	9	1.79	5.06	0.83	4.59	1.45	0.433	1.64	0.29	1.8
38	12.1	2.53	7.06	1.09	5.67	1.79	0.698	2.21	0.39	2.41
23	8.3	2.46	5.78	0.91	4.53	1.39	0.533	1.6	0.28	1.67
215	8.8	53.7	94.4	10.4	34.7	4.96	1.33	3.24	0.4	1.87
13	8	0.74	1.98	0.3	1.71	0.56	0.242	0.87	0.2	1.39
56	18.8	10.1	17.1	2.41	10.4	2.69	1.01	3.2	0.58	3.59
137	12.3	29.8	57.6	6.31	22.7	3.72	1.02	2.78	0.43	2.28
117	7.5	20.2	38.5	3.97	14	2.27	0.655	1.77	0.27	1.4
29	8.6	1.72	4.66	0.72	3.76	1.2	0.498	1.44	0.27	1.68
109	25.9	7.37	19.6	2.7	13	3.76	1.22	4.32	0.79	4.8
27	7.2	2.33	5.6	0.79	3.82	1.06	0.352	1.26	0.23	1.35
118	14.3	27.5	54.9	6.15	22.8	3.92	1.2	3.11	0.46	2.58

ACME-labs	Ho	Er	Tm	Yb	Lu	Cu	Pb	Zn	Ni	Cr
Unit	ppm	ppm	ppm	ppm	ppm	ppm	ppm	ppm	ppm	-
MDL	0.02	0.03	0.01	0.05	0.01	0.1	0.1	1	0.1	-
468646	0.37	0.94	0.15	0.95	0.14	19.8	21.9	80	15.2	-
468647	0.56	1.72	0.26	1.65	0.27	36.6	3.2	11	41.5	-
468648	0.37	1.04	0.15	0.93	0.14	16.8	3.5	70	17.1	-
468651	0.76	2.34	0.38	2.51	0.38	66.6	2.8	23	39.7	-
468653	0.39	0.90	0.13	0.93	0.13	9.4	6.1	59	6.1	-
468654	0.37	1.03	0.15	0.98	0.14	7.6	5.9	54	6.2	-
468660	1.00	2.87	0.43	2.80	0.41	12.9	1.3	19	5.8	-
468661	1.14	3.27	0.48	3.14	0.46	93.8	1.3	28	11.7	-
468662	1.27	3.73	0.55	3.72	0.54	63.6	0.8	63	22.8	-
468665	0.76	2.05	0.30	1.79	0.27	337.9	1.3	23	31.8	-
468666	0.48	1.27	0.18	1.11	0.17	150.1	0.8	7	24.7	-
468667	0.38	1.00	0.15	0.90	0.13	168.2	0.4	39	324.6	-
468668	0.39	0.94	0.15	0.80	0.12	75.3	0.9	18	130.5	-
468669	0.04	0.13	0.02	0.15	0.03	33.8	0.3	5	116.8	-
468670	0.53	1.60	0.23	1.65	0.24	85.6	2.3	16	28.0	-
468672	0.86	2.66	0.41	2.75	0.39	10.0	0.9	28	15.2	-
468673	0.88	2.41	0.35	2.24	0.33	42.2	0.7	16	41.2	-
468674	0.18	0.57	0.08	0.56	0.09	22.1	5.2	46	12.3	-
468676	0.76	2.10	0.33	2.04	0.33	35.6	1.0	9	21.6	-
468677	0.68	2.01	0.31	2.21	0.32	15.9	0.9	21	38.9	-
468678	0.47	1.20	0.19	1.08	0.18	13.6	2.8	42	4.7	-
484630	0.34	0.91	0.15	0.84	0.15	4.9	1.7	29	15.0	-
484631	0.27	0.78	0.11	0.75	0.12	4.8	2.0	42	17.1	-
484632	0.18	0.58	0.09	0.66	0.10	27.9	0.8	8	8.8	-
484633	0.36	1.02	0.14	0.89	0.13	22.8	1.7	28	12.9	-
484634	0.64	1.94	0.30	1.98	0.31	0.5	0.4	5	9.4	-
484635	0.71	2.12	0.32	2.34	0.34	16.5	0.4	14	16.5	-
484636	0.59	1.74	0.27	1.75	0.26	15.2	0.3	29	77.6	-
484638	1.07	3.16	0.50	3.14	0.49	67.0	0.4	18	24.0	-
484639	0.99	2.75	0.41	2.44	0.38	166.3	0.5	33	18.3	-
484640	0.38	1.13	0.17	1.11	0.16	11.2	6.0	74	6.6	-
484641	0.39	1.09	0.17	1.08	0.16	14.3	3.2	78	36.0	-
499168	0.34	0.94	0.15	0.86	0.14	258.9	0.5	38	406.2	-
499174	0.56	1.83	0.26	1.61	0.24	4.6	0.6	27	36.7	-
499181	0.64	1.92	0.29	1.82	0.27	131.5	0.5	23	60.3	-
499182	1.05	3.08	0.52	3.23	0.50	183.2	0.3	46	11.9	-
499183	0.28	0.92	0.13	0.93	0.13	83.4	20.4	13	12.4	-
499184	0.39	1.25	0.23	1.26	0.22	109.4	0.7	12	23.5	-
499187	0.35	0.89	0.13	0.95	0.13	10.8	1.8	43	5.8	-
499190	0.03	0.08	0.01	0.10	0.02	86.0	<0.1	1	4.2	-
4686641	0.59	1.67	0.28	1.79	0.28	33.0	2.7	10	20.0	-
4686642	0.61	1.94	0.28	1.83	0.31	69.9	1.8	15	35.0	-
4846371	0.96	2.96	0.39	2.67	0.37	76.9	0.6	18	13.9	-
4846372	0.87	2.46	0.37	2.32	0.34	149.7	0.6	14	27.4	-
4846373	0.94	2.62	0.40	2.45	0.36	122.4	0.5	25	21.8	-
4846374	0.93	2.59	0.40	2.48	0.37	124.3	0.5	21	19.0	-
4846375	1.00	2.67	0.41	2.58	0.37	131.8	0.5	23	16.2	-
Actlabs	ppm	ppm	ppm	ppm	ppm	ppm	ppm	ppm	ppm	ppm
MDL	0.02	0.03	0.01	0.05	0.01	1	5	1	20	1
499161	-	-	-	0.8	0.16	8	29	51	8	< 1
499169	0.35	0.98	0.141	0.86	0.123	120	< 5	250	1120	1790
499171	0.46	1.3	0.189	1.16	0.161	90	< 5	130	540	1730
499172	0.31	0.87	0.124	0.75	0.11	130	< 5	130	940	1550
499173	0.31	0.82	0.11	0.67	0.09	20	6	50	< 20	40
499175	0.3	0.92	0.136	0.84	0.12	< 1	< 5	70	920	2780
499176	0.7	1.99	0.285	1.79	0.28	100	< 5	90	130	490
499185	0.44	1.27	0.19	1.22	0.181	< 1	13	70	< 20	30
499186	0.26	0.73	0.105	0.67	0.103	< 1	8	50	30	30
499188	0.31	0.84	0.116	0.7	0.105	70	< 5	100	1110	1700
499189	0.92	2.61	0.371	2.33	0.334	300	< 5	120	90	100
499191	0.25	0.73	0.11	0.7	0.106	100	< 5	90	1000	3070
499192	0.48	1.36	0.203	1.3	0.188	< 1	15	110	20	30

Results for PGE/NiS-FA

		99 Ru [1]	%	103 Rh [1]	%	105 Pd [1]	%	189 Os [1]	%	193 Ir [1]	%	195 Pt [1]	%	197 Au [1]	%
SAMPLE ID	Sample Name	Conc. [ppb]	Conc. RSD	Conc. [ppb]	Conc. RSD	Conc. [ppb]	Conc. RSD	Conc. [ppb]	Conc. RSD	Conc. [ppb]	Conc. RSD	Conc. [ppb]	Conc. RSD	Conc. [ppb]	Conc. RSD
468667	OZ-4	2.341	5.213	0.703	0.640	5.915	1.440	0.333	10.404	0.377	2.902	4.125	2.000	0.878	5.237
499168	OZ-3	2.736	1.214	0.701	5.726	6.236	5.293	1.008	1.976	0.869	0.608	4.777	1.166	2.272	2.050
499171	OZ-9	1.509	5.015	0.548	3.342	6.041	0.570	0.340	9.570	0.360	2.424	3.601	2.641	<0.484	-
499172	OZ-15	1.908	3.648	0.570	3.667	4.963	2.091	0.639	11.090	0.605	2.012	3.419	2.259	2.745	3.282
499175	OZ-8	4.038	0.599	1.115	3.136	5.054	2.503	0.893	8.989	0.839	1.208	8.451	1.162	1.282	3.404
499191	OZ-11	4.810	1.601	0.814	1.870	1.796	2.597	0.533	1.545	0.852	4.795	3.213	2.959	<0.484	-
Internal STND	OZ-16-bb-235	1.816	7.237	1.607	3.597	14.900	4.063	0.149	6.714	0.133	3.609	16.064	0.639	0.673	7.025
Internal STND	OA-51-bb-235	1.824	1.757	1.531	2.130	14.319	2.025	0.133	4.401	0.129	8.434	15.170	0.495	0.520	9.818
WORKING values (+/-ppb)	Compilation	1.847	0.117	1.577	0.109	15.409	0.794	0.170	0.040	0.125	0.017	15.847	2.169	1.149	0.529

Normalisation values:

		Ru (ppb)	Rh (ppb)	Pd (ppb)	Os (ppb)	Ir (ppb)	Pt (ppb)	Au (ppb)	Cu (ppm)	Ni (ppm)
Primitive Upper Mantle	Becker et al. (2006)	1	7.1	7.21	3.92	3.5	7.73	7.21	28	2000

Supplementary data table 3 (Paper III): Interlab standard comparison

GEUS (2003-2010) ¹					ACME lab (2008-2010) ²				ACME/GEUS	
Element	Avg	±1σ (abs.)	±1σ (%)	n	Avg	±1σ (abs.)	±1σ (%)	n	(% diff.)	Isotope
Sc	40.9	1.3	3.3	32	41.8	0.9	2.2	21	2.1	45
V	412	12	2.9	32	434	17	3.9	21	5.5	51
Cr	126	3	2.5	32	129	5	3.7	21	2.7	
Co	56.7	1.0	1.7	32	51.9	4.9	9.4	21	-8.5	59
Ni	60.1	2.1	3.5	32	61.0	7.1	11.7	19	1.6	
Cu	226	3	1.5	32	222	10	4.4	21	-1.8	63
Zn	106	2	2.2	32	62.2	5.1	8.1	21	-41.1	66
Ga	20.8	0.2	1.0	32	20.1	1.0	5.0	21	-3.4	71
Rb	3.30	0.05	1.6	32	3.57	0.51	14.4	21	8.1	85
Sr	213	3	1.4	32	224	7	3.1	21	5.4	88
Y	33.8	0.6	1.7	32	30.6	1.2	3.8	21	-9.5	89
Zr	122	3	2.3	32	111	5	4.3	21	-8.7	90
Nb	4.46	0.09	1.9	32	4.16	0.35	8.3	21	-6.8	93
Cs	0.059	0.003	4.5	32	0.121	0.043	35.1	14	106.2	133
Ba	46.5	1.1	2.4	31	47.9	4.4	9.2	21	3.0	137
La	6.58	0.08	1.2	32	6.41	0.32	5.0	21	-2.6	139
Ce	17.4	0.3	1.7	32	17.9	1.0	5.5	21	2.8	140
Pr	2.87	0.07	2.4	32	2.78	0.11	4.1	21	-3.2	141
Nd	14.7	0.3	2.0	32	14.4	0.8	5.4	21	-2.1	143
Sm	4.67	0.09	1.9	32	4.43	0.20	4.4	21	-5.1	147
Eu	1.67	0.04	2.5	32	1.64	0.06	3.8	21	-2.0	153
Gd	5.54	0.32	5.8	32	5.55	0.26	4.7	21	0.1	157
Tb	0.963	0.019	2.0	32	0.991	0.040	4.0	21	2.9	159
Dy	5.86	0.10	1.6	32	5.73	0.20	3.6	21	-2.1	161
Ho	1.23	0.03	2.3	32	1.16	0.05	4.0	21	-5.9	165
Er	3.19	0.06	1.8	32	3.26	0.16	4.9	21	2.0	166
Tm	0.479	0.009	1.8	32	0.469	0.030	6.4	21	-2.0	169
Yb	2.89	0.04	1.5	32	2.81	0.14	5.1	21	-2.6	174
Lu	0.425	0.012	2.9	32	0.419	0.029	7.0	21	-1.6	175
Hf	3.26	0.06	1.8	32	3.27	0.31	9.5	21	0.3	177
Ta	0.305	0.017	5.4	32	0.276	0.089	32.2	21	-9.4	181
W	n.a.				83.3	5.2	6.2	9		
Pb	1.24	0.08	6.5	32	1.17	1.57	134.9	21	-5.9	208
Th	0.594	0.024	4.0	32	0.790	0.232	29.4	21	33.0	232
U	0.147	0.005	3.1	32	0.186	0.096	51.9	21	26.2	238

¹Based on total digestion solution ICP-MS

²Based on total fusion ICP-MS

Rock	Sample	Sm (ppm)	Nd (ppm)	¹⁴⁷ Sm/ ¹⁴⁴ Nd	Error (%)	Abs. Error	¹⁴³ Nd/ ¹⁴⁴ Nd	±2σ mean (%)	Abs. Error
Pillow Lava	468661	5.23	20.07	0.158	0.010	0.000016	0.512252	0.0016	0.0000082
Amphibolite	484637-2	3.86	13.18	0.177	0.010	0.000018	0.512333	0.0012	0.0000061
Amphibolite	484638	2.27	6.04	0.227	0.010	0.000023	0.513392	0.0008	0.0000041
Amphibolite	468651	1.59	4.35	0.221	0.010	0.000022	0.513211	0.0015	0.0000077
Amphibolite	484637-4	4.26	15.78	0.163	0.010	0.000016	0.512208	0.0008	0.0000041
Ultramafic Rock	468667	1.61	4.96	0.197	0.010	0.000020	0.512762	0.0008	0.0000041
Ultramafic Rock	468666	2.35	8.47	0.168	0.010	0.000017	0.512254	0.0009	0.0000046
Ultramafic Rock	468668	1.62	4.88	0.201	0.010	0.000020	0.512867	0.0009	0.0000046
Aplite	484641	3.29	19.59	0.102	0.010	0.000010	0.511017	0.0011	0.0000056

Supplementary data table 4 (Paper II): Sm-Nd isotope data

Supplementary data table 5 (Paper III): U-Pb isotope data

Sample	Spot	Pb _c ^a	U (ppm)	Th/U	Age (Ma)		
					²⁰⁷ Pb/ ²⁰⁶ Pb	±2σ	Conc. %
499161	9	N	849	0.48	2839	38	92
499161	10	N	995	0.15	2869	33	95
499161	15	N	231	0.76	2884	52	104
499161	16	Y	1185	0.17	2668	52	83
499161	21	Y	438	0.76	2870	62	100
499161	22	Y	131	0.61	2882	43	90
499161	23	Y	229	0.27	2876	57	96
499161	27	Y	816	0.26	2826	58	100
499161	28	N	943	0.16	2831	72	90
499161	34	Y	870	0.35	2706	98	89
499161	36	N	442	0.16	2862	40	95
499161	37	Y	316	0.37	2867	34	100
499161	38	Y	688	0.66	2834	73	98
499161	39	Y	368	0.57	2902	93	98
499161	40	N	282	0.12	2901	27	98
499161	41	Y	150	0.25	2881	40	100
499161	47	Y	375	0.92	2883	41	103
499161	48	Y	1649	0.18	2726	30	85
499161	49	N	656	0.63	2868	68	105
499161	50	Y	665	0.14	2855	20	96
499161	51	Y	481	0.43	2800	69	90
499161	53	Y	332	0.30	2852	40	102
499161	54	Y	104	0.41	2912	32	108
499161	55	N	1217	0.19	2759	41	80
499161	60	Y	131	0.28	2890	26	103
499161	61	N	1725	0.22	2670	44	87
499161	62	Y	543	0.74	2857	31	103
499161	63	Y	449	0.82	2879	35	101
499161	64	Y	531	0.85	2848	30	104
499161	65	N	699	0.24	2836	25	101
499161	66	Y	439	1.14	2878	27	103
499161	67	Y	583	0.34	2699	25	89
499161	68	Y	920	0.55	2839	27	108
499161	73	Y	933	0.32	2767	28	89
499161	74	N	899	0.16	2765	41	97
499161	75	N	459	0.38	2873	31	109
499161	76	Y	373	0.32	2808	42	109
499161	77	Y	828	0.24	2761	47	90
499161	78	Y	342	0.47	2875	12	110
499161	79	Y	434	0.21	2861	25	106
499161	80	Y	565	0.43	2832	43	105
499161	81	Y	119	0.42	2862	25	105
499161	86	Y	1042	0.27	2840	30	103
499161	87	Y	280	0.39	2887	17	109
499161	88	Y	313	1.00	2895	34	102
499161	89	N	1374	0.24	2703	37	88
499161	90	N	68	0.75	3201	22	102
499161	91	Y	740	0.63	2867	26	102
468653	9	Y	382	0.94	2849	23	108
468653	10	N	1090	0.18	2778	21	109
468653	11	N	102	0.37	2883	25	99
468653	12	N	461	0.09	2859	20	102
468653	13	N	916	0.40	2827	23	107
468653	15	N	302	0.60	2873	33	101

^bCut off at 100^aCommon lead corrected (Yes/No)

Sample	Spot	Pb _c ^a	U (ppm)	Th/U
468653	16	N	238	1.06
468653	21	N	435	1.05
468653	22	N	1024	0.23
468653	23	N	620	1.01
468653	24	N	647	0.51
468653	25	N	374	0.43
468653	26	N	1383	0.42
468653	27	N	630	0.40
468653	28	N	241	0.66
468653	29	N	2686	0.52
468653	34	N	831	0.43
468653	35	N	542	0.47
468653	36	N	1279	0.48
468653	37	N	1032	0.31
468653	39	N	554	0.49
468653	41	N	323	0.10
468653	170	Y	2635	0.41
468653	171	N	421	0.77
468653	172	Y	1573	0.29
468653	177	Y	2186	0.71
468653	178	Y	1436	0.36
468653	179	N	393	0.29
468653	180	N	1860	0.40
468653	181	Y	436	0.27
468653	185	Y	649	0.15
468653	194	Y	1126	0.62
468653	195	Y	921	0.48
468653	196	N	763	0.34
468653	197	N	1343	0.20
468653	198	N	765	0.39
468653	199	N	876	0.31
468653	200	N	601	0.35
468653	210	N	833	0.23
468653	211	Y	358	0.32
468653	213	Y	917	0.28
468657	7	N	354	0.50
468657	8	N	143	0.43
468657	10	N	152	0.53
468657	11	Y	201	0.38
468657	13	Y	256	0.47
468657	14	Y	118	0.44
468657	15	N	121	0.48
468657	16	N	151	0.33
468657	20	Y	202	0.55
468657	24	N	173	0.43
468657	27	N	173	0.50
468657	28	Y	126	0.60
468657	37	N	243	0.41
468657	38	N	338	0.27
468657	39	N	367	0.35
468646	25	N	171	0.41
468646	26	N	117	0.43
468646	27	N	130	0.46
468646	28	N	561	0.51
468646	29	N	181	0.58
468646	33	N	81	0.43
468646	34	N	227	0.48
468646	35	N	165	0.54

²⁰⁷ Pb/ ²⁰⁶ Pb	±2σ	Conc. %
2881	33	103
2857	34	103
2811	45	100
2812	44	108
2846	32	104
2868	42	106
2609	28	97
2842	30	107
2893	37	105
2579	27	83
2831	36	109
2862	27	105
2694	22	96
2794	35	108
2848	38	103
2886	23	105
2696	25	95
2883	22	103
2816	25	107
2658	30	97
2836	23	104
2868	19	85
2724	29	94
2880	21	98
2819	29	105
2789	37	95
2841	36	100
2865	36	100
2704	24	97
2879	21	101
2871	21	98
2892	18	98
2878	26	102
2821	31	104
2795	41	86
2854	14	101
2860	21	101
2866	22	101
2847	16	104
2839	16	100
2849	19	104
2860	32	100
2868	13	103
2834	16	102
2867	18	109
2858	22	105
3180	27	98
2850	29	98
2847	23	103
2840	20	105
2919	37	100
2909	34	102
2917	47	98
2900	45	102
2913	35	96
2916	37	98
2892	40	100
2921	30	101

Sample	Spot	Pb _c ^a	U (ppm)	Th/U
468646	36	N	147	0.56
468646	37	N	201	0.60
468646	38	N	218	0.76
468646	39	N	216	0.74
468646	40	N	171	0.64
468646	41	N	99	0.63
468646	42	Y	143	0.65
468646	47	N	102	0.62
468646	48	N	130	0.47
468646	49	N	152	0.51
468646	50	N	205	0.44
468646	51	N	163	0.46
468646	52	N	229	0.67
468646	53	N	155	0.64
468646	54	N	102	0.69
468646	55	N	183	0.63
468646	60	N	104	0.45
468646	61	N	191	0.52
468646	138	N	117	1.03
468646	139	N	142	0.82
468646	140	N	293	0.46
468646	141	N	234	0.54
468646	142	N	422	0.66
468646	143	N	339	0.95
468646	144	N	344	0.52
468646	145	N	181	0.70
468646	146	N	327	0.74
468646	151	N	140	0.64
468646	152	N	297	0.61
468646	153	N	490	1.04
468646	154	N	418	0.34
468646	155	N	198	0.85
468646	156	N	518	0.59
468646	157	N	137	0.58
468646	158	N	89	0.40
468646	159	N	142	0.49
468646	164	N	650	1.09
468646	165	N	161	0.73
468646	166	N	410	0.86
468646	168	N	214	0.43
468646	169	N	372	0.69
468646	170	N	549	1.15
468646	171	N	230	0.86
468646	172	Y	230	0.61
468646	178	N	89	0.60
468646	179	N	213	0.39
468646	180	N	314	1.51
468646	181	N	198	0.87
468646	182	N	132	0.79
468646	183	N	208	0.36
468646	184	N	131	0.55
468646	185	N	168	0.55
468646	193	N	225	0.84
468646	194	N	368	0.61
468646	195	N	234	0.33
468646	196	N	164	0.77
468646	197	N	321	0.75
468646	198	N	259	0.83

²⁰⁷ Pb/ ²⁰⁶ Pb	±2σ	Conc. %
2912	37	99
2888	35	100
2907	27	103
2906	30	102
2912	42	99
2926	36	97
2919	31	100
2920	28	103
2917	39	97
2918	35	99
2907	31	98
2911	32	103
2902	25	100
2918	20	105
2896	30	102
2915	27	100
2912	22	106
2905	25	106
2903	22	97
2917	17	102
2912	23	107
2911	24	109
2903	21	102
2908	19	103
2910	19	106
2961	38	103
2931	20	104
2916	26	97
2910	24	103
2902	18	98
2909	20	107
2923	38	99
2870	17	104
2912	21	104
2915	29	101
2918	26	101
2896	15	101
2902	19	102
2911	17	94
2903	31	107
2907	18	104
2906	22	95
2910	17	99
2926	30	104
2918	30	100
2913	24	106
2912	12	98
2917	26	100
2926	24	103
2899	14	102
2925	36	104
2912	16	103
2899	21	102
2923	19	101
2921	22	103
2920	28	98
2914	12	103
2908	23	107

Sample	Spot	Pb _c ^a	U (ppm)	Th/U
468646	199	N	154	0.57
468646	200	N	208	0.36
468646	201	N	429	0.79
468646	206	N	114	0.73
468646	207	N	210	0.80
468646	208	N	514	0.89
468646	209	N	225	0.29
468646	210	N	151	0.41
468646	211	N	129	0.76
468646	212	N	208	0.73
468646	213	N	321	0.47
468646	214	N	197	0.87
468646	219	N	114	0.59
468646	220	N	114	0.53
468646	221	N	189	0.53
468646	222	N	145	0.59
468646	223	N	110	0.68
468646	224	N	79	0.56
468646	225	N	108	0.56
468646	226	N	340	0.49
468646	227	N	95	0.52
468646	232	N	108	0.65
468646	233	N	236	0.49
468646	234	N	131	0.72
468646	235	N	283	0.75
468646	236	N	193	0.65
468646	237	N	551	0.47
468646	238	N	154	0.53
468646	239	N	128	0.50
468646	240	N	82	0.41
468646	245	N	221	0.64
468646	246	N	127	0.79
468646	247	N	584	1.18
468646	248	N	206	0.61
468646	249	N	883	1.44
468646	251	N	697	0.74
468646	253	N	114	0.57
468646	259	N	206	0.57
468646	260	N	138	0.65
468646	261	N	165	0.49
468646	262	N	324	0.81
468646	263	N	132	0.42
468646	264	N	224	0.34
468646	265	N	79	0.51
468646	266	N	183	0.57
468646	271	N	241	0.47
468646	272	N	307	0.45
468646	273	N	203	0.48
468646	274	N	173	0.65
468646	275	N	121	0.53
468646	276	N	65	0.25
468646	277	N	128	0.73
468646	278	N	147	0.59
468646	279	N	119	0.99
468646	284	N	213	0.63
468646	286	N	1006	0.69
484631	7	N	158	0.47
484631	8	N	209	0.47

²⁰⁷ Pb/ ²⁰⁶ Pb	±2σ	Conc. %
2911	27	98
2908	25	96
2909	17	100
2909	28	106
2924	14	103
2927	19	100
2917	24	97
2932	34	105
2925	30	105
2915	27	106
2903	23	105
2924	22	99
2926	21	100
2915	35	97
2923	35	99
2934	31	94
2919	18	104
2938	36	96
2913	32	99
2910	26	102
2920	38	97
2908	34	104
2909	21	104
2917	21	100
2903	29	103
2904	23	104
2886	33	100
2916	26	99
2903	33	102
2925	33	100
2909	28	103
2920	34	108
2898	22	102
2876	31	110
2891	20	100
2886	22	107
2894	41	104
2918	45	100
2934	35	108
2910	21	110
2917	39	94
2913	39	98
2938	20	101
2936	26	101
2917	32	93
2921	13	101
2919	42	106
2916	40	98
2920	35	102
2927	31	96
2918	36	102
2886	39	102
2899	32	103
2915	35	109
2915	32	104
2894	41	101
2924	36	98
2907	41	99

Sample	Spot	Pb _c ^a	U (ppm)	Th/U
484631	9	N	149	0.66
484631	10	N	167	0.68
484631	11	N	195	0.60
484631	12	N	264	0.47
484631	13	Y	230	0.36
484631	14	N	384	0.59
484631	15	N	260	0.35
484631	21	N	117	0.47
484631	22	N	209	0.52
484631	23	N	102	0.77
484631	24	N	106	0.52
484631	287	N	138	0.68
484631	288	N	239	0.54
484631	289	N	118	0.63
484631	290	N	91	0.62
484631	291	N	146	0.63
484631	292	N	182	0.68
484631	297	N	198	0.57
484631	298	N	212	0.65
484631	299	N	126	0.81
484631	300	N	311	0.60
484631	301	N	721	0.57
484631	302	N	207	0.51
484631	303	N	181	0.59
484631	305	N	125	0.61
484631	310	N	160	0.43
484631	311	N	177	0.51
484631	312	N	155	0.60
484631	313	N	153	0.94
484631	314	N	138	0.52
484631	315	N	76	0.57
484631	316	N	84	0.90
484633	65	N	111	0.53
484633	66	N	176	0.66
484633	67	N	120	0.54
484633	68	N	174	0.80
484633	73	N	232	0.67
484633	74	N	183	0.62
484633	75	N	190	0.57
484633	78	N	159	0.69
484633	79	N	129	0.53
484633	80	N	276	0.69
484633	81	N	209	0.71
484633	86	N	121	0.55
484633	87	N	75	0.70
484633	88	N	179	0.51
484633	89	N	430	1.11
484633	90	N	183	0.92
484633	91	N	145	0.61
484633	92	N	150	0.72
484633	93	N	190	0.89
484633	94	N	144	0.46
484633	99	N	341	0.67
484633	100	N	138	0.66
484633	101	N	236	0.50
484633	102	N	131	0.62
484633	103	N	335	0.54
484633	104	N	134	0.61

²⁰⁷ Pb/ ²⁰⁶ Pb	±2σ	Conc. %
2922	22	101
2902	24	106
2905	37	101
2716	63	80
2926	22	101
2876	33	90
2932	50	97
2918	50	98
2887	22	99
2885	27	91
2904	29	103
2921	26	102
2831	30	106
2911	40	106
2910	21	106
2879	38	108
2914	27	106
2912	32	105
2925	26	102
2917	25	98
2823	77	86
2733	31	103
2909	31	103
2922	35	99
2920	22	102
2939	32	95
2918	34	105
2931	22	106
2948	42	88
2900	40	85
2936	36	103
2929	28	98
2915	40	106
2920	20	90
2929	29	99
2915	26	99
2916	30	100
2938	24	107
2918	19	101
2911	22	102
2932	23	102
2922	35	105
2917	24	97
2906	35	106
2895	29	106
2910	34	102
2913	22	103
2912	26	104
2919	38	110
2861	43	105
2900	24	107
2901	19	109
2895	33	104
2910	40	103
2900	34	102
2906	36	98
2902	36	99
2912	40	91

Sample	Spot	Pb _c ^a	U (ppm)	Th/U
484633	105	N	111	0.52
484633	106	N	94	0.72
484633	107	N	195	0.87
484633	112	N	418	1.00
484633	113	N	182	0.83
484633	114	N	136	0.53
484633	115	N	116	0.69
484633	116	N	235	0.59
484633	117	N	149	0.57
484633	118	N	200	1.06
484633	119	N	174	0.53
484633	120	N	125	0.79
484633	125	N	256	0.55
484633	127	N	88	0.79
484633	128	N	123	0.57
484633	129	N	131	0.56
484633	130	N	120	0.68
484633	131	N	148	0.63
484633	132	N	51	0.80
484633	133	N	207	0.62

²⁰⁷ Pb/ ²⁰⁶ Pb	±2σ	Conc. %
2837	47	99
2910	28	103
2911	21	98
2895	24	96
2902	31	97
2887	39	100
2913	35	98
2890	21	101
2919	23	97
2907	30	98
2875	22	105
2911	21	105
2875	36	105
2911	41	105
2872	38	104
2909	17	109
2897	46	100
2904	29	99
2893	45	107
2895	33	108

Isotope ratio

Sample	Spot	²⁰⁶ Pb/ ²⁰⁴ Pb ^b	²⁰⁸ Pb/ ²³² Th	±2σ(%)	²³⁸ U/ ²⁰⁶ Pb	±2σ(%)	²⁰⁷ Pb/ ²⁰⁶ Pb	±2σ(%)
499161	9	65179	0.139	8.5	2.136	20.3	0.202	2.4
499161	10	2458	0.212	30.8	1.966	7.3	0.205	2.0
499161	15	28291	0.158	4.5	1.622	4.2	0.207	3.2
499161	16	20977	0.114	9.8	2.888	15.7	0.182	3.2
499161	21	10280	0.144	11.5	1.773	7.7	0.205	3.8
499161	22	2507	0.102	38.9	2.213	13.2	0.207	2.7
499161	23	643	0.129	32.0	1.957	12.5	0.206	3.5
499161	27	1871	0.139	18.8	1.824	8.9	0.200	3.5
499161	28	1523	0.274	23.6	2.277	4.6	0.201	4.4
499161	34	470	0.106	39.8	2.429	25.9	0.186	5.9
499161	36	4667	0.218	18.8	1.983	9.7	0.204	2.5
499161	37	4890	0.160	13.1	1.796	7.3	0.205	2.1
499161	38	9799	0.153	10.0	1.882	9.9	0.201	4.4
499161	39	1551	0.173	8.8	1.840	10.0	0.209	5.7
499161	40	16411	0.230	12.7	1.830	8.1	0.209	1.7
499161	41	833	0.198	19.5	1.773	7.8	0.207	2.4
499161	47	2593	0.188	10.8	1.671	5.8	0.207	2.5
499161	48	548	0.132	10.0	2.696	8.1	0.188	1.8
499161	49	16944	0.212	9.6	1.601	5.3	0.205	4.2
499161	50	848	0.198	19.6	1.948	6.1	0.204	1.2
499161	51	581	0.175	15.5	2.274	9.4	0.197	4.2
499161	53	2345	0.140	14.1	1.733	6.1	0.203	2.4
499161	54	1006	0.144	22.7	1.492	12.7	0.211	2.0
499161	55	11080	0.143	10.5	2.994	7.3	0.192	2.5
499161	60	1869	0.174	19.7	1.648	5.2	0.208	1.6
499161	61	2359	0.160	6.1	2.619	5.2	0.182	2.7
499161	62	1259	0.175	10.7	1.678	5.4	0.204	1.9
499161	63	670	0.158	10.2	1.727	3.5	0.207	2.1
499161	64	886	0.187	9.7	1.659	3.9	0.203	1.8
499161	65	7731	0.183	9.3	1.778	6.1	0.201	1.5
499161	66	18738	0.172	5.1	1.674	3.0	0.207	1.7
499161	67	2602	0.149	9.0	2.469	8.9	0.185	1.5
499161	68	983	0.202	14.8	1.534	5.2	0.202	1.6
499161	73	2264	0.153	8.5	2.367	5.1	0.193	1.7
499161	74	42531	0.159	10.5	1.999	5.9	0.193	2.5
499161	75	23151	0.200	13.5	1.496	7.8	0.206	1.9
499161	76	184	0.174	26.5	1.514	4.6	0.198	2.5
499161	77	1939	0.121	22.6	2.334	7.3	0.192	2.8
499161	78	2193	0.191	10.8	1.457	5.3	0.206	0.7
499161	79	617	0.127	26.0	1.579	2.4	0.204	1.5
499161	80	1404	0.150	22.9	1.634	9.4	0.201	2.6
499161	81	6509	0.160	15.8	1.608	7.4	0.204	1.6
499161	86	10165	0.170	3.2	1.702	5.1	0.202	1.8
499161	87	1808	0.156	33.2	1.482	4.2	0.208	1.0
499161	88	3144	0.169	5.6	1.675	3.4	0.209	2.1
499161	89	3131	0.137	15.3	2.520	7.6	0.186	2.3
499161	90	2320	0.218	7.3	1.490	4.3	0.253	1.4
499161	91	2743	0.173	7.2	1.711	7.1	0.205	1.6
468653	9	44170	0.200	8.6	1.517	2.2	0.203	1.4
468653	10	99999	0.201	5.1	1.543	0.8	0.194	1.3
468653	11	9403	0.161	6.1	1.808	1.8	0.207	1.6
468653	12	92809	0.161	4.8	1.716	1.4	0.204	1.2
468653	13	18018	0.186	3.9	1.561	1.4	0.200	1.4
468653	15	23332	0.163	6.2	1.727	3.4	0.206	2.0

Sample	Spot	$^{206}\text{Pb}/^{204}\text{Pb}^b$	$^{208}\text{Pb}/^{232}\text{Th}$	$\pm 2\sigma(\%)$	$^{238}\text{U}/^{206}\text{Pb}$	$\pm 2\sigma(\%)$	$^{207}\text{Pb}/^{206}\text{Pb}$	$\pm 2\sigma(\%)$
468653	16	14928	0.185	7.3	1.667	2.4	0.207	2.1
468653	21	11092	0.185	5.2	1.685	2.8	0.204	2.1
468653	22	8453	0.165	8.9	1.816	2.5	0.198	2.8
468653	23	24558	0.162	10.0	1.554	2.9	0.198	2.7
468653	24	25677	0.202	2.8	1.660	2.3	0.202	1.9
468653	25	20047	0.203	6.5	1.589	3.8	0.205	2.6
468653	26	7071	0.125	4.0	2.121	1.7	0.175	1.7
468653	27	42323	0.185	5.2	1.571	2.9	0.202	1.9
468653	28	6678	0.171	7.8	1.597	3.1	0.208	2.3
468653	29	5554	0.091	4.8	3.045	3.7	0.172	1.6
468653	34	99999	0.196	4.8	1.521	2.6	0.201	2.2
468653	35	15259	0.167	5.6	1.605	2.6	0.204	1.7
468653	36	7163	0.144	13.3	2.112	4.6	0.184	1.3
468653	37	99999	0.186	5.4	1.574	2.6	0.196	2.1
468653	39	6243	0.153	2.7	1.708	1.2	0.203	2.3
468653	41	3214	0.305	13.6	1.587	1.7	0.207	1.4
468653	170	8985	0.141	5.3	2.149	3.4	0.185	1.5
468653	171	1751	0.168	6.8	1.668	5.1	0.207	1.4
468653	172	23700	0.196	5.2	1.583	5.6	0.199	1.5
468653	177	8447	0.108	12.9	2.084	2.4	0.181	1.8
468653	178	23862	0.183	7.9	1.666	10.1	0.201	1.4
468653	179	7326	0.151	21.2	2.476	11.3	0.205	1.2
468653	180	24792	0.144	4.4	2.188	3.8	0.188	1.8
468653	181	6504	0.133	12.5	1.863	3.3	0.207	1.3
468653	185	5755	0.204	8.0	1.639	4.6	0.199	1.8
468653	194	1664	0.143	3.5	2.082	2.5	0.195	2.3
468653	195	2972	0.160	7.2	1.820	4.6	0.202	2.2
468653	196	10933	0.187	5.8	1.799	4.0	0.205	2.2
468653	197	22785	0.177	6.7	2.045	4.9	0.186	1.5
468653	198	25118	0.142	15.7	1.748	5.3	0.207	1.3
468653	199	25062	0.153	8.7	1.841	3.6	0.206	1.3
468653	200	27639	0.186	5.3	1.844	10.7	0.208	1.1
468653	210	17941	0.173	6.0	1.719	6.9	0.206	1.6
468653	211	26495	0.162	18.3	1.665	5.6	0.199	1.9
468653	213	10755	0.130	69.7	2.520	7.0	0.196	2.5
468657	7	12948	0.127	4.0	1.784	1.1	0.2034	0.8
468657	8	54699	0.126	7.5	1.765	2.1	0.2042	1.3
468657	10	39769	0.118	5.0	1.768	2.0	0.2050	1.3
468657	11	7879	0.125	8.6	1.711	2.2	0.2026	1.0
468657	13	96009	0.125	2.9	1.813	0.9	0.2015	1.0
468657	14	11623	0.126	5.0	1.710	1.7	0.2028	1.2
468657	15	7415	0.127	4.9	1.797	2.3	0.2041	1.9
468657	16	9148	0.126	12.0	1.719	2.6	0.2052	0.8
468657	20	18870	0.123	6.3	1.769	2.0	0.2009	1.0
468657	24	88479	0.137	3.2	1.605	1.2	0.2050	1.1
468657	27	26281	0.122	8.0	1.687	2.4	0.2039	1.3
468657	28	3262	0.158	11.4	1.619	3.5	0.2492	1.7
468657	37	24676	0.120	3.9	1.841	2.2	0.2030	1.8
468657	38	54013	0.132	4.1	1.742	1.7	0.2026	1.4
468657	39	65966	0.130	9.1	1.695	3.2	0.2018	1.2
468646	25	10353	0.153	7.2	1.741	3.6	0.212	2.3
468646	26	8181	0.149	7.6	1.683	5.9	0.210	2.1
468646	27	7104	0.146	13.4	1.827	7.8	0.212	2.9
468646	28	99999	0.161	3.2	1.692	3.9	0.209	2.8
468646	29	8726	0.152	8.0	1.917	8.9	0.211	2.1
468646	33	3711	0.146	9.2	1.813	6.8	0.211	2.3
468646	34	5928	0.150	4.2	1.770	5.1	0.208	2.4
468646	35	964	0.163	5.9	1.715	3.9	0.212	1.8

Sample	Spot	$^{206}\text{Pb}/^{204}\text{Pb}^b$	$^{208}\text{Pb}/^{232}\text{Th}$	$\pm 2\sigma(\%)$	$^{238}\text{U}/^{206}\text{Pb}$	$\pm 2\sigma(\%)$	$^{207}\text{Pb}/^{206}\text{Pb}$	$\pm 2\sigma(\%)$
468646	36	20997	0.150	5.8	1.778	5.8	0.211	2.3
468646	37	8093	0.156	9.8	1.785	12.1	0.208	2.1
468646	38	15052	0.162	4.7	1.642	4.2	0.210	1.6
468646	39	21379	0.171	5.6	1.694	5.1	0.210	1.9
468646	40	9265	0.154	7.4	1.794	4.7	0.211	2.6
468646	41	6880	0.155	7.5	1.842	5.6	0.213	2.2
468646	42	2144	0.141	9.6	1.752	6.0	0.212	1.9
468646	47	5630	0.167	4.0	1.653	4.7	0.212	1.7
468646	48	5026	0.163	4.8	1.856	4.8	0.211	2.4
468646	49	26035	0.162	5.0	1.796	4.8	0.212	2.2
468646	50	4011	0.153	6.6	1.812	5.2	0.210	1.9
468646	51	5550	0.161	5.2	1.657	4.3	0.211	2.0
468646	52	6739	0.159	22.5	1.770	6.0	0.210	1.6
468646	53	99999	0.159	6.1	1.581	8.8	0.212	1.2
468646	54	12703	0.150	4.1	1.677	3.8	0.209	1.8
468646	55	9649	0.158	4.2	1.732	5.4	0.211	1.7
468646	60	9884	0.166	8.3	1.543	4.9	0.211	1.3
468646	61	8634	0.168	5.2	1.551	3.8	0.210	1.6
468646	138	12255	0.152	7.7	1.836	6.4	0.2097	1.4
468646	139	1403	0.178	4.6	1.701	4.8	0.2114	1.0
468646	140	69373	0.180	5.5	1.610	5.0	0.2108	1.4
468646	141	9290	0.170	17.1	1.565	2.9	0.2107	1.5
468646	142	73811	0.175	5.0	1.720	4.4	0.2097	1.3
468646	143	1416	0.179	7.2	1.689	3.6	0.2103	1.2
468646	144	60342	0.176	4.6	1.632	4.4	0.2105	1.2
468646	145	3985	0.200	11.9	1.648	5.3	0.2173	2.4
468646	146	4925	0.187	4.0	1.648	4.0	0.2133	1.2
468646	151	2056	0.160	4.3	1.825	5.1	0.2114	1.6
468646	152	13555	0.173	2.5	1.694	2.6	0.2106	1.5
468646	153	99999	0.158	8.8	1.810	5.2	0.2096	1.1
468646	154	40707	0.184	4.3	1.619	3.7	0.2105	1.3
468646	155	5445	0.151	13.6	1.773	6.6	0.2123	2.4
468646	156	17223	0.166	3.8	1.708	3.5	0.2055	1.0
468646	157	7784	0.166	7.4	1.667	6.1	0.2109	1.3
468646	158	20529	0.188	13.7	1.730	6.1	0.2112	1.8
468646	159	7377	0.168	6.0	1.718	4.0	0.2116	1.6
468646	164	36309	0.150	4.4	1.732	3.1	0.2088	0.9
468646	165	5968	0.161	5.6	1.722	2.8	0.2095	1.2
468646	166	13379	0.149	8.0	1.897	4.8	0.2108	1.1
468646	168	6492	0.177	4.9	1.615	2.5	0.2097	1.9
468646	169	28084	0.174	10.7	1.663	6.8	0.2102	1.1
468646	170	20219	0.175	9.8	1.862	7.3	0.2100	1.4
468646	171	42827	0.163	3.4	1.771	3.6	0.2105	1.1
468646	172	99999	0.211	33.4	1.657	15.7	0.2127	1.9
468646	178	4044	0.163	5.5	1.747	7.6	0.2116	1.8
468646	179	22202	0.171	9.7	1.636	4.6	0.2110	1.5
468646	180	5940	0.159	12.4	1.790	4.6	0.2108	0.7
468646	181	37793	0.158	7.5	1.739	3.3	0.2114	1.6
468646	182	4909	0.159	10.2	1.683	5.4	0.2127	1.5
468646	183	14011	0.166	6.8	1.717	3.7	0.2092	0.8
468646	184	11309	0.183	7.2	1.661	6.0	0.2125	2.2
468646	185	9160	0.165	4.6	1.694	3.6	0.2108	1.0
468646	193	18849	0.172	9.5	1.714	5.3	0.2092	1.3
468646	194	10007	0.154	9.8	1.731	4.0	0.2123	1.1
468646	195	30729	0.187	12.1	1.672	3.2	0.2120	1.4
468646	196	8671	0.151	4.9	1.782	4.0	0.2119	1.7
468646	197	40228	0.154	3.7	1.688	2.7	0.2110	0.7
468646	198	11114	0.166	5.2	1.617	7.8	0.2104	1.4

Sample	Spot	$^{206}\text{Pb}/^{204}\text{Pb}^b$	$^{208}\text{Pb}/^{232}\text{Th}$	$\pm 2\sigma(\%)$	$^{238}\text{U}/^{206}\text{Pb}$	$\pm 2\sigma(\%)$	$^{207}\text{Pb}/^{206}\text{Pb}$	$\pm 2\sigma(\%)$
468646	199	3375	0.163	8.7	1.790	4.7	0.2108	1.7
468646	200	7433	0.153	13.2	1.842	8.2	0.2103	1.6
468646	201	14685	0.176	17.7	1.748	9.9	0.2105	1.1
468646	206	31759	0.156	8.9	1.624	4.7	0.2105	1.7
468646	207	26206	0.162	4.8	1.685	2.8	0.2124	0.9
468646	208	18519	0.162	8.2	1.741	5.5	0.2128	1.2
468646	209	37919	0.156	10.2	1.816	5.9	0.2115	1.5
468646	210	45379	0.184	8.9	1.642	3.0	0.2135	2.1
468646	211	5525	0.164	7.6	1.637	2.4	0.2126	1.8
468646	212	9196	0.168	10.1	1.619	7.8	0.2112	1.7
468646	213	12187	0.170	11.2	1.661	8.0	0.2097	1.4
468646	214	12527	0.155	6.8	1.769	3.6	0.2124	1.4
468646	219	3898	0.162	6.3	1.747	6.7	0.2127	1.3
468646	220	99999	0.146	8.5	1.823	4.7	0.2113	2.2
468646	221	8386	0.161	5.4	1.773	3.4	0.2122	2.1
468646	222	7156	0.154	17.9	1.878	9.8	0.2138	1.9
468646	223	8328	0.156	5.1	1.660	2.7	0.2117	1.1
468646	224	2675	0.144	13.9	1.820	6.5	0.2143	2.2
468646	225	4694	0.154	8.5	1.781	5.2	0.2110	2.0
468646	226	75001	0.158	6.2	1.708	6.6	0.2105	1.6
468646	227	27420	0.146	13.1	1.802	4.2	0.2119	2.3
468646	232	3474	0.166	13.6	1.673	9.1	0.2103	2.1
468646	233	14446	0.168	11.9	1.679	4.1	0.2104	1.3
468646	234	5009	0.160	8.1	1.749	5.2	0.2115	1.3
468646	235	16097	0.150	6.4	1.693	4.4	0.2097	1.8
468646	236	31464	0.163	12.7	1.675	8.3	0.2098	1.4
468646	237	99999	0.142	8.5	1.778	5.1	0.2075	2.0
468646	238	40288	0.152	7.3	1.768	3.6	0.2114	1.6
468646	239	12023	0.150	8.2	1.712	5.1	0.2097	2.0
468646	240	1640	0.154	12.6	1.746	6.9	0.2125	2.1
468646	245	17095	0.153	10.1	1.697	8.7	0.2104	1.7
468646	246	7815	0.170	5.4	1.580	4.9	0.2118	2.1
468646	247	49300	0.157	15.2	1.716	5.7	0.2090	1.4
468646	248	3711	0.176	15.0	1.584	8.4	0.2062	1.9
468646	249	46107	0.157	8.2	1.775	6.2	0.2081	1.3
468646	251	99999	0.167	5.3	1.624	5.4	0.2075	1.4
468646	253	3695	0.176	6.8	1.674	8.7	0.2086	2.5
468646	259	14151	0.159	5.0	1.740	5.6	0.2117	2.8
468646	260	10127	0.179	5.5	1.575	2.8	0.2137	2.2
468646	261	3628	0.185	7.7	1.559	5.0	0.2106	1.3
468646	262	10973	0.140	7.7	1.898	5.4	0.2115	2.4
468646	263	9933	0.143	28.0	1.792	10.5	0.2110	2.4
468646	264	20314	0.168	6.1	1.716	4.2	0.2142	1.3
468646	265	6933	0.161	9.3	1.707	7.3	0.2140	1.6
468646	266	5548	0.152	5.6	1.907	8.0	0.2115	2.0
468646	271	23273	0.165	4.7	1.715	4.2	0.2121	0.8
468646	272	30620	0.172	8.4	1.624	8.6	0.2118	2.6
468646	273	9321	0.148	6.4	1.782	5.7	0.2114	2.5
468646	274	23649	0.170	6.0	1.693	7.2	0.2119	2.2
468646	275	4762	0.163	6.0	1.826	6.6	0.2128	1.9
468646	276	4330	0.172	15.6	1.712	7.5	0.2116	2.2
468646	277	8502	0.157	5.8	1.718	5.2	0.2075	2.4
468646	278	2412	0.162	9.4	1.702	5.3	0.2092	2.0
468646	279	32766	0.172	9.9	1.578	6.5	0.2113	2.2
468646	284	34258	0.161	4.6	1.668	3.7	0.2113	2.0
468646	286	31544	0.323	41.4	1.752	7.6	0.2085	2.5
484631	7	4333	0.177	8.3	1.801	4.4	0.2124	2.2
484631	8	20453	0.190	9.1	1.779	8.2	0.2102	2.5

Sample	Spot	$^{206}\text{Pb}/^{204}\text{Pb}^b$	$^{208}\text{Pb}/^{232}\text{Th}$	$\pm 2\sigma(\%)$	$^{238}\text{U}/^{206}\text{Pb}$	$\pm 2\sigma(\%)$	$^{207}\text{Pb}/^{206}\text{Pb}$	$\pm 2\sigma(\%)$
484631	9	7580	0.155	6.1	1.695	3.9	0.2122	1.4
484631	10	99999	0.163	6.2	1.552	2.8	0.2096	1.5
484631	11	6136	0.155	3.9	1.735	4.1	0.2100	2.3
484631	12	9087	0.093	26.8	3.102	9.4	0.1870	3.8
484631	13	27329	0.165	13.8	1.716	3.2	0.2127	1.4
484631	14	53340	0.152	13.9	2.219	12.5	0.2062	2.1
484631	15	7005	0.172	9.5	1.866	3.4	0.2135	3.1
484631	21	9585	0.156	12.0	1.841	7.1	0.2117	3.1
484631	22	7034	0.168	8.1	1.823	3.2	0.2076	1.3
484631	23	8687	0.084	8.1	2.150	6.8	0.2074	1.6
484631	24	4970	0.166	17.9	1.667	5.8	0.2098	1.8
484631	287	5546	0.155	8.3	1.709	8.0	0.2120	1.6
484631	288	9766	0.167	6.8	1.680	2.9	0.2006	1.8
484631	289	2577	0.166	7.5	1.623	7.4	0.2107	2.4
484631	290	6054	0.164	7.8	1.626	5.1	0.2106	1.3
484631	291	12742	0.164	22.8	1.610	5.7	0.2066	2.3
484631	292	7260	0.166	3.7	1.629	4.3	0.2111	1.6
484631	297	4231	0.170	4.2	1.640	2.0	0.2108	2.0
484631	298	13540	0.166	3.6	1.699	2.8	0.2126	1.6
484631	299	8903	0.159	6.3	1.782	3.9	0.2115	1.6
484631	300	5247	0.117	11.0	2.188	9.3	0.1996	4.7
484631	301	33448	0.161	10.4	1.828	6.6	0.1889	1.9
484631	302	5359	0.173	4.0	1.697	4.0	0.2104	1.9
484631	303	99999	0.165	5.9	1.771	5.4	0.2122	2.1
484631	305	36340	0.167	4.8	1.712	5.2	0.2119	1.3
484631	310	4650	0.159	7.5	1.839	5.1	0.2144	2.0
484631	311	17782	0.179	8.0	1.645	6.3	0.2117	2.1
484631	312	8641	0.174	10.7	1.617	4.7	0.2133	1.4
484631	313	5782	0.134	7.8	2.012	4.0	0.2155	2.6
484631	314	3349	0.137	24.3	2.158	15.7	0.2093	2.5
484631	315	21344	0.175	11.5	1.673	7.3	0.2140	2.2
484631	316	8724	0.139	7.4	1.784	5.4	0.2131	1.8
484633	65	16024	0.157	7.1	1.635	4.6	0.2113	2.5
484633	66	7296	0.145	8.5	1.990	8.2	0.2119	1.3
484633	67	11430	0.150	5.6	1.766	5.8	0.2130	1.8
484633	68	5441	0.161	12.1	1.762	5.1	0.2112	1.6
484633	73	20435	0.159	7.2	1.744	4.2	0.2114	1.8
484633	74	4277	0.169	6.2	1.591	6.1	0.2142	1.5
484633	75	5895	0.156	6.1	1.733	3.1	0.2116	1.2
484633	78	4154	0.149	12.9	1.719	5.8	0.2107	1.4
484633	79	22420	0.159	4.7	1.689	4.6	0.2134	1.4
484633	80	5974	0.157	5.8	1.645	3.2	0.2122	2.2
484633	81	99999	0.145	5.9	1.803	3.8	0.2115	1.5
484633	86	26358	0.166	4.4	1.629	4.3	0.2101	2.2
484633	87	3507	0.154	8.8	1.647	5.3	0.2087	1.8
484633	88	7258	0.163	5.7	1.712	3.5	0.2106	2.1
484633	89	40480	0.160	4.5	1.694	3.6	0.2110	1.4
484633	90	42339	0.167	2.6	1.660	3.4	0.2108	1.6
484633	91	13145	0.177	39.9	1.546	10.4	0.2117	2.4
484633	92	48386	0.161	6.2	1.678	4.3	0.2043	2.7
484633	93	7020	0.165	3.2	1.626	4.3	0.2093	1.5
484633	94	13809	0.184	10.2	1.581	5.6	0.2094	1.2
484633	99	13196	0.163	6.0	1.687	3.0	0.2087	2.0
484633	100	16886	0.160	8.7	1.689	6.0	0.2105	2.5
484633	101	10197	0.157	4.4	1.711	4.8	0.2092	2.1
484633	102	5461	0.138	12.2	1.807	4.3	0.2101	2.2
484633	103	13870	0.164	6.2	1.772	5.6	0.2095	2.2
484633	104	4015	0.143	14.2	1.966	10.4	0.2109	2.5

Sample	Spot	$^{206}\text{Pb}/^{204}\text{Pb}^b$	$^{208}\text{Pb}/^{232}\text{Th}$	$\pm 2\sigma(\%)$	$^{238}\text{U}/^{206}\text{Pb}$	$\pm 2\sigma(\%)$	$^{207}\text{Pb}/^{206}\text{Pb}$	$\pm 2\sigma(\%)$
484633	105	4159	0.136	25.3	1.839	6.2	0.2013	2.9
484633	106	4352	0.154	6.9	1.698	5.4	0.2106	1.7
484633	107	7679	0.143	5.7	1.803	5.7	0.2107	1.3
484633	112	15272	0.137	15.0	1.861	5.2	0.2086	1.5
484633	113	4747	0.140	5.4	1.820	4.2	0.2095	1.9
484633	114	6800	0.149	7.5	1.776	7.9	0.2077	2.4
484633	115	11098	0.132	8.1	1.784	4.6	0.2109	2.1
484633	116	7964	0.148	5.5	1.736	5.0	0.2080	1.3
484633	117	42665	0.168	8.8	1.812	5.3	0.2118	1.4
484633	118	19334	0.142	11.7	1.789	7.3	0.2102	1.9
484633	119	10884	0.160	6.4	1.669	1.9	0.2060	1.3
484633	120	6988	0.141	3.3	1.651	2.0	0.2108	1.3
484633	125	3433	0.152	18.3	1.678	3.1	0.2061	2.2
484633	127	2818	0.156	5.4	1.656	5.5	0.2107	2.5
484633	128	7341	0.142	14.1	1.698	8.0	0.2056	2.4
484633	129	9023	0.171	5.9	1.568	2.9	0.2104	1.1
484633	130	99999	0.135	10.8	1.770	8.1	0.2089	2.8
484633	131	9718	0.156	7.6	1.774	6.3	0.2098	1.8
484633	132	3042	0.167	4.5	1.624	5.3	0.2084	2.8
484633	133	4508	0.161	10.3	1.607	5.4	0.2086	2.0

Supplementary data table 6 (Paper III): Hafnium isotope data

Sample	Spot	$^{176}\text{Hf}/^{177}\text{Hf}$	$\pm 2\sigma$	$^{178}\text{Hf}/^{177}\text{Hf}$	$\pm 2\sigma$	$^{176}\text{Lu}/^{177}\text{Hf}$	$\pm 2\sigma$
499161	2	0.281067	0.000015	1.467339	0.000026	0.001369	0.000031
499161	4	0.281007	0.000018	1.467351	0.000033	0.000639	0.000007
499161	5	0.281039	0.000014	1.467338	0.000034	0.000756	0.000050
499161	6	0.281070	0.000010	1.467329	0.000020	0.001601	0.000011
499161	7	0.281057	0.000014	1.467324	0.000022	0.001270	0.000110
499161	8	0.281055	0.000008	1.467326	0.000021	0.001446	0.000008
499161	9	0.281087	0.000012	1.467288	0.000023	0.002024	0.000030
499161	10	0.281091	0.000009	1.467335	0.000020	0.001487	0.000024
499161	11	0.281055	0.000009	1.467314	0.000016	0.001105	0.000024
499161	12	0.281063	0.000013	1.467329	0.000014	0.001343	0.000062
499161	13	0.281057	0.000014	1.467275	0.000024	0.001320	0.000047
499161	14	0.281025	0.000010	1.467277	0.000018	0.001259	0.000065
499161	15	0.280851	0.000014	1.467304	0.000023	0.001083	0.000005
468653	1	0.281011	0.000015	1.467403	0.000054	0.001074	0.000042
468653	4	0.280972	0.000014	1.467398	0.000047	0.000528	0.000053
468653	6	0.281002	0.000010	1.467326	0.000021	0.000893	0.000005
468653	9	0.280984	0.000008	1.467354	0.000018	0.000797	0.000025
468653	10	0.281073	0.000010	1.467357	0.000029	0.001624	0.000102
468653	11	0.280999	0.000011	1.467329	0.000027	0.001011	0.000033
468653	12	0.281007	0.000014	1.467393	0.000030	0.001027	0.000087
468653	13	0.281001	0.000011	1.467351	0.000026	0.001054	0.000059
468653	14	0.281045	0.000011	1.467289	0.000021	0.001343	0.000033
468653	15	0.281071	0.000010	1.467339	0.000027	0.001604	0.000075

^aZircon $^{207}\text{Pb}/^{206}\text{Pb}$ age

^bCHUR values for calculating $\epsilon\text{Hf}(t)$: $^{176}\text{Hf}/^{177}\text{Hf} = 0.282785$, $^{176}\text{Lu}/^{177}\text{Hf} = 0.0336$ (Bouvier et al., 2008)

Errors combine the internal errors and the reproducibility of the standard analyses in quadrature

Sample	Spot	$^{176}\text{Yb}/^{177}\text{Hf}$	$\pm 2\sigma$	Age Ma ^a	$\pm 2\sigma$	Conc. %
499161	2	0.04895	0.00105	2869	33	95
499161	4	0.01978	0.00015	2668	52	83
499161	5	0.02535	0.00157	2882	43	90
499161	6	0.06109	0.00053	2826	58	100
499161	7	0.04070	0.00342	2867	34	100
499161	8	0.05050	0.00058	2855	20	96
499161	9	0.05312	0.00089	2879	35	101
499161	10	0.04225	0.00091	2878	27	103
499161	11	0.03231	0.00066	2873	31	109
499161	12	0.04276	0.00193	2808	42	109
499161	13	0.04227	0.00156	2875	12	110
499161	14	0.04313	0.00222	2895	34	102
499161	15	0.03407	0.00025	3201	22	102
468653	1	0.03342	0.00184	2795	41	86
468653	4	0.01518	0.00197	2878	26	102
468653	6	0.02319	0.00032	2704	24	97
468653	9	0.02199	0.00082	2819	29	105
468653	10	0.04796	0.00339	2841	36	100
468653	11	0.02829	0.00083	2868	19	85
468653	12	0.02786	0.00238	2816	25	107
468653	13	0.03124	0.00203	2836	23	104
468653	14	0.04255	0.00129	2696	25	95
468653	15	0.05096	0.00270	2696	25	95

Sample	Spot	$^{176}\text{Hf}/^{177}\text{Hf}_{(t)}$	$\pm 2\sigma$	$\epsilon\text{Hf}_{(t)}^b$	$\pm 2\sigma$
499161	2	0.280991	0.000036	1.95	1.27
499161	4	0.280974	0.000039	-3.37	1.40
499161	5	0.280997	0.000034	2.47	1.21
499161	6	0.280983	0.000027	0.67	0.96
499161	7	0.280987	0.000035	1.75	1.26
499161	8	0.280976	0.000025	1.08	0.87
499161	9	0.280975	0.000031	1.62	1.10
499161	10	0.281009	0.000026	2.80	0.92
499161	11	0.280994	0.000025	2.14	0.89
499161	12	0.280991	0.000032	0.52	1.13
499161	13	0.280984	0.000034	1.85	1.22
499161	14	0.280955	0.000028	1.28	0.99
499161	15	0.280784	0.000033	2.43	1.19
468653	1	0.280954	0.000035	-1.13	1.25
468653	4	0.280942	0.000034	0.43	1.20
468653	6	0.280956	0.000026	-3.18	0.94
468653	9	0.280941	0.000024	-1.00	0.86
468653	10	0.280984	0.000029	1.04	1.03
468653	11	0.280944	0.000029	0.23	1.05
468653	12	0.280952	0.000035	-0.68	1.25
468653	13	0.280944	0.000030	-0.48	1.06
468653	14	0.280976	0.000029	-2.66	1.03
468653	15	0.280989	0.000029	-2.20	1.02

Oxygen isotope composition of zircons reported as $\delta^{18}\text{O}$ as ‰ SMOW

Sample	Spot	$^{18}\text{O}/^{16}\text{O}$	d^{18}O	\pm ‰	Drift corr.	Ext. err.	Comment
ID	ID	<i>Drift corr.</i>	<i>Samples</i>		<i>‰ / run</i>	<i>‰ , 1 σ</i>	
468653	1a	0.0020125	6.21	0.26	0.00	0.21	
468653	1b	0.0020050	2.44	0.24	0.00	0.21	Altered
468653	2	0.0020097	4.79	0.28	0.00	0.21	
468653	3	0.0020108	5.36	0.26	0.00	0.21	
468653	4	0.0020134	6.68	0.24	0.00	0.21	
468653	5a	0.0020113	5.62	0.23	0.00	0.21	
468653	5b	0.0020118	5.88	0.26	0.00	0.21	
468653	6	0.0020119	5.91	0.27	0.00	0.21	
468653	7	0.0020125	6.21	0.30	0.00	0.21	
468653	8	0.0020125	6.23	0.26	0.00	0.21	
468653	9	0.0020125	6.21	0.27	0.00	0.21	
468653	10	0.0020062	3.08	0.22	0.00	0.21	Altered
468653	11	0.0020133	6.62	0.26	0.00	0.21	
468653	12	0.0020042	2.06	0.26	0.00	0.21	Altered

Supplementary data table 7 (Paper III): Oxygen isotope data

Supplementary data table 8 (Paper III): Electron microprobe data

Sample	Grain no.	Sequence no.	Sector	SiO ₂	TiO ₂	Al ₂ O ₃	Cr ₂ O ₃	MgO
Tour_1390	1	1 - core	+c	35.87	0.29	31.23	0.06	7.79
Tour_1390	1	2	+c	35.58	0.32	31.16	0.04	7.76
Tour_1390	1	3	+c	35.26	0.26	31.22	0.07	7.89
Tour_1390	1	4	+c	35.65	0.29	31.05	0.05	7.87
Tour_1390	1	5	a	34.57	1.09	29.31	0.07	8.32
Tour_1390	1	6	a	34.53	1.40	29.46	0.08	7.69
Tour_1390	1	7	a	35.24	1.16	29.40	0.10	8.25
Tour_1390	1	8	a	35.41	1.24	29.31	0.11	8.27
Tour_1390	1	9	a	34.54	1.24	28.86	0.11	8.20
Tour_1390	1	10	a	35.21	1.18	29.09	0.09	8.26
Tour_1390	1	11	a	35.18	1.18	29.27	0.10	8.25
Tour_1390	1	12	a	35.48	1.22	29.26	0.10	8.28
Tour_1390	1	13	a	35.59	1.18	29.00	0.11	8.40
Tour_1390	1	14	a	35.57	1.29	29.06	0.18	8.30
Tour_1390	1	15	a	35.74	1.27	29.08	0.16	8.40
Tour_1390	1	16	a	34.85	1.23	28.94	0.19	8.44
Tour_1390	1	17	a	34.92	1.27	29.27	0.19	8.38
Tour_1390	1	18	a	35.14	1.28	29.33	0.15	8.39
Tour_1390	1	19	a	35.32	1.20	29.40	0.20	8.29
Tour_1390	1	20	a	35.01	1.26	29.67	0.15	8.21
Tour_1390	1	21	a	35.52	1.29	29.54	0.12	7.97
Tour_1390	1	22	a	35.84	1.22	29.66	0.11	8.12
Tour_1390	1	23	a	35.89	1.21	29.30	0.17	8.23
Tour_1390	1	24	a	35.39	1.29	29.28	0.09	8.12
Tour_1390	1	25	a	35.73	1.26	29.01	0.13	8.13
Tour_1390	1	26	a	35.35	1.26	29.39	0.10	7.97
Tour_1390	1	27	a	35.16	1.14	29.23	0.14	8.14
Tour_1390	1	28	a	35.61	1.24	29.30	0.15	8.10
Tour_1390	1	29	a	35.76	1.10	29.22	0.17	8.25
Tour_1390	1	30	a	35.83	1.19	29.28	0.17	8.20
Tour_1390	1	31	a	35.80	1.15	29.17	0.14	8.07
Tour_1390	1	32	a	35.53	1.21	30.47	0.07	7.94
Tour_1390	1	33	a	35.59	1.22	29.53	0.12	7.88
Tour_1390	1	34	a	35.65	1.27	30.07	0.09	7.87
Tour_1390	1	35	a	35.97	1.21	29.74	0.10	8.06
Tour_1390	1	36	a	35.68	1.29	29.99	0.04	8.03
Tour_1390	1	37	a	35.45	1.21	29.75	0.03	8.12
Tour_1390	1	38	a	35.71	1.34	29.74	0.05	7.93
Tour_1390	1	39	a	35.60	1.24	29.99	0.06	7.89
Tour_1390	1	40 - rim	a	35.24	1.18	29.90	0.03	7.89
Tour_1390	10	1 - core	a	36.63	0.68	30.75	0.06	7.81
Tour_1390	10	2	a	35.96	1.08	30.12	0.06	7.79
Tour_1390	10	3	a	35.67	1.23	30.03	0.08	7.90
Tour_1390	10	4	a	36.21	1.15	29.99	0.04	7.99
Tour_1390	10	5	a	35.89	1.20	30.05	0.05	8.03
Tour_1390	10	6	a	35.96	1.26	30.11	0.10	7.82
Tour_1390	10	7	a	35.87	1.26	30.03	0.06	7.91
Tour_1390	10	8	a	36.10	1.04	29.98	0.04	8.04
Tour_1390	10	9	a	36.39	1.03	29.86	0.05	7.98
Tour_1390	10	10	a	36.50	1.11	29.78	0.05	8.07
Tour_1390	10	11	a	35.98	1.16	29.82	0.04	8.00
Tour_1390	10	12	a	36.31	1.27	29.79	0.05	8.01
Tour_1390	10	13	a	35.85	1.30	29.90	0.02	8.04
Tour_1390	10	14	a	35.75	1.26	29.91	0.04	8.03
Tour_1390	10	15	a	36.17	1.25	29.91	0.03	7.97
Tour_1390	10	16	a	36.36	1.26	29.95	0.03	7.98

Sample	Grain no.	Sequence no.	Sector	SiO ₂	TiO ₂	Al ₂ O ₃	Cr ₂ O ₃	MgO
Tour_1390	10	17	a	35.62	1.29	29.93	0.07	7.92
Tour_1390	10	18	a	34.84	1.24	29.98	0.03	8.02
Tour_1390	10	19	a	35.68	1.24	29.80	0.03	8.02
Tour_1390	10	20	a	36.08	1.33	29.89	0.06	7.89
Tour_1390	10	21	a	36.40	1.35	29.62	0.04	7.93
Tour_1390	10	22	a	35.77	1.38	29.80	0.06	7.90
Tour_1390	10	23	a	35.98	1.32	29.82	0.09	7.95
Tour_1390	10	24	a	36.01	1.40	29.83	0.07	7.88
Tour_1390	10	25	a	36.09	1.32	29.83	0.05	7.98
Tour_1390	10	26	a	35.91	1.29	29.73	0.05	7.85
Tour_1390	10	27	a	36.13	1.30	29.87	0.05	7.94
Tour_1390	10	28	a	36.09	1.31	29.99	0.06	7.89
Tour_1390	10	29	a	36.26	1.29	29.95	0.04	7.87
Tour_1390	10	30	a	36.10	1.28	29.86	0.02	7.88
Tour_1390	10	31	a	36.36	1.26	29.78	0.03	7.95
Tour_1390	10	32	a	36.28	1.32	29.66	0.04	7.86
Tour_1390	10	33	a	35.77	1.26	29.80	0.03	7.91
Tour_1390	10	34	a	35.43	1.29	30.02	0.03	7.89
Tour_1390	10	35	a	35.27	1.24	30.01	0.02	7.86
Tour_1390	10	36 - rim	a	35.85	1.07	29.92	0.04	7.98
Tour_1390	10	1 - core	+c	36.66	0.58	31.32	0.04	7.57
Tour_1390	10	2	+c	36.38	0.76	31.01	0.06	7.53
Tour_1390	10	3	+c	36.85	0.47	31.50	0.05	7.74
Tour_1390	10	4	+c	36.55	0.62	31.06	0.08	7.68
Tour_1390	10	5	+c	36.33	0.97	30.62	0.05	7.50
Tour_1390	10	6	+c	36.39	0.90	30.84	0.04	7.60
Tour_1390	10	7	+c	36.64	0.80	31.04	0.05	7.49
Tour_1390	10	10	+c	36.64	0.40	31.48	0.05	7.81
Tour_1390	10	11	+c	36.79	0.47	30.94	0.04	7.88
Tour_1390	10	12	+c	36.52	0.39	30.98	0.03	7.78
Tour_1390	10	13	+c	36.18	0.28	31.31	0.03	7.61
Tour_1390	10	14	+c	36.76	0.27	31.84	0.03	7.90
Tour_1390	10	15	+c	36.59	0.56	31.02	0.05	7.80
Tour_1390	10	16	+c	35.52	0.38	31.60	0.04	7.74
Tour_1390	10	17	+c	36.58	0.37	31.56	0.03	7.78
Tour_1390	10	18	+c	36.60	0.69	30.80	0.07	7.88
Tour_1390	10	20	+c	36.59	0.55	30.94	0.05	7.73
Tour_1390	10	21	+c	36.18	0.63	31.04	0.04	7.68
Tour_1390	10	22	+c	36.62	0.53	31.17	0.02	7.62
Tour_1390	10	23	+c	36.20	0.42	31.45	0.02	7.74
Tour_1390	10	24	+c	36.95	0.44	31.34	0.02	7.63
Tour_1390	10	26	+c	36.79	0.87	30.86	0.06	7.61
Tour_1390	10	27	+c	36.84	0.91	30.80	0.01	7.46
Tour_1390	10	28	+c	36.72	0.69	31.17	0.01	7.55
Tour_1390	10	29	+c	36.06	0.84	31.19	0.02	7.47
Tour_1390	10	30	+c	35.85	0.80	31.25	0.02	7.45
Tour_1390	10	31	+c	36.07	0.76	31.26	0.03	7.46
Tour_1390	10	32	+c	36.78	0.83	31.21	0.02	7.42
Tour_1390	10	33	+c	36.49	0.87	30.99	0.02	7.42
Tour_1390	10	34	+c	35.82	0.92	30.73	0.02	7.67
Tour_1390	10	35	+c	36.05	0.83	31.05	0.02	7.47
Tour_1390	10	36	+c	36.31	0.67	31.22	0.01	7.49
Tour_1390	10	37	+c	36.42	0.60	31.11	0.01	7.59
Tour_1390	10	38	+c	36.29	0.46	31.25	0.01	7.65
Tour_1390	10	39	+c	36.23	0.47	31.26	0.01	7.73
Tour_1390	10	40	+c	36.06	0.62	31.02	0.04	7.84
Tour_1390	10	41	+c	36.72	0.55	30.85	0.03	7.85

Sample	Grain no.	Sequence no.	Sector	SiO ₂	TiO ₂	Al ₂ O ₃	Cr ₂ O ₃	MgO
Tour_1390	10	42	+c	36.66	0.55	31.04	0.02	7.88
Tour_1390	10	43	+c	36.51	0.59	30.88	0.03	7.88
Tour_1390	10	44	+c	36.46	0.67	30.63	0.03	7.82
Tour_1390	10	45	+c	36.21	0.72	30.72	0.03	7.95
Tour_1390	10	46	+c	35.63	0.70	30.69	0.02	7.87
Tour_1390	10	47	+c	36.59	0.71	30.33	0.04	7.93
Tour_1390	10	48	+c	36.16	0.66	30.47	0.04	7.98
Tour_1390	10	49	+c	36.46	0.68	30.43	0.02	7.82
Tour_1390	10	50	+c	36.04	0.58	30.50	0.03	7.92
Tour_1390	10	51	+c	36.19	0.59	30.37	< d.l.	8.03
Tour_1390	10	52	+c	36.27	0.68	30.25	0.02	8.02
Tour_1390	10	53	+c	36.40	0.66	30.58	0.02	7.88
Tour_1390	10	54	+c	36.44	0.66	30.54	0.02	7.90
Tour_1390	10	55	+c	36.21	0.60	30.66	0.01	7.87
Tour_1390	10	56	+c	36.58	0.76	30.50	0.02	7.71
Tour_1390	10	57	+c	36.30	0.78	30.69	0.02	7.60
Tour_1390	10	59	+c	36.10	0.95	30.39	0.01	7.62
Tour_1390	10	60 - rim	+c	36.01	1.01	30.11	0.04	7.67
Tour_1390	4	1 - core	a	33.03	1.19	27.72	0.08	7.89
Tour_1390	4	2	a	33.70	1.24	27.61	0.08	7.85
Tour_1390	4	3	a	32.94	1.26	28.16	0.08	7.79
Tour_1390	4	4	a	33.70	1.21	28.25	0.06	7.77
Tour_1390	4	5	a	32.49	1.22	28.48	0.05	7.86
Tour_1390	4	6	a	33.08	1.34	28.75	0.07	7.88
Tour_1390	4	7	a	32.83	1.25	28.46	0.03	7.89
Tour_1390	4	8	a	33.42	1.29	28.71	0.06	7.89
Tour_1390	4	9	a	33.39	1.29	28.37	0.03	7.89
Tour_1390	4	10	a	33.38	1.30	28.15	0.01	7.81
Tour_1390	4	11	a	32.81	1.25	28.24	0.01	7.87
Tour_1390	4	12	a	32.74	1.24	28.15	0.03	7.79
Tour_1390	4	14	a	33.53	1.21	28.24	0.02	7.76
Tour_1390	4	15	a	33.60	1.20	28.30	0.04	7.81
Tour_1390	4	16	a	33.42	1.25	28.39	0.04	7.92
Tour_1390	4	17	a	33.53	1.36	28.17	0.04	7.85
Tour_1390	4	18	a	32.96	1.28	27.63	0.06	8.16
Tour_1390	4	19	a	33.71	1.34	28.17	0.04	7.76
Tour_1390	4	20	a	32.92	1.38	28.09	0.04	7.83
Tour_1390	4	21	a	33.41	1.31	27.95	0.04	7.70
Tour_1390	4	22	a	33.21	1.28	28.17	0.05	7.81
Tour_1390	4	23	a	33.37	1.32	27.96	0.02	7.70
Tour_1390	4	24	a	33.94	1.30	27.85	0.05	7.67
Tour_1390	4	25	a	32.52	1.31	28.03	0.04	7.78
Tour_1390	4	26	a	31.90	1.24	27.86	0.01	7.76
Tour_1390	4	27	a	32.90	1.27	27.79	0.04	7.74
Tour_1390	4	28	a	33.86	1.21	27.51	0.03	7.77
Tour_1390	4	29	a	33.38	1.23	27.62	0.03	7.71
Tour_1390	4	30 - rim	a	32.38	1.15	27.44	0.03	7.65
Tour_1390	4	1 - core	-c	33.19	1.12	27.96	0.04	7.79
Tour_1390	4	3	-c	33.28	1.19	27.81	0.05	7.80
Tour_1390	4	4	-c	33.50	1.16	27.77	0.02	7.74
Tour_1390	4	5	-c	33.33	1.16	27.60	0.04	7.79
Tour_1390	4	6	-c	32.78	1.16	27.90	0.05	7.88
Tour_1390	4	8	-c	32.34	1.14	27.40	0.02	7.93
Tour_1390	4	9	-c	32.71	1.18	27.63	0.06	7.81
Tour_1390	4	10	-c	32.52	1.15	27.88	0.07	7.82
Tour_1390	4	11	-c	32.77	1.15	27.83	0.05	7.82
Tour_1390	4	12	-c	33.36	1.14	27.91	0.02	7.88

Sample	Grain no.	Sequence no.	Sector	SiO ₂	TiO ₂	Al ₂ O ₃	Cr ₂ O ₃	MgO
Tour_1390	4	13	-c	32.75	1.17	28.44	0.04	8.09
Tour_1390	4	15	-c	33.80	1.15	28.13	0.06	7.95
Tour_1390	4	16	-c	32.86	1.25	28.00	0.02	7.88
Tour_1390	4	17	-c	33.73	1.22	27.62	0.01	7.78
Tour_1390	4	18	-c	32.58	1.21	27.88	0.04	7.93
Tour_1390	4	19	-c	31.91	1.21	27.66	0.02	7.79
Tour_1390	4	20	-c	32.79	1.25	27.69	0.01	7.76
Tour_1390	4	21	-c	33.07	1.27	27.75	0.04	7.85
Tour_1390	4	22	-c	33.46	1.12	27.86	0.01	7.75
Tour_1390	4	24	-c	33.22	1.29	27.92	0.02	7.91
Tour_1390	4	26	-c	32.91	1.24	27.51	0.03	7.91
Tour_1390	4	27	-c	33.68	1.24	27.60	0.05	8.01
Tour_1390	4	28	-c	33.40	1.18	27.43	0.02	7.92
Tour_1390	4	29	-c	33.10	1.24	27.51	0.04	7.86
Tour_1390	4	31	-c	33.56	1.21	27.32	0.03	7.97
Tour_1390	4	32	-c	33.21	1.18	27.56	0.01	7.97
Tour_1390	4	34	-c	32.95	1.23	27.17	0.03	7.93
Tour_1390	4	35	-c	33.21	1.16	26.97	0.02	7.93
Tour_1390	4	37	-c	33.89	1.17	27.43	0.02	7.88
Tour_1390	4	39	-c	32.76	1.22	27.85	0.01	7.91
Tour_1390	4	40 - rim	-c	33.48	1.17	27.65	0.08	7.88

Grain no.	Sequence no.	MnO	FeO	CaO	Na ₂ O	K ₂ O	F	Total
1	1 - core	0.01	6.27	0.88	1.96	0.02	< d.l.	84.38
1	2	0.01	6.17	0.89	1.90	0.00	< d.l.	83.82
1	3	0.02	5.95	0.87	1.98	0.01	< d.l.	83.52
1	4	0.01	6.14	0.84	1.99	0.01	0.02	83.91
1	5	< d.l.	6.80	1.51	1.90	0.00	0.02	83.58
1	6	< d.l.	6.97	1.43	1.81	0.02	< d.l.	83.39
1	7	0.02	6.60	1.53	1.86	0.00	0.03	84.18
1	8	0.02	6.70	1.53	1.92	0.00	< d.l.	84.50
1	9	0.01	6.63	1.58	1.83	0.02	0.02	83.03
1	10	< d.l.	6.59	1.61	1.88	0.00	< d.l.	83.92
1	11	< d.l.	6.63	1.60	1.89	0.00	< d.l.	84.11
1	12	0.02	6.58	1.56	1.87	0.00	< d.l.	84.37
1	13	0.02	6.56	1.69	1.83	0.02	0.03	84.42
1	14	0.01	6.65	1.62	1.89	0.00	< d.l.	84.57
1	15	< d.l.	6.66	1.62	1.90	0.01	0.02	84.88
1	16	0.01	6.41	1.62	1.87	0.00	0.03	83.58
1	17	0.02	6.46	1.60	1.84	0.01	0.03	83.99
1	18	< d.l.	6.47	1.64	1.82	0.01	0.02	84.25
1	19	< d.l.	6.51	1.60	1.91	0.01	0.03	84.48
1	20	< d.l.	6.63	1.58	1.88	0.00	< d.l.	84.39
1	21	< d.l.	6.86	1.60	1.81	0.01	< d.l.	84.72
1	22	0.02	6.67	1.64	1.86	0.01	< d.l.	85.15
1	23	0.04	6.74	1.62	1.83	0.01	< d.l.	85.04
1	24	0.02	7.00	1.64	1.89	0.00	< d.l.	84.71
1	25	0.03	6.90	1.67	1.86	0.02	< d.l.	84.75
1	26	< d.l.	6.86	1.60	1.86	0.01	0.02	84.43
1	27	0.01	7.00	1.73	1.86	0.01	< d.l.	84.42
1	28	0.01	7.14	1.72	1.86	0.02	< d.l.	85.16
1	29	0.04	6.94	1.74	1.84	0.01	< d.l.	85.07
1	30	0.01	7.04	1.73	1.84	0.01	0.02	85.33
1	31	0.03	7.56	1.75	1.85	0.01	< d.l.	85.54
1	32	0.03	7.64	1.56	2.02	0.01	< d.l.	86.49
1	33	0.01	7.48	1.65	1.92	0.01	0.02	85.43
1	34	0.02	7.06	1.57	1.83	0.01	< d.l.	85.44
1	35	0.03	7.01	1.64	1.85	0.00	0.04	85.64
1	36	0.02	6.89	1.57	1.88	0.01	0.02	85.42
1	37	< d.l.	7.03	1.59	1.93	0.02	< d.l.	85.14
1	38	0.03	6.87	1.47	1.87	0.02	< d.l.	85.03
1	39	0.04	7.25	1.42	1.92	0.02	< d.l.	85.42
1	40 - rim	0.01	7.34	1.32	1.96	0.00	< d.l.	84.88
10	1 - core	0.02	6.82	1.23	1.89	0.00	< d.l.	85.88
10	2	0.01	7.19	1.55	1.83	0.01	< d.l.	85.60
10	3	0.03	7.03	1.57	1.81	0.01	< d.l.	85.36
10	4	0.01	7.02	1.61	1.91	0.00	< d.l.	85.94
10	5	0.01	6.80	1.61	1.82	0.01	< d.l.	85.47
10	6	0.03	7.02	1.57	1.82	0.01	< d.l.	85.69
10	7	0.01	7.23	1.57	1.88	0.02	0.02	85.86
10	8	0.01	7.39	1.60	1.87	0.00	< d.l.	86.08
10	9	0.02	7.14	1.60	1.87	0.01	0.02	85.97
10	10	0.01	7.04	1.56	1.86	0.01	0.03	86.01
10	11	0.01	6.95	1.63	1.85	0.00	< d.l.	85.44
10	12	0.04	6.95	1.59	1.84	0.01	0.02	85.88
10	13	0.01	6.95	1.56	1.88	0.01	< d.l.	85.53
10	14	0.02	7.11	1.53	1.86	0.01	< d.l.	85.52
10	15	< d.l.	7.17	1.58	1.91	0.01	< d.l.	86.00
10	16	0.01	7.15	1.56	1.88	0.01	< d.l.	86.19
10	17	0.02	7.10	1.54	1.87	0.01	< d.l.	85.37
10	18	0.04	7.03	1.58	1.91	0.01	0.01	84.69

Grain no.	Sequence no.	MnO	FeO	CaO	Na ₂ O	K ₂ O	F	Total
10	19	0.03	7.18	1.57	1.90	0.01	0.02	85.48
10	20	< d.l.	7.28	1.52	1.84	0.00	< d.l.	85.89
10	21	< d.l.	7.15	1.49	1.89	0.01	< d.l.	85.88
10	22	0.03	7.02	1.49	1.90	0.01	< d.l.	85.36
10	23	< d.l.	7.25	1.52	1.91	0.01	0.02	85.87
10	24	0.02	7.25	1.44	1.87	0.01	< d.l.	85.78
10	25	0.01	7.33	1.45	1.93	0.02	< d.l.	86.01
10	26	< d.l.	7.22	1.48	1.92	0.00	< d.l.	85.45
10	27	0.01	7.21	1.44	1.97	0.01	< d.l.	85.93
10	28	0.02	7.12	1.39	1.94	0.01	0.03	85.84
10	29	0.01	7.41	1.37	1.95	0.00	< d.l.	86.15
10	30	< d.l.	7.38	1.36	1.94	0.01	< d.l.	85.84
10	31	0.02	7.30	1.38	1.96	0.01	< d.l.	86.06
10	32	0.01	7.50	1.32	1.99	0.02	< d.l.	85.99
10	33	< d.l.	7.44	1.36	1.98	0.01	< d.l.	85.55
10	34	0.03	7.43	1.33	1.98	0.01	0.01	85.44
10	35	< d.l.	7.21	1.30	2.00	0.01	< d.l.	84.91
10	36 - rim	0.01	7.21	1.21	2.04	0.01	< d.l.	85.33
10	1 - core	< d.l.	6.80	1.06	1.87	0.00	< d.l.	85.90
10	2	0.03	6.85	1.21	1.81	0.00	< d.l.	85.64
10	3	< d.l.	6.45	1.05	1.81	0.00	< d.l.	85.92
10	4	0.01	6.60	1.17	1.81	0.01	< d.l.	85.59
10	5	< d.l.	7.16	1.24	1.82	0.00	< d.l.	85.69
10	6	0.03	7.12	1.24	1.92	0.01	< d.l.	86.08
10	7	0.01	7.01	1.10	1.83	0.02	< d.l.	85.98
10	10	0.04	6.34	1.11	1.84	0.00	< d.l.	85.71
10	11	< d.l.	6.55	1.13	1.85	0.00	0.04	85.69
10	12	0.03	6.50	1.11	1.81	0.00	0.01	85.16
10	13	0.02	6.01	1.04	1.79	0.01	< d.l.	84.27
10	14	< d.l.	6.08	1.01	1.85	0.01	0.02	85.77
10	15	0.03	6.49	1.19	1.85	0.01	0.01	85.60
10	16	< d.l.	6.49	1.11	1.85	0.00	< d.l.	84.73
10	17	< d.l.	6.54	1.11	1.88	0.01	0.01	85.87
10	18	0.02	6.81	1.31	1.87	0.01	0.04	86.11
10	20	0.02	6.59	1.13	1.86	0.01	< d.l.	85.46
10	21	< d.l.	6.74	1.15	1.92	0.00	< d.l.	85.38
10	22	0.02	6.73	1.14	1.87	0.01	0.02	85.75
10	23	0.02	6.29	1.10	1.81	0.01	< d.l.	85.06
10	24	0.02	6.58	1.12	1.78	0.00	< d.l.	85.88
10	26	0.01	6.90	1.17	1.87	0.01	< d.l.	86.14
10	27	0.01	7.07	1.10	1.82	0.01	0.03	86.07
10	28	0.03	6.84	1.11	1.85	0.01	0.01	85.98
10	29	0.01	6.68	1.06	1.88	0.00	< d.l.	85.21
10	30	0.02	6.98	1.07	1.81	0.00	< d.l.	85.25
10	31	0.03	6.77	1.09	1.84	0.00	< d.l.	85.31
10	32	< d.l.	7.10	1.06	1.90	0.01	0.01	86.35
10	33	0.02	6.94	1.08	1.87	0.01	0.03	85.73
10	34	0.02	6.96	1.12	1.90	0.01	< d.l.	85.16
10	35	0.01	6.89	1.06	1.89	0.01	< d.l.	85.27
10	36	< d.l.	6.80	1.06	1.84	0.00	0.03	85.42
10	37	< d.l.	6.69	1.05	1.86	0.02	0.03	85.37
10	38	0.02	6.49	1.04	1.87	0.00	< d.l.	85.08
10	39	0.02	6.58	1.07	1.85	0.00	< d.l.	85.22
10	40	< d.l.	6.75	1.14	1.91	0.01	0.02	85.40
10	41	< d.l.	6.47	1.14	1.88	0.01	< d.l.	85.51
10	42	0.02	6.54	1.07	1.94	0.01	< d.l.	85.74
10	43	0.02	6.45	1.09	1.89	0.00	0.05	85.39

Grain no.	Sequence no.	MnO	FeO	CaO	Na ₂ O	K ₂ O	F	Total
10	44	0.02	6.39	1.08	1.91	0.00	< d.l.	85.01
10	45	< d.l.	6.82	1.15	1.94	0.02	< d.l.	85.56
10	46	0.02	6.68	1.07	1.96	0.01	0.01	84.66
10	47	0.01	6.86	1.21	1.98	0.00	< d.l.	85.66
10	48	0.01	6.84	1.12	1.96	0.01	0.04	85.29
10	49	0.03	6.80	1.12	1.97	0.00	< d.l.	85.33
10	50	0.01	6.83	1.05	2.00	0.00	0.01	84.98
10	51	0.01	6.71	1.03	1.99	0.00	0.01	84.93
10	52	< d.l.	6.97	1.10	2.05	0.01	< d.l.	85.36
10	53	0.01	6.98	1.02	2.00	0.01	< d.l.	85.56
10	54	0.01	7.01	1.05	2.06	0.01	0.05	85.75
10	55	0.01	6.88	0.95	2.01	0.00	< d.l.	85.20
10	56	0.02	7.11	0.96	2.03	0.00	< d.l.	85.69
10	57	< d.l.	6.97	0.96	1.97	0.01	< d.l.	85.31
10	59	0.01	7.36	0.95	2.06	0.02	< d.l.	85.46
10	60 - rim	0.01	7.04	0.97	2.02	0.01	< d.l.	84.89
4	1 - core	< d.l.	7.27	1.95	1.55	0.01	< d.l.	80.69
4	2	0.01	7.18	2.02	1.54	0.02	< d.l.	81.24
4	3	0.02	7.08	1.69	1.75	0.02	< d.l.	80.79
4	4	< d.l.	7.05	1.55	1.81	0.01	< d.l.	81.42
4	5	0.01	6.93	1.61	1.81	0.01	0.04	80.50
4	6	0.02	7.04	1.59	1.91	0.00	0.01	81.69
4	7	0.02	7.04	1.62	1.84	0.00	< d.l.	80.98
4	8	0.02	6.84	1.49	1.85	0.01	< d.l.	81.58
4	9	< d.l.	7.04	1.51	1.89	0.00	< d.l.	81.41
4	10	< d.l.	7.16	1.54	1.93	0.02	< d.l.	81.30
4	11	0.03	7.02	1.54	1.90	0.01	< d.l.	80.69
4	12	0.03	7.10	1.50	1.87	0.01	< d.l.	80.46
4	14	< d.l.	7.04	1.58	1.93	0.00	0.02	81.32
4	15	< d.l.	7.04	1.46	1.90	0.01	0.02	81.39
4	16	0.01	7.05	1.45	1.85	0.01	0.04	81.43
4	17	0.03	7.03	1.44	1.84	0.01	0.02	81.32
4	18	0.01	7.54	1.47	1.82	0.02	< d.l.	80.95
4	19	0.03	7.06	1.43	1.86	0.01	< d.l.	81.40
4	20	0.02	7.07	1.41	1.93	0.00	0.01	80.71
4	21	0.03	7.07	1.41	1.96	0.01	0.02	80.90
4	22	< d.l.	7.06	1.36	1.96	0.01	< d.l.	80.91
4	23	< d.l.	7.08	1.34	1.90	0.01	< d.l.	80.70
4	24	< d.l.	7.09	1.33	1.98	0.01	< d.l.	81.21
4	25	0.02	7.16	1.35	1.95	0.01	0.05	80.21
4	26	< d.l.	7.23	1.32	1.97	0.01	< d.l.	79.30
4	27	0.03	7.29	1.29	1.98	0.01	< d.l.	80.34
4	28	0.01	7.20	1.25	1.99	0.01	< d.l.	80.84
4	29	0.01	7.13	1.25	2.01	0.01	< d.l.	80.38
4	30 - rim	0.01	7.02	1.18	2.04	0.01	0.02	78.94
4	1 - core	0.03	7.24	1.74	1.77	0.01	0.04	80.93
4	3	0.03	7.42	2.00	1.60	0.01	< d.l.	81.20
4	4	0.01	7.43	2.07	1.55	0.00	< d.l.	81.25
4	5	0.02	7.32	2.01	1.56	0.02	< d.l.	80.85
4	6	0.01	7.30	2.02	1.59	0.01	< d.l.	80.70
4	8	< d.l.	7.19	2.01	1.59	0.00	< d.l.	79.62
4	9	0.02	7.38	1.92	1.62	0.01	< d.l.	80.33
4	10	0.03	7.38	1.90	1.62	0.01	< d.l.	80.37
4	11	0.01	7.36	2.11	1.58	0.02	0.01	80.70
4	12	0.01	7.45	2.05	1.56	0.01	< d.l.	81.39
4	13	0.01	7.26	1.99	1.65	0.01	< d.l.	81.41
4	15	0.03	7.12	1.96	1.62	0.01	0.01	81.84

Grain no.	Sequence no.	MnO	FeO	CaO	Na ₂ O	K ₂ O	F	Total
4	16	0.01	7.56	1.93	1.64	0.01	< d.l.	81.16
4	17	0.03	7.69	1.94	1.64	0.02	< d.l.	81.69
4	18	0.02	7.49	1.92	1.64	0.01	< d.l.	80.72
4	19	< d.l.	7.48	1.96	1.62	0.02	< d.l.	79.66
4	20	0.02	7.37	1.91	1.65	0.01	< d.l.	80.46
4	21	0.03	7.23	1.90	1.64	0.01	0.01	80.80
4	22	< d.l.	7.38	2.01	1.56	0.01	< d.l.	81.16
4	24	< d.l.	7.44	1.94	1.64	0.02	0.03	81.43
4	26	0.02	7.21	1.94	1.67	0.01	< d.l.	80.45
4	27	0.01	7.24	1.89	1.68	0.00	< d.l.	81.40
4	28	< d.l.	7.30	1.92	1.64	0.01	0.02	80.84
4	29	0.03	7.48	1.85	1.75	0.00	< d.l.	80.86
4	31	0.01	7.47	1.77	1.69	0.01	0.01	81.06
4	32	0.01	7.28	1.81	1.73	0.01	< d.l.	80.77
4	34	0.02	7.47	1.75	1.74	0.01	< d.l.	80.29
4	35	0.06	7.46	1.72	1.79	0.01	< d.l.	80.33
4	37	0.01	7.45	1.70	1.76	0.01	< d.l.	81.33
4	39	0.03	7.83	1.68	1.75	0.01	< d.l.	81.04
4	40 - rim	0.02	7.15	1.57	1.82	0.01	< d.l.	80.83

